SPECTROCHIMICA ACTA

Founder Editor

A. GATTERER S.J. +

Editors

UNITED KINGDOM

E. H. S. van SOMEREN — *London*

H. W. THOMPSON — *Oxford*

U.S.A.

V. A. FASSEL — *Ames, Iowa*

F. A. MILLER — *Pittsburgh*

EDITORIAL ADVISORY BOARD

B. Bak, *Copenhagen*
N. S. Bayliss, *Perth, W. Aust.*
L. J. Bellamy, *Waltham Abbey*
Wallace R. Brode, *Washington, D.C.*
C. G. Cannon, *Pontypool*
C. G. Carlsson, *Stockholm*
B. L. Crawford, *Minneapolis*
G. Duyckaerts, *Liége*
C. Feldman, *Oak Ridge*
W. Gordy, *Durham, N.C.*
D. Hadzi, *Ljubljana*
D. F. Hornig, *Providence, Rhode Island*
R. N. Jones, *Ottawa*
H. Kaiser, *Dortmund*
M. Kasha, *Tallahassee*
J. A. A. Ketelaar, *Amsterdam*
J. Lecomte, *Paris*
E. Loeuille, *Paris*
R. C. Lord, *Cambridge, Mass.*
S. L. Mandelstam, *Moscow*
A. Mangini, *Bologna*
J. R. McNally, *Oak Ridge*
R. Mecke, *Freiburg*
A. C. Menzies, *London*
S. Mizushima, *Tokyo*
R. L. Mitchell, *Aberdeen*
G. Porter, *Sheffield*
W. C. Price, *London*
R. E. Richards, *Oxford*
H. Schüler, *Hechingen-Hohenzollern*
B. F. Scribner, *Washington D.C.*
N. Sheppard, *Cambridge*
H. Shull, *Bloomington, Indiana*
D. M. Smith, *Wembley*
H. Stammreich, *São Paulo*
B. Vodar, *Bellevue, S. et O.*
A. Walsh, *Melbourne*
H. L. Welsh, *Toronto*
M. Kent Wilson, *Medford, Mass.*
N. Wright, *Midland (Mich.)*

VOLUME IX

1957

PERGAMON PRESS

LONDON · NEW YORK · PARIS · LOS ANGELES

OL.
9
57

Spectrochim. Acta

SPECTROCHIMICA ACTA

EDITORS

GREAT BRITAIN AND BRITISH COMMONWEALTH OF NATIONS

Dr. H. W. Thompson, F.R.S., St. John's College, Oxford

E. H. S. van Someren, B.Sc., F.Inst.P., 4 Churchfields, Broxbourne, Herts, England

UNITED STATES OF AMERICA

Dr. V. A. Fassel, Iowa State College, Ames, Iowa, U.S.A.

Dr. F. A. Miller, Mellon Institute for Industrial Research, Pittsburgh, Penna., U.S.A.

CONTENTS OF VOLUME IX

No. 1

Page

Editors' Note 1

J. K. Hurwitz: Spectrographic analysis of segregates with a dynamic microvolume technique—I. Theory 3

Cyrus Feldman and Margaret K. Wittels: Sample transport and temperature studies in porous-cup discharges 19

K. K. Turekian, P. W. Gast, and J. L. Kulp: Emission-spectrographic method for the determination of strontium in silicate materials 40

L. P. Lindeman and M. Kent Wilson: Infra-red spectra of $GeCl_4$, $GeHCl_3$, and $GeDCl_3$ 47

M. Judith Schmelz, Tatsuo Miyazawa, San-Ichiro Mizushima, T. J. Lane, and J. V. Quagliano: Infra-red absorption spectra of inorganic co-ordination complexes—IX. Infra-red spectra of oxalato complexes 51

R. N. Dixon: The structure of some halogenated ethanes from infra-red measurements 59

C. M. Cundall and J. D. Craggs: Excitation temperatures in spark discharges . . 68

William H. Dennen: Spectrographic determination of carbon in sedimentary rocks, using direct-current arc excitation 89

Spectrochemical Note:

Foil A. Miller and William B. White: Electronic spectrum and apparent thermochromism of $VOCl_3$ 98

Meetings 101

Book Review:

Gaustav Kortüm: Colorimetry, Photometry, and Spectrometry (reviewed by E. van Someren) 104

VOL. 9 1957

Contents

No. 2

Page

CHARLES E. WHITE, DONALD E. HOFFMAN, and JOHN S. MAGEE JR: Fluorescence emission spectra, fluorescence excitation spectra, and absorption spectra of some metal chelates 105

R. C. LORD, A. L. MARSTON, and FOIL A. MILLER: Infra-red and Raman spectra of the diazines 113

HARRY C. ALLEN JR., L. R. BLAINE, and EARLE K. PLYLER: The emission spectrum of OH from 2·8 to 4·1 μ 126

R. A. RUSSELL and H. W. THOMPSON: Vibrational band shapes and band intensities . 133

JOHN W. OTVIS, HENRY STONE, and W. R. HARP JR.: Theory of radiant-energy absorption by randomly dispersed discrete particles 148

Spectrochemical Notes:

J. NOAR: An apparatus for the excitation of powders in the direct-current arc . . 157

N. W. H. ADDINK: Excitation energies in line spectra 158

Reports of Meetings 160

Notice of Meeting 174

Announcement 175

No. 3

J. E. GREENSTREET and K. P. NORRIS: The existence of differences between the infra-red absorption spectra of bacteria 177

I. NAKAGAWA, R. B. PENLAND, S. MIZUSHIMA, T. J. LANE, and J. V. QUAGLIANO: Infra-red absorption spectra of inorganic co-ordination complexes—XI. Infra-red studies of mercuric amidobromide, $Hg(NH_2)Br$ 199

PAUL A. GIGUÈRE et KENNETH B. HARVEY: Spectra d'absorption infra-rouge du protoxyde d'azote à l'état solide 204

H. W. THOMPSON, R. W. NEEDHAM, and D. JAMESON: The intensities of the carbonyl group vibration in some aromatic compounds 208

ALF LOFTHUS: The accuracy of photographic intensity measurements of absorption spectra 216

ROGER BARTEL and ALAN GOLDBLATT: The direct-reading spectrometric analysis of alloy cast iron 227

R. N. JONES: The intensities of the infra-red absorption bands of *n*-paraffin hydrocarbons 235

V. RAMAKRISHNA RAO and V. SURYANARAYANA: Analysis of the near-ultra-violet absorption spectrum of *p*-fluoroanisole 252

Spectrochemical Note:

D. HADŽI and D. JERAMIĆ: The infra-red spectrum and the O—H in-plane deformation frequency in CH_3CD_2OH 263

Papers to be published in future issues 264

Contents

No. 4

Page

CHIZUKO TANAKA, KENJI KURATANI, and SAN-ICHIRO MIZUSHIMA: In-plane normal vibrations of methanol 265

F. S. MORTIMER: Vibrational assignment and rotational isomerism in some simple organic phosphates 270

E. M. TANNER: The infra-red absorption spectra of some indole-3-ketones 282

B. J. RUSHTON and G. D. NICHOLLS: A spectrographic scheme for the determination of Al, Ti, Fe, Ca, Mg, and Mn in silicates 287

F. W. J. GARTON: The spectrographic determination of boron in graphite 297

C. GORDON PEATTIE and L. B. ROGERS: Analytical studies of the fluorescence of samarium in calcium sulphate 307

ROBERT C. FRANK, JAMES E. DALLEMAND, and DAVID L. FRY: A statistical study on the homogeneity of zinc-base spectrographic standards 323

J. R. BUTLER: The spectrographic determination of the rare earths 332

L. J. BELLAMY and R. L. WILLIAMS: The NH stretching frequencies of primary amines 341

ERIKA SMAKULA, AUGUSTUS GORI, and HERBERT H. WOTIZ: Effects of polymorphism and influence of sample preparation on the infra-red spectrum of estradiol-17β . . 346

Reports of Meetings:

The Tenth Conference on Spectroscopy in the U.S.S.R. 357

The Eighth Annual Symposium on Spectroscopy 359

Notice of Meeting 363

Announcement 363

Papers to be published in future issues 364

VOL. 9 1957

Publishing offices: 4 & 5 Fitzroy Square, London W. 1 (EUSton 4455). Subscriptions per volume (including postage) £7 7s. (U.S.A. $20.60). Back numbers £9 ($25.20) per volume.

Payment must be made in advance

Distributors: U.K. only—*Hilger & Watts Ltd. (Hilger Division), 98 St. Pancras Way, London N.W.1*

U.S.A.—*Pergamon Press, Inc., 122 East 55th Street, New York 22, N.Y.*

All other countries—*I. R. Maxwell & Co. Ltd., 4 & 5 Fitzroy Square, London W.1*

PERGAMON PRESS

4 & 5 FITZROY SQUARE, LONDON W.1 122 EAST 55th STREET, NEW YORK 22, N.Y.

24 RUE DES ÉCOLES, PARIS, Ve 10638 SOUTH WILTON PLACE, LOS ANGELES 47, CALIF.

AUTHOR INDEX TO VOLUME IX

ADDINK, N. W. H.: Excitation energies in line spectra. p. 158

ALLEN, H. C., JR., BLAINE, L. R. and PHYLER, E. K.: The emission spectrum of OH from 2·8 to 4·1 μ. p. 126

BARTEL, R. and GOLDBLATT, A.: The direct reading spectrometric analysis of alloy cast iron. p. 227

BELLAMY, L. J. and WILLIAMS, R. L.: The NH stretching frequencies of primary amines. p. 341

BLAINE, L. R.: *see* ALLEN, H. C., JR.

BUTLER, J. R.: The spectrographic determination of the rare earths. p. 332

CRAGGS, J. D.: *see* CUNDALL, C. M.

CUNDALL, C. M. and CRAGGS, J. D.: Excitation temperatures in spark discharges. p. 68

DALLEMAND, J. E.: *see* FRANK, R. C.

DENNEN, W. H.: Spectrographic determination of carbon in sedimentary rocks, using direct current arc excitation. p. 89

DIXON, R. N.: The structure of some halogenated ethanes from infra-red measurements. p. 59

FELDMAN, C. and WITTELS, M. K.: Sample transport and temperature studies in porous-cup discharges. p. 19

FRANK, R. C., DALLEMAND, J. E. and FRY, D. L.: A Statistical Study on the homogeneity of zinc-base spectrographic standards. p. 323

FRY, D. L.: *see* FRANK, R. C.

GARTON, F. W. J.: The spectrographic determination of boron in graphite. p. 297

GAST, P. W.: *see* TUREKIAN, K. K.

GIGUÈRE, P. A. and HARVEY, K. B.: Spectra d'absorption infra-rouge du protoxyde d'azote à l'état solide. p. 204

GOLDBLATT, A.: *see* BARTEL, R.

GORI, A.: *see* SMAKULA, E.

GREENSTREET, J. E. and NORRIS, K. P.: The existence of differences between the infra-red absorption spectra of bacteria. p. 177

HADŽI, D. and JERAMIĆ, D.: The infra-red spectrum of the O—H in-plane deformation frequency in CH_3CD_2OH. p. 263

HARP, W. R., JR.: *see* OTVIS, J. W.

HARVEY, K. B.: *see* GIGUÈRE, P. A.

HOFFMAN, D. E.: *see* WHITE, C. E.

HURWITZ, J. K.: Spectrographic analysis of segregates with a dynamic micro-volume technique—I. Theory. p. 31

JAMESON, D.: *see* THOMPSON, H. W.

JERAMIĆ, D.: *see* HADŽI, D.

JONES, R. N.: The intensities of the infra-red absorption bands of *n*-paraffin hydrocarbons. p. 235

KORTÜM, G.: Calorimetry, Photometry, and Spectrometry (reviewed by E. VAN SOMEREN) p. 104

KULP, J. L.: *see* TUREKIAN, K. K.

KURATANI, K.: *see* TANAKA, C. p. 265

LANE, T. J. *see* SCHMELZ, M. J.

LANE, T. J. *see* NAKAGAWA, I.

LINDEMAN, L. P. and WILSON, M. K.: Infra-red spectra of $GeCl_4$, $GeHCl_3$ and $GeDCl_3$. p. 47

LOFTHUS, A.: The accuracy of photographic intensity measurements of absorption spectra. p. 216

LORD, R. C., MARSTON, A. L. and MILLER, F. A.: Infra-red and Raman spectra of the diazines. p. 113

MAGEE, J. S., JR.: *see* WHITE, C. E.

MARSTON, A. L.: *see* LORD, R. C.

MILLER, F. A.: *see* LORD R. C.

MILLER, F. A. and WHITE, W. B.: Electronic spectrum and apparent thermochromism of $VOCl_3$. p. 98

MIYAZAWA, T.: *see* SCHMELZ, M. J.

MIZUSHIMA, S.: *see* SCHMELZ, M. J.

MIZUSHIMA, S.: *see* NAKAGAWA, I.

MIZUSHIMA, S.: *see* TANAKA, C.

MORTIMER, F. S.: Vibrational assignments and rotational isomerism in some simple organic phosphates. p. 270

NAKAGAWA, I., PENLAND, R. B., MIZUSHIMA, S., LANE, T. J. and QUAGLIANO, J. V.: Infra-red absorption spectra of inorganic co-ordination complexes—XI. Infra-red studies of mercuric amidobromide, $Hg(NH_2)Br$. p. 199

NEEDHAM, R. W.: *see* THOMPSON, H. W.

NICHOLLS, G. D.: *see* RUSHTON, B. J.

NOAR, J.: An apparatus for the excitation of powders in the direct-current arc. p. 157

NORRIS, K. P.: *see* GREENSTREET, J. E.

OTVIS, J. W., STONE, H. and HARP, W. R., JR.: Theory of radiant-energy absorption by randomly dispersed discrete particles. p. 148

PEATTIE, C. G. and ROGERS, L. B.: Analytical studies of the fluorescence of samarium in calcium sulphate. p. 307
PENLAND, R. B.: *see* NAKAGAWA, I.
PLYLER, E. K.: *see* ALLEN, H. C., JR.
QUAGLIANO, J. V.: *see* SCHMELZ, M. J.
QUAGLIANO, J. V.: *see* NAKAGAWA, I.
RAO, V. R. and SURYANARAYANA, V.: Analysis of the near ultra-violet absorption spectrum of *p*-fluoroanisole. p. 252
ROGERS, L. B.: *see* PEATTIE, C. G.
RUSHTON, B. J. and NICHOLLS, G. D.: A spectrographic scheme for the determination of Al, Ti, Fe, Ca, Mg, and Mn in silicates. p. 287
RUSSELL, R. A. and THOMPSON, H. W.: Vibrational band shapes and band intensities. p. 133
SCHMELZ, M. Z., MIYAZAWA, T., MIZUSHIMA, S., LANE, T. J. and QUAGLIANO, J. V.: Infra-red absorption spectra of inorganic co-ordination complexes—IX. Infra-red spectra of oxalato complexes. p. 51
SMAKULA, E., GORI, A. and WOTIZ, H. H.: Effects of polymorphism and influence of sample preparation on the infra-red spectrum of estradiol-17β. p. 346
STONE, H.: *see* OTVIS, J. W.
SURYANARAYANA, V.: *see* RAO, V. R.
TANAKA, C., KURATANI, K. and MIZUSHIMA, S.: In-plane normal vibrations of methanol. p. 265
TANNER, E. M.: The infra-red absorption spectra of some indole-3-ketones. p. 282
THOMPSON, H. W.: *see* RUSSELL, R. A.
THOMPSON, H. W., NEEDHAM, R. W. and JAMESON, D.: The intensities of the carbonyl group vibration in some aromatic compounds. p. 208
TUREKIAN, K. K., GAST, P. W. and KULP, J. L.: Emission spectrographic method for the determination of strontium in silicate materials. p. 40
WHITE, C. E., HOFFMAN, D. E. and MAGEE, J. S., JR.: Fluorescence emission spectra, fluorescence excitation spectra, and absorption spectra of some metal chelates. p. 105
WHITE, W. B.: *see* MILLER, F. A.
WILLIAMS, R. L.: *see* BELLAMY, L. J.
WILSON, M. K.: *see* LINDEMAN, L. P.
WITTELS, M. K.: *see* FELDMAN, C.
WOTIZ, H. H.: *see* SMAKULA, E.

VOL.
9
1957

SUBJECT INDEX TO VOLUME IX

Absorption: PAGE
Accuracy of photographic intensity measurements of absorption spectra 216
Of radiant energy by discrete particles 148
Amines, primary, NH stretching frequencies in — 341
Bacteria, Differences in the I.R. spectra of — 177
Book review:
Calorimetry, Photometry, Spectrometry (author G. KORTÜM) . 104
Boron in graphite spectrographic detn. 297
Carbon, Spectrographic determination in sedimentary rocks . . 89
Carbonyl frequencies in indole-3-ketones 282
Carbonyl group, Vibrational intensity in aromatic compounds . . 208
Cast Iron — spectrometric analysis of — 227
Chelates (metal —), Fluorescence emission and excitation spectra, and absorption spectra 105
Crystals:
I.R. spectra of some organic phosphates 270
I.R. spectra of estradiol-17β . . 346
I.R. studies of mercuric amidobromide 199
Diazines, I.R. and Raman spectra . 113
Direct Reading — analysis of cast iron 227
Discharges, Porous cup, Sample transport and temperature studies in — 19
Discharges, Spark, Line intensities and excitation temperatures in — . 68
Electronic spectrum of $VOCl_3$ . . 98
Estradiol-17β, Effects of polymorphism and sample preparation on the I.R. spectrum of — 346
Ethanol, heavy, I.R. spectrum and OH in-plane deformation frequency 263
Ethyl chloride-bromide, I.R. spectra and structure 59
Excitation energies in line spectra . 158
Excitation sources:
Excitation of powders in the d.c. arc. 157
Porous-cup discharges, Sample transport and temperature studies in— 19
Spark discharges, Excitation temperatures in — 68
Fluorescence spectroscopy:
Detn. of, and spectra of samarium in $CaSO_4$ 307
Emission and excitation spectra, and absorption spectra of some metal chelates 105
Germanium chlorides and deuterated germanes, I.R. spectra . . 47
Graphite, detn. of B in 297
Hydroxyl — emission spectrum of . 126
Hydroxyl — deformation frequency in CH_3CD_2CHOH . . . 263
Indole-3-ketones I.R. absorption spectra 282
Infra-red absorption intensity measurements: 133, 235
Band shapes and absorption intensities 133
of bands in *n*-paraffin hydrocarbons . 235
of the CO group in aromatic compounds 208
Infra-red absorption spectra:
of bacteria, differences in the — . 177
of CH_3CD_2OH and OH in plane deformation frequency . . 263
of C_2H_5Cl, C_2H_5Br and *trans* 1:2-$C_2H_4Cl_2$ 59
of estradiol-17β, Influence of polymorphism and sample preparation on the — 346
of $GeCl_4$, $GeHCl_3$ and $GeDCl_3$ . . 47
of indole-3-ketones 282
of mercuric amidobromide . . 199
of organic phosphates . . . 270
of oxalato complexes . . . 51
of solid nitrous oxide (in French) . 204
of the diazines 113
Infra-red emission spectra:
OH emission from 2·8 to 4·1 μ . . 126
Mercuric amidobromide, I.R. spectra and structure 199
Methanol, In-plane normal vibrations . 265
Methods:
for the excitation of powders in the d.c. arc 157
Point to plane method of direct spectrographic analysis of iron and steel. 227
Ultrasonic techniques . . . 359
Nitrous oxide, solid, I.R. spectrum of — (in French) 204
n-paraffin hydrocarbons, Intensity of I.R. absorption bands of — . 235

Notices of Meetings:
Seventh Colloquium Spectroscopicum Internationale, Liége, September 1958 101
Commission on Molecular Spectroscopy, Paris, July 1957 . . 102
European Molecular Spectroscopy Group, Freiburg, 9–13 July 1957 103
Institute of Petroleum Conference on Molecular Spectroscopy, London, 27–28 February 1958 . . 363
Sixth Ottawa Symposium of the Canadian Association for Applied Spectroscopy, Ottawa, 11–13 September 1957 103
Union of Chemical Societies of Yugoslavia, International Symposium on Hydrogen Bonding, Ljubljana, 30 July–3 August 1957 . . 174
Oxalato complexes, I.R. spectra of — . 51
Para-fluoro-anisole, Analysis of near U.V. absorption spectrum of — . 252
Phosphates, organic vibrational assignment and rotational isomerism in — 270
Photographic intensity measurements of absorption spectra, accuracy of . 216
Polymorphism in estradiol-17β . . 346
Raman spectra of the diazines . . 113
Rare earths, Spectrographic detn. . 332
Reports of Meetings:
Eighth Annual Pittsburgh Conference on Analytical Chemistry and Applied Spectroscopy, 3–8 March 1957 160
Eighth Annual Symposium on Spectroscopy, Chicago, Illinois, 29 April–1 May 1957. . . 359
Commission on Molecular Spectroscopy, Zürich, July 1955 . . 102
Colloquium Spectroscopicum Internationale, Amsterdam, 16 May 1956 101
Western Spectroscopy Assoc. Fourth Annual Conference, Los Angeles (Titles only) 173
Rotational isomerism in organic phosphates 270
Samarium in $CaSO_4$, Fluorescence of — 307
Segregates — spectrographic analysis of 3
Sedimentary Rocks — detn. of carbon in — 89
Silicate, Spectrographic detn. of strontium in — 40
Silicates, Spectrographic detn. of Al, Ti, Fe, Ca, Mg, Mn in — 287
Spectra (*see* I.R. —, U.V. —, Raman —, Vibrational —)
Strontium, Spectrographic detn. in silicate materials 40
Temperature studies in porous cup discharges 19
Temperatures in spark discharges . 68
Ultra-violet spectra:
Analysis of absorption spectrum of para-fluoro-anisole . . . 252
Electronic spectrum of $VOCl_3$ . . 98
Ultra-violet spectroscopy (*see* also Reports of Meetings)
Vibrational spectra:
Band shapes and absorption intensities 133
In-plane normal vibrations of methanol 265
Intensities of CO group vibrations in aromatic compounds . . 208
NH stretching frequencies of primary amines 341
Vibrational assignments in organic phosphates 270
Zinc-base spectrographic standards, Study on the homogeneity of — 323

VOL. 9 1957

EDITORS' NOTE

THE changing emphasis in spectroscopy over the past ten years, caused especially by the vast increase in measurements on molecular spectra of many kinds, has made it desirable to reorganize the operation of this journal. Originally it was mainly directed to problems of atomic emission spectroscopy and spectrographic analysis, and it is not intended that the importance of this aspect shall now be diminished. However, the impact upon chemistry, whether organic or physical, of molecular spectroscopy—emission or absorption, ultra-violet, infra-red or Raman—has been so great that many of their applications are now routine both for analysis and for work on molecular structure. They are equally significant in research, whether it be pure or applied.

It is therefore proposed to widen the scope of this international journal so as to cater for all the above lines of work. Also, it is hoped to include up-to-date reports on spectroscopic meetings held in different countries, general information of interest to spectroscopists internationally, reports of commissions, and other features. The Editorial Board has been reconstituted

so as to include recognized authorities on most aspects of the field, and its members will be replaced from time to time after a period of office. It is hoped that the journal will provide a rapid means of publication of spectrographic data of many kinds.

VOL.
9
1957

Spectrochimica Acta, 1957, Vol. 9, pp. 3 to 18. Pergamon Press Ltd., London

Spectrographic analysis of segregates with a dynamic microvolume technique—I

Theory*

J. K. HURWITZ†
Mines Branch, Department of Mines and Technical Surveys
Ottawa, Ontario, Canada

(*Received* 19 *July* 1956; *accepted for publication* 30 *October* 1956)

Abstract—To apply a dynamic microvolume technique to the analysis of segregates which are narrower than the width of the sparked crater, a theory was developed to predict the integrated intensities recorded on a photographic emulsion. Several variables in the technique are taken into account, namely, the size and shape of the sparked crater, the lengths of the spectrograph and microphotometer slits, the ratio of camera speed to sample speed, and the width of the segregate. It is shown how this theory can be conveniently applied for rapid use in the laboratory.

Introduction

MANY metallurgical samples submitted to the laboratory for segregate analysis have been rolled, forged, or extruded. The segregates or inclusions usually appear as bands or "stringers" in these products. For mathematical purposes, a suitable model on which to base a theory would be one in which the segregate is assumed to be bounded by two distinct boundaries (Fig. 1b). This situation might be called a double-boundary problem.

The ability of a dynamic or moving-plate-and-traversing-spark technique to differentiate between adjacent areas of different composition is limited [1] by

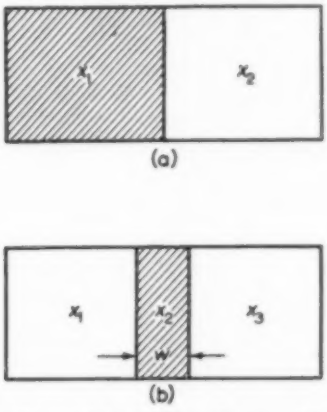

Fig. 1. (a) Boundary between two regions of different composition, (b) Model of a segregate showing boundaries separating segregate from the rest of the sample.

* Published by permission of the Acting Deputy Minister, Department of Mines and Technical Surveys, Ottawa, Ontario, Canada.
† Senior Scientific Officer, Mines.

four variables, namely, the size and shape of the sparked crater, the lengths of the spectrograph and microphotometer slits, and the ratio of camera speed to sample speed. In segregate analysis, the width of the segregate enters the problem as well. If it is narrower than the diameter of the sparked crater, a microvolume analysis will not give the true concentration in the segregate but a value somewhere between it and the concentration in the surrounding matrix.

In an earlier paper [1], the author developed the theory for a traverse across a single boundary between regions of different composition (Fig. 1a). The derived equations, although not too involved, were subsequently simplified. Also, the derivation was given only for the case where the length of the image of the spectrograph slit on the photographic emulsion was less than the product of the sparked-crater's diameter and the ratio of camera speed to sample speed. In the case where the reverse is true, the equations are similar and somewhat simpler in form. It is the purpose of this paper to show the simplification and extension of the single-boundary theory, to derive a generalized double-boundary theory for the analysis of segregated samples, and to indicate how this theory may conveniently be applied in the laboratory.

Assumptions and definition

Certain assumptions must be made concerning the sparked crater and the radiation emitted in the discharge. (a) The spark distribution on the surface of the sample is circular, and symmetrical about the centre of that circle. It has been shown [2] that this distribution is very nearly a paraboloid of revolution. (b) The intensity ratio of a spectral line pair is independent of the position on a homogeneous sample from which the emitting atoms are vaporized, that is the spectral line pair must be truly homologous. (c) The intensity ratio is proportional to the concentration ratio [3]. This means that all calculations may be performed directly in terms of concentration ratios instead of intensity ratios. (d) The spectrograph slit is assumed to be uniformly illuminated. (Although this is not a rigid requirement and although the theory could be worked out taking into account any nonuniformity in slit illumination, the theory is somewhat easier to derive and there are methods of assuring the validity of this assumption in practice.) (e) It is assumed that the sparked crater does not penetrate through the segregate. It is found in the laboratory that the maximum penetration of the crater at a very slow traverse rate is 0·008 in. for magnesium, 0·001 in. for steel, and less than 0·0002 in. for copper and brass.

The symbols used in this paper are as follows:

X_1 is the concentration ratio on the side of the boundary where the traverse is begun which will be called the initial side of the first boundary,

X_2 is the concentration ratio between the two boundaries in the two-boundary problem or the concentration ratio on the final side of the boundary in a single-boundary problem,

X_3 is the concentration ratio on the final side of the second boundary,

r is the radius of the sparked crater,

u is the distance of a boundary from the leading edge of the sparked crater when it is within the crater,

VOL. 9 1957

b is the ratio, $(r - u)/r$, and has all values between -1 and $+1$,
$V(b)$ is the volume represented by the effective spark distribution on the final side of a boundary at any instant,
V_T is the total volume represented by the effective spark distribution,
$g(b)$ is the ratio $V(b)/V_T$, which is determined by the effection spark distribution on the surface of the specimen,
$1 - g(b)$, therefore, will be the ratio of the sparked-crater's volume on the initial side of the boundary to the total volume,
v_p is the camera speed,
v_s is the sample speed
R is the ratio of camera speed to sample speed, v_p/v_s,
L is the length of the image of the spectrograph slit on the photographic emulsion,
K is the length of the microphotometer slit,
M is the magnification of the optical system in the microphotometer,
w is the distance between the two boundaries, i.e. the width of the segregate,
s is the distance on the photographic emulsion measured from A_1 in the zonal diagram (Figs. 2 and 3),
x is the distance in the zone A_1B_1 (Fig. 2) measured from A_1,
y is the distance in the zone B_1C_1 (Fig. 2a) measured from B_1,
z is the distance in the zone C_1D_1 (Fig. 2) measured from C_1,
$C_a(s)$ is the apparent concentration ratio recorded on the photographic emulsion at a point which is at a distance, s, from A_1,
C_a is the apparent concentration ratio which results from a microphotometer measurement,
t_0 is the time for a point on the photographic emulsion to be fully exposed which is the time for the emulsion to move a distance L, and
t is any time less than or equal to t_0.

The concentration ratios X_1, X_2, and X_3 may also be the concentrations of the element for which the analysis is performed if the concentration of the internal standard element is fixed. There are a few other symbols which are not defined above and which are used very little and late in the paper. These are introduced at the appropriate places.

Single-boundary traverse ($L \leqslant 2Rr$)

In carrying out the following calculations, the integrated intensity is divided into convenient parts. Each part is directly proportional to the time in which it is recorded on the photographic emulsion and to the average concentration ratio of the sample being traversed by the spark discharge during this time Zonal diagrams [1] are used extensively in order to visualize what is happening during a traverse.

Since a spark discharge covers a finite area on the surface of the specimen, the traverse across a concentration boundary will be recorded over a distance $2Rr$ on a photographic plate. This distance is shown in Fig. 2 as B_1D_1. As the leading end of the image of the spectrograph slit moves across the line A_1 and into the zone A_1B_1, all light falling on the plate will be characteristic of concentration X_1 (Fig. 1a). While the image of the slit is crossing line B_1, the spark discharge is traversing the boundary, and the spectrum recorded during this time

will be representative of both X_1 and X_2. Consequently, any point in zone A_1B_1 receives a partial exposure characteristic of X_1 and a partial exposure representative of X_1 and X_2. During the time that the image of the spectrograph slit is entirely within B_1D_1 (Fig. 2a), all light falling on the plate will be emitted from atoms vaporized from both sides of the boundary. After the leading edge of the slit reaches D_1, the spark discharge is wholly on the second side of the

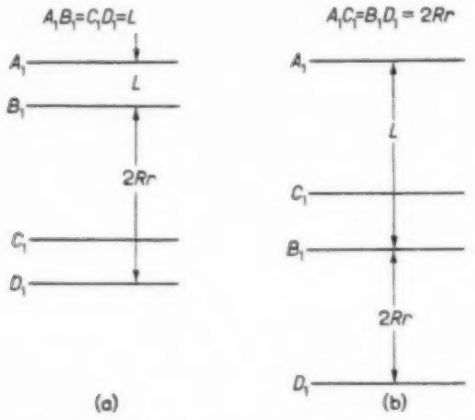

Fig. 2. Zonal diagrams for single boundary traverses.
(a) $L < 2Rr$, (b) $L > 2Rr$.

boundary. Hence as in zone A_1B_1, any point within zone C_1D_1 receives a partial exposure representative of X_1 and X_2 and partial exposure representative of X_2 only. There are certain relationships between the lengths of the zones. These are

$$A_1B_1 = C_1D_1 = L$$

$$A_1C_1 = B_1D_1 = 2Rr.$$

(a) *Zone* A_1B_1

Originally [1], the equations for each zone were expressed in a linear combination of summations. For zone A_1B_1 (Fig. 2a) the equation was given as

$$C_a(s) = X_1\frac{L-x}{L} + \frac{Rr\,.\,\Delta b}{L}\left[X_1 \sum_{b=1}^{1-\frac{X}{Rr}} 1 - g(b) + X_2 \sum_{b=1}^{1-\frac{X}{Rr}} g(b)\right] \qquad (1)$$

where Δb is the small interval in which each term of the summations is taken and into which a larger interval is divided. Since the effective spark distribution on the surface of the sample is known to be very close to a paraboloid of revolution [2], it may be assumed that it is, and therefore,

$$g(b) = \tfrac{1}{2} - \frac{2}{3\pi}b(1-b^2)^{3/2} - \frac{b}{\pi}(1-b^2)^{\frac{1}{2}} - \frac{1}{\pi}\arcsin b \qquad (2)$$

VOL. 9 1957

which is integrable. Equation (1) may be rewritten as

$$C_a(s) = X_1\frac{L-x}{L} + \frac{Rr}{L}\left[X_1\int_{1-\frac{X}{Rr}}^{1} 1 - g(b)\,db + X_2\int_{1-\frac{X}{Rr}}^{1} g(b)\,db\right] \qquad (1a)$$

There is a simple relation between the integrals in equation (1a)

$$\int_{b_1}^{b_2} 1 - g(b)\,db = (b_2 - b_1) - \int_{b_1}^{b_2} g(b)\,db \qquad (3)$$

Using equation (3) and substituting $s = x$, equation (1a) may be rewritten in a more compact form.

$$C_a(s) = X_1 + \frac{Rr}{L}(X_2 - X_1)\int_{1-\frac{s}{Rr}}^{1} g(b)\,db \qquad (4)$$

(b) *Zones B_1C_1 and C_1D_1*

Similarly, the equation applicable in zone B_1C_1 is given by

$$\left.\begin{aligned} C_a(s) &= X_1 + \frac{Rr}{L}(X_2 - X_1)\int_{1-\frac{s}{Rr}}^{1-\frac{s-L}{Rr}} g(b)\,db \\ \text{or}\qquad C_a(s) &= X_2 + \frac{Rr}{L}(X_1 - X_2)\int_{1-\frac{s}{Rr}}^{1-\frac{s-L}{Rr}} (1 - g(b))\,db \end{aligned}\right\} \qquad (5)$$

and in zone C_1D_1

$$C_a(s) = X_2 + \frac{Rr}{L}(X_1 - X_2)\int_{-1}^{1-\frac{s-L}{Rr}} (1 - g(b))\,db \qquad (6)$$

The substitutions, $y = s - L$ and $z = s - 2Rr$, were made in these equations where y and z were the distance variables used in the original equations [1].

Single-boundary traverse ($L \geqslant 2Rr$)

In zones A_1C_1 and B_1D_1 (Fig. 2*b*), the equations for $C_a(s)$ are given by equations (4) and (6) respectively. When the sparked crater reaches a sharp boundary between two regions of different concentration ratio, the image of the spectrograph slit is at A_1B_1 (Fig. 2b), and each point in the zone C_1B_1 has received an exposure proportional to X_1 for a time $t = (L - s)/v_p$. Since the time for full exposure is that which is required for the camera to move a distance, L, in a time, $t_0 = L/v_p$, each point in C_1B_1 at this instant has received a fraction of the total exposure equal to

$$t/t_0 = (L - s)/L$$

When the sparked crater has just finished crossing the boundary and the image of the spectrograph slit is at C_1D_1, a further exposure proportional to

$$\frac{1}{2}\left[X_1\int_{-1}^{1}(1 - g(b))\,db + X_2\int_{-1}^{1} g(b)\,db\right]$$

has registered on the emulsion at any point within zone C_1B_1 for a fraction of

the total exposure time equal to $2Rr/L$. After this time any point within zone C_1B_1 receives a final exposure proportional to X_2 for a time equal to $(s-2Rr)/v_p$. Therefore, the equation for the apparent concentration ratio in zone C_1B_1 is given by,

$$C_a(s) = X_1\frac{L-s}{L} + X_2\frac{s-2Rr}{L} + \frac{2Rr}{L}\tfrac{1}{2}\left[X_1\int_1^{-1}(1-g(b))\,db + X_2\int_{-1}^{1}g(b)\,db\right] \quad (7)$$

Using equation (2), it is found that

$$\int_{-1}^{1}(1-g(b)\,db = \int_{-1}^{1}g(b)\,db = 1 \quad (8)$$

Therefore, from equation (8), equation (7) becomes

$$C_a(s) = X_1 + (X_2 - X_1)\frac{s-Rr}{L} \quad (7a)$$

Double-boundary traverses

As indicated in the Introduction, a segregate may be thought of as a region of composition different from its surroundings and separated from its surroundings by two linear parallel boundaries. This is the model used in the following theoretical development of the microvolume technique for segregates and inclusions.

The zonal diagram (Fig. 3) for a traverse across two such boundaries, a distance, w, apart, is the combination of two identical zonal diagrams (one for each boundary which are displaced from each other by a distance, Rw. There are actually twenty different ways in which two zonal diagrams may overlap (Fig. 3). Close inspection reveals that the number of equations not derived so far and applicable in each zone for twenty different cases is ten, even though it might seem to be much larger. For instance, in cases I(a), II(a), III(a), and IV(a), all light falling on any point within zone D_1A_2 was emitted entirely by atoms, molecules, or ions which were vaporized from a region between the two boundaries, and hence is representative of the concentration ratio, X_2, existing between these two boundaries. Therefore, in zone D_1A_2,

$$C_a(s) = X_2 \quad (9)$$

Also, it appears plausible that a single equation would apply to the zone formed by the overlap of two particular zones, one from each zonal diagram, regardless of the case in which such an overlap occurs. This actually happens without exception. For example, an overlap of zones B_1C_1 and B_2C_2 occurs in cases I(d), I(e), and II(e), and a single equation describes the apparent concentration ratio, $C_a(s)$, at each point within the zone common to both of these zones. Hence, it is seen in Fig. 3 that there are nine different ways in which zones may overlap with nine corresponding equations. These equations consist of a linear combination of those terms occurring in equations (4), (5), (6), and (7a). The apparent concentration ratio, $C_a(s)$, in zones A_1A_2 and D_1D_2 in each of the twenty cases

VOL. 9 1957

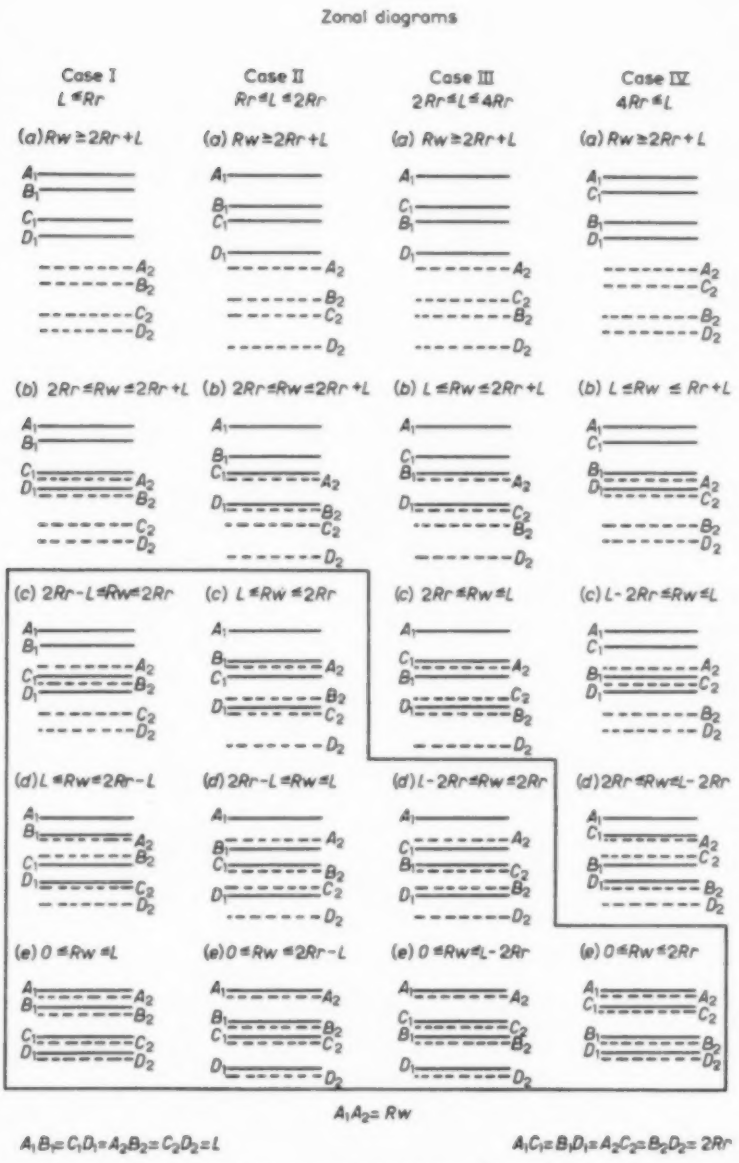
Zonal diagrams
Case I
L ≤ Rr
Case II
Rr ≤ L ≤ 2Rr
Case III
2Rr ≤ L ≤ 4Rr
Case IV
4Rr ≤ L
(a) Rw ≥ 2Rr + L
(b) 2Rr ≤ Rw ≤ 2Rr + L
(b) L ≤ Rw ≤ 2Rr + L
(b) L ≤ Rw ≤ Rr + L
(c) 2Rr - L ≤ Rw ≤ 2Rr
(c) L ≤ Rw ≤ 2Rr
(c) 2Rr ≤ Rw ≤ L
(c) L - 2Rr ≤ Rw ≤ L
(d) L ≤ Rw ≤ 2Rr - L
(d) 2Rr - L ≤ Rw ≤ L
(d) L - 2Rr ≤ Rw ≤ 2Rr
(d) 2Rr ≤ Rw ≤ L - 2Rr
(e) 0 ≤ Rw ≤ L
(e) 0 ≤ Rw ≤ 2Rr - L
(e) 0 ≤ Rw ≤ L - 2Rr
(e) 0 ≤ Rw ≤ 2Rr
A1A2 = Rw
A1B1 = C1D1 = A2B2 = C2D2 = L
A1C1 = B1D1 = A2C2 = B2D2 = 2Rr

Fig. 3. Zonal diagrams for double-boundary traverses.

where there is no overlap is given by the appropriate application of equations (4), (5), (6), and (7a).

Two of these nine equations will be derived in detail at this point and a summary of the entire double-boundary theory will be given later. The approach is the same as before, that is, the total exposure recorded at each point on the photographic emulsion is broken down into its component parts. One term always appears as a constant multiplier of the integrals at every stage in the theoretical development. This term is $t/t_0(b_2 - b_1)$. Suppose at one instant, that the sparked crater is on both sides of the boundary such that the boundary is at a distance, c, from the leading edge of the crater (Fig. 4). After a time, t, the crater has

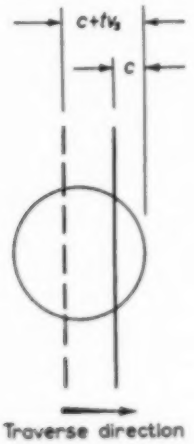

Fig. 4. Position of a boundary relative to the sparked crater at two different times.

moved a distance tv_s, and the boundary is at a distance, $c + tv_s$, from the leading edge of the crater.

$$t_0 = L/v_p = L/Rv_s$$

$$b_2 = 1 - \frac{c}{r}$$

$$b_1 = 1 - \frac{c + tv_s}{r}$$

Therefore
$$\frac{t}{t_0(b_2 - b_1)} = \frac{t}{\frac{L}{Rv_s} \cdot \frac{tv_s}{r}} = \frac{Rr}{L} \tag{10}$$

which is a constant for any given traverse.

(a) *Overlap of zones C_1D_1 and B_2C_2*

This occurs in cases I(c), I(d), I(e), II(c), II(d), and II(e) (Fig. 3). In all cases, the segregate is narrower than the sparked crater, that is, $w \leqslant 2r$. Before any point in the region common to both zones is exposed, the sparked crater has

VOL. 9 1957

begun to cross both boundaries. The light falling on a point in this region at a given instant is proportional to

$$(X_1 - X_2)(1 - g(b)) + X_2(1 - g(b^1)) + X_3 g(b^1)$$

where b refers to the first boundary and b^1 refers to the second boundary. At the instant when the sparked crater has finished crossing the first boundary

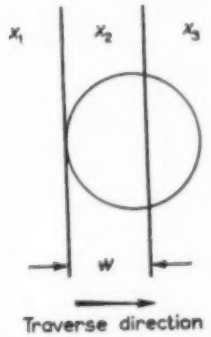

Fig. 5. Positions of the boundaries relative to the sparked crater at the instant when the initial exposure is completed in the region of overlap of zones C_1D_1 and B_2C_2.

(Fig. 5), the initial integrated intensity recorded on the photographic emulsion is proportional to

$$\frac{Rr}{L}\left[\int_{b_1}^{b_2}(X_1 - X_2)(1 - g(b))\,db + \int_{b_1^1}^{b_2^1} X_2(1 - g(b^1)) + X_3 g(b^1)\,db^1\right]$$

The first boundary has moved from a position $(s - L)/R$ to a position $2r$ from the leading edge of the crater.

Hence

$$b_2 = 1 - \frac{s - L}{Rr}$$

$$b_1 = -1$$

and

$$b_2^1 = \frac{s - Rw - L}{Rr}$$

$$b_1^1 = -1 + \frac{Rw}{Rr}$$

After this time, the final exposure occurs while the crater crosses the second boundary and is proportional to

$$\frac{Rr}{L}\int_{1-\frac{s-Rw}{Rr}}^{-1+\frac{Rw}{Rr}} X_2(1 - g(b^1)) + X_3 g(b^1)\,db^1$$

Adding these two exposures together and using equation (3), a total exposure proportional to the apparent concentration ratio

$$C_a(s) = X_2 + \frac{Rr}{L}(X_1 - X_2)\int_{-1}^{1-\frac{s-L}{Rr}}(1 - g(b))\,db$$

$$+ \frac{Rr}{L}(X_3 - X_2)\int_{1-\frac{s-Rw}{Rr}}^{1-\frac{s-Rw-L}{Rr}} g(b)\,db \qquad (11)$$

(b) *Overlap of zones B_1D_1 and C_2B_2*

This occurs in cases III(c), III(d), III(e), IV(c), IV(d), and IV(e). The equation which is applicable must be derived twice, since in three cases the segregate is

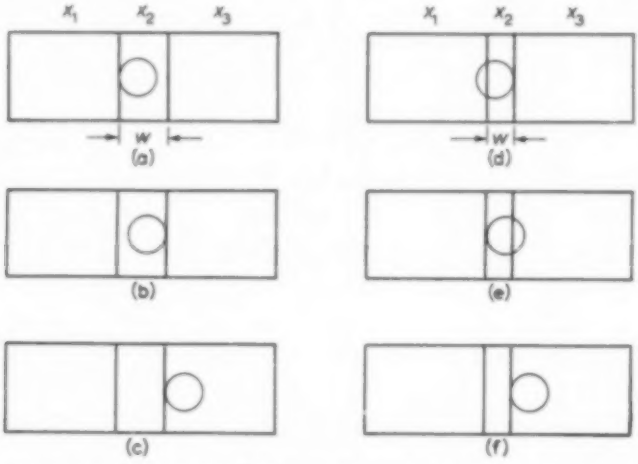

Fig. 6. Positions of the boundaries relative to the sparked crater at the times when the various partial exposures are completed in the region of overlap of zones B_1D_1 and C_2B_2.

wider than the crater and in the other three cases the segregate is narrower than the crater. Although two proofs are required, the same equation results.

(i) $w \geqslant 2r$. The following derivation applies to cases III(c), IV(c), and IV(d). The first exposure occurs entirely while the sparked crater is crossing the first boundary (Fig. 6a) and is proportional to

$$\frac{Rr}{L}\int_{-1}^{1-\frac{s-L}{Rr}} X_1(1 - g(b)) + X_2 g(b)\,db$$

The second exposure is recorded while the crater is crossing the region between the two boundaries (Fig. 6b), and is proportional to

$$X_2\frac{Rw - 2Rr}{L}$$

VOL. 9 1957

The third exposure happens while the crater is traversing the second boundary (Fig. 6c), and is proportional to

$$\frac{Rr}{L}\int_{-1}^{1} X_2(1 - g(b)) + X_3 g(b)\, db$$

The final exposure is recorded while the crater is moving in the region where the concentration ratio is X_3, and is proportional to

$$X_3 \frac{s - 2Rr - Rw}{L}$$

Using equations (3) and (8) and adding the above four terms, the apparent concentration ratio in the region common to B_1D_1 and C_2B_2 is

$$C_a(s) = X_2 + \frac{Rr}{L}(X_1 - X_2)\int_{-1}^{1-\frac{s-L}{Rr}} (1 - g(b))\, db$$

$$+ (X_3 - X_2)\left(\frac{s - Rw - Rr}{L}\right) \tag{12}$$

(ii) $w \leqslant 2r$. This occurs in cases III(d), III(e), and IV(e). The first exposure is recorded while the crater is crossing the first boundary (Fig. 6d), and is proportional to

$$\frac{Rr}{L}\int_{1-\frac{Rw}{Rr}}^{1-\frac{s-L}{Rr}} X_1(1 - g(b)) + X_2 g(b)\, db$$

The second exposure occurs while the crater is traversing both boundaries (Fig. 6e), and is proportional to

$$\frac{Rr}{L}\int_{-1}^{1-\frac{Rw}{Rr}} X_1(1 - g(b)) + X_2 g(b)\, db$$

$$+ \frac{Rr}{L}\int_{1-\frac{2Rr-Rw}{Rr}}^{1} (X_3 - X_2) g(b)\, db$$

The third exposure occurs while the crater is crossing the second boundary (Fig. 6f), and is proportional to

$$\frac{Rr}{L}\int_{-1}^{1-\frac{2Rr-Rw}{Rr}} X_2(1 - g(b)) + X_3 g(b)\, db$$

The final exposure is recorded while the crater is moving in the region where the concentration ratio is X_3 and is proportional to

$$X_3 \frac{s - 2Rr - Rw}{L}$$

Using equation (3) and adding the above four terms, equation (12) is obtained again.

The derivations of equations (11) and (12) as well as the other equations applicable where there is an overlap of two zones are summarized in Fig. 7. This

Position of sparked crater at end of partial exposure[a]	Partial exposure	Overlapped zones and limits of integration[b]								
		$A_1B_1-A_2B_2$ $A_1C_1-A_2C_2$	$B_1C_1-A_2B_2$	$B_1C_1-B_2C_2$	$C_1D_1-A_2B_2$ $B_1D_1-A_2C_2$	$C_1D_1-B_2C_2$	$C_1D_1-C_2D_2$ $B_1D_1-B_2D_2$	$C_1B_1-A_2C_2$	$C_1B_1-C_2B_2$	$B_1D_1-C_2B_2$
		b_1 b_2 b_1' b_2'	b_1 b_2 b_1' b_2'	b_1 b_2 b_1' b_2'	b_1 b_2 b_1' b_2'	b_1 b_2 b_1' b_2'	b_1 b_2 b_1' b_2'	b_1 b_2 b_1' b_2'	b_1 b_2 b_1' b_2'	b_1 b_2 b_1' b_2'
Case $W \geq 2r$					I (b), II (b), III (b), III (c), IV (a), IV (c)			III (c), IV (c), IV (a)	IV (a)	III (c), IV (c), IV (a)
X_1 X_2 X_3, W	$X_1 \frac{L-s}{L}$							✓	✓	
X_1 X_2 X_3, W	$\frac{Rr}{L}\int_{b_1}^{b_2} X_1 (1-g(b)) + X_2 g(b)\, db$				b_{12} b_{22}			b_{12} b_{21}	b_{12} b_{21}	b_{12} b_{22}
X_1 X_2 X_3, W	$X_2 \frac{Rw-2Rr}{L}$				✓			✓	✓	✓
X_1 X_2 X_3, W	$\frac{Rr}{L}\int_{b_1'}^{b_2'} X_2 (1-g(b)) + X_3 g(b)\, db$				b_{11}' b_{21}'			b_{11}' b_{21}'	b_{12}' b_{21}'	b_{12}' b_{21}'
X_1 X_2 X_3, W, $2r$	$X_3 \frac{s-Rw-2Rr}{L}$								✓	✓
Case $W \leq 2r$		I (e), II (a), II (e), III (a), III (e), IV (e)	I (c), I (a), I (e), II (c), II (a), II (e)	I (a), I (e), II (e)	I (c), II (c), II (a), III (a)	I (c), I (a), I (e), II (c), II (a), II (e)	I (e), II (a), II (e), III (a), III (e), IV (e)	III (a), III (e), IV (e)	III (e), IV (e)	III (a), III (e), IV (e)
X_1 X_2 X_3, W	$X_1 \frac{L-s}{L}$	✓						✓	✓	

VOL. 9 1957

		1	2	3	4	5	6	7	8	9
x_1 x_2 x_3 W	$\frac{Rr}{L}\int_{b_1}^{b_2} x_1(1-g(b))+x_2 g(b)\,db$	b_0 b_{21}	b_0 b_{22}		b_0 b_{22}			b_0 b_{21}	b_0 b_{21}	b_0 b_{22}
x_1 x_2 x_3 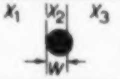 W	(a) $\frac{Rr}{L}\left[\int_{b_1}^{b_2} x_1(1-g(b))+x_2 g(b)\,db+\int_{b'_1}^{b'_2}(x_3-x_2)g(b)\,db\right]$ (b) $\frac{Rr}{L}\left[\int_{b_1}^{b_2}(x_1-x_2)(1-g(b))\,db+\int_{b'_1}^{b'_2} x_2(1-g(b))+x_3 g(b)\,db\right]$	(a) b_{11} b_0 b'_{11} b'_{21}	(a) b_{11} b_0 b'_{11} b'_{21}	(a) b_{11} b_{22} b'_{11} b'_{22}	(a) b_{12} b_0 b'_0 b'_{21}	(b) b_{12} b_{22} b'_0 b'_{22}	(b) b_{12} b_{22} b'_0 b'_{22}	(a) b_{12} b_0 b'_0 b'_{21}	(a) b_{12} b_0 b'_0 b'_{21}	(a) b_{12} b_0 b'_0 b'_{21}
x_1 x_2 x_3 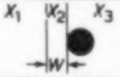 W	$\frac{Rr}{L}\int_{b'_1}^{b'_2} x_2(1-g(b))+x_3 g(b)\,db$				b'_{11} b'_0	b'_{11} b'_0	b'_{12} b'_0	b'_{11} b'_0	b'_{12} b'_0	b'_{12} b'_0
x_1 x_2 x_3 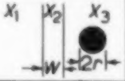 W, 2r	$x_3\,\frac{s-Rw-2Rr}{L}$						✓		✓	✓
Notes (see below)		$C_0(s)=x_1+\frac{Rr}{L}(x_2-x_1)\int_{1-\frac{s}{Rr}}^{1} g(b)\,db+\frac{Rr}{L}(x_3-x_2)\int_{1-\frac{s-Rw}{Rr}}^{1} g(b)\,db$	$C_0(s)=x_1+\frac{Rr}{L}(x_2-x_1)\int_{1-\frac{s}{Rr}}^{1-\frac{s-L}{Rr}} g(b)\,db+\frac{Rr}{L}(x_3-x_2)\int_{1-\frac{s-Rw}{Rr}}^{1} g(b)\,db$	$C_0(s)=x_1+\frac{Rr}{L}(x_2-x_1)\int_{1-\frac{s}{Rr}}^{1-\frac{s-L}{Rr}} g(b)\,db+\frac{Rr}{L}(x_3-x_2)\int_{1-\frac{s-Rw}{Rr}}^{1-\frac{s-Rw-L}{Rr}} g(b)\,db$	$C_0(s)=x_2+\frac{Rr}{L}(x_1-x_2)\int_{-1}^{1-\frac{s-L}{Rr}} 1-g(b)\,db+\frac{Rr}{L}(x_3-x_2)\int_{1-\frac{s-Rw}{Rr}}^{1} g(b)\,db$	$C_0(s)=x_2+\frac{Rr}{L}(x_1-x_2)\int_{-1}^{1-\frac{s-L}{Rr}} 1-g(b)\,db+\frac{Rr}{L}(x_3-x_2)\int_{1-\frac{s-Rw}{Rr}}^{1-\frac{s-Rw-L}{Rw}} g(b)\,db$	$C_0(s)=x_3+\frac{Rr}{L}(x_1-x_2)\int_{-1}^{1-\frac{s-L}{Rr}} 1-g(b)\,db+\frac{Rr}{L}(x_2-x_3)\int_{-1}^{1-\frac{s-Rw-L}{Rr}} 1-g(b)\,db$	$C_0(s)=x_1+(x_2-x_1)\frac{s-Rr}{L}+\frac{Rr}{L}(x_3-x_2)\int_{1-\frac{s-Rw}{Rr}}^{1} g(b)\,db$	$C_0(s)=x_1+(x_2-x_1)\left(\frac{s-Rr}{L}\right)+(x_3-x_2)\left(\frac{s-Rw-Rr}{L}\right)$	$C_0(s)=x_2+\frac{Rr}{L}(x_1-x_2)\int_{-1}^{1-\frac{s-L}{Rr}} 1-g(b)\,db+(x_3-x_2)\left(\frac{s-Rw-Rr}{L}\right)$

Notes

a The traverse direction is such that the sparked crater moves from left to right relative to the specimen.

b The presence of a partial exposure (column 2) is indicated by the mark, ✓, where no limits of integration are applicable or by the limits of integration these limits have the following values:-

$b_{11}=1-\frac{s}{Rr}$ $\qquad b'_{11}=1-\frac{s-Rw}{Rr}$

$b_{12}=-1$ $\qquad b'_{12}=-1$

$b_{21}=1$ $\qquad b'_{21}=1$

$b_{22}=1-\frac{s-L}{Rr}$ $\qquad b'_{22}=1-\frac{s-Rw-L}{Rr}$

$b_0=1-\frac{Rw}{Rr}$ $\qquad b'_0=1-\frac{2Rr-Rw}{Rr}$

Fig. 7. Summary of the derivations of equations applicable for double-boundary traverses.

figure is divided into three main parts. In the top and middle parts, the derivations of the equations are summarized for cases where $w \geqslant 2r$ and $w \leqslant 2r$ respectively. Notes and equations for all cases are given in the lower third of this diagram. The left-hand column shows the positions of the sparked craters with reference to the boundaries at the end of each partial exposure. Column 2 lists the appropriate terms for partial exposures recorded during the time taken for the sparked crater to move from one of these positions to the next. The remaining columns indicate which terms are used in the proofs of the equations for each overlapping zone. The limits of integration are listed in these columns, but where no integration is indicated, the presence of a term in a proof is indicated by the symbol. $\surd$.

The theory developed and summarized in this paper is based on the assumption that all traverses are carried out in a direction normal to the boundaries. If the direction of traverse makes an angle, θ, with the normal to the boundaries, the component of the sample speed in the direction of the normal is

$$v_s{}^1 = v_s \cos \theta$$

and the speed ratio, R, must be replaced in all equations by $R \sec \theta$. Using the same reasoning, the theory may easily be extended to the case where the two boundaries are not parallel. If the normals to the first and second boundaries make angles, θ_1 and θ_2, with the direction of traverse respectively, R must be replaced in the terms of the equations that refer to the first and second boundaries by $R \sec \theta_1$ and $R \sec \theta_2$ respectively.

VOL. 9 1957

The microphotometer slit-length

Since a finite length of spectral line must be microphotometered, the effect of microphotometer slit-length must be included in a traverse theory. Two possibilities will be considered, namely, uniform and nonuniform illumination of the slit. In the case of uniform slit illumination, the apparent concentration ratio as measured with a microphotometer is the mean value of the apparent concentration ratio recorded at each point and is given by

$$C_a = \frac{\int_{s-\frac{K}{2M}}^{s+\frac{K}{2M}} C_a(s)\, ds}{K/M} \tag{13}$$

If the slit is nonuniformly illuminated, C_a is given by the weighted mean value of $C_a(s)$, that is

$$C_a = \frac{\int_{s-\frac{K}{2M}}^{s+\frac{K}{2M}} \alpha C_a(s)\, ds}{\int_{-\frac{K}{2M}}^{\frac{K}{2M}} \alpha\, d\sigma} \tag{14}$$

where α is the fraction of the total light passing through the slit at any point and is therefore a function of the distance, σ, along the length of the slit. Therefore,

$$\int_{-\frac{K}{2M}}^{\frac{K}{2M}} \alpha\, d\sigma = 1 \tag{15}$$

and equation (14) becomes

$$C_a = \int_{s-\frac{K}{2M}}^{s+\frac{K}{2M}} \alpha C_a(s)\, ds \tag{16}$$

The dilution factor

In traversing a segregate that is narrower than the sparked crater, the crater is never wholly within the segregate at any time. Hence, the true peak-concentration ratio is never observed, instead the material vaporized from the segregate

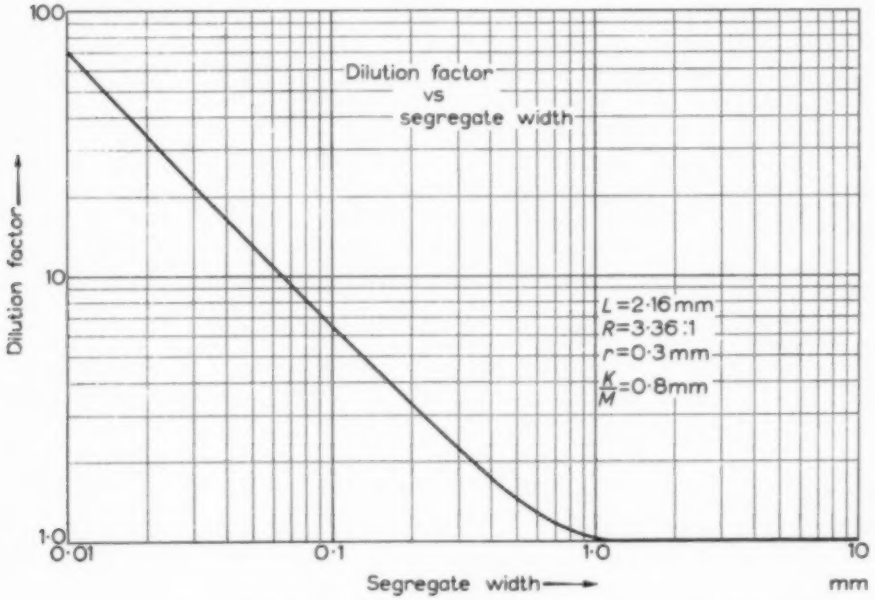

Fig. 8. Relationship of the dilution factor to the segregate width.

appears to be diluted with that from the surrounding matrix. The dilution expected in the analysis of a segregate can be calculated as follows.

If $X_1 = X_3$, the equations given in Fig. 7 can be put in the following form

$$C_a(s) = X_1 + (X_2 - X_1)X \tag{17}$$

where X is a function of s as well as the other parameters of the traverse and is not concentration-dependent. It can be easily shown that the maximum or minimum in equation (17) occurs at the point midway between A_1 and D_2 (Fig. 3).

i.e. $$s_m = \tfrac{1}{2}(2Rr + L + Rw)$$

where s_m is the distance from A_1 at which the maximum or minimum occurs.

Therefore,

$$C_a = \int_{s_m - \frac{K}{2M}}^{s_m + \frac{K}{2M}} \alpha(X_1 + (X_2 - X_1)X)\, ds$$

$$= X_1 + \int_{s_m - \frac{K}{2M}}^{s_m + \frac{K}{2M}} \alpha(X_2 - X_1)X\, ds$$

$$= X_1 + \frac{X_2 - X_1}{D} \tag{19}$$

where

$$\frac{1}{D} = \int_{s_m - \frac{K}{2M}}^{s_m + \frac{K}{2M}} \alpha X\, ds \leqslant 1 \tag{20}$$

and D is the dilution factor and is a constant for any given traverse across a particular segregate. Since X_1 is known for a particular case and since D may be calculated, the true peak concentration ratio, X_2, is a linear function of C_a

i.e.

$$X_2 = X_1 + (C_a - X_1)D$$

In practice, for a standard set of traverse conditions, D may be plotted as a function of the segregate width, w (Fig. 8). In carrying out a microvolume analysis, the width of a segregate can be measured from photomicrographs, D can be obtained from a curve such as Fig. 8, and X_2 can then be calculated by means of equation (19).

The theory presented has proven useful in segregate studies of samples submitted to the laboratory. No experimental verification has been given here, but will be presented in a later paper.

Acknowledgements—The author wishes to thank Dr. J. CONVEY and Dr. R. L. CUNNINGHAM for their encouragement and interest.

References

[1] HURWITZ J. K. *J. Opt. Soc. Amer.* 1954 **44** 30.
[2] HURWITZ J. K. *Spectrochimica Acta* 1955 **7** 1.
[3] NACHTRIEB N. H. *Principles and Practice of Spectrochemical Analysis* McGraw-Hill Book Company Inc. New York 1950 p. 269.

VOL. 9 1957

Spectrochimica Acta, 1957, Vol. 9, pp. 19 to 39. Pergamon Press Ltd., London

Sample transport and temperature studies in porous-cup discharges

CYRUS FELDMAN and MARGARET K. WITTELS
Oak Ridge National Laboratory, Oak Ridge, Tennessee

(*Received* 9 *February* 1956; *accepted for publication* 5 *November* 1956)

Abstract—High-speed colour motion pictures were taken of porous-cup discharges produced by a triggered polarized low-voltage condensed spark. These pictures indicated that soon after the trigger spark strikes the surface of the porous-cup electrode (PCE) a conical jet of solution vapour is emitted from another location on this surface. The discharge channel soon shifts to the axis of this vapour jet. The outer portions of the jet contain luminous fragments of water and solute molecules, but do not carry current. The interpretation of spectroscopic temperature measurements is discussed. A procedure is described for measuring the mean rotational temperature of the OH molecules in a transverse zone of the discharge; it is believed that these temperature values correctly reflect the excitation conditions to which vaporized solute atoms and ions are subjected. Near the PCE, where the discharge channel occupies almost all of the vapour jet, the temperature appears to be governed by a Saha equilibrium. Near the counter-electrode, where the discharge channel occupies only a small fraction of the luminous cone, temperature appears almost independent of solution composition. Most emission of metallic lines occurs in the latter zone.

1. Introduction

SPECTROCHEMICAL procedures can be designed most intelligently when detailed information is available on (1) the mechanism by which the sample is excited to luminescence, and (2) the relationships existing in the analytical gap between current, sample vapour, and atmosphere.

The present study is an attempt to provide information of this type for the discharge obtained in air with the porous-cup and similar thin-film solution excitation devices. The investigation was carried out in two phases:

1. High-speed colour motion pictures were obtained of porous-cup discharges in order to show the manner in which the sample is transported into the analytical gap, and indicate the geometrical relationships between sample vapour, discharge column, and electrodes.
2. The temperature of the discharge itself was measured at several locations in the analytical gap for solutions having a variety of solutes and concentrations. It was hoped that this information would aid in understanding and perhaps controlling the effects of sample composition, current, and electrode geometry on the spectral-line intensity ratios of metallic solutes.

2. High-speed motion pictures

A. Experimental

(1) *Apparatus*

(a) *Camera.* Exposures were taken with a Western Electric Company "Fastax" Camera which uses 100-ft reels of 16-mm film. This camera, when running at full speed, takes approximately 4000 frames per second. Each frame then receives an exposure of ~50 μsec; the elapsed "dark" time between frames is thus ~200 μsec. Since there is considerable acceleration during the course of a single run, the exposure time per frame and the time-interval between frames

were calculated for a given pulse by measuring the spacing between the 60-c.p.s. pulses at the appropriate position on the roll.

(b) *Electrode arrangement.* The arrangement used was that shown in Fig. 4, except that no reservoir was employed. Preliminary exposures showed a predominance of pinks and blues in the discharge when the solution contained no added metals (e.g. 1% $HClO_4$ soln.). In order to provide a colour (green) which was not otherwise present in the discharge and which could unequivocally be attributed to the metallic solute, subsequent exposures were made with solutions containing 1 mg/ml of silver as the perchlorate.

(2) *Excitation conditions*

Since it was planned to use a Walsh low-voltage intermittent d.c. arc[9] for the temperature measurements, a similar discharge was used here. In the present case, the polarized Λ-shaped pulse had a peak-height of ~10·7 amp; its base was ~940 μsec broad. Exposures were made of the trigger spark alone so that it could be identified in the triggered-pulse exposures.

A few runs were made with an Applied Research Laboratories Model 2025 High-voltage Spark Source, using the circuit parameters listed in Table 3.

Further details concerning the power source are given in Section 3B(3)c (p. 29).

(3) *Photographic exposure conditions*

All runs were made on 16-mm Eastman Kodak Kodachrome motion-picture film (Type A, ASA speed 16). In order to obtain proper exposure for the wide range of intensities encountered, separate runs were made at apertures of *f*/8, *f*/4, and *f*/2.

B. *Results: Description of Phenomena*

Photographs of approximately 1300 discharge pulses were examined. In the *f*/4 and *f*/8 runs, a red colour was very prominent in the images of the luminous vapour emitted from the porous cup (see Fig. 1). In view of the origin of this vapour, and the fact that the colour was passed very efficiently by an interference filter peaked for 6562 Å, this colour was assumed to be H_α radiation. The blue colour was assumed to be radiation due to CN and other carbonaceous species. The green colour apparent in runs made with silver solutions was attributed to the 5209·07-, 5465·49-, and 5471·55-Å radiation of atomic silver. This colour was not observed when silver was not present in the solution.

Taken as a whole, the photographs indicated* that the porous-cup discharge, when excited by the d.c. pulses described above, consists of the following sequence of events:

Section	Polarity of PCE	Solution	Camera aperture	Exposure per frame (μsec)	Interval between frames (μsec)
a	−	0·1% $AgClO_4$	*f*/2	100	300
b	+	0·1% $AgClO_4$	*f*/2	45	180
c	+	1% $HClO_4$	*f*/2	45	180
d	+	0·1% $AgClO_4$	*f*/8	100	—
e	+	1% $HClO_4$	*f*/2	60	—
f	+	0·1% $AgClO_4$	*f*/4	100	—
g	+	0·1% $AgClO_4$	*f*/4	45	—

* These conclusions were drawn from examination of the original films. Some details may be lost in reproduction.

VOL. 9 1957

VOL.
9
957

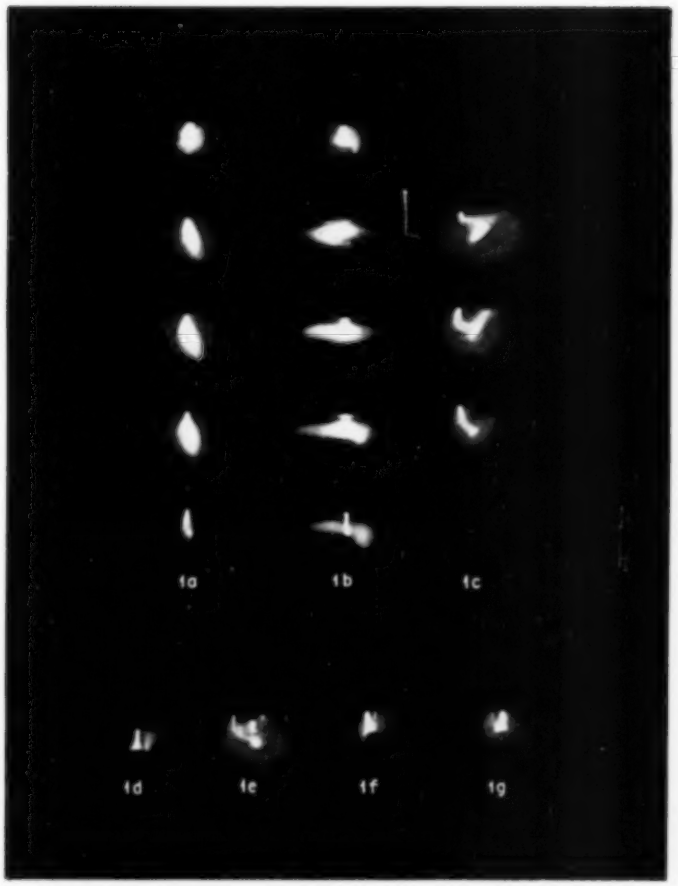

Fig. 1. High-speed photographs of porous-cup discharge. (Sections a, b, and c are consecutive (top to bottom) strip pictures of single pulses; sections d–g are single frames of interest.) PCE is upper electrode.

VOL.
9
1957

The discharge is initiated by a short-lived ($\leqslant 50$ μsec) trigger spark (pink and white spark in Figs. 1d, 1g). Without the aid of the main power pulse, however, this spark was found to be incapable of causing ejection of solution from the PCE.

When the PCE is the anode, the order of subsequent events is as follows:

As the main power pulse begins (presumably flowing through the channel of the moribund trigger spark), one or more jets of vaporized solution start perpendicularly from the PCE surface. These jets (hereinafter called the PCE jets) commonly originate at points on the PCE surface which are at a considerable distance from the point at which the trigger spark strikes (Figs. 1e, 1f). They advance into the analytical gap at a velocity of 1–3 m/sec. Their origins remain stationary throughout the pulse.

As the trigger spark strikes, or very soon afterward, a luminous jet of carbonaceous vapour is emitted from the counter-electrode. The origin of this counter-jet is often near the point at which the trigger discharge strikes (Fig. 1g), but is occasionally quite far removed from this point (Fig. 1d). This jet is propelled into the gap at a velocity which initially is considerably greater than that of the PCE jet. The origin of a counter-jet may move during the course of a pulse (Fig. 1b).

The abundance of charged particles in these jets encourages the formation of conducting paths between one of the PCE jets (usually the largest) and the cathode spot (Fig. 1e).* The anode spot is soon found at the apex of this PCE jet, and remains there for the duration of the pulse. The other PCE jets, if any, soon die away. The cathode spot unites with the apex of the counter jet. The discharge column now runs from the apex of one vapour jet to the apex of the other, although it seldom occupies the entire volume of either. It is apparent that as the conical PCE jet crosses the analytical gap, there is a steady decrease in the fraction of the jet volume occupied by the discharge column; i.e. a decrease in the fraction of the luminous vapour which is carrying current.

The discharge channel may be quite tortuous at the beginning of the power pulse, especially if the origins of the PCE and counter-jets are not directly opposite, and the counter-jet (usually much more vigorous than the PCE jet) is directed sidewise (Fig. 1c, first frame). The counter-jet spends itself comparatively soon, however, and the channel is usually fairly straight by the end of the pulse.

Normally, the PCE jet assumes a conical shape,† growing in size and emissivity until—and sometimes after—the amperage peak is reached. The outer portions of this jet may cease to be luminous some time before the current stops flowing. When this occurs, a well-defined discharge channel approximately 0·25 mm in diameter can be seen burning in the residual vapours (Fig. 1b) until the end of the current pulse. Luminous vapours excited by the discharge (e.g. Ag° vapours in Fig. 1b) can sometimes be seen in and around the analytical gap for as long as 200 μsec after the current ceases.

---

* The apparent truncation of the trigger spark in this photograph is an artifact due to rotation of the camera prism between cessation of the short-lived trigger spark and exposure of the subsequent events recorded in this frame.

† The outer portions of this jet are less luminous than the inner portions (Fig. 1b, centre frame). The overall size and shape of the cone are therefore shown best in the $f/2$ exposures (Fig. 1b).

Whereas the PCE jet in this polarity consists mainly of vaporized solution, the counter-jet consists mainly of carbonaceous vapours.

When the PCE is the cathode (Fig. 1a), the PCE jet appears to contain major amounts of both carbonaceous and solution vapours. As before, the channel occupies the axis of the PCE jet (Fig. 1a. fourth frame). This jet advances faster and farther than it did when the PCE was the anode. When the solution contains 0·1% Ag, none of the last frames of pictures of cathodic PCE shots (e.g. the last frame in Fig. 1a) show the clearly defined discharge channel evident in the late stages of anodic PCE exposures (e.g. Fig. 1b). From this fact, and from the observed lifetime of the PCE jet, it has been inferred that in this polarity and with these solutions, the emission of the PCE jet continues with almost undiminished vigour until the current ceases. In similar exposures of 1% $HClO_4$ solutions, however, the discharge channel is clearly visible in the last frame.

The counter-jet is negligible or absent when the PCE is the cathode, regardless which of these solutions is used. This indicates that consumption of the counter electrode occurs mainly while it is the cathode.

High-speed motion pictures of a PCE discharge excited by a conventional Feussner spark (see Table 3) were of no help in deducing the mechanism of this discharge, since the duration of the spark trains in this case was too short (~300 μsec) to permit resolution by the camera available.

VOL. 9 1957

C. *Conclusions*

When electrical excitation consists of a pulse of the type described, a jet of solution vapour is emitted from the PCE during most of the pulse. Although the entire conical jet is luminescent, only an axial discharge channel carries current. Thus, near the PCE, most of the sample vapour is located in or near the discharge column; near the counter electrode, most of the sample vapour is distributed in a spontaneously cooling cone-shaped jet, with the discharge channel at its centre.

The orientation and momentum of the counter-jet may play a decisive role in determining the shape and direction of the PCE jet when PCE is the anode. These factors probably also influence the energy distribution (i.e. spectral-line intensity ratios) of metallic atoms in the vapour propelled into the gap by the jet. Cf. Spark evolution studies by VAN CALKER [18].

3. Temperature measurements

A. *Thermal Equilibrium in Spark Discharges*

A gas system has a number of degrees of freedom—translational, rotational, vibrational, and electronic. If complete equilibrium exists, a single "temperature" can be used to describe the intensity ratio of any pair of spectral lines emitted by a given species. However, if the system, at the instant considered, has not yet achieved complete equilibrium, then each of these degrees of freedom, though itself having a quasi-Boltzmann distribution of energies, may temporarily be characterized by a different temperature. As an illustration, the "excitation temperature" characterizing the distribution of the atom population among the

atomic electronic energy levels might differ, until equilibrium was attained, from the "rotational and/or vibrational temperature" describing the relative populations of a given set of molecular electronic-rotation-vibration levels in the same gas.

Energy is furnished to the discharge column by only one source—the acceleration of electrons in the axial electric field. There is a finite relaxation time required for distribution of this energy among all degrees of freedom. This raises the possibility that in a continuous discharge, a steady state may be achieved in which the above-mentioned temperatures may continue indefinitely to differ to some extent. The (rotational) temperature observed by measuring molecular band systems might, for instance, differ from the (excitational) temperature characterizing, say, the FeI energy levels. Even if such a difference did exist, however, it would still be possible to make significant and useful correlations between these observed temperatures and line-intensity ratios of spectrochemical interest.

Before making such correlations in pulsed discharges, one must first have some assurance that the relaxation time of the system is short compared with the rate of change of the energy supply (i.e. current). (Spatial variations will be considered below.) If so, the observed time-averaged temperatures will still bear a definite relationship to the observed "intensity ratios" (energy ratios) of the lines of spectrochemical interest. We shall now inquire as to the degree of equilibrium to be expected in the present discharges, and thus gain a better idea of how the observed temperatures can be used.

As a result of investigations by FEDDERSEN [2], KAISER and WALLRAFF [1], and CUNDALL and CRAGGS [13], there is abundant evidence that when a spark strikes a metallic electrode, a jet of luminous vapour is emitted from the electrode at or near the point of impact. In these cases, as in the porous-cup discharge described above, much of the luminous vapour exists outside the discharge channel. The question of the existence of a steady state of energy distribution must therefore be discussed separately for the channel and extra-channel regions. The discharge channel will be considered first.

In oscillatory spectrochemical spark sources of 10 kV or over, the duration of a given half-cycle is usually 1–10 μsec, depending on the electrical parameters of the circuit. STETTER [3] has estimated that approximately 1 μsec is required to establish a steady state between the electron population (which supplies the energy) and Mg vapour at 1-atm pressure. Experiments by LEVINTOV [4], however, indicate that when an abrupt change in the current occurs ($di/dt \sim 10^9$ amp/sec), a steady state is re-established in the discharge channel within 0·2 μsec or less. The rate of change of current in the spark discharges commonly used in spectrochemistry seldom exceeds 10^8 amp/sec. In the discharge pulse used in the present temperature measurements (see Table 3), $di/dt \sim 1{\cdot}5 \times 10^4$ amp/sec. It is therefore probably safe to say that the average distribution of energy levels in the channel of these and other pulsed oscillatory discharges over a given period of say a few microseconds can be adequately described by a conventionally measured temperature.

It is even more likely that essentially complete equilibrium exists throughout

most of the remainder of the vapour jet. In conventional high-voltage spark discharges between metallic electrodes, this vapour has a "muzzle velocity" of 100–1000 m/sec [1,14]; in the present porous-cup discharges, this velocity was 1–3 m/sec. If the attainment of thermal equilibrium is assumed to require 1 μsec, the extra-channel vapours will thus have advanced only 0·001–0·1 mm into the analytical gap (depending on the type of power source used) before thermal equilibrium has been attained. Measurement of the distribution of energy levels among particles in this jet should thus yield meaningful temperature values. More detailed discussions of time and space averaging of discharge temperature were recently given by STETTER [3] and HULDT [17].

B. *Technique of Measurement*

1. *Points of observation; nature of the temperature value obtained*

It has been shown that energy distributions in porous-cup discharges can be described in terms of temperature. It must be assumed, however, that the temperature varies with both time and location in the discharge.

If metal-line intensities are to be studied as a function of discharge temperature, it is important that metal-line intensity data and temperature data be obtained from the same portion of the discharge. The smaller the area from which a given pair of observations is made, the more meaningful will be any correlation observed between variations in metallic-line intensity and temperature.

In terms of experimental technique, this means that a stigmatic image of the light source must be formed on a diaphragm, and light from only the region under study passed through the diaphragm. It is possible to restrict the area of observation in only one plane—that perpendicular to the optic axis of the spectrograph. The temperature information obtained from any one of the zones shown in Fig. 4 thus represents a time- and space-averaged value for the portions of the channel and vapour jet lying within that zone.

When a given area of the arc image is passed into the spectrograph, the light so admitted includes contributions from a tubular sector of the arc whose base area is the image area accepted, and whose height is the thickness of the discharge parallel to the optic axis. The temperature value obtained from this measurement is the mean of all of the temperature signals originating within this tube. If each element of volume within the tube emits an equal number of signals, the observed temperature is a volume-averaged value, i.e.

$$\bar{T}_{\text{vol}} = \frac{\int_{x_1}^{x_2}\int_{y_1}^{y_2}\int_{z_1}^{z_2} T(x,y,z)\,dx\,dy\,dz}{V}$$

where x_1, y_1, etc. are the boundaries of this region and V is its volume.

In spectroscopic temperature measurements, however, the signals are actually produced by some atomic or molecular species (hereinafter called the thermometric species) which may or may not be uniformly distributed within the discharge. The density n of this species in a given element of volume may vary as

VOL. 9 1957

a result of material transport phenomena (diffusion, convection, etc.) or temperature variation (creation or destruction of species by ionization, dissociation, recombination, etc.), or both. In practice, therefore, the observed temperature is a population-averaged value; i.e.

$$\bar{T}_{\text{pop}} = \frac{\int_{x_1}^{x_2}\int_{y_1}^{y_2}\int_{z_1}^{z_2} T(x,y,z)n(T,x,y,z)\,dx\,dy\,dz}{N}$$

where N is the total population of the thermometric species contained in volume V. A population-averaged temperature measurement derived from say, the rotational levels of thermometric species X will hereinafter be called the mean X rotational temperature.

The spectrochemist is not interested primarily in a volume-averaged temperature; he is interested in obtaining a temperature value which can be correlated with the excitation behaviour of certain neutral and singly ionized metallic particles which are unevenly distributed in space. Such a temperature figure would be produced by a thermometric species whose density varied with location and temperature in a manner similar to that of the metallic species. He thus finds a $\bar{T}_{\text{pop}}$ measurement most useful.

It would also be desirable to follow temperature variations at a given location in the spark discharge as a function of time. The elaborate apparatus [5, 18] required to do this was not available, however, and it was felt that the asymmetric nature of the discharge obtained when a thin film of solution was fed to one electrode would still permit the drawing of certain conclusions with regard to time-dependent variations.

2. *Selection of thermometric (temperature-indicating) species*

The temperature of a gaseous discharge which is at thermal equilibrium is measured by observing the relative intensities of two or more spectral lines emitted by a single species in the discharge, and using a relationship of the form

$$I_K = A_K g_K \nu_K e^{-\frac{E_K}{kT}} \tag{1}$$

where I_K, A_K, and ν_K are the intensity, transition probability, and frequency of line K, g_K, and E_K are the statistical weight and energy of the upper energy level, and k and T are the Boltzmann constant and absolute temperature, respectively. If the lines to be measured for a determination of T cover a very narrow wavelength range, ν_K can be omitted. If we convert to logarithmic form and set $a_K = A_K\, g_K$, we obtain

$$\log \frac{I_K}{a_K} = \left(\frac{\log_{10} e}{kT}\right) E_K. \tag{2}$$

We then plot log (I_K/a_K) against E_K, and calculate the temperature from the slope of the line obtained.

The thermometric species must satisfy the following requirements:

(a) It must be capable of existing in substantial numbers over the entire range of temperatures to be studied. An easily ionized or dissociated species

cannot exist at high temperatures; a species whose energy of formation is high is unlikely to be formed in sufficient numbers in a cool region.

(b) If the thermometric species is one which must be added to the system, its presence must not affect the temperature. This requirement can usually be met by using a sufficiently small quantity of the species.

(c) The coefficients a_K must be known for all lines used.* Since the measurement of these probabilities is often difficult, the accuracy of the published values of such coefficients varies widely, especially in the case of atomic and ionic lines.

(d) The lines emitted by the thermometric species must show negligible self-absorption.

(e) These lines must be in an accessible and interference-free wavelength region.

(f) They must be sufficiently well resolved from neighbouring lines to permit accurate photometry, including background correction.

Among these requirements, it is the need for accurately known transition probabilities which most seriously narrows the range of species which can be considered for temperature measurement. The fact that temperature values for a given discharge obtained with different thermometric species sometimes vary widely can often be attributed to the lack of accurate a_K values. At high temperatures in particular, a relatively small error in the value of a_K can lead to a considerable error in the temperature figure obtained.

In order to obtain the most accurate value possible for the slope of equation (2), as many spectral lines as possible should be used for a given measurement. This factor alone places atomic and ionic lines at a disadvantage compared with molecular band lines, since transition probabilities are seldom known accurately for many lines in a given atomic or ionic spectral series. It was therefore decided to use molecular bands, if possible.

Two obvious choices presented themselves in the present case: the cyanogen bands in the visible-blue region, and the hydroxyl bands in the near-ultraviolet. Both species are naturally abundant in porous-cup discharges, are stable over the same range of temperatures as the metallic particles of spectrochemical interest, and are in easily accessible spectral regions. Transition probabilities have been calculated for both. The hydroxyl bands have four advantages over the cyanogen bands, however: (1) Since OH and metal particles are generated from sample material by the same mechanism, their density distributions are apt to be similar within a given zone (see Fig. 4). The temperature obtained from OH bands should thus accurately reflect the temperature conditions to which the metallic particles are exposed. Much of the CN radiation, on the other hand, comes from the cathode jet, which contains little of the luminous metallic vapour whose temperature behaviour we wish to study. (2) The OH bands have a structure which is sufficiently open to permit use of a reciprocal linear dispersion of 2·5 Å/mm; the CN bands require the use of greater dispersive power. (3) The

* P. COHEUR [16] and I. I. LEVINTOV [4] have independently described a method for measuring relative temperatures in spark discharges without the use of a_K values. This advantage of their method is offset, however, by the need for a discharge of the type studied having a known temperature, and by the relative difficulty of obtaining good precision.

VOL. 9 1957

OH bands are more intense at low temperatures than the CN bands. (4) The OH bands occurring in porous-cup discharges are located in a region (3000–3200 Å) in which exposures can be obtained in a reasonable length of time with fine-grained photographic emulsions such as Eastman Kodak SA1.

Since the hydroxyl bands appeared to be the most promising of the available possibilities, they were examined in detail. All data on these bands were obtained from the tables of DIEKE and CROSSWHITE [6].

The lines found to have the most favourable combination of intensity and freedom from interference are those listed in Table 1. They constitute a portion of the R_2 branch of the (0, 0) band in the $^2\Sigma$—$^2\Pi$ system of the neutral OH molecule; i.e. each line represents an electronic transition of the molecule from the $^2\Sigma$ to the $^2\Pi$ state in which the vibrational quantum number remains zero but the rotational quantum number decreases by 1. Table 1 lists the rotational quantum numbers and energy levels associated with each line.

Table 1. Characteristics of selected lines of the R_2 branch of the $^2\Sigma$—$^2\Pi$ (0,0) band of OH

Line designation	Wavelength in Å	Energy level in cm^{-1}		Rotational quantum no.		Relative transition probability a_K
		Initial	Final	Initial	Final	
$R_2 3$	3077·028	32778·49	289·01	4	3	8·9
$R_2 4$	3074·369	32947·05	429·45	5	4	12·8
$R_2 7$	3069·177	33650·38	1077·80	8	7	24·8
$R_2 8$	3068·277	33949·67	1367·56	9	8	28·8
$R_2 13$	3069·675	35911·59	3344·34	14	13	49·1
$R_2 14$	3071·145	36393·24	3841·51	15	14	53·2
$R_2 15$	3073·028	36902·90	4371·18	16	15	57·2

A convenient atlas of OH band lines has been published by BASS and BROIDA [7]. A diagram of the spectral region including the lines in Table 1 is given in Fig. 2.

It was decided to use these bands for the temperature measurements. In accordance with the previous section, the values obtained will be called mean hydroxyl rotational temperatures, or MHR temperatures.

3. *Experimental arrangement*

(a) *Illumination optics* (see Fig. 3). A spherical quartz lens was used to form an enlarged stigmatic image of the source on the intermediate image diaphragm. A slot was cut in this diaphragm; a spherical lens at the slit formed an image of this slot on the collimating mirror of a Jarrell-Ash Wadsworth 3·4-m grating spectrograph. The dimensions and position of this slot were adjusted so that its image exactly filled the mirror aperture, thus minimizing stray light within the instrument. The degree of magnification of the image of the source on the intermediate image diaphragm was adjusted so that the image of the analytical gap on this diaphragm was five times as high as the slot. This made it possible to obtain temperature measurements from correspondingly restricted areas of the gap. The labelling of the regions represented by the various temperature measurements is shown in Fig. 4.

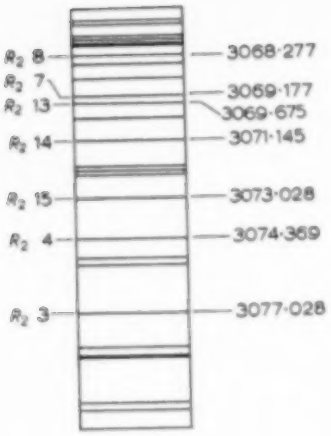

Fig. 2. OH band lines listed in Table 1.

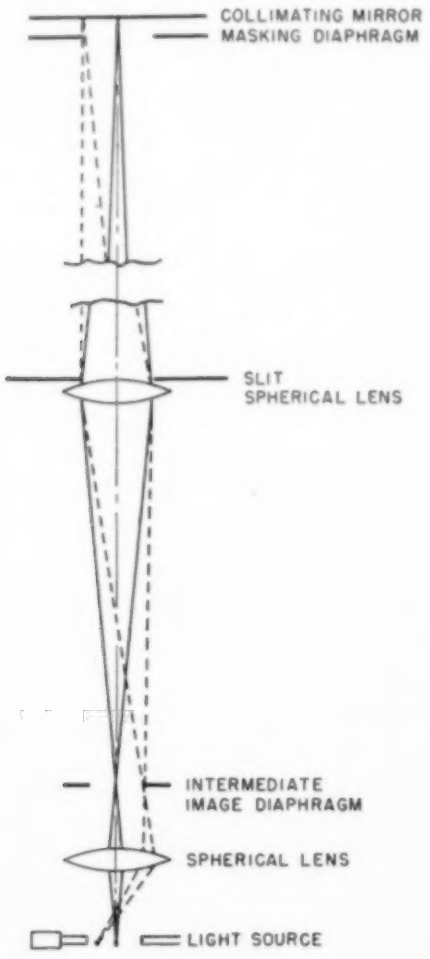

Fig. 3. Illumination optics.

VOL.
9
1957

(b) *Electrode arrangement* (see Fig. 4). Graphite porous-cup electrodes (National Carbon Co. Catalogue No. L4048) were porosified by baking 1 hour at 900°C in a fused-quartz beaker covered by a tight-fitting fused-quartz watch glass. The side walls of the electrodes were then waterproofed by grasping each electrode near the sparking surface with suitably bowed forceps and partly immersing it, open end down, in a 0·25% solution of paraffin in petroleum ether. The immersion was made as brief as possible in order to prevent the solution from reaching the floor of the electrode and rendering it impermeable.

The electrode was placed in its clamp and filled in the normal manner [8]. A 2-in. length of thick-walled plastic tubing was then fitted onto the PCE, as shown in Fig. 4. This reservoir

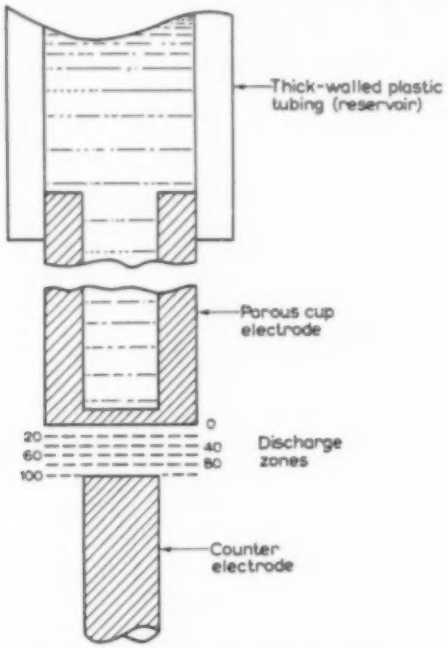

Fig. 4. Reservoir-PCE arrangement. Each temperature measurement was an average value of one of the zones marked.

was then filled to the desired height. Under the conditions used, these reservoir electrodes were found to operate continuously for 300–500 sec without refilling.*

The electrode gap was 2 mm. The counter-electrode was a $\frac{1}{8}$-in.-diameter flat-topped graphite rod.

(c) *Excitation*. In most exposures in the present series, it was desired to employ a discharge which was intermittent, yet approached thermal equilibrium as closely as possible. A Walsh [9] triggered low-voltage discharge was used for this purpose; the parameters listed in Table 2 were chosen so as to give a long pulse at a fairly low current. These values will be designated hereafter as "Standard Excitation Conditions."

The d.c. voltage was supplied by a half-wave selenium rectifier; the capacitor was charged during one half-cycle of the mains and discharged during the next.

The parameters in Table 2 correspond to an underdamped wave. Because of the comparatively low charging voltage, however, the discharge failed to re-ignite spontaneously after the first half-cycle. It was thus in effect a pulsed d.c. discharge; the porous cup was connected

* Reservoirs of this type were first employed by Dr. R. L. Mitchell, Macaulay Inst. Soil Research, Aberdeen. (Dr. R. B. Temple, private communication.)

Table 2. Standard excitation conditions (WALSH power source)

	Temp. Mmts.	Colour photos (Section 2)
Capacitance (μF)	10	25
Charging voltage (V(d.c.))	200	200
Polarity	PCE anode	as noted (Fig. 1)
Series resistance in discharge circuit (ohms)	15	0·5
Series inductance in discharge circuit (μH)	3300	3300
Peak current (see below) (amperes)	4·8	~10·7
Peak width at base (μsec)	650	940
Energy dissipated in anal. gap (watt sec) (per pulse)	0·1	0·5

as the anode unless otherwise noted. The pulse was an essentially symmetrical peak of the dimensions noted above.

Conventional high-voltage spark exposures were made with an Applied Research Laboratories Model 2025 Excitation Unit. This is a conventional Feussner high-voltage spark source with a synchronous interrupter in the secondary. In the present experiments, it was operated at approximately $\frac{1}{2}$ kVA. Exact parameters of the discharge circuit are given in Table 3.

(d) *Spectrograph*. The instrument used was a Jarrell-Ash 3·4-m Wadsworth grating spectrograph having a reciprocal linear dispersion of 2·5 Å/mm in the second order. The instrument was set for 3000 Å in the second order (i.e. 6000 Å in the first order). No spectral interference from the first or third orders was encountered, since the emulsion used (Eastman Kodak SA1) is insensitive to both 6000-Å and 2000-Å radiation. The slit was fixed, and measured 0·025 × 2·0 mm.

Table 3. Characteristics of Feussner spark circuit

Voltage on condenser at time of discharge	20,000 V
Capacitance of condenser	0·007 μF
Series inductance	360 μH
Initial amperage of train of oscillations	~90 amp
Energy dissipated in anal. gap (per spark train)	0·47 watt sec

(e) *Exposure*. The OH bands were more intense near the porous-cup surface than near the counter-electrode. Exposures therefore lasted 300 sec in zones 0–20 (see Fig. 4), 600 sec in zones 20–40 and 40–60, and 900-sec in zones 60–80 and 80–100. In the longer exposures, the spark was stopped every 300 sec and the porous cup refilled.

(f) *Photographic processing and densitometry*. All films were developed 3 min in Eastman Kodak D-19 at 20°C. Emulsions were calibrated and line intensities (corrected for background) measured according to Sections 9, 12, and 14 of reference 10.

(g) *Reduction of data*. Most of the temperature values were obtained by plotting log (I_k/a_k) against E_k (see Table 1) and calculating the temperature from the observed slope by means of equation (1). During the later stages of the study, intensity data were converted to temperature values by use of a special graph paper whose construction is shown schematically in Fig. 5.

On this graph paper, a vertical log intensity scale is located at the abscissa point corresponding to the upper energy level E_k of each of the spectral lines used. The intensity of each line (corrected for background) is plotted on the appropriate log I scale. An arbitrary fiduciary intensity is established by drawing a horizontal line (shown at the top of Fig. 5) representing the ordinate log $(I/a) = 0$. Each of the vertical logarithmic scales in Fig. 5 has been displaced downward with respect to this line by an amount equal to the logarithm of the transition probability a_k for the spectral line which the scale represents. A given point (say log 10) on

VOL. 9 1957

one scale is thus displaced downward with respect to the same point on the neighbouring scale by an amount equal to the difference between the respective log a values of the spectral lines represented by these scales (see Fig. 5). This displacement of the scale automatically subtracts the appropriate log a_K value from each log I_K value as it is plotted; with respect to the fixed scale of ordinates, as represented by the fiduciary log $(I/a) = 0$ line, the quantity actually plotted is log I_K − log a_K, or log (I_K/a_K). According to equation (1), the slope of

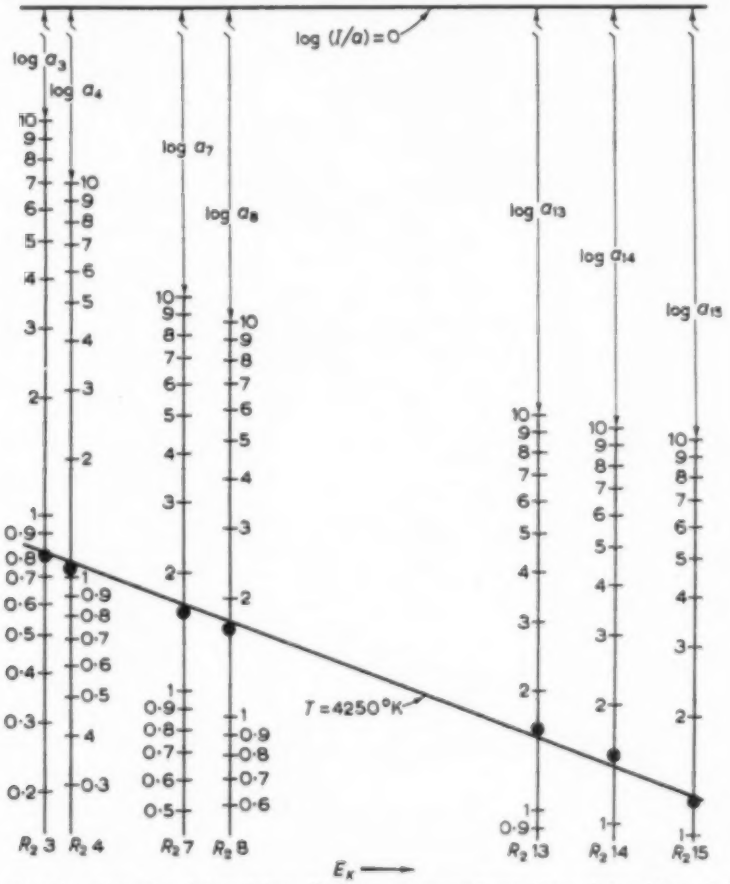

Fig. 5. Graph paper for determining discharge temperatures from intensities of OH band lines. (Schematic—see text.) The line shown represents a temperature of 4250°K.

the line through these points (corrected for the compression of the abscissa scale necessary in plotting) is equal to $\log_{10} e/(kT)$. Since $\log_{10} e$ and k are constants, this gives the temperature T. In practice, T was actually obtained by measuring the slope of this line with a protractor calibrated in terms of temperature. The temperatures obtained were "rotational temperatures" in the sense of Section 3A (p. 22).

4. *Experimental results**

(a) *Attainment of equilibrium in porous-cup discharges.* Examination of 750 temperature plots yielded only four cases (all in the 0–20 zone) which showed

* For statement on precision and accuracy, see Section i below (p. 37).

perceptible curvature. None of these four were among the twelve high-voltage spark exposures (see Table 3) included in the study. This indicates that in all of the remaining cases, thermal equilibrium existed in all five of the zones of the discharge. This statement applies rigorously only to the rotational states of the OH molecules in the discharge. In view of the length of the pulse, however, it appears safe to assume that equilibrium also exists in the present discharge among the other degrees of freedom, in particular the atomic and ionic electronic

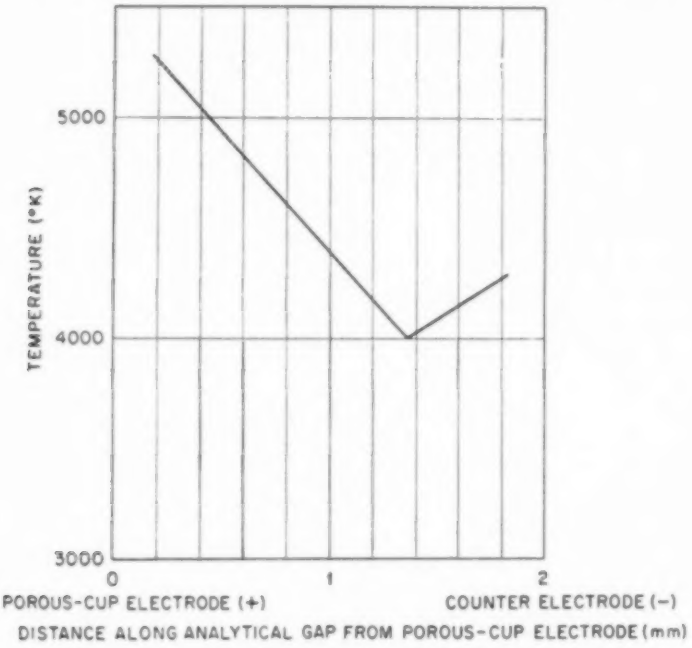

Fig. 6. Typical plot of MHR temperature vs. location in gap for porous-cup discharge (schematic).

energy levels, and that correlations may therefore be made between observed average temperatures and average intensity ratios within each zone.

The straightness of these plots also indicates absence of self-absorption.

(b) *General characteristics of MHR temperature distribution curves.* Almost all of the curves obtained showed the following characteristics (see Fig. 6).

(1) The MHR temperature of the discharge in the 0–20 zone depended on the nature and concentration of the metallic constituent of the solute.

(2) This temperature decreased linearly from this zone to a point approximately three-fifths of the way of the counter electrode. The slope of the curve became more positive at this point.

This behaviour may be explained by assuming that the observed temperature distribution resulted from the superposition of three temperature distribution curves: those of the PCE jet, the counter-jet, and the discharge channel.

The temperature of the discharge channel can be assumed to have been

VOL. 9 1957

essentially uniform all along its length. Since the temperature distribution curves in general showed a very different tendency, much emission of OH bands must occur outside the channel. (It will be remembered from Part 2, Section B (p. 22) that the discharge channel occupied a smaller and smaller fraction of the luminous PCE jet as the distance from the PCE surface increased.) The observed variation must thus be due principally to the superposition of the remaining two effects.

Since the PCE jet contains considerably more water-vapour than the counter-jet, the OH molecules found in the 0–60 region (see Fig. 4) must be principally those which originated at the PCE. This portion of the curve in Fig. 6 thus primarily represents the cooling of the PCE jet as it crosses the gap. The signals received from the 60–100 region, however, represent three contiguous or partly intermixed groups of OH molecules: (1) the leading portion of the PCE jet, emitting weakly and cooling as it travels toward the counter-electrode, (2) the OH component of the counter-jet, which is cooling as it travels away from the counter-electrode, and (3) OH molecules from the PCE jet which are reheated by contact with the counter-jet. If group (1) were not present in the 60–80 region, the MHR temperature-distribution curve in this region would have a positive slope. As it is, the slope in this region may be positive, or may merely be less negative than that of the 0–60 branch, depending on the temperature of the OH molecules in group (1) and their luminosity relative to those in groups (2) and (3).

(3) The nature and concentration of the solute had far more effect on the MHR temperature of the discharge near the surface of the PCE than on that near the surface of the counter-electrode.

(c) *Effect of variation of gap width.* MHR temperature distributions were measured across 1·5-, 2·0-, and 3·0-mm gaps under standard excitation conditions (Table 2). The results are shown in Fig. 7. Two effects are apparent:

(1) The temperature gradient of the PCE jet increases with decreasing gap width. The jet emerging from the PCE was able to lose energy in three ways: by conduction to the electrodes or atmosphere, by adiabatic expansion of the jet itself, and by diffusion of high-energy particles out of the jet. (Radiation losses are negligible.)

The effect of gap variation on temperature gradient probably did not involve conduction losses to the atmosphere, since experiments performed in helium (an excellent heat conductor) gave temperature gradients similar to those obtained in air. Since the electrode upon which each jet impinges is a heat-sink of almost infinite capacity, smaller gaps would be expected to produce steeper temperature gradients. The cooling of vapours by electrodes is vividly illustrated by Fig. 8, which is a photograph of a single pulse of a 1% $HClO_4$ solns. discharge (PCE +), in which the PCE surface has apparently cooled adjacent regions of the counter-jet below the temperature at which they can emit light. This effect was therefore presumed to be due to the cooling by the electrodes.

(2) The MHR discharge temperature in both end zones (0–20 and 80–100) varied inversely with electrode separation: The total rate of liberation of energy for the entire channel was the same for all gap separations. It is thus understandable that the temperature of the channel would vary inversely with gap separation,

and that this would change would be reflected in measurements of the present type. This fact, combined with the expected change in temperature gradients (see above), would explain the observed behaviour.

(d) *Effect of reduction of PCE surface area.* Bevelled porous cups similar to those used by SCRIBNER and BALLINGER [11], which have one-fourth the sparking surface of the type shown in Fig. 4, gave temperature-distribution curves which were indistinguishable from those given by the flat-bottom type.

(e) *Effect of preliminary ignition of PCE.* Although this step slightly increased

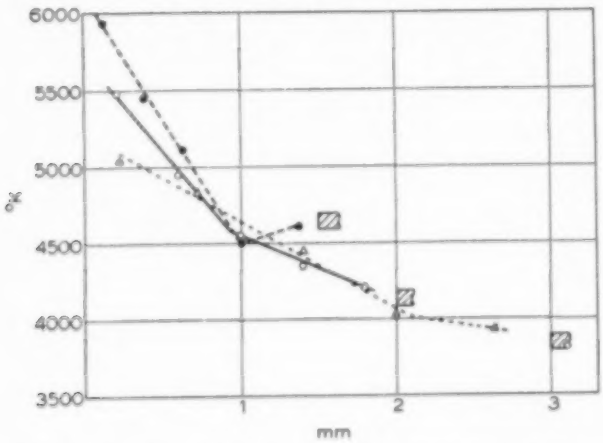

Fig. 7. MHR temperature distribution in PCE discharge for various gap widths.

Gap width (mm)	Temperature gradient of PCE branch (°K/mm)
1·5	−1600
2·0	−1200
3·0	−550

the porosity of the electrode, its effect on the temperature-distribution curve was negligible.

(f) *Effect of reversal of polarity.* All MHR temperature-distribution curves discussed up to this point were obtained with the PCE as anode. In order to study the role of polarity in determining temperature distribution, exposures of a 1% $HClO_4$ solution were made with the PCE as cathode, and with Feussner spark excitation. In the latter case, polarity was reversed approximately twenty times in each spark train, at a frequency of $\sim 10^5$ cycles per second. Fig. 9 shows that reversal of polarity had little effect on MHR temperature distribution within the analytical gap. Since an arc discharge delivers considerably less energy to the cathode than to the anode, this invariance indicates that the OH molecules must acquire most of their energy directly from the discharge column, rather than from their respective electrodes.

(g) *Effect of solutes.* (1) Nature of solute: MHR temperature-distribution curves were obtained for 1 vol. % acid solutions of salts containing 0·25 gram-atom of metal per litre. Details of composition are given in Table 4. Since all curves obtained were qualitatively similar to Fig. 6, the data were summarized in terms

VOL. 9 1957

Fig. 8. Cooling effect of PCE surface on counter-jet (single pulse; PCE (upper electrode) is anode. 1% $HClO_4$ soln.)

VOL.
9
1957

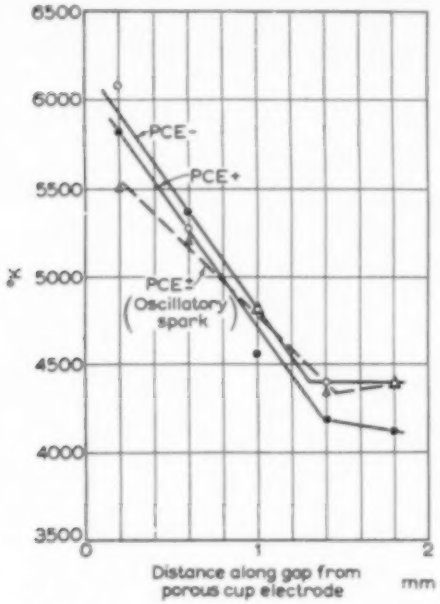

Fig. 9. Effect of electrode polarity on MHR temperature distribution in the porous-cup discharge.

Table 4. MHR temperature distributions in PCE discharges of salt solutions in 1% acid (0·25 gram-atom metal per litre)

Salt	Acid	Average discharge temp. in zone (°K)		Temperature gradient of PCE jet (°K/mm)
		0–20	80–100	
LiCl	H_2SO_4	5475	4125	−1150
NaCl	H_2SO_4	4650	4250	−400
KCl	H_2SO_4	4050	4200	−250
Rb_2CO_3	H_2SO_4	4050	4200	(nonlinear)
Cs_2CO_3	H_2SO_4	4175	4200	−750
$Mg(ClO_4)_2$	$HClO_4$	5500	4350	−1000
$Ca(ClO_4)_2$	$HClO_4$	4650	4150	−430
$Sr(ClO_4)_2$	$HClO_4$	4500	4300	−300
$Ba(ClO_4)_2$	$HClO_4$	4900	4675	−430
$Zn(ClO_4)_2$	$HClO_4$	6175	4325	−1600
$AgClO_4$	$HClO_4$	5625	4575	−880
$Cu(ClO_4)_2$	$HClO_4$	5300	4725	−880
$Be(ClO_4)_2$*	$HClO_4$	4700	3725	−850*

* Data not comparable with other data in table. Exposure made in "wind tunnel" because of possible toxicity of Be-laden mist. Temperature probably reduced considerably by cooling effect of air-current.

of "Average Discharge Temperature in the 0–20 Zone," "Average Discharge Temperature in 80–100 Zone" and "Temperature Gradient of PCE Jet" (see Table 4).

The MHR discharge temperature in the 0–20 zone is plotted against ionization potential of the metal in Fig. 10. Except for Li, the experimental points show the linear relationship which O. P. SEMENOVA [12] and her students found between ionization potential of a metal and the temperature of a continuous d.c. arc of one of its salts or oxides. The fact that these points follow the same trend as

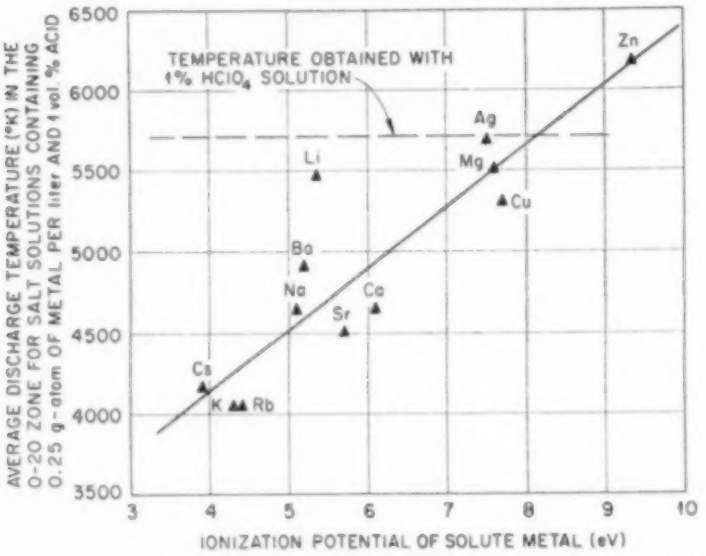

Fig. 10. Variation of average temperature in 0–20 zone with ionization potential of solute metal.

SEMENOVA'S points indicates that the mechanism regulating the discharge temperature near the PCE surface is essentially the same as that regulating the d.c. arc.* If this is the case, the failure of the Li solution to lower the temperature to the expected value (~4650°K) probably indicates a low degree of volatilization and/or dissociation of lithium-bearing particles in the 0–20 zone.

MHR temperatures near the counter-electrode surface, on the other hand, show little if any dependence on ionization potential. Within the alkali group, all such temperatures are the same within experimental limits. (Average value $T = 4170$°K). MHR temperatures in the remaining group tend to be somewhat higher, and to show real, but slight, differences. The absence of any marked tendency to follow the Semenova equation at the counter-electrode shows that

* The commonly accepted basic theory of arc temperature assumes that (1) an excess electron population of 0·001–0·01 atm is required to maintain the discharge column [14], and that (2) the discharge temperature rises only high enough to ionize the vapours present to a sufficient extent to produce this partial pressure of electrons. The higher the ionization potential of the vapour, the higher the temperature required to accomplish this. The quantitative relationship between ionization potential temperature, and degree of ionization is described by SAHA'S equation [15].

VOL. 9 1957

the temperature in this region must be determined by factors other than the mechanism described above.

This behaviour is entirely consistent with the picture of the PCE jet obtained from the high-speed motion pictures. Near the PCE surface, where the discharge channel constitutes almost the entire volume of this jet, the temperature of the vapours would be expected to be regulated by the above-described mechanism. Near the counter-electrode, however, the channel is a relatively small fraction of the volume of the vapour jet; the remainder does not carry current. This major portion of the luminous vapour in this region is thus not subject to the above-described temperature-regulating mechanism, and the vapours cool spontaneously. The population-averaged MHR temperature in this region (which is the quantity observed experimentally) is therefore largely independent of the ionization potential, and thus of the identity, of the solute.

(2) Concentration of Solute: When the ionization potential of the metal in the salt is less than $\sim$8·5 eV, an increase in salt concentration up to 0·25 M causes a decrease in discharge temperature at the PCE surface. The surface temperature at the counter-electrode is affected relatively little. An example of this variation in the case of potassium is shown in Fig. 11.

(h) *Distribution of intensity across gap.* (1) OH Bands under the excitation conditions in Table 2, the $^2\Sigma - {}^2\Pi$ bands at the PCE surface are approximately three times as intense as those at the counter-electrode surface.

(2) Metallic Lines: In general, most of the radiation from metals originates in the half of the analytical gap nearest the counter-electrode. This is probably due to the fact that the sample material has been projected well across the gap before the bulk of the solute can be vaporized and excited. With regard to spectrochemical analysis by the porous-cup technique, and probably by the rotating-disc technique as well, this fact has two implications:

(a) Metallic line-to-background ratios in OH band regions can be increased by using light only from the 50–100 zone (see Fig. 4).

(b) Fluctuations of intensity ratio due to temperature variation can be minimized by using light from the same region, since the temperature is relatively uniform throughout this region.

(c) In the continuous dry d.c. arc, the matrix affects intensity ratios in two ways: (1) Its ionization potential determines the temperature of the discharge, which in turn vitally affects almost all intensity ratios, and (2) it modifies intensity ratios through radiationless collisions which change the relative populations of the upper energy levels producing a given pair of lines. Ordinarily, the second effect is difficult to disentangle from the first, since most changes of matrix involve a change of ionization potential, and therefore a change of discharge temperature as well. In the present case, however, the 50–100 zone affords an opportunity to study the effects of metals having a wide range of ionization potentials at a given temperature (see Section (g)(1), p. 36 above).

(i) *Precision and accuracy of MHR temperature measurements.* (1) The mean of the standard errors of slope for the individual log (I_K/a_K) vs. E_K plots was equivalent to $\pm$3·6% of the temperature.

(2) Mean temperature values and standard deviations were calculated for all replicate MHR temperature measurements. The mean of the standard deviations obtained was 110°K. Precision of repeated temperature measurements was not a function of location in the analytical gap in the case of $HClO_4$ solutions. In acid-salt solutions, however, precision limits tended to be higher near the PCE surface (±200°K) than elsewhere (±50–100°K).

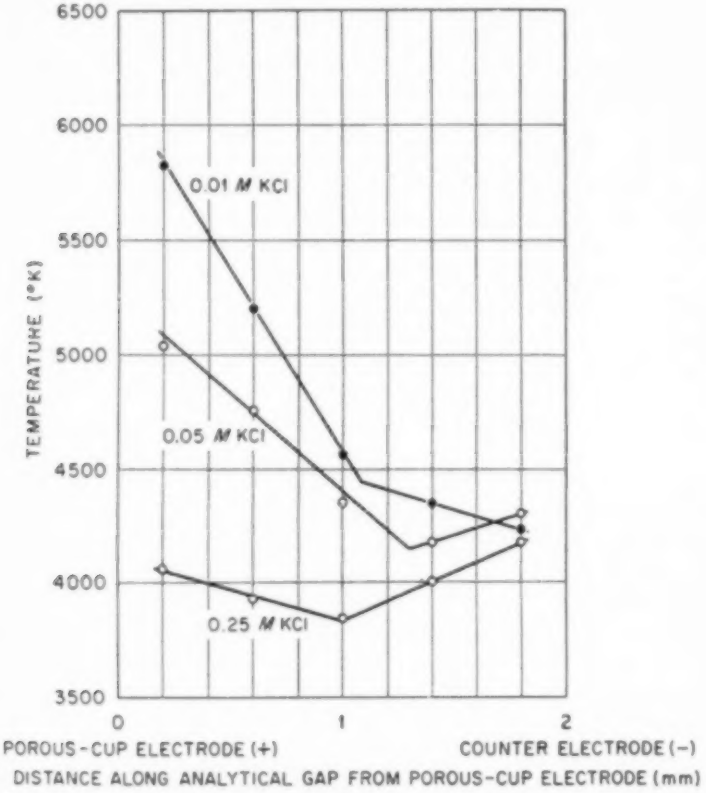

Fig. 11. Effect of potassium concentration on temperature distribution in porous-cup discharges.

(3) Since no other measurements of MHR temperatures in porous-cup discharges were available for comparison, it was not possible to estimate the accuracy of the present measurements.

(5) *Summary*

(a) Thermal equilibrium exists in porous-cup discharges excited by d.c. pulses approximately 600–900 μsec in duration and 5–10 amps in peak-height.

(b) A technique is described for measuring the mean hydroxyl rotational (MHR) temperatures of such discharges using a spectrograph of 2·5 Å/mm dispersion.

(c) At solute concentrations of 0·25 M or less, and under the above-mentioned

VOL. 9 1957

excitation conditions, the MHR temperature of the discharge decreases linearly with distance from the PCE surface until a point approximately three-fifths of the distance across the gap is reached. The slope of the temperature vs. distance curve then becomes more positive.

(d) Increasing the gap width decreases the MHR temperature gradient and the discharge temperatures near both electrodes.

(e) Reversing the polarity of the d.c. pulse has relatively little effect on the MHR temperature distribution curves.

(f) The nature and concentration of the solute has a considerable effect on the average discharge temperature in the 0–20 zone, where temperatures observed using 0·25 N solutions ranged from 4050° to 6175°K. Variations are much less marked near the counter-electrode. MHR temperatures appear to be regulated to some extent by a Saha dissociation equilibrium in the first case, but not in the second.

(g) The effect of a matrix element on the spectrum of a minor element has two aspects: (1) the promotion or suppression of radiationless transitions which either increase or decrease the population of a given excited level of the minor element, correspondingly changing the intensity of the lines originating at that level, and (2) the regulatory effect of the matrix on the discharge temperature, which in turn also affects the spectrum of the minor element. The properties of the region near the counter-electrode suggest that these two factors could be studied independently in this region.

References

[1] Kaiser H. and Wallraff A. *Ann. Physik* 1939 **34** (5) 297.
[2] Feddersen W. *Pogg. Ann.* 1861 **113** 467; 1862 **116** 132.
[3] Stetter A. *Spectrochim. Acta* 1953 **5** 350.
[4] Levintov I. I. *Zhur. Tekh. Fiz.* 1947 **17** 781.
[5] Steinhaus D. W., Crosswhite H. M., and Dieke G. H. *Spectrochim. Acta* 1953 **5** 436.
[6] Dieke G. H. and Crosswhite H. M. The Ultra Violet Bands of OH-Fundamental Data, *Bumblebee Series, Report No. 87*, The Johns Hopkins University, Baltimore, Md., Nov. 1948.
[7] Bass A. M. and Broida H. P. A Spectrophotometric Atlas of the $^2\Sigma^+ - {}^2\Pi$ Transition of OH. *Natl. Bur. of Stds. Circular 541.* (June 26, 1953).
[8] Feldman C. *Anal. Chem.* 1949 **21** 1041.
[9] Walsh A. Bull. Brit. Non-Ferrous Metals Research Assoc., 1946 No. 201 60.
[10] Suggested Practices for Photographic Photometry in Spectrochemical Analysis in *Methods for Emission Spectrochemical Analysis*, American Society for Testing Materials, Phila., Pa. (1953).
[11] Scribner B. F. and Ballinger J. C. *J. Research Natl. Bur. Standards* 1951 **47** 221.
[12] Semenova O. P. *Izv. Akad. Nauk S.S.S.R.* (Ser. Fiz.), 1945 **9** 715.
[13] Cundall C. M. and Craggs J. D. *Spectrochim. Acta* 1955 **7** 149.
[14] Rollwagen W. *Spectrochim. Acta* 1939 **1** 66.
[15] Huldt L. Thesis Univ. Uppsala 1948.
[16] Coheur P. *Mem. Soc. Roy. Sci. Liège* 1942 **5** (4) 365.
[17] Huldt L. *Spectrochim. Acta* 1955 **7** 264.
[18] van Calker J. *Z. Naturforsch.* 1955 **10a** 697.

Spectrochimica Acta, 1957, Vol. 9, pp. 40 to 46. Pergamon Press Ltd., London

Emission-spectrographic method for the determination of strontium in silicate materials*

K. K. Turekian,† P. W. Gast, and J. L. Kulp
Lamont Geological Observatory, Columbia University
Palisades, New York

(*Received* 25 *May* 1956; *accepted for publication* 13 *November* 1956)

Abstract—A technique for the emission spectrographic determination of strontium in natural silicate materials is described. The effects of a varying matrix have been diminished by the addition of strontium-free calcium carbonate. The technique, applicable to all silicate materials, gives a precision of the order of 7–12% standard deviation, Comparison analyses with the stable isotope dilution method indicate a high degree of accuracy as well.

Introduction

In order to establish the geochemistry and crustal abundance of strontium [1], it was necessary to develop a technique for the analysis of trace amounts of strontium in geologic materials (largely silicate) which would have a reproducibility of a few per cent, and would give assurance of giving accurate values. Wet chemical [2], X-ray fluorescence [3], and flame photometric [4] techniques are not generally applicable to the analysis of a large number of natural silicate samples for strontium either because of the complexities of the procedure, insensitivity, or lack of accuracy for low concentration.

The emission spectrograph provides the mechanism for rapid and precise analysis of refractory materials if adequate compensations are made for matrix and other effects which might significantly affect the accuracy.

The fact that spectrographic techniques with stated high precision can be markedly inaccurate has been demonstrated by the compilation of a series of analyses by several laboratories on a standard granite (G–1) and standard diabase (W–1). The details of these results are given in Ahrens [5]. Table 1 is taken in part from Ahrens' book and illustrates how widely the strontium determination can vary with the analyst.

In the scheme of analysis outlined below an attempt has been made to delineate and correct the causes of poor accuracy. The resulting emission spectrographic technique was employed in the analysis of seven different rock specimens in which the strontium has been determined by the inherently more accurate mass spectrometric isotope dilution method. The good agreement gives further assurance of the reliability of the method for the accurate spectrographic determination of strontium.

Matrix effects and standard preparation

Probably the two main causes for uncertainties in the accuracy of determinations of strontium made spectrographically are the ignorance of possible matrix effects and the unavailability of accurately known standards.

* Lamont Geological Observatory Contribution Number 230.
† Present address: Department of Geology, Yale University, New Haven, Connecticut.

VOL. 9 1957

Table 1. Comparison of values for strontium in standard granite G–1 and standard diabase W–1 by several laboratories

	G–1 p.p.m. Sr	W–1 p.p.m. Sr
Mitchell	900	420
Murata	120	120
Gorfinkle and Ahrens	250	250
Nockolds	280	180
Hey (Chemical)	450	450
Harvey	220	180
Herzog and Pinson (Isotope Dilution, [6])	233	177
This Paper (Emission Spec.)	287	172
This Paper (Isotope Dilution)	262	178

Preliminary exploratory experiments indicated that the effect of a varying chemical composition of the silicate material on the intensity of the strontium resonance line used in analysis might be considerable. In order to investigate the manner and magnitude of the matrix effect a series of experiments were performed. All experiments were performed with the spectrographic parameters completely described under "Method of Analysis."

In the first experiment, mixtures of quartz and calcium carbonate containing a known amount of strontium carbonate were fused in a radio-frequency induction furnace, yielding four samples with concentrations of calcium oxide being 2·85%, 5·85%, 12·3%, 27·2%. In each case the strontium/calcium ratio was the same, Fig. 1 shows the effect of the amount of calcium oxide present in the sample on the $I_{Sr\text{-}4607\cdot33}/I_{Ca\text{-}4578\cdot56}$ ratio. Next the effect of calcium and alkalies on the intensity of the Sr-4607·33 line was examined. A synthetic granite and synthetic plagioclases (feldspars containing compensating amounts of calcium and sodium) with calcium concentration ranging from 1·35 to 15·5% calcium oxide but with constant strontium/calcium ratio were made. The effect on the Sr-4607·33 line is seen (Fig. 2) to be even greater than in the first experiment. Although it is probable that the presence of the alkalies has had a marked effect it is not easily separated from the effect of the amount of calcium present.

Various silicates with known major element composition and known strontium concentrations were mixed with two parts of graphite. Accurately weighed 5 mg samples of each were then arced to completion under the same conditions described in this paper for all the other experiments. Fig. 3 shows that the effect of low calcium and high alkali is to increase markedly the intensity of the Sr-4607·33 line. This is not surprising, since the temperature of the arc column remains low if alkalies are strong. Such a situation tends to increase the probability of excitation of those lines which have their origin in the lowest possible energy level ("resonance" lines). The comparison calcium lines are high-energy lines and hence are not much affected by the same condition. Where calcium is the major material the effect of the alkalies is apparently diminished.

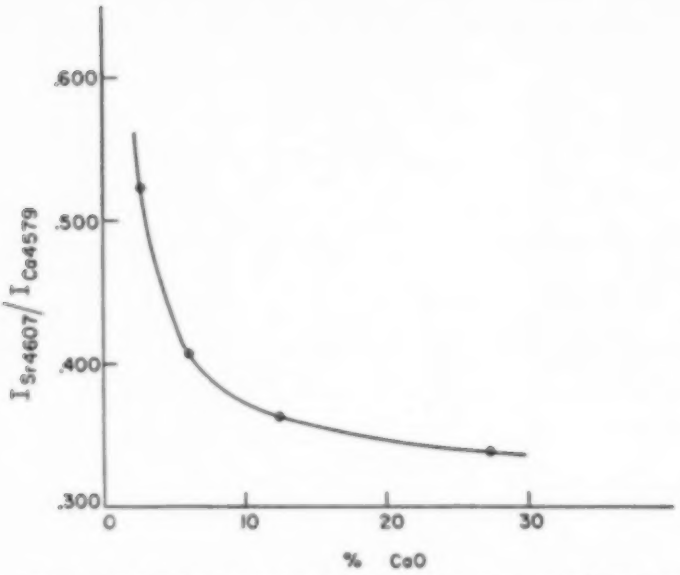

Fig. 1. The effect of the total calcium content at constant %Sr/%Ca intensity ratio Sr-4607/Ca-4579; fused $CaCO_3$ + quartz system.

VOL.
9
1957

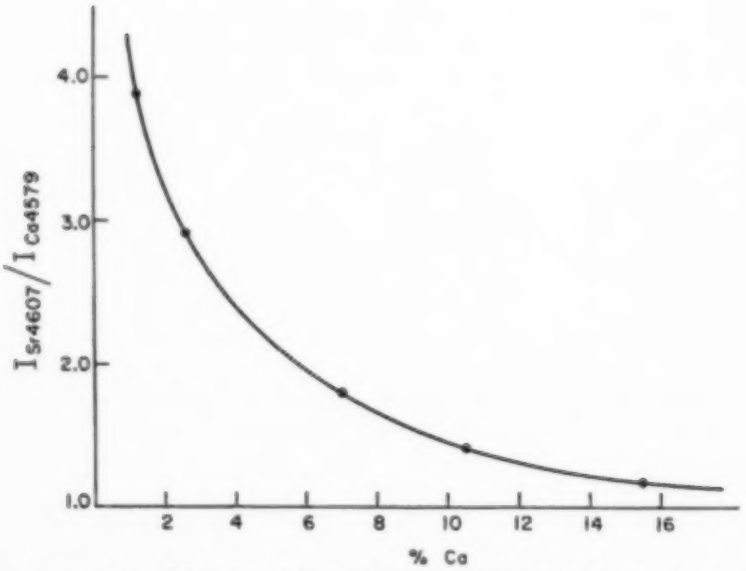

Fig. 2. The effect of the total calcium and alkalines at constant %Sr/%Ca intensity ratio Sr-4607/Ca-4579; synthetic granite and plagioclase system.

It is concluded from these experiments that there can be a wide variation in the reported values of strontium because the intensity of the Sr-4607·33 line is markedly affected by the matrix, and that the common buffering material, graphite, does not eliminate this condition.

Figs. 1 and 2 give strong indications that if the calcium concentration in the arc were high enough, the effect of small variations in calcium and alkalies due to the composition of the rock would probably have negligible effects on the intensity of the strontium line.

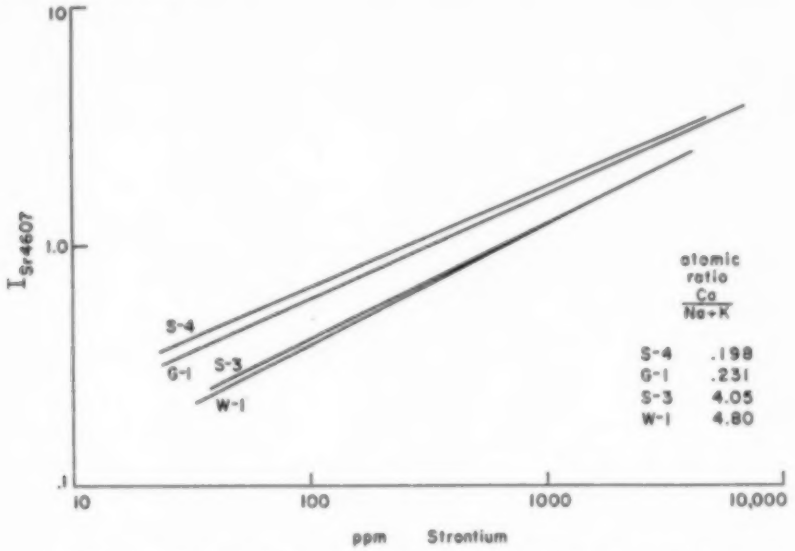

Fig. 3. Analytical curves for different matrices showing the effect of calcium and alkali concentration (graphite buffer used).

In the preparation of standards an attempt was made to select a natural silicate that would be similar to many common rocks and yet contain a minimum of strontium. Experience indicated that albite should have a minimum of strontium since it contains almost no calcium or potassium: two elements which strontium would be expected to follow on the basis of ionic size and charge [8]. Albite from a Spruce Pine, N.C., pegmatite was found to contain 20 p.p.m. strontium by the addition technique [7]. To this albite were added known amounts of strontium as strontium carbonate. The mixtures constituted standard values of strontium.

Fig. 4 is the analytical curve obtained from the standards using the technique to be described subsequently. The $\%Sr/\%Ca \times 10^3$ ratio refers to the sample diluted with an equal part of strontium-free calcium carbonate. It is to be noted that the strontium-working curve has an angle less than 45°. This may be an indication of latent self-absorption which becomes pronounced at higher strontium concentrations. However the points are reproducible as is seen in Table 2, hence the working curve is completely usable.

Method of analysis

Each silicate sample was mixed in an equal ratio by weight with strontium-free calcium carbonate.

The process of purification of the calcium carbonate was as follows: An ion exchange column 2·4 cm in diameter was prepared with 20 cm of Dowex-50, 200–400 mesh, 12% cross linkage cation resin in the ammonium form. Approximately 2·5 g of analytical grade calcium carbonate (preferably as low in strontium as possible) was dissolved in a minimum of dilute hydrochloric acid and adsorbed on the column. Elutriation was with 150 ml/l. solution of purified syrupy ammonium lactate in water. The calcium fraction was found in the second 250 ml of elutriate. Spectrographic analysis indicated the strontium content of the purified calcium carbonate to be about 5 p.p.m.

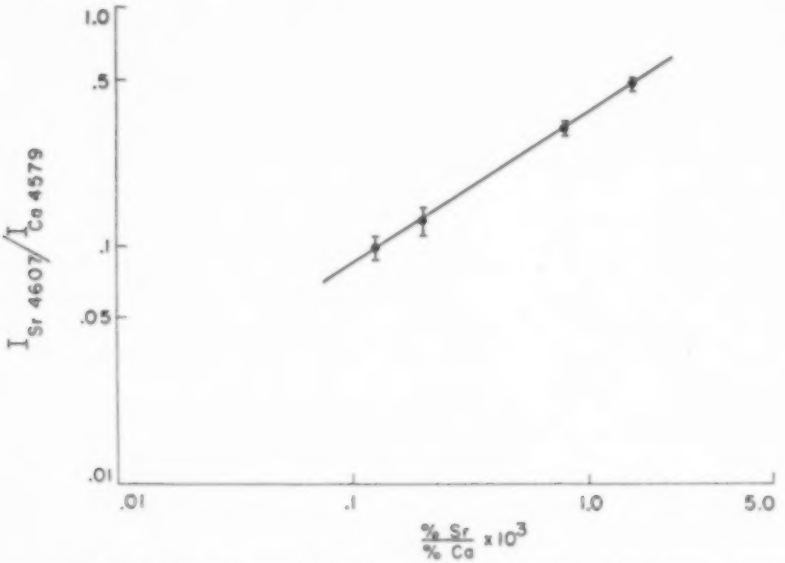

Fig. 4. Analytical curve for the determination of strontium in silicate materials.

Roughly 5-mg samples were then weighed and arced to completion (about 60 seconds) at 16·5 amp (anode excitation) in 3/16-in.-deep, necked electrodes 3/16-in. in outer diameter, 1/8-in. in inner diameter (National Carbon Co. L–4000). The deep electrodes prevented any spattering while the carbon dioxide and adsorbed water escaped during the first seconds of arcing. Using a rotating sector and a 30-μ slit, 35%–40% of the light from the arc was transmitted through the spectrograph. The spectrum was recorded on Eastman Spectrum Analysis No. 1 plates, which were processed in Kodak D-19 developer for three minutes at 20°C. The Jarrell-Ash Ebert 3·4-m plane grating spectrograph was used. A glass filter was used in the light path to absorb low wavelength ultra-violet radiation so that the second-order lines of these wavelengths would not interfere with the Sr-4607·33 line. Particularly, the Fe-2303·58 line was eliminated in the case of mafic rocks. The electrode gap was 3 mm and a cylindrical quartz lens with the axis parallel to the slit was placed in front of the slit.

A moving plate revealed that the strontium followed the calcium exclusively. During the emission of the sodium spectrum no strontium or calcium lines appeared.

It was necessary to make readings on the background blackening for both the Sr-4607·33 analysis line and the Ca-4578·56 internal standard line even though at times the background appeared light.

It has been observed that if a complete set of strontium standards is run on a plate together

VOL. 9 1957

with the samples to be analysed it is not necessary to use an internal standard provided weighings are made with great care. However, the advantages of the internal standardization are that weighings do not have to be made accurately and an analytical curve can be constructed using the intensity ratios from a large number of observations instead of depending on the few permitted on each plate. Since the strontium/calcium intensity ratio should remain constant from plate to plate it is possible to use the synoptically constructed working curve in a permanent manner (Fig. 4). The concentration function relates to the ratio of strontium to calcium in the mixed sample. The actual content of strontium in the silicate material can be obtained by compensation for the calcium addition and the calcium content of the original silicate. The calcium concentration can be determined by a rapid spectrographic technique for major element analysis in silicates which one of us (K. K. T.) will discuss in a later paper. However, it is clearly evident that for most natural silicate materials the calcium correction due to the chemical composition of the silicate will be small.

Table 2 shows the variation in fourteen replicate runs on the four standards used to construct the working curve (Fig. 4). There is no significant variation in intensity ratios for a single column from plate to plate. The precision, expressed

Table 2. Reproducibility of strontium analysis

Date	Run	$I_{Sr\text{-}4607}/I_{Ca\text{-}4579}$ %Sr/%Ca × 10^3			
		0·124	0·198	0·790	1·525
1/27/56	1	0·109	0·111	0·282	0·436
	2	0·086	0·105	0·311	0·483
	3	0·078	0·129	0·357	0·535
	4	0·105	0·145	0·335	0·525
1/4/56	5	0·101	0·134	0·322	0·472
	6	0·106	0·165	0·300	0·441
	7	0·093	0·086	0·286	0·460
	8	0·109	0·147	0·302	0·525
	9	0·105	0·129	0·310	0·465
	10	0·082	0·121	0·327	0·465
9/16/56	11	0·099	0·117	0·324	0·487
	12	0·084	0·116	0·304	0·432
	13	0·104	0·121	0·286	0·490
	14	0·109	0·115	0·309	0·452
Average		0·098	0·124	0·311	0·476
Coefficient of variation		11·3	15·8	6·7	7·0

as the coefficient of variation is obviously poorer for the lower values of strontium. It can be seen from Table 2 that for values of %Sr/%Ca × 10^3 of 0·2 and less. the coefficient of variation is about 12. For samples run in duplicate in this concentration range the per cent standard error becomes 8·5. For values of %Sr/%Ca × 10^3 greater than about 0·2 the coefficient of variation is about 6·9 and samples in this concentration range when run in duplicate will give a per cent standard error of 4·9.

In order to check the accuracy of this method, strontium was independently determined in a number of silicate samples by the stable isotope dilution technique and the emission spectrographic method. The mass spectrometric technique*

* The chemical and mass spectrometric details of analysis reported here will be published at a later date. For a general discussion of the technique of stable isotope dilution method of analysis see the review by INGHRAM [10].

is believed to be inherently the more accurate of the two and is estimated to have a precision equivalent to a standard deviation of 2% for a single determination. Table 3 shows a comparison of emission spectrographic and mass spectrometric determinations.

Table 3. Comparison of strontium values by the emission spectrographic method and the isotope dilution technique

Sample	E.S.* (p.p.m. Sr) $\bar{x}$	Number of observations–n	I.D.† (p.p.m. Sr) μ	$\bar{x}(\mu)$	s	t	ϕ	P (%)
Granite G–1	287	12	262	25	19·8	4·37	11	0·1–0·5
Granite 29A5	230	7	229	1	15·9	0·17	6	>50
Granite Gg–1	287	5	255	32	19·8	3·62	4	1–2·5
Granite NG–13 (b)	62	2	75	13	7·4	2·48	1	10–25
Diabase W–1	172	7	178	6	20·6	0·77	6	25–50
Basalt Gb–1	98	2	116	18	11·8	2·16	1	25–50
Granite Gg–2	73	10	78	3	8·7	1·09	9	25–50

* E.S.–Emission spectrograph.
† I.D.–Isotope dilution.

On the assumption that the isotope dilution value represents the true value it is possible to apply the t-test [9]. In Table 3, $\bar{x}$ represents the mean of the emission spectrographic observations and μ represents the value obtained by isotope dilution. The standard deviation, s, is calculated from the coefficient of variation values given above and ϕ represents, as usual, the degrees of freedom or $n - 1$. Then the t statistic is calculated as:

$$t = \frac{\bar{x} - \phi}{s/\sqrt{n}}$$

The last column gives the Significance Level as the probability that the observed difference might have been the result of chance and that no real difference existed.

According to the usual statistical practice, only Granite G–1 and Granite Gg–1 have significantly different values for the emission spectrographic and isotope dilution analyses. If these seven samples are a measure of the degree of accuracy of the technique described it can be seen that 71·5% of the comparisons are identical within statistics.

References

[1] Turekian K. K. and Kulp J. L. *Geochim. et Cosmochim. Acta* 1956.
[2] Wilkinson P. R., Gibson J. A., and Headlee A. J. W. *Analyt. Chem.* 1954 **26** 767.
[3] Noll W. *Chemie der Erde* 1934 **8** 507.
[4] Odum H. T. *Biogeochemistry of Strontium* Yale Univ. Ph.D. thesis, 1950.
[5] Ahrens L. H. *Quantitative spectrochemical analysis of silicates* Pergamon, London, 1954.
[6] Herzog L. F. and Pinson W. H. *Geochim et Cosmochim. Acta* 1955 **8** 295.
[7] Ahrens L. H. *Spectrochemical Analysis* Addison-Wesley, Cambridge, 1950.
[8] Goldschmidt V. M. *Geochemistry* Oxford, 1954.
[9] Davies O. L. *Statistical Methods in Research and Production* Hafner, New York, 1954.
[10] Inghram M. G. *Annual Reviews of Nuclear Science* Standford, Calif. 1954 **4** 81.

VOL. 9 1957

Spectrochimica Acta, 1957, Vol. 9, pp. 47 to 50. Pergamon Press Ltd., London

Infra-red spectra of $GeCl_4$, $GeHCl_3$, and $GeDCl_3$*

L. P. LINDEMAN† and M. KENT WILSON‡
Mallinckrodt Chemical Laboratory, Harvard University, Cambridge, Massachusetts

(*Received* 24 *October* 1956; *accepted for publication* 13 *November* 1956)

Abstract—The infra-red spectra of $GeCl_4$, $GeHCl_3$, and $GeDCl_3$ were investigated from 300 to 4000 cm^{-1}. The results for $GeCl_4$ and $GeHCl_3$ are in agreement with the previously published Raman data.

DURING the course of a spectroscopic investigation of various deuterated germanes [1], it was of interest to record the infra-red spectra of $GeCl_4$, $GeHCl_3$, and $GeDCl_3$. As only the Raman spectra of liquid $GeCl_4$ [2] and $GeHCl_3$ [3] have been published previously, the infra-red spectra of these compounds are reported here.

The $GeCl_4$ was a "pure" grade commercial sample§ which had experienced one bulb-to-bulb distillation. The $GeHCl_3$ was prepared by the series of reactions [4]

$$GeCl_4 + Ge \xrightarrow{350°} GeCl_2$$

$$GeCl + HCl \longrightarrow GeHCl_3$$

The DCl used in the analogous reaction for the preparation of $GeDCl_3$ was obtained from the reaction of D_2O and PCl_5 and contained about 5% HCl. Likewise the $GeDCl_3$ contained about 5% $GeHCl_3$.

Spectra were obtained in the region 300 cm^{-1} to 4000 cm^{-1} with a Perkin-Elmer Model 12C spectrometer modified for double-pass operation and equipped with CaF_2, NaCl, KBr, and CsBr prisms and a Perkin-Elmer Model 21 spectrophotometer equipped with NaCl optics. The NaCl prisms were calibrated with NH_3 and CO lines using the frequencies given by DOWNIE *et al.* [5]. The CaF_2 prism was calibrated in the 1600 cm^{-1} region with water vapour lines whose frequencies were taken from the work of NIELSEN [6] and BENEDICT, CLASSEN, and SHAW [7], and in the 2100 cm^{-1} region by the CO frequencies reported by LAGEMAN, NIELSEN, and DICKEY [8]. The water vapour spectra reported by RANDALL *et al.* [9] were used to calibrate KBr and CsBr prisms. Cells 10 cm in length equipped with KBr or polythene windows were used to record the spectra at pressures up to the equilibrium vapour pressures (~80 mm) at room temperature.

The observed spectra of $GeCl_4$, $GeHCl_3$, and $GeDCl_3$ are illustrated in Figs. 1, 2, and 3, respectively. Tables 1 and 2 list the observed frequencies and their assignments as well as the previously reported Raman data for $GeCl_4$, $GeHCl_3$, and $GeDCl_3$. The assignments follow readily from those proposed for similar molecules [10].

* This work was supported in part by the United States Air Force under Contract AF18(600)–590 monitored by the U.S. Office of Scientific Research.
† Present address: California Research Corporation, Richmond, California.
‡ Present address: Tufts University, Medford, Massachusetts.
§ Anderson La oratories, Adrian, Michigan.

Table 1. The observed vibrational frequencies and their assignment in $GeCl_4$

Assignment	Observed infra-red	Frequencies (cm^{-1}) Raman[a]
ν_2 (e)		132
ν_4 (f_2)		172
ν_1 (a_1)		396
ν_3 (f_2)	461	451 (508)
$\nu_1 + \nu_3$	858	
$\nu_2 + \nu_3$	918	

[a] See reference 2.

Table 2. The observed vibrational frequencies and their assignment in $GeHCl_3$ and $GeDCl_3$

Assignment	$GeHCl_3$ observed frequencies (cm^{-1})		$GeDCl_3$ observed frequencies (cm^{-1}) infra-red (gas)
	Raman (liq.)[a]	infra-red (gas)	
ν_6 (e)	149	(152)*	(150)†
ν_3 (a_1)	181	(184)*	(182)†
ν_2 (a_1)	409	423	421
ν_5 (e)	409	449	449
$\nu_6 + \nu_5$		590	590
ν_4 (e)	699	705	508
$\nu_2 + \nu_5$			865
$\nu_4 + \nu_5$		1150	958
ν_1 (a_1)	2159	2156	1552

[a] See reference 3.
* Estimated from observed Raman frequencies in liquid phase.
† Estimated.

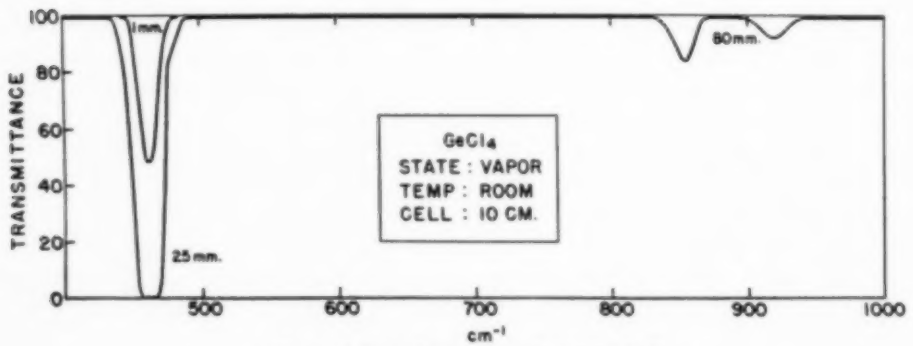

Fig. 1. Infra-red spectrum of gaseous $GeCl_4$.

VOL. 9 1957

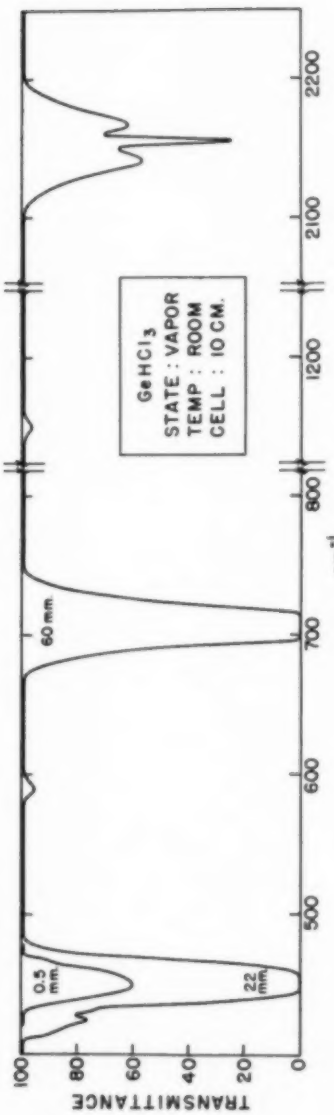

Fig. 2. Infra-red spectrum of gaseous $GeHCl_3$.

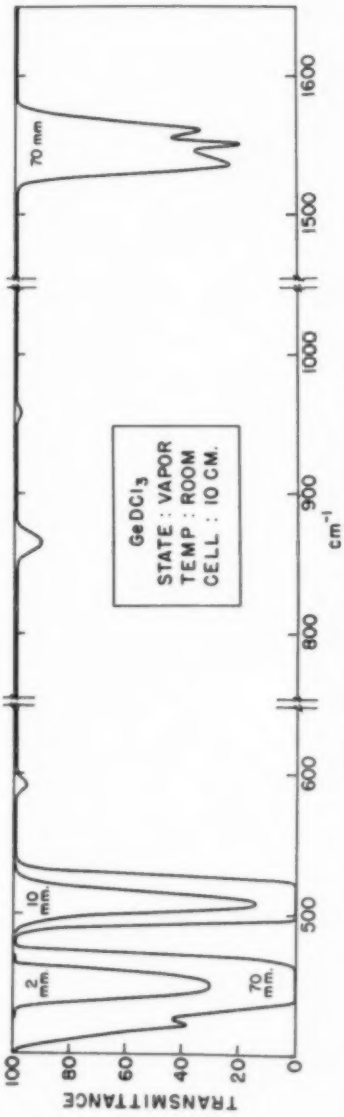

Fig. 3. Infra-red spectrum of gaseous $GeDCl_3$.

HAUN and HARKINS [2] had some doubts concerning the location of the triply degenerate GeCl stretching frequency, ν_3, which is weak in the Raman effect. The infra-red spectrum clearly indicates that their choice of 451 cm^{-1} for ν_3 is, indeed, the correct one.

References

[1] LINDEMAN L. P. and WILSON M. K. *Z. physik. Chemie* (in press).
[2] HAUN R. R. and HARKINS W. D. *J. Amer. Chem. Soc.* 1932 **54** 3917.
[3] DELWAULLE M. L. and FRANCOIS M. F. *Compt. Rend.* 1949 **228** 1007.
[4] DENNIS L. M., ORNDORFF W. R., and TABERN R. L. *J. Phys. Chem.* 1926 **30** 1049.
[5] DOWNIE A. R., MAGOON M. C., PURCELL T., and CRAWFORD B. *J. Opt. Soc. Amer.* 1953 **43** 941.
[6] NIELSEN H. H. *Phys. Rev.* 1941 **59** 565.
[7] BENEDICT W. O., CLASSEN H. H., and SHAW U. H. *J. Res. Nat. Bur. Stand.* 1952 **49** 91.
[8] LAGEMAN R. T., NIELSEN A. H., and DICKEY F. P. *Phys. Rev.* 1947 **72** 284.
[9] RANDALL H. M., DENNISON D. M., GINSBURG N., and WEBER L. R. *Phys. Rev.* 1937 **52** 160.
[10] HERZBERG G. *Infra-red and Raman Spectra* D. Van Nostrand Co. New York 1946.

VOL.
9
1957

Spectrochimica Acta, 1957, Vol. 9, pp. 51 to 58. Pergamon Press Ltd., London

Infra-red absorption spectra of inorganic co-ordination complexes*—IX

Infra-red spectra of oxalato complexes

M. Judith Schmelz,† Tatsuo Miyazawa, San-ichiro Mizushima‡
T. J. Lane,§ and J. V. Quagliano

Abstract—The infra-red spectra of simple metal oxalates have been measured and the assignment of bands has been based on the normal vibration calculation for the free oxalate ion. The infra-red spectra of oxalato complexes of Fe(III), Co(III), Cr(III), Al(III), Pd(II), and Cu(II) have been measured in the NaCl and CsBr regions. Assignment of bands has been made by the comparison of the spectra with those of alkali metal oxalates and dimethyl oxalate.

Introduction

Simple oxalate salts consist of a metal cation and the oxalate anion. Therefore, the infra-red spectra of these compounds in the NaCl and CsBr regions are considered to arise from the oxalate ion and from water of crystallization present in the compound. In most metal oxalato complexes the ligand is co-ordinated to the central metal ion through two oxygen atoms, whose oxygen-to-metal bonds have at least some covalent character. Douvillé, Duval, and Lecompte [1] have carried out a number of absorption studies of simple and complex metal oxalates. Oxalato complex salts can be explained approximately by considering the vibrations of the structure, which in some respects is similar to dimethyl oxalate. However,

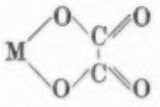

in a complex ion such as the trioxalato metal complex, coupling of similar vibrations of the same structure must also be considered.

The results of this research, based on the normal vibration calculation of the free oxalate ion, explain the nature of the vibrations of simple oxalate salts. The infra-red bands of the oxalato metal complexes are assigned by comparison with those of simple oxalate salts and of dimethyl oxalate.

Experimental

Preparation and purification of compounds. Calcium, lithium, and barium oxalates were Fisher-certified reagents; potassium oxalate was a Baker's C.P. product; and sodium oxalate was obtained from the National Bureau of Standards. Samples were dried at 110°. Iron(III), cobalt(III), chromium(III), and aluminium(III) trioxalato complexes were prepared and analysed by Dr. D. N. Sen [2]. *Trans*-potassium dioxalatodiaquochromate(III) trihydrate and *trans*-sodium dioxalatodiaquochromate(III) pentahydrate were prepared by the method of Werner [3].

---

* Paper VIII in series, *J. Amer. Chem. Soc.* 1956 **78** 889. Presented in part before the Physical and Inorganic Division of the American Chemical Society, Kansas City, Missouri, March 1954; contribution from the Department of Chemistry, University of Notre Dame.

† Sr. M. Judith, R.S.M.

‡ Visiting Professor from Faculty of Science, Tokyo University.

§ Rev. T. J. Lane, C.S.C.

Anal. calcd. for $K[Cr(C_2O_4)_2(H_2O)_2]\cdot 3H_2O$: Cr 14·56. Found: Cr 14·87. Calcd. for $Na[Cr(C_2O_4)_2(H_2O)_2]\cdot 5H_2O$: Cr 13·79. Found: Cr 13·75.

Sodium dioxalatodiaquocuprate(II) was prepared as described by RILEY [4].

Anal. calcd. for $Na_2[Cu(C_2O_4)_2(H_2O)_2]$: Cu 19·75. Found: Cu 19·50.

Potassium dioxalatopalladate(II) [5] was prepared by adding a concentrated solution of $K_2C_2O_4$ to a concentrated aqueous solution of $K_2[PdCl_4]$. $[Pd(NH_3)_2(C_2O_4)]$ was prepared by dissolving *cis*-$[Pd(NH_3)_2Cl_2]$ in a concentrated aqueous solution of $K_2C_2O_4$ [6]. The complexes precipitated in the cold.

Anal. calcd. for $K_2[Pd(C_2O_4)_2]\cdot 2H_2O$: C_2O_4 44·35. Found: 44·10. Calcd. for $[Pd(NH_3)_2C_2O_4]$: C_2O_4 38·47. Found: 37·98.

Deuteration was effected by recrystallization of the metal oxalates from 99·5% D_2O.

Table 1. Observed frequencies of simple oxalates in cm^{-1}*

$Li_2C_2O_4$	$Na_2C_2O_4$	$K_2C_2O_4\cdot H_2O$	$CaC_2O_4\cdot H_2O$	$BaC_2O_4\cdot H_2O$
—	—	3370 s	3400 s	3500 m
—	—	—	3300 s	3400 m
—	—	—	3020 s	—
1650 vs	1640 vs	1600 vs	1620 vs	1620 vs
—	—	—	—	1600 vs
1420 m	1418 m	1408 m	1365 m	1470 m
1330 vs	1338 vs	1310 vs	1316 vs	1325 vs
—	1320 vs	—	—	1310 vs
—	—	—	943 m	896 w
—	—	—	881 m	866 m
782 sh	780 sh	772 s	780 vs	771 vs
771 vs	774 vs	—	—	—
—	—	716 m	660 s	662 m
—	—	613 s	—	—
507 s	514 s	523 s	511 s	520 s
434 s	—	—	416 w	406 w
370 s	360 m	349 m	305 s	343 m

*vs = very strong, s = strong, m = medium, w = weak, sh = shoulder.

Table 2. Observed frequencies of trioxalato complexes in cm^{-1}

$K_3[Al(C_2O_4)_3]\cdot 3H_2O$	$K_3[Cr(C_2O_4)_3]\cdot 3H_2O$	$K_3[Fe(C_2O_4)_3]\cdot 3H_2O$	$K_3[Co(C_2O_4)_3]\cdot 3H_2O$
3440 w	3450 w	3450 w	3450 w
1725 vs	1710 vs	1710 vs	1710 vs
1695 vs	1680 vs	1680 vs	1680 vs
1400 vs	1400 vs	1390 vs	1397 vs
1290 s	1300 w	1265 m	1300 w
1268 s	1255 m	1248 m	1255 m
906 m	903 w	890 m	900 w
820 m	823 m	802 s	823 m
800 m	804 m	785 m	805 m
577 s	540 s	574 sh	561 s
478 s	480 m	528 s	470 s
434 m	409 s	493 s	445 s

VOL. 9 1957

Absorption measurements. Spectra were obtained by means of a Perkin-Elmer model 21 infra-red spectrophotometer using NaCl and CsBr prisms. The region from 2 to 35 microns was examined and the spectra obtained by the KBr disk method were checked using Nujol mulls. The absorption bands observed are listed in Tables 1, 2, and 3.

Table 3. Observed frequencies of mono- and dioxalato complexes in cm^{-1}

$[Pd(NH_3)_2(C_2O_4)]$	$K_2[Pd(C_2O_4)_2]\cdot 2H_2O$	$Na_2[Cu(C_2O_4)_2(H_2O)_2]$	$Na[Cr(C_2O_4)_2(H_2O)_2]\cdot 5H_2O$	$K[Cr(C_2O_4)_2(H_2O)_2]\cdot 3H_2O$
3250[a]	3460 m	3500 s	3430 s	3430 s
3150[a]	3400 sh	3400 s	3350 sh	3360 sh
—	—	—	2980 s	2960 s
1695 vs	1705 vs	1725 m	1715 vs	1715 vs
1665 vs	1680 vs	1680 vs	1690 vs	1690 vs
1630 sh[a]	—	—	1660 vs	1660 vs
1400 vs	1390 vs	1412 vs	1395 vs	1395 vs
1315 s[a]	—	—	—	—
1250 s	1240 s	1275 s	1255 s	1257 s
—	—	—	967 m	967 m
895 w	890 m	898 m	883 s	886 s
823 s	813 s	809 s	812 vs	815 vs
779 m[a]	—	—	653 m	658 m
—	600 s	—	645 m	—
549 s	570 s	558 s	543 s	540 s
467 s	454 m	497 s	424 s	422 s
374 m	374 s	387 m	398 s	399 s
363 m	357 m	346 s	315 m	315 m
299 m	—	—	—	—

[a] These frequencies are attributed to NH_3 stretching and deformation vibrations [7].

Discussion

1. *Normal vibration calculations of oxalato ion and the assignment of observed frequencies.* The calculation of normal vibrations of the free oxalate ion has been made on the basis of the Urey-Bradley type potential:

Table 4. Molecular constants and force constants (10^5 dyne/cm) of the oxalate ion

Molecular constants		Force constants	
r(C—C)	1·56 Å	K(C—C)	2·50
r(C—O)	1·27 Å	K(C—O)	7·20
(O—C—O)	124°	H(O—C—O)	0·15
(C—C—O	118°	H(C—C—O)	0·15
		F(O . . . O)	3·00
		F(C . . . O)	0·50

$V = \Sigma\frac{1}{2}K_i(\Delta r_i)^2 + \Sigma\frac{1}{2}H_{ij}r_i^0r_j^0(\Delta\alpha_{ij})^2 + \Sigma\frac{1}{2}F_{ij}(\Delta q_{ij})^2 +$ linear terms, where r_i and r_j are bond lengths with equilibrium values r_i^0 and r_j^0; α_{ij} bond angles and q_{ij} distances between nonbonded atoms. In addition, K, H, and F represent stretching-, bending-, and repulsive-force constants respectively.

The atomic distances, bond angles, and force constants used in this calculation are shown in Table 4. The molecular constants have been taken from data obtained for ammonium oxalate monohydrate [8], and the stretching-force constant K, bending-force constant H, and repulsive-force constant F have been taken from the corresponding constants of ethane [9], formate ion [10], and acetate ion [11] respectively. The frequencies calculated for the V_h model are shown in Table 5.

Table 5. Calculated and observed frequencies of the oxalate ion with point group V_h*

Symmetry of vibration		Type	Calculated	Observed†
$A_g(R)$	ν_1	ν_s (O—C—O)	1407	1489
	ν_2	ν (C—C)	973	902
	ν_3	δ (O—C—O)	412	456
A_u	ν_4	C—C torsion	inactive	
$B_{1g}(R)$	ν_5	ν_a (O—C—O)	1595	1647
	ν_6	CO_2 rocking	432	317
$B_{1u}(I)$	ν_7	CO_2 wagging	—	—
$B_{2g}(R)$	ν_8	CO_2 wagging	—	—
$B_{2u}(I)$	ν_9	ν_a (O—C—O)	1544	1600
	ν_{10}	CO_2 rocking	222	—
$B_{3u}(I)$	ν_{11}	ν_s (O—C—O)	1335	1310
	ν_{12}	δ (O—C—O)	777	772

* R = Raman active; I = infra-red active; ν = stretching; ν_s = symmetric stretching; ν_a = antisymmetric stretching; δ = in-plane deformation vibrations.
† Observed values are those for $K_2C_2O_4{\cdot}H_2O$.

In $Na_2C_2O_4$ three absorption bands have been observed at 1640, 1329, and 774 cm^{-1}. These three bands can undoubtedly be assigned to ν_9, ν_{11}, and ν_{12}, respectively. In the case of $K_2C_2O_4{\cdot}H_2O$, $Li_2C_2O_4$, $CaC_2O_4{\cdot}H_2O$, and $BaC_2O_4{\cdot}H_2O$ the corresponding three bands occur at about 1610, 1314, and 775 cm^{-1}. The band arising from the deformation frequency of water in the monohydrates overlaps the ν_9 band. Furthermore, the spectra of the monohydrates show a broad absorption band at about 680 cm^{-1} which in some way may be related to the water molecule, since this band disappeared upon deuteration.

Raman lines of $K_2C_2O_4$ in aqueous solution were reported by EDSALL [12] at 1647 ($\frac{1}{2}b$), 1489 (7), 902 (6), 456 (3) cm^{-1}, and they can be assigned to ν_5, ν_1, ν_2, and

VOL. 9 1957

ν_3, respectively. Since the latter three lines are strong Raman lines, they can be assigned quite reasonably to the A_g class.

The ν_{11} (B_{3u}) and ν_9 (B_{2u}) bands are forbidden in the Raman effect by the selection rule for the V_h symmetry. Since they were observed in the aqueous solution, however, the V_h symmetry may be changed to V in this state. That is to say, the oxalate ion is no longer planar, and consequently ν_{11} and ν_9 have been observed in aqueous solution. In this connection, Table 6 shows the corresponding vibrations for the planar V_h model and the nonplanar V model. It is to be noted that for all the B_3 vibrations, frequencies become independent of the azimuthal angle θ of the internal rotation about the central C—C axis, since the G and F matrices for B_3 do not include θ. Consequently, the B_3 frequencies of V_h become Raman-active for V without a change of frequency.

Table 6. Classification of vibration types for the planar V_h and nonplanar V models with selection rules

Planar (V_h)	Nonplanar (V)
$3A_g(R)$ $1A_u$	$4A(R)$
$2B_{1g}(R)$ $1B_{1u}(I)$	$3B_1(R, I)$
$1B_{2g}(R)$ $2B_{2u}(I)$	$3B_2(R, I)$
$0B_{3g}(R)$ $2B_{3u}(I)$	$2B_3(R, I)$

The G and F matrices of the B_1- and B_2-type vibrations contain θ and therefore change considerably with a change of internal rotation. This change is most marked for the O—C—O rocking and wagging frequencies. It would be interesting to compare the Raman effect of $K_2C_2O_4 \cdot H_2O$ in the solid state with that in aqueous solution.

Probably in aqueous solution the energy of conjugation between the two O—C—O groups is reduced and thus steric repulsion between them becomes more important, resulting in an out-of-plane twisting about the C—C bond. It is easily seen that the steric repulsion potential is a minimum when one O—C—O group is at right angles to the other.

2. *Assignment of IR bands of oxalato complexes.* To assign the bands observed in the oxalato complexes, the spectrum of dimethyl oxalate in the *cis* form together with that of the oxalate ion must be considered. Dimethyl oxalate in the liquid state was shown by one of us (MIYAZAWA) to exist in both the *trans* and *cis* forms. Of these, the *cis* form may be considered similar in vibrational spectrum to chelated oxalato metal complexes. The assignment of the spectrum of the *cis* ester was made as shown in Table 7 [13], listing only the frequencies necessary for comparison.

From these data the assignment of infra-red bands for the chelated trioxalato metal complexes can be made as follows:

(1) An intense doublet band observed at about 800 cm^{-1} is considered to correspond to the 772-cm^{-1} (B_{3u}) band of the oxalate ion of the potassium salt, and the 851-cm^{-1} (B_1) band of the *cis* ester and can be assigned to the (O—C—O) deformation vibration (B_1). The doublet structure arises from coupling of vibrations of the three oxalato groups, as will be explained later.

(2) The band at about 900 cm^{-1} corresponds to the band at 902 (A_g) of the oxalate ion and that of the *cis* ester at 862 cm^{-1} (A_1). Therefore, this can be assigned to the C—C stretching vibration (A_1).

(3) A doublet band observed between 1250 and 1300 cm^{-1} is considered to correspond to the 1310-cm^{-1} (B_{3u}) band of the oxalate ion of the potassium salt and to the 1165-cm^{-1} (B_1) band of the *cis* ester. This is the O—C—O stretching vibration in the oxalate ion. In the *cis* ester the C—O bond order is less than the C=O bond order and therefore this vibration arises mainly from the C—O vibration. However, there is a contribution of the C=O stretching vibration in the same phase as the C—O vibration, and therefore we shall denote this vibration of the oxalato complex as ν_s (O—C—O).

Table 7. Assignment of some observed frequencies of dimethyl oxalate in the *cis* form

Observed frequency	Type of vibration
404	δ(O—C=O), A_1
851	δ(O—C=O), B_1
862	ν(C—C), A_1
958	ν(CH_3—O), B_1
987	ν(CH_3—O), A_1
1165	ν(C—O), B_1
1325	ν(C—O), A_1
1770	ν(C=O), A_1
1776	ν(C=O), B_1

(4) A strong absorption observed at about 1400 cm^{-1} corresponds to the 1489-cm^{-1} band (A_g) of the oxalate ion and to the 1325-cm^{-1} band (A_1) of the *cis* ester. Therefore, this band can be assigned to the O—C—O symmetric stretching vibration (A_1). This band does not show a doublet splitting.

(5) Strong doublet bands were observed in the 1700-cm^{-1} region. Here we may expect A_1 and B_1 type O—C—O stretching vibrations. As shown below, the B_1-type vibrations appear as double bands, of which the higher frequency band is considered to overlap the A_1-type band.

(6) The band observed at about 3450 cm^{-1} can undoubtedly be assigned to the stretching vibrations of the water of crystallization.

The following explanation is proposed for the observed doublet structure of the

VOL. 9 1957

B_1-type vibrations. In the preceding discussion we have been dealing with the vibrations of oxalato complexes as a seven-body problem, taking into account one oxalato group and the central metal atom. Strictly speaking, however, the vibrations should be treated as a nineteen-body problem. In other words, in addition to the frequencies just considered, we have to take into account the coupling of three such systems.

The trioxalato metal complex ions have a symmetry of D_3. Consequently, the B_1-type vibrations of a single oxalato group are classed as symmetric to the trigonal axis (A_2) or degenerate (E), both of which are infra-red-active. On the other hand, of the A_1-type vibrations of a single oxalato group those symmetric to the trigonal axis (A_1) are inactive and those degenerate are active. Thus it is understandable that the B_1 vibrations of the oxalato group are observed as double bands, whereas the A_1 vibrations of the group are single .

The carboxylate frequencies in the spectra of the oxalato metal complexes are intermediate between those of the oxalates of the alkali metals (in which the metal-to-oxygen bonds are essentially ionic) and those of dimethyl oxalate,

Table 8. Fractional shifts of carboxylate stretching frequencies in trioxalato complexes

Type of vibration	Fe	Cr	Co	Al
$B_1\ \nu_a$(O—C—O)	0·4	0·4	0·4	0·6
$A_1\ \nu_s$(O—C—O)	0·6	0·6	0·6	0·5

suggesting a partial covalent character for the oxygen-to-metal bonds in these complexes. Using the carboxylate frequencies of sodium oxalate as the standard of reference, the ratio of the shift in these frequencies in a complex to that in the ester, which we shall term the fractional shift, may be taken as a measure of the covalent character of the M—O bonds. The relative positions of the absorption bands in $K_2C_2O_4 \cdot H_2O$ and $K_3[Al(C_2O_4)_3] \cdot 3H_2O$ are shown in Fig. 1.

For this comparison of frequencies we have chosen the O—C—O antisymmetric stretching vibration (B_1) and the O—C—O symmetric vibration (A_1), thereby avoiding the difficulty arising from coupling with the M—O stretching vibration, the CH_3—O stretching vibration, and the CH_3 rocking vibration. The result is shown in Table 8, where simple oxalate salts are assigned a value of zero and dimethyl ester a value of unity. The mean value of the fractional shift is about 0·5, which indicates that the M—O bonds in these complexes have about half the covalent character present in the C—O bond of the dimethyl ester.

Acknowledgement—This investigation was supported in part by a research grant H-2218 (C) from the Department of Health, Education and Welfare, Public Health Service.

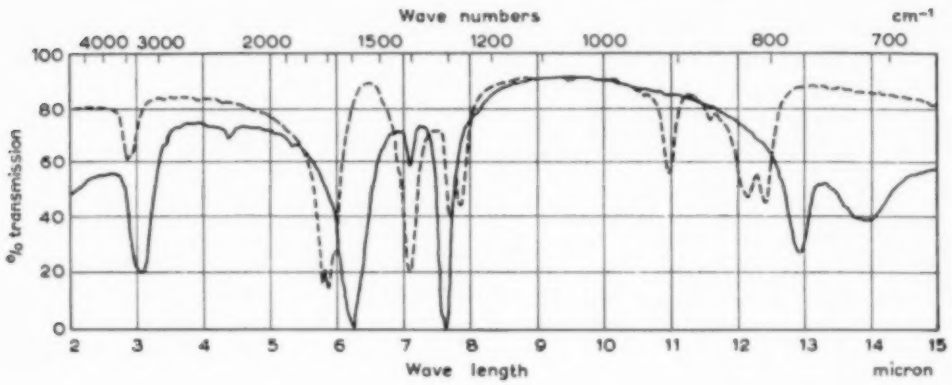

Fig. 1.

——— Potassium oxalate monohydrate, $K_2C_2O_4 \cdot H_2O$.
– – – – – – Potassium trioxalatoaluminate trihydrate, $K_3[Al(C_2O_4)_3] \cdot 3H_2O$.

References

[1] DOUVILLÉ F., DUVAL C., and LECOMPTE J. *Bull. Soc. Chim. France* 1942 **9** 548.
[2] SEN D. N. Ph.D. thesis, University of Notre Dame, 1954.
[3] WERNER A. *Ann.* 1914 **406** 261.
[4] RILEY H. L. *J. Chem. Soc.* 1929 1307.
[5] LANDESEN G. *Z. Anorg. Chem.* 1926 **154** 432.
[6] MANN F. G., CROWFOOT D., GATTIKER D. C., and WOOSTER N. *J. Chem. Soc.* 1935 1642.
[7] MIZUSHIMA S., NAKAGAWA I., and QUAGLIANO J. V. *J. Chem. Phys.* 1955 **23** 1867.
[8] JEFFREY G. A. and PARRY G. S. *J. Chem. Soc.* 1952 4864.
[9] Private communication of Dr. T. Shimanouchi.
[10] MIYAZAWA T. *J. Chem. Soc. Japan* 1956 **77** 381.
[11] MIZUSHIMA S., SHIMANOUCHI T., and NAKAMURA K. private communication.
[12] EDSALL J. T. *J. Chem. Phys.* 1937 **5** 508.
[13] MIYAZAWA T. *J. Chem. Soc. Japan* 1954 **75** 540.

VOL. 9 1957

Spectrochimica Acta, 1957, Vol. 9, pp. 59 to 67. Pergamon Press Ltd., London

The structure of some halogenated ethanes from infra-red measurements

R. N. DIXON*
Department of Colloid Science, Cambridge University

(*Received* 27 *November* 1956)

Abstract—The fine structure of some absorption bands of gaseous C_2H_5Cl, C_2H_5Br, and *trans* 1 : 2-$C_2H_4Cl_2$ has been resolved. From the spacings of the lines and, for the ethyl halides, microwave measurements, knowledge is gained of the molecular structure of these compounds.

Introduction

ALTHOUGH the theory of the structure of the rotation-vibration bands of gaseous asymmetric top molecules has been well developed, its full use has been limited to very light molecules such as H_2O [1]. With heavy molecules the pattern of lines is in general too complex and the individual lines are too closely spaced for resolution, so that band contours only are observed. Notable exceptions to this are nearly prolate or oblate symmetric top molecules in which the lines are grouped together to give spectra close to those of strictly symmetric top molecules. The halogenated ethanes described herein are almost prolate symmetric tops with $A \gg B$ and $B \simeq C$. For such molecules the expected spacing of the lines in type B and type C bands is $2(A - \tilde{B})$ cm^{-1}, where $\tilde{B} = \frac{1}{2}(B + C)$ [2], their bands approximating to perpendicular bands of symmetric tops.

A preliminary account of the main results of this study has appeared previously [3]. However, the detailed results given here, when combined with recent microwave measurements on the ethyl halides, allow considerably more accurate values of the molecular constants to be obtained.

Experimental

The spectra given in Figs. 1–4 were obtained with a grating spectrometer designed and built in this laboratory. The resolution of which this instrument was capable was 0·6 cm^{-1} at 2900 cm^{-1} and 0·5 cm^{-1} at 770 cm^{-1} with thermocouple detection. Calibration by secondary standards fixed the frequency of sharp lines to within 0·1–0·2 cm^{-1} [4, 5].

Results

Ethyl chloride. The out-of-plane CH_2 rocking vibration of ethyl chloride gives rise to a typical type C absorption band (Fig. 1). There is a strong Q branch at 785·1 cm^{-1}, and the "lines" in the P and R branches are regularly spaced, their frequencies being represented by the equation:

$$\nu = 785{\cdot}1 \pm 1{\cdot}745\, m - 0{\cdot}0014m^2 \qquad m = 0, 1, 2, \ldots$$

with a r.m.s. error of 0·14 cm^{-1}. Thus for this band $2(A - \tilde{B}) = 1{\cdot}745 \pm 0{\cdot}015$ cm^{-1}.

---

* Present address: Physics Department, University of Western Ontario, London, Canada.

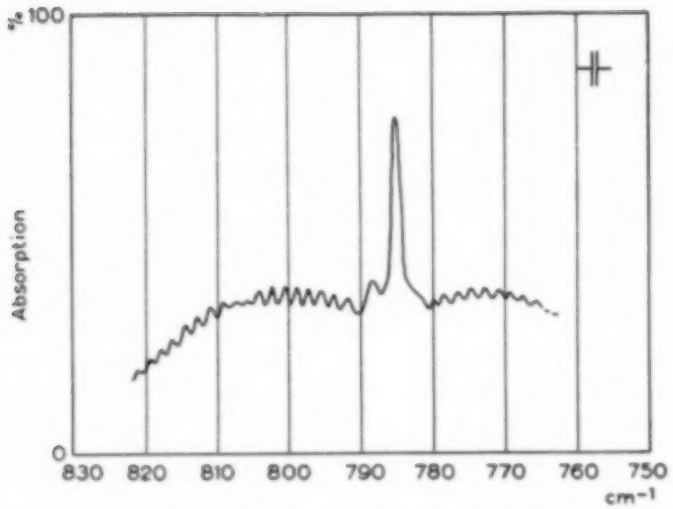

Fig. 1. The CH_2 rocking band of C_2H_5Cl.
Cell = 11 cm.
Pressure = 80 cm Hg.

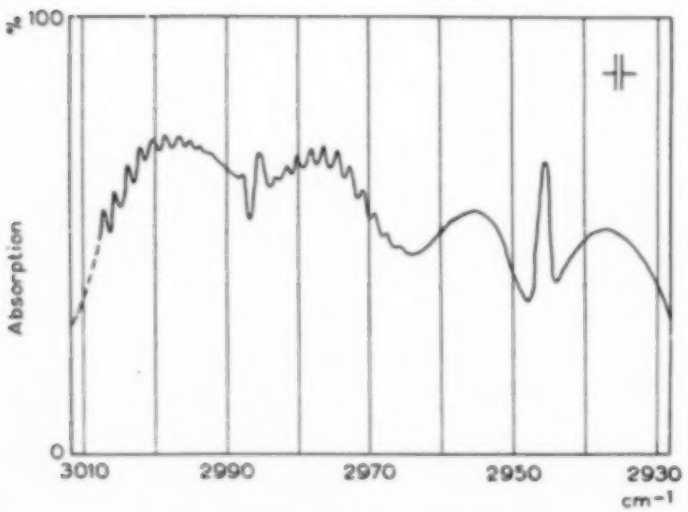

Fig. 2. The νCH_2 bands of ethyl chloride.
Cell = 10 cm.
Pressure = 1·0 cm Hg.

VOL
9
1957

The Q branch of a "hot band" transition can be seen at a slightly higher frequency than the main Q branch.

Stretching vibrations of the CH_3 group of ethyl chloride give rise to three absorption bands between 2900 and 3000 cm^{-1} (Fig. 2). The symmetric νCH_3 vibration has a contour mainly of type A and is centred about a Q branch at 2945·8 cm^{-1}. The two asymmetric νCH_3 vibrations (one in plane, mainly type B, and one out of plane, type C) would be expected to differ little in frequency and to exhibit fine structure of the same spacing. The Q branch of the type C band can be seen at 2985·3 cm^{-1} near an absorption minimum in a series of "lines". The frequencies of these lines can be expressed by the equation:

$$\nu = 2986{\cdot}5 \pm 1{\cdot}77(m - 0{\cdot}29) \qquad m = 0, 1, 2, \ldots$$

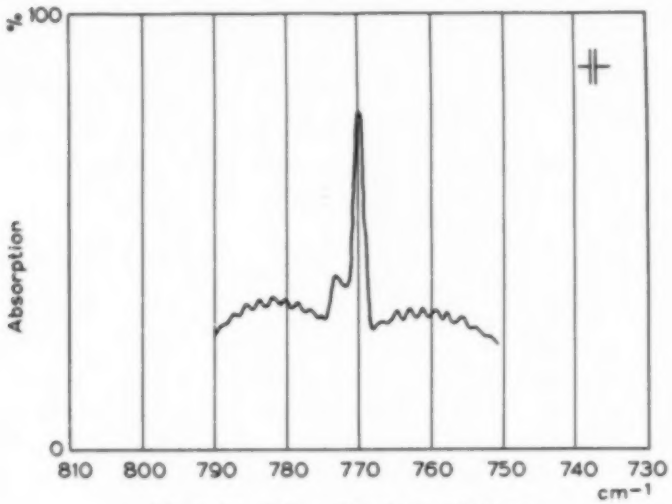

Fig. 3. The CH_3 rocking band of C_2H_5Br.
Cell = 20 cm.
Pressure = 10 cm Hg.

with a r.m.s. error of 0·11 cm^{-1}. The "origin" of these lines does not coincide with the Q branch, neither does a single plot of their frequencies against numbering include both P and R lines. This anomaly probably arises from the superposition of the two absorption bands. Nevertheless, the spacing of 1·77 $\pm$ 0·02 cm^{-1} is in close agreement with that obtained above. However, the former value of $2(A - \tilde{B})$ is to be preferred and will be used in subsequent calculations.

Ethyl bromide. The out-of-plane CH_2 rocking vibration of ethyl bromide gives rise to an absorption band very similar to that of ethyl chloride (Fig. 3). The Q branch is at 769·9 cm^{-1} and the "lines" in the P and R branches can be represented by the equation:

$$\nu = 769{\cdot}9 \pm 1{\cdot}750m - 0{\cdot}005m^2 \qquad m = 0, 1, 2, \ldots$$

with a r.m.s. error of 0·17 cm^{-1}. Hence the value of $2(A - \tilde{B})$ is 1·750 $\pm$ 0·015 cm^{-1}.

Trans 1 : 2-*dichloroethane.* 1 : 2-dichloroethane is capable of existing in two

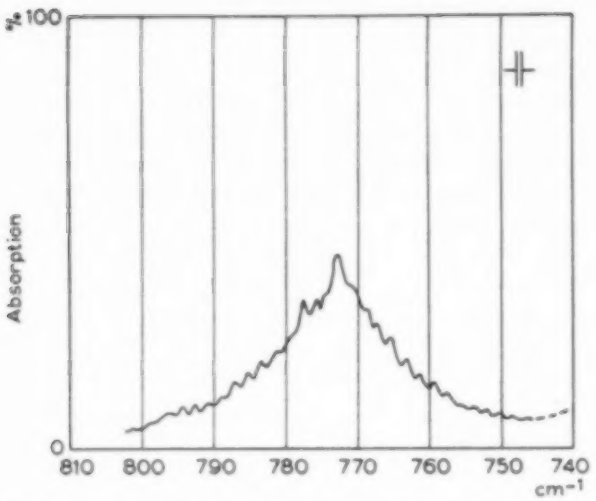

Fig. 4. The species A_u CH_2 rocking band of *trans* 1 : 2-$C_2H_4Cl_2$.
Cell = 20 cm.
Pressure = 6 cm Hg.

VOL.
9
1957

forms, the one being transformed to the other by rotation of the CH_2Cl groups about the C-C bond (rotational isomers). Brown and Sheppard [6] found that the number of infra-red bands decreased when liquid 1 : 2-dichloroethane was crystallized. In the light of Mizushima's work [7] they assigned the persisting bands to the *trans* isomer and those that disappeared to the *gauche* isomer, and were able to make a complete vibrational assignment for both isomers in the spectral region studied. The absorption curve for the species A_u CH_2 rocking vibration (out of plane) of *trans* 1 : 2-dichloroethane is given in Fig. 4. Unlike the CH_2 rocking bands of the ethyl halides, there is no strong Q branch, although there is a defined absorption peak at 772·7 cm^{-1} with regularly spaced "lines" on either side. However, this could only be a type C band of the *trans* molecule, the weakness of the Q branch being explained upon examination of the ratio of rotational constants obtained below. An approximate value for the ratio B/C is 1·03 for *trans* 1 : 2-dichloroethane, as compared with 1·10 for ethyl chloride and 1·08 for ethyl bromide. *Trans* 1 : 2-dichloroethane is therefore much closer to a symmetric top, for which this band would be of the perpendicular type.

The lines can be represented by the equation:

$$\nu = 772{\cdot}30 \pm 1{\cdot}83m \qquad m = 0, 1, 2, \ldots$$

with a r.m.s. error of 0·21 cm^{-1}, giving a value of $2(A-\tilde{B})$ equal to $1{\cdot}83 \pm 0{\cdot}02$ cm^{-1}.

Molecular structure

The ethyl halides. The microwave spectra of ethyl chloride and ethyl bromide have been published, and values of B and C in Mc/s given for $C_2H_5Cl^{35}$ and $C_2H_5Cl^{37}$ [8], and for $C_2H_5Br^{79}$ and $C_2H_5Br^{81}$ [9]. The corresponding values in cm^{-1} are

given in Table 1. The isotopic ratio $Cl^{35} : Cl^{37} \simeq 3 : 1$ and the infra-red measurements for ethyl chloride are assumed to apply essentially to $C_2H_5Cl^{35}$. For bromine, however, the ratio $Br^{79} : Br^{81} \simeq 1 : 1$, and the measurements must be considered average values for the two isotopic molecules.

Table 1. Observed and calculated rotational constants for ethyl chloride and bromide

Molecule	Constant	Observed value (cm^{-1})	Calculated value (cm^{-1})
$C_2H_5Cl^{35}$	B	0·18326	0·18320
	C	0·16553	0·16563
	$2(A - \bar{B})$	1·745 ± 0·015	1·740
$C_2H_5Cl^{37}$	B	0·18004	0·17938
	C	0·16053	0·16247
$C_2H_5Br^{79}$	B	0·12692	0·12693
	C	0·11750	0·11757
$C_2H_5Br^{81}$	B	0·12616	0·12614
	C	0·11684	0·11689
C_2H_5Br*	$2(A - \bar{B})$	1·750 ± 0·015	1·743

* Mean for the two isotopic molecules.

If the axes of least and intermediate moments of inertia of an ethyl halide (in the symmetry plane) are x and y respectively, and the z axis is perpendicular to this plane, then:

$$I_A = \Sigma my^2 + \Sigma mz^2$$

$$I_B = \Sigma mx^2 + \Sigma mz^2$$

$$I_C = \Sigma mx^2 + \Sigma my^2$$

and therefore:

$$I_A + I_B - I_C = 2\Sigma mz^2 \qquad (1)$$

Smith has shown that for ethane there is strong evidence in favour of a staggered configuration [10]. However, for either a staggered or eclipsed configuration for an ethyl halide the only atoms lying out of the symmetry plane, and therefore contributing to Σmz^2, are two of the CH_3 group hydrogen atoms and the two CH_2 group hydrogen atoms. If the C-C-H and H-C-H angles are all assumed to be tetrahedral (109° 28′) and the C-H bonds of equal length, then substituting the experimental results in the left-hand side of equation (1) leads to:

C—H = 1·080 Å for $C_2H_5Cl^{35}$

C—H = 1·079 Å for C_2H_5Br (Br^{79} and Br^{81})

The error in these values arising from inaccuracies in the experimental measurements is $\pm 0{\cdot}012$ Å, but further error might arise, as equation (1) is only exact for the non-vibrating state of the molecule. For methane the length of the C-H bond is 1·093 Å [11]. In view of the considerable error possible in the above values, and the small contribution of the hydrogen atoms to the moments of inertia, the C-H bond lengths were assumed to be 1·09 Å for subsequent calculations on both the ethyl halides, with the C-C-H and H-C-H angles tetrahedral. Rotational constants were calculated for ethyl chloride and bromide for all combinations of the additional molecular parameters given in Table 2. From these calculated rotational

Table 2. The chosen parameters for ethyl chloride and bromide

Molecule	Parameters for calculation
$C_2H_5Cl^{35}$ and $C_2H_5Cl^{37}$	C–C = 1·54 Å, 1·55 Å. C–Cl = 1·76 Å, 1·78 Å 1·80 Å. <C–C–Cl = 109° 28′, 111° 0′, 112° 30′.
$C_2H_5Br^{79}$ and $C_2H_5Br^{81}$	C–C = 1·54 Å, 1·55 Å. C–Cl = 1·92 Å, 1·94 Å, 1·96 Å. <C–C–Cl = 109° 28′, 111° 0′, 112° 30′.

VOL. 9 1957

constants and the experimental values of B, C, and $2(A - \tilde{B})$, curves were drawn up of values of the C-X bond length and the corresponding C-C-X angles consistent with each experimental measurement for the two assumed lengths of the C-C bond (chosen to bracket the length of 1·543 Å found for ethane [12]). Fig. 5 and 6 show these curves for C—C = 1·54 Å, the curves for 1·55 Å being very similar. The area of intersection of these curves gives structures consistent with all the experimental measurements.

Ethyl chloride. The data for the two isotopic chloride molecules do not agree, and the final structures (Table 3) are estimated using the data for $C_2H_5Cl^{35}$ only. It is found to be impossible to choose a molecular configuration consistent with the values of B and C for both isotopic molecules. The microwave spectrum of ethyl chloride has recently been reinvestigated and the rotational constants for $C_2H_5Cl^{37}$ given by Wagner and Dailey and quoted in Table 1 have been found incorrect, although no further values have been given [13]. The two possible structures given in Table 3 lead to essentially identical calculated rotational constants, and the mean values are compared with the experimental values in Table 1.

Ethyl bromide. The consistency curves for the two isotopic bromide molecules are identical to within the limits of representation in Fig. 6. The sets of calculated rotational constants for the two structures given in Table 3 are essentially identical, and the mean values are compared with the experimental values in Table 1.

Trans 1 : 2-*Dichloroethane.* No microwave spectrum has been published for

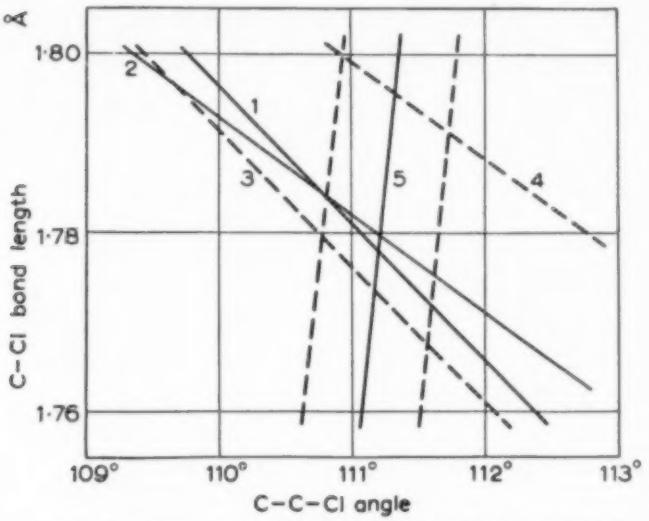

Fig. 5. Consistency curves for ethyl chloride with C–C = 1·54 Å.

Curves for:

1. *B*, $C_2H_5Cl^{35}$
2. *C*, $C_2H_5Cl^{35}$
3. *B*, $C_2H_5Cl^{37}$
4. *C*, $C_2H_5Cl^{37}$
5. Infra-red spacing with margin of error.

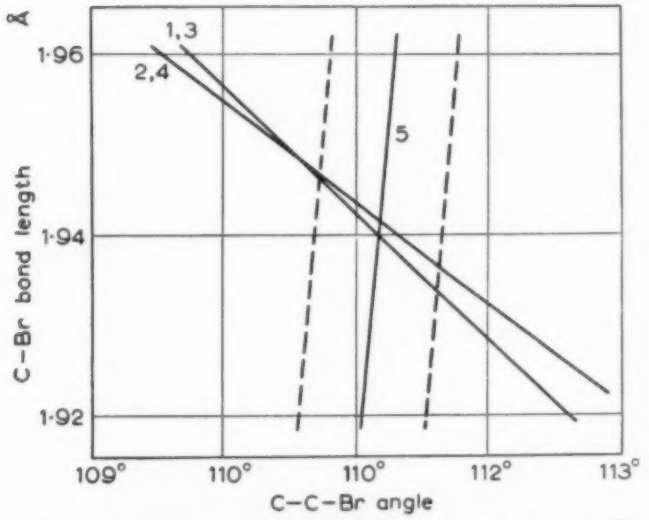

Fig. 6. Consistency curves for ethyl bromide with C–C = 1·54 Å.

Curves for:

1. *B*, $C_2H_5Br^{79}$
2. *C*, $C_2H_5Br^{79}$
3. *B*, $C_2H_5Br^{81}$
4. *C*, $C_2H_5Br^{81}$
5. Infra-red spacing with margin of error.

Table 3. Possible structures for ethyl chloride and bromide

Molecule	Assumed parameters	Calculated parameters
C_2H_5Cl	C–H = 1·09 Å <C–C–H = <H–C–H = 109° 28′ C–C = 1·54 Å	C–Cl = 1·780 ± 0·005 Å <C–C–Cl = 111° 6′ ± 25′
	as above, but C–C = 1·55 Å	C–Cl = 1·771 ± 0·005 Å <C–C–Cl = 111° 16′ ± 25′
C_2H_5Br	C–H = 1·09 Å <C–C–H = <H–C–H = 109° 28′ C–C = 1·54 Å	C–Br = 1·943 ± 0·005 Å <C–C–Br = 110° 57′ ± 25′
	as above, but C–C = 1·55 Å	C–Br = 1·933 ± 0·005 Å <C–C–Br = 111° 16′ ± 25′

The errors stated here are estimated from the experimental errors using the consistency curves, but take no account of possible errors in the assumed parameters.

VOL. 9 1957

trans 1 : 2-dichloroethane, and one experimental measurement only was available for structural calculations. The C-H bond lengths were again assumed to be 1·09 Å and the C-C-H and H-C-H angles tetrahedral. From the dimensions of molecules closely related to halogenated ethanes it was seen that the bond lengths vary but little from one molecule to another, but that there was considerable variation in the bond angles [14]. The values for the C-C and C-Cl bond lengths were therefore chosen equal to those pairs found above for ethyl chloride. Rotational constants were calculated upon these assumptions for values of the C-C-Cl

Table 4. Possible structures for *trans* 1 : 2–dichloroethane

Assumed parameters	Calculated angle C–C–Cl	Calculated rotational constants
C–H = 1·09 Å <C–C–H = <H–C–H = 109° 28′ C–C = 1·54 Å C–Cl = 1·78 Å	109° 2′ ± 45′	B = 0·05031 cm^{-1} C = 0·04871 cm^{-1}
as above, but C–C = 1·55 Å C–Cl = 1·77 Å	109° 26′ ± 45′	B = 0·05038 cm^{-1} C = 0·04876 cm^{-1}

angles equal to 108° 0′, 109° 28′, and 111° 0′. From these and the experimental value of $2(A - \tilde{B}) = 1{\cdot}83 \pm 0{\cdot}02$ cm^{-1} the C-C-Cl angle was determined for each of the above bond-length pairs, and is given in Table 4.

The two possible structures given in Table 4 have Cl—Cl distances of $4{\cdot}315 \pm 0{\cdot}016$ Å and $4{\cdot}311 \pm 0{\cdot}016$ Å respectively. These compare favourably with the value of 4·275 Å from electron diffraction measurements [15], thus leaving no doubt in the assignment of the 772·3 cm^{-1} band of this molecule to the *trans* form.

Acknowledgement—I am indebted to Dr. N. SHEPPARD for many helpful discussions during this study. I am also grateful to the Institute of Petroleum for financial aid in this work and to the Department of Scientific and Industrial Research for a maintenance grant.

REFERENCES

[1] HERZBERG G. *Infra-red and Raman Spectra of Polyatomic Molecules* Van Nostrand Inc. 1945 p. 484.
[2] MECKE R. *Hand- und Jahrb. d. Chem. Phys.* 1934 **911** 281.
[3] CUMMING C., DIXON R. N., and SHEPPARD N. *Nuovo Cimento Suppl.* 1955 **2·X** 564.
[4] BELL E. E. and NIELSEN H. H. *J. Chem. Phys.* 1950 **18** 1382.
[5] BOYD D. R. J., THOMPSON H. W., and WILLIAMS R. L. *Proc. Roy. Soc.* (Lond.) 1952 **A213** 42.
[6] BROWN J. K. and SHEPPARD N. *Trans. Faraday Soc.* 1952 **48** 123.
[7] MIZUSHIMA S., MORINO Y., WATANABE I., SIMANOUTI T., and YAMAGUCHI S. *J. Chem. Phys.* 1949 **17** 591.
[8] WAGNER R. S. and DAILEY B. P. *J. Chem. Phys.* 1954 **22** 1459.
[9] WAGNER R. S., SOLIMENE N., and DAILEY B. P. *J. Chem. Phys.* 1955 **23** 559.
[10] SMITH L. G. *J. Chem. Phys.* 1949 **17** 139.
[11] BOYD D. R. J. and THOMPSON H. W. *Trans. Faraday Soc.* 1953 **49** 1281.
[12] HANSEN G. E. and DENNISON D. M. *J. Chem. Phys.* 1952 **20** 313.
[13] BARCHUKOV A. I., MINAEVA T. M., and PROKHOROV A. M. *Soviet Physics J.E.T.P.* 1956 **2** 760.
[14] GORDY W., SMITH W. V., and TRAMBARULO R. F. *Microwave Spectroscopy* Wiley and Sons, Inc. 1953 p. 371.
[15] ALLEN P. W. and SUTTON L. E. *Acta Cryst.* 1950 **3** 46.

Spectrochimica Acta, 1957, Vol. 9, pp. 68 to 88. Pergamon Press Ltd., London

Excitation temperatures in spark discharges

C. M. CUNDALL and J. D. CRAGGS
Department of Electrical Engineering
The University of Liverpool

(*Received* 17 *October* 1956)

Abstract—The paper describes measurements of spectral line intensities in the vapour clouds emitted from the electrodes in controlled spark discharges carrying a current of rectangular pulse shape. Measurements were made during current flow and in the afterglow for the whole discharge and with spatial resolution. Currents of 200 and 600 A for pulse lengths of 3–3·5 μsec were used. Excitation temperatures deduced from the measured relative line intensities vary from 6000–40,000°K. Data were obtained for zinc, cadmium, and magnesium electrodes, and also tungsten.

1. Introduction

THIS paper describes excitation temperature measurements that have been carried out for short duration (3 and 3·5 μsec) spark discharges of rectangular current waveform, 600- and 200-A amplitude, in hydrogen at about atmospheric pressure. The results were derived by measuring the relative spectral-line intensities as a function of time for metal lines originating at the electrode vapour jets. These measurements were carried out at different points along the discharge. The hydrogen radiation was also examined in an attempt to assess the effect of the metal-vapour clouds on (i) the Balmer decrements, and (ii) the ionic concentration measured from the Stark broadening of the Balmer lines H_β and H.

Some observations have also been made on the spark-to-spark fluctuations in the light intensity from metal lines in successive electrically identical sparks. The work is of particular interest in the spectrochemical analysis of metals, where the spark-to-spark fluctuations provide a limitation to the accuracies obtainable.

A number of publications have appeared on the excitation of the Balmer-series radiation in supposedly metal-vapour free conditions [1–6], but in the present work variations along the length of the spark channel were specially studied. Excitation temperatures have also been measured by a number of workers [7–10], but in general no account has been taken of the "jet" nature of the metal vapour. This makes spatial resolution along the length of the discharge especially desirable. A review of the metal line excitation processes is given by LLEWELLYN JONES [11].

2. Description of apparatus

The 600-amp 3-μsec rectangular current waveform sparks were generated using a modified chopping circuit as described initially by DURNFORD and MCCORMICK [12]. The 200-amp 3·5-μsec sparks were generated by charging up a suitable length of coaxial cable (~360 m) and discharging it through the characteristic impedance in series with the test gap. Single sparks were used.

Light from the spark gap was examined by means of a Hilger small-quartz spectrometer with a photomultiplier fitted behind the exit slit. By passing the output pulse from the photomultiplier through a wide-band amplifier and applying it to a synchronized single-sweep high-speed C.R.O., oscillograms of the temporal variation of light intensity of a specific spectral

VOL. 9 1957

line or part of a continuum were obtained. This system, together with the calibration techniques, is described in another paper [13], and fuller details are also given elsewhere [14]. The oscillograms were recorded on 35-mm film and measurements were made by projection in an enlarger.

By using the optical system shown in Fig. 1, light could be examined from the small length of the discharge column selected by S_1. The region selected was varied by mounting the spark chamber on a platform which could be moved by means of a traversing screw. The spark gap

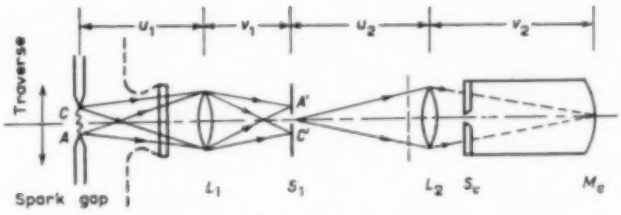

Fig. 1. The optical system.

was mounted in a vacuum-tight chamber with one electrode fitted to a rod passing through a Wilson seal. This enabled the gap length to be altered without affecting the gas inside the chamber. The pressure of hydrogen inside the chamber was maintained a little above the atmospheric value, so that any leakage would be outwards. The use of very pure gas was not attempted. Normal cylinder-grade H_2 ($>0{\cdot}5\%$ O_2) was used and other impurities were less than 1 in 10^4. Spectroscopically pure electrodes of Mg, Cd, Zn, and W were used as representing a wide range of physical properties, and in all cases they were pointed in shape. Experiments with oxygen-free hydrogen were made, but the statistical spark lags were found to be too variable for study with a high-speed synchronized time sweep, even with intense external irradiation.

3. Experimental procedure

In order to measure total line intensities, using the above techniques, it is necessary to adjust the spectrometer exit slit to receive the line concerned and to exclude any neighbouring lines and as much background as possible. The required width can be found either by opening the exit slit gradually and noting the smallest width at which further opening would cause little or no increase in intensity, or by plotting a profile of the line using a slit (~20 microns) that is narrow compared with the line width. If a typical profile is as shown in Fig. 2, where

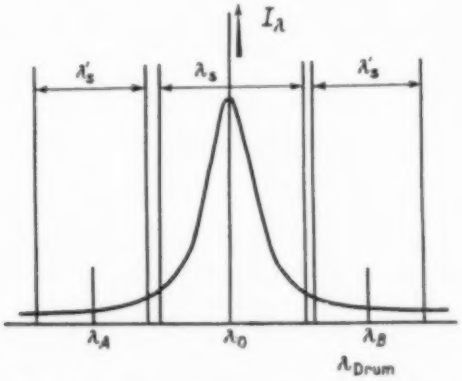

Fig. 2. To show the measurement of total line intensity.

I_λ is the measured intensity plotted against the wavelength λ, as given by the spectrometer drum, then λ_0 is the required drum setting at this line centre; and if $D(\lambda_0)$ is the dispersion of the spectrometer in Å/mm at λ_0, then the required slit-width is $s/D(\lambda_0)$ mm.

The background correction is taken as the mean of readings at λ_A and λ_B multiplied by λ_s/λ'_s, where $\frac{\lambda'_s}{D(\lambda_0)}$ is the exit slit-width used to measure the background.

Metal lines suitable for measurement are those whose transition probabilities are known and which are reasonably isolated; these were found for the metals considered by photographing the complete spectra. Similar lines, so close together that the spectrometer was unable to resolve them, were measured as the sum of a number of lines (e.g. the Mg triplet 3838, 3832, 3829 Å). For each line measured, oscillograms of at least ten successive sparks were recorded together with the oscillograms of the background.

The suitable metal lines were measured by taking the integrated light from the whole discharge. They were then measured as a function of gap position, taking light from 0·5 mm of the 7-mm gap, at 1-mm intervals along its length. Attenuating gauzes were used to keep the oscillograph deflection within the limits of the linearity of the system. Photomultiplier fatigue was approximately corrected by measuring the lines L_1, L_2, etc. in succession in the following order: $L_1; L_2, L_3, L_2, L_1$. The average was then taken for each pair.

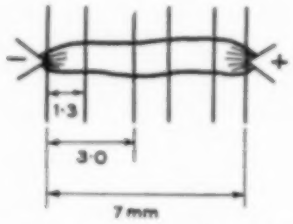

Fig. 3. Measurement positions in the discharge channel.

The Balmer-series lines H_α, H_β, and H_γ were also measured when they were not affected by the metal lines. In such cases, the profiles of H_β and H_γ were also measured by taking oscillograms with a very narrow exit slit for each of the gap positions shown in Fig. 3. Using a fairly wide exit slit, the sensitivity was sufficient to make measurements of the light from the Balmer recombination continuum over the wavelength range from the series limit (3647 Å) down to 3000 Å at the three gap positions of Fig. 3. Some trouble was encountered in the latter experiments due to the presence of vapour, since the intensity of the W lines in the region of the continuum proved to be comparable with that of the continuum. This consideration prevented the latter from being measured with electrodes of the more volatile metals. The presence of W vapour was most noticeable in this part of the spectrum and not in the visible region, since the hydrogen lines in the latter are very much more intense.

4. Experimental results

4.1. *Calibration*

Very careful calibrations were carried out, and these have been described elsewhere [13]. The spectral response of the photomultiplier tube (Type 931 A with ultra-violet glass envelope) is shown in Fig. 4 with curves corrected and uncorrected for the spectrometer dispersion. The curve is shown magnified over the region covering H_α, where the response is weak. The uncorrected curve gives the multiplier response to unit energy in a constant wavelength increment measured with a constant exit slit Δx. When measuring line intensities, this

VOL. 9 1957

response must be corrected to allow for the fact that a constant Δx covers a greater wavelength range at higher values of λ, i.e. it must be divided by the dispersion $d\lambda/dx$. Fig. 5 shows a typical profile from which the required exit slits were determined for relative line-intensity measurements.

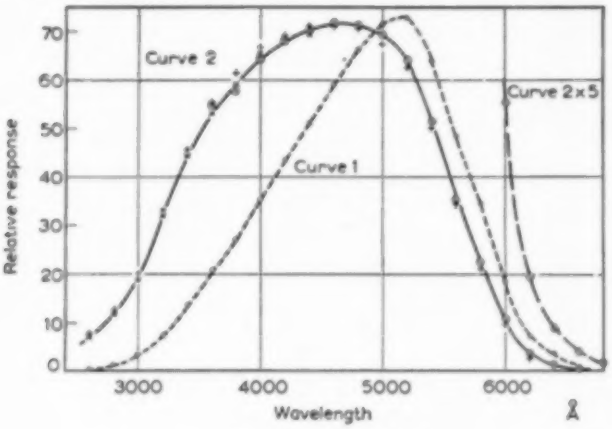

Fig. 4. Photomultiplier.
Response curves — July 1953 — × H_2 lamp
Curve 1—Uncorrected — ○ W lamp
Curve 2—Corrected for dispersion. — Jan. 1953 — +

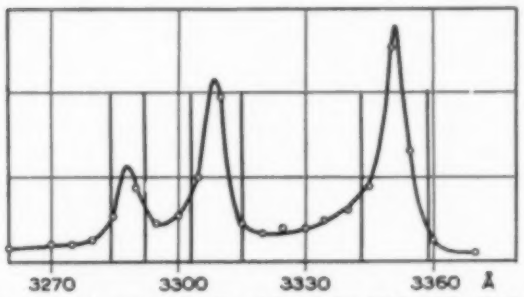

Fig. 5. 200-A spark. Profile of Zn triplet 3282, 3303, 3346 Å.
The vertical lines show the limits of the line skirts taken for line intensities.

4.2. *Metal-line intensities and the excitation temperature*

The lines in the spectra of hydrogen with various metallic electrodes chosen for measurement are listed in Table 1, with details of their transition probabilities as given elsewhere, [15, 16, 17]. Fig. 6 shows typical oscillograms of metal lines. The mean curve of ten successive oscillograms was determined for each line and its height $H(t)$ measured at 1-μsec intervals. The relative intensity of a line λ_0 is given by

$$I_{\lambda_0}(t) = \frac{1}{R'_{M2}}\left[\frac{H(t)}{G} - h(t)\frac{S_e}{S'_e}\right] \qquad (1)$$

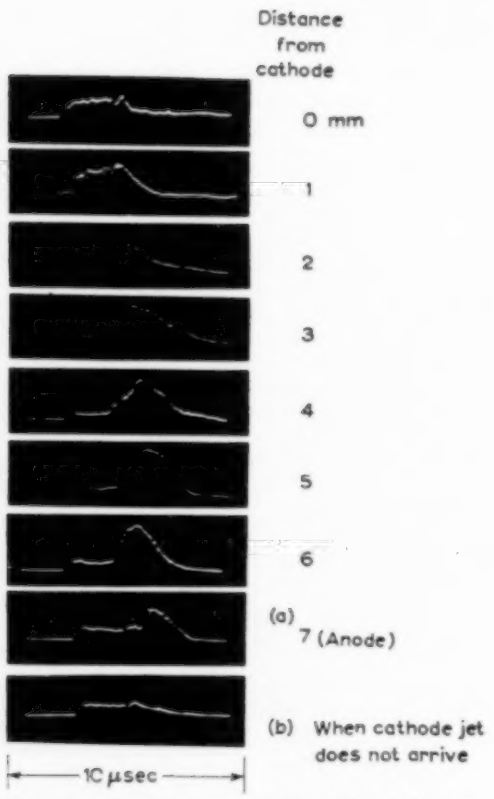

Fig. 6. Typical oscillograms of Mg triplet 3838, etc., at different gap positions for 600-A spark. Cathode Mg, anode W.

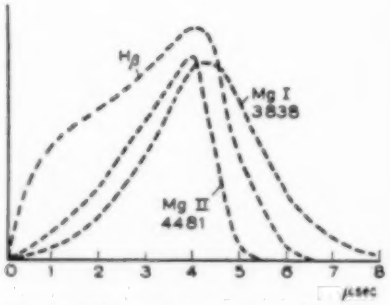

Fig. 7. 200-A spark between Mg electrodes in H_2 intensity curves for $H\beta$ and Mg lines 3838, 4481.

where $R'_{M\lambda}$ is the relative response of the multiplier corrected for dispersion (Fig. 4, curve 2),

G is the transmission of the attenuating gauze,

$h(t)$ is the height of the background,

S_e is the exit-slit width and S_e' its value when measuring the background.

The typical curves of light intensity—time for an Mg^{I} line, an Mg^{II} line, and H are shown for comparison in Fig. 7 (light taken from the whole gap). These show that the afterglow is longest for Mg^{I} lines and very short for Mg^{II}. The intensity of the metal lines is small compared with the gas lines near the beginning of the spark, since here the excited metal vapour is confined to the regions near the electrodes, whereas the gas is excited along the whole length of the discharge.

A mean excitation temperature T_x for the whole discharge is defined by the equation

$$\frac{I_{\lambda_1}}{I_{\lambda}} = \frac{A_1 g_1 \nu_1}{A_2 g_2 \nu_2} e^{(E_2 - E_1)/KT_x} \qquad (2)$$

VOL. 9 1957

where I_{λ_1} is the relative intensity of a line of wavelength λ_1 (eq. 1).

A_1 = the transition probability for that line,

g_1 = the statistical weight of the atoms in the particular excited state,

ν_1 = the frequency of line 1,

E_1 = the energy of the initial level in the transition,

K = Boltzmann's constant.

Table 1. Details of metal lines examined

Metal	Transition	Wavelength (A.U.)	Ref. No.	Transition probability Ag (relative)		Energy of initial level E (eV)	Multiplier response relative
Cd	$6\,^3S_1 - 5\,^3P_2$	5086	C_1	15·4		6·353	68
	$5\,^3D_1 - 5\,^3P_0$	3404	C_2	23·8		7·340	44
	$5\,^3D_3 - 5\,^3P_2$	3610	C_3	100	117·9	7·340	53
	$5\,^3D_2 - 5\,^3P_2$	3613		16·4		7·340	53
	$5\,^3D_1 - 5\,^3P_2$	3614		1·5		7·340	53
	$5\,^3D_2 - 5\,^3P_1$	3466	C_4	52·6	70·0	7·340	47
	$5\,^3D_1 - 5\,^3P_1$	3488		17·4		7·340	47
	$6\,^3S_1 - 5\,^3P_0$	4678	C_5	3·7		6·353	72
	$6\,^3S_1 - 5\,^3P_1$	4800	C_6	12·6		6·353	71·5
Zn	$5\,^3S_1 - 4\,^3P_0$	4680	Z_1	100		6·622	72
	$5\,^3S_1 - 4\,^3P_1$	4722	Z_2	304		6·622	72
	$4\,^3D_1 - 4\,^3P_0$	3282	Z_3	896		7·745	37
	$4\,^3D_{2,1} - 4\,^3P_1$	3303	Z_4	2500		7·745	38·5
	$4\,^3D_{3,2,1} - 4\,^3P_2$	3346	Z_5	4140		7·745	41
Mg	$3\,^3D_{3,2,1} - 3\,^3P_2$	3838	M_1	325	583·7	5·92	60
	$3\,^3D_{2,1} - 3\,^3P_1$	3832		195		5·92	60
	$3\,^3D_1 - 3\,^3P_0$	3829		63·7		5·92	60
	$4\,^3S_1 - 3\,^3P_2$	5184	M_2	50	89·6	5·08	65
	$4\,^3S_1 - 3\,^3P_1$	5173		29·7		5·08	65
	$4\,^3S_1 - 3\,^3P_0$	5167		9·9		5·08	65
	Mg^{II}	4481	M_3	—		—	71
	Mg^{II}	2929	M_4	—		—	16·5
	Mg^{II}	2915		—		—	16·5

Cd—Ornstein, v. Hengstrum, and Brinkman [15].
Zn—Schuttevaer and Smit [16].
Mg—Kersten and Ornstein [17].

Excitation temperatures are plotted as a function of time for 600-A sparks in Fig. 8 and for 200-A sparks in Fig. 9. The temperatures were determined from the line ratios indicated.

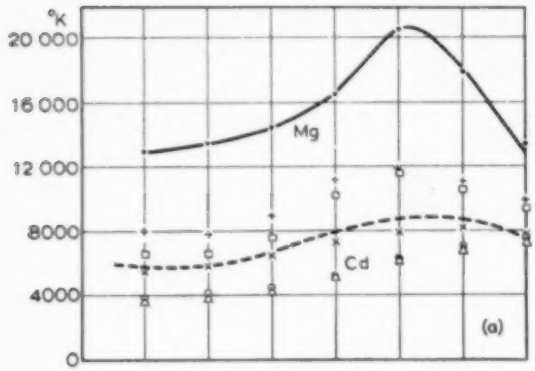

Fig. 8(a). Excitation temperatures for 600-A sparks between Cd and Mg electrodes.
● Mg 3838/5184
× Cd 4678/3404
○ Cd 4678/3466
△ Cd 4678/3610
+ Cd 5086/3466
□ Cd 5086/3610

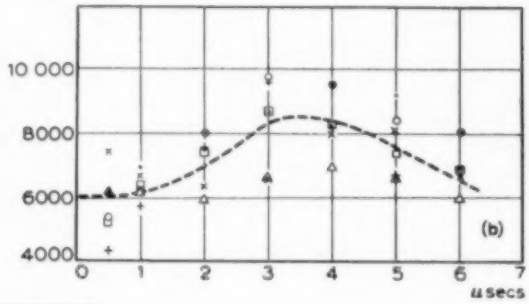

Fig. 8(b). Excitation temperatures for 600-A sparks between Zn electrodes.
× 4722/3346 △ 4680/3346
○ 4722/3303 + 4680/3303
● 4722/3282 □ 4680/3282

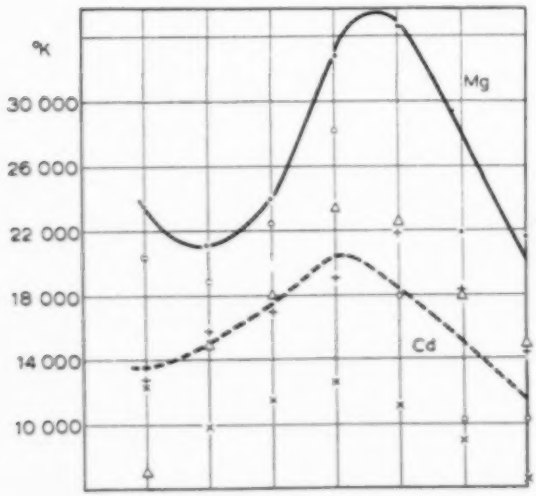

Fig. 9(a). Excitation temperatures for 200-A sparks between Cd and Mg electrodes.
● Mg 3838/5184
× Cd 5086/3610
○ Cd 5086/3466
+ Cd 5086/3404
△ Cd 4678/3404

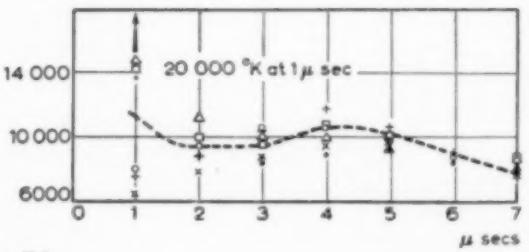

Fig. 9(b). Excitation temperatures for 200-A sparks between Zn electrodes.
× 4722/3346 ● 4680/3346
○ 4722/3303 △ 4680/3303
+ 4722/3282 □ 4680/3282

VOL. 9 1957

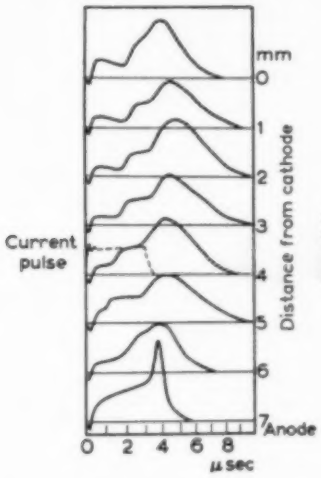

Fig. 10. Tracings of typical oscillograms of Mg triplet 3838 etc., at different gap positions for 600-A spark. Cathode W, anode Mg.

Fig. 10 shows corresponding oscillograms to those of Fig. 6, but taken with a magnesium anode. The correct time scale is given; that on the oscilloscope screen is not strictly linear. Fig. 11 shows various temperatures for various gap positions.

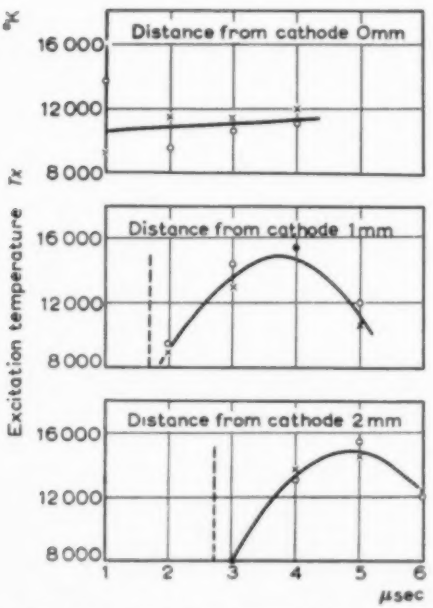

Fig. 11a. Excitation temperatures as a function of time at 0, 1, and 2 mm from a Cd cathode for 200-A, 3·5-μsec sparks in hydrogen (anode W).
× 5086/3404 ——— Jet arrival time.
○ 5086/3466

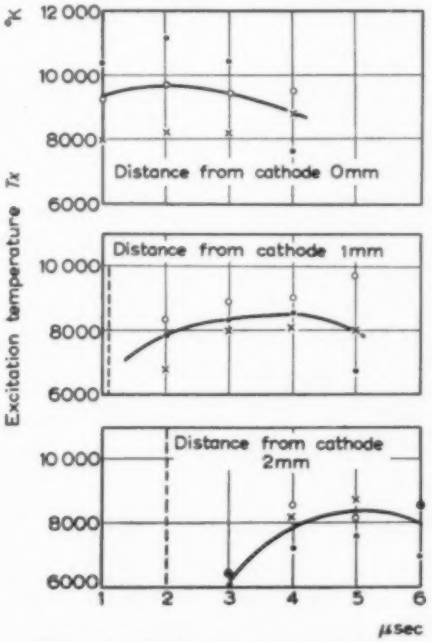

Fig. 11b. Excitation temperatures as a function of time at 0, 1, and 2 mm from a Zn cathode for 200-A sparks (anode W).
× 4722/3346
○ 4722/3303
● 4680/3346 ——— Jet arrival time.

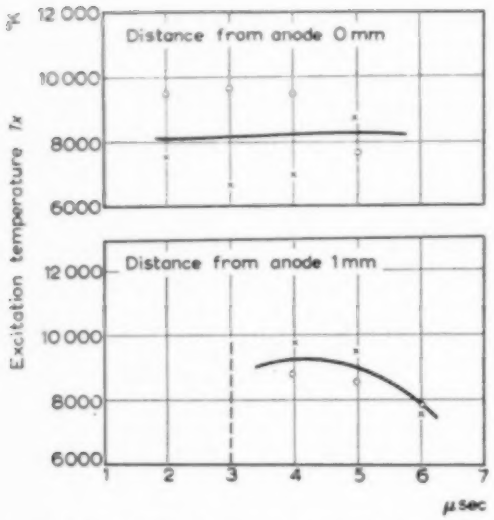

Fig. 11c. Excitation temperatures as a function of time at 0 and 1 mm from a Zn anode for 200-A sparks (cathode W).
× 4722/3346
○ 4722/3303 ——— Jet arrival time.

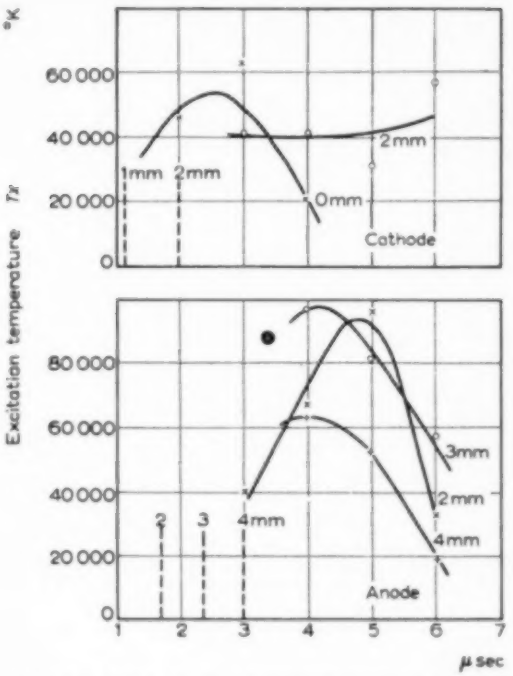

Fig. 11d. (a) Excitation temperatures as a function of time at 0 and 2 mm from Mg cathode. (b) Excitation temperatures as a function of time at 2, 3, and 4 mm from a Mg anode. 200-A, 3·5-μsec spark in hydrogen (other electrode W). ——— Jet arrival time.

Fig. 18 of our previous paper [18] shows how the spark-to-spark fluctuations vary through the gap. The curves represent the envelope of ten successive oscillograms at each gap position. It is clear that the fluctuations increase with distance from the vapour-emitting electrode. In all cases adjacent to the electrode the fluctuations were very small. The results did not differ for the 200-A discharge, and no improvement was found when electrodes composed of single crystals were used. The fluctuations were similar for both anode and cathode jets and in no particular line or metal was any reduction found.

4.3. *The hydrogen radiation*

4.3.1. *The Balmer decrements.* Light-time oscillograms were taken of the lines H_α, H_β, and H_γ at different gap positions for W and Mg electrodes in order to observe the effect of metal vapour on the hydrogen radiation. Fig. 12 shows how the H_β intensity-time profile alters in the presence of strong Mg cathode and anode vapour jets. The curves were fitted at each gap position during the time when no vapour was present at that particular position. The effect of the W vapour makes interpretation difficult, but the similarity of the curves in close proximity to the electrodes suggests (as does the H continuum work) that W

VOL. 9 1957

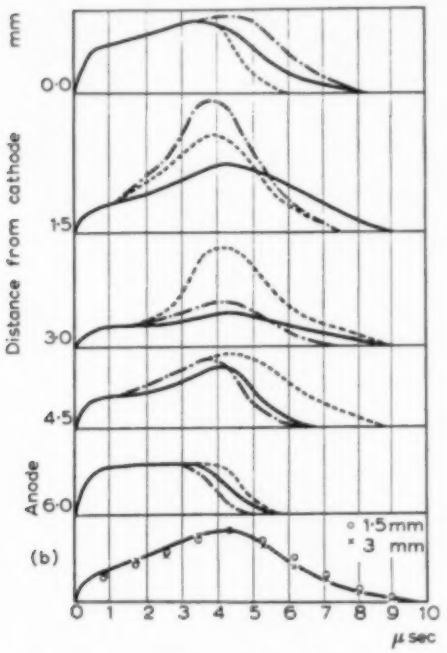

Fig. 12. (a) Light intensity vs. time curves for H_β as a function of gap position for the following electrode configurations: W electrodes, Mg cathode W anode, and Mg anode W cathode 200-A, 3·5-μsec sparks.
(b) H_β curve in the absence of metal vapour (TSUI-FANG[19]).
————W electrodes.
– – – – –Mg cathode W anode.
— · — · —Mg anode W cathode.

vapour is present in appreciable quantities. The W-electrode curves at 1·5 and 3 mm are seen from (b) in Fig. 12 to be similar to those in the apparently vapour-free gap position used by TSUI-FANG [19]. The reduction in afterglow near the anode is possibly due to the anode vapour cloud (W or Mg). At all gap positions the Mg cathode jet lengthens the afterglow and the Mg anode jet shortens it.

The values of the Balmer decrements I_{H_α}/I_{H_β} and I_{H_β}/I_{H_γ} are shown as a function of time and gap position for W and Mg electrode combinations in Fig. 13 (200-A discharges). The accuracy of the decrements was estimated on the basis of the observed spark-to-spark fluctuations and shown in the figures, and the probable shapes of the curves are drawn dotted. Strengthening of the H_α relative to H_β, denotes a decrease in the electron temperature.

Consideration of curves (a) and (b) suggests that there is an effective amount of W vapour present in the discharge which would be expected to affect the decrements. In all the cases shown, the decrements are fairly constant across the gap at 1 μsec, before the vapour has reached far into the gap. During the rest of the current pulse, an increase in I_{H_α}/I_{H_β} is observed, particularly in the centre of the gap. The change in I_{H_β}/I_{H_γ} is not so pronounced, and this decrement remains approximately constant to the end of the current pulse. In the afterglow, however,

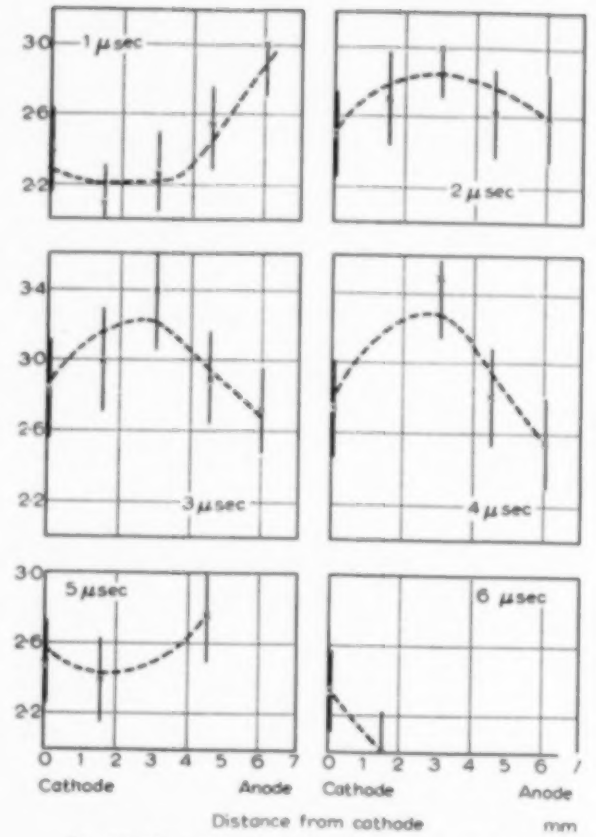

Fig. 13a. The Balmer decrement $I_{H\alpha}/I_{H\beta}$ as a function of gap position at various times during a 200-A, 3·5-μsec spark between W electrodes.

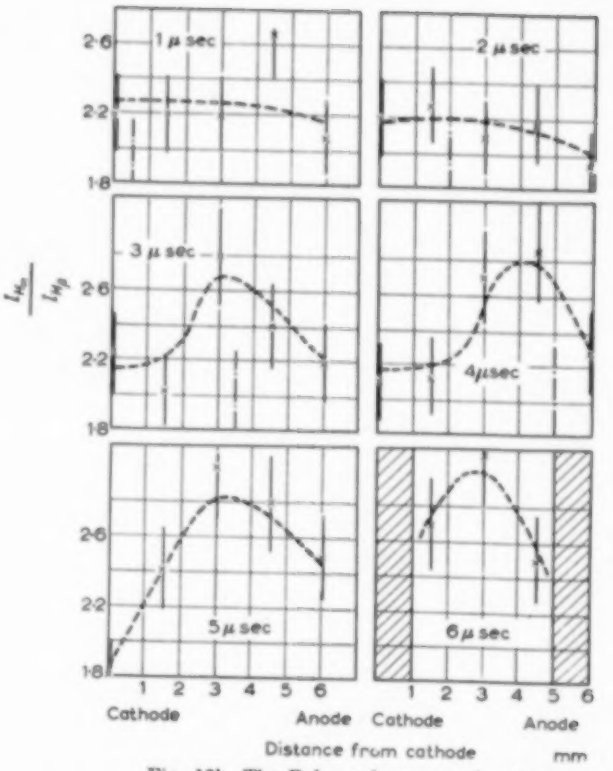

Fig. 13b. The Balmer decrement $I_{H\alpha}/I_{H\beta}$ as a function of gap position at various times during a 200-A, 3·5-μsec spark. Cathode Mg, anode W.
— . — . —Jet front position.

VOL. 9
1957

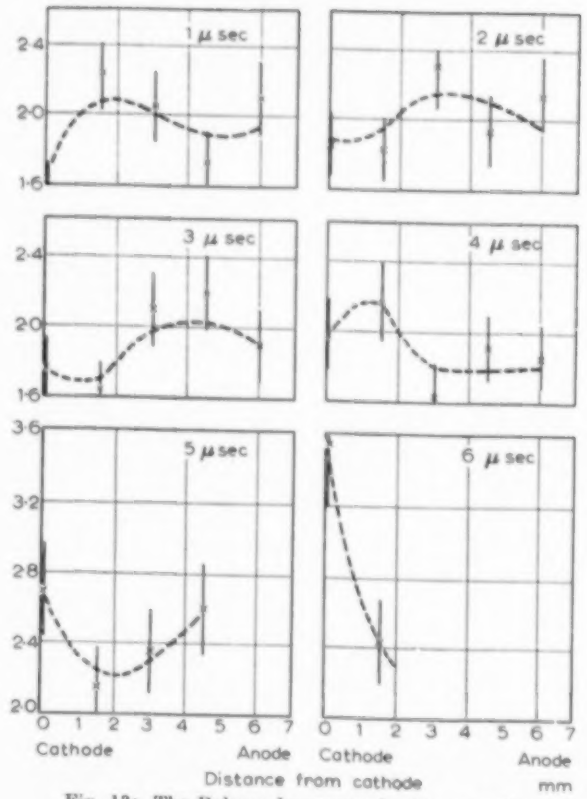

Fig. 13c. The Balmer decrement $I_{H\beta}/I_{H\gamma}$ as a function of gap position at various times during a 200-A, 3·5-μsec spark between W electrodes.

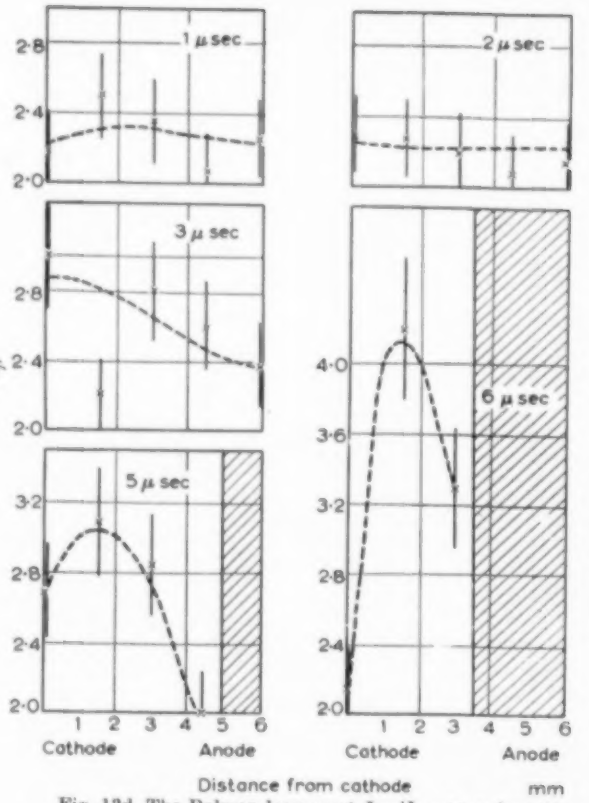

Fig. 13d. The Balmer decrement $I_{H\alpha}/I_{H\beta}$ as a function of gap position at various times during a 200-A, 3·5-μsec spark. Cathode W, anode Mg.

the radiation from near the anode becomes immeasurably small, but there is some increase in I_{H_β}/I_{H_γ} near the cathode. Particular reference to curve (c) shows I_{H_α}/I_{H_β} to increase considerably in the presence of the strong Mg vapour clouds. After the current is cut off, the ratio falls near the vapour-emitting electrode but remains high in the region of excited vapour (see the high I_{H_α}/I_{H_β} ratio in the excited vapour "suspended" in the middle of the gap at 6 μsec (c) see also the image-converter photographs of this region in ref. 18).

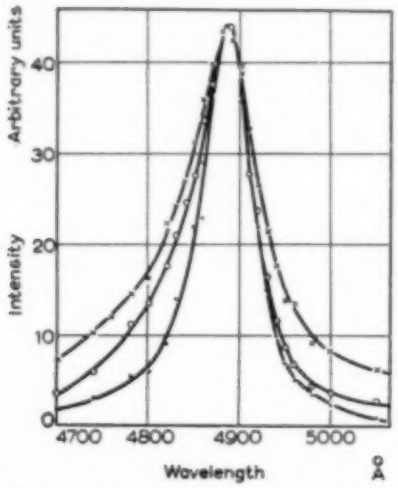

Fig. 14. Profiles of H_β near cathode. 640-A, 3-μsec spark in hydrogen. W electrodes.
× 1 μsec ○ 3 μsec ● 5 μsec

4.3.2. *The determination of ionic concentration from the Balmer line profiles.* The profiles of H_γ and H_β have been plotted for W and Mg electrodes as a range of gap positions, and a typical example is shown in Fig. 14. On the assumption that the observed broadening of the lines is due to the Stark effect of interionic fields, it is possible to determine a mean ionic concentration as a function of time and gap position. The variation of multiplier response over the wavelength range of the broadened line is such that light intensities are directly proportional to the oscillogram height (with gauze attenuator correction).

A certain lack of symmetry about the line centre may be observed, and checks were made to ensure that this was not inherent in the recording techniques. A possible explanation is the assymmetrical shift of certain components of the broadened line in a high field, as noted by BOMKE [20] and RYDE [21]. This would explain also why the asymmetry is greatest during the early stages of the spark when the field is highest.

After correction for background, the long-wavelength halves of the profiles were replotted against the wavelength displacement from the line centre, as shown in Fig. 15. The curves due to UNSÖLD [22] of $S(\alpha)$ vs. α for the Stark broadening of H_β and H_γ (further details are given elsewhere [14]) were then fitted along both axes by a process of systematic trial and error to the observed profiles. The

VOL. 9 1957

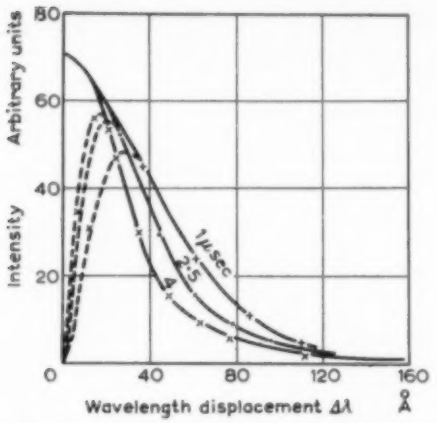

Fig. 15. Experimental and calculated profiles of H_β near the anode for 600-A sparks between Mg electrodes.
Experimental curve
1 μsec
2·5 μsec calculated
4 μsec curves.

resulting fit is seen to be good over the skirt, but not in the centre of the profile, when other effects are important.

The constant $F_0 = 2{\cdot}61en^{2/3}$, where e is the electronic charge and n is the number of singly-charged ions and electrons/c.c. (see below for a qualification of this), is given by the scaling factor $\alpha/\Delta\lambda$ on the abscissae, and hence n was derived for each time, gap position, and electrode combination. Assuming there to be an equal number of ions and electrons in the discharge, the ionic concentration is $n/2$ ions/c.c. and the derived values are given in Table 2.

Table 2. Ionic concentrations derived from hydrogen line profiles (ions/c.c.)

Near cathode	Centre of gap	Near anode
1. W electrodes (600 A)		
(a) From H_β		
(1) $4{\cdot}2 \times 10^{17}$	(1) $3{\cdot}3 \times 10^{17}$	(1) $5{\cdot}7 \times 10^{17}$
(3) $3{\cdot}3 \times 10^{17}$	(3) $3{\cdot}3 \times 10^{17}$	(2·5) $4{\cdot}2 \times 10^{17}$
(5) $3{\cdot}3 \times 10^{17}$	(5) $3{\cdot}3 \times 10^{17}$	(4) $3{\cdot}7 \times 10^{17}$
—	(7) $2{\cdot}5 \times 10^{17}$	—
(b) From H_γ		
(3) $3{\cdot}2 \times 10^{17}$	(3) $4{\cdot}2 \times 10^{17}$	—
2. Mg electrodes (600 A)		
From H_β		
(1) $4{\cdot}4 \times 10^{17}$	(1) $3{\cdot}3 \times 10^{17}$	(1) $5{\cdot}7 \times 10^{17}$
(2·5) $3{\cdot}4 \times 10^{17}$	(3) $3{\cdot}3 \times 10^{17}$	(2·5) $3{\cdot}4 \times 10^{17}$
(4) $3{\cdot}4 \times 10^{17}$	(5) $2{\cdot}5 \times 10^{17}$	(4) $2{\cdot}5 \times 10^{17}$

Numbers in brackets represent time after beginning of current pulse (μsec).

The ionic concentration is seen to be very high near the electrodes at the beginning of the current pulse. As time progresses it falls to a steady value of $\sim 3{\cdot}3 \times 10^{17}$ throughout the gap (except near the anode for W electrodes). There is seen to be little significant difference between the results with W and Mg electrodes.

4.3.3. *The Balmer ultra-violet continuum.* Using the experimental techniques described above, measurements were attempted on the Balmer continuum. Because the radiation intensity in the continuum is so weak and the sensitivity of the recording system was such that wide slits were necessary to detect the radiation, any metal-vapour lines in the range of the continuum would affect the readings. This prohibited reliable measurements even for the case of W electrodes.

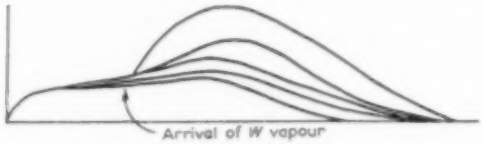

Fig. 16. Emission of radiation from tungsten vapour.

It is of interest to note the effect of the W vapour on the oscillograms of light intensity-time at points in the continuum. Fig. 16 shows a set of oscillograms taking light from the centre of the gap at 3650 Å. These were for single sparks following in rapid succession. The lowest oscillogram, in which no metal vapour is detected, was the first of the series and, as such, was fired after a time-delay. After successive sparks more and more vapour reaches the particular point of the gap. This effect is discussed later (Section 5.4).

VOL. 9 1957

5. Discussion

Some implications of the results described above, together with those of some of the effects that have been observed with vapour jets, will be discussed in this section.

5.1. *Excitation conditions in the metal-vapour jets*

Let us first consider whether the excitation of the metal atoms in the vapour jets is caused by electron-atom impacts or by atom-atom impacts. ELENBAAS [24] discusses the relative probabilities of these two mechanisms for the high-pressure Hg arc and concludes that the former predominates. We will apply a similar treatment to the discharges used in the present work.

For a discharge in which there is a thermal equilibrium (i.e. the electron temperature T_e = gas temperature T_g) he deduces that the ratio of the number of excitations by electron impact to the number of mutual atom-impact but an excited-level k is:

$$\frac{(N_e)_k}{(N_a)_k} = \frac{1}{2\sqrt{2}} \left(\frac{m_a}{m_e}\right)^{\frac{1}{2}} \frac{n_e}{n_a} \frac{(q_e)_k}{(q_a)_k} \tag{3}$$

$\frac{m_a}{m_e} = \frac{\text{mass of atom}}{\text{mass of electron}} = 4{\cdot}38 \times 10^4$ for Mg and $2{\cdot}05 \times 10^5$ for Cd.

n_e = number of electrons/c.c. from the ionic concentration work, assuming that on the average there are equal numbers of ions and electrons (see below for a further discussion).

$n_e \cong 3 \times 10^{17}$ electrons/c.c.

n_a = number of metal atoms/c.c. in the jet, assuming the jet to be at atmospheric pressure and at a temperature of 10,000°K,

$n_a = 7{\cdot}8 \times 10^{17}$ atoms/c.c.

$(q_e)_k$ and $(q_a)_k$ are the probability factors and are not exactly known. It is, however, accepted that for rare gases and alkali atoms, $(q_e)_k/(q_a)_k$ is of the order of 10^3 [25, 26]. Substituting these values in the equation gives

$$(N_e)_k/(N_a)_k = 3 \times 10^4 \text{ for Mg and } 6{\cdot}4 \times 10^4 \text{ for Cd.}$$

It is concluded from this that excitation is carried out mainly by electron impact, which is in agreement with the conclusion of Llewellyn Jones [11] in his discussion of the excitation of metal vapour in discharges.

A further possibility is the excitation of metal atoms by collision with the hydrogen atoms in the discharge. Applying equation (3) for this case, we have n_h = number of hydrogen atoms/c.c. $= 2n_e$ (assuming 33% ionization—see Section 5.3.7) $= n_a$. Also, if we assume the probabilities $(q_h)_k$ and $(q_a)_k$ to be equal, then $(N_{ah})_k/(N_a)_k = 2$. It would appear, therefore, that the number of excitations by metal-atom–gas-atom collisions can also be neglected compared with those by metal-atom–electron collisions.

5.2. *Metal-line intensities and excitation temperatures*

The excitation temperature T_x is defined from equation (2), which is derived assuming (a) that the colliding particles have a Maxwell-Boltzmann distribution of energies and (b) that collisions of the second kind predominate in the high-current density of the spark discharge. It is doubtful whether in the short-duration spark (3 μsec), (a) has time to be attained for the atoms and electrons concerned in the radiating collisions. Meek and Craggs [27] enlarge on the work of Weizel and Rompe, pointing out that for elastic-electron–atom collisions, the electron will transfer $\sim(2m/M)$ (m = mass of electron, M = mass of atom) of its excess energy, making the relaxation time for the transfer of energy from electrons to atoms $\sim M/2m$. This makes the relaxation time 5×10^{-6} sec for Cd, for example, which is of the same order as the current pulse length.

It has been suggested [11, 24] that the contributing process in the acquisition of potential energy by the metal atoms is electron impact, and if this were responsible for the major portion of the total radiation energy (i.e. kinetic energy negligible) T_x would equal the electron temperature T_e. (Section 5.1 shows that this is not the case, making a comparison between T_x and T_e difficult.)

The reasonable agreement between the value T_x derived from the different line pairs for Zn (Fig. 9b.) suggests that the assumptions (a) and (b) above may be valid to a limited extent, and in all cases the agreement improves at later times,

indicating that the assumptions are more closely approached. This agrees with the work of LANGSTROTH and MCRAE [7].

The fact that T_x rises to a peak soon after the end of the current pulse and then starts to fall, suggests that there is a fall in the total electron and/or thermal energy available for excitation in the afterglow. This would be expected, since the electrons in the discharge column, which are thought to play a predominant part in the excitation processes, receive their energy from the electric field which is zero in the afterglow (the current falls to zero within 0·2 μsec of the nominal current cut off). The energy fall in the afterglow is further illustrated by the respective shapes of the light-intensity–time oscillograms for Mg^{I} and Mg^{II} lines (see Fig. 7). For the latter, which require higher energies, the light intensity falls more rapidly after the end of the current pulse.

There is, however, a time delay of between 1 and 2 μsec after the end of the current pulse before the excitation temperature starts to fall. It is thought possible that this is due to the contribution of the kinetic energy of the metal atoms in the jet which is observed [18] to continue to move without appreciable reduction in velocity in the afterglow. The fact that the delay is longest for Mg suggests that the contribution from the kinetic energy of the jet is greatest in this case. This is based on the fact that the electron temperature T_e is found to fall immediately after the current is cut off [19]. There are probably also other effects operative in the post-current period.

VOL. 9 1957

The magnitude of the excitation temperatures is lowest for Zn and highest for Mg for both 600- and 200-A discharges, although the difference between Zn and Cd is small. This is possibly due to the fact that the velocity of the metal atoms in the Mg vapour cloud is higher than for Zn and Cd, where the velocities are little different. For it is reasonable that the presence of the high-velocity Mg atoms, whose energy is known (see Section 5.1) to be comparable with that of the other exciting particles, will, by colliding with the latter, increase the excitation temperature of the discharge. A further factor that may influence the derived values for T_x is the fact that the energy required for the excitation of the metal lines from which T_x was measured is smaller for Mg (see Fig. 5) than for Zn or Cd. There may be other influencing factors, including the possibility that T_x will depend, other things being equal, on the quantity of metal vapour in the discharge channel. The value of T_x for different metals will also depend on the elastic collision cross-sections [27], since these affect the value of T_e in relation to the gas temperature T_g. T_x was found, in all cases, to be higher for the 200-A discharges. This may be due to the reduced amount of metal vapour present, although there may be other influencing factors in the excitation mechanism.

The fact that ionized lines are observed in the Mg spark is probably due to the low ionization potential, although the higher temperature will also facilitate ionizing collisions [12]. From the excitation temperature curves (Fig. 11) taken at different gap positions (observing light from 1 mm of the gap length) it is seen that the temperature at the vapour-emitting electrode is approximately constant during the time for which emission takes place. After the current is cut off, the intensity-time oscillograms show that the light from the metal clouds falls sharply as the tail of the jet moves away from the electrode. At 1 and 2 mm from the

electrode the temperature can, of course, only be measured after the jet has arrived. After the jet arrival, T_x rises to a peak, then falls again. The peak occurs at later times at successively greater distances from the electrode. Once the jet front has passed the position of observation, the light detected is that from the body of the jet. Thus the observed results could imply that the temperature is lower at the edges of the jet and gradually increases towards the middle of the jets. The excitation temperature, as a function of time, will, however, be affected by the change in the electron temperature with time and thus the observed temperature rise may be a combination of both these effects. The same arguments apply to the fall in intensity in the afterglow, which could be due to the approach of the tail of the jet or a fall in T_e in the afterglow.

Since the vapour jets are continuously moving, it is necessary to use spatial resolution to understand fully the temperature distribution in the jet. The enhancement of the spark-to-spark fluctuations under these circumstances, however, reduces the accuracies obtainable, particularly at a distance from the electrodes. Although most previous workers have taken the integrated light from the whole discharge gap, in view of the fact that the light originates from a jet excitation temperatures measured in this way are of doubtful value. In order to advance beyond the work described here, it would be desirable to be able to measure two or more lines simultaneously.

OL.
9
57

5.3. *The hydrogen radiation*

It is seen, by comparison of results with W and Mg electrodes, that tungsten vapour is present in the discharge. This may explain, for example, why occasionally near the electrodes, where the vapour will be more dense, $I_{H_\beta}/I_{H_\gamma} > I_{H_\alpha}/I_{H_\beta}$. Referring to Fig. 14, the afterglow is found to be considerably reduced near the electrodes and there is a similarity between the hydrogen and metal-line-intensity–time oscillograms in this region. A possible explanation of the shortening of the hydrogen afterglow near a vapour-emitting electrode is that the hydrogen is swept away by the jet during the current pulse. (Calculations on the basis of FINKELNBURG'S theory [29] show that the density of metal atoms in the jet is probably greater than that of the hydrogen atoms.) When the jet tail moves away after the end of the current pulse, it will then leave behind it a region of low-hydrogen density from which the emitted light will be considerably weakened. Further evidence of this effect is given by the fact that near the electrodes the percentage increase in hydrogen radiation from, say, 1 to 4 μsec is very much less than in the centre of the gap. HAYNES [23] also found evidence that the atoms in his Hg jet swept the hydrogen away in front of it. Another possible explanation of the shortened afterglow near the electrodes is that the jet initially has a cooling effect, causing a reduction in the light output. From the Balmer decrements in the presence of both W and Mg vapour it can be deduced that the presence of metal vapour increases the I_{H_α}/I_{H_β} decrement. It was found, in particular, that a very high I_{H_α}/I_{H_β} decrement was found for Mg vapour clouds in the afterglow. This is after the sudden increase in light output from a Mg vapour cloud which occurs at the end of the current pulse. It is likely that a proportion of the Balmer radiation is due to recombination (for the presence of the ultra-violet continuum

shows this process to be operative), but the proportion has not been determined.

Considering the ionic concentrations derived from measurement of the Stark broadening of the Balmer series lines, it must first be emphasized that the derived ionic concentrations represent a mean value across the channel, since the profiles are plotted taking light from the whole cross-section and the variation across the channel is not known. Their numerical values, therefore, represent only an order of magnitude, but their comparative values as a function of time and gap-position will give an indication of the trend of variation. It is also difficult to assess the effect of the electrons in causing Stark broadening, and, it is thought now by most workers, that their influence is not negligible although they do not contribute their full effect. Thus, although here N_e was taken to equal N_i, it is possible that the total concentration contributing to broadening $= (N_i + fN_e)$ where $f < 1$.

Others workers [4, 19] have used this method to determine ionic concentrations in the absence of metal vapour, but the presence of the latter introduces uncertainties in interpretation. It is known that metal atoms are ionized, at least in the case of Mg, since strong Mg^{II} lines are observed. It is difficult to assess how the number of metal ions compares with the number of hydrogen ions, but their formation will be facilitated, particularly in the case of Mg, by the low-ionization potential of the Mg atom (7·6 eV, compared with 13·5 eV for atomic hydrogen).

Using the same method of observation, Tsui-Fang [19] found for a 200-A discharge that $N_i + fN_e = 2 \times 10^{17}$ during the current pulse falling to $1{\cdot}5 \times 10^{17}$ in the afterglow. Our values at the centre of the gap are three times these values. If this is wholly accounted for by the fact that the current used in the present experiments was three times Tsui's current, it would suggest that metal ions have negligible effect. This suggestion is supported by the fact that for Mg electrodes in the centre of the gap there is no change in N_i (Table 2) between 1 and 3 μsecs, although the jet arrives during this time. (Tsui-Fang [19] also found N_i to remain constant during the current pulse in the absence of metal vapour.)

N_i is found to fall in the afterglow, as would be expected, due to the reduction in the rate of ion production and the effect of recombination. The constancy of N_i during the current pulse suggests that the rate of ion production equals the rate at which ions and electrons are recombining.

The ionic concentration is found to be higher near the electrodes, particularly at the start of the current pulse. This could possibly be due to channel constriction near the electrode spots.

5.4. *Spark-to-spark fluctuations*

The work described here, together with that already published [18], gives some information on the fluctuations in metal-line intensity that occur for successive electrically identical sparks. That this is not a function of the recording techniques or the main spark channel is seen by the fact that the equivalent fluctuations for the hydrogen lines were about one-third of the magnitude of the metal-line fluctuations. It has been established [18] that the fluctuations are at least partially due to the different shape of the vapour jets in successive

VOL. 9 1957

sparks, since this causes the vapour to arrive at a given position at different times after the spark is initiated. The fact that more and more metal vapour was observed in successive sparks between W electrodes (Fig. 17)suggests that the amount of vapour emitted depends on the state of oxidization of the electrode surface, and this will, of course, contribute to the fluctuations.

This could explain why the fluctuations were so much larger for the repetitive sparks used by WILLIAMS *et al.* [8] than for the single sparks used by the authors, where the erosion will be slower. Since it is desirable for spectrochemical analysis to reduce the spark-to-spark fluctuations to a minimum, the following suggestions arise from the work discussed here:

(i) Light should be taken from near the electrodes where the fluctuations due to jet directions of velocity are least. For those reasons also short gaps might be advantageous.

(ii) The sparks should take place under conditions such that the oxidization of the surface remains constant. An oxygen-free atmosphere is probably the best way of achieving this.

(iii) Fluctuations due to change of electrode surface by erosion might be minimized by the use of a sample electrode in liquid form (as has been proposed by some analysts for aluminium).

6. Conclusions

The excitation temperatures measured in zinc, cadmium, and magnesium vapour clouds in sparks carrying 200 or 600 A for a few microseconds vary from 6000 to 40,000°K, depending on conditions. Spatial variations of the excitation temperatures at a given time, and for different times, are appreciable. Fluctuations of spectral-line intensities were observed and are discussed. They limit the accuracy of measurement of mean excitation temperature for a succession of sparks.

Acknowledgements—The authors wish to thank Professor J. M. MEEK for the interest he has shown in this work. They are also indebted to the British Iron and Steel Research Association for supporting this work for the award of a Bursary to one of them (C. M. C.), and for permission to publish this paper.

References

[1] CRAGGS J. D., WILLIAMS G. C., and HOPWOOD W. *Phil. Mag.* 1948 **39** 329.
[2] RAVENHILL P. and CRAGGS J. D. *Proc. Phys. Soc.* 1951 **B64** 618.
[3] ORNSTEIN L. S. and LINDEMAN H. *Z. Phys.* 1930 **63** 8.
[4] CRAGGS J. D. and HOPWOOD W. *Proc. Phys. Soc.* 1947 **59** 775.
[5] CRAGGS J. D. and HOPWOOD W. *Ibid.* 1947 **59** 771.
[6] JÜRGENS G. *Z. Phys.* 1952 **134** 21.
[7] LANGSTROTH G. O. and MCRAE D. R. *Canad. J. Res.* 1938 **A16** 17.
[8] WILLIAMS G. C., CRAGGS J. D., and HOPWOOD W. *Proc. Phys. Soc.* 1948 **B62** 49.
[9] BRAUDO C. J., CRAGGS J. D., and WILLIAMS G. C. *Spectrochim. Acta* 1949 **3** 546.
[10] BLITZER L. and CADY W. M. *J. Opt. Soc. Amer.* 1951 **41** 440.
[11] LLEWELLYN JONES F. *J. Soc. Chem. Ind.* 1945 **64** 317.
[12] DURNFORD J. and MCCORMICK N. R. *Proc. I.E.E.* II 1952 **99** 33.
[13] TSUI FANG, CUNDALL C. M., and CRAGGS J. D. *Spectrochim. Acta* 1953 **5** 452.
[14] CUNDALL C. M. Ph.D. thesis, Liverpool, 1954.

[15] ORNSTEIN L. S., VAN HENGSTRUM J. P. A., and BRINKMAN H. *Physica* 1938 **5** 145.
[16] SCHUTTEVAER J. W. and SMIT J. A. *Ibid.* 1943 **10** 502.
[17] KERSTEN J. A. H. and ORNSTEIN L. S. *Ibid.* 1941 **8** 1124.
[18] CUNDALL C. M. and CRAGGS J. D. *Spectrochim. Acta* 1955 **7** 149.
[19] TSUI FANG Ph.D. thesis, Liverpool, 1954.
[20] BOMKE H. *Phys. Zeit.* 1936 **37** 417.
[21] RYDE N. *Z. Phys.* 1938 **109** 108.
[22] UNSÖLD A. *Physik der Sternatmosphären* Springer, Berlin, 1938.
[23] HAYNES J. R. *Phys. Rev.* 1948 **73** 891.
[24] ELENBAAS W. *The High Pressure Hg Vapour Discharge* Amsterdam 1951.
[25] MAURER W. *Phys. Zeit.* 1939 **40** 161.
[26] NEUMANN V. *Ann. Phys. Leipzig* 1939 **34** 603.
[27] MEEK J. M. and CRAGGS J. D. *Electrical Breakdown of Gases* Oxford, 1953.
[28] WEIZEL W. and ROMPE R. *Theorie Elektrische Lichtdohen und Funken* Barth. Lpz. 1949.
[29] FINKELNBURG W. *Phys. Rev.* 1948 **74** 1475.

VOL.
9
1957

Spectrochimica Acta, 1957, Vol. 9, pp. 89 to 97. Pergamon Press Ltd., London

Spectrographic determination of carbon in sedimentary rocks, using direct-current arc excitation

WILLIAM H. DENNEN
Cabot Spectrographic Laboratory, Department of Geology and Geophysics,
Massachusetts Institute of Technology, Cambridge, Massachusetts

(*Received* 24 *January* 1956; *accepted for publication* 19 *November* 1956)

Abstract—Carbon may be determined in its various compounds by direct-current arc emission spectrography. When samples are excited in copper electrodes, the carbon in the sample combines with atmospheric nitrogen to form cyanogen, and the bandhead CN 3883 Å is measured. Cathode excitation at 6 A and ~50 V provides the best sensitivity for graphitic carbon and carbonates. A coefficient of variation of 13% is obtained. Marked differences of relative intensity are related to the nature of the carbon compound, to the excitation conditions, and to the presence of silica. These matrix variations are controlled by comparing unknown samples with chemically similar standards, maintaining uniform arcing conditions, and diluting samples with quartz. Separate determinations for different compounds of carbon are required.

Introduction

THE geochemistry of carbon is such that this element is largely concentrated in sedimentary rocks, where it may be found as a carbonate, a hydrocarbon, or as graphite. Carbonates (principally calcite, dolomite, and siderite) may be encountered in any sedimentary rock as minor components, and in such common rocks as limestone and dolomite they are the principal mineral. Hydrocarbons and graphite are present in many sediments as a result of the incorporation of vegetable and animal matter. Different source materials and different degrees of decomposition produce a wide variety of different compounds from this organic matter. Sedimentary rocks may be expected to contain carbonaceous material in amounts ranging from nil to greater than 90% for rocks such as coal.

The carbon content of a sedimentary rock and the distribution of this content between calcareous and carbonaceous compounds is a useful criterion in studies concerned with the geochemistry of sediments. Rapid determination of carbon by spectrographic means should be of value in such studies.

The presence of carbon in sedimentary rocks poses two problems to the spectrographer. Firstly, it should be included in the total analysis of a rock, especially if it is present in appreciable quantity; and secondly, the presence of carbonates in a sample may markedly affect the line intensities of other elements [1 (p. 115), 3] and a simple d.c.-arc technique for the determination of carbon in its various forms should thus serve as both a direct measurement of this element and as an indicator for the carbonate variations in the matrix.

Previous work

Spectrographic determination of carbon, using a spark source, is commonly employed for metallurgical samples, especially steels. However, there appears to be

no published information dealing with either d.c. arc techniques for the determination of carbon or with the spectrochemical determination of carbon in rocks.

Spectrographic considerations

The determination of carbon, using direct-current arc excitation, has probably not been considered because of the difficulty of exciting usable carbon lines and the impracticality of making electrodes of sufficiently high ionization potential. Both of these difficulties may be overcome by using copper electrodes and utilizing a cyanogen bandhead as the analysis line.

The cyanogen violet system, with principal bandheads at 3590, 3883, and 4216 Å is the most sensitive of the various cyanogen systems. In turn, CN 3883 Å is the most sensitive bandhead of this system and was, therefore, chosen as the analysis head. The excitation potential for the cyanogen violet system is ~3·2 eV. This is sufficiently below that of copper, whose minimum excitation (resonance) potential is 3·77 eV to ensure the excitation of cyanogen in a copper arc. The most intense cyanogen production was found experimentally to be obtained at higher amperages with cathode excitation, as shown in Table 1. Currents in excess of 6 A could not be used because the electrodes melt.

Table 1. Excitation conditions and cyanogen intensity

Amperage	Polarity of sample electrode	Relative intensity of CN 3883 Å
3	anode	2·6
3	cathode	3·4
6	anode	7·3
6	cathode	13·1

The complex process whereby cyanogen is formed and excited in the arc is subject to numerous variables which affect the relative intensity of the cyanogen bands arising from a given amount of carbon in the sample. The principal variables to be considered are the widely different carbon-bond strengths, the effect of excitation changes, and the control of arc temperatures by extraneous elements. These factors will all affect the rate and completeness of evolution of carbon or carbon-containing compounds from the sample.

Studies of various carbon compounds show that a large change in relative intensity accompanies changes in the nature of the carbon compound. Various carbon-containing substances were diluted with quartz in such proportions as to produce mixtures containing 10% carbon by weight. These mixtures were arced at 3 and 6 A, following the procedure later described. Relative intensities were determined from the plates and adjusted to a relative intensity of 100 for the most intense sample. The data in Table 2 show that a five- or sixfold intensity difference may be found at constant carbon content. Such large variations in relative intensity with constitution emphasize the necessity of using only standards which are very similar in nature to the material under analysis.

VOL. 9 1957

Table 2. Change in CN 3883 Å intensity with sample type and amperage

3-A cathode	Relative intensity	6-A cathode	Relative intensity
Sucrose	100	Graphitic carbon	100
Calcite	70	Calcite	85
Graphitic carbon	49	Anthracite coal	54
Anthracite coal	36	Sucrose	27
Oxalic acid	21	Silicon carbide	20
Silicon carbide	20	Oxalic acid	16

The effect of the matrix upon cyanogen intensity is further complicated by the sensitivity of different compounds to different excitation conditions, as shown by Table 2. The compounds in the table are listed in the order of decreasing cyanogen intensities at constant carbon content.

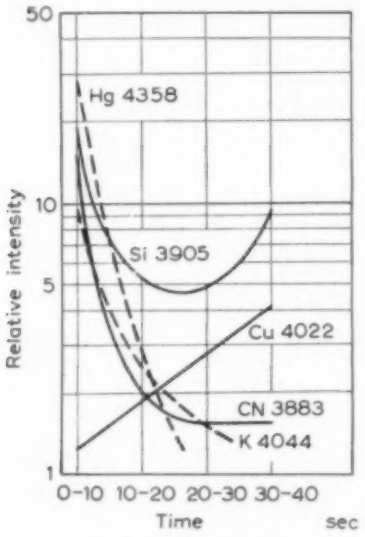

Fig. 1. Volatilization curves
(Cathode excitation, 6-A d.c. arc)
1 part SiO_2 added.

Time studies of volatilization (Fig. 1) showed that cyanogen production occurs very early in the arcing period, presumably through rapid evolution of carbon dioxide from the sample. Fig. 1 also showed a close parallelism between the volatilization curves of elements such as potassium and mercury and the appearance of CN in the arc column. Since high arc temperatures favour CN emission [1 (p.147)]. The temperature-depressant effect of these elements may in part account for observed matrix effects.

Anomalous intensity-concentration relations were found when comparisons of

silica-free and silica-bearing carbonate rocks were made. The presence of silica greatly enhances the relative intensity of CN 3883 Å, as shown in Table 3. The most likely reason for this enhancement appears to be the efficacy of reactions of the type $CaCO_3 + SiO_2 \rightarrow CaSiO_3 + CO_2$ in accelerating decomposition of carbonates in the hot electrode. The addition of one part of quartz (SiO_2) by volume to samples returns the relative intensities to their proper order.

The sensitivity of CN 3883 Å may be increased somewhat by arcing in a nitrogen atmosphere. Approximately a twofold increase in relative intensity may be obtained, depending upon the N_2 flow-rate. Arcing, however, tends to be erratic and the increased sensitivity does not warrant the loss of reproducibility.

Spectrographic techniques

A large Littrow-mounted Hilger glass-quartz spectrograph was used for all determinations. A dispersion of 7 Å/mm was provided at 3883 Å with glass optics. Photometry was done using a Jarrell-Ash JA-200 densitometer-comparator. The

Table 3. The effect of silica on CN 3883 Å intensities

Sample	% CO_2	% SiO_2	Relative intensity of CN 3883 Å with no quartz added	Relative intensity of CN 3883 Å with no quartz added
Bureau of Standards sample No. 88 dolomite	47·25	0·31	11·2	17·8
Bureau of Standards Sample No. 1a siliceous limestone	33·53	14·11	25·4	14·7

shape of the CN 3883 Å bandhead was carefully determined prior to its measurement and was found to be satisfactory, although asymmetric. No isotopic effects were noted. The rotating-sector method was used for plate calibration, each plate being individually calibrated. Curves of log per cent transmission versus log relative intensity were used for calibration. Corrections for background were made for all lines measured. Kodak type 103-0 spectroscopic plates were used and were developed for 4½ min at 18°C using Kodak D-19 developer.

The electrodes used were cut from commercial copper rod of 3-mm diameter. A cone-shaped cavity with an apex angle of 82° cut on a lathe accommodated the samples. Samples were tightly packed into this cavity, but not weighed. Counter-electrodes were made from commercial copper rod of 1·5-mm diameter.

The arc was imaged on the slit for reasons of increased spectral sensitivity. A plot of a typical pole to pole intensity distribution for CN 3883 Å is given in Fig. 2.

Time studies of volatilization (Fig. 1) showed that cyanogen production was always completed within 30 sec when the sample was excited as the cathode at 6 A

VOL. 9 1957

and 50 V. The exposure time was thus taken as 30 sec for all samples. Sectoring with aperture ratios of 1 : 1, 1 : 2, and 1 : 4 provided a sufficient latitude for densitometry at this exposure.

Operational procedures

The principal forms in which carbon is found in sedimentary rocks are as graphite, as carbonates, and as organic material of diverse nature. The determination of the latter is outside the limits of the present work because the unknown nature of this material makes standardization impossible. Organic material is, therefore, reported only as "equivalent graphite."

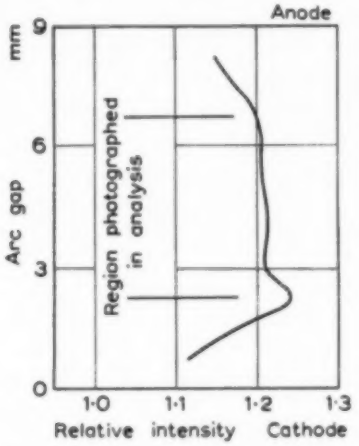

Fig. 2. Pole to pole intensity distribution for CN 3883 Å.

Determination of carbonate carbon and "equivalent graphite" carbon in the same sample requires a two-stage analytical procedure. Samples for analysis are ground to −100 mesh and dried at 110°C. The sample is then divided into two parts. The first part receives no further treatment other than the addition of one part of quartz. The second part is weighed and then treated with warm 1 N HCl to eliminate CO_2. The solution is filtered and the residue dried and weighed. Finally, one part of quartz is added to this residue.

Arcing untreated samples provides a CN 3883 Å intensity representing the total carbon content. Arcing the residue from HCl treatment gives that portion of the total intensity which is attributable to "equivalent graphite" when appropriate corrections are made. The difference is then due to carbon evolved as CO_2.

The corrections which must be applied are those for enrichment of the sample in "equivalent graphite" as a result of chemical treatment, a gravimetric factor to compensate for scale changes from CO_2 to C, and a factor to correct for matrix differences. The first correction is computed from the difference in treated and untreated sample weights. The second factor is 12/44 = 0·273. The third factor is obtained from matrix variation studies (Table 2) and is here taken as 0·85.

Calculations for the relative intensity due to $CO_2(I_{CO_2})$ and "equivalent

graphite" (I_G) may be made by using the following formulae:

$$I_{CO_2} = I_{total} - I_{residue} \times \frac{\text{weight residue}}{\text{weight sample}} \times 0{\cdot}273 \times 0{\cdot}85$$

$$I_G = I_{residue} \times \frac{\text{weight residue}}{\text{weight sample}}$$

I_{total} and $I_{residue}$ are the experimental values obtained by measurement of the CN 3883 Å bandhead, I_{CO_2} and I_G are calculated from these values as shown, and % graphitic C and % CO_2 are then obtained from the analytical curves. A sample calculation is outlined below:

CN 3883 intensity of untreated sample, $I_{tot} = 6{\cdot}00$
CN 3883 intensity of treated sample, $I_{res} = 5{\cdot}00$

$$\frac{\text{weight of residue}}{\text{weight of sample}} = \frac{0{\cdot}80}{1{\cdot}00} = 0{\cdot}80$$

$$I_{CO_2} = 6{\cdot}00 - (5{\cdot}00 \times 0{\cdot}80 \times 0{\cdot}27 \times 0{\cdot}85) = 5{\cdot}08$$
$$I_G = 5{\cdot}00 \times 0{\cdot}80 = 4{\cdot}00$$

From the analytical curves,
% $CO_2 = 8{\cdot}2\%$
% equivalent graphite $= 0{\cdot}79\%$

Standards for the determination of graphitic carbon were made by mixing pure carbon powder (from electrode cutting) with pure quartz. Standards for CO_2 were appropriate Bureau of Standards material (NBS-88 and NBS-1a), various sedimentary rocks in which the CO_2 content had been chemically determined, and mixtures of reagent grade $CaCO_3$ with quartz. All standards and samples were diluted with one part of quartz by volume before arcing. Normal precautions to prevent contamination were observed in all preparations.

Chemical determinations of CO_2 were carried out on occasional samples for control purposes. Standard solutions of ~1 N HCl and NaOH were first prepared. The HCl solution was then standardized with C.P. $CaCO_3$ in the following way: ~1-g samples of $CaCO_3$ were dried at 110°C, cooled, and weighed. Samples were then placed in a beaker, an excess of HCl was added, and the solution warmed on a hot plate to drive off CO_2. On cooling to room temperature, the excess HCl was titrated with NaOH to the methyl orange end-point. The normality of the acid was then calculated.

Unknown samples were treated by approximately the same method, except that because of the dark colour of undissolved sediments in the solution, methyl orange could not be used directly. Instead, a standard solution was prepared by titrating HCl with NaOH to the methyl orange end-point. This solution was then used in conjunction with a pH meter to obtain the end-point in the titration of the unknowns. The procedure followed was simply to record the reading of the pH meter in the standard solution and then titrate the unknown until the same reading was obtained.

The precision of this simple technique was very satisfactory for samples containing more than 3% CO_2. Comparisons of accuracy are shown as part of Table 5.

Analytical curves

Analytical curves of log relative intensity CN 3883 Å versus log per cent carbon or CO_2 are constructed as shown in Fig. 3. Inasmuch as differences in the matrix

VOL. 9 1957

do not change the slope of the analytical curves for graphitic carbon and carbon in carbonates, the same analytical curve with different abscissae may be used for these constituents. The analysis range for graphitic carbon is from about 0·1% to 50% and for CO_2 is from about 0·5% to 50%. The precision with which low-carbon

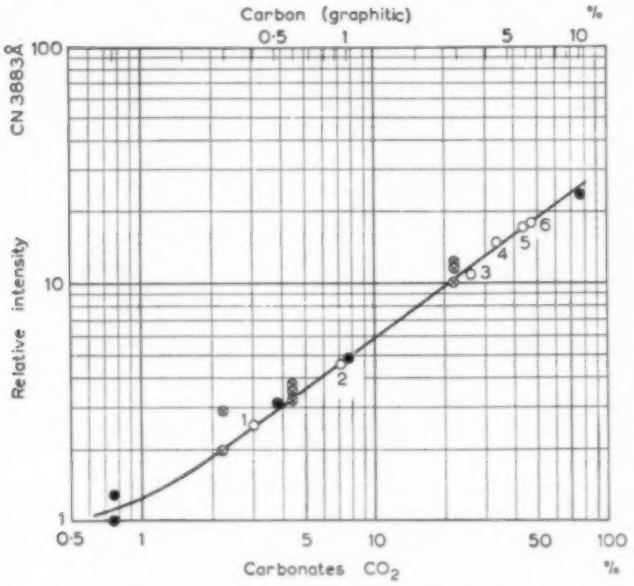

Fig. 3. Analytical curve for graphitic carbon and CO_2.
Samples
● Graphite-quartz mixtures.
⊠ $CaCO_3$-quartz mixtures.
1 Spraberry formation (sandstone).
2 Paleozoic shale composite.
3 Spraberry formation (dolomite).
4 NBS-1a, argillaceous limestone.
5 Calcite.
6 NBS-88, dolomite.

contents may be determined is somewhat decreased by the presence of small amounts of carbon dioxide in the atmosphere and adsorbed on the electrodes, samples, and quartz diluent. Corrections for this CO_2 are made by subtraction of the CN 3883 Å intensity obtained by arcing a blank, but are not entirely satisfactory.

In practice, several standards are run on each plate, and correlation of relative intensity data from plate to plate is accomplished by having at least one standard common to each plate.

Precision and accuracy

The coefficient of variation of this method as determined by replicate determinations is 13·0%. The distribution of the coefficient of variation for about thirty replicate analyses ($n = 3$ to 16) made over a two-year period on various materials was also determined. The mode of the curve so plotted is 12·9%.

Samples are commonly run in triplicate, and the expectable coefficient of variation for the average of three determinations is thus $13/\sqrt{3} = 7{\cdot}5\%$.

The accuracy of the chemical and spectrochemical methods used was investigated by comparison of results with known or chemically analysed standards. Typical results are shown in Tables 4 and 5.

Table 4. Comparison of analyses for equivalent graphite

Sample	Bureau of Standards	Cabot Laboratory spectrochemical
NBS-88 dolomite	0·08%	0·1%
NBS-1a argillaceous limestone	0·61	0·59 0·63 0·37

Table 5. Comparison of analyses for CO_2

Sample	Bureau of Standards	Cabot Laboratory chemical	Cabot Laboratory spectrochemical
NBS-1a argillaceous limestone	33·53%	34·15% 34·10%	35% 34
NBS-88 dolomite	47·25	47·77 47·52	46
APSC Paleozoic shale composite	—	7·28 6·96	7
Sl–1 Spraberry formation (sandstone)	—	2·99	3·1
Sl–2 Spraberry formation (sandstone)	—	2·27	3
Sl–6 Spraberry formation (dolomite)	—	26·28	29

Determination of nitrogen

The general approach to the determination of carbon in geological materials herein described would appear favourable for the determination of nitrogen. Samples excited in carbon electrodes in a nitrogen-free atmosphere should produce cyanogen-band spectra whose relative intensity is a measure of the nitrogen content of the sample.

VOL. 9 1957

Acknowledgements—This investigation was carried out as a part of a geochemical study of sedimentary rocks financed by a grant from the National Research Foundation. The author wishes to express his appreciation for the preparations and measurements made by Mr. F. M. WORSH and for the CO_2 determinations made by Mr. W. L. MCINTIRE.

References

[1] AHRENS L. H. *Spectrochemical Analysis* Addison-Wesley Press 1950.
[2] PEARSE R. W. B. and GAYDON A. G. *The Identification of Molecular Spectra* 2nd ed. Wiley 1950.
[3] SCOTT R. O. *J. Soc. Chem. Ind.* **64** 1945.

OL.
9
57

Spectrochimica Acta, 1957, Vol. 9, pp. 98 to 100. Pergamon Press Ltd., London

SPECTROCHEMICAL NOTE

Electronic spectrum and apparent thermochromism of $VOCL_3$

FOIL A. MILLER and WILLIAM B. WHITE
Department of Research in Chemical Physics, Mellon Institute, Pittsburgh 13, Pa.

(*Received* 15 *October* 1956; *accepted for publication* 29 *November* 1956)

Abstract—The electronic absorption spectrum of $VOCl_3$ vapour is reported, with bands at 2440 and 3330 Å. No fine structure is found with moderately high resolution. Unusual precautions are needed to avoid hydrolysis. A striking apparent thermochromism in the liquid state was found to be due to the presence of impurities.

THE vibrational spectrum of vanadium oxytrichloride has been reported [1, 2], but not its electronic spectrum. $VOCl_3$ is a clear yellow liquid which reacts avidly with water to give bright red products. This makes it extremely difficult to obtain a true spectrum, and can easily lead to false effects. An example of this is an apparent thermochromism. When a Raman tube was filled with $VOCl_3$ by vacuum transfer (after first purging the all-glass system with $SiCl_2(CH_3)_2$ to remove adsorbed water) [2], it was observed that the portion of the liquid immersed in the cold bath at −70°C had become bright red. When the liquid warmed up it returned to its normal yellow hue. This striking colour change could be repeated indefinitely. It appeared to be unique because it occurred in the liquid state, because it seemed to be due to a simple molecule, and because the colour deepened on cooling.

To our chagrin, it was later found that a very careful three-stage bulb-to-bulb distillation *in vacuo* removed the thermochromism almost completely, thus indicating that it was due to an impurity. Our present belief is that small traces of water, or perhaps even hydroxyl groups, on the glass walls will react with $VOCl_3$. The products probably have varying compositions intermediate between $VOCl_3$ and V_2O_5, and are soluble in excess $VOCl_3$. We believe that this material is in some way responsible for the thermochromism.

In view of this, it appeared that it would indeed be difficult to obtain an accurate solution spectrum in the visible and ultra-violet, because it would be almost impossible to get a solvent sufficiently free of water. It was therefore decided to obtain the electronic spectrum in the gas phase. In the first attempt, a 1-cm fused quartz cell was evacuated with a diffusion pump, purged with $SiCl_2(CH_3)_2$ vapour, re-evacuated, and filled with $VOCl_3$ vapour. Even with this treatment there was enough hydrolysis on the cell windows to form a very thin film, visible by interference colours, which absorbed completely below 3700 Å (absorbance >3). This was finally avoided by evacuating to less than 5×10^{-5} mm Hg while heating the cell almost to redness. After cooling, the cell was sealed off with a small amount of $VOCl_3$ in a side reservoir. When the vapour was allowed to diffuse into the cell, with the liquid held at 0°C, a good spectrum was obtained. From the vapour-pressure data of KOMANDIN and VLODAVETS [3] the vapour pressure in the cell was 4·6 mm Hg. The spectrum was scanned from 2200–4000 Å with a Cary model-11 spectrophotometer, and then a base line was obtained by freezing the $VOCl_3$ in liquid N_2. The resulting spectrum is shown in Fig. 1. Band peaks are at 2440 and 3330 Å.

VOL. 9 1957

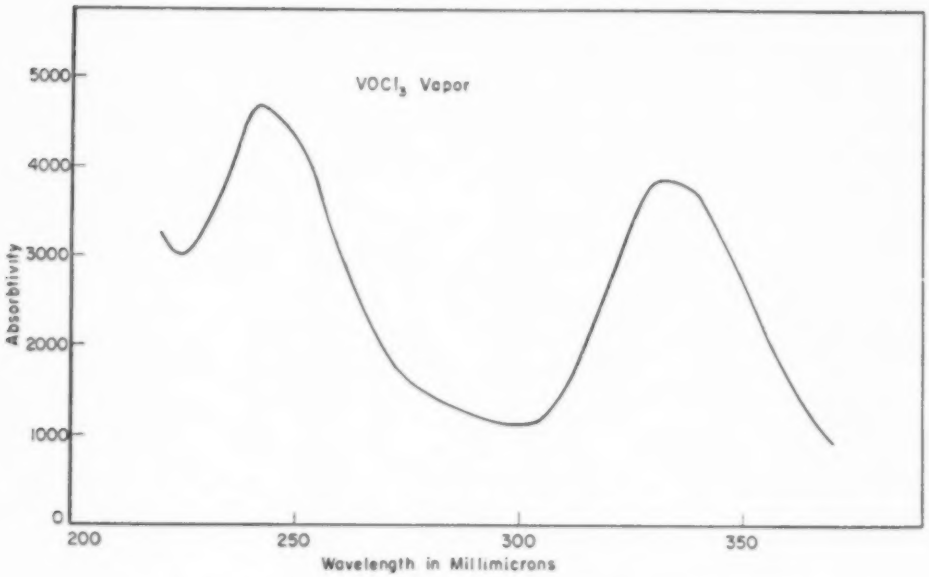

Fig. 1. Ultra-violet spectrum of $VOCl_3$ vapour. Absorptivity [$= (1/bc) \log I_0/I$] is in units of litres/mole cm.

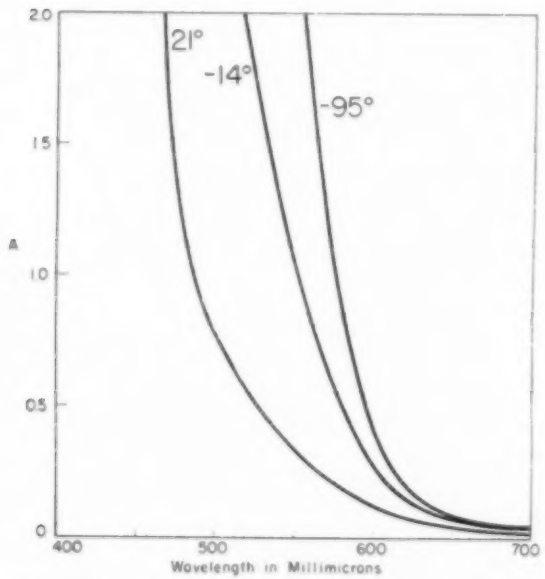

Fig. 2. Temperature dependence of $VOCl_3$ spectrum (CH_2Cl_2 solution of unknown concentration). $A = \log I_0/I$.

The same cell was used with an ARL 2-m grating spectrograph to look for vibrational fine structure in the gas spectrum under higher dispersion. None was found; the absorption appears to be truly continuous.

The reason for the thermochromism interested us, and to study it further, solutions of $VOCl_3$ in methylene chloride were prepared under dry nitrogen. These solutions were orange, indicating some hydrolysis, and were also thermochromic. They were scanned at various temperatures from 25° to −80°C. The temperature-dependent spectra (Fig. 2) showed that the visible colour change is due to a shift in the tail-off of a strong absorption which extends from the ultra-violet into the visible region. The spectrum of more dilute solutions showed that there were not distinct bands in the ultra-violet (4000–2200 Å), but only an absorption continuously increasing toward shorter wavelengths, with ill-defined shoulders at 3300, 2650, and 2390 Å.

There are several possible causes for the thermochromism, among which are: (1) a temperature-sensitive chemical equilibrium, (2) an altered population of the vibrational levels, and operation of the Frank-Condon principle, and (3) thermal transfer to a low-lying electronic state [4]. The last seems to be eliminated by the absence of a markedly temperature-dependent band. Unfortunately, the absorbing entity is not known, and may well be a mixture of several partially-hydrolysed products. It did not appear to be feasible to make Beer's law measurements, because dilution with even the most carefully dried solvent would almost certainly cause additional hydrolysis. It was therefore not possible to decide between the first two causes.

References

[1] Eichhoff H. J. and Weigel F. *Z. Anorg. Chem.* 1954 **275** 267.
[2] Miller F. A. and Cousins L. R. *J. Chem. Phys.* (in press).
[3] Komandin A. V. and Vlodavets M. L. *Zh. Fiz. Khim.* 1952 **26** 1291.
[4] Grubb W. T. and Kistiakowsky G. B. *J. Amer. Chem. Soc.* 1950 **72** 419.

VOL. 9 1957

Spectrochimica Acta, 1957, Vol. 9, pp. 101 to 103. Pergamon Press Ltd., London

MEETINGS

VI Colloquium Spectroscopicum Internationale

DISCUSSIONS on the future policy and international status of the Colloquium were held on Wednesday 16 May 1956 in Amsterdam.

There were present: KETELAAR (Netherlands), VAN SOMEREN (Britain), DUYCKAERTS (Belgium), LOPEZ DE AZCONA (Spain), MICHEL (France), LOEUILLE (France), Mme. FISCHGRUND (France), ROSBAUD (*Spectrochimica Acta*), SMITH, (Britain) MILBOURN (Britain), MECKE (Germany), KAISER (Germany), VAN CALKER (Germany), GUYER (Switzerland), KVALHEIM (Norway), ROSENBAUM (United States of America), MASI (Italy), MILAZZO (Italy), SVEJDA (Austria), KLINKENBERG (Netherlands), MENZIES (Britain), DIEKE (United States of America), CARLSSON (Sweden), GERDING, DEINUM, ADDINK, FREESE, and VAN TONGEREN (Netherlands).

The following decisions were reached:

(a) That the Belgian invitation for the seventh Colloquium to be held in Liège in 1958 should be accepted.
(b) That two-year intervals between successive Colloquia are desirable.
(c) That both emission and absorption methods belong to the field of the Colloquium (pt. 3).
(d) That it appeared desirable to have the Colloquia alternating with the meetings of the European Molecular Spectroscopy (pt. 4).
(e) That the policy of delegating Colloquia to committees appointed by national organizations should be continued.
(f) That the administrative basis ("member"-administration) should be handed over from committee to committee and no vacuum should exist between successive committees.
(g) It was decided to request that the interests of analytical (industrial) spectroscopy should be guarded by the Commission on Optical Data (chairman: Prof. DUYCKAERTS) and that co-ordination between the activities of the various groups in the domain of applied spectroscopy be also promoted by this Commission.
(h) That publication of reports as supplements to *Spectrochimica Acta* is desirable.
(i) That the limitation of the variety of subjects to be treated in any Colloquium should be left to the discretion of the proper committee.

W. VAN TONGEREN (chairman)

VII Colloquium Spectroscopicum Internationale

THE VII Colloquium Spectroscopicum Internationale will meet at Liège in September 1958:

The provisional committee consists of:

Prof. L. D'OR, président
Prof. P. COHEUR
Prof. V. DESREUX
Prof. P. SWINGS
Prof. G. DUYCKAERTS, secrétaire

The address of the administrative secretary is as follows:

VII Colloquium Spectroscopicum Internationale,
Association des Ingénieurs de Liège (A.I.L.g)
22, Rue Forgeur,
Liège, Belgique.

Scientists interested in communications concerning this and future colloquia are urgently requested to notify changes of address and possible errors in addresses of the memberlist of the VIth Colloquium to the above mentioned secretariat.

Commission on Molecular Spectroscopy

under the auspices of the International Union of Pure and Applied Chemistry

At its Zurich meeting, July 1955, the Executive Committee of the I.U.P.A.C. established a Commission on Molecular Spectroscopy under the section of Physical Chemistry, to which the following have now been appointed:

Titular members. H. W. Thompson (England, President), B. L. Crawford (U.S.A., Secretary), G. Duyckaerts (Belgium), J. A. Ketelaar (Holland), J. Lecomte (France), R. C. Lord (U.S.A.), A. Mangini (Italy), R. Mecke (Germany), S. Mizushima (Japan).

Delegate members. R. R. Brattain (U.S.A.), R. N. Jones (Canada).

G. Herzberg (Canada) has been appointed as an advisory counsellor, and to act as a liaison with the Joint Spectroscopy Commission of the I.U.P.A.C. and I.A.U. Co-ordination with the Commission on Optical Data will be ensured through G. Duyckaerts. It is hoped that a representative from the U.S.S.R. will also be appointed as titular member.

The Commission met formally at Columbus, Ohio, in June 1956, and an informal discussion among European members was held in Paris in November 1956.

It was agreed:

(1) To support fully the recommendation by the Joint Spectroscopy Commission that steps should be taken to re-introduce the symbol Å to represent the Ångström unit (wavelength) in the scientific literature;

(2) That on the question of the symbols K (Kayser) for cm^{-1} and σ (sigma) for wave number, previously recommended by the Joint Spectroscopy Commission and already to some extent in use, the Commission welcomed the decision of the Joint Spectroscopy Commission to withdraw its previous recommendations, feeling that this course would more correctly express the views of the vast majority of chemical spectroscopists;

(3) That the recent report of R. S. Mulliken on spectroscopic nomenclature and notation should be recommended for general use, and extensions prepared where appropriate.

The Commission examined schemes operating in different countries for the documentation of molecular spectra, and especially, in the first instance, for infra-red data. It was agreed that, at present, two types of card are desirable,

VOL. 9 1957

namely the I.B.M. type as supplied by the American Society for Testing Materials (A.S.T.M.), and the Keysort type being prepared by the Anglo-German Documentation of Molecular Spectra (D.M.S.) organization and by Dr. CREITZ under a Committee of the American National Research Council operated at the National Bureau of Standards, Washington (Dr. W. BRODE, Chairman). These two types of cards provide different information and fit the needs of different laboratories. It was felt desirable to aim at a co-ordination of the several schemes internationally, and in view of the more exhaustive coding adopted by the D.M.S. system this might form a basis for the Keysort-type cards. It was suggested that enquiries should be made to this effect.

Preliminary consideration was also given to a corresponding documentation of ultra-violet data, to the better co-ordination of spectroscopic symposia, and to the compilation of nuclear magnetic resonance data.

The next formal meeting of the Commission will be held in Paris during the I.U.P.A.C. Congress in July 1957. Among other matters which will be discussed are: (1) desirable extensions, if any, to the Mulliken report on notation, (2) a review and possible documentation of biological applications of infra-red spectroscopy, (3) the establishment of agreed wavelength calibration standards in the infra-red region, (4) the standardization of infra-red spectrometers as regards resolving power, effective slit-width, and intensity data.

The Commission would welcome suggestions from pure or applied spectroscopists of matters which appear to require international consideration and agreement. These should be sent as soon as possible to Dr. H. W. THOMPSON, St. John's College, Oxford, England, or to Professor B. L. CRAWFORD, Department of Chemistry, University of Minnesota, Minneapolis, U.S.A.

OL.
9
57

European Molecular Spectroscopy Group

THE next meeting of the above group will be held at the University of Freiburg, Germany, from July 9 till 13 1957. A wide range of subjects in infra-red and ultra-violet spectroscopy will be discussed, and microwave spectroscopy and nuclear magnetic resonance will also be included.

Information about the meeting can be obtained from Professor R. MECKE, Institut für physikalische Chemie, Hebelstrasse, Freiburg-i-Br., Germany.

Fourth Ottawa Symposium on Applied Spectroscopy

THE fourth Ottawa Symposium of the Canadian Association for Applied Spectroscopy is to be held at the Victoria Museum, Ottawa, on 11, 12, 13 September 1957.

Papers are invited for presentation on the subjects of applied spectroscopy and closely related fields of instrumental analysis.

Titles and brief extracts of papers should be submitted before 15 June 1957 to J. H. D. HOWARTH, Canada Metal Company, Limited, 721 Eastern Avenue, Toronto, Ontario, Canada.

Book review

GAUSTAV KORTÜM: **Colorimetry, Photometry, and Spectrometry** (an introduction to the measurement of absorbed bed, emitted, fluorescence, turbidity, scattered and reflected radiation); third revised edition, Springer, Berlin-Gottingen-Heidelberg. 1955. 458 pp. and 186 diagrams. 63s. (D.M. 36).

THIS book does not deal directly with spectrochemical analysis itself, but is valuable as a handbook of all the associated techniques of radiation measurement. It begins with a discussion of the basic laws of the absorption of radiation by matter, and then sources of radiation and methods of detection are discussed in principle. More detailed chapters follow, dealing with visual methods, photoelectric methods, thermoelectric and photographic detectors. A short section on the technique of Raman spectroscopy is included. The final chapter deals with a few selected examples of the chemical applications of some of the techniques described. The author claims that each method is described with sufficient attention to first principles to offer the physicist guidance as to which light-measuring technique should be employed in any particular case. Nevertheless, modern work on the analogy between communication channels and optical devices are not mentioned, so that the contribution which information theory can make to determining criteria of efficiency in an optical system is not discussed.

ERNEST VAN SOMEREN

VOL.
9
1957

Spectrochimica Acta, 1957, Vol. 9, pp. 105 to 112. Pergamon Press Ltd., London

Fluorescence emission spectra, fluorescence excitation spectra, and absorption spectra of some metal chelates

CHARLES E. WHITE, DONALD E. HOFFMAN,* and JOHN S. MAGEE JR.
Department of Chemistry, University of Maryland, College Park, Maryland

(*Received* 31 *July* 1956; *accepted for publication* 17 *December* 1956)

Abstract—The fluorescence emission spectra, the fluorescence excitation spectra, and the absorption spectra for the chelates of aluminium-morin, aluminium-Pontachrome-Blue-Black R, aluminium-Acid Alizarin Garnet R, beryllium-morin, beryllium-1-4-dihydroxyanthraquinone, beryllium-1-amino-4-hydroxyanthraquinone, thorium-1-amino-4-hydroxyanthraquinone, zirconium-flavonol, boron-benzoin, and lithium-8-quinolinol have been determined. The fluorescence spectrum band overlaps the longest wavelength absorption band. The wavelength for maximum excitation generally coincides with the wavelength of the absorption band nearest the fluorescence band.

Introduction

OVER a period of years one of the authors and other investigators have reported a number of fluorescence reagents for several elements. In most of these cases the fluorescence spectra were determined with a visual three-arm Bunsen spectroscope. This method was adequate to define the spectral limits of the colour of the fluorescence and for the selection of a filter. With new equipment available, we have now determined these values more accurately. Excitation-spectra and emission-spectra data are of considerable importance in the analytical application of these chelates. The chelates included in this study and references to the original papers which give details of the analytical methods are as follows: aluminium-morin (3,5,7,2′,4′-pentahydroxyflavone [12], aluminium-Pontachrome-Blue-Black R (2,2′-dihydroxy-1,1′-azonaphthalene-3-sulphonic acid, sodium salt)[10], aluminium-Acid Alizarin Garnet R (2,4,2′-trihydroxyazobenzene-5′sulphonic acid) [8, 9], beryllium-morin [7], beryllium-1,4-dihydroxyanthraquinone [4], beryllium-1-amino-4-hydroxyanthraquinone [13], thorium-1-amino-4-hydroxyanthraquinone [13], zirconium-flavonol [1, 3], boron-benzoin [15, 16], lithium-oxine (8-quinolinol) [14].

Experimental

Apparatus. The fluorometer [11] used was constructed in this laboratory and consisted of a sample holder, a 1P21 or a 1P28 photomultiplier tube (Radio Corporation of America) attached to a sensitive microammeter (Radio Corporation of America WV 84A) and a power source for the photomultiplier tube. The light source for the excitation spectra was a xenon arc. This was chosen because of its reasonably constant intensity over a wide range of the spectrum. The light from the xenon arc passed through a Bausch and Lomb grating monochromator No. 33-86-40-01. This instrument has a dispersion of 6·6 mμ/mm in the first order. Mercury-vapour lamps were used to irradiate the solutions for fluorescence spectra measurements because they are more convenient than the xenon arc and produce a more intense radiation at 253 and 365 mμ.

A Beckmann DU spectrophotometer equipped with a photomultiplier tube was used to measure the absorption spectra.

* Present address: University of Delaware, Newark, Delaware.

Reagents. Metallic salts used were all of reagent quality. Morin was the purified quality of Schuchardt (Munich, Germany). 1-Amino-4-hydroxyanthraquinone was a National Aniline product. 1,4-Dihydroxyanthraquinone was obtained from the Eastman Kodak Co. and recrystallized from acetone. Flavonol was prepared in the University of Maryland laboratories. Benzoin and 8-quinolinol were obtained from the Eastman Kodak Company. Pontachrome-Blue-Black R (PBBR) and Acid Alizarin Garnet R (AAGR) were recrystallized from E. I. DuPont de Nemours and Co. samples.

Absorption spectra. The absorption spectra of the metallic chelates were determined at a concentration of the organic reagent, as indicated in the titles of the figures. The metal-ion concentration was adjusted to three moles of metal to one of dye. The slit-width was varied usually from 0·1 to 0·2 mm. In most of the cases considered in this article the chelate complex is represented by a 1 : 1 dye-to-metal ratio [5]. For the absorption spectra and excitation spectra an excess of the metal was chosen so as to insure reasonably complete chelation of the organic reagent. If the above concentration was too small to show absorption in the desired range, a more concentrated solution was used.

Fluorescence spectra. The fluorescence spectrum represents the relative intensity of the fluorescent light over the range of 300 to 650 mμ. In the determination of the fluorescence spectra, the Bausch and Lomb monochromator was used in conjunction with the fluorometer. The fluorescent solution, in an optical glass cell, was placed at the entrance slit of the monochromator and irradiated from above with a high-pressure mercury-vapour lamp (G.E. H100B4). The envelope of this lamp is a blue filter which transmits chiefly a radiation at 365 mμ. The phototube of the fluorometer was placed at the exit slit of the monochromator. Readings were recorded generally from 350 to 650 mμ and were corrected for a blank sample and for the published response of the phototube. The latter was done as follows: If the phototube was rated at 100 for 540 mμ and 90 for 520 mμ, the reading at 520 was divided by 0·9 to obtain the value plotted on the graph. The limitations of this procedure are recognized, and the results were checked with two phototubes and also with spectroscopic observations. Readings were not taken beyond 650 mμ, because above this wavelength the correction on the phototube was so great that the significance of the values was doubtful. Some peaks were noted in readings for the fluorescent solution and not in the readings for the blank at the position of strong mercury lines. In such cases these peaks were not plotted on the curves. With some samples a short-wavelength mercury-vapour lamp equipped with a filter to transmit the 253-mμ region of the spectrum was used for irradiation and the emission spectra were examined from 300 to 650 mμ. A significant fluorescence in the ultra-violet region was not detected in any of the samples. No corrections were made for variations in intensity caused by the blaze of the grating. However, the peaks on all of the fluorescent spectra checked with those obtained on the spectroscope, and a number of the samples were run on the double-grating spectrofluorometer recently developed by the American Instrument Company [2]. The maxima points from this latter instrument on both fluorescent and excitation spectra coincided with the ones reported here. The solutions used in the determination of the fluorescence spectra were chosen at a concentration which produced a strong fluorescence.

Fluorescence excitation spectra. The excitation spectrum is represented by a plot of the exciting wavelength against the intensity of the fluorescent light. These values were determined with the combination of the Bausch and Lomb monochromator and the fluorometer. The xenon lamp was placed at the entrance slit of the monochromator and the fluorometer at the exit slit. The solution was placed in a quartz test-tube in the fluorometer and was irradiated from the monochromator. A filter was placed in front of the phototube to transmit the fluorescent light and absorb any reflected ultra-violet radiation. The filter used for this purpose was Corning No. 3060 with the following exceptions: For the compounds in Figs. 2, 6, and 7, Corning filter No.3480, and in Fig. 5 Corning filter No. 3384 were used. The phototube was at a right-angle to the incident beam. The fluorescence intensity was read on the microammeter, while the wavelength drum was rotated. These readings were corrected for the variation in intensity of the xenon lamp so that the curves represent a relatively constant intensity at each wavelength. This correction for the xenon lamp was made from a curve where adjusted microphotometer readings were plotted versus wavelengths. In this case the microphotometer readings were adjusted for the phototube response, as indicated above. The monochromator slit in these experiments was

VOL. 9 1957

generally set at 3 mm which produced about a 20-mμ band. In some cases where the fluorescence was intense, this was reduced to 1 mm, but this variation in slit-width did not seem to alter the position of the peaks of the curves. The excitation curves labelled as *B* in the figures are not continued into the region of the fluorescence emission, because beyond this point the readings have no meaning. Both the reflected incident light and the fluorescent light are transmitted by the filter when these two curves converge.

Discussion

A summation of the data taken in the course of the experiments is given in the figures and in Table 1. The absorption, emission, and excitation curves were plotted independently, and no quantitative relationship can be presumed from the vertical

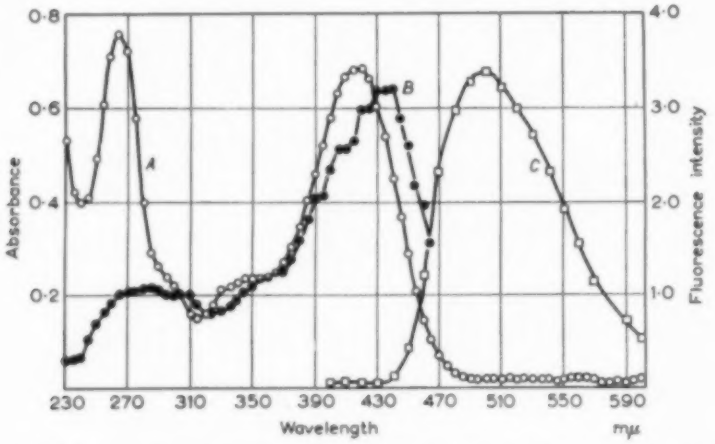

Fig. 1. Aluminium-morin: absorption spectrum, conc. 0·001% (A), fluorescence excitation spectrum (B), fluorescence emission spectrum (C).

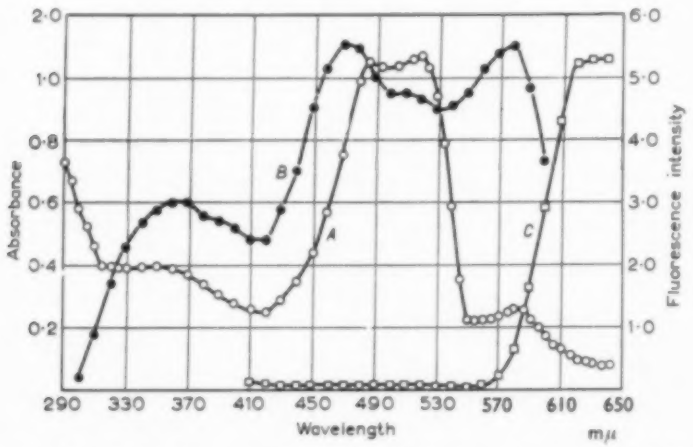

Fig. 2. Aluminium-Pontachrome-Blue-Black R: absorption spectrum, conc. 0·004%, (A), fluorescence excitation spectrum (B), fluorescence emission spectrum (C).

height of the curves. The absorbancy values were taken directly from the spectrophotometer. The fluorescence intensity values are arbitrary fluorometer readings.

The absorption readings on fluorescent solutions are always subject to question

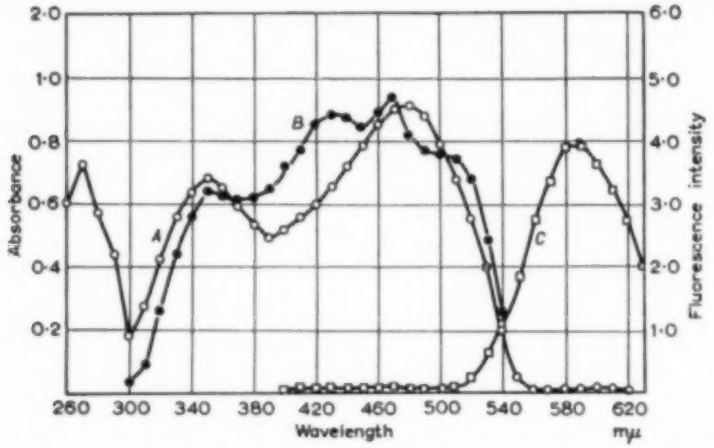

Fig. 3. Aluminium-Acid Alizarin Garnet R: absorption spectrum, conc. 0·008% (A), fluorescence excitation spectrum (B), fluorescence emission spectrum (C).

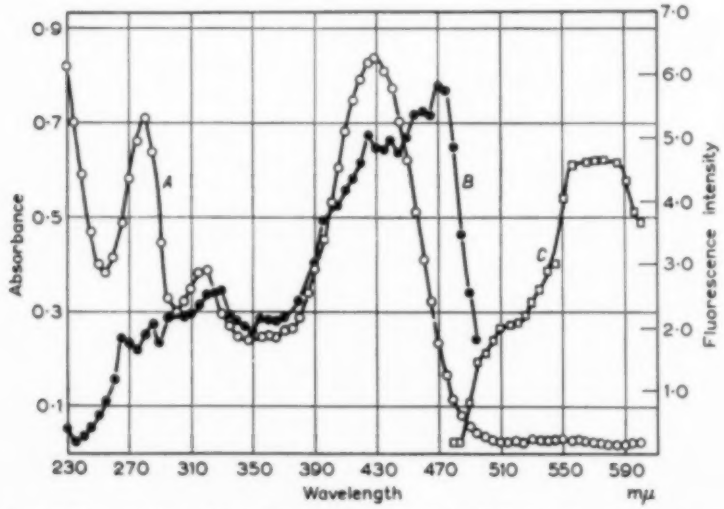

Fig. 4. Beryllium-morin: absorption spectrum, conc 0·001% (A), fluorescence excitation spectrum (B), fluorescence emission spectrum (C).

as to whether the reading represents the true absorption or is affected by the fluorescence. This effect is especially pronounced at the wavelength of greatest excitation. In very dilute solutions of low fluorescence intensity the fluorescence effect is probably negligible, but in solutions of high fluorescence intensity the absorption values are decreased by the fluorescence. This latter situation was quite evident in

VOL. 9 1957

the case of the zirconium-flavonol complex (Fig. 8). The absorption curve does not show an expected absorption peak at the wavelength of greatest excitation. The fluorescence band of this complex is very intense and overlaps the 405-mμ region;

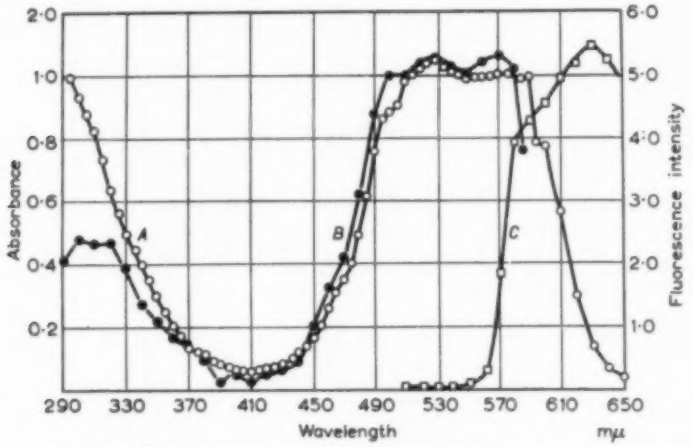

Fig. 5. Beryllium-1,4-dihydroxyanthraquinone: absorption spectrum, conc. 0·0015% (A), fluorescence excitation spectrum (B), fluorescence emission spectrum (C).

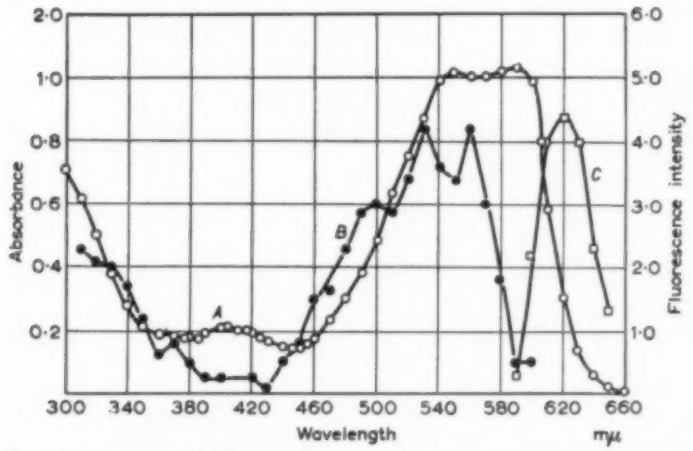

Fig. 6. Beryllium-1-amino-4-hydroxyanthraquinone: absorption spectrum, conc. 0·0015% (A), fluorescence excitation spectrum (B), fluorescence emission spectrum (C).

hence, anomalously low absorbance readings were probable at this wavelength. At concentrations slightly greater than those given on the curve the absorption of the sample was less than that of the reagent alone. Recent work with a tin-flavonol complex which is not intensely fluorescent shows a definite absorption peak at 405 mμ. The zirconium-flavonol complex which is similar to that of tin probably also has a peak in this region.

The general relationships of the parameters studied for the metal chelates follow closely those which have been reported in the literature for pure organic compounds. The following points may be observed: (1) There is good correlation

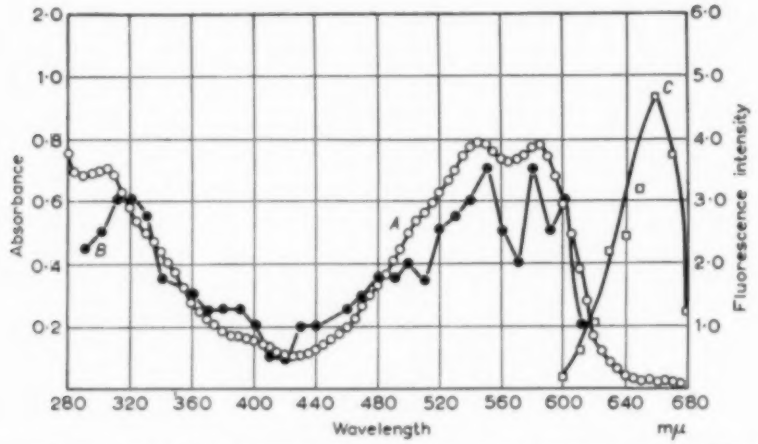

Fig. 7. Thorium-1-amino-4-hydroxyanthraquinone: absorption spectrum, conc. 0·0015% (A), fluorescence excitation spectrum (B), fluorescence emission spectrum (C).

VOL. 9 1957

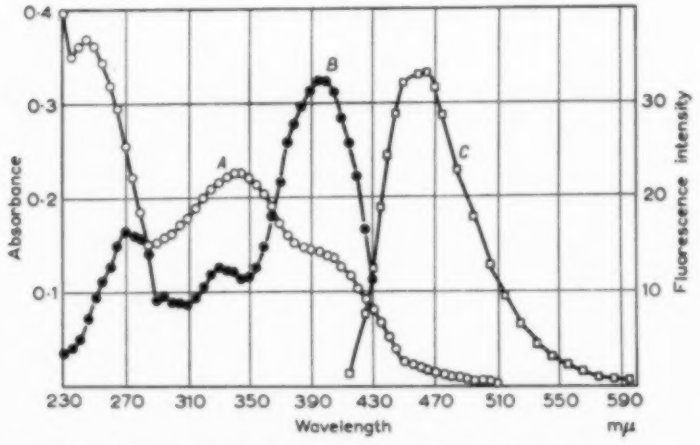

Fig. 8. Zirconium-flavonol: absorption spectrum, conc. 0·001% (A), fluorescence excitation spectrum (B), fluorescence emission spectrum (C).

between the absorption spectrum and the excitation spectrum of the complex. (2) The wavelength of greatest excitation often corresponds to an absorption peak near the fluorescence emission. (3) The fluorescence emission curve has its origin within the range of the absorption band of longest wavelength.

In routine analysis the excitation wavelength must be chosen so that it may

be completely separated from the emission by means of either a filter or a monochromator. Therefore an excitation wavelength of a reasonable distance from the emission must be chosen even though it is not at a maximum excitation point. Since, in most cases, an exciting wavelength in the ultra-violet is used for an emission in the visible range, the separation is relatively simple.

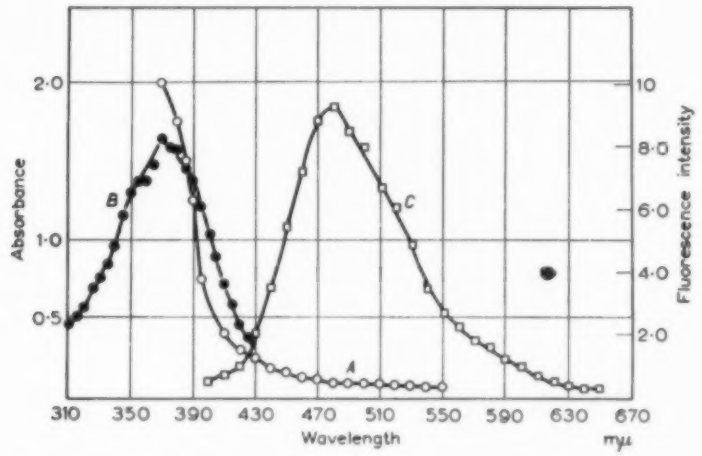

Fig. 9. Boron-benzoin: absorption spectrum, conc. 0·13% (A), fluorescence excitation spectrum (B), fluorescence emission spectrum (C).

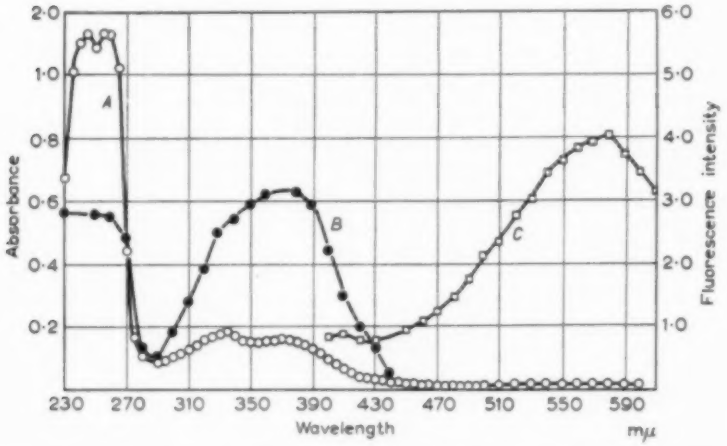

Fig. 10. Lithium-8-quinolinol: absorption spectrum, conc. 0·0002% (A), fluorescence excitation spectrum (B), fluorescence emission spectrum (C).

Acknowledgement—The authors wish to gratefully acknowledge the support of this research through a Frederick Gardner Cottrell grant from the Research Corporation.

Table 1

Complex	Acidity	Absorption band peaks (mμ)	Maximum excitation wavelength (mμ)	Fluorescence band peak (mμ)
Al-morin	pH 4·63	265, 420	430	500
Al-PBBR	pH 4·63	485, 520	470, 580	630
Al-AAGR	pH 4·63	270, 350, 480	470	590
Be-morin	pH ~11	280, 430	470	555–585
Be-1,4-dihydroxy-anthraquinone	pH ~11	510–590	530, 570	630
Be-1-amino-4-hydroxyanthraquinone	pH ~11	540–600	530, 560	620
Th-1-amino-4-hydroxyanthraquinone	pH ~2·3	545, 585	550, 580	660
Zr-flavonol	0·2 N H_2SO_4	245, 345	400	465
B-benzoin	alk.-ethanol	370	370	480
Li-oxine	alk.-ethanol	245, 255, 335, 370	370	580

REFERENCES

[1] ALFORD W. C., SHAPIRO L., and WHITE C. E. *Anal. Chem.* 1951 **23** 1149.
[2] American Instrument Co., Silver Spring, Maryland *Bull.* 2278 Mar. 1956.
[3] BOTIMER L. W. *The Zirconium-flavonol Complex* 1956 Master's thesis, University of Maryland.
[4] FLETCHER M. H., WHITE C. E., and SCHEFTEL M. S. *Ind. Eng. Chem. (Anal.)* 1946 **18** 204.
[5] FREEMAN D. C. and WHITE C. E. *J. Amer. Chem. Soc.* 1956 **78** 2688.
[6] HOFFMAN D. E. *A Study of the Benzoin Fluorometric Analysis Method for Boron* 1955 Master's thesis, University of Maryland.
[7] LAITINEN H. A. and KIVALO P. *Anal. Chem.* 1952 **24** 1467.
[8] POWELL W. A. and SAYLOR J. H. *Anal. Chem.* 1953 **25** 960.
[9] SCHUBERT LEO 2,4,2′-*Trihydroxyazobenzene-5-sulfonic acid—A Fluorometric Reagent for Aluminium and Tin* 1954 Doctoral thesis, University of Maryland.
[10] WEISSLER A. and WHITE C. E. *Ind. Eng. Chem. (Anal.)* 1946 **18** 530.
[11] WHITE C. E. Fluorescence Analysis. *Trace Analysis* (Ed. YOE J. H.) Wiley, New York, in press.
[12] WHITE C. E. and LOWE C. S. *Ind. Eng. Chem. (Anal.)* 1940 **12** 229.
[13] WHITE C. E. and LOWE C. S. *Ind. Eng. Chem. (Anal.)* 1941 **13** 809.
[14] WHITE C. E., FLETCHER M. H., and PARKS J. *Analyt. Chem.* 1951 **23** 478.
[15] WHITE C. E., WEISSLER A., and BUSKER D. *Analyt. Chem.* 1947 **19** 802.

VOL. 9 1957

Spectrochimica Acta, 1957, Vol. 9, pp. 113 to 125. Pergamon Press Ltd., London

Infra-red and Raman spectra of the diazines

R. C. Lord,† A. L. Marston,‡ and Foil A. Miller§
Department of Chemistry, Johns Hopkins University, Baltimore, Md.

(*Received* 13 *November* 1956)

Abstract—Rather complete infra-red and Raman data are presented for pyrazine, pyrimidine, and pyridazine. For pyrazine the data can be interpreted well in terms of D_{2h} symmetry. All but two of the fundamental frequencies are located. For both pyrimidine and pyridazine the complete set of fumdamental frequencies has probably been selected essentially correctly, but the low symmetry often prevents a dependable assignment of a given frequency to a specific vibration.

Introduction

The three diazines form an interesting trio of molecules, and are a logical extension

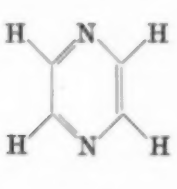

Pyrazine
1,4-diazine
m.p. 52·3°

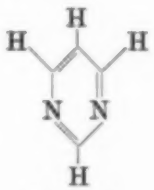

Pyrimidine
1,3-diazine
m.p. 23·5°

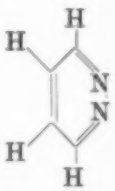

Pyridazine
1,2-diazine
m.p. −8°

of our earlier interest in benzene and pyridine and their deuterium derivatives [1–3]. Some fifteen years ago we began to accumulate data on the vibrational spectra of the diazines [4], but because of interfering circumstances these have not been published heretofore. The recent appearance of a preliminary note by Ito *et al.* [5] prompts us to present our results and conclusions for comparison with theirs.

Very little earlier spectroscopic work has been reported on the diazines. Their infra-red spectra, obtained from our samples, were first published for the limited range 750–2000 cm^{-1} in the book by Barnes, Gore, Liddel, and Williams [6]. The infra-red spectrum of pyrimidine has been given, and discussed briefly, by Brownlie [7] and by Short and Thompson [8].

Other less relevant studies include an electron diffraction investigation of pyrazine by Schomaker and Pauling [9], in which they find a planar symmetrical structure. Uber [10, 11] has studied the near ultra-violet spectrum of pyrimidine, and Halverson and Hirt [12] those of all the diazines. High-resolution ultra-violet studies on all three are also recorded in the thesis of B. J. Fax [13].

Present addresses are:
† Spectroscopy Laboratory, Massachusetts Institute of Technology, Cambridge 39, Mass.
‡ E. I. duPont de Nemours and Co., Aiken, S.C.
§ Department of Research in Chemical Physics, Mellon Institute, Pittsburgh 13, Pa.

Schneider [14] has measured their dipole moments, while Hückel and Jahnentz [15] have determined a number of physical properties of pyridazine and have measured its association.

Experimental

Origin of the samples. Pyrazine was obtained from Dr. R. C. Ellingson of Mead, Johnson and Co., who purified it by repeated vacuum distillation. The pyridazine was prepared by Dr. R. C. Evans [16] and the pyrimidine by Dr. A. L. Marston [4]. Quantities of 5 to 15 g were available for Raman studies.

Spectroscopic measurements. Raman spectra were obtained on a photographic grating instrument at Johns Hopkins University [17, 18]. The exciting line for pyrazine (molten) was Hg-5461 Å, whereas for the other two it was Hg-4358 Å. The samples, sealed under vacuum, slowly discoloured during illumination, but this did not interfere seriously. Pyridazine is the worst offender, but even with it a series of exposures totalling 15–20 hours could be taken satisfactorily. It seems essential that 4047 Å and other shorter wavelengths be heavily filtered out.

Qualitative depolarizations for pyrazine and pyrimidine were determined with the same equipment. For pyridazine they were measured on the Raman apparatus at Mellon Institute [19] by the method of Edsall and Wilson [20], using 6-hour exposures. Because the amount of sample was small (2–3 ml), only the stronger lines were observed. Lines marked *p* are clearly polarized, however.

Infra-red spectra were measured at the Stamford Research Laboratories of the American Cyanamid Co., at the University of Illinois, and at the M.I.T. Spectroscopy Laboratory. The results agreed well. The final data were obtained from 260–3800 cm^{-1} with a Perkin-Elmer Model 12-B spectrometer [21], using prisms of KRS-5, KBr, NaCl, and CaF_2. All samples were examined as pure liquids and in solution in suitable solvents. In addition, pyrazine was measured as a vapour in a variable path gas cell which is described elsewhere [21]. Pressures of 1 and 5 mm and path-lengths from 80 to 400 cm were used.

Results. The results are summarized in Tables 1, 3, and 5, and in Fig. 1. In general our data are much more extensive than those of Ito *et al.* [5], especially for pyridazine. Specific comments will be made in connection with each molecule.

Interpretation of the results

The fundamental vibrations are classified by symmetry species in Tables 2, 4, and 6. The designation of the species and the numbering of the vibrations follow Langseth and Lord's scheme for the deuterated benzenes [1]. Their schematic pictures for the vibrations of benzene are reproduced in Fig. 2 for convenience. Herzberg's tables [22] give the same species classification if, for pyrazine, the *y* axis is taken perpendicular to the molecular plane, *x* and *z* are in the plane, and *z* passes through the nitrogen atoms. For the other two molecules, *z* is the twofold axis, *y* is also in the molecular plane, and *x* is perpendicular to it.

A. Pyrazine

Our Raman spectrum does not agree well with that of Ito *et al.* [5]. They report lines at 680(0), 703(3,*dp*), and 925(1), excited by both 4047 and 4358 Å [23], which we did not find; conversely we found lines at 447, 516, 641, 1118, 1480(?), and 1628(?), which they did not. The ones at 680 and 703 were probably missed by us because of using Hg-5461 excitation. There is another mercury line at 5675·86 Å which is displaced 694 cm^{-1} from 5461 Å and which would

VOL. 9 1957

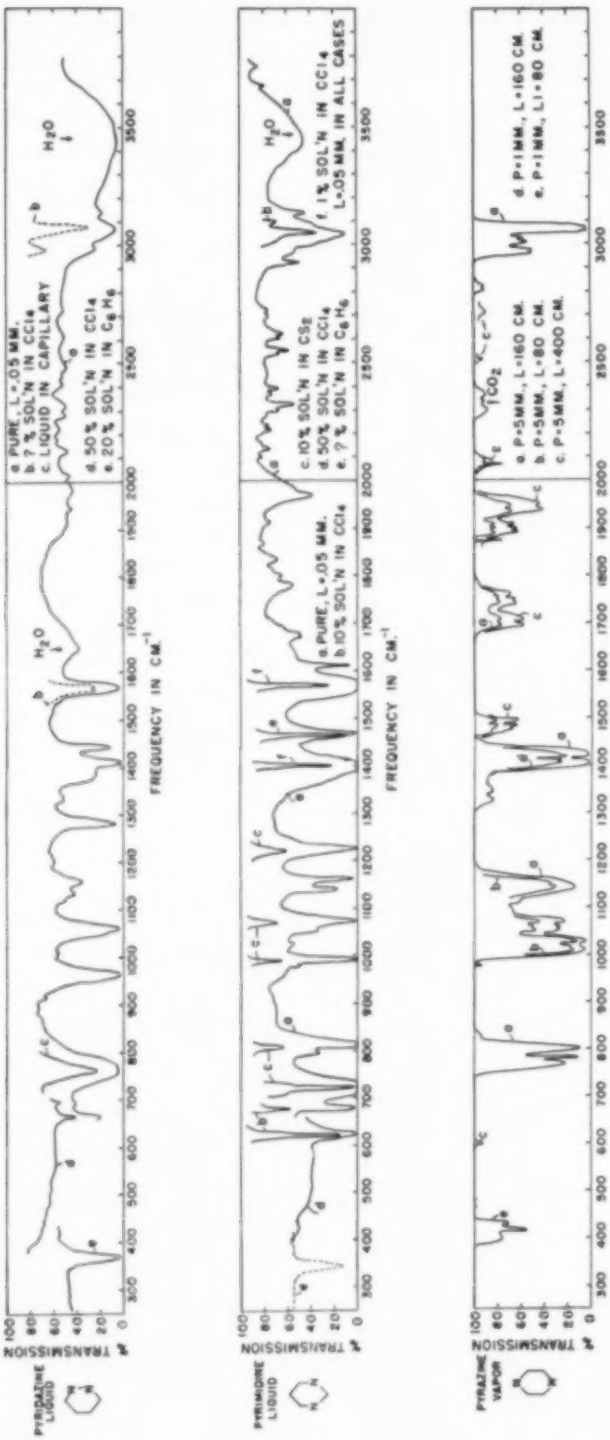
a. PURE, L=.05 MM.
b. ? % SOL'N IN CCl4
c. LIQUID IN CAPILLARY
d. 50 % SOL'N IN CCl4
e. 20 % SOL'N IN C6H6
H2O
PYRIDAZINE LIQUID
% TRANSMISSION
FREQUENCY IN CM-1
a. PURE, L=.05 MM.
b. 10 % SOL'N IN CCl4
c. 10 % SOL'N IN CS2
d. 50 % SOL'N IN CCl4
e. ? % SOL'N IN C6H6
f. 1 % SOL'N IN CCl4
L=.05 MM. IN ALL CASES
PYRIMIDINE LIQUID
% TRANSMISSION
FREQUENCY IN CM-1
a. P=5MM., L=160 CM.
b. P=5MM., L=80 CM.
c. P=5MM., L=400 CM.
d. P=1MM., L=160 CM.
e. P=1MM., L=80 CM.
PYRAZINE VAPOR
% TRANSMISSION
FREQUENCY IN CM-1

Fig. 1. Infra-red spectra of pyridazine, pyrimidine, and pyrazine.

Table 1. Observed frequencies and assignments for pyrazine (1,4-diazine)

Raman (liq.) cm^{-1}	*I*	Infra-red (liq.) cm^{-1}	*I*	Infra-red (vapour) cm^{-1}	*I*	Assignment	Symmetry of components
				400			
		417	(s)	418	vvs	ν_{16b}	
				432			
477	1					1118 − 641 = 477	$B_{2g} \times B_{2g} = B_{1g}$
516	1+					ν_{6b}	
		597	w	600	vvw	1015 − 417 = 598	$A_g \times B_{2u} = B_{2u}$
609	1+					ν_{6a}	
641?	1−					ν_4	
680[d]	0					2 × 340 = 680	$A_u \times A_u = A_g$
						1022 − 340 = 682	$B_{1u} \times A_u = B_{1g}$
703[d]	3*dp*	700	vw			ν_5[c]	
753	1	752	vw			ν_{10a}[c]	
		789	w			ν_{11} of C_{13} isotope	
				772			
		804	vs	785	s	ν_{11}	
				803			
		823	vw			1342 − 516 = 826	$B_{2u} \times B_{2g} = B_{1u}$
925[d]	1	926	vvw			1342 − 417 = 925	$B_{2u} \times B_{2u} = B_{1g}$[c]
1015	9*p*					ν_1	
		1006	w	1010		?	
		1022	m	1020	vs	ν_{18}	
		1032	vw	1030		?	
		1048	vw	1055		?	
				1060	m	641 + 417 = 1058	$B_{3g} \times B_{2u} = B_{1u}$
		1067	vs	1070		ν_{18a}	
		1110	m	1110	w, sh	703 + 417 = 1120 ?	$B_{3g} \times B_{2u} = B_{1u}$
1118	1+					ν_3	
		1125	w			?	
		1148	vs	1144	s	ν_{15}	
		1178	m			753 + 417 = 1170 Fermi resonance with 1148 ?	$B_{1g} \times B_{2u} = B_{2u}$
1232	2					ν_{9a}	
		1342	m			ν_{14}	
				1407			
				1413			
		1418	vs	1419	vvs	ν_{19b}	
				1422			
1480 ?	1−					340 + 1148 = 1488	$A_u \times B_{2u} = B_{2g}$
				1476			
		1490	s	1484	w	ν_{19a}	
				1494			
1523						ν_{8b}	
1584	3*p*					ν_{8a}	
		1623	vw			609 + 1022 = 1631	$A_g \times B_{1u} = B_{1u}$
1628 ?	1−					609 + 1015 = 1624 (?)	$A_g \times A_g = A_g$
				1697			
				1707	w	641 + 1067 = 1708	$B_{3g} \times B_{1u} = B_{2u}$
				1740			
		1745	w	1750	w	609 + 1148 = 1757	$A_g \times B_{2u} = B_{2u}$
				1760			
		1775	w			753 + 1022 = 1775	$B_{1g} \times B_{1u} = A_u$[c]
		1875	w	1874	vw	?	
				1893			
				1901	w	753 + 1148 = 1901	$B_{1g} \times B_{2u} = B_{2u}$
				1911			
		1935	m	1938	m	516 + 1418 = 1934	$B_{2g} \times B_{2u} = B_{1u}$
				1952		609 + 1342 = 1951	$A_g \times B_{2u} = B_{2u}$
		1985	m			641 + 1342 = 1983	$B_{3g} \times B_{2u} = A_u$[c]
				2065	w		
				2075			
				2288			
				2303	w	1232 + 1067 = 2299	$A_g \times B_{1u} = B_{1u}$

VOL. 9 1957

Table 1—*continued*

Raman (liq.) cm^{-1}	*I*	Infra-red (liq.) cm^{-1}	*I*	Infra-red (vapour) cm^{-1}	*I*	Assignment	Symmetry of components
				2514	vvw		
				2705	vvw	3045 − 340 = 2705	$B_{2g} \times A_u = B_{2u}$
				2813	vw		
				2829			
				2963	m		
		2973	(b)	2977			
				3010	w		
				3026			
3038–3051	5					ν_{7b}	
3051–3069	9*p*					ν_{2}	
		3066	(b)	3065	vs	ν_{13}, ν_{20b}	

(a) Benzene solution
(b) CCl_4 solution
(c) Forbidden in infra-red. Allowed in liquid?
(d) From Ito *et al.* [5]. Not observed by us.
w = weak m = medium s = strong v = very sh = shoulder *p* = polarized *dp* = depolarized

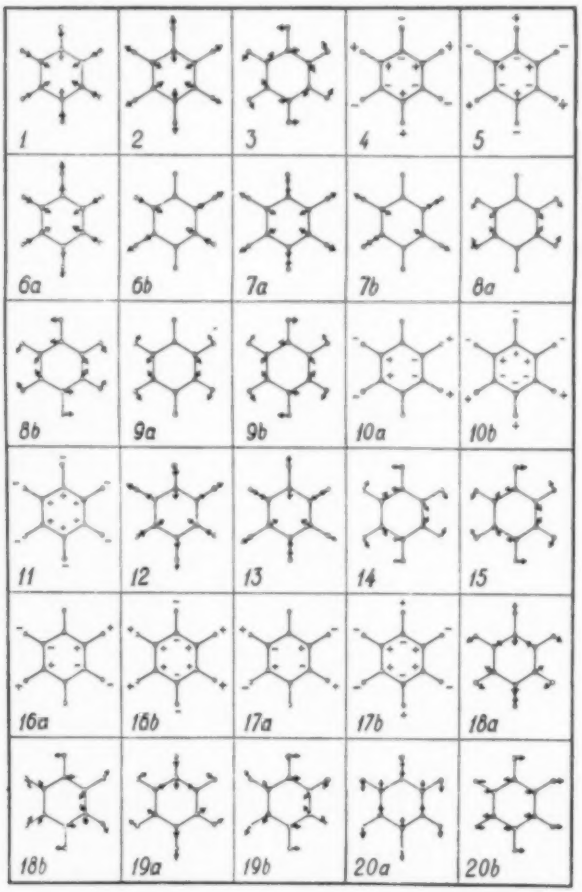

Fig. 2. Vibrations of benzene (schematic). For degenerate modes, the *a* form is symmetric to a twofold axis passing through *para* carbon atoms; the *b* form is antisymmetric. (Reproduced from reference 1 by courtesy of the publisher.)

Table 2. Summary of the fundamental vibrations of pyrazine (1,4-diazine)

D_{2h} species	Activity	Notation	Schematic description	Pyrazine	Pyridine-4-*d* [27]	*p*-Benzene-d_2 [25, 26]	Benzene [24]
Planar vibrations							
A_g	$R(p)$, —	1	Ring	1015	989	978	992
		2	H stretch	3060	3033[a]	3055	3062
		6*a*	Ring	609	597	597	606
		7*a*	H stretch	—	—	2280	3047
		8*a*	Ring	1584	1575	1587	1596
		9*a*	H bend	1232	1215	1173	1178
B_{2g}	R, —	3	H bend	1118	1215	1309	1340
		6*b*	Ring	516	645[b]	601	606
		7*b*	H stretch	3045	3069[a]	3042	3047
		8*b*	Ring	1523	1559	1569	1596
		9*b*	H bend	—	—	909	1178
B_{1u}	—, I·	12	Ring	1022	1015	992	1010
		13	H stretch	3066	2285	3060	3060
		18*a*	H bend	1067	1068	1033	1037
		19*a*	Ring	1490	1476	1469	1485
		20*a*	H stretch	—	3019[a]	2275	3080
B_{3u}	—, I	14	Ring	1342	1347	1335[c]	1310
		15	H bend	1148	1086	1106	1152
		18*b*	H bend	—	862	814	1037
		19*b*	Ring	1418	1413	1413	1485
		20*b*	H stretch	3066	3069[a]	3079	3080
Nonplanar vibrations							
B_{1g}	R, —	10*a*	H bend	753[d]	890[b]	850	850
B_{3g}	R, —	4	Ring	641	660–70	634	703
		5	H bend	703	834	967	995
		10*b*	H bend	—	743	736	850
A_u	—, —	16*a*	Ring	[340]	365[b]	405	405
		17*a*	H bend	[950]	968	975	975
B_{2u}	—, I	11	H bend	804	633	597	673
		16*b*	Ring	417	383[b]	367[b]	405
		17*b*	H bend	—	—	876	975

[ ] Estimated.
[a] Tentative assignment.
[b] Frequency is approximate.
[c] Assignment by present authors.
[d] See discussion.

VOL. 9 1957

Table 3. Observed frequencies and assignments for pyrimidine (1,3-diazine)

Raman (liq.) cm^{-1}	*I*	Infra-red (liq. or soln.) cm^{-1}	*I*	Assignment
		344	vs	ν_{16b}
394	2			ν_{16a}
567	0			ν_{6b}
623	2*p*	624	vs	ν_{6a}
679	6	679	vs	ν_4
		710	m, sh	1055 − 344 = 711
724	1 −	722	vvs	ν_{11}
		795	w	
814	0	806	vs	ν_{10b}
870	0			ν_{17a}
		980	w, sh	ν_5
991	10*p*	991	vs	ν_1
1021	0	1021	vw	ν_{18b}
1053	8*p*	1055	m	ν_{12} in Fermi resonance with
1074	8*p*	1071	vs	344 + 722 = 1066
1137	4*p*	1141	m	ν_{9a}
1160	1 −	1161	s	ν_{15}
1227	3	1227	vs	ν_3
1371	0			ν_{14}
1398	0	1402	vvs	ν_{19b}
1466	1 −	1467	vs	ν_{19a}
1566	5	1570	vvs	ν_{8a}, ν_{8b}
		1612	s	2 × 806 = 1612
		1672	vw	
		1678	vw	
		1780	vw	
		1914	vw	
		1971	m	
		2140	w	
		2215	w	
		2300	w	
2316	1 −			
		2325	w	
		2367	w	
		2392	vw	
		2537	w	
		2553	m	
		2609	w	
		2622	w	
2917	1 −	2925	m	2 × 1467 = 2934
3001	1 −			ν_{13}
		3027	m	ν_3 1467 + 1570 = 3037
3048	10*p*	3047	s	ν_2
3038	1			ν_{20a}
		3095	m	ν_{7b}
3129	2	3135	m	2 × 1570 = 3140

w = weak m = medium s = strong v = very sh = shoulder *p* = polarized

Table 4. Summary of the fundamental vibrations of pyrimidine (1,3-diazine)

C_{2v} species	Activity	Notation	Schematic description	Pyrimidine	Pyridine-3-*d* [27]	Benzene [24]
Planar vibrations						
A_1	$R(p)$, I	1	Ring	991	980	992
		2	H stretch	3048	3038[a]	3062
		6*a*	Ring	624	599	606
		7*a*	H stretch	—	—	3047
		8*a*	Ring	1570	1570	1596
		9*a*	H bend	1141	1195	1178
		12	Ring	1066[b]	1033	1010
		13	H stretch	3001	3053[a]	3060
		18*a*	H bend	—	1050	1037
		19*a*	Ring	1467	1468	1485
		20*a*	H stretch	3083	3022[a]	3080
B_1	R, I	3	H bend	1227	1217	1340
		6*b*	Ring	567	650[b]	606
		7*b*	H stretch	3095	2289[a]	3047
		8*b*	Ring	1570	1570	1596
		9*b*	H bend	—	—	1178
		14	Ring	1371	1337	1310
		15	H bend	1161	1108	1152
		18*b*	H bend	1021	848	1037
		19*b*	Ring	1402	1416	1485
		20*b*	H stretch	—	3077[a]	3080
Nonplanar vibrations						
A_2	R, —	10*a*	H bend	—	823	850
		16*a*	Ring	394	350[b]	405
		17*a*	H bend	870	965	975
B_2	R, I	4	Ring	679	670[b]	703
		5	H bend	980	902	995
		10*b*	H bend	722	717	850
		11	H bend	806	632	673
		16*b*	Ring	344	404	405
		17*b*	H bend	—	—	975

[a] Tentative assignment.
[b] Frequency is approximate.

VOL. 9 1957

Table 5. Observed frequencies and assignments for pyridazine (1,2-diazine)

Raman (liq.) cm^{-1}	I	Infra-red (liq. or soln.) cm^{-1}	I	Assignment
367	2dp	370	s	ν_{16b}
421	1 –			ν_{16a}
619	2dp	619	vvw	ν_{6a}
661	2dp	664	m	ν_{6b}
689(?)	1 –	696	w	ν_{11}
751	1			ν_4
		760	vs	ν_{10a}
863	1 –			ν_5
		891	vw	
906	1			962 from Hg 4348 ?
		916	w	
936(?)	1 –			ν_{17a}
962	7p	964	s	ν_1
		987	w, sh	367 + 619 = 986
1006	2	1009	vw	ν_{12}
		1052	m, sh	
1063	8p	1063	s	ν_{15}
1117	3p	1119	vw, sh	ν_{9a}
		1132	w	
1158	6p	1160	m	ν_{14} ?
		1201	vw	
1239	2			ν_{18a} ?
1238	3dp ?	1283	s	ν_3 ?
		1330	vw	Real ?
		1340	vw	
		1386	m, sh	
		1414	s	ν_{19b}
1446	1	1444	s	ν_{19a}
1503	1			2 × 751 = 1502 (?)
1565	3 dp	1565	s	ν_{8b}
1578	2	1572		ν_{8a}
		1916	vw	
		1945	vw	
		1982	vw	
		2023	vw	
		2129	w	
		2180	vw	
		2223	vw	
		2284	w	
		2323	w	
		2411	vw	Real ?
		2444	vw	
		2485	vw	
		2609	vw	
		2730	vw	
2817–50	1 –			
2855–82	1 –			
2953	2, br			
		2980	m	
2995	3, br	2990	vw, sh	
3043	6, br dp?			ν_2, ν_{7b}
3063	5, br p			ν_{20b}
		3075	vs	ν_{13}
3119	3			
3129	3			2 × 1565 = 3130
		3138	s	1565 + 1578 = 3143

w = weak m = medium s = strong v = very sh = shoulder br = broad
p = polarized dp = depolarized

Table 6. Summary of the fundamental vibrations of pyridazine (1,2-diazine)

C^*_{2v} species	Activity	Notation	Description	Pyridazine	Pyridine-2-*d* [27]	Benzene [24]
Planar vibrations						
A_1	*R(p), I*	1	Ring	964	989	992
		2	H stretch	3043	3040[a,b]	3062
		6*a*	Ring	619	600	606
		7*a*	H stretch	—	—	3047
		8*a*	Ring	1572	1576[b]	1596
		9*a*	H bend	1160	1149	1178
		14	Ring	1283	1357	1310
		15	H bend	1063	1112[b]	1152
		18*b*	H bend	—	834	1037
		19*b*	Ring	1414	1424	1485
		20*b*	H stretch	3063	3075[a]	3080
B_1	*R, I*	3	H bend	1239	1212	1340
		6*b*	Ring	664	640[b]	606
		7*b*	H stretch	3043	3068[b]	3047
		8*b*	Ring	1565	1570[b]	1596
		9*b*	H bend	—	—	1178
		12	Ring	1009	1029	1010
		13	H stretch	3075	3051[a]	3060
		18*a*	H bend	1052	1059	1037
		19*a*	Ring	1444	1461	1485
		20*a*	H stretch	—	2258[a]	3080
Nonplanar vibrations						
A_2	*R*, —	4	Ring	751	660–70	703
		5	H bend	863	901	995
		10*b*	H bend	—	748	850
		16*a*	Ring	421	360[b]	405
		17*a*	H bend	936	970	975
B_2	*R, I*	10*a*	H bend	760	814	850
		11	H bend	696	638	673
		16*b*	Ring	370	405	405
		17*b*	H bend	—	—	975

[a] Tentative assignment.
[b] Frequency is approximate.

therefore interfere seriously. The 925 line is more puzzling, for it is said to be as intense as 609 and 753, which we found readily. We have no explanation for why it was missed. These three frequencies have been included in Table 1 for completeness.

It is quite clear from the lack of coincidences between the Raman spectrum and the infra-red vapour spectrum that pyrazine has a centre of symmetry.

VOL. 9 1957

Its aromatic nature and the electron diffraction results both indicate that it is planar. We therefore take the symmetry to be D_{2h}, and proceed to assign the frequencies as shown in Tables 1 and 2. Included in Table 2 for comparison are the assignments for benzene [$^{4}_{27}$], *p*-benzene-d_2 [25, 26], and pyridine-4-*d* [27]. The analogy with *p*-benzene-d_2 is particularly helpful. For the infra-red frequencies liquid-state values will be used where possible to make them directly comparable to the Raman frequencies.

Species A_g. The polarized Raman lines at 1015, 1584, and 3060 are undoubtedly ν_1, ν_{8a}, and ν_2 respectively. The lines at 1118 and 1232 must be the two planar hydrogen bending frequencies ν_{9a} and ν_3. Because Ito *et al.* [5] found 1232 to be polarized, we assign it to ν_{9a} and attribute 1118 to ν_3. ν_{6a}, a ring frequency, is taken as 609 cm^{-1}.

Species B_{2g}. ν_{7b} must be 3045 cm^{-1}, ν_{8b} is undoubtedly 1523, and ν_3 has already been put at 1118. This leaves only ν_{6b}, which is presumably either 516 or 641. We select 516, and attribute 641 to the remaining Raman-active ring frequency ν_4. If they are reversed, the infra-red bands at 823, 1060, and 1935 cannot be explained by the binary combinations shown in Table 2, because they become inactive. It seems quite clear that the three Raman-active ring vibrations ν_{6a}, ν_{6b}, and ν_4 must be chosen from 516, 609, and 641, but we would not insist on the specific assignments given above.

Species B_{1g} *and* B_{3g}. There are two Raman-active fundamentals remaining to be chosen (the nonplanar hydrogen modes ν_{10a} and ν_5) from among the three possible frequencies 703, 753, and 925. It is interesting to note that all of these appear very weakly in the infra-red spectrum of the liquid, presumably because of the breakdown of selection rules; they are the only Raman-infra-red coincidences. The first two are taken as the fundamentals, because we are not certain of the validity of the 925 line, and because if 925 is real it can be explained as 1342–417 = 925. Consequently, we assign 703 to ν_5 and 753 to ν_{10a}, although they could equally well be reversed. However, both are surprisingly low, for they were expected to be around 900 cm^{-1}. For this reason an alternative assignment is possible with 703 and 925 as the fundamentals, and 753 explained as [340] + 417 = 757. [340] is the estimated value for ν_{16a}, to be discussed shortly.

Infra-red-active fundamentals. 417 is undoubtedly ν_{16b}. The strong bands at 1490 and 1418 are certainly ν_{19a} and ν_{19b}. The former is assigned to ν_{19a} by analogy with pyridine and pyridine-4-*d*. (In both pyridine and pyridine-d_5 the higher of these two is stronger in the Raman effect and is slightly polarized.) The two C—H stretching modes are presumably superimposed at 3066 cm^{-1}. This leaves four strong infra-red bands (804, 1022, 1067 and 1148) and five fundamentals (ν_{12}, ν_{18a}, ν_{14}, ν_{15}, ν_{11}). 804 is assigned to ν_{11}, 1022 to ν_{12}, 1067 to ν_{18a}, and 1148 to ν_{15}. The assignment of 1022 to ν_{12} and 1067 to ν_{18a} is of course arbitrary, since both belong to the same species. It is further possible that one or the other might be interchanged with 1148, assigned to ν_{15}. It is clear, however, that all these frequencies are fundamentals. The remaining fundamental, ν_{14}, is reasonably taken as the medium intensity band at 1342 cm^{-1}.

Totally-inactive fundamentals. The two vibrations of species A_u are totally inactive. A postulated frequency of 340 for ν_{16b} is useful in explaining the weak

Raman lines at 680 and 1480, which we have been unable to account for otherwise. Presumably ν_{17a} is in the vicinity of 950 cm^{-1}. Neither of these is at all certain.

Remaining bands. Table 1 lists our explanation for most of the remaining bands below 2000 cm^{-1}, using only binary combinations.

B. Pyrimidine

Pyrimidine is assumed to have symmetry C_{2v}. The observed data and assignments are given in Tables 3 and 4. Because species A_2 is infra-red-inactive, ν_{16a} is undoubtedly 394, and ν_{17a} is probably 870. Most of the A_1 fundamentals can be chosen with fair certainty with the help of the polarization properties and the analogy to benzene and pyridine-3-*d* [27]. It may be noted that whereas we found 1137 to be polarized, Ito *et al.* [5] report it as depolarized. The remaining assignments are made by analogy with the corresponding frequencies of benzene, pyridine, and their various deuterium derivatives, but in view of the uncertainties of such a procedure, detailed discussion is not warranted.

C. Pyridazine

Our data for pyridazine are much more complete than those of Ito *et al.* [5]. The molecule is assumed to have symmetry C^*_{2v}, where the asterisk indicates that the twofold axis bisects bonds rather than atoms as it does in C_{2v}. The data and assignments are given in Tables 5 and 6. The assignments for species A_1 are not wholly satisfactory. One would like to use 1283 for ν_{14}, but if this were done there would be an extra polarized line in the range 1000-1200 cm^{-1}. This extra line would have to be 1117, for 1063 and 1158 are so intense that they must be fundamentals. Since we have not been able to find a satisfactory explanation for 1117 as a combination tone, we conclude that it is an A_1 fundamental, and attribute 1283 to a B_1 vibration. The frequencies for species A_2 can be located by their infra-red inactivity. They are taken to be 421, 751, 863, and 936. The remaining assignments are made by analogy, and will not be discussed.

VOL.
9
1957

Acknowledgements—The authors are most appreciative to Dr. R. C. Ellingson and Dr. R. C. Evans for providing purified samples of pyrazine and pyridazine, respectively. Drs. R. Bowling Barnes and Van Zandt Williams very kindly obtained the initial infra-red spectra at the Stamford Research Laboratories of the American Cyanamid Co. We are particularly indebted to Dr. Ellis R. Lippincott for Raman data on pyrazine and pyridazine, and to Dr. Betty J. Fax, who redetermined the infra-red spectra at M.I.T. and plotted Fig. 1.

References

[1] Langseth A. and Lord R. C. *Kgl. Danske Videnskab. Selskab, Mat.-fys. Medd.* 1938 **16** No. 6.
[2] Miller F. A. and Crawford B. L. jr. *J. Chem. Phys.* 1946 **14** 282; 1949 **17** 249.
[3] Corrsin L., Fax B. J., and Lord R. C. *J. Chem. Phys.* 1953 **21** 1170.
[4] Marston A. L. *The Preparation and Vibrational Spectrum of Pyrimidine* 1943 Ph.D. thesis, Johns Hopkins University.
[5] Ito M., Shimada R., Kuraishi T., and Mizushima W. *J. Chem. Phys.* 1956 **25** 597.
[6] Barnes R., B. Gore R. C., Liddel U., and Williams V. Z. *Infra-red Spectroscopy* p. 97. Reinhold, N.Y. 1944.

[7] Brownlie I. A. *J. Chem. Soc.* 1950 3062.
[8] Short L. N. and Thompson H. W. *J. Chem. Soc.* 1952 168.
[9] Schomaker V. and Pauling L. *J. Amer. Chem. Soc.* 1939 **61** 1769.
[10] Uber F. M. and Winters R. *J. Amer. Chem. Soc.* 1941 **63** 137.
[11] Uber F. M. *J. Chem. Phys.* 1941 **9** 777.
[12] Halverson F. and Hirt R. C. *J. Chem. Phys.* 1949 **17** 1165; 1951 **19** 711.
[13] Fax B. J. *Near Ultraviolet Absorption Spectra of Pyridine, Pyridine-d_5, and the Diazines under High Dispersion* 1950 Ph.D. thesis, Massachusetts Institute of Technology.
[14] Schneider W. C. *J. Amer. Chem. Soc.* 1948 **70** 627.
[15] Hückel W. and Jahnentz W. *Ber. Deut. Chem. Ges.* 1942 **75B** 1438.
[16] Evans R. C. and Wiselogle F. Y. *J. Amer. Chem. Soc.* 1945 **67** 60.
[17] Lord R. C. jr. and Miller F. A. *J. Chem. Phys.* 1942 **10** 328.
[18] Harrison G. R., Lord R. C., and Loofbourow J. R. *Practical Spectroscopy* pp. 515–17. Prentice-Hall, N.Y. 1948.
[19] Miller F. A. and Inskeep R. G. *J. Chem. Phys.* 1950 **18** 1519; Miller F. A., Hannan R. B., and Cousins L. R. *ibid.* 1955 **23** 2127.
[20] Edsall J. T. and Wilson E. B. jr. *J. Chem. Phys.* 1938 **6** 124 method 1.
[21] Lord R. C., McDonald R. S., and Miller F. A. *J. Opt. Soc. Amer.* 1952 **42** 149.
[22] Herzberg G. *Infra-red and Raman Spectra* Van Nostrand, N.Y. 1945.
[23] Ito M. Private communication.
[24] Miller F. A. *J. Chem. Phys.* 1956 **24** 996. Table 2.
[25] Herzfeld N., Hobden J. W., Ingold C. K., and Poole H. G. *J. Chem. Soc.* 1946 272.
[26] Bailey C. R., Carson S. C., Gordon R. R., and Ingold C. K. *J. Chem. Soc.* 1946 288. Their assignment for ν_{14} (1413) is wrong.
[27] Anderson F. A., Bak B., Broderson S., and Rastrup-Anderson J. *J. Chem. Phys.* 1955 **23** 1047.

Spectrochimica Acta, 1957, Vol. 9, pp. 126 to 132. Pergamon Press Ltd., London

The emission spectrum of OH from 2·8 to 4·1 μ*

HARRY C. ALLEN JR., L. R. BLAINE, and EARLE K. PLYLER
National Bureau of Standards, Washington, D.C.

(*Received* 3 *December* 1956; *accepted for publication* 26 *January* 1957)

Abstract—The emission spectrum of an oxyacetylene flame has been measured from 2·8 to 4·1 μ. The most prominent features of the spectrum in this region arise from the 3 → 2, 2 → 1, and 1 → 0 vibrational transitions of OH in the ground electronic state. Most of the observed emission can be accounted for by the *P* branches of these three transitions, although transitions in other branches are observed for some of the vibrational bands. Strong emission by water vapour precludes observation of the OH spectrum at wavelengths shorter than 2·8 μ.

Introduction

PREVIOUS work [1] on the emission sprectra of flames has shown that many of the regions of the characteristic emission in the infra-red region arise from CO, OH, H_2O, and CO_2 molecules. In another investigation with a grating spectrometer [2] the emission spectrum of an oxyacetylene flame was studied in the region from 2750 to 3000 cm^{-1}, and many components of the *P* branch of the OH fundamental band were observed, including lines of the 1 → 0 and 2 → 1 transitions. The present work was undertaken to identify as many lines produced by OH as possible in the region from 2·7 to 4·1 μ and to make a precise measurement of the positions of the lines so that the molecular constants for the ground state could be determined. The molecular constants determined from the infra-red spectrum could then be compared with those obtained from the ultra-violet spectrum.

Experimental procedure

The emission spectra were measured from an oxyacetylene flame. The gases were first supplied to the flame in a stoichiometric mixture, but it was found that an increase in the intensity of the lines could be obtained when there was a slight increase in the oxygen. All of the spectra represented in the figures were obtained with a lean mixture of the fuel.

An infra-red spectrometer with a 7500-line/in. grating was used in the observation of the spectrum. The lines were measured in wavenumbers by the use of the fringe system of a Fabry-Perot interferometer. The instrument and the method of measurement have been described previously [3].

The emission spectrum of OH is of low intensity. In order to avoid wide slits with the resulting low resolution, the available energy on the slit of the spectrometer was increased by use of a greater solid angle from the flame through the use of mirrors. Fig. 1 shows the optical system used in increasing the available energy. The radiation from four solid angles is utilized in this arrangement.

In the figure the spherical mirror M_1 is positioned so that the flame *F* is imaged on itself. Mirror M_2 is placed with its axis slightly off the flame at a distance somewhat less than its radius of curvature producing the virtual image, E_v, as shown. A plane mirror M_3 projects this image E_v on the flame. By tracing the cones emanating from the flame it can be seen that the system

* This work was supported in part by the Geophysics Research Directorate, Air Force Cambridge Research Center.

VOL. 9 1957

is closed; that is, radiation emitted into any of these four solid angles about the flame reaches the slit.

With this optical system, nearly four times the intensity of the radiation was observed. This indicates that the absorption of the flame for the frequencies emitted by OH is small.

Figs. 2, 3, and 4 are photographs of the recorder trace of the spectrum from 2·7 to 4·1 μ. The results shown in Fig. 2 were measured in the second order with a 7500-lines/in. grating and the effective slit-width was about 0·35 cm^{-1}. Many of the lines in this region arise from the H_2O molecule, but several of the lines are identified as belonging to the $1 \rightarrow 0$, $2 \rightarrow 1$, and $3 \rightarrow 2$ transitions of the molecule. The identified lines are labelled on the figure.

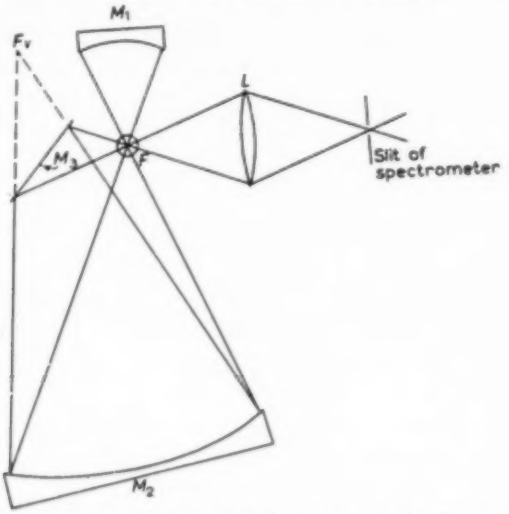

Fig. 1. An optical system for increasing the energy on the slit of the spectrometer from a transparent source.

In Fig. 3 the region from 3·1 to 3·65 μ is shown. The spectra in Figs. 3 and 4 were obtained with a 7500-lines/in. grating in the first order, with an effective slit-width of about 0·6 cm^{-1} This region is almost devoid of H_2O emission lines and the OH lines of the P branches stand out clearly.

The spectrum shown in Fig. 4 is a continuation of Fig. 3, except that the slits had to be widened to observe the lines in the tail of the band. The average effective slit-width was 0·8 cm^{-1} in this region. The OH lines of the P branch were observed to the beginning of the CO_2 emission band at about 4·1 μ.

Discussion

The molecular constants and energy levels of OH have been obtained from the analysis of extensive electronic transitions [4]. In the present work only the P-branch region and a portion of the Q-branch region of the $1 \rightarrow 0$ transition are sufficiently free from overlapping water-vapour emission to enable specific identification of transitions. The spectrum due to the $1 \rightarrow 0$ transition was calculated using the term values given in ref. [4]. It was possible on this basis to assign 122 Q- and P-branch lines in the $1 \rightarrow 0$ transition, with a mean deviation of 0·09 cm^{-1}. For the $2 \rightarrow 1$ transition 79 Q-, P-, and R-assignments could be made with the same average deviation. About 30 assignments could be made for the $3 \rightarrow 2$ transition, although these lines were much weaker than in the other two transitions and the measurements more uncertain. Such remarkable agreement between the

observed and calculated spectra serves to emphasize the excellence of the analysis of the electronic spectra. The molecular constants found in ref. [4] cannot be

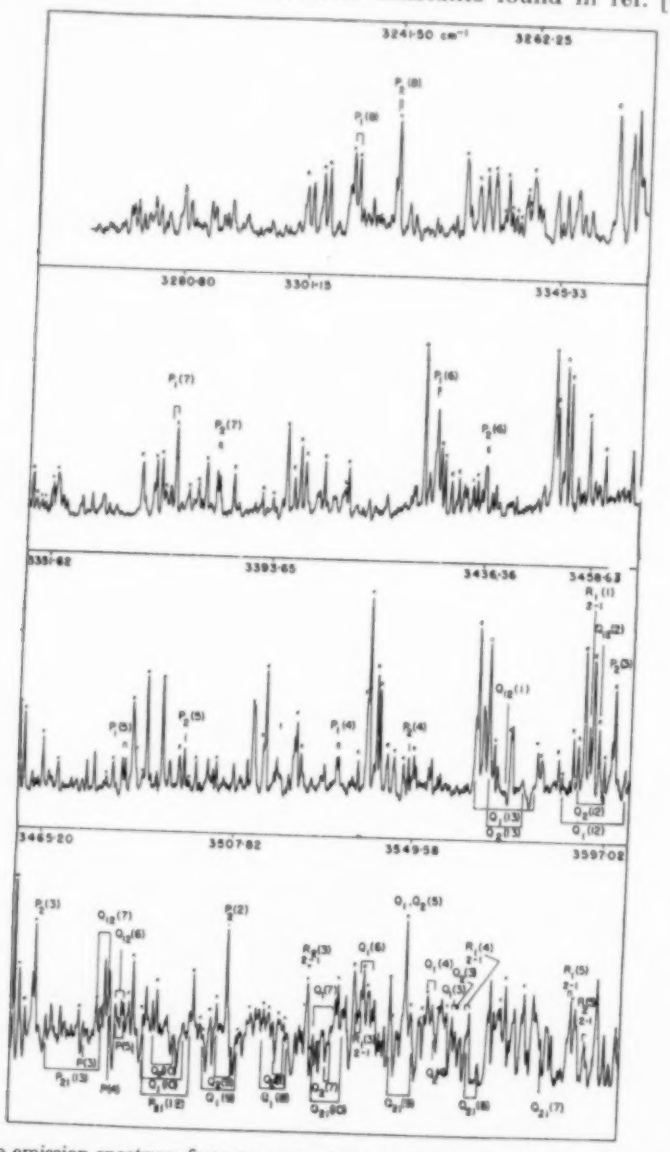

Fig. 2. The emission spectrum from an oxyacetylene flame from 3200 to 3600 cm^{-1}. The more intense rotational lines of H_2O are labelled by an asterisk, and the OH rotational lines are identified.

improved on from the present infra-red data. These constants from ref. [4], as quoted in HERZBERG [5], are $\omega_e = 3734{\cdot}09$, $\omega_e x_e = 82{\cdot}81$, $B_e = 18{\cdot}871$, and $\alpha_e = 0{\cdot}714$, all in cm^{-1}. The comparison between the observed and calculated spectra is

given in Table 1 and the identification of the various transitions is given in Figs. 2, 3, and 4. It is unfortunate that the R-branch of the $1 \rightarrow 0$ transition could not be

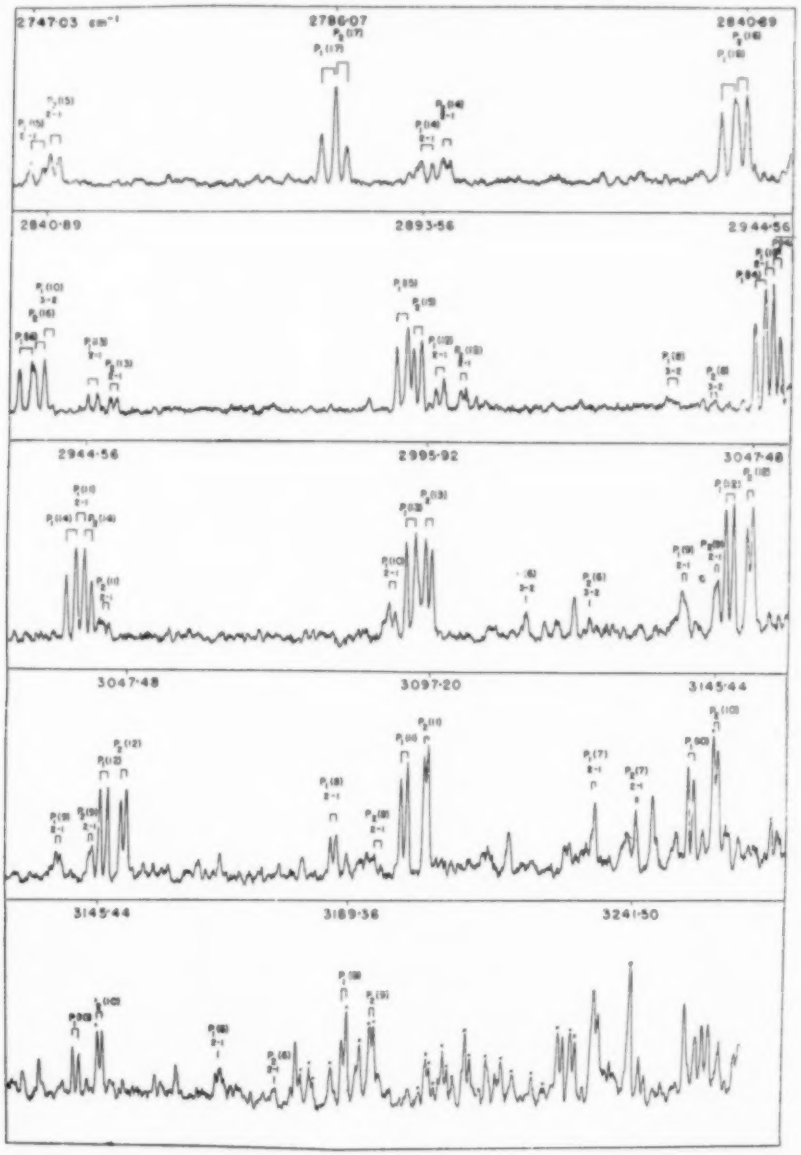

Fig. 3. The emission spectrum from the flame from 2740 to 3270 cm^{-1}. Most of the intense lines in this region belong to the P branches of the OH spectrum.

observed, but the excellent agreement found in the accessible regions indicates that such observations would add little to the knowledge about OH.

Table 1. Main branches OH $1 \rightarrow 0$ band

K	P_1		P_2		Q_1		Q_2		R_1		R_2	
	Calc.	Obs.	Calc.	Obs.	Calc.	Obs.	Calc.	Obs.	Calc.	Obs.	Calc.	Obs.
1					3568·49		3568·60		3649·10		3627·72	
					3568·28		3569·22		3649·25		3627·83	
2	3484·61 }	3484·60	3507·63	3507·82	3565·58		3566·24					
	3484·59 }		3507·56		3565·20		3566·68					
3	3447·20		3465·14	3465·20	3561·50	3561·56	2563·09					
	3446·91		3465·12		3560·66	3560·80	3562·55					
4	3407·94 }	3407·64	3421·93	3421·98	3556·17	3556·19	3556·54 }	3556·72				
	3407·53 }		3421·87		3554·68	3554·88*	3556·91 }					
5	3367·01	3367·04	3377·99 }	3377·98	3549·56	3549·58*	3549·60					
	3366·44	3366·48	3377·83 }		3547·13		3549·64	3549·58*				
6	3324·50	3324·36	3333·31	3333·37	3541·58	3541·60	3540·39	3540·59*				
	3323·93	3324·05	3332·99	3333·16	3538·22		3540·86	3540·82				
7	3280·70	3280·80	3287·82	3287·91	3532·35		3531·84	3531·75				
	3279·93	3280·04	3287·41	3287·53	3527·70	3527·60*	3530·55					
8	3235·55	3235·62*	3241·46	3241·50	3521·73	3521·69	3520·96	3520·94*				
	3234·80	3134·83*	3240·98	3241·14	3515·84		3518·79					
9	3189·34	3189·36	3194·30	3194·28	3509·85		3508·80					
	3188·48	3188·52	3193·67	3193·64	3502·45	3502·54*	3505·55	3505·57*				
10	3141·97	3142·03	3146·14	3146·14	3496·57		3495·09					
	3141·06	3141·03	3145·49	3145·44	3487·68	3487·64	3490·92	3491·02				
11	3093·70	3093·70	3097·23	3097·20	3482·16		3480·42	3480·42				
	3092·50	3092·64	3096·30	3096·50	3471·30		3474·72	3474·72				
12	3044·34	3044·44	3047·31	3047·48	3466·11		3464·13	3464·14				
	3043·31	3043·24	3046·61	3046·62	3443·68		3457·31	3457·33*				
13	2994·21	2994·34	2996·93 }	2995·92	3448·97		3446·83					
	2992·81	2993·03	2995·84 }		3434·50		3438·28					
14	2943·21	2943·34	2945·52	2945·61	3430·47		3428·01	3428·10				
	2941·79	2941·91	2944·53	2944·56	3414·07		3418·04					
15	2891·31	2891·54	2893·50	2893·56	3410·98		3408·01	3408·02				
	2889·88	2890·04	2892·21	2892·44	3492·21		3496·25					
16	2838·87	2839·12	2840·70	2840·89	3389·56		3386·72					
	2837·44	2837·48	2839·54	2839·55	3369·03		3373·28					
17	2785·80	2786·07	2787·43	2787·49								
	2784·04	2784·21	2786·05	2786·07								
18	2731·97	2732·12	2733·36	2733·52								
	2730·29	2730·31	2732·14	2732·12								
19	2677·70	2677·69	2679·02	2679·10								
	2675·83	2675·93	2677·44	2677·46								
20	2622·77	2622·76	2623·94	2624·08								
	2620·88	2621·01	2622·53	2622·76								
21	2567·46	2567·55	2568·48	2568·70								
	2565·41	2567·29	2566·83									
22	2511·51	2511·80	2512·65	2512·72								
	2509·58	2509·66	2510·94	2510·90								
23	2455·50	2455·65	2456·42	2456·32								
	2453·31	2453·25	2454·48	2454·48								
24	2398·88	2398·90	2399·62	2399·82								
	2396·62		2397·91									
25	2341·97		2342·55									
	2339·62		2340·59									
26	2284·83		2285·24									
	2282·50		2283·42									

VOL. 9
1957

Table 1 (*continued*)

K	P_1		P_2		Q_1		Q_2		R_1		R_2	
	Calc.	Obs.	Calc.	Obs.	Calc.	Obs.	Calc.	Obs.	Calc.	Obs.	Calc.	Obs.
1					3402·87	3402·70	3401·96		3480·54	3480·42	3459·77	3459·73
					3400·53		3402·35		3480·67			
2	3321·92		3343·23		3400·06				3509·50		3494·05	3494·20
	3321·90		3343·75		3399·57		3401·16		3509·72		3494·07	
3	3285·82	3285·79	3303·73		3395·97		3396·64		3537·47	3537·46	3526·10	3526·00*
	3285·76	3285·87	3304·10	3304·01	3395·20		3397·10		3537·84	3537·85	3526·22	3526·31*
4	3248·05		3262·02	3262·25	3390·69		3391·18		3564·43	3564·22	3555·96	3555·95
	3247·74		3262·03		3389·24		3391·49		3564·78	3564·96	3556·11	3556·19
5	3208·55	3208·72	3219·68	3219·59	3384·09	3384·12*	3384·30		3590·19	3590·12	3583·82	
	3208·14	3208·08	3219·57		3381·88		3384·35		3590·53	3590·32*	3584·14	3584·12
6	3167·59		3176·48	3176·53	3376·24		3376·23					
	3167·01		3176·22		3373·11		3375·74					
7	3125·34	3125·23	3132·60		3367·13	3367·04*	3366·74					
	3124·59	3124·71	3132·25	3132·28	3362·75		3365·58					
8	3081·71	3081·87	3087·77	3087·80	3356·61		3355·95					
	3080·95	3081·00	3087·24	3087·24	3351·01		3353·91					
9	3037·04	3037·06	3042·03	3042·05	3344·90		3343·88					
	3036·10	3036·27	3041·45	3041·55	3337·77		3340·84					
10	2991·15	2991·29	2995·41		3331·70		3330·44					
	2990·30	2990·37	2994·93	2995·09	3323·24		3326·54					
11	2944·44	2944·56	2948·12	2948·16	3317·42		3315·88					
	2943·24	2943·36	2947·25	2947·34	3307·07		3310·43					
12	2896·70	2896·76	2899·73	2899·88	3301·58		3299·72					
	2895·65	2895·60	2899·06	2899·12	3289·84		3293·29					
13	2848·15	2848·17	2850·85	2850·86	3284·54		3282·53					
	2846·82	2846·82	2849·82	2850·01	3271·05		3274·61					
14	2798·77	2798·71	2801·10	2801·05	3267·27		3263·96					
	2797·28	2797·28	2800·04	2797·28	3250·75		3254·53					
15	2748·42	2748·55	2750·75	2750·56								
	2746·87	2747·03	2749·45	2749·46								
16	2697·44	2697·44	2699·38	2699·48								
	2695·94	2696·02	2698·19	2698·20								
17	2645·89	2646·15	2647·56	2647·58								
	2644·19	2644·30	2646·22	2646·15								
18	2593·55		2595·05	2595·29								
	2591·96	2591·94	2593·82	2593·84								
19	2540·85	2540·84	2542·27	2542·27	2542·32							
	2538·98	2539·23	2540·68	2540·84								
20	2487·45	2487·40	2488·59									
	2485·52	2485·67	2487·27	2487·40								
21	2433·68	2433·60	2434·76	2434·80								
	2431·49		2433·08									
22												

• Partially H_2O

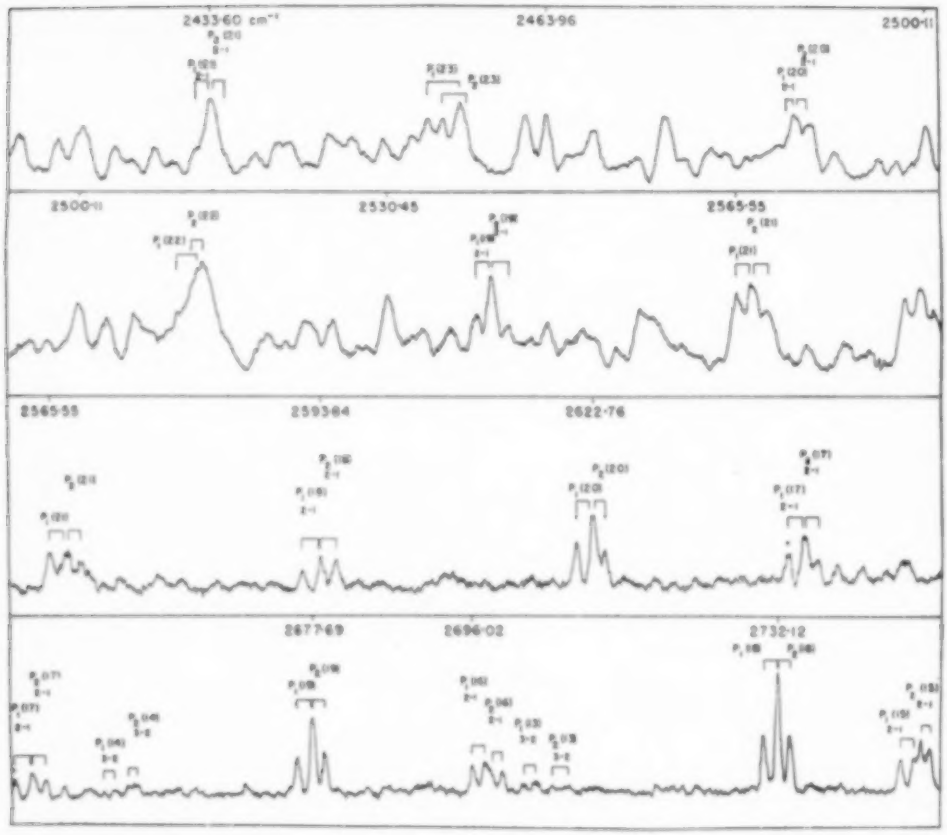

Fig. 4. The emission spectrum of the flame from 2400 to 2750 cm^{-1}, showing a continuation of the P branches at smaller wave numbers.

References

[1] PLYLER EARLE K. *J. Research, Natl. Bur. Standards* 1948 **40** 113.
[2] PLYLER EARLE K., and BALL J. J. *J. Chem. Phys.* 1952 **20** 1178.
[3] PLYLER E. K., BLAINE L. R., and CONNOR W. S. *J. Opt. Soc. Amer.* 1955 **45** 102.
[4] DIEKE G. H. and CROSSWHITE H. M. *Bumblebee Report* No. 87. Johns Hopkins University, 1948.
[5] HERZBERG G. *Spectra of Diatomic Molecules* p. 560. Van Nostrand, New York, 1950.

VOL. 9 1957

Spectrochimica Acta, 1957, Vol. 9, pp. 133 to 147. Pergamon Press Ltd., London

Vibrational band shapes and band intensities

R. A. Russell* and H. W. Thompson
The Physical Chemistry Laboratory, Oxford

(*Received 5 February* 1957)

Abstract—The influence of spectrometer slit-widths upon the shapes of some vibrational absorption bands has been examined. The apparent band widths, apparent extinction coefficients at band peaks, and integrated band areas were measured under different conditions. The relative significance of extinction coefficients and integrated intensities for quantitative work has been considered, and some general conclusions have been drawn about the difficulties of applying the convenient procedures previously worked out by Ramsay for determining the true band intensities.

The accurate determination of the positions (frequencies) of vibrational absorption bands now presents no great difficulty, and their use for qualitative analysis and for structural diagnosis is firmly established. The intensity of an absorption band is another property of comparable significance, for it is not only required as a basis for most quantitative analysis but it may also provide structural information about atomic groupings and the polar characteristics of individual bands [1].

At present there is some uncertainty about the accurate determination of band intensities, and it is not clear how far they can be used in diagnostic work. In most quantitative analysis it has been customary to use the extinction coefficients at band peaks. However, the value for a given band as measured in different laboratories is often very different, and it is not yet possible to lay down acceptable reference data for common use. The difficulty arises mainly through variations in instrumental factors which markedly affect the band shapes and "apparent" peak optical densities, and which to some extent are difficult to control.

It is therefore desirable to determine the experimental conditions which are necessary for obtaining reliable and reproducible values for the intensities, so that detailed calibrations by individual laboratories may be avoided. Specifically, the question is whether it is possible under normal working conditions to use the peak-extinction coefficients at all, or whether the integrated true band intensities must be determined.

As far as structural diagnosis is concerned, much essential information about band intensities is still lacking. For example, it is still not known how far they can be used to characterize particular types of a chromophore, or to estimate the number of groups of a given kind in a compound, although some progress has been made in both these directions [1, 2, 3]. In fact, a survey of vibrational band intensities is needed, along the same lines as the empirical survey of vibrational frequencies which led previously to the structural correlation rules. It is also possible that the inherent relationship between the electrical characteristics

* Now at Imperial Chemical Industries Ltd., Alkali Division, Northwich, Cheshire.

of molecular vibrations and the band intensities may in certain circumstances lead to correlations between these intensities and the reactivity of certain groups.

During the course of a larger programme of work on band intensities we have obtained some data which are relevant to the general problem of band shapes, and to the significance of experimental conditions. The main instrumental factor which affects the values of the extinction coefficients at the band peaks is the finite spectrometer slit-width, and its value in relation to the intrinsic width of the bands. The standard absorption law,

$$I = I_0 e^{-\alpha c l}$$

applies strictly only for monochromatic radiation, whereas it is necessary in most infra-red work to use slit-widths which pass a comparatively large band of wavelengths. In consequence, the band contour is affected, and intensity measurements are complicated by the slit function. We have therefore first examined the effect of slit-widths upon the widths and shapes of some absorption bands. Several vibration bands of a number of molecules in the pure liquid phase, in solution and in solid layers, have been studied, using both grating and prism spectrometers to obtain a large range of slit-widths.

The prism spectrometer was a Perkin-Elmer 12C model, with prisms of rock-salt, potassium bromide, and lithium fluoride. The grating spectrometer has been described elsewhere [4]. It is necessary to calculate the "effective" slit-width for the actual working conditions from the mechanical slit-widths and general instrumental properties and geometry. This problem has been discussed by Williams [5] and by Brodersen [6], but it is still not satisfactorily settled. It is usually accepted that for a prism spectrometer with Littrow mounting, the effective slit $s = s_g + s_0$, the first term arising from the finite slits and the second from the diffraction effects. Further, it has been assumed that, in the terminology of Williams,

$$s_g = \frac{v^2 \sqrt{\left(1 - n^2 \sin^2 \frac{\alpha}{2}\right)}}{4 \sin^2 \frac{\alpha}{2} \cdot \frac{dn}{d\lambda}} \cdot \frac{s}{f}$$

and

$$s_0 = F(s) \cdot \frac{v}{2b \cdot \frac{dn}{d\lambda}}$$

There is some doubt about the exact value of $F(s)$, but for our present work it was taken as 0·85. In fact, however, it must be realized that the true value of s will be greater than $(s_g + s_0)$ by an indeterminate amount arising from instrumental imperfections of slit-misalignment. For the present, this factor, which has been denoted as ϕ by Jones and Sandorfy [3], has been neglected.

For the grating spectrometer, s_g was calculated from a corresponding relation set up for the particular optical arrangement and grating properties, and s_0 from $0{\cdot}85v/mN$, in which N is the total number of rulings and m the spectral order.

The results for some liquids and thin solid layers are given in Table 1. The

VOL. 9 1957

Table 1. S and $\Delta\nu^a_{1/2}$ are given in cm^{-1}
$\varepsilon^a_{max} = \log (T_0/T)_{max}$

(a) *Cyclohexane*. Liquid 0·00646 cm

Band 903 cm^{-1} Extrapolated $\Delta\nu^l_{1/2} = 5{\cdot}0\ cm^{-1}$			Band 861 cm^{-1} Extrapolated $\Delta\nu^l_{1/2} = 9{\cdot}5\ cm^{-1}$		
S	$\Delta\nu^a_{1/2}$	ε^a_{max}	S	$\Delta\nu^a_{1/2}$	ε^a_{max}
Grating			Grating		
0·46	5·02	1·12	0·42	9·59	1·04
0·9	5·23	1·10	0·82	9·77	0·95
1·34	5·33	1·08	1·22	9·68	0·95
1·79	5·64	1·01	1·63	9·63	0·94
2·24	6·05	0·93	2·04	9·80	0·93
Prism			Prism		
2·0	5·8	1·07	1·9	10·1	0·98
3·6	6·6	0·92	3·1	10·3	0·93
5·5	7·4	0·80	4·5	10·9	0·88
6·9	8·8	0·68	6·0	11·4	0·82
9·6	11·7	0·54	8·4	13·1	0·75
12·3	14·5	0·44	10·7	15·2	0·65
15·2	18·4	0·39	13·2	17·1	0·58
18·1	20·2	0·34	15·5	19·1	0·52
20·8	23·2	0·31	18·0	21·0	0·48
23·4	25·5	0·28	20·3	22·6	0·45

(b) *Acetonitrile*. Liquid 0·00646 cm

Band 750 cm^{-1} Extrapolated $\Delta\nu^l_{1/2} = 15{\cdot}60\ cm^{-1}$			Band 861 cm^{-1} Extrapolated $\Delta\nu^l_{1/2} = 7{\cdot}4\ cm^{-1}$		
S	$\Delta\nu^a_{1/2}$	ε^a_{max}	S	$\Delta\nu^a_{1/2}$	ε^a_{max}
Grating			Grating		
0·32	5·60	0·38	0·47	7·51	1·00
0·62	15·67	0·35	0·92	7·26	0·99
0·94	15·56	0·37	1·39	7·62	0·93
1·25	15·58	0·37	1·85	7·96	0·90
1·56	15·50	0·37	2·31	8·01	0·88

VOL. 9 1957

Table 1 (*continued*)

(c) 2·4 *Dimethyl pentane*. Liquid 0·00646 cm

Band 919 cm^{-1} Extrapolated $\Delta\nu^{i}_{1/2}$ = 8·8 cm^{-1}			Band 986 cm^{-1} Extrapolated $\Delta\nu^{i}_{1/2}$ = 7·5 cm^{-1}		
S	$\Delta\nu^{a}_{1/2}$	ε^{a}_{max}	S	$\Delta\nu^{a}_{1/2}$	ε^{a}_{max}
Grating			Grating		
0·93	8·86	0·31	1·07	7·69	0·37
1·39	9·06	0·31	1·60	8·11	0·36
1·86	9·11	0·31	2·14	8·70	0·34
2·32	9·35	0·29	2·67	9·53	0·34
Prism			Prism		
2·1	10·3	0·32	2·6	8·2	0·35
3·7	11·0	0·30	4·6	9·2	0·32
5·7	11·7	0·28	6·8	10·8	0·30
7·1	12·6	0·26	8·5	12·3	0·27
7·1	12·7	0·25	8·5	12·2	0·25
10·0	14·6	0·23	12·1	15·7	0·21
12·8	17·6	0·20	15·7	19·3	0·18
15·8	20·8	0·17	19·4	22·6	0·16
18·8	21·9	0·16	22·9	26·1	0·14
21·6	23·8	0·15	26·3	28·5	0·13
24·3	25·9	0·14	29·7	31·6	0·12

(d) *Methylene chloride*. Liquid 0·00646 cm

Band 896 cm^{-1} Extrapolated $\Delta\nu^{i}_{1/2}$ = 9·2 cm^{-1}		
S	$\Delta\nu^{a}_{1/2}$	ε^{a}_{max}
Grating		
0·45	9·34	0·54
0·88	9·25	0·53
1·32	9·40	0·52
1·76	9·96	0·50
2·20	9·80	0·50

(e) *Diphenyl*. Solid film

Band 904 cm^{-1} Extrapolated $\Delta\nu^{i}_{1/2}$ = 6·0 cm^{-1}		
S	$\Delta\nu^{a}_{1/2}$	ε^{a}_{max}
Grating		
0·90	6·12	0·28
1·36	6·26	0·27
1·81	6·28	0·26
2·26	6·81	0·24

VOL. 9 1957

Table 1 (*continued*)

(f) *Naphthalene.* Solid film

Band 981 cm^{-1} Extrapolated $\Delta\nu^{i}_{1/2} = 2{\cdot}5$ cm^{-1}			Band 1009 cm^{-1} Extrapolated $\Delta\nu^{i}_{1/2} = 1{\cdot}8$ cm^{-1}		
S	$\Delta\nu^{a}_{1/2}$	ε^{a}_{max}	S	$\Delta\nu^{a}_{1/2}$	ε^{a}_{max}
Grating			Grating		
0·42	2·74	0·23	0·43	2·08	0·52
0·54	3·26	0·22	0·57	2·08	0·52
1·06	3·45	0·19	1·12	2·84	0·41
1·59	4·18	0·16	1·68	3·54	0·33
2·12	4·49	0·15	2·24	4·35	0·29
2·65	5·16	0·13	2·80	4·93	0·26

(g) *"Impurity" band at 588 cm^{-1} in potassium bromide disc*
Extrapolated $\Delta\nu^{i}_{1/2} = 0{\cdot}7$ cm^{-1}

S	$\Delta\nu^{a}_{1/2}$	ε^{a}_{max}	S	$\Delta\nu^{a}_{1/2}$	ε^{a}_{max}
Grating					
0·21	0·84	0·55	1·4	2·3	0·20
0·30	0·85	0·49	2·3	3·6	0·14
0·39	1·06	0·45	3·1	4·7	0·10
0·58	1·20	0·38	3·1	4·6	0·10
0·77	1·42	0·30	4·2	5·5	0·08
0·97	1·55	0·27	4·9	6·3	0·07

apparent half-band widths $\Delta\nu^{a}_{1/2}$ (width at half-peak optical density), and peak optical densities $\log (T_0/T)_{max}$ are given for different calculated effective slit-widths. Typical data are plotted in Figs. 1a, 1b. It is seen that $\Delta\nu^{a}_{1/2}$ is markedly dependent upon s, and by extrapolation to $s = 0$ the values of $\Delta\nu^{i}_{1/2}$ are obtained. The true half-band widths differ considerably in value, even among different vibrations of the same molecule. The intrinsically narrower bands are, as might be expected, rather more sensitive to changes in slit-widths than the broader bands. For values of $s \geqq \Delta\nu^{i}_{1/2}$, the apparent half band width is roughly proportional to s with a proportionality factor close to unity. More significant of all, perhaps, is the result that if the observed band is to have a half-width close to its limiting true value $\Delta\nu^{i}_{1/2}$, the calculated effective slit-width must not exceed about one fifth of $\Delta\nu^{i}_{1/2}$. With pure liquids or solutions, limiting half-band widths

as small as 5 cm^{-1} are found. Hence the limiting conditions for measurement will not be obtained in general, unless the effective spectrometer slits are 1 cm^{-1} or less. With solids, when the bands are often intrinsically sharper, very narrow slits will be necessary.

The variation of peak optical density ε^a_{max} with slit-width follows a similar trend, shown typically in Fig. 2. As the actual slit-width is diminished gradually

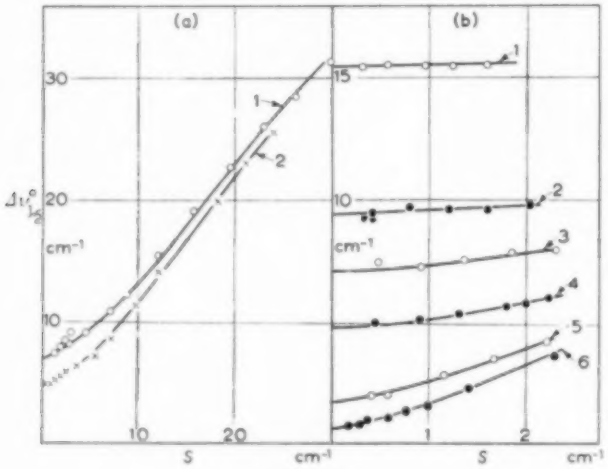

Fig. 1.

(a) Plots of $\Delta\nu^a_{1/2}$ against calculated slit-width: (1) 2·4 dimethylpentane 986 cm^{-1}, (2) cyclohexane 903 cm^{-1}.

(b) Plots of $\Delta\nu^a_{1/2}$ against calculated slit-width: (1) acetonitrile 750 cm^{-1}, (2) cyclohexane 861 cm^{-1}, (3) acetonitrile 918 cm^{-1}, (4) cyclohexane 903 cm^{-1}, (5) naphthalene 1009 cm^{-1}, (6) bromide disc impurity 588 cm^{-1}.

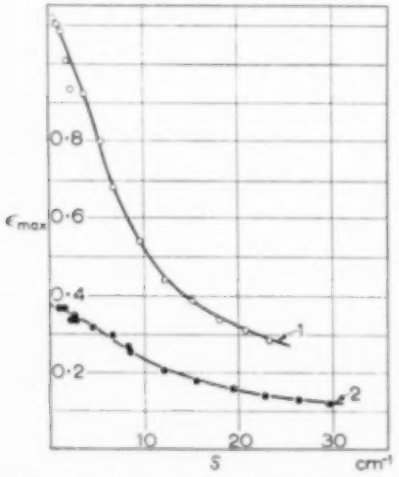

Fig. 2. Plots of ε^a_{max} against calculated slit-width: (1) cyclohexane 903 cm^{-1}, (2) 2·4 dimethyl pentane 986 cm^{-1}.

VOL. 9 1957

Table 2. Diphenylamine in carbon tetrachloride. Path-length 2 cm. Band at 3434 cm^{-1}. Extrapolated $\Delta\nu^{i}_{1/2} = 24{\cdot}5\ cm^{-1}$. B in cm^2 molecule^{-1} sec^{-1} ($\log_e$), E^{a}_{max} in cm^2 $mole^{-1}$ ($\log_{10}$)

Slit (cm^{-1})	c (molar)	$B \times 10^7$	$\log (T_0/T)_{max}$	$E^{a}_{max} \times 10^{-5}$	$\Delta\nu^{a}_{1/2}$
8·5	0·00268	2·29	0·314	0·585	25·0
	0·00444	2·24	0·519	0·584	27·2
	0·00222	2·17	0·263	0·593	25·3
	0·00682	2·18	0·781	0·573	25·1
	0·00341	2·15	0·395	0·579	25·2
	0·00460	2·19	0·525	0·571	25·8
	0·00745	2·15	0·834	0·559	25·5
	0·00324	2·19	0·366	0·565	25·8
	0·00352	2·17	0·397	0·564	25·7
	0·00627	2·22	0·708	0·565	25·6
	0·00158	2·26	0·183	0·579	26·7
13·9	0·00460	2·14	0·496	0·540	26·8
	0·00745	2·08	0·777	0·521	26·4
	0·00324	2·15	0·352	0·544	27·1
	0·00157	2·25	0·174	0·558	27·3
	0·00352	2·23	0·382	0·542	27·0
	0·00627	2·11	0·663	0·529	26·7
	0·00158	2·26	0·176	0·557	27·6
23·2	0·00460	2·12	0·434	0·472	30·6
	0·00745	2·07	0·682	0·457	30·0
	0·00324	2·18	0·307	0·474	31·0
	0·00157	2·20	0·156	0·497	31·8
	0·00627	2·08	0·581	0·463	30·2
	0·00158	2·24	0·157	0·497	31·9
44·4	0·00460	1·99	0·308	0·335	43·4
	0·00745	1·84	0·466	0·313	42·6
	0·00324	2·07	0·222	0·343	43·6
	0·00157	2·17	0·114	0·363	45·3
	0·00627	1·93	0·403	0·321	42·5
5·8	0·00460	—	0·530	0·576	25·5
	0·00745	—	0·832	0·558	25·5
	0·00324	—	0·385	0·594	25·3
	0·00157	—	0·186	0·593	25·4
	0·00352	—	0·410	0·582	25·3
	0·00627	—	0·699	0·557	25·6
	0·00158	—	0·188	0·595	26·1
11·1	0·00460	—	0·513	0·558	26·1
	0·00745	—	0·810	0·543	25·8
	0·00324	—	0·362	0·559	26·9
	0·00157	—	0·182	0·580	26·6
	0·00352	—	0·393	0·580	26·6
	0·00627	—	0·680	0·542	26·7
	0·00158	—	0·179	0·567	26·8

Table 2 (*continued*)

Slit (cm^{-1})	c molar	$B \times 10^7$	$\log (T_0 T)_{max}$	$E^a_{max} \times 10^{-8}$	$\Delta\nu^a_{1/2}$
17·8	0·00460	—	0·476	0·518	28·7
	0·00745	—	0·746	0·500	27·7
	0·00324	—	0·338	0·522	28·3
	0·00157	—	0·171	0·545	30·0
	0·00627	—	0·628	0·501	28·0
	0·00158	—	0·168	0·532	28·4
33·8	0·00460	—	0·359	0·390	37·2
	0·00745	—	0·559	0·375	35·8
	0·00324	—	0·265	0·409	38·3
	0·00157	—	0·137	0·437	37·5
	0·00215	—	0·184	0·428	37·9
	0·00627	—	0·478	0·381	35·8
	0·00158	—	0·134	0·426	38·2

from very large values, $\varepsilon_{max}{}^a$ at first increases slowly, then more rapidly, finally reaching a limiting value when s is less than about $\frac{1}{2}\Delta\nu'_{1/2}$. The data suggest that, in general, the following relations apply:

$$s = \Delta\nu'_{1/2}, \qquad \varepsilon^a_{max} = 0{\cdot}62\ \varepsilon^{limit}_{max}$$

and for $$s = 1/2\ .\ \Delta\nu'_{1/2}, \qquad \varepsilon^a_{max} = 0{\cdot}82\ \varepsilon^{limit}_{max}$$

in which $$\varepsilon^{limit}_{max} = \lim_{s \to 0} \varepsilon^a_{max}$$

Thus, if the values of $\Delta\nu'_{1/2}$, were known for a given band, it might be possible to calculate the limiting value of ε_{max} without actually using very narrow slit-widths.

Similar measurements were made with solutions. Tables 2 and 3 give data for the fundamental N-H stretching vibration band with solutions of diphenylamine and indole in carbon tetrachloride.

Fig. 3a shows plots, for diphenylamine, of the apparent half-band widths as a function of slit-widths for three different concentrations. When the slits are fairly wide, $\Delta\nu^a_{1/2}$ is somewhat dependent upon c at a given slit-width, but as the slit-width approaches very small values the apparent half-band width approaches the same value for all concentrations. The same point is demonstrated by the plots of Fig. 3b, which show $\Delta\nu^a_{1/2}$ as a function of concentration for each of a number of slit-widths.

A result of perhaps more direct significance for analytical measurements is shown by Fig. 3c, in which the molecular extinction coefficient ε^a_{max} is plotted as a function of concentration for each of a number of slit-widths. These plots show that the extrapolated value of E^a_{max} at $c = 0$ depends markedly upon the value of the slit-widths, and only when the latter is very small does this extrapolated measure of E_{max} reach its limiting value. The plots illustrate clearly

VOL. 9 1957

Table 3. Indole in carbon tetrachloride. Path-length 2 cm. Band at 3490 cm^{-1}. Extrapolated $\Delta\nu^{l}_{1/2} = 11{\cdot}0\ cm^{-1}$. B in cm^2 $molecule^{-1}$ sec^{-1} ($\log_e$), E^{a}_{max} in cm^2 $mole^{-1}$ ($\log_{10}$)

Slit (cm^{-1})	c (molar)	$B \times 10^7$	$\log (T_0/T)_{max}$	$E^{a}_{max} \times 10^{-5}$	$\Delta\nu^{a}_{1/2}$
6·0	0·00237	5·10	1·093	2·31	12·7
	0·00160	5·56	0·782	2·44	12·7
	0·00079	5·97	0·428	2·70	12·5
	0·00032	6·21	0·190	2·93	12·6
	0·00151	5·28	0·750	2·48	12·5
	0·00065	6·39	0·369	2·84	12·5
	0·00309	4·85	1·296	2·09	13·1
	0·00038	6·46	0·231	3·02	13·1
	0·00096	5·74	0·519	2·71	12·3
	0·00177	5·20	0·870	2·45	12·5
	0·00089	—	0·492	2·76	12·5
	0·00046	—	0·279	3·00	12·5
	0·00024	—	0·153	3·12	12·6
8·6	0·00271	4·56	1·087	2·00	13·3
	0·00217	4·81	0·926	2·14	14·0
	0·00157	5·30	0·744	2·37	14·0
	0·00126	5·55	0·614	2·44	14·0
	0·00054	6·20	0·293	2·70	14·0
	0·00063	6·04	0·333	2·65	14·0
	0·00237	5·09	0·994	2·10	13·7
	0·00160	5·39	0·742	2·31	13·2
	0·00079	5·63	0·400	2·52	13·6
	0·00032	6·57	0·180	2·78	14·1
	0·00151	5·45	0·701	2·32	13·6
	0·00065	6·09	0·338	2·60	13·6
	0·00310	4·92	1·176	1·90	14·7
	0·00038	6·46	0·215	2·81	14·5
	0·00096	5·62	0·482	2·51	13·6
	0·00177	5·09	0·788	2·22	13·6
	0·00089	—	0·454	2·54	13·3
	0·00046	—	0·260	2·80	13·7
	0·00024	—	0·140	2·86	—
11·4	0·00237	4·87	0·890	1·88	15·4
	0·00160	5·37	0·668	2·08	15·3
	0·0079	5·71	0·364	2·29	15·3
	0·00032	6·13	0·162	2·50	15·4
	0·00151	5·29	0·636	2·11	15·4
	0·00065	5·99	0·311	2·40	15·4
	0·00310	4·64	1·093	1·76	15·4
	0·00038	6·23	0·199	2·60	15·3
	0·00096	5·64	0·440	2·29	15·2
	0·00177	4·92	0·720	2·03	15·0
	0·00089	—	0·410	2·30	14·9
	0·00046	—	0·231	2·48	15·2
	0·00024	—	0·127	2·60	—

Table 3 (*continued*)

Slit (cm^{-1})	c (molar)	$B \times 10^7$	$\log (T_0/T)_{max}$	$E^a_{max} \times 10^{-5}$	$\Delta\nu^a_{1/2}$
18·4	0·00237	4·67	0·694	1·46	19·7
	0·00160	5·18	0·528	1·64	19·6
	0·00079	5·59	0·299	1·88	19·5
	0·00032	6·43	0·137	2·14	20·2
	0·00151	5·26	0·505	1·67	19·6
	0·00065	6·04	0·250	1·93	19·7
	0·00310	4·42	0·847	1·37	20·1
	0·00038	6·06	0·164	2·15	19·2
	0·00096	5·42	0·352	1·84	19·4
	0·00177	4·72	0·563	1·59	19·3
	0·00089	—	0·330	1·85	19·2
	0·00046	—	0·190	2·04	19·7
	0·00024	—	0·107	2·18	—
(in 5·39-cm path)					
	0·00080	4·47	0·662	1·54	—
	0·00088	4·43	0·696	1·47	—
	0·00043	5·19	0·419	1·80	—
	0·00051	5·04	0·475	1·73	—
	0·00026	5·73	0·238	1·99	—
	0·00020	5·73	0·220	2·03	—
4·0	0·00310	—	1·376	2·22	12·0
	0·00028	—	0·236	3·09	11·9
	0·00096	—	0·530	2·76	11·5
	0·00177	—	0·857	2·42	12·2
	0·00089	—	0·482	2·70	12·0
	0·00046	—	0·290	3·12	12·1
	0·00024	—	0·155	3·16	—
14·3	0·00310	—	0·956	1·54	17·9
	0·00038	—	0·182	2·38	16·6
	0·00096	—	0·407	2·12	16·8
	0·00177	—	0·648	1·83	16·1
	0·00089	—	0·378	2·12	16·9
	0·00046	—	0·214	2·30	17·3
24·0	0·00310	—	0·696	1·12	24·6
	0·00038	—	0·142	1·87	24·5
	0·00096	—	0·287	1·50	22·1
	0·00177	—	0·476	1·34	24·4
	0·00573	—	1·000	0·87	26·6
	0·00429	—	0·853	0·99	24·8
	0·00089	—	0·280	1·57	24·7
	0·00046	—	0·166	1·78	24·5
	0·00024	—	0·094	1·92	—

VOL. 9 1957

Table 3 (*continued*)

Slit (cm^{-1})	c (molar)	$B \times 10^7$	$\log (T_0/T)_{max}$	$E^a_{max} \times 10^{-5}$	$\Delta\nu^a_{1/2}$
34·9	0·00310	—	0·523	0·84	33·3
	0·00038	—	0·106	1·39	33·3
	0·00096	—	0·218	1·14	31·7
	0·00177	—	0·349	0·98	32·1
	0·00573	—	0·755	0·66	34·1
	0·00089	—	0·210	1·18	32·5
	0·00046	—	0·123	1·32	32·4
	0·00024	—	0·073	1·49	—
45·8	0·00310	—	0·408	0·66	41·1
	0·00038	—	0·087	1·14	42·5
	0·00096	—	0·180	0·94	38·9
	0·00177	—	0·280	0·79	40·0
	0·00573	—	0·603	0·53	41·6
	0·00089	—	0·170	0·95	40·2
	0·00046	—	0·101	1·09	40·9
	0·00024	—	0·058	1·18	—

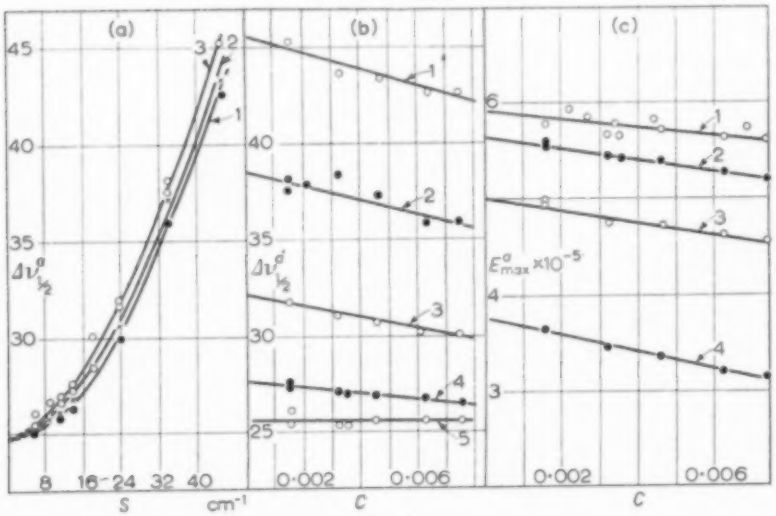

Fig. 3.

(a) Plots of $\Delta\nu^a_{1/2}$ against calculated slit-width for diphenylamine (ν_{NH}): (1) 0·0075 molar, (2) 0·0046 molar, (3) 0·0016 molar in carbon tetrachloride.

(b) Plots of $\Delta\nu^a_{1/2}$ against concentration for diphenylamine solutions at different slit-widths: (1) 44·4 cm^{-1}, (2) 33·8 cm^{-1}, (3) 23·2 cm^{-1}, (4) 13·9 cm^{-1}, (5) 5·8 cm^{-1}.

(c) Plot of molecular extinction coefficient for diphenylamine solutions as a function of concentration, at different slit-widths: (1) 8·5 cm^{-1}, (2) 13·9 cm^{-1}, (3) 23·2 cm^{-1}, (4) 44·4 cm^{-1}.

why values of E_{max}, determined arbitrarily without special care in the choice of slit-widths, even after extrapolation to zero concentration, will usually be unsatisfactory for universal use.

Now, if certain conditions are fulfilled, Wilson and Wells [7] have shown that the true band intensity A can be obtained as the limiting value of B, where

$$A = \lim_{cl \to 0} B = \lim_{cl \to 0} \frac{1}{cl} \int \ln (T_0/T)_\nu \, . \, d\nu$$

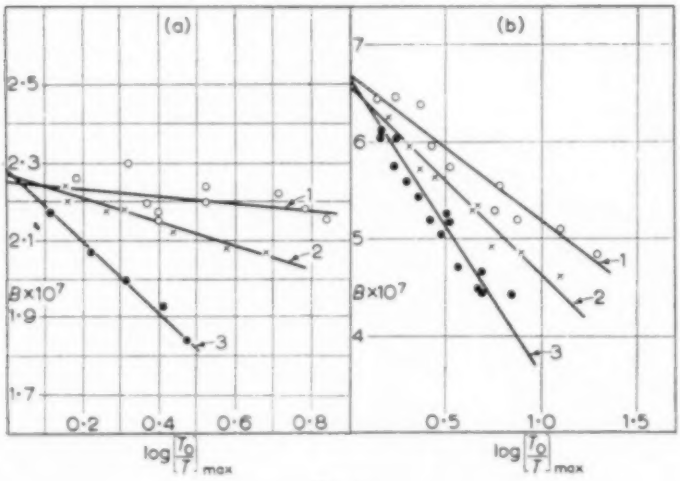

Fig. 4.

(a) Diphenylamine (ν_{NH}). Plots of B against log $(T_0/T)_{max}$ for different slit-widths; (1) 8·5 cm^{-1}, (2) 23·2 cm^{-1}, (3) 44·4 cm^{-1}.
(b) Indole (ν_{NH}). Plots of B against log $(T_0/T)_{max}$ for slit-widths: (1) 6·0 cm^{-1}, (2) 11·4 cm^{-1}, (3) 18·4 cm^{-1}.

More conveniently, the extrapolation of B can be carried out as a function of apparent optical density ln $(T_0/T)_{max}$, according to the relation discussed by Ramsay [8], namely,

$$B = A + A\theta \ln(T_0/T)_{max}$$

Fig. 4a shows plots of B against $\log(T_0/T)_{max}$ for three different slit-widths in the case of diphenylamine. It is seen that all three lines lead to almost the same value of the intercept A. Fig. 4b shows similar plots for the solutions of indole. In both the examples shown, the extrapolated values of A obtained from the measurements at different slit-widths agree to within a few per cent. The data for other slit-widths are not plotted in Fig. 4 but a least-squares treatment leads to values of the intercept A which agree very closely.

The plots of Fig. 4 can also be used to derive values or θ in the above equation, and these are listed in Table 4.

Fig. 5 shows how these derived values of θ compare with the values predicted by Ramsay on the basis of a Lorentz band contour and the slit function adopted by him. In making this comparison, it must be remembered that the calculated

VOL. 9 1957

Table 4

	s (cm^{-1})	$s/\Delta\nu'_{1/2}$	$A \times 10^7$	$2{\cdot}303A\theta$	$-\theta$
(a) Diphenylamine	8·5	0·34	2·25	0·10	0·019
	13·9	0·56	2·28	0·26	0·05
	23·2	0·94	2·27	0·32	0·06
	44·4	1·8	2·26	0·93	0·18
(b) Indole	6·0	0·54	6·78	1·7	0·10
	8·6	0·78	6·80	1·98	0·125
	11·4	1·03	6·58	1·9	0·125
	18·4	1·7	6·70	3·05	0·19

experimental slit-widths may have been in error by the unknown amount mentioned earlier. The value of θ found for the band of diphenylamine agree satisfactorily with RAMSAY'S computations, but those for indole deviate noticeably. It may be noted that with indole the band is intrinsically much narrower, and there are also signs of a shoulder on the lower frequency side. The sharper nature of the band implies a more rapid change of the absorption coefficient across the

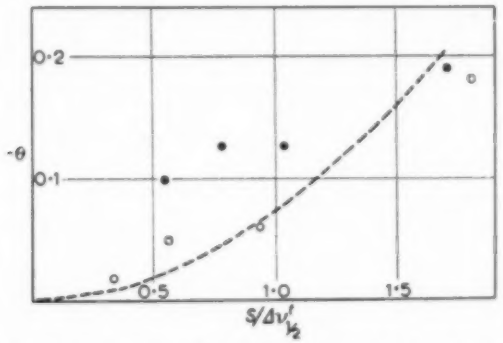

Fig. 5. Plot of θ, determined and predicted from RAMSAY'S data, as function of $S/\Delta\nu_{1/2}$.
○ Diphenylamine, ● Indole.

width of slit, and this may be relevant to the basic assumption made in the Wilsen Wells method of extrapolation. The assumption of a Lorentz band shape is also uncertain, for apart from the inherent form of the true functions for this shape, the presence of underlying "hot" transitions on other bands appears often to cause asymmetry, the precise reason for which is difficult to determine in a given case. Some earlier results of PHILPOTTS, THAIN, and SMITH [9] also suggest that the discrepancy between the calculated and measured values of θ may arise in other cases.

It may be desirable to summarize the main conclusions reached from the above work.

(1) The intrinsic true half-band widths of different vibration bands differ

considerably, not only as between different types of vibration of the same molecule, but also as between the corresponding vibration of a given group in different molecules. The factors which control these band widths have not yet been disentangled, but it seems possible that, when more information becomes available, the widths may also be useful for structural determinations. Recently, some variations of band widths in a related series of molecules have been examined by Orr [10].

(2) It seems probable that if the extinction coefficients at band peaks are to be used for quantitative work, the slit-widths employed must be at least five times smaller than the true half-band widths (widths at half-peak optical density). This means that when liquids or solutions are being studied, the spectrometer slit-widths must be 1 cm^{-1} or less. With most prism spectrometers working under normal conditions, the "true" limiting values of E_{max} will not be obtainable by extrapolation procedures.

(3) The integrated band areas A, on the other hand, may be satisfactorily determined by a Wilsen Wells extrapolation method for bands which are not specifically complicated by overlap, using any normal slit-width. With spectrometers which present a spectral record which is linear in wave numbers, automatic mechanical or electrical integrating devices can be built, and we have for some time used such a mechanical device based upon a ball-disc integrater quite satisfactorily.

(4) Quick methods have been suggested by Ramsay [8] for determining the true intensities A from single measurements made with a normal working slit-width. On the basis of a Lorentz band shape, $A = K \,.\, E^a_{max} \,.\, \Delta\nu^a_{1/2}$, and values of K can be used according to the apparent peak density log $(T_0/T)_{max}$ and the ratio $S/\Delta\nu^i_{1/2}$. Alternatively, a value of θ can be adopted according to the value of $S/\Delta\nu^i_{1/2}$. While these relations may be applicable in some cases, it seems that they must be used with much caution, for the assumption of a Lorentz band shape is uncertain, and an exact evaluation of the ratio $S/\Delta\nu^i_{1/2}$ is also difficult for reasons explained above. Further, the frequent occurrence of overlapping bands giving rise to shoulders, complicates the problem.

More measurements designed to examine band shapes and to extend our knowledge of the factors relevent to intensity determinations are needed, and the values for the intrinsic band intensities and also for the true half-band widths should prove useful in structural investigations.

Acknowledgement—We are grateful to the Hydrocarbon Research Group of the Institute of Petroleum for financial support, and to the Department of Scientific and Industrial Research for a maintenance allowance to one of us (R. A. R.)

References

[1] Thompson H. W. *Molecular Spectra* p. 94. Institute of Petroleum 1955.
[2] Russell R. A. and Thompson H. W. *J. Chem. Soc.* 1955 483; *Proc. Roy. Soc.* 1956 **A234** 318.
[3] Jones R. N. and Sandorfy C. *Techniques of Organic Chemistry* Vol. IX; *Chemical Applications of Spectroscopy* Chap. IV. Interscience, New York 1956.
[4] Miller C. H. and Thompson H. W. *Proc. Roy. Soc.* 1949 **A200** 1.

VOL. 9 1957

[5] Williams V. Z. *Rev. Sci. Instrum.* 1948 **19** 135.
[6] Brodersen S. *J. Opt. Sci. Amer.* 1953 **43** 877, 1216; 1954 **44** 22.
[7] Wilson E. B. and Wells A. J. *J. Chem. Phys.* 1946 **14** 578.
[8] Ramsay D. A. *J. Amer. Chem. Soc.* 1952 **74** 72.
[9] Philpotts A. R., Thain W., and Smith P. G. *Analyt. Chem.* 1951 **23** 268.
[10] Orr S. F. D. *Spectrochim. Acta* 1956 **8** 218.

OL.
9
57

Spectrochimica Acta, 1957, Vol. 9, pp. 148 to 156. Pergamon Press Ltd., London

Theory of radiant-energy absorption by randomly dispersed discrete particles*

JOHN W. OTVOS, HENRY STONE, and W. R. HARP JR.
Shell Development Company, Emeryville, California

(*Received* 15 *August* 1956)

Abstract—By the application of simple laws of probability, an expression is derived for the absorption of radiant energy by randomly dispersed, discrete particles in a non-absorbing medium. For spherical particles of diameter, d, and density, ρ, the transmittance is given by

$$\frac{I}{I_0} = e^{-a(1-\theta)}, \qquad a = 3cl/2\rho d$$

where c is the mass of sample per unit volume of the system, l is the thickness of the system, ρ is the density of the particles, and θ is the transmittance of a single particle averaged over all trajectories of a ray through the particle. The absorbance is then given by

$$\ln \frac{I_0}{I} = \frac{3cl}{2\rho d}(1-\theta)$$

From the last expression, it is seen that the absorbance is proportional to both concentration and thickness for uniform particle size. Thus the derived absorption law is exactly consistent with BEER's law, the linear absorptivity being given by

$$k_d = \frac{3(1-\theta)}{2d}$$

The present treatment is compared to previously published treatments of the absorption by discrete particles and errors in the previous treatments are discussed. The relationships derived here have been experimentally tested, using quartz particles of uniform size with the aid of the KBr pressed-plate technique. The difficulties of making quantitative applications of theoretical absorption laws to infra-red data are discussed in light of the MIE theory.

1. Introduction

THERE have been a number of attempts to treat theoretically the problem of radiant-energy absorption by discrete particles randomly dispersed in a non-absorbing medium [1, 2, 3]. Although certain aspects of these treatments have agreed with experiments designed to show the interdependence of particle size and absorbance, the derivations of the theories themselves are incorrect in principle, since it is assumed that the absorbing system may be divided into layers in which the particles are close-packed. It is the purpose of this paper to show in what way they are incorrect, and to present a new and consistent treatment of the subject.†

In 1926, Soos [1] tried to account for results he obtained on gold sols by a theory

* Presented in part by W. R. HARP JR. at the Pittsburgh Conference on Analytical Chemistry and Applied Spectroscopy March 1954.

† Since this paper was prepared for publication an article has appeared by L. N. M. DUYSENS *Biochimica et Biophysica Acta* **19**, 1, 1956, which treats the problem in a similar way but with a different emphasis on applications.

VOL. 9 1957

in which he considered the solution to be made up of layers, each of which contained just enough particles to give a total cross-sectional area equal to the area of the absorption cell. His theory predicted a discontinuous dependence of transmittance on concentration, the discontinuities occurring when the number of layers was integral. LANGE [4] showed later that no such discontinuities actually existed. He also demonstrated experimentally that BEER's law* was obeyed by sols of uniform particle size as far as the concentration dependence of absorbance was concerned.

More recently a treatment by DUYCKAERTS [3] has appeared of the radiant-energy absorption by particles in a potassium bromide pellet, which is similar to Soos's in that layers are again postulated. The particles are treated as being in close-packed layers, and because of their physical dimensions they can pack so as to cover only a fraction of the cross-sectional area of the pellet. DUYCKAERTS's derivation, if followed literally, also leads to a discontinuous dependence of transmittance on concentration, although he later makes the assumption that incomplete layers and complete layers may be treated alike, which then permits his expression to agree with BEER's law. JONES [2], in his treatment of the potassium bromide pellet system, did not assume layers of particles normal to the direction of the energy beam, but he did consider the pellet, or cell, as made up of two parts: one through which energy could pass without encountering any particles and the other in which all the particles were contained. He then assumed BEER's law was obeyed in the second part only. JONES's results are qualitatively correct in predicting changes in shapes and relative intensities of absorption bands due to particle-size variations. The result of his assumption, however, is that BEER's law is not followed by the pellet as a whole, even with respect to changes in the cell length at constant concentration (Fig. 2). Thus neither theory meets the minimum requirement that one must impose, namely, that absorbance be proportional to cell-length, with other variables being held constant. The reasons for their failure are, first, it is incorrect to say, as DUYCKAERTS does, that when there are not enough particles to form a complete layer no ray encounters more than one particle. Indeed, one can show that even when only one-half a layer is present more than 9% of the rays will strike two or more particles. Again, the restriction of BEERS's law to only part of the cell, according to JONES, is an unnecessary and artificial one. Actually, the "free space" (the fraction of the cell where no absorption takes place) is always greater than zero, even in solutions, and the energy that goes through it is part of the total, which follows the exponential absorption law. The derivation that follows is based on simple laws of probability and results in an expression that is exactly consistent with BEER's law for constant particle size.

2. Derivation of the absorption law for discrete particles

Let us consider a mass, m, of sample having a density, ρ, dispersed as spheres of uniform diameter, d, in a supporting medium that has faces of area, s, perpendicular to the direction of a parallel radiant-energy beam. The thickness of the

* The usage of BEER's law is consistent with that suggested by the Joint Committee on Nomenclature in Applied Spectroscopy. *Anal. Chem.* **8**, 1349, 1952.

system is l. We shall assume that the index of refraction of the sample is the same as that of the supporting medium, so that we shall not be concerned with scattering effects. (In practice, with use of the KBr technique, scattering usually contributes very little to loss of intensity from the beam. In those instances when it does, the effect is obvious from either a gradual decrease of transmittance toward the shorter wavelength or from the appearance of unsymmetrical absorption bands.)

In order to compute I/I_0, the ratio of the transmitted to the incident

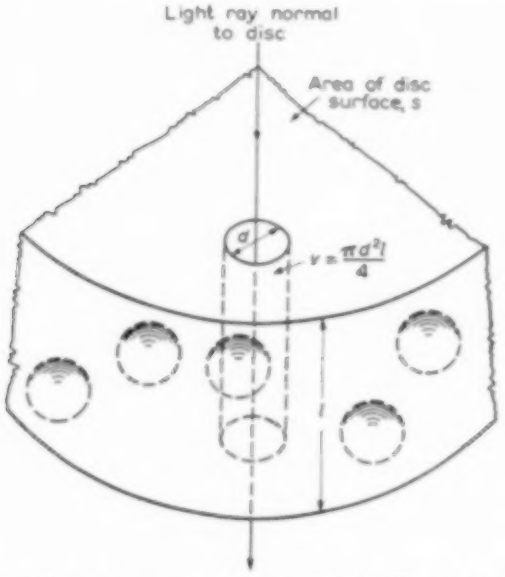

Fig. 1. Light-ray penetrating a disc containing discrete particles.

radiant power, we shall first calculate the fraction of the incident radiant power that passes through the disc without encountering any particles, the fraction that encounters one, two, three, etc. Consider an arbitrarily chosen ray through the system, as shown in Fig. 1. It will strike any particle whose centre is within the cylinder of radius $d/2$ around the ray as an axis, or, in other words, within a volume, v, where

$$v = \frac{\pi d^2 l}{4}. \tag{1}$$

Now, if the particles are randomly dispersed, the probability of finding 0, 1, 2, . . . , or n particles in this volume is given simply by the Poisson distribution, P_n, where

$$P_n = \frac{a^n e^{-a}}{n!} \tag{2}$$

Here a is the average number to be found in the volume, and a may be expressed as

$$a = \frac{tv}{V} \tag{3}$$

VOL. 9 1957

where t is the total number of particles and V is the total volume of the system. Substitution of (1) as well as

$$t = \frac{6m}{\rho\pi d^3} \tag{4}$$

and

$$V = sl \tag{5}$$

in (3) gives

$$a = \frac{3m}{2\rho sd} \tag{6}$$

Thus the freely transmitting area referred to by JONES is $P_0 = e^{-a}$, while the fraction of the radiant power that encounters 1, 2, etc., particles is $P_1 = ae^{-a}$, $P_2 = (a^2/2)e^{-a}$, etc. If we take θ as the transmittance of a single spherical particle, averaged over all trajectories of the ray through the sphere, then the overall transmittance of the system is given by the sum

$$\begin{aligned} \frac{I}{I_0} &= P_0 + \theta P_1 + \theta^2 P_2 + \dots \\ &= \sum_{n=0}^{\infty} \theta^n \cdot \frac{a^n}{n!} e^{-a} \\ &= e^{-a} \sum_{n=0}^{\infty} \frac{(a\theta)^n}{n!} \\ &= e^{-a} \cdot e^{a\theta} \end{aligned} \tag{7}$$

whence

$$\frac{I}{I_0} = e^{-a(1-\theta)} \tag{8}$$

or

$$\ln \frac{I_0}{I} = \frac{3m}{2\rho sd}(1 - \theta) \tag{9}$$

The dependence of θ on particle diameter, d, and on the true linear absorptivity, k, of the solid sample is given by DUYCKAERTS as

$$\theta = \frac{1 - (1 + kd)\, e^{-kd}}{\frac{1}{2}k^2d^2} \tag{10}$$

The concentration of sample in the system is $c = m/sl$, so

$$\ln \frac{I_0}{I} = \frac{3cl}{2\rho d}(1 - \theta) \tag{11}$$

The absorbance is therefore seen to be proportional to both concentration and thickness at constant particle size. This is an exact expression as long as the main assumption is true, namely, that the Poisson distribution holds. It is of interest to examine this assumption under typical conditions in the use of the KBr pressed-plate technique.

In order for the Poisson distribution to be strictly applicable [5], three conditions must be fulfilled:

(1) v/V must be small compared to 1. This is certainly true in practice. If, for example, $s = 5$ cm^2 and d is even as large as 50 microns, then $v/V = 0{\cdot}000004$.

(2) t must be large enough that $t(t-1) \cong t^2$. This is also true, since, for example, 10 mg of 50-μ spheres when $\rho = 1$ g/cm^3 makes $t = 160{,}000$.

(3) The particles must be randomly situated throughout the system, i.e. they must not get in one another's way. Therefore, the probability of finding no

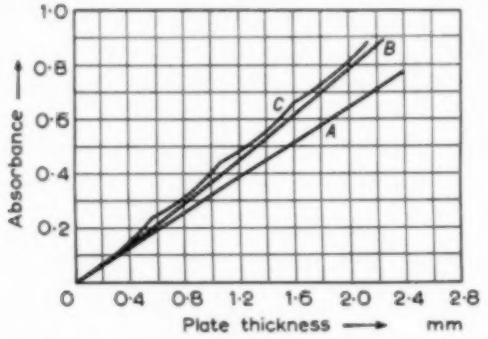

Fig. 2. Absorbance versus plate thickness for a typical case.
Curve *A*: Present theory.
Curve *B*: JONES [2].
Curve *C*: DUYCKAERTS [3].
Sample concentration = 0·01 g/cm^3;
Particle diameter = 10 μ;
Particle density = 1·0 g/m^3;
Transmission of each particle = 0·50.

particles within a distance of 2 radii from a given particle should be very nearly 1. We can apply the Poisson distribution itself to test the validity of this condition for the typical numerical values given above. The probability that a volume $v' = 4/3\ \pi d^3$, which is the volume of a sphere of radius, d, around a given particle, will be free of other particles is

$$P'_0 = \exp\left(-\frac{tv'}{V}\right) = \exp\left(-\frac{8m}{\rho s l}\right) \tag{12}$$

This is seen to be independent of particle size, but dependent on l. Actually, the quantity $m/\rho s l$ is the volume fraction of sample in the system. For $l = 2$ mm and m, s, and ρ as above, the volume fraction is 0·01, a typical value in practice and $P'_0 = 0{\cdot}925$. So 92·5% of the particles will be "undisturbed," that is, they will be randomly dispersed. The "crowding" of the other particles probably has a negligible effect on the absorption. However, for strict adherance to the Poisson distribution, the volume fraction of the sample should be kept small and the thickness, l, of the system adjusted to get desirable values of transmittance.

3. Discussion

The results of this derivation are compared in two ways with the theories of JONES and DUYCKAERTS [2, 3] in Figs. 2 and 3. First, in Fig. 2, the predicted absorbance is plotted versus plate thickness for a system of constant composition, having

VOL. 9 1957

a sample concentration of 0·01 g/cm³, and particles 10 μ in diameter with a density of 1·0 g/cm³. The transmittance, θ, of each sphere is taken as 0·50. To get the data from JONES's equation, the free space $(1 - X)$ was taken to be equal to e^{-a} and the "true "absorptivity was set in such a way that the absorbance agreed with that predicted by our theory at very small plate thicknesses. Fig. 2 shows clearly the nonlinear dependence of absorbance on plate thickness predicted by

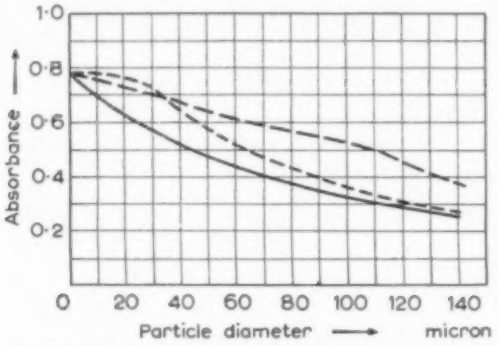

Fig. 3. Absorbance versus particle diameter for a typical case.
———————— Present theory.
— — — — DUYCKAERTS [3].
- - - - - - - - JONES [2].
True absorptivity = 0·030 μ-1;
Pellet 5 cm² in cross-section 2 mm thick;
Sample weight = 30 mg.

the other two theories. The points at the discontinuities of the curve for DUYCKAERTS's theory, where there are an intergal number of "layers," do, however, fall on a straight line.

In Fig. 3 the dependence of absorbance on particle size is shown as it is predicted by the three theories for a typical case.* A pellet 5 cm² in cross-section and 2 mm thick is assumed to contain 30 mg of a sample. The true linear absorptivity of the solid sample is taken to be 300 cm^{-1}, or 0·0300 μ^{-1}. Although the three curves all approach the same limit at small particle sizes, i.e. true solutions, it is evident that they are widely different elsewhere. In using such a curve to determine the true absorptivity of an absorption band, as BONHOMME [6] did with the theory of DUYCKAERTS, one would ordinarily measure absorbance and particle size and then, from a plot of the predicted absorbance versus the product, kd (since θ is a function of kd only), find the value of k that gives the best fit of the experimental points to the curve. Hence, if the wrong curve is used, the calculated absorptivity can be greatly in error.

Furthermore, even if the correct theory is used, there is yet another pitfall in its application to experimental data. Throughout the derivation of equation (11) it was implicitly assumed that the diameter, d, defined as the physical size of the particle, was the same as the effective optical diameter for absorption. This is not necessarily true, however, when the wavelength of the radiation being

* The Duyckaerts equation for a large number of layers n was used when $n > 1$ and the equation for a partial layer was used when n was less than 1.

considered is of the same order of magnitude as the particle size. Indeed, according to the MIE theory [7], it is possible for the optical cross-section to be several times the physical cross-section under some conditions. The relative sizes of the two cross-sections depend in a complex manner on wavelength, particle size, absorptivity of the particle, and the refractive indices of particle and medium. It will be shown in the experimental section below that the 9·1-μ band of the quartz exhibits such an anomalous behaviour and that at least the 6·98-μ band of the three bands of calcite examined by BONHOMME [6] does likewise.

4. Experimental

A finely ground grade of quartz was obtained, in which more than 90% of the particles were below 50 μ in diameter. A particle size separation was effected by allowing the particles to settle through water for various lengths of time and thirteen fractions of uniform particle diameter in the range from 6 to 45 μ were obtained. Microscopic examination showed that the particles were roughly uniform in cross-section under all orientations. It is thus reasonable to assume that a large number of them will behave like spheres of some average size. Further, the average particle diameters measured using a microscope equipped with a micrometer eyepiece was the same as the diameters predicted from the Stokes equation relating settling time to particle size.

KBr plates were prepared from each of these fractions. The plates were 2·5 cm in diameter and 0·11 cm thick. The concentration of quartz varies from 2×10^{-3} to 8×10^{-3} g/cm^3. The "natural" linear absorptivity k_d, at the particle diameter d, defined by

$$k_d = \frac{\rho^g}{m} \ln \frac{I_0}{I} \tag{13}$$

was calculated from the measured transmittance of the absorption bands. The strong band at 9·1 μ was selected for measurement.

According to (9) and (13), the linear absorptivity k_d is related to the particle size d, and the fraction of light θ transmitted by each particle by

$$k_d = \frac{3}{2d}(1-\theta). \tag{14}$$

5. Calculations and conclusions

The 9·1-μ band was so intense that it was suspected to be essentially totally absorbing over the range of particle sizes used. If a band is totally absorbing, θ must be zero for all values of d and (14) reduces to

$$k_d = \frac{3}{2}\left(\frac{1}{d}\right) \tag{15}$$

i.e. a straight line in the variables k_d and $1/d$ passing through the origin and with slope 3/2. A plot of k_d versus $1/d$ is shown in Fig. 4 for the 9·1-μ band of quartz. It is seen that a straight line passing through the origin is obtained, but with a slope of 4·8 instead of the predicted 1·5. The straight line shows that the band is indeed essentially totally absorbing. In such a case it is obvious that no measure of the true absorptivity can be obtained. The fact that the slope is larger than the predicted value means that the absorbance of the plate at every particle size is greater than should be observed for opaque particles. This can only mean that the optical cross-section of the particles is actually greater than their

VOL. 9 1957

Stokes cross-section, a conclusion that is qualitatively in accord with the Mie theory, as discussed above. The actual value of the slope indicates a ratio of optical to Stokes cross-sections of 4·8/1·5, or 3·1. Also shown in Fig. 4 are the data obtained by BONHOMME [6] for the strong band of calcite at 7 μ over the

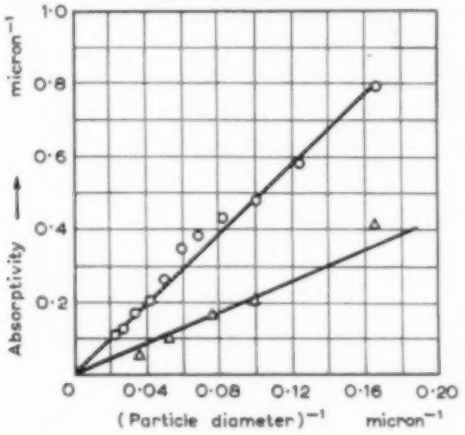

Fig. 4. Absorptivity versus inverse of particle diameter for totally absorbing bands.
——○—— 9·1-μ band of quartz.
——△—— 6·98-μ band of calcite (BONHOMME [6]).

same particle size range. The points fall on a straight line of slope 2·2, showing again that the band is essentially totally absorbing. Here, the ratio of optical to Stokes cross-sections is 2·2/1·5, or 1·5. The difference in slope between quartz at 9·1 μ and calcite at 7 μ illustrates the point mentioned above, namely, that the anomalous absorption effects predicted by the Mie theory are dependent upon many factors about which there is in practical cases no available information.

Thus, even if one is willing to make the unsupported assumption that the optical cross-section, as calculated from essentially totally absorbing bands in the manner shown here, is the same for weaker bands of the same substance, and one then uses the corrected "optical" diameter in expressions (10) and (14), a calculation of the true absorptivity, k, by curve fitting is still meaningless. This is so because the expression for θ was derived by averaging the absorption of all trajectory rays through the particle. In such a derivation, an implicit assumption is that the wavelength is much smaller than the particle, a condition that is not fulfilled when the optical cross-section is different from the geometrical cross-section. Furthermore, in fitting experimental points to a curve such as is shown in Fig. 3, one must make the particle size a variable and therefore the ratio of optical to Stokes cross-section must also vary. Hence, the curve itself is not applicable, since it stems from a derivation that takes no account of anomalous absorption effects.

As stated earlier, these anomalous effects are expected to be most pronounced when the wavelength and particle size are nearly the same. Since most investigators in this field work with particles in the 1–50-μ range, which extends over the most useful infra-red wavelengths, all quantitative applications of theoretical

absorption laws to experimental infra-red data should be thoroughly examined with respect to the consequences of the MIE theory. Undoubtedly the chances for error are not so great in this respect in ultra-violet absorption spectrometry.

References

[1] SOOS A. *Koll. Z.* 1926 **38** 300.
[2] JONES R. N. *J. Amer. Chem. Soc.* 1952 **74** 2681.
[3] DUYCKAERTS G. *Spectrochim. Acta* 1955 **7** 25.
[4] LANGE B. *Z. Physik. Chem.* 1932 **A159** 277.
[5] MOOD A. M. *Introduction to the Theory of Statistics* p. 431. McGraw-Hill 1950.
[6] BONHOMME Mlle. J. *Spectrochim. Acta* 1955 **7** 32.
[7] MIE G. *Ann Phys.* 1908 **25** 377.

VOL.
9
1957

Spectrochimica Acta 1957, Vol. 9, pp. 157 to 159. Pergamon Press Ltd., London

SPECTROCHEMICAL NOTES

An apparatus for the excitation of powders in the direct-current arc

J. NOAR
Thornton Research Centre, Chester

(*Received* 3 *December* 1956)

Abstract—The apparatus described employs a motor-driven mechanism which feeds the pelleted sample into the arc through a hollow electrode.

ONE approach to the quantitative spectrographic analysis of diverse powder samples is to try to regulate the supply of sample, or sample-mixture, to the arc so that each mixture component is vaporized completely and at constant rate. The apparatus described here achieves a fair degree of regulation while retaining operational simplicity. Figs. 1 and 2 are largely self-explanatory, relevant details being as follows:

(a) Pellet mixture is 1 part sample, 3 parts lithium carbonate (containing cobalt), and 36 parts cellulose powder.

(b) A pellet, weighing about 40 mg, is made by filling a tube (former) loosely and compressing to 1-cm length. The pellet is pushed directly from the former into the lower electrode.

(c) Electrodes, lower carbon tube, and push rod are made from Champion 5·5-mm carbon.

(d) Arc current is 12 amperes and arc length 4 mm.

(e) Sequence after striking arc is as follows: 5 sec with pellet at lowest point, and 3 sec to raise the pellet from lowest point to point at which it starts to enter arc with shutter closed. 45 sec feed of pellet into arc with shutter open.

The apparatus has proved very simple to use, and cleaning (after 50–100 exposures) takes about half an hour. Analytical accuracy has been generally good for the elements determined, results in the range 0·1% upwards being within $\pm 10\%$ of chemical, but there are exceptions. Sodium and calcium are less accurate; this being expected because of photometric difficulties (lines too intense and in region of varying photographic contrast) and some improvement is possible if so required. Determination of silicon is not accurate below about 1% because of the contribution of the cellulose powder used. Other elements, notably magnesium and vanadium, give less exact results above about 15%, and although this may be overcome by further dilution, the reason is as yet obscure, and therefore of interest. The effect may be concerned with atom depletion (probably by molecule formation) in the arc column and not with excitation or self-absorption, but so far no attempt has been made to elucidate the underlying physical or chemical reactions. The use of the apparatus as indicated also gives good sensitivity of detection (about that of the cathode layer arc) and samples of less than 1 mg have been analysed by decreasing the sample content of the mixture.

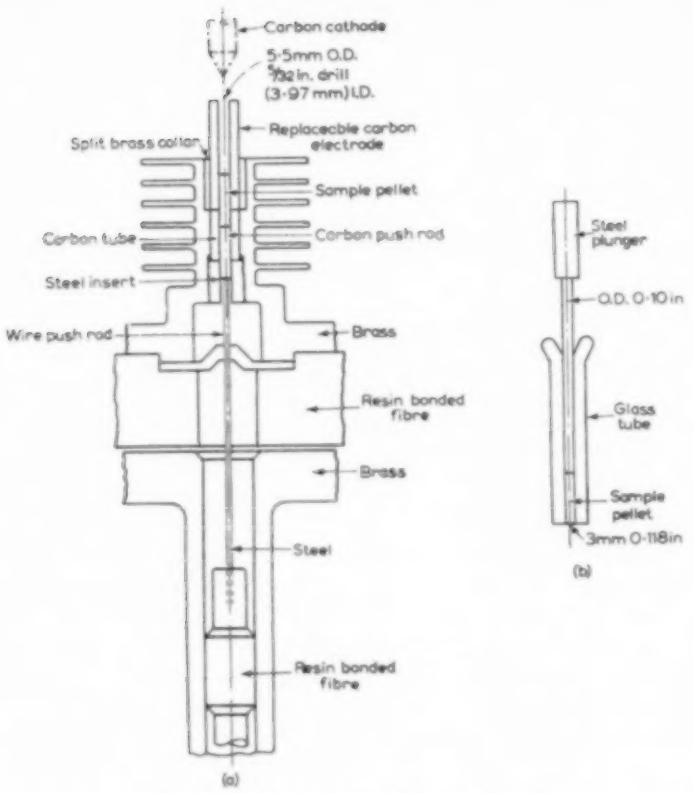

Fig. 2. (a) Detail of lower electrode system.
(b) Pellet former.

Acknowledgement—The author wishes to thank the Directors of "Shell" Research Ltd. for permission to publish this note.

Excitation energies in line spectra

N. W. H. Addink
N. V. Philips' Gloeilampenfabrieken, Eindhoven, Netherlands
Philips Research Laboratories

(*Received 6 November* 1956)

In the introduction of *Tables of Spectrum Lines* by Saidel, Prokofjew, and Raiski (VEB Verlag Technik Berlin 1955) the following passage occurs on page xxxvii: "To obtain the values for the excitation energies of the lines of the ion spectra, the value of the ionization

VOL. 9 1957

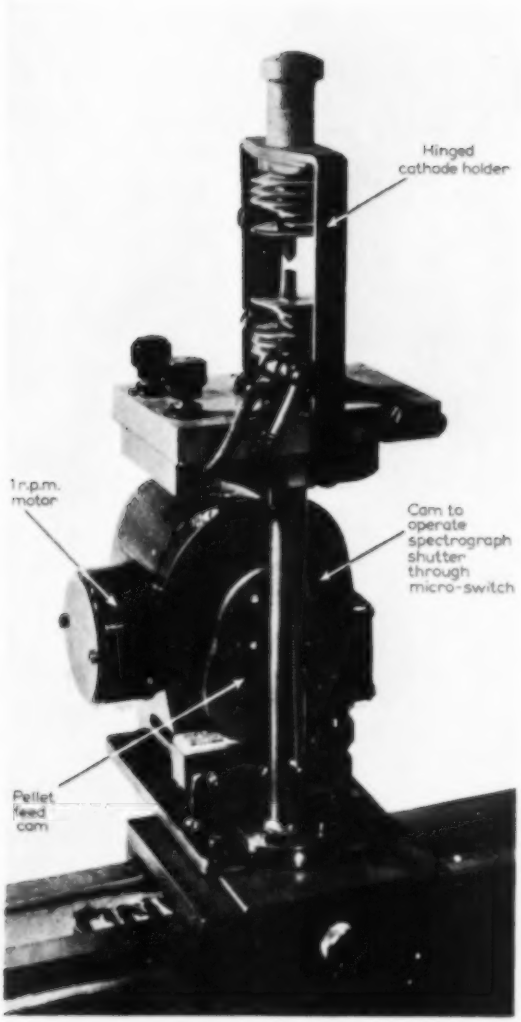

Fig. 1. General view of apparatus.

VOL.
9
1957

potential of the respective element should be added to the number mentioned in the table."

On page 539 *et seq.* various examples appear, in which the excitation energy of an ion line is reported to be the *sum* of the ionization energy of the element and the excitation energy of the ion.

Quite apart from the fact that it is difficult to picture a collision process in which an electron from an atom is transferred right outside the attractive field and at the same time, moreover, a second electron is raised to a higher state of energy, conclusions might be drawn which are quite at variance with what is observed. To mention one example, let us compare the energy of excitation of the argon arc lines situated in the red part of the spectrum (about 13·1–13·5 eV) and the summated energy of ionization and excitation (13·2 eV) of the Be-II lines 3130·4 and 3131·1 Å. The lower limits of detection for the two elements in a carbon arc differ very markedly; 0·5 gamma of Be is quite sufficient for both lines to appear sharply in the spectrum, while this is certainly not the case with argon.

It is correct to bear the ionization energy in mind when investigating spark lines, but it must be considered in the same way as AHRENS considers it in his book [1], where, according to SAHA's equation [2], for a given temperature the ionization energy is a measure of the degree of ionization. BOLTZMANN's equation can then be applied to the number of ions determined in this way, this giving the ratio of the excited ions and the total number of ions at a given temperature.

References

[1] AHRENS L. H. *Spectrochemical Analysis* p. 23. Cambridge (Mass.) 1950 (K_2 in formula (3–1) on that page should be K^2).

[2] *Phil. Mag.* 1920 **40** 472.

Spectrochimica Acta, 1957, Vol. 9, pp. 160 to 174. Pergamon Press Ltd., London

REPORTS OF MEETINGS

8th Annual Pittsburgh Conference on Analytical Chemistry and Applied Spectroscopy

THE conference was held at Pittsburgh, Pennsylvania, March 3 to 8, 1957. An exposition of modern analytical equipment was held in connection with the conference. The Pittsburgh Spectroscopy Award for outstanding achievement in the field of Spectroscopy was awarded to Dr. GEORGE R. HARRISON, Dean of Science, Massachusetts Institute of Technology.

The following papers were presented at the spectroscopic sessions.

Emission

The Quantovac, a direct-reading polychromator for the 1600 Å to 3000 Å region. G. ANDERMANN, J. W. KEMP, and M. F. HASLER.

The Quantovac, which is basically a concave grating, vacuum spectrometer, suitable for work in the range from 1600 Å to 3000 Å, and equipped with a number of photoelectric detectors, is described in detail.

Its performance is evaluated particularly with reference to the measurement of carbon, sulphur, and phosphorus in ferrous materials.

Its possible performance down to 1100 Å is discussed.

Vacuum fluorite spectrographs. A. C. MENZIES and J. SKINNER.

A description is given of two versions of an instrument for spectroscopy in the Schumann region. In both versions the instrument is evacuated and the spark chamber is flushed with nitrogen.

(a) A three-prism spectrograph, in which the spectrum may be photographed from 1600 Å to 1850 Å. Spectra will be shown of steels containing carbon, phosphorus, and sulphur in varying proportions.

(b) A direct-reading version, employing the same optics, but with four E.M.I. multipliers, set on lines of the three elements named above, and one on an iron line.

Efficient continuous arc excitation. J. T. ROZSA, L. E. ZEEB, and O. W. UGUCCINI.

While d.c. arc excitation has been conventional for many types of analysis, the erratic volatilization characteristics have always demanded rigidly standardized methods and an unnecessarily high amount of preliminary development. A high amperage a.c. arc (sustaining arc) has been developed for maximum output at high electrical efficiency. The unit exhibits the greatest improvement for heavy or refractory elements. In general, background is reduced more than 20 per cent, sensitivity improved by 10 to 30 per cent, and reproducibility enhanced by 30 to 100 per cent over a wide range of materials encountered in a commercial laboratory.

Narrow wavelength interval direct-reading spectrometer. LOUIS E. OWEN.

Further progress on the spectrometer assembly described at the 1956 Conference is given. The electronic read-out has been coupled with a B and L Dual Grating spectrograph using mechanical scanning. The use of electronic scanning with a Vidicon tube is under investigation.

VOL. 9 1957

A direct-reading approach to semi-quantitative analysis. P. E. Lemieux.

A method in which samples are mixed with CuO and graphite in the proportions 1:9:20 (cf. Jaycox, ASTM E-2 SM 10-9) has been tested on a wide variety of non-metallics, using an ARL Quantometer. The technique yields results accurate within a factor of 1·2 for a majority of determinations ranging from traces (order of 0·01 per cent level) to major constituents. When applied to one class of material, viz. bauxites of different origins having varied mineral structures, the method gives much improved accuracy without evidence of appreciable matrix effects. Advantages and limitations of direct-reading instrumentation for semi-quantitative analysis will be discussed.

New spectrographic laboratory instrumentation. Louis E. Owen.

A completely mechanized arc-spark stand, a pacing type timer for photographic processing, and a constant current d.c. arc source unit are described. The mechanized stand is based upon the model developed at Iowa State College. The photographic timer provides visual or aural signals for all steps of the photographic process. The constant current arc source employs grid controlled rectifiers. A similar source was developed concurrently at the Carborundum Company at Niagara Falls.

Spectral character as a function of source parameters. T. P. Schreiber and D. L. Fry.

The $\frac{\text{FeI } 3016{\cdot}185}{\text{FeIII } 3013{\cdot}12}$ intensity ratio was measured under a variety of source conditions using an air-gap type source. With steel samples and point-to-plane excitation the following relationship was obtained:

$$\frac{\text{FeI}}{\text{FeIII}} \sim \frac{L}{VC}$$

where L = inductance in the range 10 to 500 μH, V = breakdown voltage in the range 8,000 to 18,000 volts, and C = capacitance in the range 0·0025 to 0·015 μF. The intensity ratio is independent of resistance and discharges per half cycle except that the latter showed some sensitivity to the other parameters.

The average current (see K. Laqua, *Spectrochimica Acta*, Vol. IV, No. 6, 1952) was measured and found to bear a direct relationship to the over-all spectral intensity.

The average current can be used to calculate the power dissipated in the analytical gap ($P = I_{av}v$, where v is the arcing potential of the electrode system, usually 50 to 100 volts).

There are indications that source conditions can be duplicated on different units by obtaining the same I_{av} and $\frac{\text{FeI}}{\text{FeIII}}$ values.

The identification by emission spectroscopy of foreign objects damaging compressor blades in turbojet engines. A. E. Spakowski and J. Graab.

Damage to the compressor blades of turbojet engines due to ingestion of foreign objects is a growing problem with aircraft using this type of propulsion system. The solution of the problem has been made more difficult by the large percentage of damaging materials that have remained unknown. A rapid emission spectroscopic method has been set up to identify the chemical composition of these foreign objects from the trace of material left behind on the damaged blade. Results were obtained on laboratory prepared specimens and on the damaged compressor blades from turbojet engines with known histories. The results show that the method can be utilized to determine the nature of the ingested foreign objects.

Punched card data correlation for the identification of samples of unknown origin. John C. Bartlet and Charles G. Farmilo.

The identification of samples of unknown origin depends on the simultaneous comparison of

many characteristics with those of known samples. A hand-sorted punched card system has been developed for the identification of opium origin which permits the rapid comparison of any combination of parameters. Prior to the identification step, over 50 qualitative and quantitative characteristics for each of 300 known samples were determined, in order to form the basis for classification according to geographical type. The chemical composition ranges and sub-ranges for opium were established, coded and punched on cards. A type of coding was developed for this purpose.

In determining the geographical origin of an unknown sample, graphical methods were tested, and it was found that not more than three parameters for a given sample could be compared at one time. Mathematical methods were also tested, and up to eleven variables have been used in three populations. This procedure proved cumbersome because of the involved mathematical calculations. On this basis the punched card technique was found superior to other methods investigated.

The techniques reported here, using opium identification as an example, may also be extended to many fields where taxonomic problems are involved such as in botany, zoology and forensic science. The method would also be applicable in certain problems in metallurgy and geology.

Segregation studies in titanium alloys using the spectrographic micro-volume technique. J. K. Hurwitz.

The spectrographic micro-volume technique has been applied to two titanium alloys. In one alloy containing 4 per cent manganese and 4 per cent aluminium, segregation exists as an increase in manganese content from the outside to the inside of the bar with severe banding superimposed on this concentration gradient. The validity of applying this technique to these alloys was verified by analysing synthetic segregates which were assembled from chemically analysed alloys.

VOL. 9 1957

A study of the influence of electrode form on selective volatilization occurring in d.c. arc–II. Graphite electrodes, sample electrode as cathode. D. O. Landon and J. M. Siomkajlo.

In the first paper of a series, work was reported on selective volatilization in the d.c. arc with the sample electrode positive. Several shapes of electrodes were studied at varying currents. The present paper is based on further work in which the same electrode types and samples were studied, but with the sample electrode as the cathode of the arc. The data are presented in the form of time-intensity curves.

The effects of various oxidizing atmospheres on the spark excitation of a nickel-base alloy. R. F. Majkowski and T. P. Schreiber.

Samples of a nickel-base alloy (GMR 235) were sparked with a series of oxygen-nitrogen and oxygen-argon gas mixtures. The gases were introduced into the analytical gap by means of a tube placed so that the gas impinged upon the sample surface as well as enveloped the gap.

Large changes were observed in the spectral intensity, the $\frac{\text{NiIII } 2448{\cdot}35}{\text{NiI } 2472{\cdot}06}$ intensity ratio, and the $\frac{\text{Al } 30821{\cdot}6}{\text{Ni } 3064{\cdot}62}$ intensity ratio. An attempt will be made to explain these changes on the basis of oxidation reactions taking place in the spark crater.

Spectrometric analysis of high purity argon. Bourdon F. Scribner and Barry W. Mulligan.

The increasing use of high purity argon in applications for which the total of impurities is specified to be less than 100 parts per million has posed a difficult problem for elemental analysis. The possibility of applying emission spectrometric procedures to this low range of concentrations has been investigated with promising results. A glow discharge in the flowing gas, excited by a microwave field, is viewed end-on for maximum sensitivity and the spectrum is observed with an automatic scanning photoelectric spectrometer. The gas handling system and techniques

employed were designed to minimize the troublesome effect of contamination, and to provide the necessary control of pressure and flow rate of the gas. With this system a detectability of 1 ppm has been attained for nitrogen. Because of the high speed of the spectrometric measurement, the procedure is particularly well adapted for monitoring a continuous flow of gas. The equipment, techniques, and applications will be described.

The spectrochemical determination of fluorine in porcelain enamel frits. DONALD C. SPINDLER and MONA L. FRANCK.

The rapid comparison of porcelain enamel frits is facilitated by a spectrochemical determination of fluorine. Calcium carbonate and ammonium chloride are mixed with the sample to produce CaF bands with heads at 5291 and 6064 Å. The intensities of various band components, corrected for background, are compared with chemical standards or addition standards. The usual range of fluorine covered is from a few tenths to 6 per cent in frits.

Some of the factors considered in this procedure are emulsions, amperages, amounts and kinds of additives, times of exposure, and band components. Emphasis is given to an evaluation of previously reported work on fluorine determination.

Spectrographic determination of the major constituents of coal ash. C. H. ANDERSON and R. A. HEIN.

This paper is concerned with the spectrographic determination of the common constituents of coal ash, except the alkalies, present in amounts over 0·5 per cent, with particular attention given to the determination of silicon, iron and aluminium. The sample is buffered with NiO and graphite. D.C. arc excitation is used. Nickel serves as the internal standard for iron, titanium, calcium and magnesium. Germanium and chromium are added to serve as internal standards for silicon and aluminium respectively, The effect of variable amounts of iron, calcium, and sodium on determining the other elements was studied. Results agree satisfactorily with wet chemical analysis.

Emission spectrometric determination of oxygen in titanium and titanium alloys. VELMER A. FASSEL and WILLIAM A. GORDON.

An emission spectrometric method for the determination of oxygen in titanium and titanium alloys will be presented. The procedure is based on the d.c. carbon arc excitation of a special electrode assembly which provides a molten platinum bath after the arc is initiated. The oxygen content of the titanium sample is rapidly liberated from this bath into an argon atmosphere which supports the arc discharge. The intensity ratio of the line pair $\frac{\text{O } 7771 \text{ Å}}{\text{A } 7891 \text{ Å}}$ is related to the oxygen content of the titanium sample. This procedure provides oxygen determinations with a precision comparable to the vacuum-fusion or bromination-reduction techniques, but with greatly reduced time requirements. Other recent developments on the spectroscopic determination of gases in metals will also be discussed.

The analysis of lateritic ores and metal salt solutions for nickel and associated elements by the rotating disc technique. MILTON E. SLAGEL.

Use of the rotating disc technique in the analysis of salt solutions and lateritic ores with a Jaco 3·4 metre Ebert Spectrograph and Varisource is discussed. Spectrographic results are compared with both gravimetric and colorimetric chemical results with very acceptable agreement. This work covered the analysis of ten elements with emphasis on nickel and cobalt. The method has been successfully applied to a wide range of element concentrations with only a minimum amount of interelement effect.

High temperature alloy 5376. J. T. ROZSA, J. D. GOLLAND, J. CANNON,

This routine type spectrographic technique utilizes a stabilized high frequency a.c. spark and a 0·5 A/mm dispersion spectrograph for the determination of tungsten, manganese, molybdenum,

columbium, titanium, and silicon in a very complex alloy. Results on the analysis of chromium, nickel and cobalt appearing in major concentrations will also be given. Overall accuracy appears to be about 1 to 3 per cent and long range uncorrected reproducibility about 5 per cent. The method is essentially a modified point to plane approach and exhibits normal high speed. Cost savings for complete analysis are significant.

Spectrographic analysis of silicon-germanium alloys. MARVIN C. GARDELS and HUBERT H. WHITAKER.

A spectrographic method was developed for the analysis of the silicon-germanium binary system over a concentration range of 1 to 99 mole per cent Si. The samples were finely ground, mixed with graphite, and burned to completion in a 10 A d.c. arc. The exposure was controlled with a rotating sector. No other element was added as an internal standard. Instead, germanium served as a variable internal standard for silicon determinations up to 70 mole per cent silicon, and silicon served as a variable internal standard for germanium up to 30 mole per cent germanium. Line pairs were chosen according to the range under investigation. Two line pairs were sufficient to cover the silicon analysis and one was sufficient for the germanium. The standard deviation was ± 4 per cent to ± 8 per cent over the entire range.

Spectrochemical determination of bismuth and magnesium in cast iron. ALBERT C. OTTOLINI.

The determination of bismuth in cast iron presents a special challenge because of the absence of reliable chemical methods of analysis.

This paper describes two spectrochemical methods for the determination of bismuth in cast iron in the range of 0·01 per cent to 0·08 per cent. A point-to-plane, unidirectional arc method employing a nitrogen atmosphere was developed for the rapid control analysis of routine samples. In addition, a solution method, required for the certification of a proposed series of standards, was developed. The success of the solution method depends on the preliminary chemical removal of iron by ether extraction.

A solution method for the determination of magnesium in cast iron is reviewed with special emphasis on time requirement and repeatability studies.

The determination of boron and silicon in steel using copper fluoride. J. E. PATERSON and W. F. GRIMES.

Copper fluoride decomposes when heated by relatively low amperage arcs to provide a labile fluorine which will combine with boron and silicon to form the volatile fluorides. The fluorides can be distilled preferentially to most other compounds giving a spectrum essentially free of lines other than those of boron and silicon. This system has been applied to the determination of boron and silicon in thin sheets of steel. It is indicated that it may be applied to other materials as well as steel.

Determination of traces of boron in silicon. GEORGE H. MORRISON and RICHARD L. RUPP.

A method is described for the determination of traces of boron in silicon covering the concentration range of 0·001 to 1 ppm. The procedure involves a chemical concentration step followed by spectrographic analysis and has a precision of ± 25 per cent.

Infra-red

Near-infra-red spectroscopy. ROBERT J. MANNING.

A project has been undertaken in our laboratories which has been designed to provide a library of near-IR spectra (0·7–3·2 μ). These spectra are being used to explore this relatively unknown region to see what advantages it offers in analytical and structural work. The first phase of this investigation has been confined to solvents and the more common organic liquids. Analytical possibilities, solvent effects, choice of solvents, concentrations, path lengths, etc., will be detailed. A number of representative near-IR spectra will be shown.

VOL. 9 1957

Near-infra-red analysis of N-alkyl and N-alkyl-N-hydroxyalkyl aromatic amine mixtures. KERMIT WHETSEL, WILLIAM E. ROBERSON, and MAX W. KRELL.

Mixtures of N-alkyl and N-alkyl-N-hydroxyalkyl aromatic amines are often difficult to analyse by infra-red spectroscopy since the N-H stretching band near 3 μ is obscured by the stronger O-H band. The application of near-infra-red spectroscopy to the analysis of such mixtures was investigated. By utilizing the O-H and N-H overtone bands near 1·4 and 1·5 μ, respectively, methods were developed for the analysis of N-ethylaniline and N-ethyl-N-2-hydroxyethylaniline. Separate procedures are presented for the analysis of mixtures covering the entire concentration range and for the more precise determination of small amounts of the secondary amine. The standard deviation is approximately ± 1 per cent for the determination of both components and $\pm 0{\cdot}1$ per cent for the determination of N-ethylaniline only. Similar methods for the analysis of mixtures of N-ethyl-*m*-toluidine and N-ethyl-N-2,3-dihydroxypropyl-*m*-toluidine are discussed briefly.

Ulvir gas and stream automation analyser and processor for continuous analysis in the ultra-violet to near infra-red. M. H. AXLER.

In recent years, process stream analysers have become prominent in industry because of the increasing tendency to automation. Axler Associates is manufacturing a double beam analyser for use in liquid or gas streams, operating in the ultra-violet, visible, and near infra-red (0·220 to 2·7 microns).

The instrument utilizes the standard narrow band interference filters manufactured by this company for the particular application. This instrument has the advantage of low cost, small size, and portability and can be used in conjunction with a standard recorder-controller. Its simplicity of operation enables it to be used by non-technical personnel.

Control of concentration of an absorbing component can be accomplished by differential comparison of a known concentration standard with the process stream concentration. Alternatively it may be used as an ordinary colorimeter for determining the concentration of a substance over a wider range.

A typical application is the determination of trace amount of water in Freon 21. Air pollution studies will find this instrument useful in determination of ozone, SO_2, and other atmospheric impurities. Manufacturers of pharmaceuticals, food, paper, cosmetics, petroleum, rubber, plastics, and chemicals can use this instrument for the analysis and automatic control of their products.

Infra-red studies of metal urea complexes of Pt(II), Pd(II), Cr(III), Fe(III), Zn(II), and Cu(II). R. B. PENLAND, S. MIZUSHIMA, BROTHER COLUMBA, C.S.C., and J. V. QUAGLIANO.

Infra-red spectra of some urea metal co-ordination compounds have been measured in the 2–35-micron region. From a comparisn with the result of the calculation of the normal vibration of urea, absorption bands observed in these metal urea complexes have been assigned. The spectroscopic evidence, the presence or absence of the carbonyl band near 1700 cm^{-1}, the presence or absence of bands in the the 3-μ region at frequencies lower than those of the N-H stretching vibrations of urea, permits dividing the urea complexes into two groups. Urea forms nitrogen-to-metal bonds with Pt(II) and Pd(II), and oxygen-to-metal bonds with Cr(III), Fe(III), Zn(II) and Cu(II).

Infra-red spectra of some xanthates and related compounds. F. G. PEARSON and R. J. BUSER.

The infra-red spectra of nujol mulls of several xanthates ROC(=S)SK, oxyxanthates, ROC(=O)SK and dixanthates, $ROC(=S)S{-}M{-}SC(=S)OR$, where M is Pb, Cu, or Zn, will be presented. A discussion of the constancy of characteristic frequencies within each group will be presented. Correlation of characteristic frequencies with molecular structure will be attempted.

Infra-red absorption studies of complex cyanides, metallic soaps, and commercial soap greases. STEPHEN E. WIBERLEY and WALTER H. BAUER.

The spectra of potassium ferrocyanide and ferricyanide, sodium ferrocyanide and sodium nitroferricyanide have been obtained using both sodium chloride and lithium fluoride prisms. The compounds show distinct differences in the C≡N stretching region. In this region the spectrum of potassium ferricyanide in KBr has been found to change markedly with grinding time.

The infra-red spectra of the laurate soaps of barium, calcium, magnesium, strontium, aluminium, manganese, mercury, zinc, and cadmium have been obtained. The main differences are in the C=O region. However, the C=O frequency does not decrease with increase in the atomic weight of the metal in a regular fashion. The commercial soap greases can be readily distinguished from one another by certain characteristic bands. All of the greases show distinct differences in the C=O region.

Infra-red and ultra-violet spectra of metal chelate compounds of 2-pyrrolealdehyde derivatives. SISTER MARY IRMA GERBER, O.P. and BROTHER COLUMBA CURRAN.

Infra-red absorption spectra have been obtained in KBr disks for co-ordination compounds of some aldimines derived from 2-pyrrolealdehyde and from N-methyl-2-pyrrolealdehyde with copper, nickel, and zinc. The ring N-H bond is replaced by nitrogen-to-metal bonds on chelation with copper and nickel, but the N-H bond is retained in complexes with zinc chloride. In every instance the frequency of the C=N stretching vibration is reduced on co-ordination with metals. The C=N absorption band is split when two C=N groups are in *cis* positions in complexes. Spectra reveal that bis-(2-pyrrolealdimine) nickel(II) has a *trans* planar configuration. Nitrogen-to-metal frequencies have been observed in the cesium bromide region.

The ultra-violet absorption maxima are shifted to longer wavelengths on replacement of a ring N-H bond by a nitrogen-to-metal bond, as also in complexes in which only the side chain nitrogen is involved in co-ordination. The absorption maximum of N-methyl-2-pyrrolealdehyde dichlorocopper(II) is shifted to a shorter wavelength relative to the maximum in the spectrum of the free aldehyde. This shift is attributed to the blocking of resonance within the ring by chelation.

Infra-red studies of methylthiourea and some of its metal complexes. JAMES A. RYAN and THOMAS J. LANE.

The infra-red spectra of methylthiourea and some of its metal complexes have been measured in the 2–15-micron region, using the KBr disk method. The frequencies of the normal vibrations of methylthiourea have been assigned by comparison with previously calculated and observed values for the urea, formamide, acetamide, N-methyl-acetamide, N-methylformamide, oxamide, and methylamine molecules. The absorption bands observed in the methylthiourea complexes have been assigned, using the normal vibration frequencies of methylthiourea as a basis for assignment.

Infra-red spectroscopy for the chemical laboratory. JOHN U. WHITE, NELSON L. ALPERT, and SEYMOUR WEINER.

The requirements of a modern chemical laboratory for infra-red instrumentation are considered in terms of performance, complexity, and operator skill required. A new instrument has been built to satisfy these requirements. Its design and features are described and its performance illustrated.

Design and performance of a new infra-red spectrophotometer. E. H. SIEGLER, J. G. ATWOOD, T. F. FLYNN, and H. W. MARSHALL.

A new infra-red spectrophotometer has been designed with emphasis on operator convenience, simplicity of controls, reliability, and low cost.

VOL. 9 1957

The instrument has a fixed programme of operation with the following characteristics:
Wavelength range: 2·5 to 15 μ.
Scan time: 15 minutes, programmed for maximum efficiency.
Resolution: 0·05 μ at 10 μ (5 cm^{-1} at 1000 cm^{-1}).
Photometry: Double beam, optical null.
Slit control: Programmed for normal scanning, manual control for differential analysis.
Chart presentation: Linear wavelength, linear percent transmission.
Chart size: Spectrum 10 × 25 cm on 8½ × 11-inch paper.

The instrument design incorporates the latest production techniques. Printed circuits and a new long life source lead to reliability and compactness. Aspheric optics are used throughout to provide high quality optical performance. The system is designed as a compact single unit requiring only 28 × 17 inch of bench space.

A simplified double-beam infra-red spectrophotometer. E. DuBois, R. H. Packard, and E. H. Merrill.

A new double-beam infra-red recording spectrophotometer is described. The emphasis of design has been on simplicity with the object of making the instrument available to laboratories with limited budgets. In spite of the simplification, there is no sacrifice of important operational parameters. The result, as illustrated by spectra and performance specifications, is an extremely stable and easy-to-operate instrument that can be used for both qualitative and quantitative analysis.

Details of design are illustrated. These include large optics, permanently evacuated bolometer, and an electronic system which is compact and designed for minimum maintenance. Physically the instrument fits on a table top and the sample space is exposed and easily accessible from the front of the instrument.

Also discussed is a series of accessories which may be added to the basic instrument to increase versatility. These accessories provide variability in prism material, scan drive-speed, slit-width, servo parameters, programming, and data presentation.

A new low-cost double-beam infra-red spectrophotometer as a general tool in the chemical laboratory. Helene Sternglanz and V. Z. Williams.

The performance and application capability of a new low-cost double-beam infra-red spectrophotometer are discussed. The progress of an organic synthesis from starting materials to intermediates and final products is illustrated by infra-red. A typical quantitative analysis and a differential analysis are shown. Results are compared with those obtained using a higher priced instrument.

Laboratory gas analyser. G. E. Smith.

A portable, infra-red gas analyser of the negative filter, non-dispersive type is described physically and functionally. A typical application is presented together with some examples of its sensitivity.

Improving the measurement of weak infra-red absorption bands using expanded-scale double-beam spectrophotometry. Vincent J. Coates and Robert Anacreon.

The consideration of Beer's law indicates that the absorbance of an infra-red band at a given wavelength is directly proportional to the number of molecules present in the radiation beam. The extinction coefficient is a constant for a given wavelength, being a fixed property of the vibrational group in the molecule. The number of molecules in the radiation beam can be increased by increasing the thickness of the sample, the concentration in the case of solutions and mixtures, and/or the pressure in the case of gases.

It will be the purpose of this paper to discuss means of improving sensitivity of measurement in several cases where the practical limits in the adjustment of the various parameters discussed above are reached. Furthermore, it will be shown that a large gain in sensitivity results from the simple modification of a flexible double optical null spectrophotometer.

Rapid sorting of unknown infra-red spectra. PHILIP SADTLER.

Rapid sorting of unknown infra-red spectra based on largest band per micron have been described. These include Keysort, IBM, Major Band, etc.

The method is based on the selection of the strongest band of the spectra and further arranging all bands in each micron in ascending order. These may be further broken down when required to prevent ambiguity.

The spectra, although coded from 2 to 15 microns, generally single out to one spectrogram after 5 or 6 of the micron areas have been examined. When two or more answers are obtained, the compounds are closely related. The spectra should be examined whenever a single number is obtained on all spectra with similar bands.

The spectra may be examined rather than the location of the bands. Accuracy is 75 per cent.

Rapid sorting of unknown infra-red spectra based on major bands. PHILIP SADTLER.

Sorting methods have been in the state of flux for a period of years, as evidenced by different types of papers presented.

Keysort methods have been described by several workers. These have been superseded by IBM sorting as described by Kuentzel. There is a recent tendency to arrange spectra by prearranged chemical type.

The paper describes a simple book method of locating unknown infra-red spectra. It is based upon punching this spectra on IBM cards according to the ASTM—E-13 Committee procedure.

Selecting the longest band and those which are 80 per cent of this band and calling all such major bands and coding the card with an over punch in each micron region and each of these major bands. The cards are then arranged in a systematic order and printed. Examples are given.

A master list of 10,000 standard spectra would have too many numbers with similar bands so a further subdivision may be required such as the exact location of the strongest band, or by the elements present, or by chemical classification.

The accuracy is 60 per cent. It is increased by subdividing.

Crystallinity of polymers by infra-red methods. R. E. MOYNIHAN.

Crystallinity is an important and often studied variable in the physical behaviour of semi-crystalline polymers. While X-ray techniques are more commonly used in such studies, in many cases information concerning crystallinity can be obtained from a study of the infra-red spectrum of a polymer. Changes in infra-red spectra with crystallinity provide a means for making quantitative measurements of crystallinity that are generally more rapid, and sometimes more precise than X-ray determinations. Some general aspects of this technique are discussed with application to polytetrafluoroethylene and nylon.

Study of the decomposition of polyvinyl chloride by means of infra-red spectrophotometry. ROBERT STROMBERG, CHARLES BERSCH, MARY HARVEY, SIDNEY STRAUS, and BERNARD ACHHAMMER.

The changes in chemical structure occurring in polyvinyl chloride as a result of exposure to heat in the temperature range 100 to 400°C, ultra-violet radiant energy and oxygen were studied using infra-red spectrophotometry. The polyvinyl chloride powder was prepared for infra-red analysis by a pelleting technique. When the polymer was treated with heat at 100°C or with ultra-violet radiation, only small changes in the spectrum were observed. These minor differences were studied by a compensation technique using untreated polymer. Among the structural alterations observed after pyrolysis with heat *in vacuo* was a change from an aliphatic spectrum to one showing aromatic absorptions.

An infra-red study of solvent-extracted materials from wire enamels. RUDOLPH P. ARNDT.

Formvar and polyurethane wire enamels were baked on copper wire at a series of appropriate

VOL. 9 1957

temperatures. Extractions were obtained from each baked condition with toluol using a soxhlet assembly. The enamels studied contain more than one resinous component. Infra-red curves of the extracted materials indicate the extent of relative cure of enamel components. The results are useful in formulation, choosing suitable baking temperatures, troubleshooting, and predicting performance of enamels under special conditions.

The infra-red spectra of some halogen carriers. Sister Miriam Michael Stimson, O.P., and Dorothy M. Richardson.

The effect of bromination, chlorination and mixed halogenation on 5,5-dimethylhydantoin and 5,5-diphenylhydantoin has been studied with particular reference to the effect of halogenation on C—H. C=O and for the monohalogen compounds on N—H frequencies. Replacement of the imide hydrogen, only, causes a shift of the 4-position carbonyl band to lower frequencies, whereas replacement of both the amide and imide hydrogen atoms causes the 4-position carbonyl band to shift toward higher frequencies. The extent of these shifts is greater for bromo than for chloro compounds. The brom-chloro compound is anomolous.

The C—H deformation frequencies are moved to lower values with increasing halogenation, the extent of the shift being independent of the nature of the halogen.

Application of the potassium bromide disc technique to infra-red micro analysis of water-insoluble single and multiple component systems.* H. P. Schwarz, R. Childs, L. Dreisbach, S. V. Mastrangelo, and A. Kleschick.

Infra-red micro analysis of water-insoluble compounds with the potassium bromide disc technique was tested on a relatively large scale. 50 to 150 micrograms of the samples were dissolved in benzene, benzene-methanol or other solvent mixtures and suspended in 50 milligrams of solid potassium bromide of small particle size by means of the two step freeze drying procedure demonstrated previously. Examination of discs prepared from pure complex lipids showed general agreement of band frequencies with those obtained by other infra-red techniques, examination of solutions or Nujol pastes. Duplicate analysis of single components gave satisfactory results. The method has been tested for multiple component analysis and found useful for analysis of small chromatographic fractions.

Semi-micro KBr unit for use with Perkin-Elmer model 21 infra-red spectrophotometer.† W. B. Mason and H. N. VanSlyke.

A simple unit is described which makes possible good infra-red spectra with 10–25 μg of sample in 8–10 mg of KBr. There is no beam condensing unit. Using an evacuable die and a total pressure of 600 pounds, the prepared KBr is compressed into a 0·065″ diameter hole in a 0·625″ diameter steel disc measuring 0·08″ in thickness. This disc containing the pellet is then placed at a focal plane in the sample beam. An off-axis position is necessary for good compensation of atmospheric bands, and the best position seems to be in the plane of the slits approximately 0·14″ above the optical centre. The reference beam is brought to the desired intensity by means of an adjustable "perforated attenuator." The air line falls off slightly at both long and short wavelengths, but is quite reproducible. Some operating compromise is necessary to cover the 5–6 fold reduction in beam energy imposed by the semi-micro unit. We prefer increasing the slit programme to 970, which provides ample energy for scanning at the rate of 0·5 microns per minute and gives adequate resolution for most work which can be accomplished by the KBr technique. Interconversion between macro and semi-micro operation requires less than one minute.

Quantitative analysis of pesticides by the KBr technique. H. Susi and H. E. Rector.

Random testing of the KBr technique showed it to be particularly useful in the infra-red

---

* This work was carried out under Contract with the U.S. Atomic Energy Commission.

† This paper is based, in part, upon work done at The University of Rochester Atomic Energy Project under contract with the U.S. Atomic Energy Commission.

spectroscopy of relatively insoluble organic fungicides and insecticides. It offers significant improvement over mulling for general qualitative work. Its quantitative application has been tested satisfactorily for several single component types and is demonstrated for a two-component example system. No internal standard is necessary. Plots of absorbance vs. concentration × thickness resulted in straight lines in all cases studied. Deviations from linearity were within 5 per cent relative.

The results suggest that rigorous quantitative analysis of pesticides is feasible by these methods. Light scattering and distribution effects which might interfere with analytical determinations are briefly discussed and evaluated. Particle size is the critical factor. Reproducibility of grinding is both necessary and sufficient for quantitative applications. An adequate, simple procedure will be described.

X-ray Fluorescence

The determination of iron in sphalerite by X-ray fluorescence spectrography. A. A. Chodos, A. W. Rose, and E. Godijn.

The determination of iron in sphalerite is of importance in the suggested use of the FeS-ZnS system as a geological thermometer.* A rapid, non-destructive method has been developed for the determination of iron in 5–10 mg samples of sphalerite obtained by drilling from a polished section. The sample is not contaminated and may be used for trace element analyses by emission spectrography.

The counting rates for the iron and zinc peaks and their respective backgrounds are obtained and the Zn/Fe intensity ratio plotted against the ZnS/FeS concentration ratio. This application of the relative standard principle compensates for many variables. Standardization of the method was based on chemically analyzed samples as appreciably different results were obtained using synthetic mixtures. The method has been used in the range from 0·2 per cent Fe to 20 per cent Fe. Total analysis time is 15 minutes per sample. The method has a coefficient of variation of 3 per cent.

VOL. 9 1957

X-ray fluorescent spectrometric determination of yttrium in rare-earth mixtures. Robert H. Heidel and Velmer A. Fassel.

The great similarity in the chemical properties of yttrium and the rare-earth group of elements prevents the use of classical chemical methods for the separation and determination of yttrium. In this paper an X-ray fluorescent method for determining yttrium in mixtures of rare earths and thorium is described. For the determination of yttrium in ores, a preliminary rare-earth group separation is required. The samples are analysed in solution form, using added strontium as an internal standard. At 50 per cent yttrium oxide content the coefficient of variation is ±5 per cent of the amount present. About 10 minutes are required for a single determination.

Sample preparation for accurate X-ray fluorescence analysis†. Fernand Claisse.

The method consists in fusing the sample in a suitable glass, making disks out of it, and analysing these by X-ray fluorescence. When the glass has the following composition, 1 part of sample, 100 parts of barium peroxide, 100 parts of barium sulphate and 1000 parts of fused borax, it has been observed that the matrix effect is practically negligible. The line intensities (background included) are almost linearly related with percentages, up to 100 per cent. With this method, only one reading per sample is needed to obtain a result of analysis with an accuracy of the order of ±0·3 per cent absolute in less than 2 minutes. For concentrations below 3 to 5 per cent a better accuracy is obtained by fusing 1 part of sample with 20 parts of borax and using an internal standard. A simple technique for making the glass disks is described. The method can be used for ores and rocks (including sulphides), and possibly for metals and alloys.

* Kullerud, G. The FeS-ZnS system. A geological thermometer. *Norsk. geol. tidsskrift* **32**, 61–147 (1953).

† Published by the permission of the Deputy-Minister of Mines of the Province of Quebec.

Determination of uranium in solution by X-ray spectrometry.* HARRY M. WILSON and G. V. WHEELER.

A method is presented for the analysis of uranium in nitric acid solution by X-ray fluorescence The sample contained in a simple bottom window cell is excited by radiation from a molybdenum target X-ray tube. The intensity of the uranium L-spectra is measured by means of a scintillation counter with pulse height analysis and compared to reference standards.

The concentration range, the precision of measurements, the effects of interfering elements and the effects of radioactive materials present are described.

Reduction of interelement effects in fluorescent X-ray spectrography. WILLIAM J. CAMPBELL and MELVIN LEON.

A dilution technique was developed which reduces the samples, regardless of composition, to a common matrix, water. Since the interelement effects, differential absorption and mutual excitation, increase with the concentration of the element, dilution lessens these effects.

By this dilution technique elements found in high concentration in a low absorbing matrix can be readily determined, since the relationship of intensity to concentration of dilute solutions is linear over the range of 0 to 100 per cent. This is not true of solid samples as the concentrational response varies with the matrix and concentration.

This technique also facilitates the analysis of samples of very different matrices. Dilute solutions containing equivalent amounts of bromine gave bromine K_α line intensities to within ± 5 per cent while the line intensities in undiluted powdered samples varied as much as 400 per cent.

The principal limitations are that (1) the sample must be soluble in water or in a dilute acid or base, and (2) it must be possible to dilute the sample while still maintaining a reasonable line intensity above background.

Analysis of clays, bauxites and other silicates by the X-ray spectrograph. R. K. SCOTT.

With the development of the flow proportional counter tube, the range of X-ray spectroscopy has been extended to allow the detection of sodium. Of particular interest to analysts in the mineral industries is the determination of aluminium and silicon. Estimation of major amounts of these elements, along with iron, titanium, potassium and calcium in clays, bauxites, refractories and some other silicate minerals are presented. Pulse height discrimination against higher order lines has been accomplished, in the General Electric XRD-5, by use of a "reverter," which rejects pulses above a certain level. Interelement effects, techniques of sample preparation, and the relative magnitude of errors from different sources are discussed.

Instrumental design factors in X-ray polychromators. J. W. KEMP, ERNEST DAVIDSON, and J. L. JONES.

X-ray polychromators are instruments designed to provide a number of fixed monochromators receiving radiation from a single sample. Each monochromator is designed to detect the radiation from a single element. This technique allows the simultaneous determination of a number of elements in considerably less time per sample than the one-element-at-a-time technique practised with scanning X-ray monochromators.

An important additional advantage of the polychromator technique is that it allows each monochromator to be designed for maximum efficiency at one wavelength. This means that the best optical system, crystal and detector, can be used for the wavelength for which the monochromator is designed.

Relative detector efficiencies are well known but crystal monochromator efficiencies have received little attention. Studies of optical efficiencies and optical reflectivities will be reported.

In order to remove cost and complexity and to improve reliability, physical methods of improving line-to-background ratios have been investigated. Some of these show promise for replacing the complex circuits sometimes used for this purpose.

---

* Work done under the auspices of U.S. Atomic Energy Commission.

Semi-automatic data reduction of X-ray powder patterns.* CARL CLARK and LOUIS KAPLAN.

Using a manually operated line positioning device, powder X-ray diffraction data have been transcribed automatically by electric typewriter and punch cards for subsequent utilization in semi-automatic qualitative analyses. Possible modifications for automatic qualitative and semi-quantitative analyses of mixtures and the proposed applications to automatic biochemical analyses of fractionation products of biological fluids, extracts, and hydrolysates will be discussed.

Flame Photometry

Determination of sodium in epoxy resins by flame photometry. MYRL R. ADAMS and RICHARD M. JONES.

This investigation describes the application of a Beckman Model B flame photometer to the determination of sodium in epoxy resins. The sodium line at 589 millimicrons is used. The procedure is applicable for resins melting as high as 120°C and containing as much as 700 ppm. All values are expressed as ppm NaCl. A precisely prepared solution of approximately 1 per cent of the resin in a solvent of benzene and glacial acetic acid (3–1 by volume) is used. Because of traces of sodium in the acetic acid a blank on the solvent must be run and corrections applied. The corrected reading is then referred to a calibration graph to get ppm in the solution. Multiplication by reciprocal of concentration gives the ppm in the original sample. Reproducibility was considered satisfactory for the purpose under study when the difference between duplicates was no greater than 5 per cent of their average.

Flame photometric determination of sodium and potassium in coal ash. C. H. ANDERSON and E. Q. WEIMER.

This paper describes the flame photometric determination of sodium and potassium in coal ash. Since preliminary studies showed that iron, aluminium, calcium, and magnesium in concentration ranges expected in coal ash had little effect on the sodium and potassium determination, the determination is carried out with a minimum of preliminary chemical separations. Results of flame photometric determinations are compared with alkali determinations by the J. Lawrence Smith and Berzelius methods.

Flame spectrophotometric study of barium. JOHN A. DEAN and J. C. BURGER JR†.

This investigation involves a flame spectrophotometric study of barium, in both oxy-hydrogen and oxy-acetylene flames. The emission of the barium atomic line at 553·6 mμ and the barium ionic lines at 455·4 mμ and 493·4 mμ as well as the barium oxide band head at 515 mμ was studied in relation to position in flame mantle, fuel flow rates, and monochromator slit width.

Various types of interferences were investigated. The emission intensity minus flame background radiation method and the standard addition method for evaluation of the amount of barium present in a sample are discussed.

Miscellaneous

Qualitative and quantitative analyses through the combined technique of ultra-violet and chromatography. CHARLOTTE LUTINSKI.

The use of an automatic recording ultra-violet spectrophotometer for qualitative identification of components isolated by chromatographic techniques is discussed. The high sensitivity to ultra-violet active materials makes it particularly suited to column chromatographic analysis where very low concentrations of sample in gas or liquid solvents are encountered. The direct analysis of paper chromatograms is also illustrated.

* This study is supported in part by a research grant from the American Cancer Society.

† Present address: Westinghouse Electronic Tube Division, Elmira, N.Y.

VOL. 9 1957

A new direct-reflectance recording spectrophotometer for use between 230 and 2200 millimicrons. B. D. HENDERSON.

A new direct-reflectance recording spectrophotometer and a reflectance attachment for the Beckman DK-1 and DK-2 Spectrophotometers are described. An integrating sphere is used with ports for a sample and a reference. A simple rotation of the sample and reference mounts converts the system from total reflectance performance to total diffuse reflectance. Mountings are also provided at the entrance ports of the sphere for transmittance measurements of samples up to 1 cm path length. Three detectors are available to give a usable spectral range from 230 to 2200 millimicrons.

As a second mode of operation special irradiating sources are used to illuminate the sphere directly, and the reflected plus fluorescent energy of the sample and reference is passed through the monochrometer. This is the preferred mode of operation for samples which are fluorescent.

Fluorescence spectrophotometry. WILLIAM F. ULRICH.

The design and use of a new fluorescence attachment for the Beckman DU and DK Spectrophotometers are discussed. With its use, high resolution and sensitivity are combined into one instrument. The monochromator system can be employed either to isolate selected wavelength radiation for excitation or to analyse the fluorescence radiation. This flexibility is highly desirable for establishing optimum conditions for fluorescence measurements. Various practical applications of fluorescence spectrophotometry are described.

Improvements in the Todd Spectranal for rapid identification of metals. REGINALD STABLER and CLIFFORD W. MELL.

The Todd Spectranal has been developed by the Todd Scientific Company for the rapid detection of metallic elements by a visual spectroscopic method. Tables of the spectranal identification lines have been prepared by the Todd Company which serve as a reference for the excited spectra. Even though this instrument has been designed for the untrained operator, it has been found that unless the operator is familiar with element spectra, he misidentifies elements in metals because of the many spectral lines present. This paper discusses the use of element comparators which can be placed at the collimater tube. The standard lines of hydrogen and sodium are used to align the comparator. When the four principal lines of an element are covered, the element can be identified. This device has been very useful in the rapid identification of elements in metals for quality control work.

Western Spectroscopy Association Fourth Annual Conference

University of California, Los Angeles

Professor GEORGE C. PIMENTEL, University of California, Berkeley: "The Matrix Isolation Technique and Spectroscopic Study of Free Radicals."

Dr. HERBERT P. BROIDA, National Bureau of Standards, Washington: "Spectroscopy of Free Radicals in Solids at Very Low Temperatures."

Professor MICHAEL KASHA, Florida State University: "Molecular Parameters Affecting Light Emission Properties of Molecules."

Professor W. D. HERSHBERGER, University of California, Los Angeles: "Current Microwave Studies on Smog."

Professor GEORGE E. PAKE, Stanford University: "Relaxation Mechanisms."

Dean KENNETH S. PITZER, University of California, Berkeley: "Spectral Studies in the Far Infra-red."

Dr. EUGENE B. TURNER, The Ramo-Wooldridge Corporation: "The Shock Tube as an Instrument for Spectroscopic Research."

Professor R. W. NICHOLLS, University of Western Ontario, Canada: "Recent Experimental and Theoretical Work on the Excitation of Molecules of Importance in Auroral and Atmospheric Physics, Astrophysics, and Combustion."

NOTICE OF MEETING

International Symposium on Hydrogen Bonding

AN International Symposium on Hydrogen Bonding will be held at Ljubljana from 30 July to 3 August. It will be organized by the Union of Chemical Societies of Yugoslavia under the auspices of the I.U.P.A.C. The papers and discussions should cover all aspects of hydrogen bonding (spectroscopic, crystallographic, dielectric, theoretical interpretations, influence of hydrogen bonding on various physicochemical processes).

Additional information may be obtained upon request from the Slovenian Chemical Society, Hajdrihova 19, Ljubljana, or directly from Professor D. HADZI, University of Ljubljana, Institute of Organic Chemistry, Ljubljana, Vegova 4, Yugoslavia.

VOL. 9 1957

ANNOUNCEMENT

Le G.A.M.S. et l'Enseignement des méthodes physiques d'analyse

Les méthodes physiques d'analyse et plus particulièrement la Spectroscopie d'Émission et d'Absorption demandent pour leur application des connaissances très diverses : atomistique, électrique, électronique, photographique, chimique. Seules quelques grandes écoles donnent l'enseignement correspondant. De plus, ces sciences évoluent vite et les connaissances acquises sont rapidement périmées.

Or, l'industrie a un besoin impérieux d'ingénieurs et de techniciens connaissant les possibilités de ces méthodes et étant capables de les mettre en oeuvre. C'est pourquoi un enseignement post-scolaire était nécessaire; le G.A.M.S. organe de liaison entre les milieux industriels et scientifiques, a donc créé une Commission de l'Enseignement, dans le but d'organiser l'Enseignement des Méthodes Physiques d'Analyse à deux niveaux différents:

(1°) *Formation de techniciens*

Cet enseignement, particulièrement important, a pour but de former des techniciens de laboratoire, échelon intermédiare entre le simple manipulateur et l'ingénieur.

Il ne comporte aucun développement mathématique et peut être suivi par des personnes ayant une instruction du niveau "Brevet Elémentaire."

Il comporte 30 cours d'une heure et demie sur les sujets suivants:

— Bases physiques de la Spectroscopie,
— Spectroscopes,
— Générateurs,
— Méthodes d'analyse qualitative et quantitive, par voies photographique et photoélectrique,
— Spectroscopie infra-rouge et Raman,
— Méthodes électriques d'analyse.

Il comporte en outre 25 séances de travaux pratiques de 2 heures, sur tous les sujets étudiés et des visites de laboratoires industriels. Il est à noter que les Constructeurs d'appareils d'analyse comprenant l'importance de cet enseignement et faisant confiance au G.A.M.S. ont mis bénévolement à la disposition de la Société, pendant la durée des Cycles d'enseignement, du matériel dont l'importance atteint une valeur d'environ 40 millions de francs; nos élèves peuvent ainsi manipuler euxmêmes les appareils les plus modernes.

3 cycles d'enseignement ont déjà été organisés sur ce schéma:

— En 1954 Le cycle s'est déroulé suivant un horaire conforme à l'intérêt des industries de la région Parisienne. Durée 3 mois—séances en fin de journée.
— 1955 Cycle rapide de 3 semaines à temps plein, destiné aux techniciens éloignés (Belgique—Sarre—Algérie—Maroc).

— En 1956 Cycle étudié pour l'industrie de grande Banlieue Parisienne 2 fois par semaine à temps complet.

Chaque cycle a eu en moyenne 25 auditeurs.

Le G.A.M.S. délivre un certificat d'assiduité aux élèves ayant suivi les cours et travaux practiques de ces cycles.

Enfin, les anciens élèves de cette école de techniciens sont groupés en une Association Amicale qui se réunit trois fois par an et poursuivent leur enseignement post-scolaire par des conférences d'actualité faites par des spécialistes.

(2°) *Enseignement complémentaire pour Ingénieurs Spécialistes*

Une "Semaine Internationale d'Études Supérieures des Méthodes Physiques d'Analyse" fut organisée en février 1955. Elle comportait 10 conférences magistrales sur les développements nouveaux de la Spectroscopie sous toutes ses formes. Ces conférences furent effectuées par des Professeurs de Faculté ou des Directeurs de laboratoires particulièrement compétents.

Des démonstrations et des visites de laboratoires furent en outre effectuées.

Cette semaine qui a présenté la synthèse des derniers progrès théoriques et pratiques, fut suivie par plus de 50 Ingénieurs parmi lesquels quelques Ingénieurs non Français.

En résumé, le G.A.M.S. en accord avec l'industrie s'éfforce de répondre à un besoin réel de l'industrie en organisant ces cycles d'enseignement élémentaire et supérieur.

Dans l'immédiat un cycle à temps plein de 3 semaines pour techniciens n'habitant pas la région Parisienne est prévu en 1957.

Rappelons que notre enseignement est ouvert à toute personne possédant le niveau d'instruction nécessaire, s'inscrivant en temps voulu, française ou étrangére, membre du G.A.M.S. ou non.

M. Michel

Président, Groupement pour l'Avancement des Méthodes Spectrographiques

VOL. 9 1957

Spectrochimica Acta 1957, Vol. 9, pp. 177 to 198. Pergamon Press Ltd., London

The existence of differences between the infra-red absorption spectra of bacteria

J. E. S. Greenstreet and K. P. Norris
Microbiological Research Establishment, Ministry of Supply, Porton, Wilts

(*Received* 18 *February* 1957)

Abstract—The infra-red absorption spectra of 136 strains of bacteria have been examined. The attempt is made to show that bacteria can be differentiated by their infra-red absorption spectra (5–15 μ). The difficulties and the means adopted to overcome them are discussed. A statistical method of comparing spectra is described and results quoted to show that similarity between bacteria on biological grounds is paralleled by similarity between their spectra, and vice versa. Genera are easily distinguished. Species can be distinguished with more difficulty, but the spectral differences between strains are of the same order of magnitude as those arising from errors of the technique as yet uncontrolled. However, there is evidence that it is possible to distinguish strains.

It is also shown that the spectrum of *Bacillus megatherium* varies with the morphology of the organism. It appears possible that differential spectroscopy may help to elucidate the changes which occur in such bacteria.

Introduction

The first applications of infra-red spectrophotometry to bacteriology were essentially extensions of its use as an analytical tool. Randall, Smith, Colm, and Nungester [1, 2] showed that, whereas the spectra of a virulent and an avirulent strain of *Mycobacterium tuberculosis* were very similar, extracts isolated in the same way from each strain had quite different spectra. It has been suggested [3] that such fractions may be used to control the preparation of antigenic fractions of bacteria.

In a similar manner, Shirk and Greathouse [4] isolated samples of cellulose from the pellicles produced by *Acetobacter xylinum* grown on six media each containing a different carbohydrate, and they were able to show that the spectrum of the cellulose was independent of the carbohydrate in the medium.

The capsular polysaccharides of *Streptococcus pneumoniae* have been divided by serological methods into a number of types. The polysaccharides from strains of a given type were shown [5, 6] to have similar infra-red absorption spectra, indicating that there may be some association between serological behaviour and infra-red absorption.

These experiments are of a completely different nature from those described by Stevenson and Bolduan [7], who maintained that it is possible to identify bacteria by their infra-red absorption spectra. Identification is based upon differences in the shape and relative intensity of the absorption bands, because the main bands in the spectra of the bacteria examined occur at the same frequencies. The spectral differences between different genera were much smaller than those

normally regarded as significant by spectroscopists engaged upon analytical work. This is the first recorded case in which conclusions are based upon such small spectral differences.

It has been realized for many years [8] that a spectrometer does not reproduce a spectrum without distortion, and more recently Brodersen [9] has advanced a simple theory to show how band shape and intensity depend upon slit-width. Despite the difficulties associated with work involving small spectral differences, much has since been done to study the differentiation of bacteria both in England [10] and in the United States of America [11, 12]. The method has even been extended to classify virus preparations [13, 14].

In previous work, the differentiation of bacteria was achieved by personal judgement of the strength of very weak absorption bands or by an examination of a restricted spectral region. In view of the difficulties associated with the measurement of small absorption bands, it was thought desirable in the present work to have a method of comparing spectra which eliminates personal judgement as far as possible. To achieve this, a correlation method has been devised which can be applied to the spectra in a mechanical way. The method has been used to compare the spectra of bacteria from different species and genera, and it has been possible to show that the spectral differences between different genera are significantly greater than those between different species of the same genus. It must be emphasized that the method was devised solely to show that the differences in spectra exist; it can in no way be regarded as a generally applicable method for the comparison of dissimilar spectra.

The object of this paper is twofold: (i) To show that the spectra of similar organisms are more alike than are those of dissimilar organisms; (ii) to discuss methods of interpreting differences in the spectra of bacteria in terms of chemical composition.

The work is a continuation of that described by Thomas and Greenstreet, who emphasized the importance of standardizing each part of the technique in order to obtain reproducible results. It is for this reason that the experimental methods are described here in such detail. The methods selected have no particular merit other than that they were chosen so as to reduce to a minimum possible variations in the resulting spectra.

Although this paper is concerned with the infra-red absorption of bacteria, the specimens examined did not consist of pure cell substances, for, no matter how bacteria are grown, they are more or less contaminated with components from the medium and with products of their own metabolism. To remove such contamination, it is necessary to wash with an aqueous medium and in doing so, cell components themselves are likely to be extracted. It has been shown, for instance, that washing suspensions of bacteria with distilled water or physiological saline reduces the intensity of the absorption band at about 9·3 micron (μ), which is probably due to carbohydrate.

It is desirable for many purposes to work on single colonies of bacteria, and throughout the present work an attempt has been made to use the minimum possible amount of material, although at the present time is it still not possible to obtain satisfactory spectra from a single colony.

VOL.
9
1957

For this study of differentiation the bacteria examined were obtained from cultures having confluent growth, so as to have as uniform a population as possible.

The preparation of samples, the obtaining of spectra, and the comparison of spectra will be described consecutively, different possible procedures for some of the stages being discussed.

Materials and methods

Strains of bacteria were obtained from various sources either as vacuum-dried samples or as growing cultures. The strains were subjected to appropriate bacteriological tests to confirm that they were what they purported to be and that they were pure, and any available data concerning them were noted. Stock cultures were then made in suitable media and stored at 4°C.

In a separate series of experiments one strain of a coliform organism was grown in twenty-five fluid media and on twelve media solidified by the addition of agar. Some of these were complex classical media of the types based on tryptic digest of meat and on peptone, and some were of the synthetic type of which the components were exactly known. Growth on the classical media resulted in more reproducible spectra than growth on the synthetic media. It was found that the addition of fermentable carbohydrate, even to the classical media, made the spectra more complex.

Differences between the spectra of an organism grown on tryptic meat agar (TMA) and peptone agar (PA) were very small indeed. For instance, two cultures could be distinguished as belonging to different genera, even if one had been grown on TMA and the other on PA.

Usually it was easier to obtain sufficient material for examination by growing on a solid medium rather than in liquid. Since it was desired to make the method as simple as possible, aeration and agitation to increase the amount of growth was not undertaken on a large scale.

All solid media were assessed by inoculating the agar surface directly, and in addition many were inoculated after laying a disk of Cellophane or Millipore filter material (Millipore Filter Corp., Watertown, Mass., U.S.A.) on the agar.

In previous work, slopes of solid medium in test-tubes were used, but these were discarded in favour of Petri plates because the depth of solid medium has an effect on growth. It has already been reported [7, 10] that the spectra obtained from bacteria may change if the temperature or duration of incubation is changed. Experiments to confirm this were repeated, but are not further discussed here. The effect of temperature is not surprising, since it is known for instance that the metabolism of *Pasteurella pestis* changes if the temperature of incubation is changed [15, p. 876, etc.]. An attempt was made to control the humidity at which cultures were incubated. An ordinary electrically-heated water-jacketed incubator of about 4 ft^3 capacity was used and a recording thermohygrograph was placed inside it. Opening both the incubator doors for a few seconds caused a very small fall in temperature, but opening for a minute or longer caused a fall of 2°C or more, after which the incubator took at least 1 hour to reach its normal working temperature. The humidity in the incubator was markedly affected by opening the doors: even with an open beaker of water in the incubator, equilibrium humidity was not regained for several hours. When the incubator doors were kept shut with the beaker of water inside, the temperature and humidity varied very little indeed during quite large changes in the state of the air in the laboratory.

The earlier samples were prepared by placing a small volume of water on a silver chloride disk, transferring into it live bacteria from colonies on a solid medium, and mixing. The suspension was allowed to dry in air, and then a second disk of silver chloride was placed on the top so as to make a sandwich which was then sealed round the edge with tape. This technique was not thought suitable for three reasons: (i) The quantity of material transferred was not controlled, so that the production of usable films was subject to the experience of the operator; (ii) work with pathogenic bacteria was to be done and there seemed some risk in working in such a way with live bacteria; and (iii) the sandwich required the use of two thicknesses of silver chloride. The best silver chloride in the form of sheet 1 mm thick has a transmission of about 80% from 5 μ to about 12 μ, after which it falls, so that two layers transmit about 65% at best. This causes a reduction in the sensitivity of the instrument, particularly in the water vapour region and beyond 12 μ.

Some work with non-pathogenic bacteria was attempted by smearing the growth of bacteria from an agar surface straight on to silver chloride, allowing it to dry in air, but not covering it with a second plate. It was found that during the exposure of such smears to infra-red radiation while obtaining a spectrum, they tended to flake and fall away from the silver chloride. We decided to use suspensions of bacteria to provide some control over film thickness and to kill the bacteria to allow pathogens to be freely manipulated. The commonly used ways of killing bacteria are by means of chemicals, of radiation, or of heat. It is clearly desirable either that the killing agent should not absorb in the infra-red or that if it does it should be easily removed from the dead bacteria. Chemical sterilization was not adopted because of the difficulty of removing completely even gases or volatile liquids from bacteria. The literature suggests that the killing of bacteria by irradiation is an exponential process, so that it may be dangerous to assume that complete sterilization is ever achieved.

Sterilization by heat in its various forms has been used with confidence for many years, and so this method was adopted. Most bacteria of medical interest are fairly easily killed by heat. Published conditions for killing vegetative cells range from less than 5-min exposure at 55°C to 60 min at 60°C, with a few exceptions such as some particularly resistant strains of *Streptococcus faecalis*. Spores are more difficult to kill; some have to be exposed to steam at 18 lb/in.^{2} (*c.* 125°C) for 60 min.

Heat-killed bacteria have a slightly different spectrum from live ones, but this is not important for the present purpose. It is only necessary for their spectra to be reproducible; they have been found to be so.

Since the bacteria were manipulated wholly in aqueous media, all suspensions were made either in distilled water or in physiological saline. It is difficult to decide which of these is the better. If distilled water is used, there may be some cell lysis, but the whole of the added liquid is removed by drying. If saline is used, then although there may be little damage to cells while the suspension is still liquid, during drying the cells are subjected to increasingly concentrated salt solution and the dry sodium chloride remains with the cells in the film. Despite these possible happenings, there seems to be little difference between spectra obtained from aqueous suspensions and from saline suspensions. The sodium chloride left in films made from saline suspensions does not seem to increase the amount of radiation scattered by the film.

Taking account of all these considerations and desiderata, the following scheme was adopted for the preparation of bacteria.

Final method of specimen preparation

The **medium** (usually TMA or PA) was melted, cooled to about 55°C, and poured into uniform 4 in. Petri dishes. The cooling was necessary to avoid excessive condensation and to avoid the creeping of the medium up the walls of the dish and the danger of consequent sealing to give anaerobic conditions. Swirling of the medium in the plates was avoided also. The plate-pouring was standardized so as to obtain the same uniform depth of medium in each dish; in practice, there were about 20 ml of medium in each. The medium was allowed to set, the plates were incubated at 37°C overnight to reveal contamination, and then dried at 37°C for a further 2 hours. They were allowed to cool to room temperature and then stored in a large cold room at 4°C. When various strains of a species or various species of a genus were grown for comparison, the same batch of the same medium was used for the whole group.

For use, the plates were put in a hot room or incubator at 37°C and left for about 2 hours to warm and dry. Plates more than 5 days old were not used.

The organisms were grown first in the fluid medium analogous to the solid medium to be used for the preparation of the samples. Fluid media were used as 5 ml quantities in test-tubes and were warmed to the requisite incubation temperature before use. The first set of fluid cultures was incubated for about 24 hours, mixed well, and one drop of each transferred to a second set of warm broths which were incubated for 24 $\pm \frac{1}{4}$ hour. Warmed plates of the solid medium were inoculated each with 0·5 ml from the second set of fluid cultures. This was spread as uniformly as possible over the surface of the medium with an L-shaped glass spreader, care being taken not to damage the agar surface. The plates were left at room temperature until the inoculum was absorbed and then incubated at the chosen temperature for 24 $\pm \frac{1}{4}$ hour. They were incubated

VOL. 9 1957

spread out in a single layer and not piled one on the other. The incubator contained a beaker of water and the doors were not opened during the incubation.

Afterwards the growth was washed off without delay. Physiological saline (1·5 ml) at 4°C was added to each plate and the growth emulsified in it with an L-shaped glass rod. The accumulation of a mass of bacteria on the rod was avoided so as not to dilute the suspension. The plates were set on a rack at an angle of about 10° with the horizontal, the suspension swept gently down the surface with the rod and left to drain. The suspension was removed with a bent capillary pipette and placed in a sterile $\frac{1}{4}$ oz screw-capped bottle. As far as possible, the time interval between adding the suspending fluid to the plate culture and removing the suspension to a bottle was kept constant. This was accomplished by an orderly rhythmic method of working, subservience to a stop-watch being quite unsatisfactory. At this stage, films of many of the suspensions were stained by suitable methods for microscopical examination. The suspensions in their bottles were then killed by immersing them in a water-bath at 60°C for 60 min. Spore-bearing bacteria were autoclaved in steam at 20 lb/in.^{2} for 30 min. The success of the killing was always confirmed by subculturing the heated bacteria.

When suspensions of bacteria were accepted as sterile, standard films were made on silver chloride and the spectra obtained between 5 and 15 μ. This was done as soon as possible after the suspensions were prepared, most of the delay being due to the safety precaution of confirming the success of killing. During the period of waiting the suspensions were stored at 4°C.

For particular experiments, other than those concerned with the differentiation of bacteria, this procedure was modified, e.g. by growing in liquid media, centrifuging, and resuspending the deposited bacteria, or by centrifuging and resuspending suspensions obtained from plate cultures.

Instrument conditions

The infra-red absorption spectrum of a single molecule is unique for the molecule and in many cases it is possible to interpret the spectrum in terms of interatomic vibrations. For larger molecules there is often a correlation between the presence of specific atomic groupings within the molecule and absorption bands in the spectrum. Absorption bands within the region 5–15 μ are associated with the stretching vibrations of double bonds, the bending vibrations of single bonds involving hydrogen, and skeletal vibrations of the molecule.

All bacteria are similar in that most of the dry weight is contributed by protein, carbohydrate, lipid, and nucleic acid. Different bacteria may have small differences in each of these classes of component, but infra-red absorption bands due to all of them appear in the spectra of all the bacteria examined. For these reasons the spectra differ only in the shape and relative intensity of the absorption bands.

The absorption spectra were recorded between 5 and 15 μ as percentage transmission versus wavelength, using a Grubb-Parsons S4 double-beam spectrophotometer equipped with a rock-salt prism. The shape and apparent intensity of absorption bands measured in this way are dependent upon the instrument settings, and before any reliance can be placed upon them it is necessary to consider all the possible factors which influence them. The performance of a servo system such as that used in the spectrophotometer can be expressed in terms of the output torque of the motor driving the beam attenuator for a given optical unbalance between the beams of the radiation unit. This will be referred to as the stiffness. The speed of response of the recording pen is the important factor which determines how faithfully the pen follows the shape of the band. Provided friction and the moment of inertia of the recording system are constant, the speed of response is proportional to the stiffness. Thus if servo-mechanical errors are to be standardized, it is essential to keep the stiffness constant.

It has been realized for many years that owing to the finite slit-widths used in spectrometers, the spectrum is not reproduced without distortion [8]. The effect of slit-width on optical density measurements was studied by Philpotts, Thain, and Smith [16] and Robinson [17]. Their results and the theory given by Brodersen [18] showed that the true optical density and shape of a band can be measured only if the slit-width is considerably smaller than the width of the band. Some of the bands resolved in bacteria are only 5 to 6 wave numbers (cm^{-1}) apart, and to measure these accurately would require effective slit-widths of approximately 1 cm^{-1}. As it is not practicable to work with slit-widths as small as this, it is necessary to accept an error

on the sharpest bands caused by using larger slit-widths. The difficulty is that in general it is not known which bands are sharp. For this error to be constant, the slit programme must be reproducible. The programme was chosen so that no spectral information was lost at the high speed of scan used (1 min per micron). The effective slit-width [9, 19] was 5 cm^{-1} at 5 μ, 2 cm^{-1} at 10 μ, and 5 cm^{-1} at 15 μ. Bands resolved in practice had separations of about twice these values. Some of our bacterial films have been examined with a high-resolution grating spectrometer by the courtesy of Dr. L. A. Sayce and Mr. A. Jackson of the Light Division of the National Physical Laboratory. In no case was any further band resolved.

To achieve constant stiffness over a long period of time with a fixed slit programme means that careful check has to be kept on the optical and electronic components of the instrument. Tests were devised to enable the following to be checked for constancy: the gain of the head amplifier; the gain of the servo amplifier; the friction in the recording system; the slit programme, and the overall performance of source, monochromator, and detector.

The complex spectrum of water vapour present in the atmosphere is eliminated by a double-beam instrument, but the presence of absorbing material in both beams of the instrument affects the stiffness of the servo system. The stiffness at 6 μ decreases by a factor of 2 when the relative humidity changes from 23% to 80%, and this change results in detectable differences of band shape in the water vapour region. The loss in available energy at 6–7 μ due to water-vapour was considerably reduced by circulating air at a relative humidity of 30% derived from the laboratory compressed-air supply. The monochromator was kept at a relative humidity of less than 35% by desiccating with potassium hydroxide pellets. It seems unlikely that the small changes in relative humidity ($<5\%$) from day to day affect the shape of bands in the water vapour region of the spectrum.

Particular attention was paid to controlling the temperature of the prism. So far in this work it has not been thought necessary to have the wavelength calibration absolutely accurate. It was necessary, however, that the calibration with its errors should remain constant, so that the spectra could be compared directly. It was found that the variation of the prism temperature was the factor contributing most to variations in wavelength calibration, so the thermostat was modified as described by Norris [20] to improve the control of the prism temperature.

The spectrum of polystyrene obtained at intervals of several days was used to check the reproducibility of the instrument alone. Careful attention to all instrument settings combined with the use of the tests already mentioned resulted in reproducible spectra.

Preparation of bacterial films

Various possible materials were considered as a support for the bacterial film, but most had to be discarded because of softness, susceptibility to attack by water, toxicity, or unsuitable range of transmission. The pressed potassium bromide disk method may be applicable to frozen-dried bacteria, but freeze-drying viable pathogenic bacteria is hazardous and either the bacteria would have to be killed before weighing, grinding, and pressing, or these processes made cumbersome in order to be safe. Silver chloride was eventually chosen because of its suitable range of transmission and its insolubility in water. It is not ideal, however, in that its absorption spectrum changes with age and it is very difficult to keep it highly polished. For these reasons it is difficult to obtain spectra which are independent of changes in the absorption and scatter of the window material. The relative absorption at 5·5 and 11·5 μ and the slope of the background absorption between 11 and 15 μ change with the age of the silver chloride. By cutting the windows in pairs from adjacent parts of the stock silver chloride sheet and using them alternately in the sample and reference beams, it is possible to reduce the errors due to silver chloride to a level where they do not interfere with the results. Despite these precautions, however, it is difficult to obtain well-matched pairs of silver chloride windows, and they have to be replaced frequently.

Rock-salt has ideal optical properties, but attempts so far made to dry aqueous suspensions on it have not been successful.

Silver chloride windows of constant area were employed. It was thought that reproducible spectra might result if a constant volume of bacterial suspension, already standardized to a defined optical opacity, were spread over this area and dried. Experiments with *Bacterium coli* suggested that if the windows were 23 $\times$ 6 mm, 0·06 ml of suspension containing 4 $\times$ 10^{10} cells

VOL. 9 1957

per millilitre produced suitable films. For purposes of comparison, acceptable films are defined as having a transmission of 10–20% at 6·1 μ and 40–50% at 9·3 μ. Much work was done on this basis, using BROWN's tubes [21] as reference standards. These opacity standards were used whatever the bacterium being investigated, since the important thing is the concentration of bacterial substance, not the cell count.

This principle was put on a more exact basis by calibrating a nephelometer, measuring the light scattered by a dilution of each bacterial suspension, and calculating from calibration graphs the volume of undiluted suspension to be placed on a window of standard area. This volume was transferred using a 0·5 ml graduated pipette controlled by a micrometer screw.

This method of standardization worked well for many strains, but has the inherent weakness that the density of the suspensions is measured in visible light, whereas it is the density in the 5–15 μ region which must be controlled. The method failed when it was applied to bacteria which produce varying amounts of metabolites transparent in the visible but absorbing in the infra-red. In such circumstances, suspensions which matched very well by eye or by nephelometer, gave spectra in the infra-red of different apparent optical transmissions. It was then necessary to use the spectrophotometer to control the film thickness and so produce acceptable films.

This could be achieved rapidly because there is an empirical relationship between the measured optical density of certain bands in the spectrum and the thickness of the film.

For the first experiments with dried films of bacteria a fixed volume of standardized suspension was placed on a silver chloride window of prescribed size and dried on a metal platform suspended above an electric heater dissipating 1000 W. This dried the films too quickly and tended to overheat them. Films were then dried by placing the silver chloride on a metal block and exposing to the radiation from infra-red drying-lamps. The rate of drying could be varied by moving the lamps with respect to the block. It was found that rapid drying resulted in a film of rough opaque appearance. Such films had a high apparent optical density due to the increase in scattered light. Overheating caused the films to discolour and also resulted in the loss of reproducibility of spectra.

If the films were dried slowly and heating was stopped as soon as they appeared to be dry, smooth clear films were obtained which gave reproducible spectra. Films are now dried by placing them on a metal block on a hot-plate maintained at 50°C. This is found to give very satisfactory films, except from suspensions of spores, which seem always to give granular scattering films.

It was found that when a visibly wet film was compared with one dried as described above, there were marked differences in the spectra in the range 5·5 to 7·0 μ, but no further change was detected when a dry film was exposed to infra-red radiation in the instrument for up to 10 min.

The method of film preparation described has a drawback in that in section the film is not uniform along its short axis. Small changes in spectrum have been found, particularly with films of spores, when a given film is traversed across the sample beam. The effect of this upon results will be discussed later.

For comparison purposes it is necessary to examine the spectra only for differences. Sometimes the difference may be due to a small absorption band being present in the spectrum of one organism and absent in that of the other. More often the difference is due to only dissimilarities in the shape and relative intensity of bands present in both spectra.

The spectra have been examined in two ways:

(i) The main features of the spectrum were classified into a given number of types depending upon shape, and by comparison of five or six of these main features it was possible to decide whether two spectra were similar or dissimilar.

(ii) Any two spectra can be compared by forming a correlation coefficient between pairs of ordinates. To do this, the percentage transmission of the specimen was read from the chart (to the nearest 1%) at intervals of 0·2 μ between 5·0 and 14·4 μ, i.e. forty-eight measurements were made.

A correlation coefficient between the two sets of transmissions gives a measure of the similarity between the two spectra. In the first instance Pearson product-moment correlation coefficients were formed between sets of optical densities. Optical densities were used to overcome the difficulties arising because the films being compared had slightly different thicknesses.

The Pearson coefficient was evaluated for several pairs of spectra, but it was found that a small difference in transmission or a slight error in measurement at one wavelength could have a large effect upon the coefficient. If, however, the transmissions are ranked according to their magnitudes and a correlation coefficient formed between the ranks, it is possible to change the transmission at some wavelengths appreciably without altering the order. A rank correlation is thus less sensitive to small errors in measurement and to small changes of transmission. For this reason a Spearman rank correlation was used to compare the spectra; it has the added advantage that it is possible to use spectra from films of different thickness because the order of ranks is the same whether the transmission or optical density is used; furthermore the coefficient is easier to compute than the product-moment.

The Spearman correlation coefficient ρ is defined by

$$\rho = 1 - \frac{6\Sigma\,(d^2)}{n^3 - n}$$

where $\Sigma\,(d^2)$ is the sum of the squares of the difference between corresponding values of the ranks from any two spectra and n is the number of observations, i.e. for the work described $n = 48$. The values of the ordinates obtained as above were ranked in order of magnitude, allowance being made for tied ranks. The difference (d) in the values of the allotted ranks for any two spectra were then written down for each wavelength. The values were squared and summed to give $\Sigma\,(d^2)$.

The correlation coefficient formed by comparing bacterial films is nearly always greater than 0·9. With such high correlation coefficients, the sampling distribution of the correlation coefficient is very skew.

If the Fisher transformation, $z = \tanh^{-1}\rho$ [22], is applied to Pearson product-moment correlation coefficients, the function z is approximately normally distributed and has the usual sampling variance $1/(n - 3)$, even for small sample sizes. When $\rho = 1$, $z = +\infty$, and when $\rho = -1$, $z = -\infty$.

Some experimental work by Hartley, Pearson, and Fieller (personal communication) shows that the sampling variance of the transformed Spearman rank correlation coefficient is about $1/(n - 5)$ for $\rho \leqslant 0{\cdot}9$. In our application the tranaformation of Spearman coefficients to z has the advantage that it spreads out the numerical values and makes the handling of them more convenient.

Since transmissions are estimated to only 1% at each wavelength, two spectra may be assigned transmissions differing by as much as 1% even though they can in fact be superimposed to within line thickness. A large addition to $\Sigma(d^2)$ results if this happens at wavelengths for which the ranks of the transmissions are tied. In practice, the largest z we have found is 3·7 for duplicate spectra. Measuring transmissions to $\frac{1}{2}$% leads to a small increase in ρ, and this in turn to a much larger increase in z. So much extra work is necessary to effect this improvement that it has not been attempted. Inspection by eye is still necessary to appreciate all the distinguishing features. Measuring ordinates to 1% at 0·2 μ intervals and ranking these figures does not take into account quite large changes in the shape of the bands. Thus the present method of comparison does not use all the information in the spectra.

It is convenient at this stage to introduce symbols for the various comparisons which can be made. A comparison between spectra of two organisms from different genera is called a G comparison; a comparison between spectra of two organisms from different species of the same genus an Sp comparison; that between the spectra of two strains of the same species an St comparison, and between replicate spectre of the same organism an R comparison. Corresponding values of z are called z_G, z_{Sp}, z_{St}, and z_R respectively.

The way in which the z can be used to test the significance of differentiation at the various levels (genus, species, strain) is best described by means of an example.

Twelve strains of *Chromobacterium* were examined, and from these it is possible to make $\binom{12}{2}$, i.e. sixty-six comparisons in all. There were five strains of *Chr. prodigiosum* and seven of *Chr. violaceum* from which it is possible to make $\binom{5}{2} + \binom{7}{2}$ = thirty-one St comparisons and 5×7 = thirty-five Sp comparisons. If the distinction between the St and the Sp comparisons were ideal,

VOL. 9 1957

the z_{St} would all be greater than the z_{Sp}. In practice, however, the distributions of z overlap, and a value of $z(z_c)$ can be chosen such that there are thirty-one z greater than z_c and thirty-five smaller than z_c. We found that there were twenty-five St comparisons and six Sp comparisons with $z > z_c$, and twenty-nine Sp comparisons and six St comparisons with $z < z_c$. These values can be used in a 2×2 bivariate table (Table 1), from which the usual χ^2 can be calculated to see

Table 1. Bivariate table for Sp and St comparisons of genus *Chromobacterium*

	St comparison	Sp comparison	Totals
$z > z_c$	(a) 25 (31)	(b) 6 (0)	31
$z < z_c$	(c) 6 (0)	(d) 29 (35)	35
Totals	31	35	66

A bivariate table showing the numbers of z_{St} and z_{Sp} with values greater than or less than z_c. The values in brackets are those to be expected if the distinction is perfect.

$$\chi^2 = (ad - bc)^2(a + b + c + d)/(a + b)(b + d)(c + d)(a + c).$$
$$N = a + b + c + d$$

whether or not the actual distributions of z_{St} and z_{Sp} could have arisen from one population by random sampling. $P(\chi^2)$ represents the probability that the observed value of χ^2 could be equalled or exceeded in a similar dissection of a similar sample from a population homogeneous in z. $P(\chi^2)$ gives an objective method of judging whether or not there is an association between the value of z and the relative taxonomic position of the two organisms from which the z is derived; it does not, however, provide an indication of the strength of the association. A convenient measure of this is provided by YULE's [23] coefficient of association V. ($V^2 = \chi^2/N$) Only if V is high and $P(\chi^2)$ low can the data be used with any certainty to predict the class to which a given z belongs. Values of χ^2, $P(\chi^2)$, and V for G, Sp, St, and R comparisons are given in Tables 3, 5, and 6. Where necessary, a correction for continuity has been applied to the values of χ^2. We do not know that the organisms used in this work represent a random sample, if such a concept has any meaning in bacteriology. As a consequence, the values of $P(\chi^2)$ quoted in the tables refer only to the organisms used and not necessarily to bacteria in general. Thus from these results only tentative predictions can be made about strains of organisms not included amongst those we have studied.

Results

1. *Reproducibility of technique*

Correlation coefficients have been used to study the reproducibility of each stage in the production of a spectrum. There are so many different manipulations between obtaining a seed culture and recording the spectrum that it is essential to know what reliance can be placed upon each stage of the procedure. One of the overriding considerations is that the experimental technique should be as simple as possible. An attempt has been made to keep it so.

Duplicate spectra obtained from the same film of bacteria on the same day can be superimposed to within line thickness. When such spectra are correlated, however, the resulting z is 3·6. The implication of this value will be seen by reference to Table 2, which summarizes the statistical information.

To investigate the uniformity of the film along the short axis of the support, the film was traversed across the beam and five spectra were recorded; from these it is possible to make ten comparisons which have a mean $z(\bar{z})$ of 3·35 (Table 2). It should be noted that not all these comparisons are independent. The $\bar{z}$ of 3·35 supports the view that there are small changes in film-thickness across the specimen.

When a given organism is grown in replicate at the same time and under the same conditions and the spectra are obtained at the same time, it is found that there are small differences in the spectra. The $\bar{z}$ obtained by comparing the spectra of replicate specimens of one strain is 3·08 (Table 2). It seems unlikely therefore that the small spectral variations arising from non-uniform films cause any difficulty, because the errors in specimen preparation are larger.

Table 2. Summary of statistical information on comparison of spectra

Comparison	Number of comparisons	Mean value of z
Duplicate spectra	2	3·60
Uniformity of film	10	3·35
Replicate samples of same strain grown at same time	30	3·08
Different samples of same strain grown at different times	21	3·06
Different strains of same species	229	3·00
Different species of same genus	276	2·74
Different genera	599	2·39

VOL. 9 1957

An attempt was made to check the overall reproducibility of the method by making films of a killed spore suspension at regular intervals over a period of months. This was abandoned because of the difficulty of making good films from spore suspensions. Instead, *Staphylococcus aureus* R113T was grown and examined at weekly intervals for several months. The small differences in spectra gave a $\bar{z}$ of 3·06 (Table 2). This value is a little lower than that obtained for different samples of the same strain examined at the same time, but the difference is so small as to be negligible. Two years elapsed between two examinations of *Staph. albus* Bale, and a comparison of the spectra gave a z of 3·07. Whilst this is only a single observation, it shows that spectra may still be very similar even though a long period of time separates the two examinations. On one occasion the spectrum of *Staph. aureus* Denham was obtained, the optics of the double-beam unit were removed, replaced, and adjusted, and a second spectrum obtained from the same film. A comparison of these two spectra gave a z of 3·11, suggesting that errors arising from such disturbances are smaller than those arising in specimen preparation.

2. *Strain differences*

If the spectra of two strains of *Staph. aureus* are compared, the general shape of the absorption bands is the same for each, but small differences are found. These differences are slightly greater than those due to the unevenness of the film. If, however, the same two strains are grown again, the spectra are slightly different

from those obtained previously and the small differences between them are changed. The following experiment was performed in an attempt to decide what weight can be attached to the spectral differences between two strains of an organism.

Two strains of *Staph. aureus* were each grown in quadruplicate at the same time and under the same conditions. The differences between the four spectra of each strain alone were smaller than those between spectra of the two strains. It was thus possible to separate the eight spectra into two groups of four corresponding to the two strains. Four of us, with differing degrees of familiarity with spectra, have in fact succeeded in sorting such spectra by inspection into the correct groups. It appears, therefore, that when similar organisms are grown at the same time it is possible to differentiate between them by infra-red spectrophotometry, but it must be emphasized that it is not yet possible to do so if the samples are not grown at the same time.

All possible R and St comparisons were made for the two strains. The $P(\chi^2)$ for such comparisons are listed in Table 3. It will be seen that for the strains of *Staph. aureus* $P(\chi^2)$ is not small and so it cannot be inferred that the replicates of any one strain are more alike than are the strains themselves. For the two strains of *Salm. typhi* treated in the same way $P(\chi^2)$ is 0·011. It seems likely therefore in this instance that the difference between the strains is greater than that between replicates of the same strain.

Table 3. Significance of strain differences

		N	$P(\chi^2)$	V
Salmonella typhi TY2–T6S	3 × 3*	15	0·011	+0·722
Staphylococcus aureus Oxford H–R113T	4 × 4	28	0·62	−0·167
Staphylococcus aureus 84T–Denham	3 × 4	21	0·57	+0·222

* Three replicates of strain TY2 and three replicates of strain T6S.

In many cases, however, the χ^2 test and the values of $\bar{z}$ (Table 2) do not distinguish between different strains. It must be remembered that this statistical method does not make use of all the information in the spectra, and when the spectra of different strains are compared by eye it is possible to differentiate them.

In order to assess the spectral differences between different strains of a given species, we have examined 136 strains from 29 species belonging to 10 genera, of which 98 different strains from 10 different genera have been used in statistical comparisons (Table 4).

The spectra of these organisms were obtained under the standard conditions already described, the strains of any one species being grown on the same day and under the same conditions. For any species except *Chr. violaceum* the spectra of strains within the species are very similar.

The following results are instructive as an example of what the technique can achieve in strain differentiation. It was found that the spectrum of a strain

Chr. prodigiosum 2 was identical by inspection with that of a strain *Chr. prodigiosum* 4. To rule out the possibility of error, fresh samples of these two strains were prepared from fresh dried cultures, and their spectra examined. Once again the two spectra were identical, but the second pair differed slightly from the first pair. A very comprehensive bacteriological examination of the two strains failed to show any difference between them. When a pair of the spectra were compared statistically, the z obtained was 3·28, whereas $\bar{z}$ for the comparison of all pairs of the strains of *Chr. prodigiosum* was 2·86.

Table 4. Species used in correlations

Genus	Species	Number of strains
Bacterium	*aerogenes*	2
	cloacae	2
	coli	9
Brucella	*abortus*	1
	suis	2
Chromobacterium	*prodigiosum*	6
	violaceum	7
Corynebacterium	*diphtheriae*	7
	hofmanni	1
	xerosis	2
Pasteurella	*pestis*	6
Proteus	*vulgaris*	1
Salmonella	*london*	1
	montevideo	1
	newport	1
	typhi	14
	typhi-murium	3
Shigella	*alkalescens*	2
	dispar	1
	flexneri	1
	schmitzi	2
	dysenteriae	7
	sonnei	1
Staphylococcus	*albus*	2
	aureus	6
Streptococcus	*haemolyticus*	10

The evidence thus points to the fact that strain differentiation is possible, but that if it is to be made a reliable method much more work must be done to determine whether spectral differences arising in specimen preparation are due to inadequate technique, to bacterial variation, or to a combination of both. Using the methods now described, such differences are of the same magnitude as those associated with strain differences.

3. *Species and genus differences*

By a visual examination of the spectra of the bacteria used for studying strain differences it was obvious that there was a tendency for the spectra of organisms

VOL. 9 1957

of the same genus to be more alike than those from different genera. The main spectral features which demonstrate this are:

(i) The shape of the absorption bands at 6·0–6·4 μ.
(ii) The ratio of the intensity of the bands at 7·0 and 7·2 μ.
(iii) The shape of the bands at about 7·6 μ.
(iv) The relative intensity of the band at 8·1 μ.
(v) The shape of the strong band at 9·3–9·5 μ.

Fig. 1 shows the spectral shapes characteristic of certain genera.

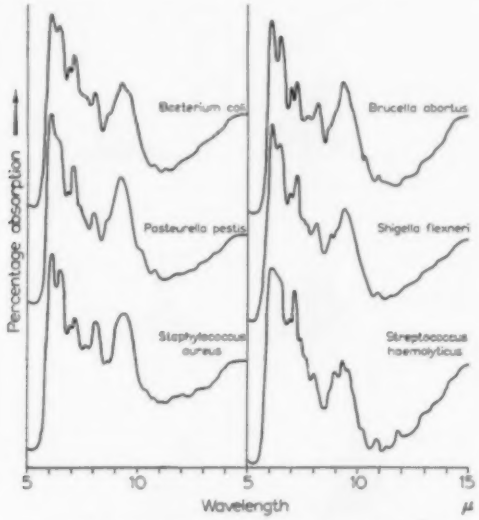

Fig. 1. Spectra typical of certain genera. (The spectra are displaced vertically).

When bacteria are grown on a given medium, the shape of the band at 9·3–9·5 μ, which is probably due to carbohydrate, tends to be characteristic of the genus. The addition of any fermentable carbohydrate to the medium results in the shape of this strong band being changed. Comparison of spectra obtained after growth on PA and on TMA does not show any change in the shape of this or of any other prominent band. This is borne out by the fact that when an organism is grown on PA and TMA, z for the comparison of the two spectra is high. For several such comparisons $\bar{z}$ is 3·11.

The fact that organisms of a given genus are more alike than those from different genera is shown by the values of $\bar{z}$ in Table 2. The $\bar{z}$ obtained by comparing strains from different genera is 2·39, whereas the comparison of strains within a given species gives a value of 3·00. The difference between different genera may readily be seen by inspection of the spectra, but the difference between different species of the same genus is not so obvious. Despite this, the $\bar{z}$ obtained by inter-comparing strains of different species of a given genus is 2·74. The possibility of species differentiation is shown more clearly by a detailed study of strains within the genera *Salmonella* and *Chromobacterium*. The genus *Salmonella* is represented by fifteen strains from two species. For the St comparisons $\bar{z}$ is 3·07, whereas for

the Sp comparisons $\bar{z}$ is 2·84; this is further reduced to 2·44 for the G comparisons when all the strains are compared with strains of *Staph. aureus*. The corresponding values of $\bar{z}$ for strains of *Chromobacterium* are $\bar{z}_{St} = 2{\cdot}86$, $\bar{z}_{Sp} = 2{\cdot}29$, and $\bar{z}_{G} = 2{\cdot}13$ respectively. The actual distribution of z is shown in histogram form in Fig. 2. The distributions overlap, and the χ^2 test can be used as already described to test the significance of the difference.

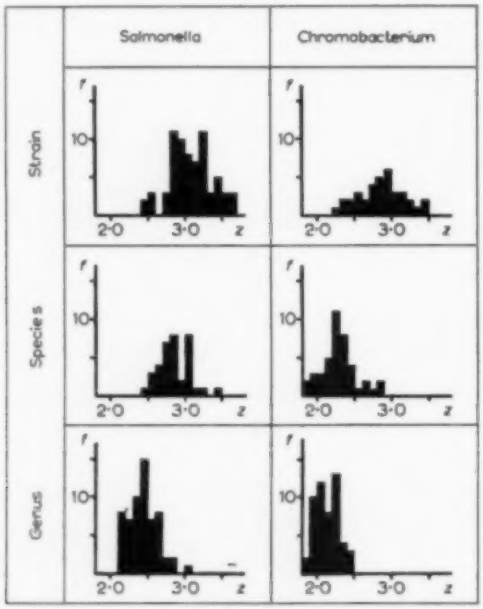

Fig. 2. Frequency distribution of z for strain, species, and genus differences. Ordinate, class frequency. Abscissa, value of z.

For the Sp comparisons of the Salmonellae, $P(\chi^2)$ is $<0{\cdot}001$, and likewise for the G comparisons of the genera *Salmonella* and *Staphylococcus* $P(\chi^2)$ is $<0{\cdot}001$; the corresponding values for the genus *Chromobacterium* are $<0{\cdot}001$ and 0·003. These results show that there is little chance of the different distributions having arisen by random sampling even though there is overlap in the distribution of z.

In Table 5 none of the values of $P(\chi^2)$ much exceeds 0·01, except that for the comparison of *Staph. aureus* with *Staph. albus*. There were five strains of *Staph. aureus* and only two of *Staph. albus*, and it is felt that here there are too few values of z for the χ^2 test to have much meaning. By visual examination of the spectra of strains of these species it is possible to differentiate them.

Among the coliform organisms used there is one strain of *Bact. cloacae*, and as this has a spectrum markedly different from the others, there is some scatter in the values of z for coliform-coliform comparisons. The $\bar{z}$ for these comparisons when *Bact. cloacae* is included is 2·82, but if *Bact. cloacae* is excluded, $\bar{z}$ rises to 2·91, although it is admitted that this change is not significant.

For the comparison of *Chr. prodigiosum* with *Chr. violaceum* $\bar{z}$ is 2·29, and it has

VOL. 9 1957

been seen that for the comparison of different genera $\bar{z} = 2{\cdot}39$. The spectral differences within the genus *Chromobacterium* are therefore greater than those normally occurring between different genera. These results are reflected in the values of $P(\chi^2)$ for species differences of *Chromobacterium* and the genus difference of *Chromobacterium* and *Staphylococcus* given in Tables 5 and 6 respectively. The

Table 5. Significance of species differences

		N	χ^2	$P(\chi^2)$	V
Shigella species	6 × 2 × 2 × 1 × 1 × 1*	78	6·4	0·011	0·323
Bacterium species	9 × 2 × 2	78	7·4	0·0065	0·333
Staphylococcus species	5 (in duplicate) × 2 (1 in duplicate)	72	0·24	0·62	0·0857
Chromobacterium species	5 × 7	66	24·4	<0·001	0·635
Salmonella species	12 × 3	105	12·5	<0·001	0·366
Corynebacterium species	5 × 2 × 1	28	11·0	<0·001	0·702

* Six strains of *Shig. dysenteriae*, two each of *Shig. alkalescens* and *Shig. schmitzi*, one each of *Shig. dispar*, *Shig. flexneri*, and *Shig. sonnei*.

classification of bacteria on the basis of pigment production seems to result in the inclusion of organisms of widely different composition in the same genus (see, for instance, [15, p. 726, 24]).

Whilst the spectra of different genera tend to have characteristic shapes, it is found that the genera *Salmonella*, *Proteus*, and *Shigella*, and the coliform bacteria give rise to similar shapes. Only one strain of *Proteus* was examined, but its

Table 6. Significance of genus differences

	N	χ^2	$P(\chi^2)$	V
Shigella—Salmonella	113	30·1	<0·001	0·535
Shigella—Bacterium	97	0·35	0·55	0·0806
Salmonella—Bacterium	71	7·71	0·0052	0·358
Salmonella—Staphylococcus	68	24·1	<0·001	0·626
Brucella—Staphylococcus	28		<0·001	1·0
Corynebacterium—Shigella	85	46·6	<0·001	0·765
Corynebacterium—Staphylococcus	73	53·0	<0·001	0·8783
Chromobacterium—Staphylococcus	128	8·8	0·003	0·28

spectrum was so similar to that of *Salm. typhi* that comparison gave $\bar{z} = 3{\cdot}08$. The spectra of strains of *Shigella* and of many of the coliform organisms have a shoulder at about 8·7 μ on the large absorption band centred at 9·3–9·5 μ. This feature, which may be used to distinguish the spectra visually, has an effect on the correlation coefficient. Thus for the G comparison of *Shigella* and *Bacterium* (Table 6), $P(\chi^2)$ is 0·55. However, other G comparisons involving *Salmonella*,

Shigella, and the coliform bacteria result in low values of $P(\chi^2)$, that is to say, the spectra can be distinguished with a high degree of confidence. In Table 6 none of the values of $P(\chi^2)$, except that for the comparison *Shigella-Bacterium*, is greater than 0·01.

Table 2 is a summary of all the results obtained. It has already been seen that $\bar{z}$ decreases progressively for comparisons of duplicate spectra, traversal of specimen (evenness of film), replicate specimens of the same strain grown at the same time, different samples of the same strain grown at different times, different strains of the same species, different species of the same genus, and finally different genera. The probability that the seven means in Table 2 should appear by chance in this logical order is only 1/5040. In particular, the order of the means for St, Sp, and G comparisons is of great importance. As the data for Table 2 have been collected and the number of comparisons has increased, the means for these three kinds of comparisons have changed very little. The stability of the means in conjunction with the values of χ^2 in Tables 3, 5, and 6 is strong evidence for saying that the spectral difference between dissimilar organisms is greater than that between similar ones. Thus the correlation coefficients between pairs of spectra and the relative positions of the corresponding organisms in the hierarchical classification appear to be related.

Other applications of infra-red spectrophotometry

1. *Interpretation of spectra*

Because there are significant differences in the spectra of different organisms, it is pertinent to enquire what these differences are due to.

The spectra of bacteria contain several strong bands in the 3 μ region which may be attributed to the stretching of carbon-hydrogen and nitrogen-hydrogen bonds. In early work, little or no information was found in this region useful for the differentiation of bacteria, so that most of the spectra were recorded from 5–15 μ. In any future work concerned with relating spectrum to structure it will be necessary to record from 2–15 μ.

The bands in the spectrum from 6 to 10 μ are superimposed on a strong background absorption due to protein. The peptide link of the protein itself gives rise to strong absorption bands at about 6·1 and 6·5 μ. Other strong bands in the spectra of bacteria occur at 6·9 ,7·1, 8·1, and in the region 9·3–9·5 μ. The last is thought to be due to carbohydrate, while both ribonucleic acid and deoxyribonucleic acid give rise to bands at 8·1 μ. Each of these strong bands probably represents the sum of contributions from more than one class of compound. Goulden [25] made the observation that when casein and sugar are mixed dry, the spectrum of the mixture contains all the bands due to casein and the sugar. When, however, solutions are mixed and then dried, many of the bands become so broad and diffuse as to lose their identity. These effects, which can be explained in terms of the change of state of the lactose with the amount of water present (Norris and Greenstreet, unpublished), make it extremely difficult to interpret the spectra of bacterial films. The situation is even further complicated by the large background absorption in the spectra.

VOL. 9 1957

Despite these difficulties, a certain amount of progress can be made in studying the structure of cells by examining the spectra of pure known substances of biological importance, examining known compounds derived from bacteria, and treating films of bacteria with enzymes and solvents and trying to interpret the consequent changes in the spectra.

The small differences in spectra between two bacteria may be enhanced by one or both of two methods: (i) Isolating the components responsible for the spectral difference [2]; (ii) Differential spectroscopy in which bacterial films are compared directly by putting one film in the sample beam and the other in the reference beam. Alternatively, they may each be compared with a standard film. In this way, minute bands in the spectra of ordinary bacterial films have been amplified tenfold and doubtful bands clearly demonstrated as being true absorption bands.

2. *Aerobic spore-forming bacilli*

An attempt was made to bring the aerobic spore-forming bacilli into the scheme already described, but it was found that such organisms gave variable spectra. This can be attributed to the fact that the physiological state of the organisms changes profoundly during growth. This change is reflected in the absorption spectrum (Fig. 3), and there is a distinct correlation between the infra-red absorption spectrum and the morphology of the organisms. To study this problem it is necessary to arrange if possible for all the organisms to be in a similar state of development. This can be achieved by suitable choice of medium and conditions of growth. The spectral changes are blurred if the organism is grown on a medium on which it does not develop uniformly throughout the culture.

The change in spectrum between 5 hour vegetative cells and resting spores is greater than any difference we have observed between films of vegetative bacteria. Reference has already been made to the difficulties in interpreting such changes in spectrum. As an example of the usefulness of differential spectroscopy, the following example can be quoted. It was shown by Powell [26] that when spores of *Bacillus megatherium* germinate, calcium dipicolinate (calcium salt of pyridine-2:6-dicarboxylic acid) separates from the spore suspension. There are only a few small differences between the spectra of resting and germinated spores of *B. megatherium*. The spectrum of the resting spores shows bands at 13·1, 13·9, and 14·4 μ, which are not obvious in the spectrum of germinated spores but which appear in the spectrum of calcium dipicolinate. If the spore films are made thicker, the film of the resting spores placed in the sample beam and the film of the germinated spores in the reference beam, then in the resulting differential spectrum these three bands are more prominent and ten other bands due to calcium dipicolinate become visible. The differential spectrum between 6 hour vegetative cells and resting spores is very complex, and much more work is necessary to understand it.

Discussion

Reproducible spectra of bacterial films can be obtained when careful attention is paid to standardizing every experimental procedure. The experimental methods used in this work have been discussed at great length to emphasize the point that small variations in any one of the operations can lead to different spectra. The

methods adopted by us are not ideal, but were selected for their simplicity and reproducibility. It is known that the spectra of live and heat-killed bacteria are different, but for reasons of safety we elected to kill the organisms. It may be that the spectral differences between live organisms are greater than those between dead ones, but there is a greater possibility of live organisms changing with time.

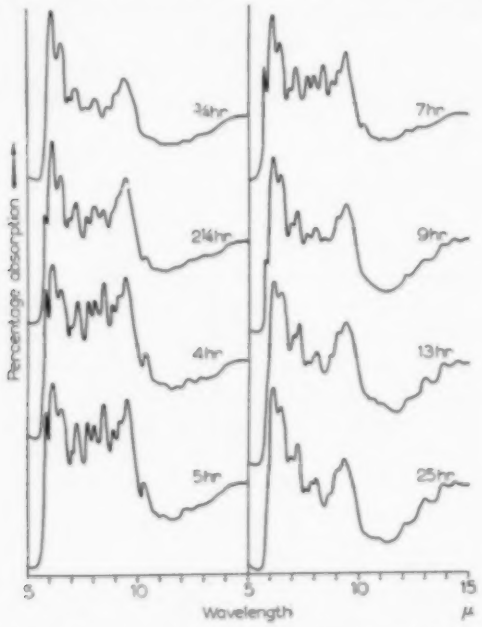

Fig. 3. Changes in spectra of *Bacillus megatherium* with incubation time (Hills' glucose lactate medium).

Whilst the use of suspensions makes the handling of bacteria more convenient and helps in the preparation of uniform films, it places some restriction on the technique, because it is found that spectra produced from a suspension of an organism known to produce a capsule (e.g. *Past. pestis* grown at 37°C) do vary slightly amongst themselves. This is almost certainly because such organisms stick to the walls of containing vessels, and so change the composition of the suspension. The resulting changes in spectrum are of the same order of magnitude as the differences exhibited by two strains of a given species. It may be that some refinement of the original smear technique such as that used by Stevenson and Bolduan [7] may be successful in such circumstances.

The potassium bromide pressed-disk technique [27] is a further method of preparing bacteria for examination in the infra-red. To incorporate bacteria into a disk with potassium bromide requires that the bacteria be frozen-dried and ground into a fine powder. This presents considerable difficulties, because frozen-dried bacteria cannot easily be ground and they are strongly hygroscopic. Perhaps the greatest source of variation in the method used by us lies in the use of silver chloride as a support for the bacterial film. Silver chloride, being soft, is easily

VOL. 9 1957

scratched and its absorption spectrum changes with age. Barium fluoride, by contrast, is a hard crystalline substance and it may be better to use it as the support for obtaining the spectra of bacteria and to accept the resulting restriction of the wavelength range. The difficulties associated with recording the spectra have already been discussed. With prism spectrophotometers small changes in band shape can be recorded, but grating instruments may make the process more reliable because for the same resolving power wider slits can be used than on a prism instrument. If the technique is to be applied to a systematic study of bacteria, it would seem desirable to develop an instrument specifically for that purpose.

The results presented here can be deduced by a visual examination of the spectra; the correlation coefficients were used to express mathematically what had already been seen by eye. The Spearman rank correlation coefficient is not ideal for this purpose, because it attaches equal significance to the measurement at each wavelength, whereas it is known that the ranks of the ordinates at some wavelengths are nearly the same for many bacteria. If some method of comparing spectra at points of significant difference can be found, then such correlations will differ much more than do the transformed Spearman coefficients. It might be possible by multivariate analysis [28] to calculate a single coefficient which takes simultaneous account of a number of features of importance. This has not been done in the present work because it is the object here to show that there is sufficient information in the infra-red absorption spectrum of bacteria for the spectra to be used as the basis of a scheme of identification. The treatment of spectra so that they may be compared with one another deserves more study, and if the infra-red method is to be used on a large scale for comparing bacteria it may be necessary to use machine-sorting equipment such as that used by Riddle *et al.* [29] to differentiate between clinically important bacteria.

Several methods may be used to enhance the spectral difference between two bacteria and so make differentiation easier.

The inclusion of carbohydrate in the medium can result in large changes in the spectra of bacteria. Species which were difficult to differentiate when grown on a medium with no carbohydrate were more easily differentiated when a carbohydrate utilized by the one but not by the other was included in the medium [30].

The spectra of bacteria are dominated by that of protein, and if the protein or a large part of it could be removed, the spectrum of the remaining bacterial substance would show greater differences. It seems unlikely that any chemical process will be satisfactory for this purpose, but it may be done by differential spectroscopy. A differential spectrum between bacteria and protein will probably contain much more information upon which to base an identification scheme. A disadvantage of this method is that greater amounts of bacterial substance are necessary to produce satisfactory differential spectra. This is not important for research purposes, but poses further difficulties for any practical scheme for the identification of single colonies.

It could be argued that it should be possible to compensate for material in the suspensions other than cell substances by putting something in the reference beam. Neither washing sterile medium nor washing medium after bacteria have been

grown on it will supply just the right mixture of extracts from the medium and of bacterial products. The nature of such a mixture will change for each organism examined. It is difficult to see how compensation can be accomplished without introducing another uncontrolled variable.

The results do show that the spectra of different genera tend to have characteristic shapes, and it is our opinion that species differentiation will be possible. The classification and nomenclature in bacteriology are not yet as ordered as those existing in botany and zoology [15, p. 370, etc.], although the attempt to improve is going on constantly. Bacteria of medical importance and such others as may be confused with them have been widely studied, and these are classified largely on physiological characteristics, antigen-antibody reactions, and pathogenicity. The commonly used classifications tend to have identification as their object rather than the logical reflection of a natural order. Whilst some genera have been closely studied, others have received very little attention. Consequently, it is possible that in some instances bacteria may temporarily have been classified as congeners on inadequate grounds. A further difficulty arises in the definition of a species. For instance, among the organisms of the genus *Salmonella* many antigenic patterns have been identified and, until recently, each of these was given a specific name. On the other hand, certain of the streptococci have been differentiated by antigen-antibody reactions and the resulting subdivisions identified by type numbers only.

These two points—the variation in the extent of our knowledge about each of the groups of bacteria called genera and the inconsistency from genus to genus of the grounds upon which specific rank is accorded, reflect the difficulty of classifying bacteria at the present time.

For the identification of the strains used in this infra-red study, the nomenclature used by Wilson and Miles [15] has been followed.

It is interesting and encouraging to find that, as far as it goes, the statistical comparison of the spectra of bacteria leads to conclusions very similar to those reached on the evidence supporting classification. Three points may be emphasized.

The strains of *Salm. typhi* resemble one another much more closely than do for instance the strains of *Chr. violaceum*.

The organisms of the genus *Salmonella* are more similar than are the *Chromobacterium* species.

The Salmonella, Shigella, Proteus, and coliform strains all resemble one another very closely: on biological grounds these are classified together, forming the tribe *Bactericae* [15, p. 380].

Insufficient data have been obtained to judge how useful infra-red spectrophotometry may be in elucidating the structure of cells, but the indications are that it will be of great use to the bacterial chemist. Only milligram quantities of a substance are required to obtain satisfactory infra-red absorption spectra, and by comparison with the spectra of pure substances it may be possible to identify components isolated from cells. The fractionation of bacteria accompanied by infra-red examination of the fractions may result in a fuller understanding of cell composition. The examples quoted in the introduction and in the paper are the start of what may be a very profitable field of study. Even though it may not be possible to break down bacteria and identify their components, it may be possible

VOL. 9 1957

to study the differences between bacteria by differential spectroscopy coupled with the examination of pure cell substances. As the spectrum of an organism changes with the environment in which it multiplied, the latter technique may be applicable to the study of the metabolism of bacteria under different conditions. This change in spectrum is most marked with the aerobic spore-forming bacilli. In growing these organisms it was essential for the conditions to be so chosen that all the individuals grew and developed at about the same rate. Only by doing this could the spectral changes be followed satisfactorily. Perhaps the best way of obtaining cells in a uniform state is to grow them in continuous culture, and preliminary results indicate that infra-red spectrophotometry may be of some value in studying cells grown in this way.

We wish to thank Dr. D. W. HENDERSON, Director, M.R.E., for his constant advice and encouragement. Also we are greatly indebted to Mr. E. O. POWELL for suggesting the statistical treatment of our results and for much helpful advice and criticism, and to Dr. H. W. THOMPSON, F.R.S., for constructive criticism of the work and the manuscript. We are grateful to Mr. E. C. FIELLER for helpful discussions of the statistical methods, and to Mr. S. PETO, both for discussing the statistics and doing much of the calculation for us. We wish to acknowledge with gratitude the invaluable technical assistance rendered by Mr. D. A. V. JOHNSON and Miss JEAN M. SCOTT. Finally, we wish to thank Lt.-Col. E. J. BOWMER, R.A.M.C., and Dr. I. H. PATTISON for supplying us with strains of bacteria.

References

[1] RANDALL H. M., SMITH D. W., COLM A. C., and NUNGESTER W. J. *Amer. Rev. Tuberc.* 1951 **63** 372.
[2] RANDALL H. M., SMITH D. W., COLM A. C., and NUNGESTER W. J. *Amer. Rev. Tuberc.* 1952 **65** 477.
[3] RANDALL H. M. and SMITH D. W. *J. Opt. Soc. Amer.* 1953 **43** 1086.
[4] SHIRK H. G. and GREATHOUSE G. A. *Analyt. Chem.* 1952 **24** 1774.
[5] STEVENSON H. J. R. and LEVINE S. *Science* 1952 **116** 705.
[6] LEVINE S., STEVENSON H. J. R., and KABLER P. W. *Arch. Biochem. Biophys.* 1953 **45** 65.
[7] STEVENSON H. J. R. and BOLDUAN O. E. A. *Science* 1952 **116** 111.
[8] SLATER J. C. *Phys. Rev.* 1925 **25** 783.
[9] BRODERSEN S. *J. Opt. Soc. Amer.* 1954 **44** 22.
[10] THOMAS L. C. and GREENSTREET J. E. S. *Spectrochim. Acta* 1954 **6** 302.
[11] LEVINE S., STEVENSON H. J. R., CHAMBERS L. A., and KENNER B. A. *J. Bact.* 1953 **65** 10.
[12] LEVINE S., STEVENSON H. J. R., BORDNER R. H., and EDWARDS P. R. *J. Infect. Dis.* 1955 **96** 193.
[13] BENEDICT A. A., POLLARD M., and ENGLEY F. B. *Tex. Rep. Biol. Med.* 1954 **12** 21.
[14] BENEDICT A. A. *J. Bact.* 1955 **69** 264.
[15] WILSON G. S. and MILES A. A. Topley and Wilson's *Principles of Bacteriology and Immunity* (4th ed.) Vol. 1. Edward Arnold, London, 1955.
[16] PHILPOTTS A. R., THAIN W., and SMITH P. G. *Analyt. Chem.* 1951 **23** 268.
[17] ROBINSON D. Z. *Analyt. Chem.* 1951 **23** 273.
[18] BRODERSEN S. *J. Opt. Soc. Amer.* 1953 **43** 877.
[19] WILLIAMS V. Z. *Rev. Sci. Instrum.* 1948 **19** 135.
[20] NORRIS K. P. *J. Sci. Instrum.* 1956 **33** 125.
[21] BROWN H. C. and KIRWAN E. W. O'G. *Indian J. Med. Res.* 1915 **2** 763.
[22] FISHER R. A. *Statistical Methods for Research Workers* (10th ed.) p. 197. Oliver and Boyd, London, 1946.

[23] Yule G. U. *J. Roy. Statist. Soc.* 1912 **75** 579.
[24] Sneath P. H. A. *J. Gen. Microbiol.* 1956 **15** 70.
[25] Goulden J. D. S. *Nature, Lond.* 1956 **177** 85.
[26] Powell J. F. *Biochem. J.* 1953 **54** 210.
[27] Ford M. A. and Wilkinson G. R. *J. Sci. Instrum.* 1954 **31** 338.
[28] Wishart J. *Applied Statistics* 1955 **4** 103.
[29] Riddle J. W., Kabler P. W., Kenner B. A., Bordner R. H., Rockwood S. W., and Stevenson H. J. R. *J. Bact.* 1956 **72** 593.
[30] Levine S., Stevenson H. J. R., Tabor E. C., Bordner R. H., and Chambers L. A. *J. Bact.* 1953 **66** 664.

VOL.
9
1957

Spectrochimica Acta, 1957, Vol. 9, pp. 199 to 203. Pergamon Press Ltd., London

Infra-red absorption spectra of inorganic co-ordination complexes—XI

Infra-red studies of mercuric amidobromide, $Hg(NH_2)Br$*

I. Nakagawa, R. B. Penland, S. Mizushima,†
T. J. Lane, and J. V. Quagliano

(*Received* 19 *February* 1957)

Abstract—Infra-red spectra of the cubic and rhombic modifications of $Hg(NH_2)Br$ have been measured in the 2–35-μ region. From the result of the normal vibration calculation made for the $HgNH_2^+$ ion, the infra-red absorption bands of these modifications have been assigned.

Introduction

X-ray diffraction studies of the cubic and the rhombic modifications of $Hg(NH_2)Br$ have been made by Brodersen and Rudorf [1], and Nijssen and Lipscomb [2], respectively. The structure of the $Hg(NH_2)^+$ ion present in $Hg(HN_2)Br$ is similar to that of $Hg(NH_2)Cl$ and consists of infinite chains of alternating Hg and NH_2 with linear bonds about Hg and tetrahedral bonds about the nitrogen.

In a previous paper [3], the calculation of the normal vibrations of the $HgNH_2^+$ infinite chain and the comparison of these results with the infra-red frequencies observed for $Hg(NH_2)Cl$ were reported.

We made a similar investigation of the cubic and rhombic modifications of $Hg(NH_2)Br$, and after its completion a paper published by Brodersen and Becher on the same subject [4] was brought to our attention. However, our interpretation of the spectra, based on our calculation [3], is quite different from that of Brodersen and Becher. Our assignment of the bands of the two modifications is discussed in this paper.

Experimental

Preparation of compounds. Cubic mercuric amidobromide, $Hg(NH_2)Br$, prepared by the method of Brodersen and Rudorff [5], was dried for 2 hours at 100 C.

Anal.—Calcd. for $Hg(NH_2)Br$: N 4·72. Found: N 4·42.

Rhombic mercuric amidobromide, $Hg(NH_2)Br$, prepared by the method of Lipscomb [2], and Brodersen [5], was dried for 2 hours at 100°C and then over P_2O_5. As reported by Brodersen and Rudorff, the rhombic complex contains about 5% $HgBr_2$, which stabilizes this modification [5]. The spectrum of this impurity shows no absorption band in the NaCl region.

Absorption measurements. The infra-red spectra were obtained by means of a Perkin-Elmer infra-red spectrophotometer model 21 with sodium chloride and caesium bromide prisms over their regions of greatest resolution. The spectra of the solid complexes were obtained by the potassium bromide disk technique [6] and checked in Nujol mulls.

---

* For paper X in this series see *J. Amer. Chem. Soc.* 1957 **79** 1575. Contribution from the Department of Chemistry, University of Notre Dame, Indiana, U.S.A.

† Visiting Professor from the Faculty of Science, Tokyo University.

Results

The absorption spectra observed for cubic and rhombic modifications of $Hg(NH_2)Br$, shown in Fig. 1, are in general agreement with those reported by Brodersen and Becher. In some bands considerable differences in frequency have been observed between the two modifications. The largest differences are those observed between the 510 cm^{-1} band (cubic) and the 560 cm^{-1} band (rhombic), and between the 950 cm^{-1} band (cubic) and the 1005 cm^{-1} band (rhombic). Smaller but definite differences in frequency have been observed for all other bands.

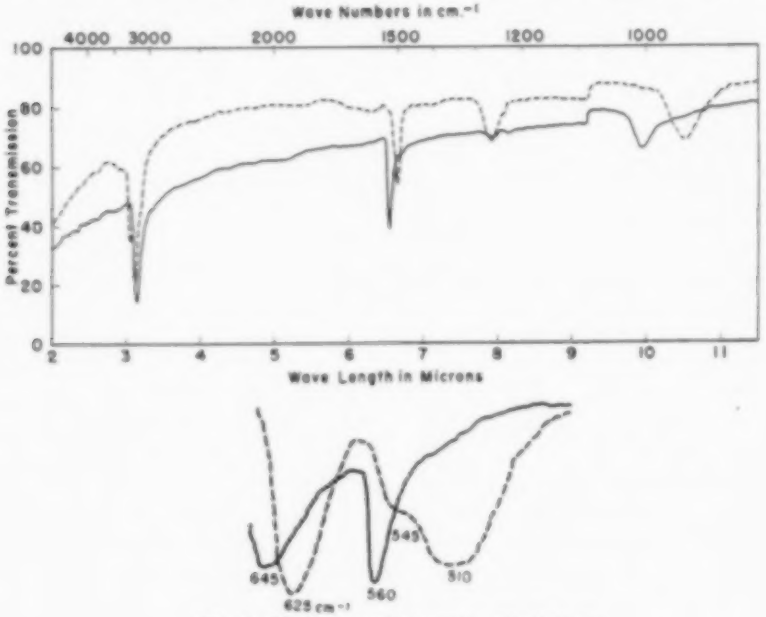

Fig. 1. Mercuric amidobromide, $Hg(NH_2)Br$.
– – – – cubic; ——— rhombic.

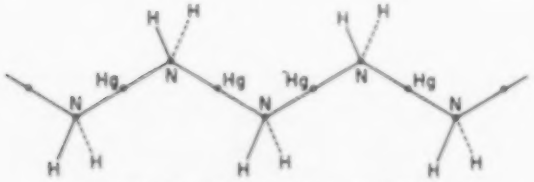

Fig. 2. The infinite chain of $HgNH_2^+$.

Discussion

The infinite chain of the $HgNH_2^+$ ion has the structure as shown in Fig. 2. The normal vibrations of this chain were calculated by Mizushima, Nakagawa, and Sweeny [3]. Based on the result of this calculation, the assignment of the observed frequencies of $Hg(NH_2)Br$ can be made as shown in Table 1. The bands observed in the 3 μ region, not listed in Table 1, undoubtedly can be assigned to the NH stretching vibrations.

VOL.
9
1957

Table 1. Assignment of the observed frequencies of cubic and rhombic $Hg(NH_2)Br$

Class	Type of vibration	Calc.	Obs. cubic	Obs. rhombic
A_{1g}	NH_2 bending	1535	i.r.—inactive	
	chain vibration	668		
A_{1u}	Hg-N stretching	522	—	—
	NH_2 bending	1540	1505	1528
	chain deformation	123	Outside the observable region	
B_{1g}	Hg-N stretching	542	i.r.—inactive	
	NH_2 wagging	1022		
B_{1u}	Hg-N stretching	588	510	560
	NH_2 wagging	1025	950	1005
	N-Hg-N deformation	74	outside the observable region	
B_{2g}	NH_2 rocking	638	i.r.—inactive	
B_{2u}	NH_2 rocking	651	620	647
	N-Hg-N deformation	207	outside the observable region	
A_{2g}	NH_2 twisting	978	i.r.—inactive	
A_{2u}	NH_2 twisting	979	i.r.—inactive	
	N-Hg-N deformation	63		

The observed frequencies of $Hg(NH_2)Br$, shown in Table 1, are consistently lower than those of $Hg(NH_2)Cl$ [3], and, since the difference in frequency values is not large, the values calculated for $Hg(NH_2)Cl$ [3] could be used in the above assignment of the bands observed for cubic and rhombic $Hg(NH_2)Br$. The calculation was made by using the potential function of the Urey-Bradley type:

$$V = \sum \tfrac{1}{2}K_i(\Delta r_i)^2 + \sum \tfrac{1}{2}H_{ij}r_i^0 r_j^0(\Delta\alpha_{ij})^2 + \sum \tfrac{1}{2}F_{ij}(\Delta q_{ij})^2 + \text{linear terms}$$

where r_i and r_j are bond lengths with equilibrium values r_i^0 and r_j^0, α_{ij} bond angles, q_{ij} distances between nonbonded atoms, and K, H, and F stretching, bending, repulsive-force constants, respectively.

The largest difference in frequency, amounting to some 10%, between the cubic and rhombic modifications of $Hg(NH_2)Br$, occurs for the Hg-N stretching vibration. This is explained by the difference in the Hg-N bond length of the two modifications (cubic 2·17 Å and rhombic 2·07 Å) [1, 2]. Consequently, a considerable difference in the value of the stretching force constants K(Hg-N), which in turn largely affects the value of the Hg-N stretching frequency, can be expected.

The next largest difference in frequency value, amounting to about 5%, was found for the NH_2 wagging and NH_2 rocking vibrations. These vibrations are

mainly concerned with the bending-force constant H(HNHg), and the repulsive-force constant between the non-bonded H and Hg atoms, F(H···Hg). Therefore, this difference in frequency mainly arises from the change in these force constants, insofar as the intramolecular forces are concerned.

The difference in the NH_2 bending-frequency values between the cubic and rhombic modifications was found to be the least among the NH_2 deformation vibrations. This is also understandable, because the NH_2 bending vibration is mainly determined by the bending-force constant H(HNH) and the repulsive-force constant of the interaction between nonbonded hydrogen atoms, F(H···H). It is reasonable to assume that these force constants have almost the same values for the two modifications.

In addition to the change in the intramolecular force constants noted above, the difference in the N···Br distance [1, 2] between the cubic and the rhombic modifications, probably caused by the difference in hydrogen bonding [2], must be taken into account. The difference in the NH stretching frequencies will be due largely to this difference in hydrogen bonding. The difference in hydrogen deformation vibrations explained above also arises in part from this difference.

Our observed frequencies are in agreement with those reported by BRODERSEN and BECHER, but our assignments differ. For example, they assigned the bands at 1260 cm^{-1} (cubic) and 1267 cm^{-1} (rhombic) to the NH_2 wagging frequency. According to our calculation of normal vibrations of the $HgNH_2^+$ infinite chain, we calculated two wagging frequencies as 1022 cm^{-1} (B_{1g}) and 1025 cm^{-1} (B_{1u}), of which B_{1g} is infra-red inactive. The calculated value 1025 cm^{-1} for B_{1u} is much closer to the observed values, 1005 cm^{-1} and 950 cm^{-1}, than 1260 cm^{-1} and 1267 cm^{-1}. The values of the force constants used in our calculation are transferable to other molecules with similar structures. For example, employing values of H(HNH), H(HgNH), F(H···H), and F(Hg···H) given above, we have calculated the frequencies of NH_3 [7], NH_4^+ [7], $Co(NH_3)_6^{+++}$ [8], and $Hg(NH_3)_2^{++}$ [9], and found them to be in good agreement with those observed. Therefore, such a large discrepancy between the calculated and observed frequencies, 1025 cm^{-1} and 1260 cm^{-1}, is not to be expected.

BRODERSEN and BECHER assigned the 950 cm^{-1} (cubic) and 1005 cm^{-1} (rhombic) frequencies to the NH_2 twisting vibrations. However, the twisting vibrations belong to the A_{2g} and A_{2u} types of the vibration of the infinite chain, both of which are inactive in the infra-red absorption.

As to the two bands present at about 1260 cm^{-1}, also observed by us, we consider these to be due to an impurity of $(Hg(NH_3)_2)Br_2$ contained in the sample of $Hg(NH_2)Br$, similar to the presence of an impurity of $(Hg(NH_3)_2)Cl_2$ in $Hg(NH_2)Cl$ [10].

Support for this conclusion is as follows: (1) Our spectra reveal that the intensity of the band at about 1260 cm^{-1} of the rhombic form is extremely weak compared with that of the cubic form, whereas the intensities of all other corresponding bands of the two modifications are almost the same. (2) The frequency difference between the two bands at about 1260 cm^{-1} is insignificant, whereas the frequency difference of other similar bands is considerable. In other words, if the 1260 cm^{-1}-bands were to be assigned to the NH_2 wagging frequency of $Hg(NH_2)Br$,

VOL. 9 1957

its frequency values should be appreciably different in the two modifications of $Hg(NH_2)Br$. (3) We prepared $(Hg(NH_3)_2)Br_2$ and found its strongest absorption to appear at 1245 cm^{-1}, and the difference between this value and 1260 cm^{-1} may arise from the dispersion of $(Hg(NH_3)_2)Br_2$ in the solid $HgNH_2Br$.

BRODERSEN and BECHER considered the Hg-N-Hg angle of the cubic modification to be 90° and that of the rhombic form to be a tetrahedral angle. Our calculation of the infinite chain of $(HgNH_2^+)$ was made with a Hg-N-Hg tetrahedral angle [2]. However, in the G matrix for the NH_2 deformation vibrations no diagonal terms concerning the Hg-N-Hg angle are present. Therefore, the calculated frequencies using a 90° bond angle for the cubic modification will differ only slightly from those listed in Table 1, and no ambiguity arises concerning the assignments.

As referred to above, we have also calculated the normal vibrations of the $(Hg(NH_3)_2)^{++}$ ion, and according to this calculation the 1245 cm^{-1} band is the NH_3 symmetric deformation vibration of the A_2 type [9].

Acknowledgement—We are indebted to Professor W. N. LIPSCOMB for informing us of the difference in structure between the two modifications of $Hg(NH_2)Br$ observed by X-ray diffraction studies.

This investigation was supported in part by a research grant H-2218 (C) from the Department of Health, Education and Welfare, Public Health Service.

References

[1] BRODERSEN K. and RUDORFF W. *Z. Anorg. Chem.* 1952 **270** 145.
[2] NIJSSEN L. and LIPSCOMB L. *Acta Cryst.* 1952 **5** 604.
[3] MIZUSHIMA S., NAKAGAWA I., and SWEENY D. M. *J. Chem. Phys.* 1956 **25** 1006.
[4] BRODERSEN K. and BECHER H. H. *Ber. Dtsch. Chem. Ges.* 1956 **89** 1487.
[5] BRODERSEN K. and RUDORFF W. *Z. Anorg. Chem.* 1954 **275** 141.
[6] STIMSON M. M. and O'DONNELL M. J. *J. Amer. Chem. Soc.* 1952 **74** 1805.
FAUST J. P. and QUAGLIANO J. V. *Ibid.* 1954 **76** 5346.
[7] NAKAGAWA I. and MIZUSHIMA S. *Bull. Chem. Soc. Japan* 1955 **28** 589.
[8] MIZUSHIMA S., NAKAGAWA I., and QUAGLIANO J. V. *J. Chem. Phys.* 1955 **23** 1367.
[9] BERTIN E., NAKAGAWA I., MIZUSHIMA S., LANE T. J., and QUAGLIANO J. V. To be published.
[10] LIPSCOMB W. N. *Anal. Chem.* 1953 **25** 737.

Spectrochimica Acta, 1957, Vol. 9, pp. 204 to 207. Pergamon Press Ltd., London

Spectre d'absorption infra-rouge du protoxyde d'azote à l'état solide

PAUL A. GIGUÈRE et KENNETH B. HARVEY*
Laboratoire de chimie physique, Université Laval, Québec, Canada

(*Received* 19 *October* 1956; *accepted for publication* 8 *February* 1957)

Abstract—The infra-red spectrum of solid nitrous oxide at −175°C was measured in the range 2 to 25 μ. In addition to the three fundamentals, four overtones and six combinations were observed. Four very weak bands are assigned to the isotopic molecules $N^{14}N^{15}O$ and $N^{15}N^{14}O$. Certain features of the spectrum may be due to some disorder in the crystal.

LE spectre infra-rouge du protoxyde d'azote N_2O à l'état gazeux a fait l'objet de nombreuses recherches depuis le travail original de PLYLER et BARKER [1]. Quant au liquide, il a été étudié dans le proche infra-rouge, entre 1 et 2,5 μ par VODAR et TA [2]. Par contre aucun travail n'avait encore été publié sur le spectre d'absorption du solide. Cette substance présente un intérêt particulier en raison de son entropie résiduelle aux très basses températures et sa faible polarité, malgré sa formule asymétrique.

Le tube à absorption était semblable à celui déjà employé dans ce laboratoire [3], moins le tube à décharge électrique. La température de l'échantillon était mesurée au moyen d'un petit thermocouple cuivre-constantan encastré dans le disque de chlorure d'argent portant l'échantillon. Le protoxyde d'azote gazeux à 98% de pureté provenait d'une bombonne pour fins médicales. La seule impureté décelable consistait en trace de N_2O_4 dont les bandes les plus intenses à 653, 768, 1286, 1747, 1870, et 2360 cm^{-1} [4] apparaissaient à peine dans les spectres. Outre celles-ci nous avons remarqué occasionnellement deux bandes très faibles (à 840 cm^{-1} et 1370 cm^{-1}) de l'ion NO_2^- provenant, sans doute, de l'attaque des fenêtres de KCl qui servaient à fermer le tube à absorption. Ces bandes parasites ont déjà été signalées dans les spectrographes utilisant comme source un filament de NERNST [5]. Pour éliminer ces impuretés il suffisait de faire passer le gaz très lentement dans un piège refroidi avec de la neige carbonique. Les films de N_2O solide étaient transparents à la température de l'air liquide. Leur épaisseur était contrôlée empiriquement d'après la quantité de gaz introduit dans l'appareil. Les spectres d'absorption furent enregistrés au moyen d'un appareil de Perkin-Elmer, modèle 12C, avec prisme de NaCl, $CaCl_2$, ou KBr suivant la region étudiée. L'air à l'intérieur du spectrographe était désséché par circulation continue dans une tour d'alumine activée.

La plupart des bandes observées (Fig. 1) peuvent être attribuées immédiatement par simple comparaison avec le spectre d'absorption du gaz [1]. En effet, on retrouve ici toutes les combinaisons actives dans le gaz avec des fréquences presque inchangées et des intensités relatives toujours dans le même ordre (Tableau 1). ce qui est assez surprenant. Comme pour la molécule libre, les harmoniques $2\nu_2$ et $2\nu_1$

*Boursier des Canadian Industries Ltd.

VOL. 9 1957

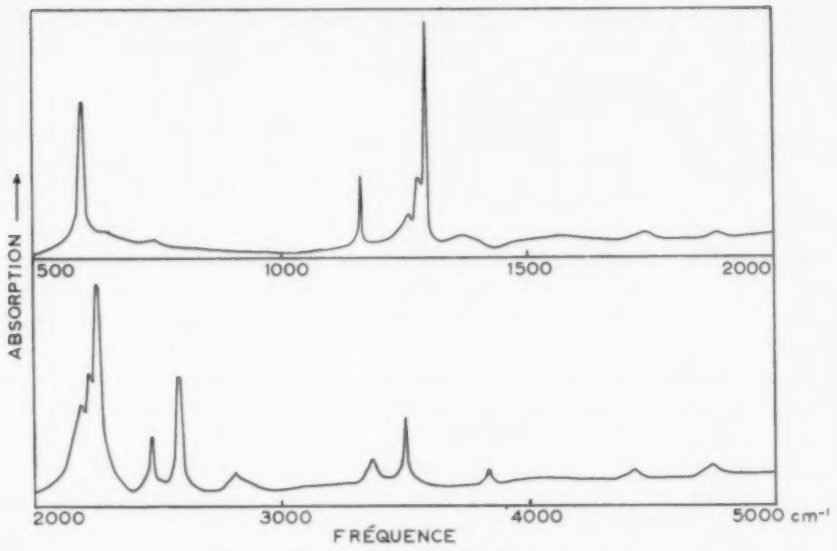

Fig. 1. Spectre infra-rouge de N_2O solide.

ainsi que la combinaison ternaire $\nu_1 + 2\nu_2$ sont remarquablement intenses, sans doute à cause de la résonance de Fermi avec les vibrations fondamentales voisines ν_1 et ν_3 respectivement. Aucune des fondamentales n'apparaît dédoublée, ce qui, dans le cas de ν_2 semble en contradiction avec les prévisions de la théorie. On sait que N_2O cristallise dans le système cubique [6] avec la symétrie du groupe T^4. Or la

Tableau 1. Bandes d'absorption de N_2O dans l'infra-rouge

Gaz*		Solide		Classification	Décalage (cm^{-1})
(cm^{-1})	Intensité	(cm^{-1})	Intensité		
588,8	*F*	595	*F*	ν_2	6
1167,0	*m*	1166	*m*	$2\nu_2$	
		1256	*ff*	ν_1 $N^{14}N^{15}O$	
		1280	*ff*	ν_1 $N^{15}N^{14}O$	
1285	*FF*	1295	*FF*	ν_1 $N^{14}N^{14}O$	10
1867,5	*f*	1890	*ff*	$\nu_1 + \nu_2$	22
		2196	*ff*	ν_3 $N^{14}N^{15}O$	
		2219	*ff*	ν_3 $N^{15}N^{14}O$	
2223,5	*FF*	2244	*FF*	ν_3 $N^{14}N^{14}O$	20
2461,5	*m*	2468	*m*	$\nu_1 + 2\nu_2$	6
2563,5	*m*	2580	*m*	$2\nu_1$	16
2798,3	*f*	2813	*f*	$\nu_2 + \nu_3$	15
3365,6	*f*	3380	*f*	$2\nu_2 + \nu_3$	14
3481,2	*m*	3500	*f*	$\nu_1 + \nu_3$	19
		3850	*ff*	$3\nu_1$	
4419,5	*f*	4440	*ff*	$2\nu_3$	20
4734,7	*f*	4750	*ff*	$2\nu_1 + \nu_3$	15

*D'après PLYLER et BARKER [1].

symétrie locale des molécules de N_2O dans cette maille est C_3 et, d'après les règles de corrélations [7], la vibration de déformation ν_2 devrait donner naissance à deux composantes. Cependant aucune indication de ce phénomène n'a pu être décelée même avec des échantillons très minces et un pouvoir de résolution de 3 cm^{-1} ou moins. Rappelons ici que CO_2, qui cristallise avec la même symétrie, montre pour ν_2 deux composantes séparées d'environ 7 cm^{-1} [8]. Il est vrai que la séparation pourrait être moindre dans le cas de N_2O parce que le rayon de van der Waals de l'azote est plus petit que celui du carbone et, partant, le couplage entre les vibrations de l'atome central des quatre molécules dans la maille cristalline de N_2O doit être un peu plus lâche que dans celle de CO_2. Mais la différence ne saurait être tellement marquée; en fait la bande ν_2 (Fig. 1) semble presque aussi fine que les deux autres fondamentales.

Une autre explication également plausible repose sur l'orientation désordonnée des molécules, NNO, ONN, etc, qui détruirait la symétrie des sites dans la maille cristalline. Cette hypothèse a déjà été avancée pour rendre compte de l'entropie résiduelle de N_2O au zéro absolu [9]. Le mode de préparation de nos échantillons par condensation brusque du gaz pourrait bien favoriser ce désordre. Quoiqu'il en soit nous nous proposons d'étudier cette question davantage.

Les quatre bandes très faibles à 1256, 1280 2196, et 2219 cm^{-1} visibles seulement dans des films très épais, appartiennent certainement aux molécules isotopiques $N^{14}N^{15}O$ et $N^{15}N^{14}O$. En effet, leur intensité était indépendante du degré de pureté des échantillons; en outre elle était égale pour les quatre bandes et correspondait assez bien à l'abondance naturelle de N^{15}, soit 0,36%. Enfin les fréquences sont toutes décalées de la bande principale, non seulement dans le même sens, mais encore de quantités presque identiques à celles prévues par la théorie [10], comme l'indique le Tableau 2. Les déplacements isotopiques de ν_2 n'ont pu être

VOL. 9 1957

Tableau 2. Décalages des fréquences de vibration des molécules isotopiques de N_2O

	$N^{14}N^{15}O$		$N^{15}N^{14}O$	
	calculé	observé	calculé	observé
ν_1	—	40 cm^{-1}	17 cm^{-1}	15 cm^{-1}
ν_2	13 cm^{-1}	—	4 cm^{-1}	—
ν_3	46 cm^{-1}	48 cm^{-1}	22–29 cm^{-1}	25 cm^{-1}

décelés parce que cette bande est sensiblement moins intense que les deux autres fondamentales. D'ailleurs, dans le cas de $N^{15}N^{14}O$ le pouvoir de résolution de l'appareil était du même ordre que la valeur calculée pour le déplacement. On n'a pas encore réussi à mesurer ces bandes isotopiques dans le gaz à cause de l'enchevêtrement de la structure fine.

Quant aux décalages gaz-solide, ils sont tous de même signe (sauf pour $2\nu_2$), soit de signe contraire à ceux de CO_2, ce qui est assez remarquable. Suivant l'analyse de HORNIG [11] les perturbations qui amènent ces décalages sont de deux

sortes. Les premières (V_j') sont dues au champ de force des autres molécules dans leur position d'équilibre à l'intérieur de la maille cristalline. Ce terme est évidemment très petit dans le cas de N_2O vu la faible polarité de la molécule (0,16 debye). Aussi les fréquences de vibration dans le liquide [2, 12] sont elles presque identiques à celles de la molécule libre. Le second facteur (V_{jk}''), résultant du couplage entre les vibrations des diverses molécules, est plus important que le premier, quoiqu'encore assez faible en valeur absolue.

Résumé

On a mesuré le spectre d'absorption infra-rouge du protoxyde d'azote à l'état solide à −175°C. Outre les trois fondamentales on a trouvé quatre harmoniques et six bandes de combinations. La présence de 0,4% de molécules isotopiques $N^{14}N^{15}O$ et $N^{15}N^{14}O$ est révélée par quatre bandes très faibles. Quelques particularités du spectre peuvent provenir d'un certain désordre dans le cristal.

Bibliographie

[1] Plyler E. K. et Barker E. F. *Phys. Rev.* 1931 **38** 1827.
[2] Vodar B. et Ta Y. *J. Phys. Radium* 1940 **1** 378.
[3] Giguère P. A. et Secco E. A. *J. Phys. Radium* 1954 **15** 508.
[4] Falk M. Résultats inédits.
[5] Launer P. J. *J. Opt. Soc. Amer.* 1952 **42** 359.
[6] de Smedt J. et Keesom W. H. *Akad. Amsterdam Versl.* 1924 **33** 573 889.
[7] Hornig D. F. *J. Chem. Phys.* 1948 **16** 1063.
[8] Osberg W. E. et Hornig D. F. *J. Chem. Phys.* 1952 **20** 1345.
[9] Blue R. W. et Giauque W. F. *J. Amer. Chem. Soc.* 1935 **57** 991.
[10] Bigeleisen J. et Friedman L. *J. Chem. Phys.* 1950 **18** 1656.
[11] Hornig D. F. *Disc. Faraday Soc.* 1950 **9** 115.
[12] McLennan J. C., Smith H. D., et Wilhelm J. O. *Trans. Roy. Soc. Can.* 1930 **24** 3 197.

Spectrochimica Acta, 1957, Vol. 9, pp. 208 to 215. Pergamon Press Ltd., London

The intensities of the carbonyl group vibration in some aromatic compounds

H. W. Thompson, R. W. Needham, and D. Jameson
The Physical Chemistry Laboratory, Oxford

(*Received* 22 *February* 1957)

Abstract—The effect of aromatic-ring substituents upon the frequency and intensity of the carbonyl group in compounds of the type C_6H_5·CO·R has been examined. Ethyl benzoates, benzaldehydes, acetophenones, benzophenones, and propiophenones were used. Some regular shifts of frequency can be correlated with the Hammett factor σ of the substituent group, but the intensity of the carbonyl-group band is hardly affected. Some data have also been obtained about the apparent half-band width and the influence of substituents upon it.

1. Introduction

Some recent publications have described how the characteristic vibration frequencies of groups attached to a benzene ring are influenced by the nature and position of other substituent groups [1]. In most cases, and especially those in which the particular vibration concerned is mainly determined by the stretching of a bond or bonds rather than by their bending, a regular relationship has been found between the position of the key infra-red absorption band and the Hammett σ factor of the substituent present. The variation of band intensity along a series of molecules containing different substituents has been examined in only a few cases. However, it was noticed recently [2] that with substituted benzonitriles, a substantial change of intensity of the cyanide group vibration is caused by variation of other substituents in the aromatic nucleus and the results appeared to fit roughly a linear relation between log (intensity) and σ.

The factors which determine the characteristic absorption frequency of a particular chromophore on the one hand, and its absorption band intensity on the other, are different. All concern the electronic structure of the bond or bonds in which the vibration is localized. Substituent groups may affect the force constant, static dipole moment or dipole derivative with respect to bond-length, either through inductive effects or by affecting the relative contributions of different forms to the resonance hybrid. Before these structural factors can be disentangled, therefore, it is desirable to measure both the frequencies and intensities and to assemble a larger selection of typical data.

We have therefore continued the program by measuring the effect of aromatic-ring substituents upon the frequency and band intensity of the carbonyl-group stretching vibration in compounds of the type C_6H_5·CO·R, in which R = OC_2H_5, H, CH_3, C_2H_5, or C_6H_5. The intensities of this carbonyl-group band in some of the parent compounds have already been determined by other workers [3].

VOL. 9 1957

2. Experimental method

Most of the measurements were made with a Perkin Elmer 21 spectrometer, with rock-salt prism, calibrated with standard lines of water vapour and ammonia in the usual way. A few were checked using a single-beam 12C instrument. A variable path-length absorption cell was used, the thickness being fixed by measurement of interference fringes. The compounds studied were commercial products, repurified by appropriate recrystallization or refractionation. Some difficulty was found due to rapid oxidation of the benzaldehydes, but this was minimized by redistillation just before use. Carbon tetrachloride and chloroform were dried and redistilled before use.

With each compound the band intensity was determined using a series of different concentrations and path-lengths. The quantity

$$B = \frac{1}{cl}\int \ln\left(\frac{T_0}{T}\right)_\nu . \, d\nu$$

was then plotted against $\ln (T_0/T)_{max}$, and the true intensity A obtained by extrapolation as the intercept on the B axis. Apart from a single set of measurements made with ethyl benzoate using several different slit-widths, all the work was carried out with a fixed value of the latter, which was too large to reveal the true half band widths (width at half-peak optical density). However, although these true half band widths were not obtained, comparisons could be made on the same experimental basis of $\Delta\nu_{1/2}^a$ in each compound of a series. The values of $\Delta\nu_{1/2}^a$ varied little with concentration over the range used, and a mean value is quoted below.

In some cases there were difficulties due to overlap with other bands not connected with the carbonyl group, and this made it impossible to derive satisfactory estimates of the band required. Occasionally, when one half of the band lay clear, the integrated area of this half was doubled.

3. Results

On theoretical grounds we should expect the true integrated band intensity A obtained by the above extrapolation to be independent of the slit-widths used, and this was recently confirmed experimentally in actual examples [4]. A series of measurements were made with solutions of ethyl benzoate in carbon tetrachloride, using four different values for the calculated effective slit-widths between 5 and 20 cm^{-1}. With increasing slit-width, the apparent half-band width of the carbonyl group absorption at 1719 cm^{-1} increases as would be expected, but the extrapolated value of the intensity A remains the same within the limits of accuracy of the measurements, which was about 5%.

Experimental conditions were then chosen for all the measurements corresponding to a calculated effective slit-width of about 8 cm^{-1}. Table 1 gives the results for substituted ethyl benzoates in carbon tetrachloride and chloroform. With ethyl benzoate the values 16·1 and 18·5 $\times 10^{-7}$ cm^2 $molecule^{-1}$ sec^{-1} are to be compared with 16·7 and 17·7 $\times 10^{-7}$ obtained earlier by BARROW [3]. Some of the bands, particularly in chloroform, were found to have an unsymmetrical contour, occasionally with apparent shoulders. The significance of this from

Table 1. Ethyl benzoates

Substituent	σ	In carbon tetrachloride			In chloroform		
		ν (cm^{-1})	$\Delta\nu^{e}_{1/2}$	$A \times 10^{7}$	ν (cm^{-1})	$\Delta\nu^{e}_{1/2}$	$A \times 10^{7}$
m-NO_2	0·71	1727	13	13·8	1722	22	17·2
p-Br	0·23	1720	18·5	15·0	1711	29	18·1
p-F	0·06	1721	16·5	14·6	1709	28	19·2
H	0	1719	15	16·1	1711	24	18·5
p-CH_3O	−0·27	1710	20	16·7	1704	26	19·2
p-NH_2	−0·66	1708	17	17·6	1694	32	21·0

Table 2. Benzaldehydes

Substituent	σ	In chloroform		In carbon tetrachloride	
		ν (cm^{-1})	$\Delta\nu^{e}_{1/2}$	$A \times 10^{7}$	ν (cm^{-1})
p-NO_2	0·78	1711	12·5	9·7	1713
3:4-di-Cl	0·52	1704	15·5	11·3	1707
p-Cl	0·23	1702	15·5	10·4	1708
H	0	1701	14	10·6	1708
m-C-$H_4(CH_3)$	−0·07	1700			
p-$CH(CH_3)_2$	−0·15	1700		11·2	1705
p-CH_3O	−0·27				1699
p-OH	−0·36	1686	19	12·6	1698

Table 3. Acetophenones

Substituent	σ	In chloroform			In carbon tetrachloride	
		ν (cm^{-1})	$\Delta\nu^{e}_{1/2}$	$A \times 10^{7}$	ν (cm^{-1})	ref (9)
m-NO_2	0·71	1693	15	8·5	1703	1701
p-Br	0·23	1684	19	10·5	1695	1693
p-Cl	0·23	1683	18	10·6	1694	1692
H	0	1680	19	9·8	1693	1692
m-NH_2	−0·16	1677	20	9·9	1689	
p-CH_3	−0·17	1677	16	10·3	1690	
p-CH_3O	−0·27	1672	19	10·7	1682	1684
3·4-di-CH_3	−0·30	1674	19	10·8	1687	
p-NH_2	−0·66	1663	24	11·1	1676	1677
2:4-di-CH_3		1678	21	9·8	1687	

VOL. 9 1957

Table 4.

Substituent	σ	In chloroform			In carbon tetrachloride	
		ν (cm^{-1})	$\Delta\nu^a_{1/2}$	$A \times 10^7$	ν (cm^{-1})	ref. (9)
Propiophenones						
p-Cl	0·23	1687	20	9·7	1696	
H	0	1683	22	9·0	1694	1692
p-OH	−0·36	1672	25	9·5	1684	
p-NH_2	−0·66	1665	29	9·4	1678	
Benzophenones						
m-NO_2	0·71	1667	19·5	10·4	1671	
p-Br	0·23	1659	20·5	10·9	1668	1665
H	0	1657	18·5	10·8	1665	1664
p-CH_3	−0·17	1653	20	10·4	1664	1661
pp'-di-CH_3O	−0·54	1645	22	10·4	1657	1655
Phenacyl bromides						
p-Br	0·23	1684		7·1		
p-Cl	0·23	1684		7·1		
p-C_2H_5	0·01	1681		6·3		
H	0	1682		6·2		
Butyrophenone		1680	23	9·1		1690
n-Valerophenone		1680	23	9·4		1690
Methyl benzyl ketone		1709	25	7·1		
Acetone		1710	15	9·7		
Methyl *n*-propyl ketone		1709	21	9·8		
Methyl *n*-hexyl ketone		1708	20	9·3		
Stearone		1706	22	9·7		

the standpoint of the estimated intensities needs further consideration, but its occurrence makes some of the measured half-band widths a little uncertain. However, it seem clear that the bands are broader in chloroform. Also, the intensity of a given band is always higher, and the frequency lower, in chloroform than in carbon tetrachloride, as noticed by BARROW for a wide range of compounds containing the carbonyl group.

Tables 2–4 summarize the results obtained for the other compounds studied, and Fig. 1 shows some typical extrapolations for obtaining A. Where comparisons of the intensity with the earlier data of BARROW are possible, close agreement is found. In some cases, again, the occurrence of overlap or of shoulders made it impossible to estimate $\Delta\nu^a_{1/2}$, or even the intensity. The frequencies in chloroform were always lower than those in carbon tetrachloride.

4. Discussion

Several features emerge from these measurements. The fall in frequency and rise in band intensity of the carbonyl group on passing from carbon tetrachloride to chloroform could be interpreted in terms of a weak hydrogen bonding with

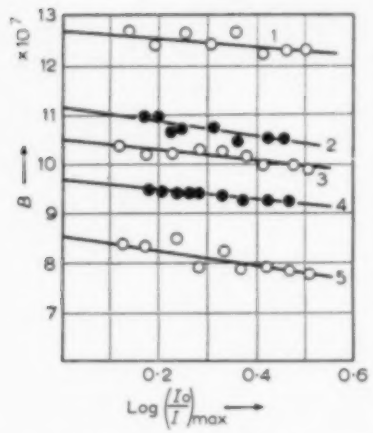

Fig. 1.
(1) *p*-Hydroxy benzaldehyde.
(2) *p-Iso*propyl benzaldehyde.
(3) *p*-Bromo acetophenone.
(4) *p*-Nitro benzaldehyde.
(5) *m*-Nitro acetophenone.
All solutions in chloroform.

the solvent, but in view of much recent information about solvent effects it may be unwise at present to generalize about this.

In each of the series of related compounds, there is a regular displacement of the carbonyl-group frequency with aromatic-ring substituent. The plots of ν against Hammett factor σ, shown in Fig. 2, are roughly linear. This result corresponds to those already found with substituted phenols, anilines, and cyanides. The rough slope of these plots ($\Delta\nu/\Delta\sigma$) is about the same, +16. for all

VOL. 9 1957

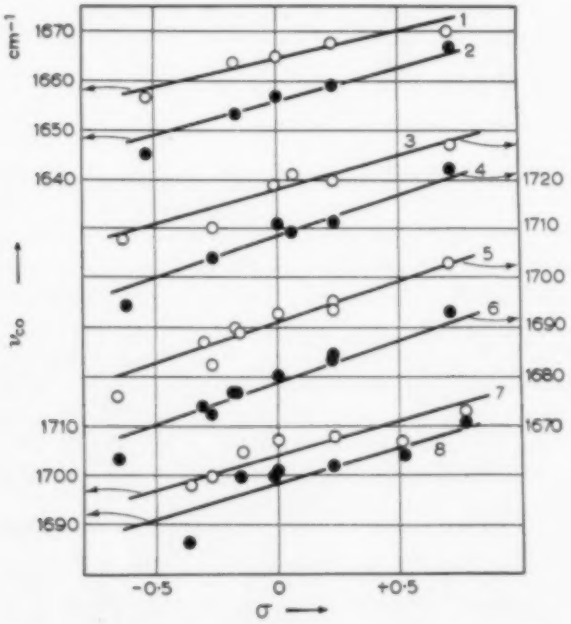

Fig. 2.
(1) (3) (5) (7), solutions in carbon tetrachloride of benzophenones, ethyl benzoates, acetophenones, benzaldehydes. (2) (4) (6) (8) ditto, in chloroform.

the series of the type ⟨⬭⟩—CO—R now examined, and this value seems also to hold for the carbonyl-group vibration of substituted benzoic acids studied by FLETT [5]. Whether this roughly linear plot of ν against σ has much physical significance is questionable, for the substitution will affect the vibration frequency by alteration of a linkage force constant, and it might therefore be more appropriate to plot ν^2 against σ. In fact, all the data so far accumulated suggest a slight curvature of the ν/σ plot which might disappear in a ν^2/σ plot, but the variation of ν is within such a small range that it is impossible to decide. Although

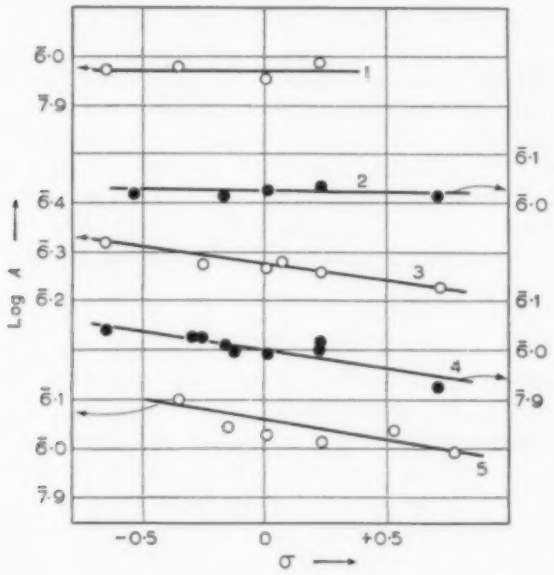

Fig. 3.
(1) Propiophenones. (4) Acetophenones.
(2) Benzophenones. (5) Benzaldehydes.
(3) Ethyl benzoates.
Solutions in chloroform.

the present data suggest that the slopes of the ν/σ plots are about the same in value for the different series of molecules now examined, this slope varies considerably in magnitude and also in sign with other series of substances which have been measured earlier, according to the particular group frequency concerned. It is hoped to discuss this relationship more fully in a later paper.

The effect of substituent group upon the intensity of the carbonyl-group vibration is surprisingly small. With substituted benzonitriles, it has been found that aromatic-ring substituents affect the intensity of the cyanide-group band markedly, and for a change of substituent corresponding to $\Delta\sigma = 1$, the change in transition moment exceeds 100%. This result has been confirmed by SENSI and GALLO [6], and by LIPPERT [7], whose intensity data on a few molecules also reveal a similar strong effect of substituents upon the symmetrical mode of the NO_2 group in nitrobenzene, although not upon the antisymmetrical mode.

With the compounds $C_6H_5{\cdot}CO{\cdot}R$ now studied, substituents have little effect on the carbonyl-group band intensity. It was shown previously that, with the benzonitriles, log A appears to vary linearly with σ, suggesting an analogy with the Hammett equation which relates reactivity constant and σ. The slope of this plot, for solutions in chloroform, was about $-0{\cdot}7$. With the compounds $C_6H_5{\cdot}CO{\cdot}R$ now examined, the plots of log A against σ shown in Fig. 1 have zero slope for propiophenone and benzophenone, and a very small slope ($-0{\cdot}05$ to $-0{\cdot}08$) for benzaldehydes, acetophenones, and benzoic esters. In later papers from this laboratory, other examples of a marked effect of substituent will be described, and the significance of the results with different structural types will be considered.

The measured values for the apparent half-band widths are, as already explained, not very precise, but if $\Delta\nu^a_{1/2}$ is plotted against ν, the carbonyl-group band frequency, for any given series $C_6H_5{\cdot}CO{\cdot}R$, a definite trend is seen, $\Delta\nu^a_{1/2}$ decreasing with increasing frequency. The slope of these plots is roughly the same for different classes of compound, and implies a fall of about 6 cm^{-1} in $\Delta\nu^a_{1/2}$ for a rise of 10 cm^{-1} in ν. There is, of course, a similar variation of $\Delta\nu^a_{1/2}$ with σ.

The extrapolations of Fig. 1 can be represented by equations of the form

$$B = A + A\theta \ln\left(\frac{T_0}{T}\right)_{max}$$

and assuming a Lorentz band shape, Ramsay [8] has computed values of θ for different slit conditions. The slopes derived from our plots, which give a value of θ, agree roughly with the computed values, but are usually rather higher than the latter. This might arise, in part, since in computing the effective slit-widths no allowance can be made for incorrect slit alignment and similar factors. On the other hand, it is not yet established that the bands have intrinsically a contour which follows the Lorentz formula, and in practice they are certainly often asymmetrical.

Further information is being sought by a study of the overtones of the carbonyl group vibration in some of these molecules.

Acknowledgement—We are grateful to the Hydrocarbon Research Group of the Institute of Petroleum for financial help.

References

[1] Brown J. F. *J. Amer. Chem. Soc.* 1955 **77** 6341.
Ingraham L. L., Corse J., Bailey G. F., and Stitt F. *J. Amer. Chem. Soc.* 1952 **74** 2297.
Randle R. R. and Whiffen D. H. *J. Chem. Soc.* 1952 4153.
Flett M. St. C. *Trans. Faraday Soc.* 1948 **44** 767.
Goulden J. D. S. *Spectrochim. Acta* 1954 **6** 129.
Fuson N., Josien M. L., and Shelton E. M. *J. Amer. Chem. Soc.* 1954 **76** 2526.
Davison J. *J. Chem. Soc.* (London) 1951 2456.
Kron R. D. and Fassel V. A. *J. Amer. Chem. Soc.* 1956 **78** 4225.
Margoshes M. and Fassel V. A. *Spectrochim. Acta.* 1955 **7** 14.
Steel G. and Thompson H. W. *Trans. Faraday Soc.* 1956 **52** 1451.
Bellamy L. J. *J. Chem. Soc.* 1955 2818.

VOL. 9 1957

[2] Steel G. and Thompson J. W. *Trans. Faraday Soc.* 1956 **52** 1451.
[3] Barrow G. M. *J. Chem. Phys.* 1953 **11** 2008.
Francis S. A. *J. Chem. Phys.* 1950 **18** 861; 1951 **19** 942.
[4] Russell R. A. and Thompson H. W. *Spectrochim. Acta*, in press.
[5] Flett M. St. C. *Trans. Faraday Soc.* 1948 **44** 767.
[6] Sensi P. and Gallo G. G. *Gaz. Chim. Ital.* 1955 **85** 224, 235.
[7] Lippert E. and Vogel W. *Z. Phys. Chem.* 1956 **9** 133.
[8] Ramsay D. A. *J. Amer. Chem. Soc.* 1952 **74** 72.
[9] Fuson N., Josien M. L., and Shelton E. M. *J. Amer. Chem. Soc.* 1954 **76** 2526.

OL.
9
57

Spectrochimica Acta, 1957, Vol. 9, pp. 216 to 226. Pergamon Press Ltd., London

The accuracy of photographic intensity measurements of absorption spectra

ALF LOFTHUS
Department of Physics, University of Oslo, Blindern, Oslo, Norway

(*Received* 25 *February* 1957)

Abstract—Some of the experimental methods used in photographic absorption spectroscopy are discussed, with special emphasis on the sources of error associated with them. On the basis of these discussions, the experimental conditions leading to the smallest total error of intensity measurements can be found. The application of the results to chemical analysis is discussed. A comparison between the photographic and the photoelectric methods is made.

1. Introduction

THE knowledge of absorption intensities connected with electronic transitions is of fundamental importance for an understanding of the electronic structure of atoms and molecules. In addition to its theoretical interest, absorption intensity measurements have found widespread applications in various fields of physics and chemistry, notably in the chemical analysis of organic molecules. However, the potentialities of absorption spectroscopy applied to chemical analysis, especially in the vacuum ultra-violet region, have not yet been fully explored.

Using the commercial photoelectric spectrometers, recording of absorption spectra is nowadays an easy and straightforward task, and can be performed with a fairly high degree of accuracy. However, these instruments are chiefly designed for spectra of liquid only, have rather low resolution, and can seldom be used in the vacuum region. For these and other reasons, photographic recording of absorption spectra is still of great importance.

The photographic method is almost exclusively used for the study of molecular gas spectra where high resolution and/or precision wavelength measurements are required, but can also be used with advantage for obtaining all kinds of survey spectra, and is still extensively used for measuring atomic line intensities and transition probabilities. Using available spectrographs for emission spectroscopy, photographic absorption measurements should prove valuable to chemical analysis also, even of atoms.

It is a well-known fact that photographic intensity measurements are encumbered with serious sources of error, and are considerably inferior to photoelectric measurements. However, by a careful design and performance of the measurements, it should prove possible to reduce the errors involved to a tolerable level. It is the purpose of this paper to discuss some of the experimental methods used in absorption spectroscopy, with special emphasis on the sources of error associated with them, and to determine the experimental conditions which give the smallest possible errors of the measurements.

Some applications of atomic absorption spectra to chemical analysis have been discussed by WALSH [1], and of vacuum ultra-violet absorption spectra to organic

VOL. 9 1957

analysis, using photoelectric spectrometers, by JONES and TAYLOR [2]. A general review of experimental methods and techniques in the vacuum ultra-violet spectroscopy has recently been given by INN [3].

2. Definitions and theoretical considerations

The *absorption coefficient* k_ν of a substance is defined by the relation

$$I_\nu = I_{0_\nu} e^{-k_\nu d} \tag{1}$$

where I_ν is the intensity of the transmitted part of a light beam with incident intensity I_{0_ν} and frequency ν, and d is the thickness of the absorbing substance.

The *total absorption* of a particular transition $n \leftarrow m$ is given by

$$I^{nm}_{\nu_{\text{abs}}} = \int (I_{0_\nu} - I_\nu)\, d\nu \tag{2}$$

where the integration is to be taken over the entire absorption region corresponding to the particular transition under consideration. Assuming that I_{0_ν} is constant over the integration range, and the absorption is not too strong, this expression can be reduced to

$$I^{nm}_{\nu_{\text{abs}}} = I_{0_\nu} d \int k_\nu\, d\nu \tag{3}$$

On the other side, the total absorption can be expressed by

$$I^{nm}_{\nu_{\text{abs}}} = I_{0_\nu} N_m B_{mn}\, dhc\nu_{nm} \tag{4}$$

where N_m is the number of absorbing atoms or molecules per cm^3 in the initial state m, ν_{nm} the absorbed frequency, B_{mn} the Einstein transition probability coefficient of absorption, h Planck's constant, and c the velocity of light. Comparing equations (3) and (4), we get for the *integrated absorption coefficient*

$$\int k_\nu\, d\nu = N_m B_{mn} h\nu_{nm} \tag{5}$$

In many cases, notably in atomic spectroscopy, it is useful to express the absorption in terms of the *oscillator strength* f^{nm}, which represents the average number of electrons per atom capable of being excited by the incident radiation, and can be shown to be related to the transition probability coefficient by the expression

$$f^{nm} = \frac{mhc^2\nu_{nm}}{\pi e^2} B_{mn} \tag{6}$$

where m and e are mass and charge of an electron. Comparing equations (5) and (6), we get

$$f^{nm} = \frac{1}{N_m} \frac{mc^2}{\pi e^2} \int k_\nu\, d\nu \tag{7}$$

In practical applications of absorption spectroscopy, and also in the general study of liquid and gas spectra, it is customary to express the absorption law (1) in a slightly different form, namely

$$I_\nu = I_{0_\nu} 10^{-\alpha_\nu d} \tag{8}$$

where the new absorption coefficient α_ν is connected to the former through the simple relation

$$\alpha_\nu = k_\nu \log_{10} e = 0{\cdot}434 k_\nu \tag{9}$$

In the following we shall assume that Beer's law is valid, which expresses that the absorption coefficient α_ν is proportional to the concentration c of the absorbing substance,

$$\alpha_\nu = \varepsilon_\nu c \tag{10}$$

If c is given in moles per litre, d in centimetres, the proportionality factor ε is called the *molecular extinction coefficient*, or in short, *the extinction coefficient*, and $\varepsilon cd = -\log_{10} I/I_0$ the total *extinction*. The molecular extinction coefficient is a function of the frequency or wavelength of the absorbed radiation, and of the temperature, but is otherwise a characteristic constant for the absorbing substance.

In the following we shall limit ourselves mainly to a discussion of how to obtain good molecular absorption spectra from which the molecular extinction coefficient

$$\varepsilon = -\frac{1}{cd}\log_{10}\frac{I}{I_0} \tag{11}$$

can be determined as a function of frequency or wavelength with the highest obtainable accuracy; i.e., determine the experimental conditions rendering the relative error $\Delta\varepsilon/\varepsilon$ a minimum.

The present discussions are mainly dealing with gases, but can readily be applied to liquids and solids as well. Regarding methods of determinations of the total absorption and f-values from the ε-curves or from more direct measurements, reference should be made to MITCHELL and ZEMANSKY [4], where the theoretical relations used in the present discussions are also evaluated, and to numerous papers in the astrophysical journals (see, for instance, KING and STOCKBARGER [5]).

VOL. 9 1957

3. Experimental methods

The common method of photographic recording of absorption spectra uses a continuous light source, the light from which is transmitted through a cell or longer tube containing the absorbing medium before entering the spectrograph; however, an exception is sometimes met in vacuum spectroscopy, where the entire spectrograph can be filled with absorbing gas. As light source a simple incandescent lamp can be used in the visible, and a hydrogen discharge in the ultra-violet region. More recently, the continuous discharge from the noble gases, excited by microwave sources, has proved intense and useful [6, 7].

Since the intensity of the light source and the sensitivity of the photographic emulsion may depend strongly on the wavelength, it is always necessary to expose on the same plate a spectrum of the light source (I_0) alone, without an interposed absorbing medium, and then compare the photographic density of this spectrum (D_0) with the density of the absorption spectrum (D). If a prism spectrograph or a stigmatic grating spectrograph is used, it might be of advantage to split the beam from the light source into two parallel beams of equal intensity, one being transmitted through the absorption cell and the other through a matched cell containing no absorbing medium (but of course the pure solvent in the case of solution spectra). Thereafter the two beams are projected on each half of the length of the spectrograph slit. Using this method, a variation in the incident light intensity during the exposure is of minor importance.

The relation between intensity and photographic density is given by

$$D_0 - D = -\gamma \log_{10} I/I_0 \tag{12}$$

provided we are working on the straight part of the characteristic curve of the

photographic emulsion. This expression inserted into equation (11) gives

$$\varepsilon = \frac{D_0 - D}{\gamma c d} \tag{13}$$

The curve of extinction coefficient is thus readily obtained, provided D_0 and D are known from densitometer tracings of the spectra, the contrast factor γ from some kind of emulsion calibration, and the product of concentration and absorption length are chosen appropriately (cf. equation 15).

A probably more accurate, but also more laborious version of this method is to find the $D_0 - D$ curve for a series of different concentrations, and then, by using equation (13) in the form

$$D_0 - D = \varepsilon \gamma c d \tag{14}$$

plot $D_0 - D$ against c for every wavelength for which an ε-value is wanted. If BEER's law is valid, and the density measurements accurate enough, a straight line should result, the slope of which is equal to $\varepsilon \gamma d$. γ and d being known, ε is thus determined. The measured points may of course be somewhat off a straight line, but with sufficiently many points a well defined line might be drawn. This method has been used by WEISSLER, PO LEE, and MOHR [8, 9] for the measurement of the absolute absorption coefficients of N_2 and O_2 in the vacuum ultra-violet region.

Relation between concentration and absorption length. It is very important that for all ε-values under consideration we choose the product cd such that the observed densities fall inside the straight part of the characteristic curve for the emulsion type in use. Further, for a good determination of weak lines, a certain minimum density is required which seems to have a value about 0·6, i.e. a density usually falling on the straight part of the curve.

The maximum density which can be used depends on the extent of the straight part, and on the sensitivity of the densitometer. Most emulsions have a straight characteristic curve up to $D \approx 2{\cdot}5$, but for such high values the densitometer readings are rather uncertain. A density value $D = 1{\cdot}2$ seems to be reasonable in most cases.

The relation between concentration and absorption length which, for a certain range of the extinction coefficient, must be fulfilled in order to get a spectrogram well suited for absorption intensity measurements is now readily given:

$$\begin{aligned} D_{\max} - D_{\min} &= 0{\cdot}6 \\ &= \log_{10} I_{\max}/I_{\min} \\ &= (\varepsilon_{\max} - \varepsilon_{\min}) cd \end{aligned}$$

i.e.

$$(\varepsilon_{\max} - \varepsilon_{\min})\, \gamma c d = 0{\cdot}6 \tag{15}$$

The extinction coefficients usually vary considerably even within a short wavelength region (e.g. sharp lines). Therefore, the interval $(\varepsilon_{\max} - \varepsilon_{\min})$, for a fixed cd, can not be chosen too large, since this would, as will be discussed more fully in the next section, lead to a high error limit. A spectrum where ε varies much must thus be taken in more steps, for each step a new value of cd being chosen.

Gas concentrations. In case of solution spectra the sample concentration should readily be known. In the case of gas spectra the concentration c is most conveniently given by the gas pressure p, between which there is the simple relation

$$c = \frac{1}{22{\cdot}4}\,\frac{273}{T}\,\frac{p}{760} = 0{\cdot}016\,\frac{p}{T} \tag{16}$$

where c is measured in moles per litre, p in mm Hg, and T is the gas temperature in °K. The problem of gas concentration measurement is thus reduced to a problem of pressure measurement.

An accurate determination of gas pressure may be a rather difficult problem, especially for very low pressures, and no satisfactory single method is applicable in all cases.

Probably the most accurate method, where usable, is to fill a small volume, e.g. a gas pipette, and then release the gas into a larger, evacuated volume. Also, a small, weighed amount of liquid can be volatized in an evacuated volume.

In some cases, notably where the exposure times are long enough so that noticeable photodissociation or liberation of impurities can take place, a continuous gas stream through the absorption tube is necessary. The rate of flow and the pressure in the absorption tube can then be regulated by means of needle valves. However, in such cases an accurate pressure measurement is of course more difficult.

In the case where the gases under investigation are vapours of condensable compounds, a reservoir containing the liquid can be connected to the absorption tube. If the reservoir is held at a fixed temperature, the gas pressure can thus be defined by this temperature. The success of this method is wholly dependent on the existence of reliable pressure vs. temperature curves.

For a somewhat more detailed discussion on gas-handling systems and pressure determinations, reference should be made to JONES and TAYLOR [2].

Relation between gas pressure and absorption length. If equation (16) is inserted into (15) we get

$$(\varepsilon_{\max} - \varepsilon_{\min})\,\gamma p d = 37{\cdot}5\,T \tag{17}$$

which in the cases of gas spectra is the requirement to be fulfilled.

Usually the absorption tube will be maintained at room temperature, i.e. $T \approx 290$°K, and consequently

$$(\varepsilon_{\max} - \varepsilon_{\min})\gamma p d \approx 10^4 \tag{18}$$

The final choice of p and d will be discussed in the last section.

4. Sources and magnitudes of errors

The various sources of error which are present in photographic photometry can be divided into (a) those associated with the photographic emulsions and with the processing, (b) those associated with the densitometer readings, (c) those which have their origin in uncertainties in concentrations and in absorption lengths, and (d) those connected with variations in source intensities (I_0) from one exposure to the other. In addition, considerable errors may be introduced through various

VOL. 9 1957

circumstances within the spectrograph itself, such as stray light and aberrations due to imperfections in the optical components.

The total relative error or uncertainty in the determination of the extinction coefficient ε is, according to equation (13), in general given by the expression

$$\frac{\Delta\varepsilon}{\varepsilon} = \frac{\Delta c}{c} + \frac{\Delta d}{d} + \frac{\Delta\gamma}{\gamma} + \frac{\Delta D_0 + \Delta D}{D_0 - D} \tag{19}$$

where the Δ's indicate the uncertainties in the various factors to be measured.

The uncertainties in the density determinations are composed of other contributions:

$$\Delta D_0 = \Delta D_{ph} + \Delta D_d \tag{20a}$$

$$\Delta D = \Delta D_{ph} + \Delta D_d + \Delta D_s \tag{20b}$$

where ΔD_{ph} indicate photographic errors, ΔD_d uncertainties in densitometer readings, and $\Delta D_s = \partial D/\partial I_0 \, \Delta I_0 = \gamma \, 0{\cdot}434 \, \Delta I_0/I_0$ is the uncertainty due to variations in the light source intensity from one exposure to the other.

Equation (19) now reads

$$\frac{\Delta\varepsilon}{\varepsilon} = \frac{\Delta c}{c} + \frac{\Delta d}{d} + \frac{\Delta\gamma}{\gamma} + \frac{0{\cdot}434}{\varepsilon_{cd}} \frac{\Delta I_0}{I_0} + \frac{2\Delta D_{ph} + 2\Delta D_d}{\varepsilon\gamma_{cd}} \tag{21}$$

From this equation it looks as if the relative error were smallest if γcd is chosen as large as possible. However, as already stated by equations (15) and (17), a certain restriction is imposed on these factors in order to obtain spectra suited for intensity measurements.

It is now seen that the relative error will be smallest for ε_{max} and largest for ε_{min} Therefore, as already stated in connection with equation (15), the interval $\varepsilon_{max} - \varepsilon_{min}$ can not be chosen too large for one and the same exposure, since this would lead to large errors for ε-values near ε_{min}.

In the following, the various sources of error will be given a more detailed discussion.

Photographic factors. The contributions to the total relative error from photographic factors are numerous and by far the most serious ones. The so-called macroscopic errors are direct imperfections in the emulsion, such as scratches, dark or light pointlike impurities, and variations of the thickness and sensitivity over the plates. These points must be carefully avoided when the density is measured. The microscopic errors are statistical fluctuations in the blackening due to the graininess of the emulsion. The graininess can to some extent be influenced by the processing, but will substantially be given by the choice of emulsion type. Fast plates are usually very grainy, and must be avoided where the exposure times are not unreasonably long. Also, fast plates are more liable to background density and fogging than slow plates.

It is essential for good developing that the specified processing conditions be followed strictly. Of special importance for a faultless and uniform development is that the developer be agitated vigorously during the development. The best means to obtain this is continuous stroking with a soft camel-hair brush: just rocking the developer tray is not enough. (In the cases of very thin emulsions, such as the special coated vacuum plates, brushing during the development is of course prohibited).

Some references to estimations of the uncertainties in the photographic density measurements corresponding to a certain exposure exist [10], indicating that for densities between 0·3 and 1·6, ΔD_{ph} is between 0·5 and 2 per cent in the most favourable cases.

The uncertainties in the densitometer readings will for good instruments probably be about 2 per cent or better.

Contrast factor. According to equation (13), the contrast factor γ must be known for the evaluation of the extinction coefficient. Apart from being strongly dependent on the wavelength, γ will usually vary appreciably from plate to plate, and even within the same plate. Therefore, every plate must be calibrated by some means for the actual conditions.

Where step sectors or step filters can be used, the calibration of a plate is easiest, since every line on the spectrum will serve as a calibration mark, and just for the wavelength it represents.

In the cases where stepped spectrograms cannot be obtained, e.g. for astigmatic spectrographs, a series of density strips may be impressed on the plates with the aid of the same light source, or a stronger source, and as near the absorption spectrograms as possible. These density strips must be exposed in a fixed ratio. A disadvantage with separate calibration marks is that possible variations of γ within the same plate are less under control.

In order to illustrate this last point, the writer measured the variation of γ within a plate for two typical emulsions, namely Kodak Spectrum Analysis No. 1, and 103 a-0, the first one a somewhat slow plate with high contrast and low background density, and the latter a high-speed plate with medium contrast, but rather liable to background density and fogging. Using a stepsector, six exposures of the iron spectrum in the range 2400–3200 Å were impressed at equal intervals over the entire plates. It was found that the variations in γ over the plate were at a maximum 4·5 per cent and in the mean 2·6 per cent for Spectrum Analysis No. 1, and 9·4 per cent and 4·6 per cent for 103 a-0. In both cases the plate was brushed during the development . For Spectrum Analysis No. 1 the same experiment was repeated, omitting the brushing (but rocking). In this case the maximum and mean variation was 10·7 per cent and 7·9 per cent respectively, that is, about three times as large. The uncertainty associated with the measurement of a specific γ was far less than the variation of γ over the plate.

The abovementioned examinations clearly illustrate the necessity of a proper choice of emulsion type and of carefulness in the development process. However, only a few of the most important points could be mentioned here; for a more detailed discussion of the photographic factors, reference should be made to the photographic handbooks [11, 12].

Gas concentrations. An accurate determination of the concentrations of substances in solution should not give rise to any major problem; however, the determination of gas concentrations or pressures may be encumbered with significant uncertainties.

When the gas concentration is measured by the pressure p and the temperature T in the absorption tube, the uncertainties associated with this measurement will, according to equation (16), be

$$\frac{\Delta c}{c} = \frac{\Delta p}{p} + \frac{\Delta T}{T} \tag{22}$$

VOL. 9 1957

or simply

$$\frac{\Delta c}{c} = \frac{\Delta p}{p} \tag{23}$$

since $\Delta T/T$ might always be regarded as small.

By means of the usual direct-reading pressure meters, the accuracy can be fairly high for higher pressures, but definitely less so for lower pressures.

In the case of vapours, where the pressure is determined by the temperature of the condensed compound contained in a reservoir, a fairly good estimate of the error $\Delta p/p$ can be given by the usual pressure versus temperature relation

$$\ln p = -\frac{\Lambda}{RT_1} + B \tag{24}$$

where R is the gas constant, Λ the heat of vaporization, T_1 the temperature of the reservoir, and B a constant. It readily follows that the contribution to the error in p from the uncertainty in the temperature of the reservoir is

$$\frac{\Delta p}{p} = \frac{\Lambda}{RT_1}\frac{\Delta T_1}{T_1} \tag{25}$$

For many organic liquids Λ/R is about 6000, so that for temperatures around 300°K we get

$$\frac{\Delta p}{p} = 20\,\frac{\Delta T_1}{T_1} \tag{26}$$

We thus see that in order to keep $\Delta p/p$ within, say 1 per cent, the temperature in the reservoir must be held constant to 0·15°.

It is clearly seen from this example that the gas pressure is strongly dependent on the temperature in the liquid reservoir, consequently this temperature must be held strictly constant, which can best be maintained by keeping the reservoir immersed in a bath controlled by a thermostat, or by some substance at a fixed temperature, e.g. dry ice, melting ice, etc.

It must here be recalled that equation (25) gives only the change in pressure corresponding to a certain change in temperature. The absolute value of the pressure is only approximately given by equation (24); for more accurate pressure determinations, reliable pressure vs temperature curves must be known for the particular substance in question, otherwise a large systematic error may be introduced.

In the cases where a continuous gas flow is maintained through the absorption tube, an accurate pressure measurement is, as already mentioned, very difficult. If the gas comes from a liquid reservoir, and the rate of flow is not greater than the rate of vaporization, the pressure may to a good approximation be given by the temperature in the reservoir as just described. Where the gas is a permanent gas, the pressure meters have to be relied upon.

Where the method of introducing known amount of gas at higher pressures into larger evacuated volumes can be used, this method seems to be by far the most reliable one.

Even though significant uncertainties in concentration may be introduced by all the methods discussed above, $\Delta c/c$ has of course the same sign for all wavelengths and thus only the absolute values of ε are affected, not the relative values which often are the only ones needed.

Absorption lengths. Many cells and tubes of various lengths are usually needed in absorption spectroscopy. For liquids and solutions the lengths may vary from a fraction of a millimetre to several centimetres, and gas tubes from some centimetres, to some metres. Exceptionally long tubes and multipass tubes may sometimes be needed.

Only for the very thinnest cells should $\Delta d/d$ have any appreciable value. JONES and TAYLOR [2], however, have described a simple method of measuring the thickness of these cells. The thickness was determined by measurement of the total extinction at 2500 Å of the cells filled with a solution of diphenyl. An aliquot of the diphenyl solution was then diluted quantitatively so that its extinction at the same wavelength might be measured in the 10·0-mm Beckman cells. The cell thickness could then be calculated from Beer's law. All of these measurements were made with a Beckman DU quartz spectrometer.

Stability of light sources. Where separate exposures for I_0 and I are made, the spectral distribution and the total intensity of the light source must be held strictly constant. The intensity of incandescent lamps and the small commercial hydrogen discharge fed by voltage regulated power units can probably be held constant to a few per cent.

Heavier gas discharge tubes are usually very hard to run under complete control, and can thus easily make intensity measurements illusory, for instance for large grating spectrographs where such tubes are needed.

VOL. 9 1957

5. Comparison between photographic and photoelectric measurements

It might here be of value to give a brief comparison between the photographic and the photoelectric methods of intensity measurements.

Two different types of instruments are usually used for the photoelectric recording of absorption spectra. In the one case a blank run (I_0) must be made with an empty cell, or in the case of solutions the pure solvent only. Thereafter the same spectrum must be rescanned with the cell filled with the absorbing medium (I). In the other case the instruments measure the transmission I/I_0 directly.

Applying equation (1), the relative error in ε is in these two cases given by

$$\frac{\Delta\varepsilon}{\varepsilon} = \frac{\Delta d}{d} + \frac{\Delta c}{c} + \frac{0{\cdot}434}{\varepsilon c d}\left[\frac{\Delta I}{I} + \frac{\Delta I_0}{I_0}\right] \tag{27}$$

and

$$\frac{\Delta\varepsilon}{\varepsilon} = \frac{\Delta d}{d} + \frac{\Delta c}{c} + \frac{0{\cdot}434}{\varepsilon c d}\frac{\Delta(I/I_0)}{I/I_0}, \tag{28}$$

respectively.

If ΔI and $\Delta(I_0/I_0)$ can be assumed to be constant, the last term in equations (26) and (27) is smallest when $\varepsilon cd \,.\, 10^{-\varepsilon cd}$ is largest. It is readily seen that this expression has its minimum for

$$\varepsilon cd = 0{\cdot}434 \tag{29}$$

Fig. 1 shows a graphical representation of $0{\cdot}434/\varepsilon cd \,.\, 10^{-\varepsilon cd}$ as function of εcd. It is seen that this curve has a rather flat minimum, consequently, the choice of εcd is not very critical. If

we for instance choose εcd between 0·2 and 0·8, the relative error will fall between 2·7 and 3·4 times $[\Delta I/I + \Delta I_0/I_0]$ or $\Delta(I/I_0)$. Then

$$(\varepsilon_{max} - \varepsilon_{min})cd = 0{\cdot}6, \tag{30}$$

which now is the requirement to be fulfilled in order to get the best spectrogram for intensity evaluations.

Comparing equations (30) and (15), we see that for emulsions with a contrast factor around 1, which is often the case, the two equations become identical. That is to say that the experimental conditions leading to the best absorption spectra are much the same for both methods, and the same considerations as to the errors can be applied. However, the value of the last term in equations (27) and (28) is considerably smaller than the corresponding four terms in equation (21) for the photographic method.

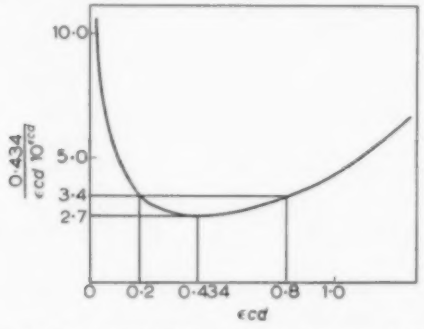

Fig. 1. Curve showing the contribution to the relative error in the extinction coefficient due to error in the photoelectric intensity measurements. The working range for the total extinction, εcd, is chosen such that the error is near its minimum.

6. Discussion

In the preceding discussions an attempt was made to estimate the various sources of error associated with photographic intensity measurements of absorption spectra. A rigorous treatment of these problems, applicable in all cases, can, however, hardly be given. The various set-ups and procedures used in such experiments will necessarily be rather diversified in details, consequently the estimate of the error limit must be done for the individual cases, along such lines as those outlined here. However, these discussions indicate clearly enough that the order of magnitude of the errors is large, and that the errors can be reduced significantly only by the utmost carefulness in design and performance of the experiments.

By far the most serious sources of error are those associated with the photographic part of the experimental procedure, especially in the vacuum ultra-violet region, where the special photographic emulsions may be of rather poor reproducibility. The preceding discussions indicate that the largest single contribution to the photographic errors is the variation of the contrast factor over the plate. This fact may explain why often so widely divergent values of extinction coefficients (20 per cent to 50 per cent off) given by occasional plates have been reported in the literature, and apparently this question has not been paid sufficient attention to earlier.

The superiority of the photoelectric method is due to the fact that the intensity is measured directly, eliminating the complexity of density measurements.

The accuracy of the intensity measurements might thus be compared with that of densitometer readings in the photographic method. The other factors contributing to the total error are much the same in these two cases, and can thus be treated in the same way.

Equations (15) and (29) put a restriction only on the product of concentration, c, and absorption length, d; the final choice of the value of the individual factors thus being left open.

In the case of solution spectra, where the fine structure usually is smeared out anyway, relatively high concentrations may be used; only it must be remembered that deviations from Beer's law may occur for higher concentrations. On the other hand, for small concentrations, with accompanying long absorption cells, the amount of impurities may become significant.

Gas concentrations are measured most accurately when the pressures are high, but also in these cases a possible failure of Beer's law must be taken into account. An important reason for choosing low pressures is that the fine structure usually shows up much sharper than in the case of higher pressures.

No strict rule for the choice of gas pressure, applicable in all cases, can be given. However, numerous measurements reported in the literature indicate that gas pressures of the order of 2 mm Hg and lower have been found useful for absorptions of ordinary intensities.

Throughout these discussions the problem was how to measure extinction coefficients. In chemical analysis, however, the problem is to measure concentrations, assuming extinction coefficients to be known within a certain limit of accuracy. Since concentrations are readily given from equation (11) just by interchanging c and ε, the subsequent discussions as to errors are directly applicable in this case also.

Acknowledgement—The author is indebted to Mrs. and Dr. J. G. HAUGE for a critical reading of the manuscript.

References

[1] WALSH A. *Spectrochim. Acta* 1955 **7** 108.
[2] JONES L. C. and TAYLOR L. W. *Anal. Chem.* 1955 **27** 228.
[3] INN E. C. Y. *Spectrochim. Acta* 1955 **7** 65.
[4] MITCHELL A. C. G. and ZEMANSKY M. W. *Resonance Radiation and Excited Atoms* Cambridge University Press, 1934.
[5] KING R. B. and STOCKBARGER D. C. *Astrophys. J.* 1940 **91** 488.
[6] WILKINSON P. G. and TANAKA Y. *J. Opt. Soc. Amer.* 1955 **45** 344.
[7] WILKINSON P. G. *J. Opt. Soc. Amer.* 1955 **45** 1044.
[8] WEISSLER G. L., LEE P., and MOHR E. T. *J. Opt. Soc. Amer.* 1952 **42** 84.
[9] WEISSLER G. L. and LEE P. *J. Opt. Soc. Amer.* 1952 **42** 200.
[10] SCHONTAG A. *Z. wiss. Photogr.* 1941 **40** 233; 1942 **41** 116.
[11] *Kodak Photographic Plates for Scientific and Technical Use* (7th ed.) Eastman Kodak Company, 1953.
[12] *Kodak Materials for Spectrum Analysis* (2nd ed.) Eastman Kodak Company, 1954.

VOL. 9 1957

Spectrochimica Acta, 1957, Vol 9, pp. 227 to 234. Pergamon Press Ltd., London

The direct-reading spectrometric analysis of alloy cast iron

ROGER BARTEL and ALAN GOLDBLATT
Chicago Spectro Service Laboratory, Chicago, Illinois, U.S.A.

(*Received* 4 *August* 1956)

Abstract—Excitation conditions have been established which eliminate the metallurgical effects of carbon in the emission spectrometric analysis of iron and steel by the point-to plane technique. As a result of this, iron and steel standards can be used interchangeably to prepare analytical curves for analysing alloy cast iron.

SPECTROGRAPHIC methods for the analysis of cast iron have not been adapted industrially on a wide, universal scale. Three factors are primarily responsible for this seemingly high degree of inertia. These are:

(1) The difficulties encountered in producing homogeneous samples.

(2) Insufficient accuracy by photographic spectrography for determining silicon at the 2 to 3 per cent concentration level.

(3) No source of primary and/or secondary standards.

In recent years much progress has been made in minimizing factors 1 and 2. The use of single-plane chilling techniques by pouring the molten sample into ceramic rings to form disks, provides samples of markedly improved homogeneity. At the same time, the advent of direct-reading spectrographs permits silicon to be determined with twice the accuracy of photographic spectrographic methods. Factor 3, the problem of procurement of standard samples, still presents itself as a serious handicap. While primary iron standards are in the planning stage, it will be at least 2 to 3 years before they become available.

Source parameters have been found in the Applied Research Laboratories, Multisource [1], which permit the use of steel standards interchangeably with iron standards. This facilitates the preparation of analytical curves for the analysis of alloy irons and thus materially minimizes factor 3.

When iron and steel samples are excited by Fuessner type high-voltage spark discharges, the spectra produced show intensity differences and individual analytical curves are required for iron and steel. This is due to the difference in carbon content. Ferrous samples containing more than 1 per cent carbon produce spectra of greater intensity than those containing less than 1 per cent carbon. This effect appears to be metallurgical in character, since many of the alloying elements in iron exist as carbides.

The unidirectional critically damped Multisource discharge [2], which has been recommended for the analysis of stainless steel, minimizes the metallurgical effects of carbon. This discharge with the sample disk as the positive electrode provides continuous analytical curves for ferrous samples. Table 1 lists the excitation constants, the electrode system and the exposure conditions used.

Table 1. Excitation conditions for the analysis of alloy cast iron

Capacitance, μF	12
Inductance, μH.	50
Resistance, ohms	5
Discharges per second	60
Output voltage, V	1000
Type of Sample	chill cast disk $1\frac{1}{2}$" dia. $\times \frac{1}{4}$" thick
Sample Finish	100 Grit grind
Upper Electrode (positive)	Disk
Lower Electrode	120° cone, $\frac{1}{4}$" graphite rod
Preburn, seconds	10
Exposure, seconds	25

A model No. 7200 Applied Research Laboratories 1·5-m Quantometer was used in this study. This instrument using a strip chart recorder provides a direct intensity ratio measurement, since the internal standard iron line is charged to the same constant value each time. The concentration ranges covered and the analytical line pairs that were selected are in Table 2.

Table 2. Line pairs used for the analysis of alloy cast iron

Element	Analytical line (Å)	Iron internal standard line (Å)	Concentration range (per cent)
Manganese	2933·2	3205·4	0·4 to 1·4
Silicon	2881·6	3205·4	0·1 to 3·0
Nickel	3414·7	3205·4	0·1 to 1·0
Nickel	2316·0	3205·4	0·5 to 3·5
Chromium	2677·0	3205·4	0·1 to 3·5
Molybdenum	3170·3	3205·4	0·1 to 3·0

Analytical curves for Manganese, Silicon, Nickel, Chromium, and Molybdenum have been prepared using secondary iron standards, National Bureau of Standards 800 series primary steel standards and a group of 8 secondary steel standards prepared by the Republic Steel Corporation. The Analytical curves shown in Fig. 1. through 5, demonstrate that iron and steel standards fall on a single curve.

The Multisource discharge used produces a heavy black deposit of graphite on the disk specimens during the excitation cycle. Fig. 6 shows the appearance of this discharge pattern and that obtained with a Feussner type high-voltage discharge on a cast-iron sample. It appears that the elimination of the metallurgical effect of carbon with the critically damped discharge is due to the formation of the graphite deposit on the sample electrode. Apparently an excess of carbon is always present so that irons and steels showing extremes of from 3·5 per to 0·05 per cent carbon still respond similarly. To examine this phenomenon experimentally, a study was made in which the polarity of the electrodes was reversed. All parameters were kept constant, except for a change in polarity. With the sample disk negative,

VOL. 9 1957

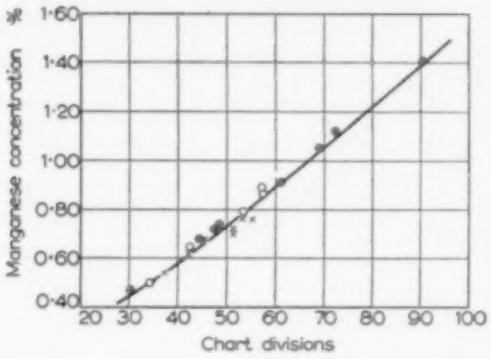

Fig. 1.
× Secondary cast-iron standards.
⊕ Secondary Steel standards.
○ National Bureau of standards, 800 series. Primary Steel standards.

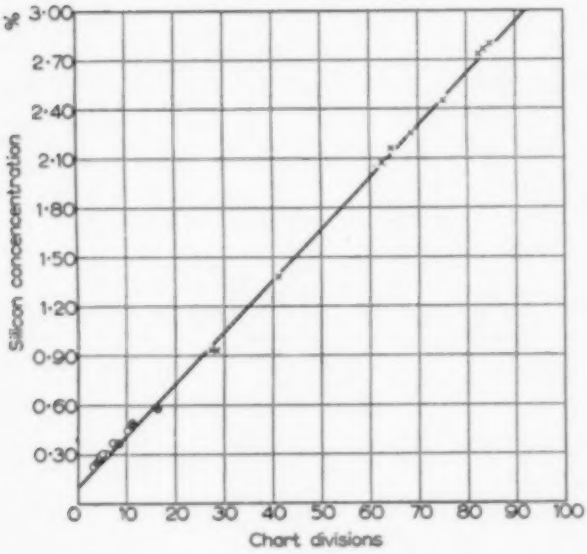

Fig. 2.
× Secondary cast-iron standards.
⊕ Secondary steel standards.
○ National bureau of standards, 800 series. Primary steel standards.

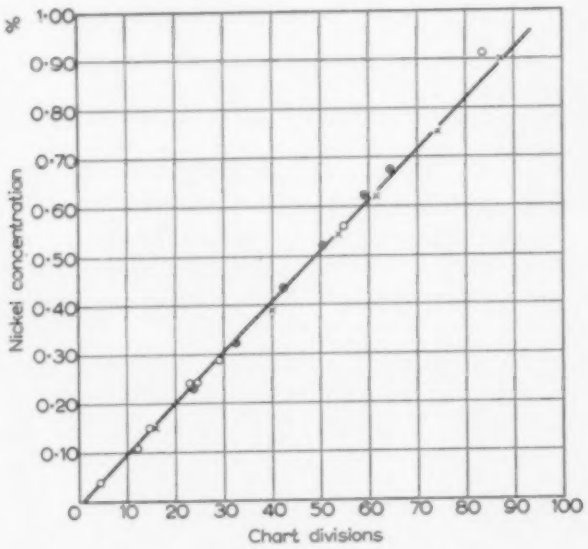

Fig. 3.
× Secondary cast-iron standards.
⊕ Secondary steel standards.
○ National bureau of standards, 800 series. Primary steel standards.

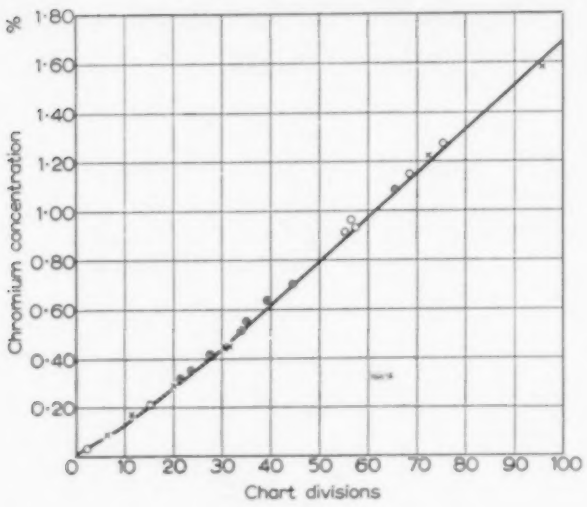

Fig. 4.

× Secondary cast-iron standards.
⊙ Secondary steel standards.
○ National Bureau of Standards, 800 series. Primary steel standards.

VOL. 9 1957

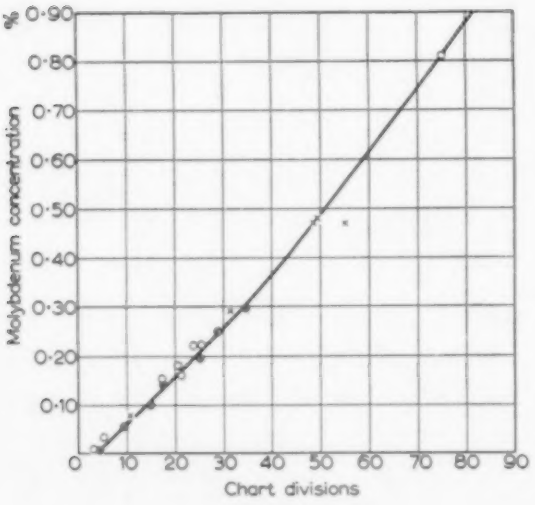

Fig. 5.

× Secondary cast-iron standards.
⊙ Secondary steel standards.
○ National Bureau of Standards, 800 series. Primary steel standards.

graphite is not deposited on the sample. The analytical curves prepared from the iron and steel standards that were used in making the curves shown earlier, are shown in Fig. 7 through 11. The iron and steels show two distinct curves for each

OL.
9
57

Fig 6. Crop as shown.

VOL.
9
1957

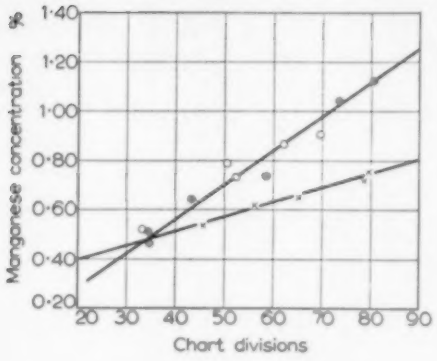

Fig. 7.
× Secondary cast-iron standards.
⊕ Secondary steel standards.
○ National Bureau of Standards, 800 series. Primary steel standards.

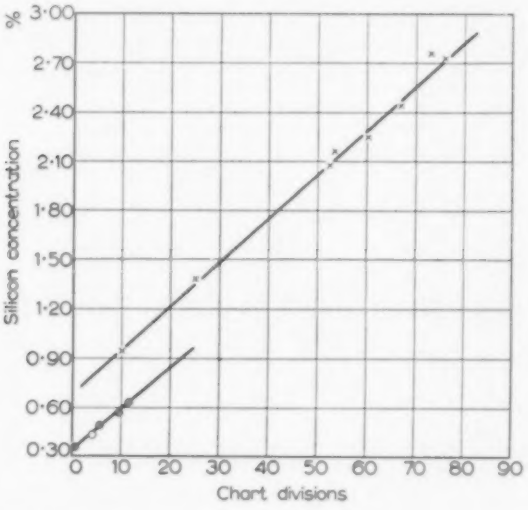

Fig. 8.
× Secondary cast-iron standards.
⊕ Secondary steel standards.
○ National Bureau of Standards, 800 series. Primary steel standards.

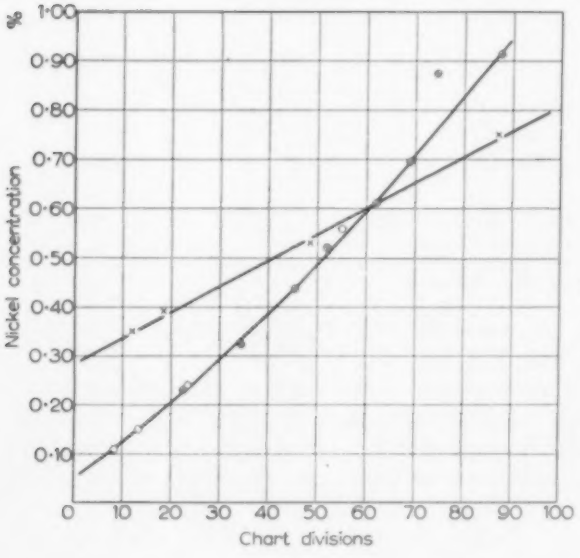

Fig. 9

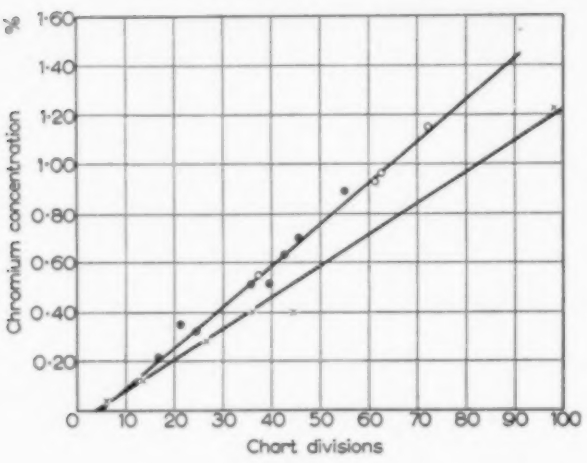

Fig. 10.

× Secondary cast-iron standards.
⊙ Secondary steel standards.
○ National Bureau of Standards, 800 series.
Primary steel standards.

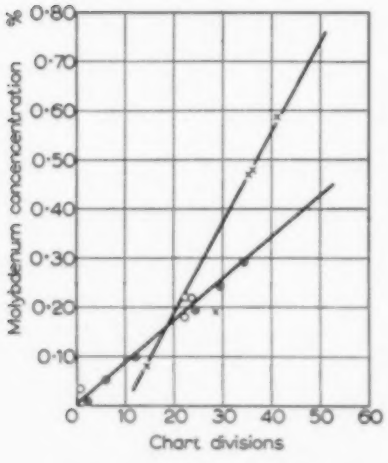

Fig. 11.

× Secondary cast-iron standards.
⊙ Secondary steel standards.
○ National Bureau of Standards, 800 series.
Primary steel standards.

element indicating that the deposit of graphite on the sample electrode is necessary to eliminate the metallurgical effects of carbon.

Table 3 summarizes a study of the precision of the method, using the critically damped case, with the sample as the positive electrode.

Cast iron standards containing high levels of nickel, chromium, and molybdenum were not available for preparing concentration curves in the ranges of 1·0 to 3·5

VOL. 9 1957

Table 3. Precision data

Element	Average concentration (per cent)	Coefficient of variation	Number of determinations
Manganese	0·46	3·44	50
	0·64	3·44	50
	0·80	1·37	50
	0·82	0·61	50
Silicon	0·86	2·10	50
	1·93	1·81	50
	2·27	1·41	50
	2·37	1·51	50
Nickel	0·16	3·15	50
	0·45	0·88	50
	0·59	0·84	50
	3·09	2·53	50
Chromium	0·45	1·12	50
	1·05	0·76	50
	1·60	1·00	50
	2·98	1·54	50
Molybdenum	0·05	13·3	50
	0·43	1·85	50
	0·57	2·10	50
	4·07	0·91	50

Table 4. Comparison of chemical and spectrographic analytical results

Per cent manganese		Per cent silicon		Per cent nickel		Per cent chromium		Per cent molybdenum	
Q	*C*	*Q*	*C*	*Q*	*C*	*Q*	*C*	*Q*	*C*
0·60	0·58	0·74	0·72	3·01	3·06	1·66	1·64		
0·64	0·65	0·75	0·78	2·95	2·93	1·60	1·61		
0·55	0·51	1·89	1·89			3·13	3·13	4·19	4·24
0·58	0·57	2·01	1·95			2·95	3·00	4·18	4·12
0·55	0·52	1·91	1·93			2·90	2·96	4·28	4·33
0·46	0·46	1·79	1·78			2·95	2·96	4·25	4·21
0·74	0·76	2·09	2·11	0·58	0·62	1·12	1·16	0·66	0·64
0·76	0·76	2·12	2·15	0·56	0·60	1·16	1·17	0·63	0·63
0·87	0·87	2·29	2·30	0·50	0·49	0·68	0·70	0·42	0·42
0·69	0·69	2·24	2·23	0·57	0·57	0·22	0·23	0·53	0·51
0·69	0·71	2·01	2·04	0·61	0·64	1·05	1·04	0·59	0·56

Q—Quantometer analysis.
C—Chemical analysis

per cent nickel, 1·5 to 3·5 per cent chromium, and 1·0 to 5 per cent molybdenum. Primary and secondary steel standards were used to draw curves covering these ranges. The validity of this follows since the effect of carbon has been eliminated. Table 4 provides a comparison of chemical determinations and routine direct-reading analysis made on the same group of unknown specimens.

It must be pointed out that this study covers chill-cast samples of iron. Sand-cast iron specimens have been analysed using these curves with appropriate bias factors. The bias factors used are plus 0·15 per cent on silicon, minus 0·08 per cent chromium and minus 0·06 per cent on molybdenum. Nickel and manganese did not require a bias correction.

Chill-cast alloy iron samples of suitable homogeneity can also be prepared by pouring molten metal into a carbon mould. This type of mould can be reused and simplifies sample-taking in the foundry.

References

[1] HASLER M. F. and DIETERT H. W. *J. Opt. Soc. Amer.* 1943 **33** 218.
[2] HASLER M. F. *Trans. Inst. Meas. Conf.* Stockholm, 1949.

VOL.
9
1957

Spectrochimica Acta, 1957, Vol. 9, pp. 235 to 251. Pergamon Press Ltd., London

The intensities of the infra-red absorption bands of *n*-paraffin hydrocarbons*

R. N. JONES
Division of Pure Chemistry,
National Research Council of Canada, Ottawa, Canada

(*Received* 26 *March* 1957)

Abstract—The first part of this paper is concerned with the measurement of molecular extinction coefficients in the infra-red region of the spectrum, using both single-pass and double-pass prism spectrometers of conventional design. The absolute accuracy of such measurements cannot be evaluated at present, as suitable reference standards are not available. Several factors are discussed which must be taken into consideration before such standards can be established.

The second part of the paper deals with the molecular extinction coefficients of the principal absorption bands in the spectra of the homologous series of *n*-paraffin hydrocarbons from hexane to hexatriacontane. The values of $\epsilon_{max}^{(a)}$, when plotted against the number of methylene groups in the chain, yield linear graphs with positive slopes. The significance of these slopes, and of the intercepts of the lines with the zero ordinate axis are considered in relationship to the vibrational assignments of the bands. Particular interest is attached to the region between 1490 and 1440 cm^{-1}. An analysis of the band envelope indicates the presence of a third peak near 1460 cm^{-1}, in addition to the well-established methylene and methyl bands at 1467 and 1457 cm^{-1}.

Measurement of infra-red band intensities

INTEGRATED absorption intensities are theoretically preferable to molecular extinction coefficient measurements as criteria of infra-red band intensities, but the area measurements can be obtained only for bands that are sensibly free from overlap, such as the —N—H, —C≡N, and —C=O stretching bands [1, 7, 15, 17, 18], whereas extinction coefficients can be measured through regions of complex absorption.

The true molecular extinction coefficient $|\epsilon_\nu|$ at the wave number ν is defined as

$$\epsilon_\nu = 1/cl \cdot \log (I_0/I)_\nu$$

where c is the solute concentration in moles per liter of solution, l the cell length in cm, and $\log (I_0/I)_\nu$ the optical density (absorbance) at the wave number ν.

To allow for errors associated with the use of finite spectral slit-widths, the *apparent* molecular extinction coefficient ($\epsilon_\nu^{(a)}$) was introduced [7, 13].

$$\epsilon_\nu = 1/cl \cdot \log (T_0/T)_\nu$$

Here $\log (T_0/T)_\nu$ is the observed optical density when the spectrometer is set at the wave number ν, though the radiation passing through the slit need not necessarily be monochromatic. The substitution of $(T_0/T)_\nu$ for $(I_0/I)_\nu$ takes account of the fact that the true molecular extinction coefficient is defined in terms of monochromatic radiation. The definitions of the apparent intensity units were later broadened

* Published as Contribution No. 4348 from the Laboratories of the National Research Council of Canada.

to take cognizance of other instrumental errors affecting the accuracy of the intensity measurements [8, pp. 276, 287]. These errors have been discussed elsewhere [8, p. 261–287], and it is necessary here to deal only with certain practical points that require more detailed consideration.

(a) *The Finite Slit Error*

When the conventional prism spectrometers are used to investigate the spectra of organic compounds in solution, the band-widths are commonly of the same order of magnitude as the spectral slit-widths. Under these circumstances the band contour is distorted and $\epsilon_{max}^{(a)}$ is diminished.

By assuming that the absorption band conformed to a Lorentz curve, RAMSAY [13] was able to express this discrepancy quantitatively. His calculations suggested that under these conditions the finite slit error on the integrated absorption intensity would be not more than 1 per cent provided $S/\Delta\nu_{\frac{1}{2}}^{(a)} \geqslant 0{\cdot}2$, S being the spectral slit-width in cm^{-1} and $\Delta\nu_{\frac{1}{2}}^{(a)}$ the apparent half-intensity band-width. The effect of the finite slit is greater on $\epsilon_{max}^{(a)}$ than on the integrated absorption intensity, and at $S/\Delta\nu_{\frac{1}{2}}^{(a)} = 0{\cdot}2$, RAMSAY's tables give the ratio of $\epsilon_{max}/\epsilon_{max}^{(a)}$ as 1·03. In setting up specifications for spectral slit schedules, we have accepted this 3 per cent error in ϵ_{max} as the maximum which can be tolerated without correction. For most bands in the spectra of organic compounds in solution, $\Delta\nu_{\frac{1}{2}}^{(a)}$ is rarely less than 8–10 cm^{-1} from which we conclude that the finite slit error can be neglected, provided we can operate with spectral slit-widths in the range 1·6–2·0 cm^{-1}. This is a premise which will need re-examination at a later date when improved instrumental techniques and accumulated experience will allow more exact evaluation. The Ramsay corrections were originally developed to deal with larger errors associated with higher values of $S/\Delta\nu_{\frac{1}{2}}^{(a)}$, and their validity at lower values of $S/\Delta\nu_{\frac{1}{2}}^{(a)}$ needs to be more thoroughly examined.

Unfortunately, there are also ambiguities in the evaluation of the spectral slit-width. For prism spectrometers with Littrow mounting, the spectral slit-width is given by an expression of the form:

$$S = \Sigma + F(s)\,\Pi + \Phi$$

where Σ and Π are functions of the optics and geometry of the spectrometer. $F(s)$ is a proportionality factor, and Φ a correction for aberration, misalignment of slits and optics, etc. Uncertainty is introduced in the computation of S because of uncertainty in the selection of the proper values for $F(s)$ and Φ. Theoretically $F(s)$ should take on values in the range 0·9–0·5, depending on the mechanical slit-widths and the dispersion of the prism material [8, p. 274, 19]. To provide a basis for comparison, the quantity *computed spectral slit-width*, S', has been defined [8, p. 274], where $F(s)$ is taken as unity and Φ as zero:

$$S' = \Sigma + \Pi$$

The errors so introduced are of opposite sign.

The significance of these considerations when applied to conventional types of commercial prism spectrometers operated under routine laboratory conditions is illustrated by the curves in Fig. 1, where the computed spectral slit-widths are

VOL. 9 1957

plotted against wave number. On the right-hand side of the diagram are shown the correction factors for the finite slit effect ($\epsilon_{max}/\epsilon^{(a)}_{max}$) for apparent half-band widths of 10 and 15 cm^{-1}, computed from RAMSAY's tables [13] for an optical density of

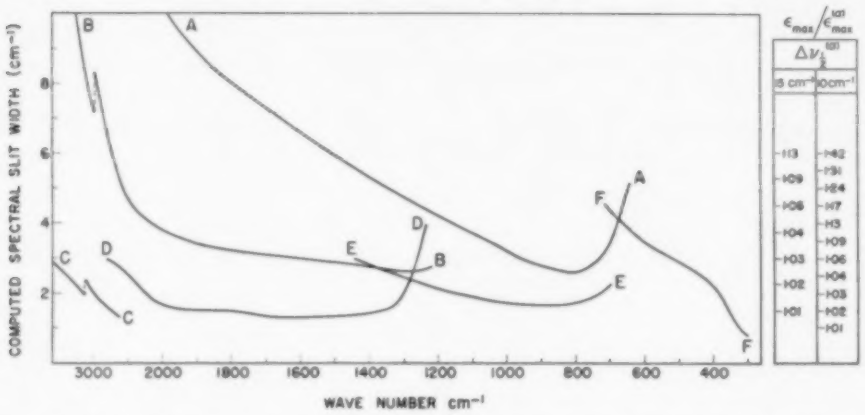

Fig. 1. Typical spectral slit schedules for various types of spectrometers (see Table 1).

0·43. The operating conditions under which these curves were obtained are summarized in Table 1.

This diagram illustrates that, using a double-pass prism spectrometer, it is possible to operate at computed spectral slit-widths of 1·5–2·0 cm^{-1} from 3000 to 650 cm^{-1} (curves *C*, *D*, *E*).

Using the conventional types of single-pass prism spectrometers, the optimum

Table 1. Slit schedules employed to obtain spectral slit curves shown in Fig. 1

Curve	Spectrometer	Prism	Slit schedule	Wave number range* (cm^{-1})
A	Perkin-Elmer Model 21	NaCl (single-pass)	17 μ–683 μ	3800–650
B	Perkin-Elmer Model 12†	CaF_2 (single-pass)	34 μ	3760–3000
			44 μ	3000–2476
			88 μ–266 μ	1900–1225
C	Perkin-Elmer Model 112	LiF (double-pass)	45 μ	3800–3150
			55 μ	3150–2625
D	Perkin-Elmer Model 112	CaF_2 (double-pass)	33 μ–445 μ	2820–1244
E	Perkin-Elmer Model 112	NaCl (double-pass)	60 μ–475 μ	1445–695
F	Perkin-Elmer Model 112	CsBr (double-pass)	170 μ–2000 μ	720–325

* The slit programmes associated with curves *A*, *B*, *E*, and *F* were obtained by the use of a string-operated cam; an electronically operated camming system was used for curve *D*, although a string cam was used satisfactorily in earlier work. The single-beam measurements (curves *B*–*F*) were obtained while operating at a gain of 0·25 μV for full-scale deflection of a Brown 2-sec Elektronik strip-chart recorder, and a noise level of about 1·5 per cent.

† The Model 21 spectrophotometer with CaF_2 prism should exhibit approximately the same spectral slit characteristics when operated under routine laboratory conditions.

operating conditions with sodium chloride and calcium fluoride prisms will conform approximately with curves *A* and *B* of Fig. 1 to provide spectral slit-widths of 4–2 cm^{-1} between 2000 and 650 cm^{-1}. In our experience, the $\epsilon_{max}^{(a)}$ values obtained under these conditions for *n*-paraffin hydrocarbons, saturated fatty acids, and esters agree quite well between 1350 and 650 cm^{-1} with the measurements made at higher dispersion. This is illustrated in Table 2 for the methylene rocking bands of

Table 2. Comparison of extinction coefficients for the methylene rocking band (722–719 cm^{-1}) of *n*-paraffin hydrocarbons as obtained under the conditions of curves *A* and *E* of Fig. 1

Hydrocarbon	Curve *A* Model 21 spectrophotometer	Curve *E* Model 112 spectrometer
	$S' = 3{\cdot}1$ cm^{-1}	$S' = 2{\cdot}0$ cm^{-1}
	$S'/\Delta\nu_{1/2}^{(a)} = .0{\cdot}19$	$S'/\Delta\nu_{1/2}^{(a)} = 0{\cdot}125$
Heptane	15	14
Octane	17·5	17
Decane	20	20
Dodecane	24·5	25
Tetradecane	28	29
Hexadecane	34	36
Octadecane	39·5	40
Octacosane	66	63·5

n-paraffin hydrocarbons, for which $\Delta\nu_{\frac{1}{2}}^{(a)} \approx 16$ cm^{-1}. It would be anticipated, however, that such good agreement would not be obtained for narrower bands, such as the C—H out-of-plane bending bands of aromatic and unsaturated compounds. The discrepancies in C=O stretching band intensities at spectral slit-widths in the range 4–8 cm^{-1} have been discussed previously [7].

(b) *Errors due to Scattered Radiation*

The significance of scattered radiation in single-pass single-prism instruments is well recognized, and methods for its evaluation and correction have been discussed [12]. In Fig. 2 the $\epsilon_{max}^{(a)}$ values for the 1379-cm^{-1} methyl band of *n*-paraffin hydrocarbons as measured on single-pass and double-pass spectrometers are compared. These were obtained under the conditions of curves *B* and *D* of Fig. 1 respectively. The broken curve of Fig. 2 shows the single-pass data after applying the Ramsay correction for the spectral slit error, and it is apparent that a large systematic error still remains; this is most probably attributable to scattered radiation in the single-pass spectrometer; the double-pass measurements were subsequently confirmed by measurement on a second spectrometer of the same type. The virtual elimination of scattered radiation in double monochromators and

VOL. 9 1957

double-pass single monochromators is of considerable importance in making measurements of absolute band intensities, apart from the additional resolution which these instruments provide.

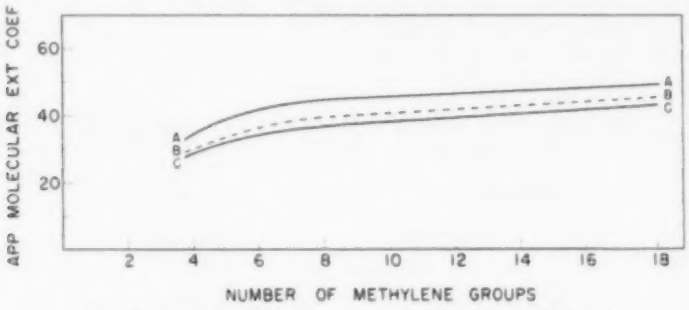

Fig. 2. $\epsilon^{(a)}_{max}$ for 1379-cm^{-1} band of *n*-paraffins in CCl_4 solution
Curve *A*. Double-pass spectrometer.
Curve *B*. Single-pass spectrometer corrected for slit error.
Curve *C*. Single-pass spectrometer uncorrected.

(c) *Errors Due to Electronic and Mechanical Inertia in the Recording System*

In principle, intensity measurements of the highest precision should be made by a point-by-point plotting technique, which allows the spectrometer to reach complete equilibrium at a given frequency setting before a measurement is taken. In survey studies of large numbers of spectra over extended frequency ranges this is too time-consuming to be practicable, and a maximum scanning speed must be determined. In any continuously recording instrument, errors in the peak intensity measurements will be introduced if there is appreciable electrical or mechanical inertia in the recording system. If the time-constants of the electronic system are known, the maximum permissible scanning speed for a given type of input signal can be computed, but this will not take account of the mechanical inertia and play in the recording system or the beam compensating comb mechanism, etc. Errors in the recorded peak heights will depend on the rate of change of the signal strength; this may be limited by avoiding measurements at extreme optical densities. Such extreme measurements will also be very sensitive to small errors in the reproducibility of the I_0 and 100 per cent absorption curves, and it is good practice to adjust concentrations and cell lengths so that all measurements fall within the range 0·2–0·8 optical density units. To determine the limiting scanning speed, it is advisable to select the sharpest band in the spectral range to be measured, and retrace it at progressively slower scanning speeds until further speed reduction ceases to yield a higher peak intensity.

(d) *Other Factors Affecting Intensity Measurements*

It is advisable to measure spectra in duplicate, using large (1–5 ml) samples of solution, prepared separately, and to average the $\epsilon^{(a)}_{max}$ values from the two curves. We prepare solutions gravimetrically in a constant temperature room at

23 ± 1°C, and calculate the molar concentration on the basis of specific gravities of 1·26 and 1·59 for solutions in carbon disulfide and carbon tetrachloride respectively. The cell thicknesses are averaged from several readings with a travelling micrometer observed at random positions across the cell face. A control solvent spectrum is recorded on each chart. The small systematic zero drift is measured at the end of each run and assumed to vary linearly with change of prism angle (i.e. Veeder counter number).

Table 3. Comparison of duplicate intensity measurements on the infra-red spectrum of Δ^5-androsten-3β-ol*

Instrument P Operator M. A. M. 11 June 1954.		Instrument E Operator H. H. 4 September 1956	
ν_{max} (cm^{-1})	$\epsilon^{(a)}_{max}$	ν_{max} (cm^{-1})	$\epsilon^{(a)}_{max}$
1216	31·0	1216	32·1
1172	25·5	1171	26·8
1132	25·0	1133	28·0
1027	63·0	1028	62·2
1020	60	1020	59·2
1008	40·5	1008	41·5
979	34·0	979	32·9
954	52·5	955	52·4
942	29·0	942	30·2

* The measurements were made in carbon disulfide solution by different operators on two Perkin-Elmer Model 112 single-beam double-pass spectrometers.

The operating conditions outlined above have been used routinely in our laboratory in band intensity measurements. The reproducibility obtained under these conditions is illustrated by the $\epsilon^{(a)}_{max}$ values for Δ^5-androsten–3β-ol solutions reported in Table 3. These are typical results, obtained by independent investigators using separate spectrometers at an interval of 2 years. The major source of error is probably the uncertainty introduced by the comparatively high noise level (about 1·5 per cent) which is unavoidable at the narrow spectral slit schedules employed. This should be eliminated by the substitution of the prisms by a grating which should provide more energy at the same spectral slit-widths.

At the present time no standards of infra-red band intensity are available, so that it is not possible to evaluate the absolute accuracy of these measurements. It is to be hoped that other investigators will repeat some of these measurements so that a body of comparative data can be compiled from which some absolute intensity standards may later be established.

Spectra of *n*-paraffin hydrocarbons

Qualitative and semi-quantitative spectra of the *n*-paraffin hydrocarbons have been studied extensively and the curves for many (as pure liquids) are listed in the

VOL. 9 1957

catalog of the American Petroleum Institute. Structure–spectra correlations and vibrational assignments have been based mainly on the solid-phase spectra, notably by SHEPPARD and collaborators [2, 3, 16].

In 1938 ROSE [14] measured the molecular extinction coefficients of a large number of hydrocarbons in the region of the first and second overtones (5400–8900 cm^{-1}) and observed that for normal paraffin hydrocarbons the extinction coefficients of the bands at 8254, 8300, 8400, 8680, and 8750 cm^{-1} increased linearly with the addition of each methylene group to the chain. The slopes of the 8680 and 8750 cm^{-1} lines, assigned to methyl-group vibrations, were very slight. The only published work on the molecular extinction coefficients of homologous series of

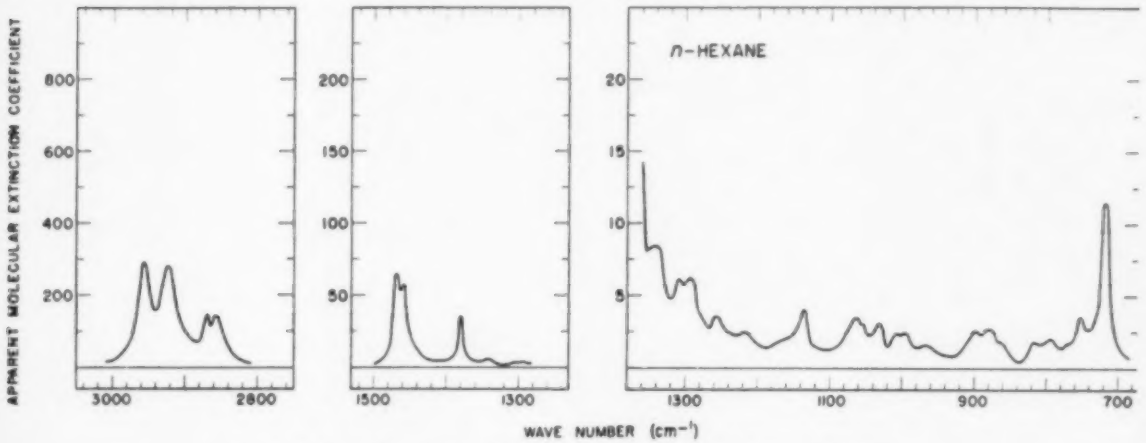

Fig. 3. Infra-red spectrum of *n*-hexane. (3000–1300 cm^{-1} CCl_4 solution; 1350–700 cm^{-1} CS_2 solution.)

hydrocarbons in the fundamental region would appear to be by MCMURRY and THORNTON [9] who computed the molecular extinction coefficients for the hydrocarbons in the A.P.I. collection of spectra and reported the increments per methylene group for some of the bands in homologous series. FRANCIS [4], using a high-resolution grating spectrometer, has established relationships between the number of $-CH_3$, $>CH_2$, and $-CH$ groups in hydrocarbons and the integrated absorption under the various C—H stretching and C—H deformation bands.

It appeared to us that a detailed analysis of the molecular extinction coefficients of the bands in an homologous series, such as the *n*-paraffin hydrocarbons, apart from its intrinsic interest, would provide a useful test of the practicability of the transfer of such data between different laboratories and different types of spectrometers. Accordingly, using the techniques described above, we have measured the apparent molecular extinction coefficients of seventeen *n*-paraffin hydrocarbons in the fundamental region. The $\epsilon^{(a)}_{max}$ values of the principal bands are summarized in Table 4. Representative spectra are shown in Figs. 3–5, and the complete set of spectra will be published separately [6]. The compounds were standard samples supplied by the U.S. National Bureau of Standards and the American Petroleum Institute.

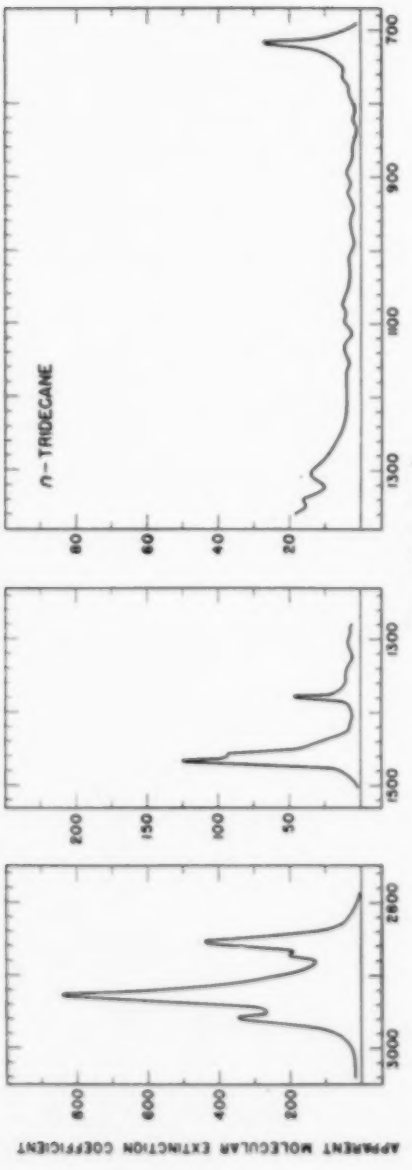

Fig. 4. Infra-red spectrum of n-tridecane (see Fig. 3).

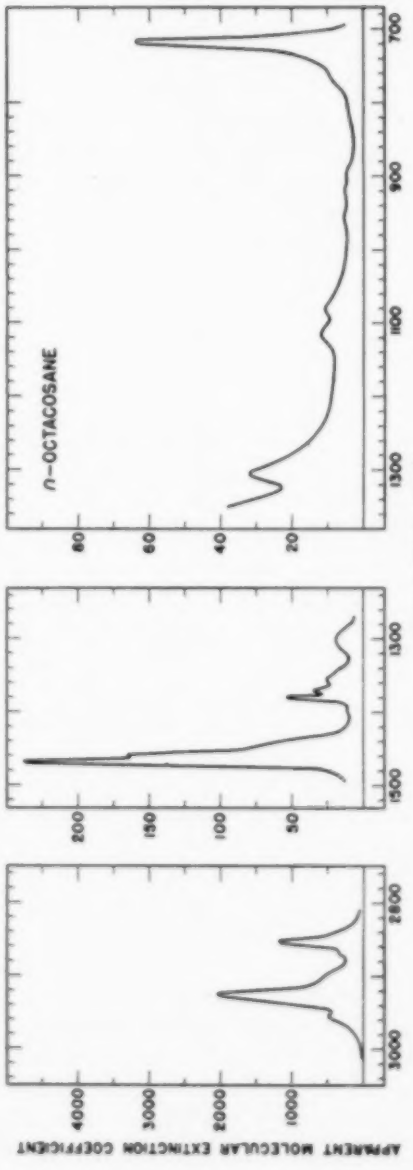

Fig. 5. Infra-red spectrum of n-octacosane (see Fig. 3).

VOL.
9
1957

Table 4. Intensities ($\epsilon^{(a)}_{max}$) of the principal bands in the infra-red spectra of *n*-paraffin hydrocarbons*†

ν_{max}	2958–2954	2927	2872–2869	2855–2853	1467	1460†	1458–1457	1457–1455‡	1379	1307–1304	1140–1130	1090–1070	900–890	722–719
Hexane	287	280	142	142	64·5	—	57	41	34·5	5·5	3·5	3·0	3·0	10·5
Heptane	297	356	148	178	73	—	61	47	38·5	7·0	4·5	3·5	3·5	14
Octane	305	435	156	217	81	—	66	50	42·0	8·5	4·5	4·5	—	16
Nonane	—	—	—	—	—	—	—	—	—	—	—	—	—	—
Decane	318	563	163	306	102	—	77	61	44·5	10·5	4·0	4·5	3·5	20
Undecane	—	—	—	—	—	—	—	—	—	—	—	—	—	—
Dodecane	337	721	192	398	117	(64)	83	71	44·5	12·5	4·5	5·5	5·0	25
Tridecane	344	840	201	437	126	(60)	96	78	45·5	14	5·0	5·5	4·0	27
Tetradecane	354	900	203	490	131	(72)	99	86	44·5	16	4·5	6·0	3·5	29
Pentadecane	364	993	208	540	140	77	98	82	46	16·5	5·0	6·0	4·0	32
Hexadecane	367	1010	228	582	150	70	111	88	47	18·5	—	6·5	4·0	36
Heptadecane	365	1107	222	612	159	90	111	94	46·5	19·5	—	6·5	4·0	37
Octadecane	382	1215	238	670	163	82	119	100	48·5	20	—	6·5	4·0	40
Eicosane	389	1331	(254)	758	185	107	131	111	48·5	21	—	7·0	4·0	44
Tetracosane	444	1740	(293)	951	211	118	146	127	49·5	26	—	8·0	5·0	53
Hexacosane	437	1810	(320)	1036	229	134	157	132	49·5	29	—	11·5	6·0	59
Octacosane	480	2005	(334)	1145	241	140	163	137	53	32	—	11·0	6·0	63·5
Dotriacontane	490	2270	(344)	1291	269	148	193	168	52	36	—	11·0	6·0	73
Hexatriacontane	(530)	2590	(398)	1503	302	186	211	180	55·5	41·5	—	13·0	7·0	83

* 3000–1300 cm^{-1} in CCl_4 solution. 1300–700 cm^{-1} in CS_2 solution.
† Figures in parentheses indicate points of inflection.
‡ There are $\epsilon^{(a)}_{max}$ values for graphically resolved bands (see Fig. 9).

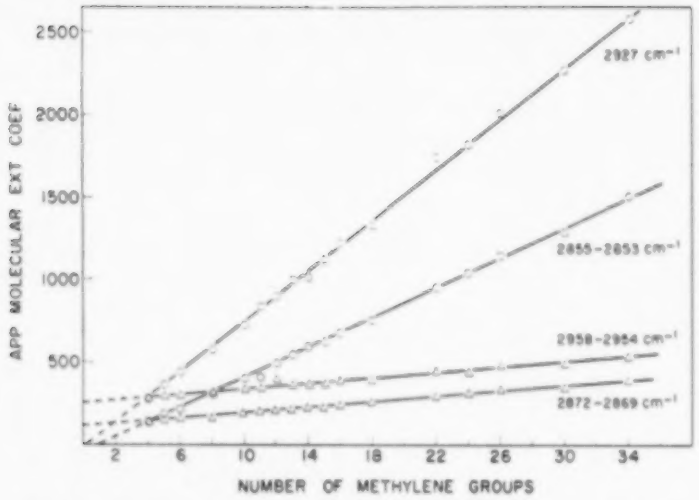

Fig. 6. $\epsilon^{(a)}_{max}$/chain-length relation for C—H stretching bands (CCl_4 solution.)

Table 5. Summarizing table of relationships between band intensity and chain length for *n*-paraffin hydrocarbons

Absorption band	Position (ν_{max}) (cm^{-1})	Intensity* ($\epsilon^{(a)}_{max}$)
Methylene vibrations		
Asym. C—H stretch	2927	$77n - 18$
Sym. C—H stretch	2855–2853	$46n - 64$
Scissor	1467	$8{\cdot}0n + 35$
Wag	1307–1304	$1{\cdot}15n + 1{\cdot}5$
Rock	722–719	$2{\cdot}4n + 1$
Methyl vibrations		
Asym. C—H stretch	2958–2954	$8{\cdot}0n + 258$
Sym. C—H stretch	2872–2869	$8{\cdot}3n + 110$
Asym. C—H deformation		
observed	1458–1457	$5{\cdot}2n + 35$
corrected for overlap	1457–1455	$4{\cdot}7n + 24$
Sym. C—H deformation	1379	$0{\cdot}4n + 41$ $(n > 8)$
Unassigned		
Isolated by curve analysis	1460	$5{\cdot}25n + 6$

* n = number of methylene groups in the chain; unless otherwise indicated the measurements cover the range $5 < n < 37$. Measurements above 1350 cm^{-1} are in carbon tetrachloride solution and below 1350 cm^{-1} in carbon disulfide solution.

VOL. 9 1957

(*a*) C—H *Stretching Region* (3050–2800 cm^{-1})

The asymmetrical and symmetrical C—H stretching peaks for the methylene groups are observed at 2927 and 2855–2853 cm^{-1} respectively. For both bands $\epsilon^{(a)}_{max}$ increases linearly with the number of methylene groups in the chain (Fig. 6), and both lines on extrapolation make small negative intercepts with the zero ordinate axis. The slopes and intercepts are summarized, together with similar data for other bands, in Table 5.

The asymmetrical and symmetrical C—H stretching bands of the terminal methyl groups occur at 2958–2954 and 2872–2869 cm^{-1}. The asymmetrical methyl band is resolved in all hydrocarbons except hexatriacontane, but the symmetrical methyl band appears only as an inflection in the spectra of the homologs above octadecane. The plots of $\epsilon^{(a)}_{max}$ against chain length (Fig. 6) are linear with small positive slopes (Table 5). As these are end-group vibrations, the slopes are due principally to the increasing intensity of the underlying shoulders of the methylene bands. The intercepts of 258 and 110 with the zero ordinate axis suggest contributions of 129 and 55 from each methyl group. This might be checked by observations on a suitable homologous series of hydrocarbons with a long-branched chain, providing three terminal methyl groups in essentially similar environments, or from measurements on a series of *n*-paraffin hydrocarbons with one terminal —CD_3 group. The synthesis of suitable compounds is being investigated. It is likely that absorption in this region will also receive contributions from overtones of C—H deformation vibrations. There is evidence of this in the spectra of the homologs above tetracosane, which exhibit a pronounced inflection at 2900 cm^{-1} (see octacosane in Fig. 5). Absorption attributed to such overtones is very prominent in the spectra of oxygenated compounds such as diethyl ketone and simple alkyl esters [10, 11]. Weak unresolved absorption of this kind may play a part in enhancing the methyl peaks and contribute to the positive slope of the lines in Fig. 6.

(*b*) C—H *Deformation Vibrations Between* 1500 *and* 1400 cm^{-1}

All *n*-paraffin hydrocarbons exhibit a prominent band at 1467 cm^{-1} assigned to the scissoring vibration of the methylene groups. For this band, $\epsilon^{(a)}_{max}$ increases linearly with the chain length (Fig. 7), but the line extrapolates to make an appreciable positive intercept with the zero ordinate axis. This would suggest that the methylene scissoring band is superimposed on other absorption. Although this is probably true, difficulties arise when an attempt is made to consider the band envelopes quantitatively.

Inspection of the curves in Figs. 3–5 suggests that the intensity of the 1467-cm^{-1} band is enhanced by a contribution from the shoulder of the 1458–1457-cm^{-1} band which has been assigned to the asymmetrical C—H deformation vibration of the methyl group. The plot of $\epsilon^{(a)}_{1458-1457}$ against the chain length is also linear (Fig. 8). This line, however, intercepts the zero ordinate axis at +35, and the shoulder of this band can account for only part of the zero ordinate intercept of +35 for the 1467-cm^{-1} line. The presence of additional absorption in this region of the spectrum is therefore suspected, and this indeed is quite evident in the spectra of the higher homologs, where the 1467-cm^{-1} band shows distinct asymmetry on the low-frequency side of the maximum.

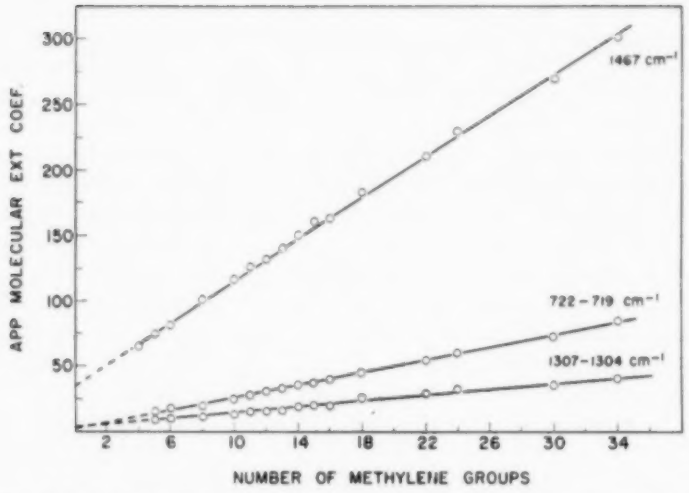

Fig. 7. $\epsilon^{(a)}_{max}$/chain-length relation for C—H deformation bands of methylene groups. (1467-cm^{-1} CCl_4 solution; 1307–4, 722–719 cm^{-1} CS_2 solution.)

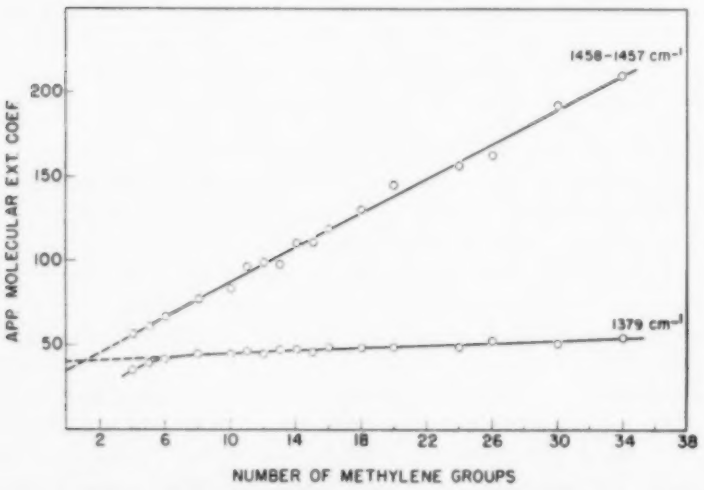

Fig. 8. $\epsilon^{(a)}_{max}$/chain-length relation for C—H deformation bands of methyl groups (CCl_4 solution).

In an initial endeavor to analyse these bands in more detail, an attempt was made to fit the high-frequency half of the 1467-cm^{-1} band envelope to a Lorentz curve based 35 units above the abscissa axis. This proved unsatisfactory, but it was established that the high-frequency half of the 1467-cm^{-1} band envelope could

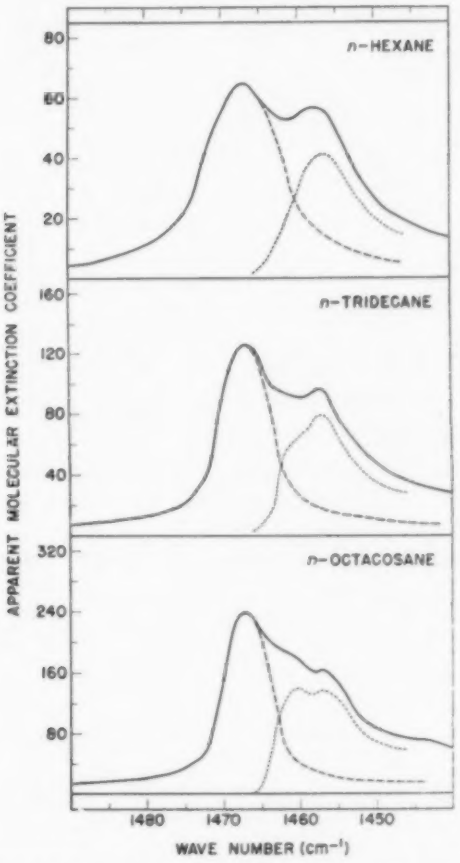

Fig. 9. Graphical analysis of 1480–1450-cm^{-1} absorption (CCl_4 solution).

be fitted fairly well by a Lorentz curve *based on the abscissa axis*, with a peak height at 1467 cm^{-1} equal to $\epsilon^{(a)}_{max}$ and a half-width of 10 cm^{-1}. This empirical observation suggested that the whole of the high-frequency side of the 1467-cm^{-1} band is probably derived from superimposed methylene scissoring absorptions, but it leaves unexplained the +35 zero ordinate intercept of the $\epsilon^{(a)}_{1467}$ line of Fig. 7.

Accepting the above as evidence for the homogeneity of the absorption on the high side of the 1467-cm^{-1} peak, the 1490–1467-cm^{-1} band envelope was reflected about the ordinate through 1467 cm^{-1} and the image subtracted from the 1467–1444-cm^{-1} envelope. The complete series of these curves will be published elsewhere [6], but the representative curves shown in Fig. 9 demonstrate that there is

an additional band in the higher homologs with a maximum near 1460 cm^{-1}. By this method of graphical curve analysis, the band is resolved in pentadecane and higher homologs, and is detected as an inflection in dodecane, tridecane, and tetradecane. The peak of the methyl band is shifted by 1–2 cm^{-1} to lower frequency

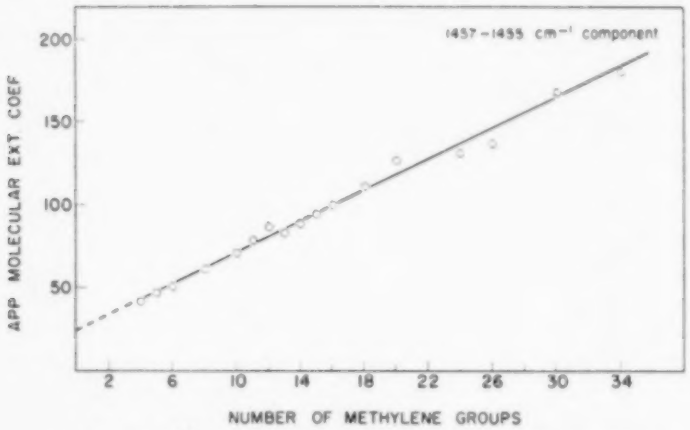

Fig. 10. $\epsilon^{(a)}_{max}$/chain-length relation for 1457–5-cm^{-1} component.

and the plots obtained for these component band intensities against chain length are shown in Figs. 10 and 11. It is not surprising that the points show more scatter than the experimentally observed $\epsilon^{(a)}_{max}$ values, but even allowing for the assumptions on which these graphical constructions are based, the 1457–1455 cm^{-1} component peak probably represents the position and intensity of the methyl absorption better than the observed maximum at 1458–1457 cm^{-1}.

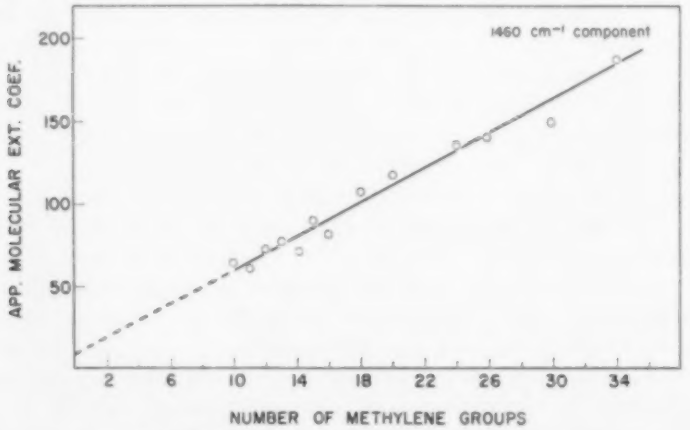

Fig. 11. $\epsilon^{(a)}_{max}$/chain-length relation for 1460-cm^{-1} component.

The 1460-cm^{-1} component band gains in relative prominence as the chain lengthens and the plot in Fig. 11 extrapolates back to the neighborhood of the origin, suggesting that this band is probably associated with methylene absorption.

VOL. 9 1957

It could result from coupling between the methylene scissoring vibrations of suitably oriented vicinal methylene groups in the randomly coiled chains, or from coupling of a methylene scissoring vibration with the first overtone of the rocking vibration at 722–719 cm^{-1}. These vibrations do not interact in the solid-phase spectra, where the fixed orientation of the chain puts them into different symmetry classes, but the selection rules may break down when the chain orientation is randomized. If this should be the case, such coupled vibrations should become statistically more probable as the chain is lengthened. This might be accompanied by a fall-off in the rate of increase of $\epsilon^{(a)}_{1467}$ with chain length, if the scissoring vibration is directly involved, but there is no evidence of this over the range of chain lengths covered by these investigations.

The band at 1379 cm^{-1} is assigned to the symmetrical C—H bending vibration of the methyl group. The plot of $\epsilon^{(a)}_{max}$ against chain length (Fig. 8) is linear for homologs above decane, with very small positive slope, but for this band there is a notable fall-off in the intensity for hexane, heptane, and octane. This is apparent also in the single-pass measurements illustrated in Fig. 2, and was noted independently by McMurry and Thornton [9]. If the straight line is extrapolated back, a value of 20·5 is obtained for the $\epsilon^{(a)}_{max}$ contribution of each methyl group in the long-chain compounds. McMurry and Thornton reported a value of 18.

(c) *Low-frequency Vibrations* (1350–700 cm^{-1})

Below 1350 cm^{-1} the spectra of the crystalline solids exhibit a great deal of structure which becomes broad and diffuse when the solids are melted or dissolved. Much of this absorption is associated with C—C stretching vibrations; when the chain orientation is randomized in the liquid phase it will become smeared out and only the characteristic vibrations localized in the individual methylene groups and the end groups will persist.

The most prominent absorption is the methylene rocking band at 722–719 cm^{-1}, which shows normal intensity behavior with $\epsilon^{(a)}_{max}$ extrapolating back near the origin (Fig. 7). The same is true also for the next strongest band at 1307–1304 cm^{-1} assigned to the methylene wagging mode. All other absorption becomes extremely diffuse in the higher members of the series, while the intensity of the background absorption, as observed in the absorption minima, rises. This rising background absorption must be derived largely from skeletal vibrations in the randomly oriented chains. In all compounds there is a broad band at 1090–1080 cm^{-1}, with $\epsilon^{(a)}_{max}$ increasing from 3·5 to 13 with lengthening chain (Table 4), and there is also a weaker band at 900–890 cm^{-1}, with $\epsilon^{(a)}_{max}$ increasing from 3·5 to 7. Most of the intensity increase observed for both these bands can be attributed to the rise in the general background absorption, and if allowance is made for this, the elevation of the two peaks above the general background is constant at about five and two intensity units respectively throughout the homologous series. This would suggest that they may be methyl absorptions. The shorter-chain compounds below eicosane also exhibit a band at 1135–1132 cm^{-1} which may also be associated with a methyl vibration. The 900–890-cm^{-1} band may correspond with the band R_3 which Brown, Sheppard, and Simpson [3] observe in the solid-phase spectra. These investigators, also assigned absorption at 1150–1120 cm^{-1} in the solids to two methyl vibrations

(R_1 and R_2), and a band at 1060 cm^{-1} to a C—C skeletal vibration. From its position, the latter band might be identified with our 1090–1080-cm^{-1} absorption, though the assignment would not be consistent with our interpretation of the intensity behavior.

The spectra of these hydrocarbon solutions compare closely in general appearance with the spectra of the pure liquids reported in the A.P.I. catalog, though the diffuse structure is better defined for the pure liquids.

Conclusions

Generally speaking, these intensity measurements substantiate the conclusions from group-frequency analysis, that the principal bands in the liquid-phase spectra are localized within the individual methyl and methylene groups. It is consistent with the accepted assignments that the methylene group absorptions at 2927, 2855–2853, 1307–1304, and 722–719 cm^{-1} increase uniformly as the chain lengthens and that the plots of $\epsilon_{max}^{(a)}$ against chain length extrapolate near zero for zero methylene groups. The measurements were limited to hexane and the higher homologs because the extreme volatility of the shorter-chain hydrocarbons make it difficult to control the concentration. It would not be surprising if these linear relations failed for the very short-chain hydrocarbons. In the first overtone region GAUTHIER has shown that the methylene groups vicinal to methyl groups show perturbed vibration frequencies [5], but the effect must be fairly small in the region of the fundamental vibrations, as otherwise the plots of $\epsilon_{max}^{(a)}$ against chain length would intercept the zero abscissa near $n = 2$. The breakdown in the linearity of these plots for short chains will be considered further when dealing with fatty acids and methyl esters in a later publication.

To a first approximation the methyl group vibrations would be expected to show bands of constant intensity, independent of the chain length. This is not the case, and for all methyl bands $\epsilon_{max}^{(a)}$ increases slowly as the chain lengthens. The plots of $\epsilon_{max}^{(a)}$ against chain length extrapolate back to make appreciable intercepts with the ordinate axis, and half of this intercept probably provides a reasonable measure of the actual contribution of the methyl-group absorption to the total intensity at the maximum, over regions where the relationship is linear. For the methyl bands at 2958–2954, 2872–2869, and 1458–1457 cm^{-1} the absorption increase with chain length can be attributed largely to the fact that the bands lie on the shoulders of methylene bands, while for the bands at 1379, 1090–1080, and 900–890 cm^{-1} the greater part of the increase must derive from the increasing intensity of the general background absorption.

The absorption is most complex in the region between 1467 and 1457 cm^{-1}, and we cannot account satisfactorily for the appreciable positive intercept which the 1467-cm^{-1} methylene scissoring line makes with the zero ordinate axis.

In regard to the more general aspects of infra-red intensity measurements, it is apparent that the techniques described in the earlier part of this paper are too time-consuming for routine laboratory use. Nevertheless, the infra-red spectrum has now become the most important single physical constant for the identification of an organic compound, and it is necessary that these spectra be recorded with the greatest possible precision in a form suitable for rapid and reliable data transfer

VOL. 9 1957

between laboratories, and for coding and sorting by electronic means. The $\nu/\epsilon^{(a)}$ curves are ideally suited for this purpose, and it should be possible to build into the amplifier-recorder a unit which would introduce the $1/cl \cdot \log |x|$ function and plot the $\epsilon^{(a)}_{max}$ curve directly. Pending such developments, it must be urged that those concerned with the recording of infra-red spectra for documentation purposes pay due attention to the importance of eliminating the major causes of error in intensity measurements. This involves using a spectrometer with adequate resolution, scanning sufficiently slowly, taking all possible precautions to minimize scattered radiation in the spectrometer, and maintaining an accurate control of the cell thickness and sample concentration. Unless these precautions are observed, the spectrograms now being recorded may fail to meet the more exacting specifications which future applications may demand.

Acknowledgements—We wish to thank Dr. R. W. SCHIESSLER for providing us with samples of the longer-chain hydrocarbons, synthesized under Project 42 of the American Petroleum Institute. We are also grateful to Mr. A. NADEAU and Mrs. M. A. MACKENZIE for technical assistance with the measurement of the spectra.

References

[1] BARROW G. M. *J. Chem. Phys.* 1953 **21** 2008.
[2] BROWN J. K., SHEPPARD N., and SIMPSON D. M. *Disc. Faraday Soc.* 1950 **9** 261.
[3] BROWN J. K., SHEPPARD N., and SIMPSON D. M. *Phil. Trans.* 1954 **A247** 35.
[4] FRANCIS S. A. *J. Chem. Phys.* 1950 **18** 861.
[5] GAUTHIER G. *C. R. Acad. Sci. Paris* 1950 **231** 1138.
[6] JONES R. N. *Nat. Res. Coun. Can. Bull.* No. 5 1957.
[7] JONES R. N., RAMSAY D. A., KEIR D. S., and DOBRINER K. *J. Amer. Chem. Soc.* 1952 **74** 80.
[8] JONES R. N. and SANDORFY C. The application of infra-red and raman spectrometry to the elucidation of molecular structure. *Technique of Organic Chemistry* (Ed. A. WEISSBERGER) Vol. IX. Interscience, New York, 1956.
[9] MCMURRY H. L. and THORNTON V. *Anal. Chem.* 1952 **24** 318.
[10] NOLIN B. and JONES R. N. *J. Amer. Chem. Soc.* 1953 **75** 5626.
[11] NOLIN B. and JONES R. N. *Can. J. Chem.* 1956 **34** 1382, 1392.
[12] OPLER A. *J. Opt. Soc. Amer.* 1950 **40** 401.
[13] RAMSAY, D. A. *J. Amer. Chem. Soc.* 1952 **74** 72.
[14] ROSE F. W. JR. *J. Res. Nat. Bur. Stand.* 1938 **20** 129.
[15] RUSSELL R. A. and THOMPSON H. W. *J. Chem. Soc.* 1955 483.
[16] SHEPPARD N. and SIMPSON D. M. *Quart Rev. Chem. Soc.* 1953 **7** 19.
[17] SKINNER M. W. and THOMPSON H. W. *J. Chem. Soc.* 1955 487.
[18] THOMPSON H. W. and STEEL G. *Trans. Faraday Soc.* 1956 **52** 1451.
[19] WILLIAMS V. Z. *Rev. Sci. Instrum.* 1948 **19** 135.

Spectrochimica Acta. 1957. Vol. 9, pp. 252 to 262. Pergamon Press Ltd., London

Analysis of the near-ultra-violet absorption spectrum of *para*-fluoro-anisole

V. Ramakrishna Rao and V. Suryanarayana*
Physics Department, Andhra University, Waltair, India

(*Received* 23 *January* 1957)

Abstract—The near ultra-violet absorption spectrum of *para*-fluoro-anisole has been studied. The discrete bands were analysed and attributed to an allowed transition $^1A_1 \rightarrow {}^1B_1$. Most of the 180 observed bands could be explained on the basis of nine fundamentals in the upper state (229, 391, 548, 720, 810, 1042, 1280, 1299, and 1367) and eight in the ground state (236, 435, 843, 857, 1116, 1275, 1308, and 1428). These fundamentals were correlated mutually, and with Raman data, and possible assignments discussed. The occurrence of the CH_3 bending frequency in all the substituted anisoles was discussed and established.

Introduction

Among the halogen-substituted benzenes, the fluoro substitutions have special spectroscopic interest. The so-called violet shift of the (0,0) band [1] in disubstituted benzenes and the more extensive nature of the spectrum obtained are among the topics of interest. In our work on substituted anisoles the fluoro-anisole assumes additional importance on account of the C–F frequency which occurs in the same region (1250 to 1300 cm^{-1}, as the CH_3 bending frequency.

Raman data with depolarization factors were given for *para*-fluoro-anisole by Paulsen [2]. Infra-red measurements were refuted by Lecomte [3]. No studies on the fluorescence or ultra-violet absorption appear to have been made. We have found that, like *para*-chloro-and *ortho*-chloro-anisoles, [4,5] *para*-fluoro-anisole also does not fluoresce. Our measurement on the near ultra-violet absorption of *para*-fluoro-anisole are described in the following pages.

Experimental

Full experimental details are given elsewhere [5,6]. The substance was obtained from Eastman Kodak Co. and purified by distillation in vacuum. Using pathlengths of 25 cm and 75 cm, spectra were recorded with saturated vapour pressures for temperatures in the range −20°C to 120°C. A Hilger medium quartz instrument and a Hilger E1 spectrograph were used.

Results

The absorption was found to consist of two regions, as with other substituted anisoles namely (a) a continuous absorption below 2300 Å and (b) a band system between 2965 and 2428 Å. At higher vapour pressures the two regions merge into one single continuous absorption.

With the lowest pressures of vapour, only five bands were distinctly recorded at 2843·4, 2779·4, 2743·5, and 2683·8 Å. From there the (0,0) band was fixed at 2843·4 Å (35159 cm^{-1}). At higher pressures, more bands develop with greater

* Formerly Junior Research Assistant in C.S.I.R. Scheme.

VOL. 9 1957

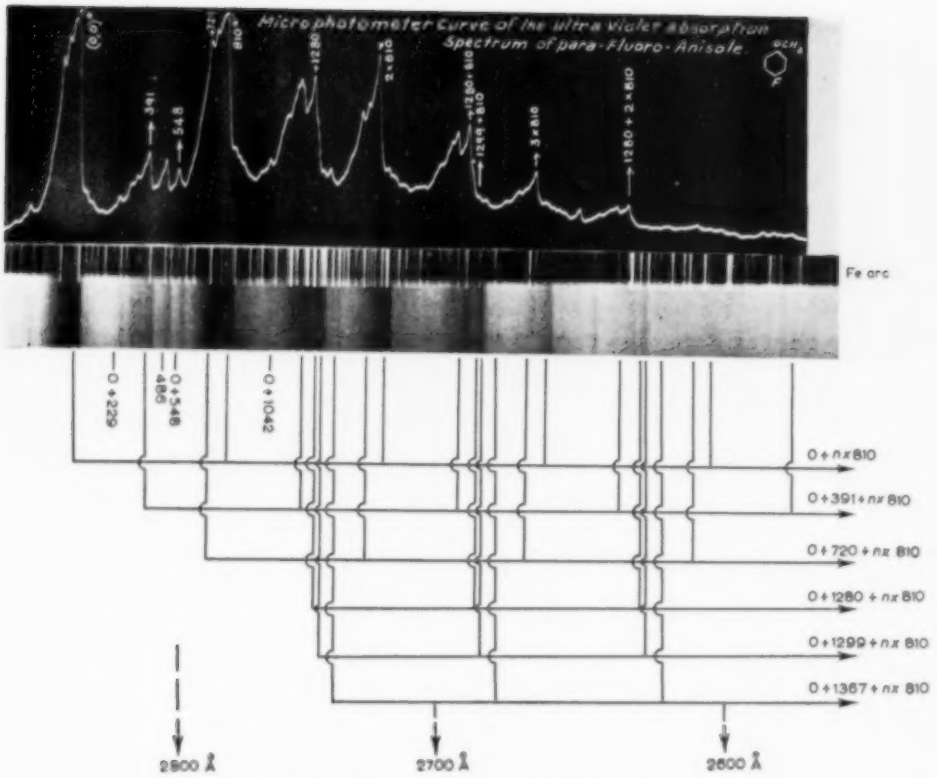

Fig. 1. Ultra-violet absorption spectrum of para-fluoro-anisole.

VOL.
9
1957

intensity. Fig. 1 shows the spectrum measured, using a pathlength of 25 cm and a reservoir temperature of 0°C. The bands are far sharper than those of the chloro-anisoles. At higher pressures, there is continuous absorption below 2843 Å. Bands begin to develop more towards the longer-wavelength side of the (0,0) band. With 75-cm path and a reservoir temperature of 70°C there is complete absorption below 2964 Å. The bands appear in groupings with characteristic repeating patterns. The intense groups are in the regions 2840–2850, 2779–2786, 2740–2750, at 2717, 2683–2688, 2659, and 2626 Å. From a consideration of these groupings and intensities, the following analysis and interpretation was arrived at. Intensities are only visual estimates in the Scale 1 to 10. The positions, intensities, and assignment of bands are given in Table 1.

Analysis and discussion

Para-fluoro-anisole, like other *para*-substituted benzenes, approximates to the point group C_{2v} and is subject to all the well-known selection rules. The transition A_1–B_1 is permitted.

The intense band at 2843·4 (35159 cm^{-1}) is chosen as (0,0) band. Frequency shifts from this band are given in Table 1. Nine fundamentals in the upper state and eight in the ground state are found to explain about 150 of the 180 bands observed. Some weak bands have not been assigned. The fundamentals in both states with corresponding Raman lines and their possible assignments are given in Table 2. There are four intense satellites on the long-wavelength side of the (0,0) band at intervals of 36, 46, 66, and 94 cm^{-1}.

The most important fundamental in the upper state appears to be 810 cm^{-1}. Five overtones of this interval are observed, and all these overtones superpose upon other fundamentals. About 70 bands in the spectrum could be interpreted in terms of this fundamental, which appears also to combine with all the other fundamentals. There are two fundamentals in the ground state namely 857 and 843 cm^{-1}, of which 857 gives the sharper and the more intense band. It is impossible to decide which of these corresponds to the upper-state frequency 810 cm^{-1}. In the Raman spectrum there are two intervals, 831 and 852 cm^{-1}, the former being the more intense and corresponding to the Raman intervals, 755 in guaicol, 796 in *para*-chloro-anisole, 793 in *para*-bromo-anisole and 796 in *ortho*-chloro-anisole This line is very strongly polarized with a depolarization factor of 0·08, whereas that at 852 is weaker and recorded by PAULSEN as being polarized. In fact, it is recorded possible that the intensity of the 852 Raman line may be partly due to Fermi resonance between 852 and $2 \times 428 = 856$. 428 is possibly the α component of E_g^+ vibration in benzene. A comparison of the ultra-violet absorption and Raman data suggests that the interval 857 corresponds to the Raman interval of 831. This set of lines may now be correlated with the very prominent upper state fundamental 810 cm^{-1}. It is found that equally prominent fundamentals in other substitutions of anisole are 767 in *ortho*-chloro-anisole, 779 in *para*-chloro-anisole, 771 in *para*-bromo-anisole, 721 in guaicol, [7] and 755 in anisole [8]. With *para*-chloro-anisole [4] we attributed these frequencies to a C–OCH_3 valence vibration. Fundamentals in the region 600 cm^{-1} were found only with chloro substituents. This would mean that C–OCH_3 vibrational frequency increases in its value even

Table 1. *Para*-fluoro-anisole: ultra-violet absorption bands

Wavelengths (Å)	Intensity	Wave numbers (cm^{-1})	Assignment
2963·8	—	33731	0 − 1428
2953·3	—	33851	0 − 1308
2950·4	—	33884	0 − 1275
2948·9	—	33901	
2942·0	—	33981	
2936·6	4	34043	0 − 1116
2922·3	½	34210	
2921·7	1	34217	
2920·3	1½	34233	0 − 1308 + 391
2918·9	½	34249	0 − 2 × 857 + 810
2917·1	1D	34271	0 − 857 − 843 + 810
2916·6	1½	34276	0 − 843 − 435 + 391
2915·2	1½	34293	0 − 2 × 435
2914·4	4S	34302	0 − 857
2913·2	2	34316	0 − 843
2887·0	2½	34628	0 ← 1308 + 2 × 391
2885·5	1	34646	
2883·7	1	34668	0 ← 1308 + 810 ?
2879·1	1	34724	0 ← 435
2876·1	½	34759	0 ← 1116 + 720 0 − 857 − 843 + 1299
2872·7	1	34800	
2872·3	1	34807	0 − 1116 − 435 + 810 + 391
2868·1	2	34856	0 − 1116 + 810
2866·0	1	34881	
2865·1	3	34892	0 − 1308 + 1042
2862·6	4	34923	0 − 236
2860·9	2	34944	0 − 94 − 2 × 46 − 36?
2858·8	1½	34970	0 − 2 × 94
2857·1	1	34990	0 − 94 − 46 − 36 ?
2855·9	½	35004	0 − 2 × 435 + 720
2855·7	1D	35007	
2854·8	2	35018	0 − 857 + 720 0 − 94 − 46
2853·7	1D	35032	0 − 94 − 36 0 − 1428 + 1299 0 − 843 + 720
2851·1	4	35065	0 − 94
2848·7	3	35093	0 − 66
2847·1	2	35113	0 − 46 0 − 857 + 810 0 − 435 + 391
2846·3	2	35123	0 − 36
2843·4	10	35159	(0,0)
2839·6	4	35205	
2836·8	3D	35241	
2825·0	4	35388	0 + 229 0 + 2 × 391 + 720 − 1275 0 + 720 + 810 − 1308

VOL. 9 1957

Table 1 (*continued*)

Wavelengths (Å)	Intensity	Wave numbers (cm^{-1})	Assignment
2823·4	2	35407	
2820·4	3	35446	$0 + 720 - 435$
2819·2	3	35461	$0 + 1280 + 810 + 391 - 2 \times 435 - 1308$
2817·5	4	35482	$0 + 2 \times 391 + 810 - 1275$
2815·3	2	35510	$0 + 391 - 36$ $0 + 2 \times 391 - 435$
2814·5	2	35520	$0 + 391 + 1280 - 1308$
2813·7	2	35530	$0 + 810 - 435$
2812·8	2	35541	$0 + 391 + 1299 - 1308$
2812·1	5	35550	$0 + 391$
2809·3	2	35586	$0 + 1280 - 857$
2806·8	2	35618	$0 + 1299 - 843$ $0 + 2 \times 229$
2804·6	5	35645	$0 + 720 - 236$
2799·7	5	35707	$0 + 2 \times 391 - 236$ $0 + 548$
2797·8	3	35733	$0 + 2 \times 720 - 435 \times 2$ $0 + 810 - 236$?
2795·0	1	35768	
2790·9	1	35821	$0 + 720 + 810 - 2 \times 435$
2786·3	4	35879	$0 + 720$
2783·8	4	35912	$0 + 2 \times 810 - 435 \times 2$
2782·7	2	35925	$0 + 2 \times 810 - 857$ $0 + 810 - 46$
2781·7	2	35939	$0 + 810 - 36$ $0 + 2 \times 391$ $0 + 1280 + 810 - 1308$
2779·4	7	35969	$0 + 810$
2778·5	3	35981	$0 + 1280 + 810 - 1275$
2777·6	1	35992	$0 + 1299 + 810 - 1275$
2775·6	2	36018	$0 + 3 \times 720 - 435 \times 3$
2774·7	1	36029	
2773·7	2	36042	$0 + 2 \times 1299 - 857 \times 2$
2769·3	1	36100	$0 + 548 + 391$
2765·1	2	36154	$0 + 1042 + 810 - 857$ $0 + 1042 - 46$
2763·5	2	36175	
2761·5	3	36201	$0 + 1042$
2758·7	1	36238	$0 + 391 + 720 - 36$
2757·2	1	36259	$0 + 720 + 810 - 435$
2756·0	1	36273	$0 + 391 + 720$
2755·1	1	36286	
2754·4	1	36296	$0 + 4 \times 720 - 435 \times 4$
2750·7	3	36343	$0 + 1280 - 94$
2749·2	4	36363	$0 + 1299 - 94$ $0 + 391 + 810$
2748·1	4	36378	$0 + 1280 + 810 - 2 \times 435$
2745·9	2	36407	$0 + 1280 - 36$
			$0 + 1299 - 36$ $0 + 548 + 720$

Table 1 (*continued*)

Wavelengths (Å)	Intensity	Wave numbers (cm^{-1})	Assignment
2743·5	8	36439	0 + 1280
2742·1	4	36458	0 + 1299
2739·7	2D	36489	0 + 1367 − 36
2736·9	3D	36526	0 + 1367
2735·5	1D	36546	
2728·5	1	36639	0 + 720 + 2 × 810 − 2 × 435
2724·4	3	36694	0 + 720 + 810 0 + 2 × 810 − 94
2722·5	3	36720	0 + 2 × 391 + 810 − 36 0 + 3 × 810 − 2 × 435
2721·8	2	36729	0 + 2 × 810 − 46 0 + 3 × 810 − 857
2721·1	2	36740	0 + 2 × 810 − 36 0 + 548 + 1042
2720·0	3	36753	0 + 391 + 1299 − 94 ? 0 + 1280 + 2 × 810 − 1308 0 + 2 × 391 + 810
2719·3	2	36764	
2718·6	3	36773	0 + 1280 + 810 + 391 − 2 × 435
2717·8	6	36784	0 + 2 × 810 0 + 1280 + 2 × 810 − 1275
2716·3	1	36804	0 + 1299 + 2 × 810 − 1275
2715·7	1½	36813	0 + 391 + 1299 − 36 0 + 1280 + 810 − 435
2714·3	2	36830	0 + 1299 + 810 − 435 0 + 391 + 1280
2712·7	½D	36853	0 + 391 + 1299
2708·5	1D	36909	0 + 1042 + 810 − 94
2707·0	1D	36930	0 + 1042 + 810 − 36 − 46
2704·0	2D	36971	0 + 1042 + 810 − 36
2701·0	2D	37013	0 + 1042 + 810
2696·5	1½	37075	
2695·7	1½	37086	0 + 391 + 720 + 810
2694·4	1½	37103	0 + 1280 + 720 + 810 − 2 × 435
2693·0	1½	37123	
2692·3	1½	37132	0 + 391 + 2 × 810 − 36
2691·0	2	37150	0 + 1280 + 810 − 94
2690·0	2D	37163	0 + 1280 + 720
2688·9	2D	37179	0 + 391 + 2 × 810 0 + 1299 + 810 − 94
2688·8	2	37181	0 + 2 × 391 + 1280 − 36
2688·1	4	37191	0 + 1280 + 2 × 810 − 435 × 2
2685·8	1½	37222	0 + 2 × 391 + 1280
2685·3	D	37229	0 + 810 + 1299 − 36
2684·4	3	37241	0 + 2 × 1042 0 + 2 × 391 + 1299
2683·8	6	37249	0 + 1280 + 810
2683·0	2	37261	0 + 1299 + 810
2680·2	2	37300	0 + 1367 + 810 − 36
2677·0	2D	37344	0 + 1367 + 810

VOL. 9 1957

Table 1 (*continued*)

Wavelengths (Å)	Intensity	Wave numbers (cm^{-1})	Assignment
2666·6	1	37490	$0 + 3 \times 810 - 94$ $0 + 2 \times 391 + (810 - 36)\,2$
2665·6	1½	37503	$0 + 720 + 2 \times 810$ $0 + 1042 + 1299$
2663·0	1	37540	$0 + 4 \times 810 - 857$
2661·9	1	37556	$0 + 3 \times 810 - 36$
2661·2	2D	37566	$0 + 2 \times 391 + 810 \times 2$
2660·5	1D	37576	
2659·9	2	37585	$0 + 1280 + 2 \times 810 + 391 - 2 \times 435$
2659·3	5	37593	$0 + 3 \times 810$
2655·6	1	37645	$0 + 391 + 810 + 1280$
2654·8	1	37656	$0 + 391 + 810 + 1299$
2652·9	D	37684	$0 + 2 \times 1280 - 36$
2651·0	2	37711	$0 + 2 \times 1280$ $0 + 2 \times 1280 + 1299 - 1308$
2648·9	1	37740	$0 + 1280 + 1299$ $0 + 2 \times 1280 + 1299 - 1275$
2648·3	1	37749	$0 + 2 \times 1299$
2643·5	4	37817	$0 + 1042 + 2 \times 810$ $0 + 1367 + 1299$ $0 + 1280 + 1367$
2635·7	D	37930	
2632·8	1½	37971	$0 + 391 + 3 \times 810$ $0 + 1280 + 2 \times 810 + 2 \times 391 - 2 \times 435$
2630·5	4	38004	$0 + 1280 + 3 \times 810 - 2 \times 435$
2628·5	1D	38034	$0 + 1280 + 2 \times 810 - 36$ $0 + 2 \times 391 + 810 + 1280$
2626·5	5	38062	$0 + 1280 + 2 \times 810$
2625·3	2	38080	$0 + 1299 + 2 \times 810$
2623·4	V.D.½	38107	$0 + 1367 + 2 \times 810 - 36$
2619·9	V.D.½	38158	$0 + 1367 + 2 \times 810$
2612·2	2D	38271	$0 + 810 + 1299 + 1042 - 36$
2608·6	V.D ½	38323	$0 + 810 + 1299 + 1042$
2605·2	1D	38374	$0 + 4 \times 810 - 36$ $0 + 2 \times 391 + 3 \times 810$
2602·9	3	38407	$0 + 4 \times 810$
2598·6	2	38471	$0 + 391 + 1299 + 2 \times 810$
2597·0	1½	38494	$0 + 2 \times 1280 + 810 - 36$
2595·0	3	38524	$0 + 2 \times 1280 + 810$
2593·6	1	38545	$0 + 1280 + 1299 + 810$
2589·6	V.V.D ½	38604	$0 + 1280 + 2 \times 1299 - 435$
2581·3	V.D	38729	
2577·4	1½	38787	$0 + 391 + 4 \times 810$
2575·7	1½	38813	$0 + 1280 + 4 \times 810 - 2 \times 435$
2571·6	3	38875	$0 + 1280 + 3 \times 810$
2562·0	1½	39020	$0 + 2 \times 1280 + 1299$
2560·3	1	39046	$0 + 1280 + 2 \times 1299$
2558·1	3	39080	$0 + 1367 + 2 \times 1280$
2548·9	1½	39221	$0 + 5 \times 810$

Table 1 (*continued*)

Wavelengths (Å)	Intensity	Wave numbers (cm^{-1})	Assignment
2544·8	1½	39284	0 + 391 + 1299 + 3 × 810
2541·2	2	39340	0 + 2 × 1280 + 3 × 810
2527·6	1	39551	
2523·0	1	39623	0 + 1280 + 5 × 810 − 2 × 435
2518·7	2D	39691	0 + 1280 + 4 × 810
2518·0	1	39702	0 + 1299 + 4 × 810
2511·7	½D	39802	
2506·1	1½D	39891	
2493·2	V.D	40097	0 + 391 + 1299 + 4 × 810
2489·7	½D	40153	0 + 2 × 1280 + 3 × 810
2484·0	½V.D	40245	
2480·6	½V.D	40301	0 + 3 × 1280 + 1299
2476·7	1½	40364	
2472·3	½V.D	40436	
2468·3	½V.V.D	40501	0 + 1280 + 5 × 810
2464·9	½V.D	40557	
2460·1	1V.V.D	40636	0 + 1299 + 2 × 1280 + 2 × 810
2456·1	1 Shp	40703	
2444·1	½V.D	40902	0 + 391 + 1299 + 5 × 810
2440·2	½V.D	40968	0 + 2 × 1280 + 4 × 810
2434·8	½V.D	41059	
2431·6	½V.V.D	41113	0 + 3 × 1280 + 1299 + 810
2428·0	1½ Shp	41174	

Table 2. Identified frequencies and their assignment in *para*-fluoro-anisole

Raman data with depolarization factors	Ultra-violet absorption data		Assignment
	Lower state	Upper state	
244 (0·6)	236	229	
428 (0·49)	435	391	Totally symmetric component of 606 E_g^+ vibration in benzene
638 (0·8)	—	548	β_1 component of 606 E_g^+ vibration in benzene.
852 (polarized)	843	720	C–F in plane bending
831 (0·08)	857	810	C–OCH_3 stretching
1151 (0·41)	1116	1042	C–C
1249 (0·09)	1275	1280	C–F valence vibration
1297 (0·22)	1308	1299	C–H_3 bending
1455 (0·72) ?	1428 ?	1367	Aliphatic O–C frequency in OCH_3 unit

VOL. 9 1957

over that in anisole (755) on substitution with halogens; namely, *para*-fluoro-anisole 810, *ortho*-chloro-anisole 767, *para*-chloro-anisole 779, and *para*-bromo-anisole 771. We might finally associate the 810 (upper state), 857 (lower state), and 831 (Raman) with this C–OCH_3 vibration in para-fluoro-anisole.

Just on the long-wavelength side of the 810 fundamental there is another strong band which probably corresponds to another fundamental of 720 cm^{-1}. It could also be explained by the combination $0 + 810 - 94 = 716$, and a few combination bands that are observed with this fundamental might also be explained in a similar way. However, this need not preclude the possibility of 720 being also an independent fundamental and the ground-state frequency 843 cm^{-1} may be correlated with it. From our earlier discussion, the only Raman line to be associated with this is that at 852 cm^{-1}. It is possible that these frequencies (720, 843, 852) may be connected with totally symmetric C–F in-plane bending mode of vibration, as suggested in our preliminary note. KRISHNAMACHARI [9] suggested the possibility of a similar vibration of *ortho*-chloro-fluoro-benzene with values 755 (Raman), 751 (ground state), and 651 (upper state).

The totally symmetric α component of the E_g^+ vibration (606) in benzene is represented in *para*-fluoro-anisole by a medium-intensity band at 391 cm^{-1}. This upper-state fundamental occurs in combination with almost all other fundamentals like 810, 1280, etc. In the ground state the fundamental is 435 cm^{-1}. The corresponding Raman line at 428 cm^{-1} is of medium intensity with $\rho = 0{\cdot}49$. Its overtones are found in both the Raman spectrum and in ultra-violet absorption form $2 \times 435 = 870$ cm^{-1} in the ground state. The Boltzmann factors for the second overtone of 435 and the 857 fundamental are about the same.

The other component (β type) of this E_g^+ nitration in benzene may be 548 cm^{-1}, which gives rise to a band of medium intensity. Only one band could be found in combination with this, namely $0 + 548 + 391 = 939$. No ground-state frequency could be established corresponding to it. In the Raman spectrum there is only one depolarized line, 638 ($\rho = 0{\cdot}80$) in this region. If this represents the β component, there must be an increase of 32 cm^{-1} above the value 606 in benzene. If these correlations are correct, it may be concluded that in the ultra-violet absorption of *para*-fluoro-anisole there is not much contribution from the so-called forbidden part of the spectrum.

The frequency 1042 in the upper state is another fundamental giving rise to bands of medium intensity. It occurs in combination with the fundamentals 810 cm^{-1} and 1299 cm^{-1}. In the ground state the corresponding value is 1116 cm^{-1}. There is a polarized ($\rho = 0{\cdot}41$) medium intensity line in the Raman spectrum at 1151. The frequencies may possibly correspond to the totally symmetric carbon ring vibrations in the phenyl radical. In ortho-chloro-anisole two C–C vibrations have been found at 948 cm^{-1} and 1060 cm^{-1} (upper state). With *para*-chloro-anisole, *para*-bromo-anisole, and guaicol only one appears to be found, namely 1053, 989, and 946 cm^{-1} respectively.

There is a pair of vibration frequencies 1280 and 1299 cm^{-1} in the upper electronic state. Of the two, the lower-frequency band is very intense and very sharp, and the higher-frequency band is comparatively weaker. We find the identical structure unmistakably repeating itself at wavelengths 2684 and 2627 Å

and more weakly at shorter wavelengths. These repeated patterns are due to the superposition of a progression of 810 on these frequencies. On the higher-frequency side of the spectrum we find many more bands being explained by the frequency 1280 cm^{-1} or its overtones. While the frequency 1299 also plays an important role in the explanation of some bands, the analysis indicates the predominance of the frequency 1280. In the ground state there are two possible intervals to be correlated with these, namely 1275 cm^{-1} and 1308 cm^{-1}, and the latter appears to be comparatively more important in the interpretation of the bands observed. A correlation between the two pairs of frequencies can be made only from the consideration of the order of magnitude in the absence of any striking difference in the appearance of these bands in the ground state. From the nearness of the values we can say that 1280 and 1275 cm^{-1} represent the same mode of vibration and 1299 and 1308 another mode of vibration. In the Raman spectrum there are two fairly strong lines at 1249 ($\rho = 0{\cdot}09$) and 1297 ($\rho = 0{\cdot}22$). Both are polarized and 1249 is the more intense, and sharp. For these reasons we might correlate 1249 (Raman) with 1275 (lower state) and 1280 (upper state), and 1297 (Raman) with 1308 (lower state) and 1299 (upper state).

It is well known that C–F frequency in substituted benzenes lies in the region 1200 to 1300 cm^{-1}. It is, for instance, 1279 (Raman), 1288 (lower state), and 1269 (upper state) in *meta*-difluoro-benzene [10]. In *para*-chloro-fluoro-benzene [11] the values are 1229 (Raman), 1239 (lower state), and 1233 (upper state). The bands of the upper-state frequency are in most cases very intense, sharp, and prominent. Thus we can definitely attribute the values 1249 (Raman), 1275 (lower state), and 1280 (upper state) with the C–F valence vibration. The variable nature of the values in the lower states is generally found in fluoro compounds. The other set of fundamentals, 1297 (Raman), 1208 (lower state), and 1299 (upper state), are to be attributed to CH_3 symmetric bending in the methoxy radical. In our paper on *ortho*-chloro-anisole we have shown how an upper-state fundamental in this region has been a regular feature of all substituted benzenes containing O–CH_3 unit. The upper-state values are 1267 in anisole [8], 1274 in *ortho*-chloro-anisole, 1271 in *para*-chloro-anisole, and 1297 in *para*-dimethoxy benzene [8]. In toluenes also we have, possibly, 1262 in toluene (Sponer and Lowe, 1949), 1250 in *meta*-dimethyl benzene [12] and unexplained frequencies in this region in fluoro-toluenes [13]. For instance, in *para*-fluoro-toluene the band at 35636 cm^{-1} may be explained with a ground-state fundamental 1240 and that at 38123 cm^{-1} with an upper-state value of 1247 instead of the combination given by Cave and Thompson. Thus we might consider the frequency in this region to be a characteristic of all substituted benzenes which contain a CH_3 unit. The corresponding Raman lines are all strong and polarized. Comparing the anisoles and toluenes, we can draw the necessary conclusion that these frequencies must belong to a mode of vibration common in both and that can be either in the phenyl radical or CH_3 unit. The frequency values do not change much from lower state to upper state, and appear to be independent of the nature of the second substitution. We naturally expect the vibration in the phenyl radical to be quite sensitive to the changes in the nature of the substituents. Further, we do not find such fundamentals in some simple derivatives like *meta*-and *ortho*-di-chloro benzene. Thus we

VOL. 9 1957

might conclude that the frequency may be characteristic of the CH_3 bending mode. This view is further strengthened by a similar observation made by KOHLRAUSCH [14] from the Raman spectra of various substituted benzenes containing a methyl radical. To confirm this further, we studied the work on benzotrifluoride [12] which contains a CF_3 unit. A frequency in this region is absent in the list of fundamentals given for benzotrifluoride. We consider this evidence for rejecting the possibility of a phenyl radical vibration being associated with these frequencies. In their paper on benzotrifluoride, SPONER and LOWE seem to have considered the possibility of a CH_3 frequency being obtained in case of toluene and its derivatives with a possible value of 1228 or 1262 cm^{-1}. They mention the occurrence of CH_3 deformation in upper state at 1090 cm^{-1} and in the ground state at 1237 cm^{-1} in the ultra-violet absorption of methyl iodide [12]. In our work on acetaldehyde we [15] also observed CH_3 frequency at 1363 cm^{-1} (lower state) and 975 cm^{-1} (upper state), though the transition is confined to electrons in the C=O bond. SPONER and COOPER [16] again mention such a possibility in connection with their work on dimethyl benzenes. Our present work on anisoles, combined with earlier work on toluenes, etc., and the resulting comparative studies, aided by Kohlrausch's similar work in Raman spectra (*loc. cit.*) may be taken as adequate support for the view that these above-mentioned frequencies represent a CH_3 bending in all these cases. Thus we conclude that in *para*-fluoro-anisole 1297 (Raman), 1308 (lower state), and 1299 (upper state) bands represent the CH_3 (symmetric) bending mode of vibration.

There is another upper-state fundamental 1367 cm^{-1}. Corresponding bands are probably 1389 in *ortho*-chloro-anisole, 1345 in *para*-chloro-anisole, and 1328 in anisole. The band in anisole was left uninterpreted by SREERAMAMURTY [8]. Assuming this as a fundamental, it was found to combine with six others observed by SREERAMAMURTY, thus explaining some uninterpreted bands and giving a reasonable alternative to his original assignments. Among all these, however, in fluoro-anisole the band is more prominent in the analysis. It is found to combine with 1299, 810, and its progression, 1280, etc. A corresponding ground-state fundamental was not definitely observed. The correlation between 1428 band and Raman lines is not satisfactory. Frequencies of this order are not found in other substituted benzenes, and the possibility is that these frequencies may represent O–C aliphatic stretching mode of vibration. Hence the suggested assignment in Table 2 for 1367. This, however, needs more evidence for confirmation.

We are now left with another possible fundamental 229 in the upper state. In the lower state its value is 236. The Raman-line 244 may possibly correspond to this. Such low-lying fundamentals are also found in *para*-chloro- and *ortho*-chloro-anisoles. Their nature is not understood.

Finally, there are a few intense bands accompanying the (0,0) band and some prominent fundamentals. They are −34, −46, −66, and −94 cm^{-1}. These are generally taken to be due to *vv* transitions of some low-lying non-totally symmetric fundamentals. However, −46 may be also due to $0 - 857 + 810 = -47$ and $0 - 435 + 391 = -44$. It is not easy to suggest the fundamental responsible for these *vv* transitions.

This work was carried out under the C.S.I.R. Scheme on "Fluorescence and

Absorption Spectra of Organic Molecules" granted to one of us (V. Ramakrishna Rao). The authors express their thanks to Prof. H. W. Thompson and Prof. K. R. Rao for their kind interest in the work.

References

[1] Sponer H. *J. Chem. Phys.* 1954 **22** 234.
[2] Paulsen O. *Monat. Chemie* 1939 **72** 244.
[3] Lecomte Par Jean *J. Phys. Rad.* 1938 **9** 13–26.
[4] Suryanarayana V. and Ramakrishna Rao V. *J. Sci. Industr. Research* 1955 **14B** 128–129.
[5] Suryanarayana V. and Ramakrishna Rao V. *Ind. J. Phys.* 1956 **30** 117–128.
[6] Suryanarayana V. and Ramakrishna Rao V. *J. Sci. Indust. Research* 1955 **14B** 36–37.
[7] Suryanarayana V. and Ramakrishna Rao V. *J. Sci. Indust. Research* 1956 **15B** 260–262.
[8] Sreeramamurty K. *Ind. J. Phys.* 1950 **24** 421.
Sreeramamurty K. 1950. D.Sc. thesis submitted to the Andhra University in 1950.
[9] Krishnamachari S. L. N. G. *Ind. J. Phys.* 1955 **29** 603.
[10] Rao V. R. and Sponer H. *Amer. Phys. Soc.* meeting at Washington, D.C. PA8 1952.
[11] Krishnamachari S. L. N. G. *Ind. J. Phys.* 1956 **90** 319.
[12] Sponer H. and Lowe D. S. *J. Opt. Soc. Amer.* 1949 **39** 840–846.
[13] Cave W. T. and Thompson H. W. A general discussion of the Faraday Society on Spectroscopy and Molecular Structure and Optical Methods of Investigating Cell Structure 1950.
[14] Kohlrausch K. W. F. *Monat. Chemie* 1946 **76** 231.
[15] Rao V. R. and Rao I. A. *Ind. J. Phys.* 1954 **28** 491–510.
[16] Cooper C. D. and Sponer H. *J. Chem. Phys.* 1952 **20** 1248.

VOL.
9
1957

Spectrochimica Acta, 1957, Vol. 9, p. 263. Pergamon Press Ltd., London.

SPECTROCHEMICAL NOTE

The infra-red spectrum and the OH in-plane deformation frequency in CH_3CD_2OH

(*Received* 26 *March* 1957)

In a recent communication, Krimm, Liang, and Sutherland [1] have pointed out that the two broad bands at about 1410 and 1330 cm^{-1} in the spectra of primary alcohols in the associated state may be due to coupled δ(OH) and $\delta(CH_2)$ vibrations. Working on similar lines, we have recorded previously the spectrum of the heavy ethanol, CH_3CD_2OH, amongst other relevant alcohols. As expected, the spectrum of CH_3CD_2OH contains but one broad band near 1400 cm^{-1}, the maximum of which cannot be determined accurately because of the overlapping bands

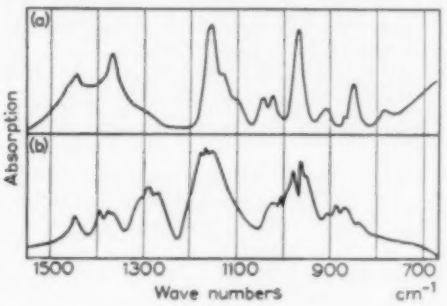

Fig. 1.

at 1370 and 1445 cm^{-1} (Fig. 1a). The latter two are due to the deformation vibrations of the methyl group, and the broad band underneath is very probably the OH in-plane deformation. It is replaced by a narrow band at 1212 cm^{-1} in a CC_4 solution and similarly in the vapour by a band with the central maximum at 1285 cm^{-1} (Fig. 1b). Although no satisfactory spectrum of the hydroxyl-deuterated alcohol CH_3CD_2OD could be obtained with the sample which we had prepared, the reduction of the broad band between 1440 and 1370 cm^{-1} is clearly observable, which is in agreement with the above assignment.

Also interesting are the differences between the ordinary and the heavy ethanol CH_3CD_2OH in the region 900–1200 cm^{-1}. The spectrum of the latter shows here two bands at 1175 and 936 cm^{-1}, respectively, neither of them undergoing appreciable changes on association. They are probably due to the skeletal vibrations, but the large difference in position with respect to ordinary ethanol suggests strong coupling with the deformation vibrations of the methylene group $\delta(CD_2)$.

A detailed account of our work on the infra-red spectra of alcohols will be published at a later date.

Our sincere thanks are offered to Prof. G. M. Schwab (München) for the generous gift of heavy ethanol.

Reference

[1] Krimm S., Liang C. Y., and Sutherland G. B. B. M. *J. Chem. Phys.* 1956 **25** 778.

D. Hadži
D. Jeramić
University Chemical Laboratory and Institute "B-Kidrič," Ljubljana, Yugoslavia.

Spectrochimica Acta, 1957, Vol. 9, p. 264. Pergamon Press Ltd., London

Papers to be published in future issues

D. F. C. Morris: Approximate spectral sensitivities of detection of sulphide mineral trace elements using the cathode-layer carbon arc.

Chizuko Tanaka, Kenji Kuratani and San-ichiro Mizushima: In-plane normal vibrations of methanol.

Forrest S. Mortimer: Vibrational assignment and rotational isomerism in some simple organic phosphates.

S. Mandelshtam: Excitation of the spectrum in a spark discharge.

E. M. Tanner: The infra-red absorption spectra of some indole-3-ketones

B. J. Rushton and G. D. Nicholls: A spectrographic scheme for the determination of Al, Ti, Fe, Ca, Mg, and Mn in silicates.

F. W. J. Garton: The spectrographic determination of boron in graphite.

Erika Smakula, Augustus Gori, and Herbert H. Wotiz: Effects of polymorphism and influence of sample preparation on the infra-red spectrum of estradiol-17β.

Michio Hayasha, Isao Ichishima, Takehiko Shimanarch, and San-ichiro Mizushima: Internal rotation in 1,2-dichloro-2-methylpropane.

Robert C. Frank, James E. Dallemand, and David L. Fry: Revision III. A statistical study on the homogeneity of zinc-base spectrographic standards.

L. B. Rogers and C. Gordon Peattie: Analytical studies of the fluorescence of samarium in calcium sulphate.

L. J. Bellamy and R. L. Williams: The NH stretching frequencies of primary amines.

M. St. C. Flett: Studies of the band near 3 μ in some hydroxy compounds.

A. Fiorenza and M. Lachin: La mesure de la "Largeur effective" des raies dans l'analyse des substances en poudre.

K. D. Mielenz: Zur Ausleuchtung von Spektrographen durch Zwischenabbildung der Lichtquelle.

William G. Fateley and Ellis R. Lippincott: Normal co-ordinate analysis of the vibrational spectrum of iron pentacarbonyl.

José R. Barceló: The infra-red spectrum of some metallic chelate compounds—I. Rubeanates.

K. Bunge: Materialabbau in Funkenentladungen. Experimentelle Untersuchungen an Zinkkathoden.

J. R. Butler: The spectrographic determination of the rare earths.

J. F. Richardson and E. R. Wooding: Concentration changes in an aerosol.

D. Hadži and D. Prevoršek: Infrared absorption bands associated with the NH Group—III. Hydroxamic acids and derivatives.

J. G. Hawkins, E. R. Ward, and D. H. Wiffen: Characteristic infra-red absorption frequencies of substituted naphthalenes.

P. J. Stone and H. W. Thompson: Vibrational band intensity of the hydroxyl group in phenols.

VOL. 9 1957

Spectrochimica Acta, 1957, Vol. 9, pp. 265 to 269. Pergamon Press Ltd., London

In-plane normal vibrations of methanol

CHIZUKO TANAKA, KENJI KURATANI, and SAN-ICHIRO MIZUSHIMA
Institute of Science and Technology and Faculty of Science, Tokyo University

(*Received* 11 *March* 1957)

Abstract—Infra-red spectra of CH_3OH and CH_3OD have been measured in the vapour and liquid states and in non-polar solutions. Normal modes of vibrations of CH_3OH, CH_3OD, and CD_3OH have been calculated. Based on the results, the complete assignment of the A' vibrations of methanol have been made.

MANY papers have appeared dealing with the OH bending frequency (A') of methanol CH_3OH (point group C_s). For free molecules, some authors have assigned this frequency to a band at 1340 cm^{-1} [1, 2], whereas others preferred a value in the region of 1060–1030 cm^{-1} [3, 4]. According to the former view, the ratio of the product of the OH and OD frequencies (stretching and bending) becomes 1/2·09, and according to the latter it is 1/1·6. Neither agrees with the value 1/1·87 calculated from Teller–Redlich's product rule, assuming other A' frequencies remain unchanged on deuteration. STUART and SUTHERLAND [5] and KRIMM, LIANG, and SUTHERLAND [6] have recently done interesting work on this subject, but there still remains a discrepancy between the calculated and observed ratio of the product of the A' vibrations for the isotopic molecules, although there is hardly doubt about the assignment of the OD bending frequency of CH_3OD to a band at 865 cm^{-1}.

Some time ago one of us measured the isotopic shift of the infra-red spectra of CCl_3COOH and C_6Cl_5OH [7]. From the result it was concluded that a strong coupling exists between the OH in-plane bending motion and the C–O stretching vibration. It seemed likely that for methanol there would be a considerable coupling between the OH bending vibration and CH_3 deformation vibrations (degenerate deformation and rocking), resulting in the two absorption bands at 1344 and 1057 cm^{-1}. The normal vibration calculations to be described below show that this is actually the case. The existence of the 1057 cm^{-1} band was first pointed out by IVASH, LI, and PITZER [8], who considered this band would be buried under the R branch of the very strong C–O stretching band centered at 1033 cm^{-1}. In dilute carbon bisulphide solution, where the 1033 cm^{-1} band is much narrower, we could show the existence of the 1060 cm^{-1} band which will correspond to the 1057 cm^{-1} band of the vapour. Therefore, it is reasonable to conclude the existence of this band in the vapour state. Our assignment of the A' vibrations shown in Table 4 can then be brought into agreement with that of IVASH, LI, and PITZER, if we take into account the coupling between the O–H bending and the CH_3 deformation vibrations stated above.

The corresponding coupling between the OD and CH_3 vibrations of CH_3OD has been shown to be weak by our calculation. These two vibrations are separated in frequency much more than those of methanol. Thus the 865 cm^{-1} band is

assigned to the OD bending vibration and the 1206 cm^{-1} band to CH_3 deformation vibration, which is hardly affected by the OD bending vibration.

The calculation of normal vibrations was based on the following potential function:

$$V = \Sigma\tfrac{1}{2}K_i(\Delta r_i)^2 + \Sigma\tfrac{1}{2}H_{ij}r_i^0r_j^0(\Delta\alpha_{ij})^2 + \Sigma\tfrac{1}{2}F_{ij}(\Delta q_{ij})^2 + \text{linear terms},$$

where r_i and r_j are bond lengths with equilibrium values r_i^0 and r_j^0; α_{ij} bond angles and q_{ij} distances between non-bonded atoms. In addition, K, H, and F represent stretching, bending, and repulsive force constants, respectively [9]. Their numerical values in 10^5 dyn/cm are shown in Table 1. The intra-molecular tension κ is given in

Table 1. Force constants K, H, F, F' (in 10^5 dyn/cm) and intra-molecular tension κ (in 10^{-11} dyn cm)

K(C—O) = 2·430	F(C . . . . H) = 0·598
H(C—O—H) = 0·325	F(O . . . . H) = 1·288
H(O—C—H) = 0·180	
H(H—C—H) + 0·4F(H . . . . H) = 0·403	
F' = −0·1F*	
κ = −0·0408	

* F' is the force constant of the linear term.

10^{-11} dyn cm [9]. Using these values, we have calculated the normal frequencies of CH_3OH, CH_3OD, and CD_3OH as shown in Table 2, in which the frequencies of CH_3OH and CH_3OD observed by us and those of CD_3OH given by IVASH, LI and PITZER are also listed. (The high-frequency OH, CH, OD, and CD vibrations have been split off in the secular equation.) The agreement between the calculated and observed values are satisfactory and justify the assignments.

Table 2. Calculated and observed frequencies of CH_3OH, CH_3OD, and CD_3OH in cm^{-1}

CH_3OH		CH_3OD		CD_3OH	
Obs.	Calcd.	Obs.	Calcd.	Obs.	Calcd.
1033	1037	1036	1035	990	1027
1344	1287	865	896	1289	1275
1458	1505	1458	1502	1080	1099
1057	1125	1206	1197	856	895
1430	1480	1427	1478	1055	1050

We have also calculated the potential energy distribution $F_{ii}L_i^2$ for each normal vibration, where F_{ii} is a diagonal term of the F matrix or the potential energy matrix and L_i is an element of the L matrix [10]. The result is shown in Table 3, by which we can make an accurate assignment of the normal vibrations. Here the

VOL. 9 1957

Table 3. The potential energy distribution for each normal vibration

(a) CH_3OH

Vibrational mode	Symmetry co-ordinate \ Calculated normal frequency (cm^{-1})	1037	1287	1505	1125	1480
C–O stretching	Δr_4	0·814	0·000	0·000	0·000	0·000
OH bending	$\Delta\alpha_{45}$	0·023	0·663	0·033	0·212	0·010
CH_3 symmetric deformation	$\Delta(\alpha_{12}+\alpha_{13}+\alpha_{23}-\alpha_{14}-\alpha_{24}-\alpha_{34})/\sqrt{6}$	0·172	0·016	1·249	0·001	0·035
CH_3 rocking	$\Delta(2\alpha_{14}-\alpha_{24}-\alpha_{34})/\sqrt{6}$	0·000	0·099	0·021	0·308	0·606
CH_3 degenerate deformation	$\Delta(2\alpha_{23}-\alpha_{31}-\alpha_{12})/\sqrt{6}$	0·000	0·207	0·009	0·243	0·589

(b) CH_3OD

Vibrational mode	Symmetry co-ordinate \ Calculated normal frequency (cm^{1})	1035	896	1502	1197	1478
C–O stretching	Δr_4	0·812	0·000	0·000	0·000	0·000
OD bending	$\Delta\alpha_{45}$	0·019	0·429	0·008	0·072	0·003
CH_3 symmetric deformation	$\Delta(\alpha_{12}+\alpha_{13}+\alpha_{23}-\alpha_{14}-\alpha_{24}-\alpha_{34})/\sqrt{6}$	0·170	0·002	1·285	0·002	0·015
CH_3 rocking	$\Delta(2\alpha_{14}-\alpha_{24}-\alpha_{34})/\sqrt{6}$	0·000	0·029	0·009	0·393	0·602
CH_3 degenerate deformation	$\Delta(2\alpha_{23}-\alpha_{31}-\alpha_{12})/\sqrt{6}$	0·000	0·015	0·005	0·411	0·617

(c) CD_3OH

Vibrational mode	Symmetry co-ordinate \ Calulated normal frequency (cm^{-1})	1027	1275	1099	895	1050
C–O stretching	Δr_4	0·769	0·000	0·023	0·000	0·010
OH bending	$\Delta\alpha_{45}$	0·027	0·857	0·017	0·023	0·015
CD_3 symmetric deformation	$\Delta(\alpha_{12}+\alpha_{13}+\alpha_{23}-\alpha_{14}-\alpha_{24}-\alpha_{34})/\sqrt{6}$	0·273	0·042	0·544	0·001	0·001
CD_3 rocking	$\Delta(2\alpha_{14}-\alpha_{24}-\alpha_{34})/\sqrt{6}$	0·001	0·059	0·020	0·215	0·294
CD_3 degenerate deformation	$\Delta(2\alpha_{23}-\alpha_{31}-\alpha_{12})/\sqrt{6}$	0·003	0·002	0·001	0·252	0·297

significance of symmetry co-ordinates expressed in terms of internal co-ordinates will be clear from Fig. 1. For the sake of convenience, approximate designations of the A' vibrations are shown in Table 4. The ratio of the product of all the A' vibrations now becomes:

$$\frac{2730 \times 2965 \times 2870 \times 1458 \times 1427 \times 865 \times 1206 \times 1036}{3680 \times 2960 \times 2860 \times 1458 \times 1430 \times 1344 \times 1057 \times 1033} = \frac{1}{1{\cdot}83}$$

which is close to the theoretical value 1/1·87 referred to above.

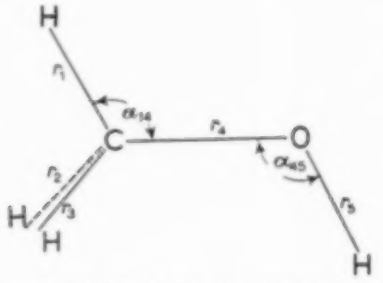

Fig. 1. Internal co-ordinates of methanol.

Table 4. Assignment of the A' vibrations

CH_3OH		CH_3OD	
3680	OH stretching	2730	OD stretching
2960	CH degenerate stretching	2965	CH degenerate stretching
2860	CH symmetric stretching	2870	CH symmetric stretching
1458	CH_3 symmetric deformation	1458	CH_3 symmetric deformation
1430	CH_3 deformation (degenerate and rocking)	1427	CH_3 deformation (degenerate and rocking)
1344	OH bending and CH_3 deformation (degenerate and rocking)	865	OD bending
1057	CH_3 deformation (degenerate and rocking) and OH bending	1206	CH_3 deformation (degenerate and rocking)
1033	C–O stretching	1036	C–O stretching

We have also measured the change of intensity of some monomeric and association bands with concentration in non-polar solvents (carbon bisulphide and carbon tetrachloride). The result is shown in Table 5. The numbers in parentheses refer to the apparent molar absorptivity.

One of us measured the Raman spectra of CH_3OH and CH_3OD in the liquid state [11]. The result is in good agreement with that obtained by us in the liquid state from infra-red absorption. It is to be noted that the ratio of the product of frequencies of the association band to that of the monomeric band of CH_3OH shown

VOL. 9 1957

in Table 5 is equal to the corresponding ratio of CH_3OD: i.e.

$$\frac{1412 \times 1112}{1344 \times 1057} = 1{\cdot}11$$

$$\frac{1228 \times 940}{1206 \times 865} = 1{\cdot}11$$

This provides us with another proof for the correctness for the assignment made in this paper.

Table 5. Monomeric and association bands of methanol between 1410 and 860 cm^{-1}

CH_3OH	Association band		Monomeric band	
liquid	1412 (strong)	1112 (medium)		
0·96 mole/l.	1412 (16)	1110 (12)		
0·24 mole/l.	1412 (10)	1110 (8)	1337 (10)	
0·012 mole/l.			1337 (13)	1060 (11)
vapour			1344 (medium)	1057*

CH_3OD	Association band		Monomeric band	
liquid	1228 (medium)	940 (strong)		
0·96 mole/l.	1227 (6)	938 (13)		865 (11)
0·24 mole/l.	1227 (4)	938 (11)		865 (29)
0·011 mole/l.			1210 (2)	865 (35)
vapour			1206 (very weak)	865 (strong)

* This band is overlapped by the *R* branch of a strong band centred at 1033 cm^{-1}.

References

[1] Noether H. D. *J. Chem. Phys.* 1942 **10** 693.
[2] Herzberg G. *The Infra-red and Raman Spectra of Polyatomic Molecules* p. 334. Van Nostrand, New York, 1945.
[3] Davies M. M. *J. Chem. Phys.* 1948 **16** 267.
[4] Borden A. and Barker E. F. *J. Chem. Phys.* 1938 **6** 553.
[5] Stuart A. V. and Sutherland G. B. B. M. *J. Chem. Phys.* 1956 **24** 559.
[6] Krimm S., Liang C. Y., and Sutherland G. B. B. M. *J. Chem. Phys.* 1956 **25** 778.
[7] Kuratani K. *J. Chem. Soc. Japan* 1952 **73** 258, 928.
[8] Ivash E. V., Li J. C. M., and Pitzer K. S. *J. Chem. Phys.* 1955 **23** 1814.
[9] Shimanouchi T. *J. Chem. Phys.* 1949 **17** 245, 734, 848.
[10] Sweeny D. M., Nakagawa I., Mizushima S., and Quagliano J. V. *J. Amer. Chem. Soc.* 1956 **78** 889.
[11] Mizushima S., Morino Y., and Okamoto G. *Bull. Chem. Soc. Japan* 1936 **11** 698.

Spectrochimica Acta, 1957, Vol. 9, pp. 270 to 281. Pergamon Press Ltd., London

Vibrational assignment and rotational isomerism in some simple organic phosphates

F. S. Mortimer
Department of Colloid Science, The University, Cambridge, England*

(*Received* 24 *October* 1956; *amended* 1 *March* 1957)

Abstract—The infra-red spectra (1600–450 cm^{-1}) of both liquid and crystalline solid samples of trimethyl phosphate, triethyl phosphate, and triphenyl phosphate are discussed. It is shown that the presence of more than one rotational isomer is the probable explanation of the double P=O stretching band that is observed in the spectra of the liquid samples. Certain other bands observed for the liquid samples but not for the crystalline solids are best explained in the same manner. Vibrational assignments are proposed for the 1600–650 cm^{-1} region and for certain of the lower-frequency absorption bands. The assignments are related to empirical correlations in the spectra of similar compounds, as reported by other authors.

VOL. 9 1957

There has been considerable interest recently in the infra-red spectra of organophosphorus compounds, but few detailed assignments for individual compounds have been attempted. Except for trimethyl phosphine oxide, studied recently by Daasch and Smith [1], no complete assignments of organic phosphorus compounds have come to the author's attention, although empirical correlations between structure and spectra of such compounds have been reported by numerous authors [2–4]. For this reason, three moderately simple phosphates: trimethyl phosphate, triethyl phosphate, and triphenyl phosphate, have been chosen for this study. At the same time the possibility of explaining by rotational isomerism the double P=O stretching band that occurs in the spectra of many phosphates has been investigated. A comparison of the spectrum of the crystalline solid with that of the liquid (and of a solution) has confirmed that rotational isomers do exist in these phosphates and that they are the cause of the doubling of the P=O stretching band. In some cases other simplifications in the spectra also occur on freezing.

Experimental

The samples of the three phosphates were commercial ones, and, except for the triphenyl phosphate, were subjected to additional purification, mainly to remove water. The spectra of samples from different commercial sources have been compared in each case, and the spectra reported here show no significant differences from those published previously for these compounds by Daasch and Smith [3]. The infra-red spectra of the liquid samples and solutions of the trimethyl and triethyl phosphates, and of the solid preparations for triphenyl phosphate were recorded in the 1650–650 cm^{-1} region by a Perkin-Elmer Model 21 spectrophotometer. The spectra determined at other than room temperature and in the 650–450 cm^{-1} region were recorded by a Hilger D209 spectrophotometer under conditions that have been described previously [5]. The simple low-temperature cell that was used to obtain the low-temperature spectra of the crystalline solids and for the above-room-temperature spectrum of the liquid

* Present address: Shell Development Company, Emeryville, California.

triphenyl phosphate has also been previously described [6]. The spectra of the liquids and crystalline solids are shown in Fig. 1. Tables 1 to 3 give the positions of the observed absorption bands along with Raman data from the literature [7, 8].

Discussion

Empirical correlations by previous authors, as described by BELLAMY [2], have located the P=O stretching band without any doubt. It is to be found somewhere between the limits of *c.* 1170 and 1400 cm^{-1}, the exact position depending on the electronegativity of the groups attached to the phosphorus atom [3, 4]. Similarly, various other bands have been ascribed to the P—O—R linkage, such as the strong band commonly occurring near 1030 cm^{-1} in compounds where R is aliphatic. It has also been remarked that when R is aromatic this band moves to *c.* 1200 cm^{-1}. Other correlations are outlined by BELLAMY, including a P—O—CH_3 band at *c.* 1190 cm^{-1}, a P—O—C_2H_5 band at *c.* 1165 cm^{-1}, and a second strong band adjacent to the 1030 cm^{-1} band in many aliphatic esters at *c.* 980 cm^{-1}. The remarkable constancy of many of these bands makes them valuable tools in the identification of R groups in phosphorus esters, and simultaneously suggests that the modes of

Table 1. The observed frequencies below 1500 cm^{-1} in the infra-red and Raman spectra of trimethyl phosphate

Infra-red frequency (cm^{-1})				Raman frequency‡ (cm^{-1})	
Liquid	Intensity†	Solid	Intensity†	Liquid	Intensity†
not investigated		not investigated		188 241 368	1*b* 1*b* 2
459	5	464	7	455	2
500	3*b*	510	8	498	1*b*
526	3*b*	533	4	523	1*b*
740 755	3 4	750	4	734 750	6 5
c. 845*	4*s*	858	10	848	3
852*	10	865	5*s*		
1045*	10*b*	*c.* 1045 1060?	10 0*s*?	1037	2*b*
c. 1080*	3*s*	1080	3	1079	1*b*
1190	4	1165 1190 1200?	1/2*s* 4 0*s*	1155 1187	1/2 1*b*
1273* 1290*	10	1290	10	1275	3
1460	8	1460	8	1460	4*b*

* Values taken from the spectrum of a solution in CS_2; however, there is no evidence for any serious frequency shifts relative to the liquid.

† Relative intensities are given on an approximate scale of 0–10. *b* = broad; *s* = shoulder.

‡ Several Raman spectra have been reported in the literature. The data given here are from SIMON and SCHULZE [7]. The more recent paper by BAUDLER [8] gives a spectrum including lines at 1211, 1252, 1375, and missing the lines at 1079 and 1187 cm^{-1}. From our infra-red data it would seem that his sample was impure; therefore the older data of SIMON and SCHULZE are quoted.

Table 2. The observed frequencies below 1500 cm^{-1} in the infra-red and Raman spectra of triethyl phosphate

Infra-red frequency (cm^{-1})				Raman frequency† (cm^{-1})	
Liquid	Intensity*	Solid	Intensity*	Liquid	Intensity*
not investigated		not investigated		287	0
				328	4*d*
c. 465	2*vb*	465	4	463	1
525	4*b*	525	6	514	1
545	4*b*	548	7		
c. 720	1*s*	740	3	734	8
740	3				
800	4	*c.* 810	4*s*	809	5*b*
823	4	823	6		
				911	0
c. 950	1*s*	955	2*s*	948	3*d*
975	10	980	10		
1030	10	1030	10	1033	5*b*
c. 1075	1*s*	1075	2	1080	3
1100	2*s*	1100	4	1102	8
1163	3	1163	3		
1260	10	1270	10	1283	6*b*
1270	10				
c. 1290	0*s*	1290	2*s*		
1368	5	1368	4	1370	2
1390	6	1390	6	1397	3
1442	5	1442	5	1453	8
1477	4	1477	4	1484	4

* Relative intensities are given on an approximate scale of 0–10. *b* = broad, *vb* = very broad, *d* = diffuse, *s* = shoulder.

† The Raman data are from the paper by Baudler [8].

vibration to which they are due do not interact strongly with each other; otherwise, they would not be so characteristic regardless of the other groups present.

Little is known concerning the structure or the nature of the bonds in the organic esters of the phosphorus acids. Daasch and Smith [1] have shown that the force constant of the P=O bond in trimethyl phosphine oxide is *c.* 8·0 x 10^5 dynes/cm and that the P=O stretching frequency occurs at 1170 cm^{-1}. In the spectrum of POF_3, where the P=O frequency lies at the other extreme of the observed range for this bond, Gutowsky and Liehr [9] report it at 1415 cm^{-1} and calculate the P=O force-constant to be 11·4 $\times$ 10^5 dynes/cm. A reasonably accurate P=O bond length has been calculated from microwave moments of inertia and electron diffraction data for POF_3 by Hawkins, Cohen, and Koski [10], and by Williams, Sheridan, and Gordy [11]. Their values are 1·48 Å and 1·45 $\pm$ 0·03 Å respectively, and the latter report the same value for $POCl_3$. By Badger's rule [12] the P=O distance in $PO(CH_3)_3$ should then be *c.* 1·52 Å, which is just that predicted from the Schomaker–Stevenson rule [13], as modified by Gordy [14], for a P=O bond. However, the exact nature of the bond remains obscure. There is no spectral evidence for conjugation with groups having π

VOL. 9 1957

Table 3. The observed frequencies between 1650 and 450 cm^{-1} in the infra-red spectrum of liquid and solid triphenyl phosphate

Infra-red frequency (cm^{-1})				Infra-red frequency (cm^{-1})			
Liquid	Intensity†	Solid	Intensity†	Liquid	Intensity†	Solid	Intensity†
470	4	470	4	1012	5	1010	5
497	5	493	5 { 0s*	1029	4	1027	3,4*
		503	6*			1034	3,0s*
518	2s	517	5	1074	2	1074	3,4*
c 565	1s	562	6			1080	1,0*
579	5	578	5	?		1110	0,1/2*
		597	2	1164	5	1155	4
620	3	617	2			1165	5
687	6	690	7			1177	7 { 0*
720	1/2	729	1/2	1192	10b	1187	7*
754	6	756	5			1197	7,6*
777	5b	774	8,9*	1235	1	1232	1
		790	4,0s*	1298	7	1296	7
845	0s	840	1/2, 1/2*	1314	7	1315	1/2s, 1*
854	1	850	1/2, 0s*			1467	3,5*
903	1	916	3			1486	7 { 7*
935	1/2	934	3			1495?	0s*
962	10b	960	10vb	1590	6	1590	7 { 7*
						1600	0s*

* The relative intensities of some bands observed in the crystalline solid change with orientation of the crystal. The intensities marked with the asterisk are those from the partially oriented sample. The others come from the randomly oriented sample.

† Relative intensities are given on an approximate scale of 0–10. b = broad; s = shoulder.

bonds; the P=O frequency in triphenyl phosphine oxide shifts to 1190 cm^{-1} rather than to a frequency lower than 1170 cm^{-1}, as might be expected. (See spectra of reference [3].) For this and other reasons Daasch and Smith have preferred to emphasize its highly polar nature by writing it $P^+—O^-$, thus avoiding the π-bond implications of the usual double-bond symbol. This notation is awkward to write, however, and does not emphasize its high force constant, so P=O is retained here as the symbol for the bond.

There seem to be no published data giving structural parameters for any simple organic phosphorus esters. However, it may reasonably be assumed that, in the phosphates, the PO_4 group is roughly tetrahedral. It is also to be expected that the P—O force constants and bond lengths will correspond to single-bond values. The Stevenson–Schomaker rule and Badger's rule predict values of $c.$ 1·71 Å and 4×10^5 dynes/cm for this bond. By comparison with other compounds containing the C—O bond, one predicts a force-constant for this bond of $c.$ 5×10^5 dynes/cm [15], and a C—O—P angle of about 100°. On the other hand, the angle that the C—O—P plane will make with the O—P=O plane cannot be predicted with any certainty. In fact, more than one stable rotational isomer might be expected in the liquid or in solutions for such compounds. For trimethyl phosphate, these angles may be $c.$ 90°, resulting in a molecule with C_3 symmetry in its most probable

configuration, but other configurations with C_{3v} or with lower symmetry are also possible.

A molecule such as trimethyl phosphate, in which the masses and force-constants differ so markedly in the various bonds, would be expected to have skeletal modes of vibration that could be characterized approximately as follows: one P=O stretching mode; three P—O(—C) stretching modes, one pair being degenerate and asymmetric, the other symmetric; three (P—)O—C stretching modes nearly superimposed, but possibly split, by interaction with the P—O modes, into a degenerate pair of out-of-phase stretching modes and one in-phase stretching mode; and eleven low-frequency bending modes. The last are more difficult to

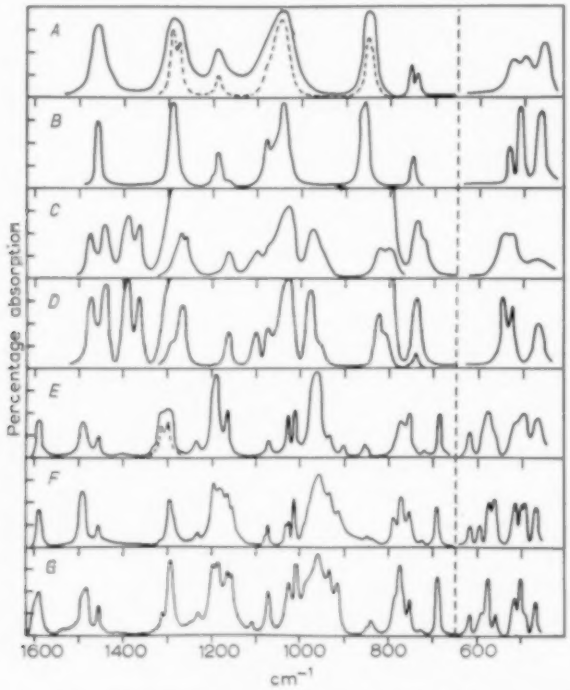

Fig. 1. The infra-red spectra of trimethyl phosphate: liquid (*A*), polycrystalline solid (*B*); triethyl phosphate: liquid (*C*), polycrystalline solid (*D*); triphenyl phosphate: liquid (*E*), polycrystalline solid, random orientation (*F*), and partially oriental (*G*).

visualize, but one possible description is given in Table 4. The splitting between the asymmetric and the symmetric modes would be largest for those involving the greatest PO_3 deformation, but some splitting is expected for the modes that are mainly P—O—C bending, since the interaction between the various bending modes would probably be larger than for the stretching modes. If one assumes there is no interaction between the P—O and O—C stretching modes, one predicts, on the basis of the above force-constants, that the absorption bands corresponding to these modes will lie near 800 cm^{-1} and 1050 cm^{-1}, respectively.

VOL. 9 1957

Table 4. Vibrational assignments in trimethyl and triethyl phosphate

Description of mode	Trimethyl phosphate			Triethyl phosphate		
	Number of modes	Wave number (cm^{-1})		Number of modes	(cm^{-1})	
		Liquid	Solid		Liquid	Solid
Skeletal modes						
P=O stretch	1	1290, 1275	1290	1	1270, 1260	1268
(P)—O—C stretching						
out-of-phase	2	c. 1045	1080	2	1075	1075
in-phase	1		1045	1	1030	1030
P—O—(C) stretching						
asym.	2	850	865, 858	2	800	c. 810
sym.	1	755, 740	750	1	740, 727	740
P—$(O—C)_3$ bending						
sym.	1	526	533	1	545	548
asym.	2	500	510	2	525	525
O=P—$(OC)_3$ bending	2	459	464	2	c. 465	465
P—O deformation						
sym.	1	367(R)	*	1	328(R)	*
asym.	2	239(R)	*	2	287(R)	*
O=P—O—C torsion						
sym.	1	184?(R)	*	1	?	
asym.	2	?		2	?	
Additional skeletal modes for C_2H_5 group						
C—C stretching	—			3	975	980, 955
O—C—C bending	—			3	c. 328?(R)	
P—O—C—C torsion	—			3	?	
CH_3 and CH_2 modes						
C—H stretching	9	2900, 3050*	*	15	2900, 3050*	*
CH_3 deformation						
asym.	6	1460	1460	6	1442	1442
sym.	3			3	1365	1365
CH_2 deformation	—	—	—	3	1477	1477
CH_3 rocking						
(in-plane)†	3	c. 1190	1190, 1165	3	1100	1100
(out-of-plane)†	3	c. 1190	1190, 1200?	3	1163	1163
CH_2 wagging	—			3	1390	1390
CH_2 twisting	—			3	c. 1290	1290
CH_2 rocking	—			3	823	823
CH_3 torsion	3	?	?	3	?	?

(R) Refers to Raman data, see Tables 1 and 2.
* Not investigated.
† The plane referred to is that of the adjacent three atoms, P—O—C, or O—C—C.

Vibrational assignments

Trimethyl phosphate

A comparison of the spectrum of crystalline solid trimethyl phosphate with that for the liquid or solution indicates that more than one isomer is present in the fluid phases: two major simplifications have occurred on freezing, near 1290 cm^{-1} and 750 cm^{-1}. In other respects the changes are just those resulting from a narrowing of the absorption bands, thus revealing bands that were only seen in the spectrum of the liquid as an asymmetry of the absorption band.

In order further to confirm the conclusion that more than one rotational isomer is present, several other experiments have been performed on one or both of the two pairs of bands that simplify on freezing. It has been shown that the relative intensities of the two components of the P=O stretching band near

Table 5. Relative intensities of bands in trimethyl phosphate when dissolved in various solvents

Solvent	Ratios of peak absorbances	
	1290 cm/1275 cm^{-1}	735 cm^{-1}/755 cm^{-1}
*iso*Octane	0·93	0·26
Carbon tetrachloride	1·03	interference
Carbon disulphide	1·40	0·49
Acetone	2·7	0·67
Chloroform	4·5	interference
Pure liquid	*c.* 3·5	0·77

1290 cm^{-1} are independent of dilution (in CS_2), thus ruling out solvent effects as a cause of the doubling of this band. Furthermore, a study of this band in a series of solvents shows that the relative intensities of the two components change in different solvents. It has been possible to obtain similar data for three of the same solvents on the pair of bands near 750 cm^{-1}. These data are illustrated in Table 5. It has also been shown that upon heating above room temperature (to *c.* 125°C) the components of the bands of each pair are broadened and that their intensities are altered so that the lower-frequency component at 1275 cm^{-1} and the higher-frequency component at 755 cm^{-1} are increased relative to their companion bands. This is consistent with the low-temperature spectra in which the other component of each pair is the one that remains in the crystalline solid.

It is thus possible to identify the 1290 cm^{-1} and the 735 cm^{-1} bands with the isomer that is more stable at low temperatures, while the 1275 cm^{-1} and 755 cm^{-1} bands belong to the isomer(s) having appreciable concentration at higher temperatures. It seems likely that the more stable form is the one having C_3 symmetry, in which the three P—O—C planes are roughly perpendicular to the corresponding O=P—O planes, thus allowing some overlap between the electronic cloud of the P=O bond and the $2p_z$ orbitals of the remaining three oxygen atoms. It is not clear whether there is only one other isomer, or whether all other isomers that are

VOL. 9 1957

sterically likely have nearly the same spectrum, though the latter explanation may be the correct one. In compounds of this complexity, one can probably expect a clear indication of more than one isomer only when, in one form, the nature of the bonding is somewhat altered relative to that in the others. Then this isomer stands out from all the others, and those bands are affected that are closely associated with the altered bonds. In the discussion of the vibrational assignments that follow, however, the symmetry of the molecule will be considered to be at least approximately C_3.

The skeletal stretching modes may be expected to give moderate to strong Raman lines and, because of the polar oxygen atoms, also to give strong infra-red bands. Clearly the bands near 1290 cm^{-1} in the various spectra are caused by the P=O stretching mode, and, since the band is double in the spectra of the fluid samples, this bond is one that is in some manner affected by the orientation of the O—C bonds relative to it. Because of its position and its intensity in the infra-red spectrum, the broad asymmetric band near 1045 cm^{-1} is assigned to the three modes that are mainly O—C-stretching. The presence of two bands in the solid phase and in the Raman spectrum probably indicates some splitting of the *A* and *E* vibrational modes for C_3 symmetry. The strongest Raman lines are the pair at 734 and 750 cm^{-1}, but the low-temperature spectrum indicates that only one fundamental lies in this region, the splitting presumably again being caused by the rotational isomerism. Because of its Raman intensity this band is assigned to the symmetric stretching of the P—O bonds in the P—$(OC)_3$ structure. The asymmetric mode is then assigned to the band near 850 cm^{-1} in the various spectra. The slight splitting of this band in the solid spectrum may indicate that the stable form has a lower symmetry than C_3, but it could equally well be caused by crystal effects.

The lower-frequency bending modes are more difficult to assign without a clearer picture of their form. One possible assignment is given in Table 4. If the assignment thus far is correct, then the remaining bands must result from modes associated with the CH_3 groups (or overtones and combinations). The C—H stretching modes will not be considered, as they will be clustered near 3000 cm^{-1}. In addition to these, there will be symmetric and asymmetric CH_3 deformations, the CH_3 rocking modes and the very low-frequency torsional modes, which are seldom observed. Sheppard [16] has shown that the frequency of the symmetric CH_3 deformation mode depends on the electronegativity of the attached group and that, for CH_3—O—, it may be expected nearly to coincide with the asymmetric modes near 1460 cm^{-1}. One rather broad band is indeed observed and is assigned to modes of both types. This leaves only the two types of CH_3 rocking modes to be assigned, those in the P—O—C plane and those perpendicular to it. Again some splitting may be expected for the former but little or none for the latter. In fact, for C_{3v} symmetry some of the latter modes are infra-red-inactive. One strong rather broad and asymmetric infra-red band at 1190 cm^{-1} is observed in the liquid phase, but in the solid phase the presence of a second band near 1165 cm^{-1} is revealed, apparently corresponding to the Raman line observed at 1155 cm^{-1}. The sharpening of the strong absorption bands in the solid has also revealed a weak band near 1200 cm^{-1} and possibly another in the O—C stretching region,

near 1060 cm^{-1}, between the stronger absorption bands at 1080 cm^{-1} and 1045 cm^{-1}.

It is assumed that both the in-plane and out-of-plane CH_3 rocking modes will lie in the 1200–1165 cm^{-1} region, though the region near 1060 cm^{-1} could also obscure one of the bands. Both 1190 and 1165 cm^{-1} are assigned to in-plane modes, since Raman lines have been observed at both positions. The out-of-plane mode is also tentatively placed at 1190 cm^{-1}. The presence of only a single band at 1460 cm^{-1} and the 1190 cm^{-1} band are typical of all compounds containing the P—O—CH_3 group. The complete assignment is given in Table 4.

Triethyl phosphate

The assignments for triethyl phosphate follow more or less readily from those for the methyl derivative. New absorption bands are to be expected for C—C stretching modes and for CH_2 bending, wagging, twisting, and rocking motions. Additional bending modes will also occur, but these will interact strongly with those already present, making unreliable any assignments below *c.* 450 cm^{-1}.

The P=O and O—C bands are assigned as for the trimethyl phosphate (see Table 4). The P—O stretching modes are assigned to the pair of bands near 800 cm^{-1} and 740 cm^{-1}, the latter again appearing double in the liquid. In the spectrum of the solid, the 800 cm^{-1} band shifts to *c.* 810 cm^{-1} and appears as a strong shoulder on the adjacent band at 823 cm^{-1}. The band at 800 cm^{-1} is preferred over that at 823 cm^{-1} for this assignment, because skeletal modes are more apt to give Raman lines than CH_2 rocking modes.

The pair of bands at about 975 cm^{-1} and 950 cm^{-1} (the latter conspicuously in the Raman effect) are probably associated with the C—C bonds, which must certainly interact with the adjacent O—C modes so that an accurate description of the motion is no longer possible. They will be referred to as C—C absorption bands, however, since, in aliphatic esters, bands in this region seldom occur unless there is a C—C bond next to an O—C bond.

The assignment of the modes associated with the CH_3 and CH_2 groups remain to be considered. There are two CH_3 deformation frequencies and one CH_2 bending frequency to be located, and there are four infra-red bands and Raman lines in the region between 1360 and 1480 cm^{-1}, where these bands are expected. The fourth band is most likely the CH_2 wagging frequency which has shifted into this region because of the proximity of the oxygen atom. It is difficult to be sure of the exact assignment of these bands; however, one might expect the two CH_3 bands to be near their position in hydrocarbons, so the band at 1442 cm^{-1} is assigned to the asymmetric modes, and the band at 1365 cm^{-1} to the symmetric modes. The CH_2 bending modes are then assigned to the highest frequency band, at 1477 cm^{-1}, and the CH_2 wagging modes to that at 1390 cm^{-1}. The band at 1290 cm^{-1} is assigned as the CH_2 twisting mode, again shifted to somewhat higher frequencies than in most hydrocarbons. The CH_3 rocking modes are then assumed to be the cause of the two bands at 1163 cm^{-1} and 1100 cm^{-1}, and the latter is assigned to the in-plane modes, since, because of interactions with the skeletal modes, it may be expected to have the greater intensity in the Raman effect. Finally, the band at 823 cm^{-1} is assigned to the CH_2 rocking modes. This band

VOL. 9 1957

also is at higher frequencies than it is in hydrocarbons, presumably because of the adjacent oxygen atom. All of these bands are typical of the P—O—C_2H_5 group and can usually be located in the spectra of compounds containing this group. The complete assignment is given in Table 4.

Triphenyl phosphate

The assignment of frequencies in triphenyl phosphate is complicated by the fact that interactions can occur between the skeletal frequencies and those arising from internal vibrations of the phenyl group itself. Unfortunately, there are no Raman data for this compound to aid in the assignment. RANDLE and WHIFFEN [17] have identified the major mass-sensitive absorption bands of mono-substituted benzenes. Of these, the only ones important in the stretching region are the strongly interacting pair made up of the Ph—X stretching mode and the mode arising from the B_{1u} ring breathing mode of benzene. (A third band, an in-plane ring deformation, is also mass-sensitive, but it lies below 450 cm^{-1}, so it is not considered.) In phenol the two bands corresponding to these modes lie at 1250 cm^{-1} and 812 cm^{-1}, respectively. In diphenyl ether there must be four coupled bands because of the two Ph—O bonds, and these lie at *c.* 1240, 1195, 900, and 800 cm^{-1} respectively. The low-frequency members of this system lie in the region where one expects the P—O stretching bands, so further interactions involving these vibrations must be expected. Indeed, three broad and rather intense regions of absorption are observed, near 1190, 965, and 772 cm^{-1}. The assignments are indicated in Table 6. Again a splitting into asymmetric and symmetric modes may be expected to be significant in the P—O stretching modes and to a lesser extent in the other two modes. However, it is not possible to identify unambiguously the second P—O stretching frequency, though it is probably a major contributor to the complex 780 cm^{-1} region. Raman data are needed to locate this frequency with certainty.

There is also an out-of-plane ring deformation mode for monosubstituted benzenes that will probably interact with the six groups of bending, deformation, and torsional modes expected for the P—$(O—Ph)_3$ skeleton of triphenyl phosphate. Nearly all of these may split into at least two components, and in addition there are the P=O bending and two other ring modes that will occur below 650 cm^{-1}. For these reasons, no attempt is made to assign frequencies lower than *c.* 650 cm^{-1}.

A reasonable assignment can be made for nearly all the remaining bands in the 1600 cm^{-1} to 650 cm^{-1} region of the spectrum, however. The P=O stretching frequently appears as a double band near 1305 cm^{-1} in the liquid phase and simplifies on freezing to a single strong band at 1296 cm^{-1} with a weak shoulder near 1315 cm^{-1}. Though this might imply continued splitting of the P=O band in the solid, the weak band seems to be better assigned as the ring mode expected in this region [17]. Other assignments for the bands associated with the phenyl group follow closely those outlined by RANDLE and WHIFFEN.

It will be noted that, with the exception of the P=O stretching band, the solid spectrum is significantly more complicated than that for the liquid and that the relative intensities of some of the bands seem to depend on the orientation of the crystal. These complications of the spectrum are probably largely caused by

Table 6. Vibrational assignments in triphenyl phosphate

Description of mode	Number of modes	Wave number (cm^{-1})	
		Liquid	Solid
Modes largely skeletal in nature			
P=O stretching	1	1314, 1298	1296
(P)—O—Ph stretching (out-of-phase)	2	*c.* 1190*	1187, 1177
(P)—O—Ph stretching (in-phase)	1		1197
P—O—(Ph) stretching (asym.)	2	962	960
P—O—(Ph) stretching (sym.)	1	777	774
O=P—$(O—Ph)_3$ bending	2	470?	470?
P—O—Ph bending, deformation, and torsional modes†	18	not assigned	not assigned
Modes largely associated with benzene ring			
Ring modes			
C—C stretching $a_1(e_{2g})$	3	*c.* 1590	1600
C—C stretching $b_1(e_{2g})$	3		1590
C—C stretching $a_1(e_{1u})$	3	1490	1486, 1495?
C—C stretching $b_1(e_{1u})$	3	1457	1467
in-plane C—C—C bending and ring breathing modes $b_1(b_{2u})$	3	*c.* 1315	1315
in-plane C—C—C bending and ring breathing modes $a_1(a_{1g})$	3	1012	1010
in-plane C—C—C bending and ring breathing modes $a_1(b_{1u})$	3	*c.* 780*	790
in-plane C—C—C bending and ring breathing modes $b_1(e_{2g})$	3	620	617
in-plane C—C—C bending and ring breathing modes $a_1(e_{2g})$	3	prob. <450*	prob. <450
out-of-plane C—C—C bending $b_2(b_{2g})$	3	687	690
out-of-plane C—C—C bending $a_2(e_{2u})$	3	450	450
out-of-plane C—C—C bending $b_2(e_{2u})$	3	†	†
Modes involving H			
C—H stretching	15	not assigned	not assigned
in-plane bending $b_1(a_{2g})$	3	1235	1232
in-plane bending $a_1(e_{2g})$	3	*c.* 1164	1165
in-plane bending $b_1(e_{2g})$	3		1155
in-plane bending $b_1(b_{2u})$	3	1074	1074, 1080
in-plane bending $a_1(e_{1u})$	3	1029	1027, 1034
out-of-plane bending $a_2(e_{2u})$	3	†	†
out-of-plane bending $b_2(e_{2u})$	3	935	934
out-of-plane bending $b_2(b_{2g})$	3	903	916
out-of-plane bending $a_2(e_{1g})$	3	854	850
out-of-plane bending $b_2(e_{1g})$	3	754	756

* These modes form an interacting set of stretching and planar ring deformation frequencies.
† These modes form an interacting set of bending and non-planar ring deformation frequencies.

VOL. 9 1957

interactions within the unit cell of the crystal, though some, particularly those for the skeletal stretching frequencies, may represent a splitting of degenerate or close-lying modes of these types.

Conclusions

It has been shown that the simple organic phosphates, such as trimethyl, triethyl, and triphenyl phosphates have at least two rotational isomers in the liquid phase. These are most strikingly demonstrated by the presence of a double P=O stretching frequency, but in some cases the P—O stretching bands may also show additional components not present in the crystalline solid.

In addition, bands that have previously been demonstrated to be characteristic of certain types of P—O—R groups in phosphorus compounds have been identified with appropriate skeletal and CH_3, CH_2, and phenyl vibrational modes. A comparison of these assignments with similar but more complicated esters should allow further useful correlations between structures and spectra to be deduced.

Acknowledgements—The author particularly wishes to thank Dr. N. SHEPPARD for many helpful discussions during the course of this work and for a number of valuable suggestions regarding the assignments. He also wishes to thank members of the Department of Colloid Science for the hospitality they have shown him during his stay at Cambridge. Finally, he wishes to thank the Shell Development Company, Emeryville, California, and R. R. BRATTAIN for the encouragement given to him during the initial stages of this work and for permission to publish that part of the data and assignments completed while he was at Emeryville.

References

[1] DAASCH L. W. and SMITH D. C. *J. Chem. Phys.* 1951 **19** 22.
[2] For a general review of this work see BELLAMY L. J. *The Infrared Spectra of Complex Molecules* pp. 257–268. Methuen, London; Wiley, New York.
[3] DAASCH L. W. and SMITH D. C. *Analyt. Chem.* 1951 **23** 853.
[4] BELL J. V., HEISLER J., TANNENBAUM H., and GOLDENSON J. *J. Amer. Chem. Soc.* 1954 **76** 5185.
[5] SHEPPARD N. and SUTHERLAND G. B. B. M. *J. Chem. Soc.* 1947 1540.
[6] BROWN J. K. and SHEPPARD N. *Trans. Faraday Soc.* 1952 **48** 128.
[7] SIMON A. and SCHULZE G. *Naturwissenschaften* 1937 **25** 669; *Z. Anorg. Chem.* 1939 **242** 313.
[8] BAUDLER M. *Z. Elektrochem.* 1955 **59** 173.
[9] GUTOWSKY H. S. and LIEHR A. D. *J. Chem. Phys.* 1952 **20** 1652.
[10] HAWKINS N. J., COHEN V. W., and KOSKI W. S. *J. Chem. Phys.* 1952 **20** 528.
[11] WILLIAMS W., SHERIDAN J., and GORDY W. *J. Chem. Phys.* 1952 **20** 164.
[12] BADGER R. M. *J. Chem. Phys.* 1935 **3** 710.
[13] SCHOMAKER V. and STEVENSON D. P. *J. Amer. Chem. Soc.* 1941 **63** 37.
[14] GORDY W. *J. Chem. Phys.* 1947 **15** 81.
[15] SHELINE R. K. *J. Chem. Phys.* 1950 **18** 602.
[16] SHEPPARD N. *Trans. Faraday Soc.* 1955 **51** 1465.
[17] RANDLE R. R. and WHIFFEN D. H. *Molecular Spectroscopy* pp. 111–128. Report of a conference organized by The Spectroscopic Panel of the Hydrocarbon Research Group, Institute of Petroleum, London, 1955.

Spectrochimica Acta, 1957, Vol. 9, pp. 282 to 286. Pergamon Press Ltd., London

The infra-red absorption spectra of some indole-3-ketones

E. M. Tanner
Research Department, Parke, Davis & Co. Ltd.,
Hounslow, Middlesex

(*Received* 19 *March* 1957)

Abstract—The infra-red spectra of some indole-3-ketones have been recorded from 4000 cm^{-1} to 700 cm^{-1} in Nujol mulls and the NH and C=O stretching regions have been re-examined in tetrahydrofuran solution. The very low C=O frequencies shown by some of the simple 3-ketones in Nujol have been attributed to strong hydrogen bonding. The origin of a band near 1550 cm^{-1} and the high frequencies of the *N*-carbonyl vibrations in *N*-acyl-3-ketones have been discussed.

Introduction

Although a number of references have been made [1, 2, 3, 4, 5] to the infra-red absorption spectra of indole and its derivatives, as far as is known no work has

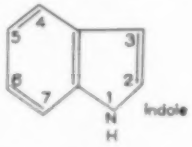

been published on the spectra of the indole-3-ketones. During the course of an investigation on indole derivatives [6] it became necessary to examine the infra-red spectra of some of the products. Since many of the 3-ketones exhibited unusual spectral properties, it seemed worthwhile to record their irregularities.

Experimental

All spectra were scanned in a Grubb Parsons' S3A spectrometer equipped with a sodium chloride prism. Single-beam recording was used for the region 1350–700 cm^{-1}, but double-beam operation was employed from 4000 to 1350 cm^{-1}. The compounds were prepared by Ames, Bowman, Evans, and Jones [6], and their purity established by elementary analysis.

Results and discussion

Owing to their insolubility in the more usual infra-red solvents, the compounds were examined first of all in Nujol mulls. The wave-numbers of the spectral bands obtained are given in Table 1, the bands obscured by Nujol absorption having been omitted. It will be seen that while the NH stretching frequencies near 3150 cm^{-1} are not abnormal for secondary amines examined in the solid state, many of the frequencies of the carbonyl group at position 3 are very low. Unsaturated and aromatic ketones generally have their C=O stretching frequencies above 1660 cm^{-1} in solution [7] and a little lower in the solid state, but some compounds in Table 1 which contain only 3-position carbonyls and no others, have their C=O frequencies much lower than this. Extreme examples are seen in the case of 3-formyl- (compound 1)- and of 3-acetyl-(compound 4)-indole with carbonyl frequencies of 1631

VOL.
9
1957

Table 1. Infra-red spectra of some indole-3-ketones (cm^{-1}). In Nujol

Compound no.	1	2	3	4	5	6	7	8	9	10	11
Substituent 1 Substituent 3	H CHO	CH_3 CHO	$COCH_3$ CHO	H $COCH_3$	$COCH_3$ $COCH_3$	H $COCH_2N(CH_3)_2$	H $COCH_2\overset{+}{N}(CH_3)_3\,I^-$	$COCH_2Cl$ $COCH_2Cl$	H $COCH_2NHCOOCH_2C_6H_5$	H $COCON(CH_3)_2$	$COCH_3$ CH_2OH
	3140	3160 *w*		3130 *s*		3110	3170		3310 *sh* 3220 *s*	3020	3530
	1631 *s* 1609 *d*	1682 *w* 1640 *s*	1747 *s* 1682 *s*	1614 *s*	1718 *s* 1662 *s*	1645 *s*	1662 *s*	1747 *s* 1670 *s*	1699 *s* 1650 *s*	1619 *s*	1691 *s*
	1572	1610 *sh*	1612 *w*		1604 *w*	1614	1614	1607 *w*	1583 *w*	1607 *d*	1601
	1514	1575 1520	1550 *s*	1576 1523 1490	1547 *s*	1579 1512	1579 *w* 1523	1547 *s* 1518 *w*	1550 1523	1575 *sh* 1512 1497 *d*	1578 1547 *w*
	1392 *s*	1395 *s*									1398 *s*
	1362	1365 *s*	1341	1339	1351 *s*	1341		1339	1333	1334 *w*	1388 *s*
	1333	1339 *s*	1319	1310	1326	1307	1310 1274 *cx*	1300	1305	1307	1353 1342
	1295 1250	1255	1254	1256 *w*	1301 1262 *s*	1281 1274 *d*	1242	1254	1260 1243 *d*	1250 *w*	1296 1250
	1213 *w* 1146 *sh* 1133 *sh* 1120 *s*	1188 1159 *cx*	1210 1172 1150 *w* 1126	1240 1138 1102	1222 *s* 1195 1164 1144 *d*	1235 1175 1143 1117 *d*	1205 *w* 1183 *w* 1146 1126 *d*	1210 1176 1132	1202 *w* 1167 1136 *w* 1097 *w*	1242 1186 1139 1120	1222 1210 *d* 1173 *w* 1148 *w* 1122
	1080 1037 *w* 1004	1070 1031 1009	1087 1039 1011	1027 1009 *d*	1035 *w* 1003	1096 *d* 1042 1012	1096	1080 1015	1078 1038 1008 *w*	1088 1059 *w* 1004	1086 1040 1007 *s*
	968 950	967 *w* 935	955 *w* 939	972 *w* 941 *s*	972 *w* 949	974 934 *s*	994 953 940 *w*	957	997 *w* 978 942 *w*	974 939 *w*	974 *s* 935
	884 867 *w*	866 857 *cx* 845	842	933 *sh* 877	923 844	881 *w* 859 812	923 894 872 848	922 *d* 868 *w* 848 *w* 807 *cx*	927 891 *w* 875 *w* 853 *w*	879 867 858	867 *w*
	790 *s*	788 *s*	786 772	803 773	769		803 770 *sh*	800 *s* 764 *sh* *cx*	824 *w* 807 *w*	810 *w* 790	820
	756 *s*	742 *s* 729 *s*	751 722	756 *s* 722 *w*	743 722	759 *s* 724	761 750 *w* 722	756 *s* 723 *s*	746 *s* *cx* 739 *sh* 701	776 754 *s* 745 *cx* 732	779 *w* 755 *s*

s = strong; *w* = weak; *d* = doublet; *cx* = complex band; *sh* = shoulder.

cm^{-1} and 1614 cm^{-1} respectively. Compound 10, 3-indolylglyoxilic acid-*NN*-dimethylamide, also shows only one carbonyl absorption which occurs at the very low frequency of 1619 cm^{-1}. The question therefore arose as to whether the indole-3-ketones were chelating in the same way as $\alpha\beta$-unsaturated β-amino-ketones in which carbonyl shifts, to lower frequency, of the order of 20–80 cm^{-1} can occur [8].

As it seemed essential to obtain the true frequencies of the NH and C=O vibrations unaffected by hydrogen bonding and crystal lattice effects in general, it was decided at this stage to attempt to use tetrahydrofuran as a solvent. Most of the indoles were known to be soluble in this solvent, and it was found that, provided it had not been allowed to oxidize and that no more than 0·1 mm thickness was used, tetrahydrofuran was sufficiently transparent from 3400 to 3000 cm^{-1} and from 1850 to 1500 cm^{-1} to be used for this purpose.

The results of the solution studies are compared with the corresponding frequencies in Nujol in Table 2. Some unusually large shifts of frequency are observed

Table 2. NH and C=O stretching frequencies of indole-3-ketones (cm^{-1}) in Nujol and in tetrahydrofuran

Compound number	Substituents		NH frequencies		C=O frequencies	
	1	3	Solid	Solution	Solid	Solution
1	H	CHO	3140	3250	1631	1679
2	CH_3	CHO			1640	1670
3	$COCH_3$	CHO			1747 1682	1740 1691
4	H	$COCH_3$	3130	3290	1614	1662
5	$COCH_3$	$COCH_3$			1718 1662	1736 1674
6	H	$COCH_2N(CH_3)_2$	3110	3250	1645	1654
7	H	$COCH_2N^+(CH_3)_3I^-$	3170		1662	1658*
8	$COCH_2Cl$	$COCH_2Cl$			1747	1751, 1737 *d*
					1670	1696, 1686 *d*
9	H	$COCH_2NHCOOCH_2C_6H_5$	3310 *sh* 3220	3270	1699 1650	1734 1662
10	H	$COCON(CH_3)_2$	3020	3320	1619	1649
11	$COCH_3$	CH_2OH	3530 (OH)	3570 (OH)	1691	1721

* In methylcellosolve *d* = doublet

VOL. 9 1957

in passing from solid to solution which are most marked in the compounds having the lowest C=O frequency in the solid state, i.e. in 3-formyl- and 3-acetyl-indoles, and the shifts affect both NH and C=O vibrations. In these compounds, shifts of over 100 cm^{-1} for NH absorptions and as much as 48 cm^{-1} for C=O bands are found. This effect appears to be due to extremely strong intermolecular hydrogen bonding, and the very low solubility of these compounds in the more usual organic solvents would support this view. On the other hand, compounds such as 9 showing smaller shifts in the NH and C=O frequencies in passing from solid to solution, are found to be more soluble in organic solvents. The shifts observed serve as a renewed warning of the danger of placing too great a reliance on carbonyl frequencies obtained on solids and of the necessity for making additional measurements in solution whenever practicable.

The figures for solutions in Table 2 show that the carbonyl frequencies are above 1650 cm^{-1} and the NH frequencies are normal, namely, neither group is so low as to bear direct comparison with the $\alpha\beta$-unsaturated β-amino-ketones. In contrast, however, many compounds have a strong or medium-strength band near 1550 cm^{-1} which persists in solid and in solution spectra, and this appears to be similar to the 1540 cm^{-1} absorption found by CROMWELL and his co-workers [8] in $\alpha\beta$-unsaturated β-amino-ketones. For lack of a more adequate explanation, this group of workers suggested that the band near 1540 cm^{-1} might be due to a lowered C=C vibration or an enhanced C—N stretching mode, probably the former, caused by resonance between the structures *A* and *B* below. The ionic-resonance form *B* could con-

tribute appreciably to the ground state and this would have the effect of lowering the C=O frequency, lowering the C=C frequency, and raising the C—N frequency. In the indole-3-ketones there is the possibility that the 1550 cm^{-1} band is due to a ring vibration of the indole fused-ring system as a whole, and in view of the evidence obtained from the carbonyl frequencies this seems the more likely explanation, although the coincidence is rather marked.

N-*Acylindole*-3-*ketones*

Some of the compounds investigated contained *N*-acyl- in addition to the 3-ketone-substituents. Compounds 3, 5, and 8 (Table 1) all contain a carbonyl adjacent to the nitrogen in addition to that at position 3. These three compounds each show two carbonyl absorptions, one of which lies between 1670 and 1690 cm^{-1} while the other is much higher, in the region 1730–1750 cm^{-1} (solution frequencies Table 2). The lower-frequency band is probably the 3-carbonyl and the higher the *N*-carbonyl by analogy with (1) the compounds unsubstituted at position 1 and (2) the carbonyl frequency of the model compound 11, 1-acetyl-3-hydroxymethylindole (1721 cm^{-1} in tetrahydrofuran). In addition, the presence of the hydrogen atom adjacent to the carbonyl in 1-acetyl-3-formylindole (compound 3) should tend to raise the frequency of the 3-carbonyl when compared with 1:3-diacetylindole (compound 5). It is seen (Table 2) that the higher carbonyl frequencies are approximately

the same in both compounds, 1740 and 1736 cm^{-1} respectively, but the lower carbonyl frequencies show greater difference, being 1691 cm^{-1} in 3-formyl-1-acetyl- and 1671 cm^{-1} in 1:3-diacetyl-indole. This, again, is in agreement with the lower frequency being assigned to the 3-carbonyl.

The frequencies of the *N*-acyl-carbonyls are worthy of comment, because they are extraordinarily high. Some model compounds were examined for comparison and of these *N*-acetylpiperidine was found to have its C=O stretching mode at 1658 cm^{-1} in tetrahydrofuran, and appears, therefore, as a normal tertiary amide. Investigation of tetrahydrofuran solutions of structures 12 and 13 showed the C=O

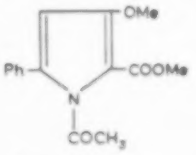

Compound 12

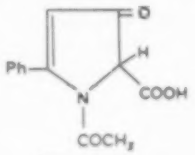

Compound 13

of the *N*-acetyl group to be at 1766 cm^{-1} in compound 12 and 1778 cm^{-1} in compound 13, approximately 100 wave numbers higher than in normal amides. The conclusion must be reached that this large increment is in some way connected with the presence of the five-membered ring, both in the pyrrole derivatives (compounds 12 and 13) and in the *N*-acylindoles (compounds 3, 5, 8, and 11). It is well known that the frequency of the carbonyl in a cyclic amide present in a five-membered ring is increased to varying extents according to the surrounding structure, above that of a normal amide or one in a larger ring. Evidently a similar correlation holds when the carbonyl is adjacent to the ring.

VOL
9
1957

Low-frequency Region

There is little of interest in the lower-frequency region of the spectra with the exception of the C—H out-of-plane deformation vibrations of the benzene ring. LEETE and MARION [5] have found these to occur between 735 cm^{-1} and 738 cm^{-1} in some simple derivatives of indole. For the compounds detailed in Table 1 the mode lies somewhat higher, but all are within the range 751 $\pm$ 7 cm^{-1} quoted by RANDLE and WHIFFEN [9] for *ortho*-substituted benzenes.

Acknowledgements—The author is indebted to Dr. D. E. AMES and Dr. D. D. EVANS for many helpful discussions, to Mrs. D. M. TEMPLE for the preparation of *N*-acetylpiperidine, and to Dr. J. DAVOLL for the model compounds 12 and 13.

REFERENCES

[1] SNYDER H. R. and ELIEL E. L. *J. Amer. Chem. Soc.* 1948 **70** 1857.
[2] BROWN J. B., HENBEST H. B., and JONES E. R. H. *J. Chem. Soc.* 1952 3172.
[3] GEISSMAN T. A. and ARMEN A. *J. Amer. Chem. Soc.* 1952 **74** 3916.
[4] NEUSS N., BOAZ H. E., and FORBES J. W. *J. Amer. Chem. Soc.* 1954 **76** 2463.
[5] LEETE E. and MARION L. *Canad. J. Chem.* 1953 **31** 778.
[6] AMES D. E., BOWMAN R. E., EVANS D. D., and JONES, W. A. *J. Chem. Soc.* 1956 1984.
[7] BELLAMY L. J. *The Infra-red Spectra of Complex Molecules* p. 114. Methuen, London, 1954.
[8] CROMWELL N. H., MILLER F. A., JOHNSON A. R., FRANK R. L., and WALLACE D. J. *J. Amer. Chem. Soc.* 1949 **71** 3337.
[9] RANDLE R. R. and WHIFFEN D. H. *Molecular Spectroscopy* p. 111. The Institute of Petroleum, London. 1955.

Spectrochimica Acta, 1957, Vol. 9, pp. 287 to 296. Pergamon Press Ltd., London

A spectrographic scheme for the determination of Al, Ti, Fe, Ca, Mg, and Mn in silicates

B. J. Rushton and G. D. Nicholls
Department of Geology, The University, Manchester 13

(*Received* 27 *February* 1957; *amended* 20 *March* 1957)

Abstract—A technique is described which enables Fe, Mg, Mn, Ca, Al, and Ti to be determined in silicates by spectrographic means employing low-voltage d.c. anodic excitation in a carbon arc.

On the grounds of volatility the major elements are divided into two groups, viz. Fe, Mg, Ca, and Mn, and Al and Ti. Separate arcing conditions are chosen for each group, the former being standardized by strontium (after Kvalheim) and the latter by yttrium. The relative error in the mean of triplicate arcings is estimated to be about $\pm 3{\cdot}5$ per cent in most cases.

Introduction

Three procedures are in common use for the chemical analysis of rocks and related materials. They are: (1) gravimetric methods [1, 2]; (2) rapid titrometric and colorimetric methods [3, 4, 5]; and (3) spectrochemical methods [6, 7, 8]. It is not unusual for analysts to select different procedures for different elements, and individual analysts frequently evolve their own scheme appropriate to the problem under investigation. Gravimetric methods are usually adopted for Ca and Mg, colorimetric methods for Ti and Mn, and titrometric methods for Fe. The determination of Al is normally made by precipitation of this element together with Fe, Ti, P, and Mn, weighing the ignited precipitate and correcting for the contaminants. Consequently it is probably the least satisfactory determination in a rock analysis. Nevertheless, such methods are generally considered the most accurate when the elements in question, expressed as oxides, are present in amount greater than 5 per cent of the rock. Where some accuracy can be sacrificed to speed (as in many rock analyses), Ca and Mg may be determined by titrometric methods [3, 4]. The accuracy of gravimetric procedures decreases as the amount of the element determined as oxide falls below 5 per cent and for amounts less than 1 per cent oxide they are generally less accurate than spectrochemical methods [9]).

Spectrochemical procedures have been extensively used for the determination of trace elements in rocks and minerals. The convenience of using similar procedures for both major and trace elements has inspired the evolution of schemes for the spectrochemical analysis of major elements which, although less accurate than gravimetric methods, are much faster. Kvalheim [10] used internal standardization methods with Sr as the internal standard for the elements considered in this paper. He reported that the relative error on triplicate analyses seldom exceed 10 per cent and was frequently less than 5 per cent. Various modifications to Kvalheim's scheme by several workers have been summarized by Ahrens [6]. Relative deviations are rarely better than 4–5 per cent. For the analysis of slags, Price [10] fused his material with borax and pelleted the powdered fusion cake with carbon before arcing. Using Co as internal standard he reported relative deviations of ± 4 per cent. Hawley and

MacDonald [11] determined the principle oxides in many igneous and metamorphic silicates, employing strontium as an internal standard and using the air-jet first designed by Stallwood [12]. Results indicated an accuracy of close to 5 per cent for the constituents present in large amounts and a suitable accuracy for others. This paper presents the results of an attempt to improve still further the procedures for the spectrographic determination of some of the major elements in rocks, viz. Al, Ti, Fe, Mg, Ca, and Mn, whilst retaining the simple conditions used for trace analysis—notably anode excitation in a carbon arc.

Relative volatilization

Among the factors to be considered in the selection of a suitable internal standard for the spectrochemical determination of a chosen element is the similarity or otherwise of the volatilization rates of the element to be determined and the

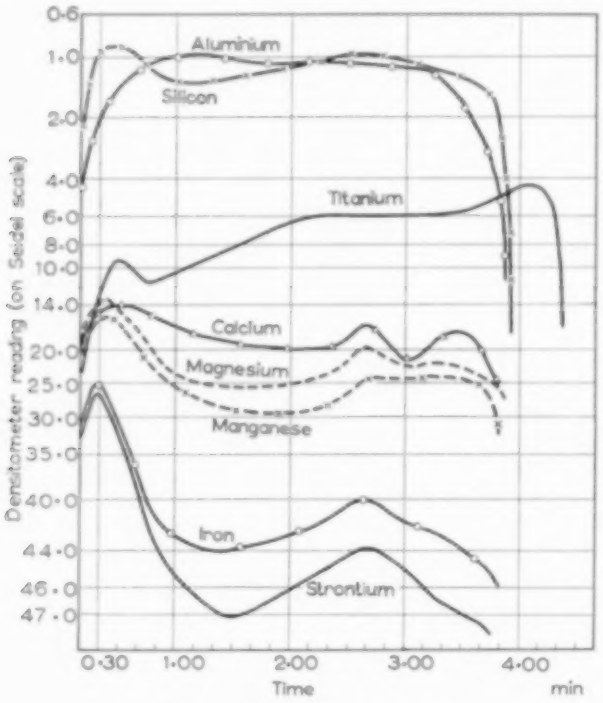

Fig. 1. The volatility of major elements.

proposed internal standard. The term "volatilization rate" is defined as the relative rate at which the respective elements are distilled into the arc at any time during the burn and is simply an attempt to classify an element by its dominant arcing characteristic. By racking a plate down through the light path, the intensity of light of a given wavelength emitted during different stages of the burn can be recorded and thus curves prepared showing how such intensity varies during the burn. The curves in Fig. 1 were prepared by plotting the Seidel function $\log \{(d_0/d) - 1\}$* against time, and illustrate that the elements considered here can

* d and d_0 are the microphotometer deflections of the line and "clear glass" respectively.

VOL. 9 1957

be split into two groups—a less volatile group Ti and Al (also Si, not considered in this paper) and a more volatile group Fe, Mn, Mg, and to a lesser extent Ca, which show maximum intensity of emission early in the burn. Sr behaves as a member of the second group and would appear to be a suitable internal standard for elements as far as rates of volatility are concerned. On the other hand, it is much less suitable for Ti and Al.

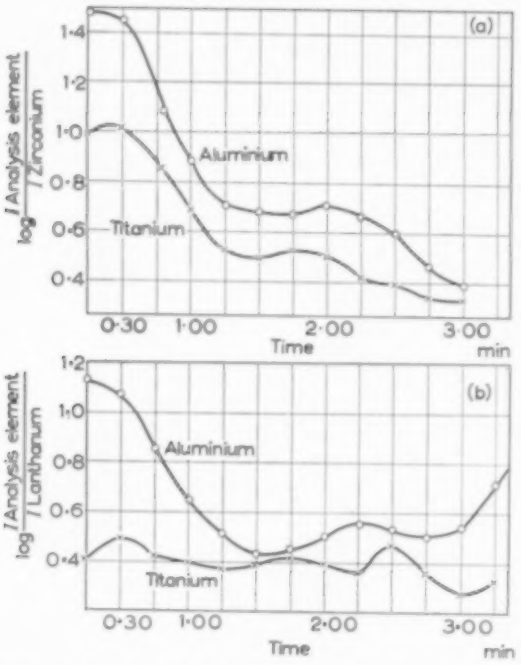

Fig. 2(a). Relative volatility of Al, Ti, and Zr from a charge consisting of ZrO_2 : rock : carbon of $\frac{1}{2}$: 1 : 10; (b) Relative volatility of Al, Ti, and La from a charge consisting of La_2O_3 : rock : carbon of $\frac{1}{2}$: 1 : 10.

The known involatile character of La, Ce, Sc, Y, and Zr prompted an examination of the rates of volatilization of these elements when incorporated in charges as internal standards. If volatilization rates were identical, it is clear that the intensity ratio for analysis line against internal standard line would not vary during the burn and a graphical illustration of the similarity of volatilization rates can take the form of a plot of this ratio against time. This has been done in Fig. 2 for results obtained with Y, Zr, and La. Zr (Fig. 2a) and to a lesser extent La (Fig. 2b) showed a marked tendency to be emitted in proportionally greater amount in the later stages of the burn, thus causing a fall in the ratio. Volatilization rates for Y, Al, and Ti were so similar under the working conditions used as to suggest Y as a possible internal standard for Al and Ti. Sc and Ce resembled La in their behaviour.

The effect of carbon dilution in reducing volatilization differences is well known, and to explore its effect on the use of Y as an internal standard for Al and Ti, charges were prepared in which the proportion of rock to carbon was always 1 : 10

but the proportion of Y_2O_3 to carbon was varied. Plots of intensity ratio against time were prepared, two of which are shown in Fig. 3 (a,b). A slight improvement in the constancy of the intensity ratio is apparent when smaller amounts of Y_2O_3 are used, and it was finally decided to use charges in which the ratio Y_2O_3 : rock : carbon was 0·23 : 1 : 10.

Similar studies indicated that the value of Sr as an internal standard for the more volatile group could be enhanced by increasing the carbon content of the charge, and the proportions of $SrCO_3$: rock : carbon finally adopted were 1 : 1 : 6.

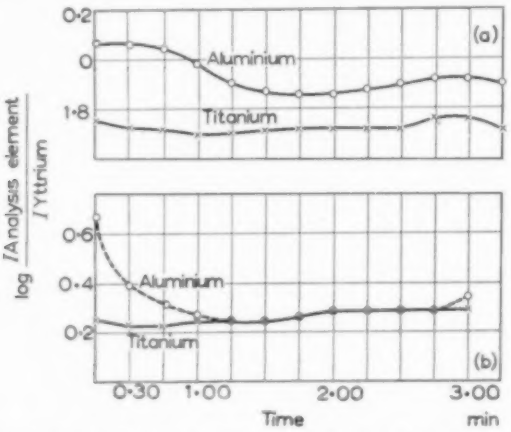

Fig. 3(a). Relative volatility of Al, Ti, and Y from a charge consisting of Y_2O_3 : rock : carbon of $\frac{1}{4}$: 1 : 10; (b) Relative volatility of Al, Ti, and Y from a charge consisting of Y_2O_3 : rock : carbon of $\frac{1}{2}$: 1 : 10.

Standards used

The Centerville diabase (W.1) and the Westerly granite (G.1), exhaustively investigated by replicate analyses [9], were obvious choices for standards, and intermediate compositions were prepared by mixing powders of these rocks in different proportions. The range of composition variation was extended by the similar use of the British Chemical Standard specimen B.C.S. 267—a silica brick of which replicate analyses are available.

Mixtures of oxides were also prepared having compositions within the range of variation it was desired to examine, with the intention of examining the effect, if any, of the different structural environments of the elements in the silicate standards from those in the oxides. Such an effect may be termed a "structural matrix effect."

Analytical technique

All weighings were made on an Oertling torsion balance which over the range 15—500 mg gave readings within $\pm\frac{1}{2}$ per cent of those obtained on a normal analytical balance.

The arcing charge was prepared by grinding standard mixture, internal standard, as oxide or carbonate, and carbon in an agate pestle and mortar for 25 min. Complete homogeneity was attained in the mix in this time when all constituents were fine enough to pass a 100-mesh sieve and the total weight of the mix did not exceed 1 g.

Electrodes were turned from "Ship" pure carbons manufactured by Champion and Co. of London. The cathodes were carbon rods of about 50 mm length and 7 mm diameter, the

VOL. 9 1957

end 12 mm of which were cut to a conical point. The anodes were made by drilling a cylindrical cavity of 0·320 ± 0·004 mm diameter and 6·00 ± 0·05 mm depth in a carbon rod of length 65 mm. The outer wall of the rod was turned to a diameter of 4·80 ± 0·05 mm extending from the lip of the cavity a distance of 8·0 ± 0·2 mm down the rod. Using a simple jig attached to a normal engineer's lathe, an inexperienced operator could cut 60 anodes per hour, of which 90 per cent were within tolerable deviation of the desired dimensions [13].

The arcing mixture was compressed to fill the cavity of the anode, no attempt being made to regulate the weight introduced. A test on five loaded anodes showed that the amount only varied from 65 to 67 mg.

Anode excitation in a d.c. (230–250 V) was used, the current being controlled at 7 A by a hand-operated rheostat. An image of the arc projected onto a fixed scale was used to control the position of the arc relative to the slit of the spectrograph and to maintain the distance between the electrode tips at 8 mm.

A Hilger E-492 spectrograph was employed with slit-width 0·020 mm, slit-height 13 mm, and camera aperture 13 mm. By means of an aluminized concave mirror, a diaphragm, and a quartz lens, the central 4 mm of the arc were collimated onto the slit. A seven-step sector was interposed in the light train, giving exposure ratios of 1 : 2 : 4 : 8 : 16 : 32 : 64. The range 2500–3650 Å was recorded.

Ilford chromatic (G.30) plates were used and developed for 2 min at 68°F (thermostatically controlled) in Ilford ID–2 dish-strength developer. The developer was violently agitated during the whole period of development. There was no evidence of any manifestation of the Ebhard effect.

The lines used are listed subsequently. Their densities were measured with a Hilger non-recording microphotometer (H.451) and galvoscale (H.671) adjusted to give a clear-glass reading (d_0) of fifty divisions. Galvanometer readings were plotted directly on a special graph-paper prepared for this department by Halden and Co. of Manchester. The abscissa scale on this graph paper is $\log\{(d_0/d) - 1\}$—the Seidel function—but the divisions marked correspond to microphotometer readings of different values and are so numbered. The use of this graph paper reduces the time required for plotting characteristic curves to less than half that required by more conventional methods. Separation of characteristic curves at a given value of $\log\{(d_0/d) - 1\}$ was used as a measure of intensity ratio. The evaluation of background and the subsequent correction for it have been the subject of much discussion. In this work, background was measured where significant in the most intense step adjacent to the line in question, plotted on the graph paper, and a characteristic curve drawn through this point parallel to that of the line. Log intensity of line and background at the given $\log\{(d_0/d) - 1\}$ value were converted to arbitary intensity values and arbitrary background intensity subtracted from arbitrary line intensity to make the background correction.

The more volatile group of elements (Fe, Mg, Ca, and Mn)

The main modifications to KVALHEIM's procedure [14] have been the use of a larger anode, and increased proportions of carbon and internal standard in the charge. The arc was struck at 3 A and raised to 7 A within 10 sec. Charges were burned to completion in 4 min. Smooth burns were usual, but subject to bursts of "instantaneous current." This effect was found to be minimized by carefully wiping the outside of the anode with clean filter paper and heating the loaded anodes for a short period at 105–110°C before arcing.

Table 1 records the lines used, their range of application expressed as a percentage as oxide, and the relative deviations obtained. Four analysis lines and the internal standard line are atom lines, the other two ion lines. Line profile studies indicated that none of the lines was prone to self-absorption or interference from neighbouring lines.

The working curves obtained are given in Fig. 4(a–d). Points corresponding to

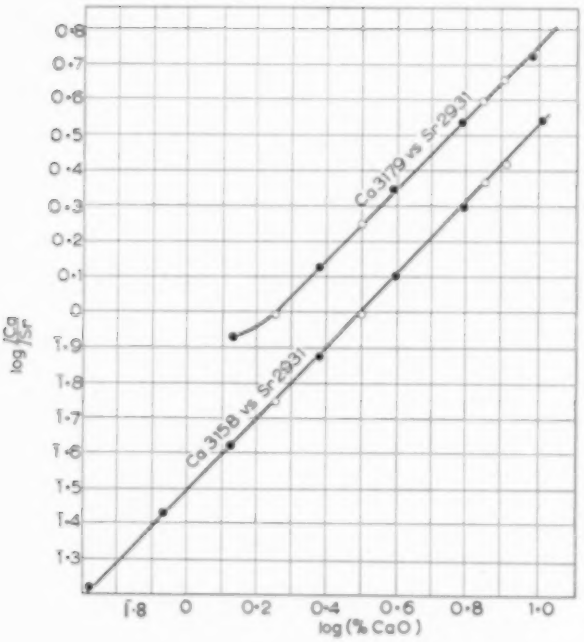

Fig. 4(a). Working curve, calcium vs. strontium.

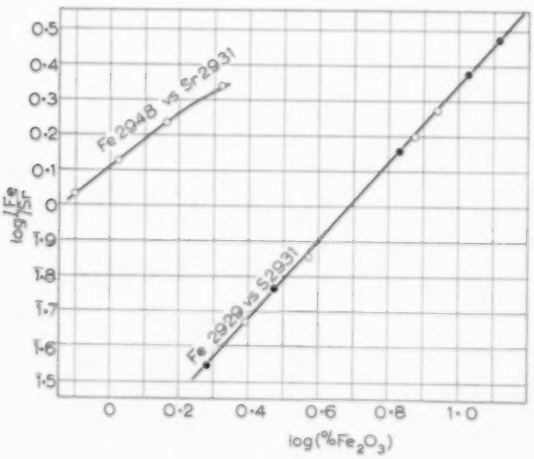

Fig. 4(b). Working curves, iron vs. strontium.

VOL. 9 1957

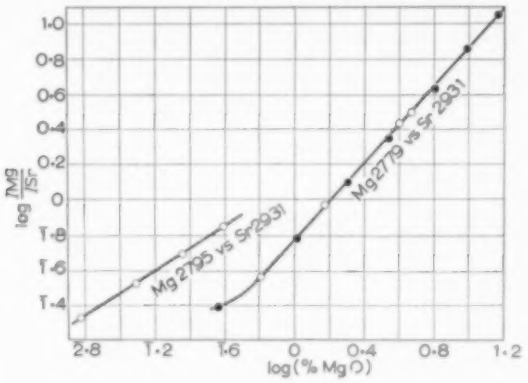

Fig. 4(c). Working curves magnesium vs. strontium.

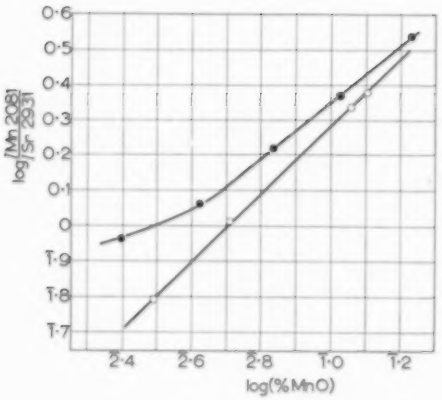

Fig. 4(d). Working curves, manganese vs. strontium.

Table 1

Element	Line pairs		Range of application (% oxide)	Relative deviation (%)
Ca	Ca I 3158·9	Sr I 29318·8	0·5–10	±3·5
	Ca II 3179·3		1·8–18	±3·5
Mn	Mn I 2801·1	Sr I 2931·8	0·025–0·15	±2·5
Fe	Fe I 2929·0	Sr I 2931·8	1·9*–11*	±3·0
	Fe I 2947·9		0·7*–2*	±3·5
Mg	Mg I 2779·8	Sr I 2931·8	0·4–15	±3·5
	Mg II 2795·5		0·05–0·4	±3·5

* Total iron expressed as Fe_2O_3.

Table 2

Element	Line pairs		Range of application (% oxide)	Relative deviation (%)
Al	Al I 2652·5	Y I 2948·4	8–25	±3·2
Ti	Ti II 3088·0	Y II 3086·9	0·5–2·0	±3·0

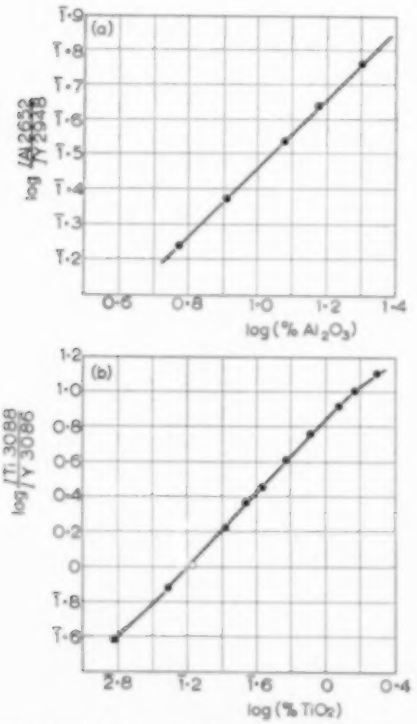

Fig. 5(a). Working curve, aluminium vs. yttrium; (b) working curve, titanium vs. yttrium.

silicate standards are ringed; unringed points correspond to oxide standards. Except for Mn, the working curves based on silicate standards were found to be coincident with those based on oxide standards. It was known that Mn impurities occurred in the oxides other than MnO, so coincidence could not be expected for this element. The higher values of the intensity ratios log ($I_{\text{Mn-2981}}/I_{\text{Sr-2931}}$) are thus to be attributed to the presence of impurities in the oxides employed in the preparation of the standard mixtures, as is suggested by the increasing divergence of the working curves at low concentrations of MnO. For Mn, therefore, the working curve based on silicate standards is preferred. The coincidence of the working curves for the other elements indicates that any effect due to the different mineral structures present in the silicate standards from those in the oxides must be so small as to be negligible. Thus for these elements oxide standards are quite suitable for the compilation of working curves.

The less volatile group of elements (Al and Ti)

In view of the doubt surrounding the determination of Al by the method commonly used and outlined in the introduction to this paper, oxide standards only were used for the determination of the working curve for this element. The assumption that there is no structural matrix effect for Al is inherent in this procedure, but in view of its negligible effect for the more volatile elements it was thought that it was unlikely to be very significant for any element. Any error in the positioning of the working curve due to neglect of a possible structure matrix effect is probably no greater than would be introduced by using the Al_2O_3 figures of analysed standards. For Ti, oxide standards were used to extend the range of compositional variation beyond that which could be obtained by mixing analysed samples.

The arc was struck at 6 A and raised to 7 A during the first 2–3 sec of the burn.

Table 2 records the lines used, their range of application expressed as a percentage as oxide, and the relative deviations obtained. Atom lines were used for the Al–Y pairing, ion lines for Ti–Y.

The working curves obtained are shown in Fig. 5(a,b).

Discussion of results

The working curves are linear over considerable ranges of concentration covering those normally encountered in the analysis of igneous rocks. The relative deviations, while higher than is desirable, represents some improvement on earlier procedures. Errors in spectrochemical results may arise through unstable arcing conditions resulting in rough burns or in the methods of recording and measuring the intensity of the emitted light. The former difficulty has been reduced though not eradicated by the use of the procedure adopted here, and it seems probable that most of the error is to be attributed to the second of the above factors. This makes it imperative that standards should occasionally be arced in a run of a number of analyses, and variation in response that may occur even between two plates of the same batch makes it desirable that one standard should be included in each plate set of analyses.

References

[1] Washington H. S. *The Chemical Analysis of Rocks* Wiley, New York, 1931.
[2] Groves A. W. *Silicate Analysis* 2nd ed. Allen and Unwin, London, 1951.
[3] Shapiro L. and Brannock W. W. *U.S. Geol. Survey Circ.* 1952 165
[4] Shapiro L. and Brannock W. W. *U.S. Geol. Survey Bull.* 1956 1036–C (Revision of circular 165).
[5] Mercy E. L. P. *Geochim. et Cosmochim. Acta* 1956 **9** 161–173.
[6] Ahrens L. H. *Spectrochemical Analysis* Addison-Wesley, Cambridge, Mass., 1950.
[7] Ahrens L. H. *Spectrochim. Acta* 1951, **4**, 302–306.
[8] Ahrens L. H. *Quantitative Spectrochemical Analysis of Silicates* Pergamon Press, London, 1954.
[9] Fairbairn H. W. *et al. U.S. Geol. Survey Bull.* 1950 980.
[10] Price W. J. *Spectrochim. Acta* 1953 **6** 26–38.
[11] Hawley J. E. and MacDonald G. *Geochim. et Cosmochim. Acta* 1956 **10** 197–223.
[12] Stallwood B. J. *J. Opt. Soc. Amer.* 1954 **44** 171–176.
[13] Scott R. O. *Spectrochim. Acta* 1950 **4** 73–84.
[14] Kvalheim A. *J. Opt. Soc. Amer.* 1947 **37** 585–592.

VOL.
9
1957

Spectrochimica Acta, 1957, Vol. 9, pp. 297 to 306. Pergamon Press Ltd., London

The spectrographic determination of boron in graphite

F. W. J. GARTON
U.K. Atomic Energy Authority, Research Group (Woolwich Outstation)
Royal Arsenal, London, S.E.18

(*Received* 22 *February* 1957)

Abstract—The development of a sensitive arc method for the routine determination of boron in graphite over the range 0·2–1·5 p.p.m. is described. The sample in the form of powder is compressed into pellets with the aid of a phenol–formaldehyde resin as binding medium, and these are arced in graphite holders at 7 A (d.c.). The density of the B I 2497·73 is compared with that of the NO(γ) band component at 2497·14.

The effects of possible disturbing factors are considered, and the extension of the method, by means of cathode-ray microphotometry, down to a lower limit of 0·01 p.p.m. boron, is described. The method can be applied to coke and pitch with suitable modifications.

Introduction

EARLY in 1946 the need arose to determine the boron content of the graphite intended for use in nuclear piles, and as it was calculated that 1 p.p.m of boron would have a significant effect upon the neutron absorption properties of the graphite, this level of concentration was the original target set for the determination. At a later stage this was lowered, particularly for the examination of raw materials and determination of "blanks" in pure graphite electrodes.

Previous work had been by chemical means [1,2,3], thus involving concentrational methods. As pointed out by FELDMAN and ELLENBURG [4], the determination is rendered difficult by the fact that boron combines with carbon at graphitization temperatures (2500—2600°C) to form boron carbide (B_4C), which is extremely involatile and inert. Any chemical method must therefore depend upon removal of the graphite by ashing and subsequent conversion of the boron carbide to a reactive compound.

Two lines of approach were available, therefore, in the spectrographic determination, i.e. a direct method using the graphite without preliminary concentration, or an indirect method involving concentration. Initial experiments soon showed that it was uneconomical to concentrate by ashing, which is a time-consuming process. Furthermore, the chemical method also involved ashing, and the indirect method would lead to little gain, coupled with the fact that independence of approach would be lost.

The main effort was therefore expended in developing a completely independent direct spectrographic method.

Development of standard technique

(a) *Excitation*

Preliminary experiments showed that of the various means of excitation available, viz. spark, a.c. intermittent arc, and d.c. arc, only the last method was suitable, as it was necessary to secure complete burning of a relatively large amount

of sample for the reasons pointed out by Feldman and Ellenburg. Various arc currents were tried, but it was found that 7A represented a good compromise between sensitivity, stability, and line/background ratio, coupled with a reasonable exposure time. Polarity had little effect, but for convenience in securing a smooth burn and avoidance of overheating of electrode holders, the top electrode was made positive.

(b) *Spectrograph*

A Hilger medium quartz and a Hilger large automatic quartz (Littrow) spectrograph were available, and were both tried, using as criterion the line/background ratio.

The nature of the background is a fairly strong discontinuous matrix of molecular bands superimposed upon a fainter continuum, and the B I line at 2496·78 is inconveniently close to one of the fainter band components, while the other B I line at 2497·73 is very close to the Fe II line 2497·82.

Various optical screening arrangements were tried in an attempt to reduce the background, but without success, as it was found that both types of background, i.e. molecular bands and continuum, had their origin in the arc itself and not in the hot electrode tips.

Experiments demonstrated clearly that the larger dispersion (3Å/mm at 2500A) of the Littrow instrument was necessary, and this was therefore used in all subsequent work.

(c) *Photographic Conditions*

In order to achieve a high contrast with reasonable sensitivity, Kodak B.10 plates were used in conjunction with a high-energy developer (Kodak D.19b or Ilford ID2), but exposure times had to be increased to $2\frac{1}{2}$ min under these conditions to give satisfactory line strength.

(d) *Form of Sample*

Although it was realized that samples would be available in solid form, the use of this form would necessitate chemically analysed samples for standardisation. These were not available at the time, and the possibility of using the sample in powder form was therefore considered, since in this case standards could be synthesized by grinding or similar means from pure graphite and a boron compound.

As attempts to arc the powdered sample in shallow graphite cups were not successful owing to considerable loss of sensitivity and reduction in line/background ratio, the possibility of making the powder into pellets was investigated. Pile-graphite powder will not compress into pellets even with the use of a hydraulic press, and it was necessary to use a binding agent. A suitable one was found in phenol–formaldehyde resin, and this, with a simple curing process, formed hard and mechanically strong pellets which could be mounted in holders and arced directly.

The resin used was originally made in the laboratory, but it was later found possible to use a proprietary brand (Damarda Lacquer, Grade L.3128, from Bakelite Ltd.).

The procedure for making pellets can be summarized as follows:

The sample, in block form, was filed with a 12 in. smooth file, kept for that

VOL. 9 1957

purpose only, and the filings bottled after discarding the surface material. 5 g of the filings were weighed out, and 1 g of a 25 per cent solution of phenol–formaldehyde resin in boron-free alcohol added, the mixture being thoroughly homogenized by grinding. Pellets were made in a steel die having six holes each $1\frac{1}{16}$ in. long and $\frac{1}{4}$ in. diameter. Each hole was loosely filled with a damp powder, the punches inserted, and the whole compressed in a 5 ton hydraulic press to a total pressure of 6000 lb. A heating coil maintained a temperature of 150°C throughout. The pressure was released after 30 sec and the punches removed to allow alcohol vapour and decomposition products of the resin to escape, since these tended to weaken the resultant pellet if retained within the graphite. The punches were

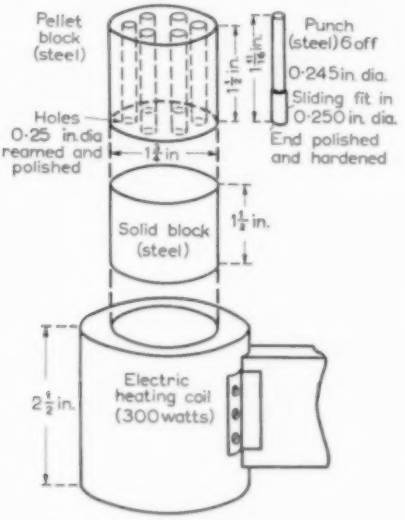

Fig. 1.

replaced and the pressure applied for a further 3 min. The finished pellets, $\frac{1}{4}$ in. in diameter and approximately $\frac{1}{4}$ in. long, were removed and bottled ready for use. They were found to be extremely strong, and could be handled as easily as graphite rod.

For spectrographing, the pellets were mounted in recesses $\frac{1}{8}$ in. deep and $\frac{1}{4}$ in. diameter in $\frac{3}{8}$ in. diameter H.S. graphite rods. A pair of pellets was used for each exposure, i.e. both electrodes had graphite pellets as tips, since this had been found to increase sensitivity. Fig. 1 shows the pelleting block and heating coil.

(e) *Standards*

Synthetic standards were prepared by adding boron carbide to pure graphite, to give concentrations of 0·1, 0·2, 0·5, 1·0, and 1·5 p.p.m of boron, and spectrographed to give a standard working curve. It was found essential that the boron carbide should be carefully standardized chemically for boron content, and that it should be very finely divided; furthermore, the mixture should be given at least 15 min grinding in agate, in quantities not greater than 5 g.

Standards were also made, using borax and boric acid instead of boron carbide,

both by dry grinding and addition in the form of solutions. Calibration curves obtained were identical with that for the boron carbide standards.

It was subsequently found that these synthetic standards gave somewhat high results and consequently were later abandoned in favour of chemically analysed

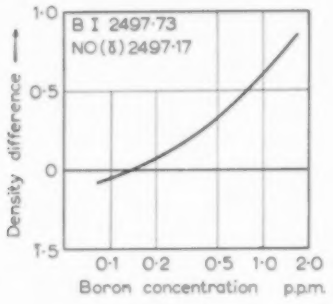

Fig. 2.

samples when sufficient of these had been collected and when differences between chemical and spectrographic results had been satisfactorily resolved (*vide infra*).

(f) *Selection of Lines*

The only two boron lines suitable were the B I 2496·78 and B I 2497·73 (excitation potential 4·94 V). The former lies close to a background line and therefore gives a rather flat working curve, whereas the latter gives a reasonably good curve down to 0·2 p.p.m. In both cases there is distinct curvature due to background, but although a linear working curve can be obtained by the use of background correction, no improvement in results was obtained, probably owing to the stability of the background, and the correction was not employed in routine practice.

Choice of internal standard proved to be a matter of some difficulty, since the only atomic carbon line in the vicinity was not only too strong, but has an excitation potential of 7·65 V.

Various background lines were therefore investigated for suitability as internal standards, and two due to the NO(γ) band system [5] were finally adopted, at wavelengths of 2497·17 and 2456·8 respectively. Of these two, the former proved more reliable in routine practice, although the index point was at a less suitable concentration (0·13 p.p.m. as compared with 0·4 p.p.m. for the 2456·8).

Beryllium, chromium, and antimony were also tried as added internal standards, but no improvement was obtained. The C I 2478·6 was also tried using a local filter to reduce its intensity, but once again no improvement resulted. The use of iridium by Feldman and Ellenburg was, of course, not known at the time the investigation was made.

(g) *Calculation of Results*

A number of methods of plate calibration and calculation of results have been studied and have been used in routine practice for varying periods.

The final method, adopted for simplicity and reliability, was to measure in a

VOL. 9 1957

Hilger non-recording microphotometer the densities of the lines B I 2497·73 and NO(γ) 2497·17 and to plot the density difference against log concentration of boron. A standard was incorporated on each plate, and this was used to obtain the plate factor in the usual manner. After correction, results were read directly from the standard curve, shown in Fig. 2.

Effects of possible disturbing factors

During the period covered by the foregoing work a parallel investigation on the chemical determination of boron in graphite was in progress. The result of a series of chemical and spectrographic analyses showed the spectrographic figures to be on an average about 1·3 times as great as the chemical. For some time this position was accepted, as it was anticipated that losses might occur in the chemical method, but later it became clear that the spectrographic results were definitely high. A full investigation into possible causes of this was made, and although eventually it was found to be attributable to a single factor, brief mention is made of other factors investigated.

(a) *Effect of Impurity Elements other than Boron*

In routine samples of pile graphite the impurities most commonly found were silicon (50–250 p.p.m.), calcium (100–600 p.p.m.), and iron (10–100 p.p.m.). In the pure graphite used for synthetic standards these impurities are almost completely absent. A standard was made up containing 1·0 p.p.m. boron, 500 p.p.m. silicon, 1000 p.p.m. calcium, and 100 p.p.m. iron, and spectrographed against the pure 1·0 p.p.m. standard. No effect due to these impurities was observed.

(b) *Effect of Pelleting Pressure*

Since the pure graphite used for standardization was of different texture and bulk density from the sample graphite, experiments were made on the possible effect of variation of pelleting pressure

A strong correlation was found between the pelleting pressure and the density of the pellets produced, for both pile graphite and that used for making standards. In neither case, however, was any correlation found between pellet density and apparent boron content, which was constant over the whole range of usable pelleting pressures.

(c) *Consumption of Graphite in the Arc*

At the same time the consumption of graphite in the arc was measured for pellets of different density, and no correlation was found between sample consumption and either pellet density or apparent boron content. There was, however, a consistent difference of about 10 per cent in the consumption of standard and sample graphite, which appeared to be a function of texture rather than density.

(d) *Particle Size and Form*

Experiments were carried out to determine the effects, if any, of particle size and method of production of the powder, but no effect was observed over a wide range of particle sizes and with various methods of preparation.

All the foregoing experiments were carried out over an extreme range of conditions either side of those used in the standard method, and as they proved to be negative, no alteration in conditions was judged to be necessary.

(e) *Rate of Emission of Boron in the Arc*

Moving-plate experiments showed that a difference in the rate of emission of boron was observable between samples and synthetic standards, and that this difference was the same whatever method was used to prepare the standards. The effect is illustrated in Fig. 3.

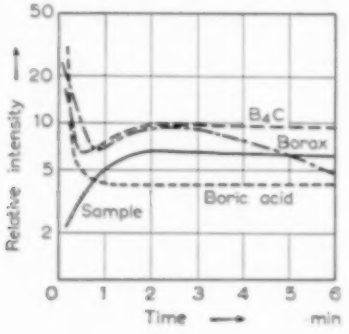

Fig. 3.

A confirmatory experiment on this effect in the case of standards was made, in which the arc was allowed to cool after 1½ min and then re-struck. There was no strong re-emission of boron, showing that the effect was confined to the initial burning period during which the pellets were brought rapidly up to the normal running temperature.

As it was thought possible that the boron might tend to concentrate on the surface of the pellets in the case of the synthetic standards due to flow during curing, trials were made on scraped pellets, but no such effect was observed.

As an additional confirmatory experiment, chemical analyses were made on portions of pellets remaining after the preliminary exposure, and they were found to be deficient in boron content to the extent of about 20 per cent.

The mechanism by which boron is volatilized by the arc from a graphite matrix is considered fully by FELDMAN and ELLENBURG, and the above experiments indicate that the general conclusions drawn by them are substantiated. It would appear, however, that the mechanism may be slightly different for pellets made from standards prepared by mixing from that for samples in which the boron, in the form of carbide, may be considered to be uniformly distributed throughout the bulk of the graphite.

Since boron carbide is extremely hard and in an extremely fine state of subdivision, it is reasonable to suppose that in the synthetic standards it is interspersed between the particles of graphite and that the process of compression into

VOL. 9 1957

pellets causes the particles of carbide to embed themselves into the surface of the graphite.

On striking the arc, rapid volatilization of the boron carbide on the exposed surface of the electrode takes place due to the formation of local hot spots on the electrodes; during this initial period some diffusion of the now molten carbide into the graphite takes place, in the underlying surface, so that after the preliminary heating the pellet simulates the "natural" graphite as far as distribution of boron is concerned, from which excitation of the boron lines occurs by the entrainment process suggested by FELDMAN and ELLENBURG. In the case of standards prepared from borax and boric acid, during the initial period the boron compound is converted into carbide and then behaves in the same manner as natural graphite although a small amount may be volatilized in the air before conversion to carbide.

Once the experimental facts had been established, it became necessary to abandon the use of synthetic standards in favour of analysed samples, which were thereafter used for establishment of standard curves. This was made possible by improvements in the chemical method of analysis, and once this was done a fairly exact correlation was obtained between chemical and spectrographic results.

Results obtained

From the outset the spectrum of a control sample was included in every routine plate and a quality control chart was kept. The control limits were set from the first 32 plates (about 300 samples), the standard deviation being 0·035 p.p.m. on the control sample, which had a nominal boron content of 1·07 p.p.m., i.e. the coefficient of variation was 3·3 per cent on duplicate exposures. This was adequate for the purpose. A deterioration then set in on the next 55 plates (about 600 samples). The possibility of personal errors was eliminated, as a statistical survey of the results obtained from seven operators showed no significant influences.

Another effect, which was not negligible, was working curve shift, which has been observed by other experimenters [6,7]. However, it was noticeable on only one of the two internal standard lines, and, as stated earlier, all subsequent work was done using the more reliable line, i.e. NO(γ) 2497·17, which showed no observable shift of the index point over a long period.

However, a further survey of the results showed that the apparent deterioration could be attributed to variation in plate-to-plate sensitivity, which caused a greater number of exposures to fall on the toe of the photographic curve. If these exposures were ignored, all results came within the original control limits.

Extension to low boron contents

The method as originally developed for and used in routine practice was designed to cover the range 0·5—1·5 p.p.m; below 0·5 p.p.m. the calibration curve flattened considerably and showed more variation than could be tolerated.

Use of Scanning Technique

The boron lines at concentrations of 0·2 p.p.m. or less were almost inseparable from the background, which, as stated, was principally due to the NO(γ) system, and a scanning method of reading the spectra became necessary.

The particular method used, namely cathode-ray display microphotometry, is described elsewhere [8]. The principal advantages of this apparatus over the conventional pen-recording microphotometers are the speed with which a scan is obtained and the ability to obtain greatly enlarged scans of small portions of very faint spectra. Interpretation of the latter is also very simple and convenient [9],

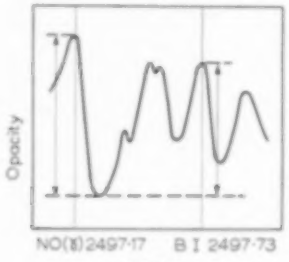

Fig. 4.

since at low densities a straight line is obtained by plotting peak-height ratios against concentration.

The scan obtained in the case of boron in graphite is shown in Fig. 4.

Effects of Electrode Holders

The electrode holders used up to this time had been H.S.-brand graphite having a boron content of about 2–3 p.p.m., and it was thought that this might be the cause of some of the variation of the lower end of the curve. Some electrode holders were therefore made from graphite having a boron content of less than 0·2 p.p.m. and a comparison was made between spectra from pellets of a 0·1 p.p.m. standard and N.C.C. spectroscopically pure graphite. A difference in apparent boron content was found, which indicated a variable "blank," due to the holders, of about 0·02 p.p.m.

Results Obtained

Fig. 5 shows the calibration curve obtained by the scanning method using the low-boron holders, over the range 0·01–0·2 p.p.m., from which it is seen that the method is usable down to 0·01 p.p.m. At this concentration the boron line is invisible on the plate using an ordinary spectrum viewer.

An investigation into the various sources of error at this low concentrational range showed that the variances due to excitation and plate emulsion were the controlling errors, those due to scanning microphotometry and preparation of samples being of a lower order.

In all this work, spectra were excited by the d.c. arc in air, and since the limit of sensitivity is set by the line/background ratio, it is possible that a further improvement in sensitivity might result from the use of a controlled atmosphere,

VOL. 9 1957

e.g. argon-oxygen as used by FELDMAN and ELLENBURG. Furthermore, the use of an added internal standard such as iridium would then become necessary owing to elimination of nitrogen and therefore of the NO(γ) system which has been used hitherto as internal standard.

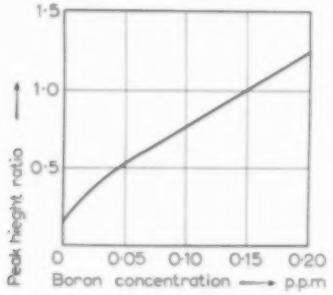

Fig. 5. Ratio = $\frac{\text{height of B I 2497·73}}{\text{height of NO}(\gamma)\ 2497{\cdot}13}$.

Extension to cokes and pitches

Simultaneously with the examination of the finished graphite it became necessary to examine the raw materials used in its manufacture, since control of boron content of graphite is confined to choice of raw materials [4].

It was found that coke could be readily examined by the method used for graphite by simply mixing it with an equal weight of boron-free graphite to ensure good pelleting and burning properties.

The method of examining pitch was a little more involved, as it was necessary to remove volatile constituents before making into pellets. Some doubt was felt as to the validity of a simple baking process, owing to possible loss of volatile boron compounds. After a series of experiments had been performed it was found possible to avoid this by first mixing the pitch with pure graphite, covering with another layer of graphite, and heating gently until all volatile matter had been removed. After grinding, the resultant coke–graphite mixture could be satisfactorily made into pellets and arced in the normal manner. Results obtained agreed closely with those obtained by chemical analysis.

Acknowledgements—The work described was carried out over a long period by a varying team of experimenters who were at the time members of the Chemical Inspectorate, M.O.S. They were, in addition to the author, Dr. F. J. BRYANT, Mr. R. A. MOSTYN, Mr. R. J. WEBB, Mr. C. E. AUSTING, and others. Grateful acknowledgement is made to these workers, also to Dr. J. H. MARTIN for advice in connection with the pelleting procedure.

Acknowledgement is also made to the Director, A.E.R.E., Harwell, for permission to publish this paper.

References

[1] MCHARGUE J. S. and CALFEE R. K. *Industr. Engng. Chem.* (*Anal.*) 1932 **4** 385–8.
[2] MCHARGUE J. S., OFFUTT E. B., and HODGKISS W. S. *Proc. Soil Sci. Soc. Amer.* 1939 **4** 308.
[3] SMITH F. M., SCHRENK W. G., and KING H. H. *Analyt. Chem.* 1948 **20** 941–3

[4] Feldman C. and Ellenburg J. Y. *Analyt. Chem.* 1955 **27**(11) 1714–1721.
[5] Pearse R. W. B. and Gaydon A. G. *The Identification of Molecular Spectra* Chapman and Hall, London, 1941.
[6] Smith R. W. and Hoagbin J. E. *Analyt. Chem.* 1947 **19**(2) 86.
[7] de Waal D. M. and Strasheim A. *Spectrochim. Acta* 1948 **3**(2) 141–158.
[8] Davis H. M. and Webb R. J. *Spectrochim. Acta* 1950 **4** 13–20.
[9] Garton F. W. J. and Webb R. J. *Colloque International de Spectrographie de Strasbourg* G.A.M.S., 1950.

VOL.
9
1957

Spectrochimica Acta, 1957, Vol. 9, pp. 307 to 322. Pergamon Press Ltd., London

Analytical studies of the fluorescence of samarium in calcium sulphate

C. Gordon Peattie*† and L. B. Rogers
Department of Chemistry and Laboratory for Nuclear Science Massachusetts Institute of Technology, Cambridge, Massachusetts

(*Received* 27 *December* 1956)

Abstract—Co-precipitation of samarium (III) with calcium sulphate, followed by partial reduction to samarium (II) using a $7{\cdot}0 \times 10^6$ rep dosage of 3 MeV electrons from a Van de Graaff accelerator makes possible the fluorimetric detection of about 10^{-3} μg of samarium and the determination of microgram amounts when originally present in 5 to 10 ml of solution. Nearby trivalent rare earths produced high negative interference in 100-fold excess but only a very small effect in ten-fold excess. Under similar conditions for the precipitation and electron bombardment, about 6×10^{-2} μg of europium can be detected using 2536-Å radiation instead of the 3650 Å used for the samarium.

The goal of the present study was to devise a practical fluorimetric procedure for the determination of microgram amounts of samarium in aqueous solutions. As pointed out in a recent survey [1], the reports existing in the literature were unsatisfactory from the analytical viewpoint because the experimental details concerning the preparation of the fluorophors were scanty or sometimes omitted entirely. In addition, many of the early fluorescence spectra were obtained under low resolution using rare earths of undetermined purity. As a result, re-examination of the data using a spectrograph seemed warranted even though it was hoped that the final procedure would require the use of only a filter photometer.

In a previous study, solutions of samarium were slurried with calcium tungstate following which the preparations were dried and ignited before measuring the fluorescence. Unfortunately, the fluorescence of samarium was very sensitive to the presence of neighbouring rare-earth elements. Furthermore, it appeared that the sensitivity might be improved by using a flux which would permit reduction of samarium (III) to (II). It also appeared that added sensitivity might be gained if rare earths were concentrated from a larger volume of solution by co-precipitation. A recent survey of some twenty potential base materials for samarium (III) fluorophors showed that only two substances, calcium and barium sulphate, were suitable for preparation by co-precipitation [1]. Of these, the calcium sulphate appeared better because of greater sensitivity and ease of handling. It filtered much faster and could be removed from the paper quickly in one piece, while the barium sulphate had to be scraped off. Moreover, the calcium sulphate remained fibrous, whereas barium sulphate became brittle upon being dried at 128°C.

* This paper was taken from a thesis submitted by C. Gordon Peattie to the Massachusetts Institute of Technology in partial fulfilment of the requirements for the Ph.D. degree in May 1952. The results were presented in part before the Conference on Analytical Chemistry and Applied Spectroscopy in Pittsburgh, Pennsylvania, March 1953.

† Present address: Texas Instruments Inc., 6000 Lemmon Avenue, Dallas 9, Texas.

Calcium sulphate has been used by several workers as a base material for samarium fluorophors [2–8], excitation having been achieved both by cathode rays [2, 4, 8] and by ultra-violet light [3, 5, 6, 7].

The methods of preparation of the fluorophors usually involved co-precipitation of the samarium (III). Bruninghaus [2] co-precipitated with calcium carbonate by adding ammonium carbonate to a calcium chloride solution containing samarium. The precipitate was ignited at 1000°C and the resulting calcium oxide converted to calcium sulphate by treating with sulphuric acid and igniting at red heat. No concentration data were given for the preparations of these fluorophors, though Bruninghaus reported being able to detect 10 μg of samarium per g of calcium oxide. Tomaschek [6, 7] prepared calcium sulphate fluorophors by adding a drop of samarium nitrate solution "of suitable concentration" to calcium chloride in a platinum dish, grinding with a pestle, fuming to dryness with sulphuric acid, and igniting at 900°C for 10 min. Lenard, Schmidt, and Tomaschek [4] used both the method just described and co-precipitation, followed by ignition. Karlik and Przibram [3] and Merkader [5] prepared fluorophors which gave a red fluorescence under "filtered ultra-violet light" by taking calcium solutions containing samarium, fuming to dryness with sulphuric acid, igniting the residues at 500°C for 15 min, and exposing the residues to radium for at least 12 hr. They attributed a peak in the spectrum at 5650 Å to samarium (III), while a band with a flat maximum at 6190 Å was assigned to samarium (II). The intensity of the latter band was not weakened by heating to 100°C. It showed no fine structure at −50°C and disappeared at −100°C. Karlik and Przibram [3] reported a concentration of 1000 μg Sm (II, III)* per g of calcium sulphate to be optimal, the intensity of fluorescence being weaker for samples containing 100 or 10,000 μg of samarium (II, III) per g of calcium sulphate.

Butement [9] confirmed the assignment of the 6190-Å band to samarium (II) after study of the fluorescence spectra of fluorophors made by fusing samarium (III) oxide with alkali and alkaline earth chlorides in hydrogen atmosphere. Butement also pointed out that the fluorescence of samarium (II) should be considerably more intense than that of samarium (III), since the probability of transitions giving rise to samarium (II) fluorescence was 10^3–10^4 times greater than of those producing samarium (III) fluorescence.

Merkader [5] reported the quantitative determination of samarium in calcium sulphate over the range, 0·10–10 μg per g of calcium sulphate. The samples were exposed for three days to 615 mg of radium at a distance of 1 cm. The fluorescence was then excited with "filtered ultra-violet light" and the spectra photographed with a Leiss spectrograph (glass). The exposure times varied from 38 sec for the sample containing 10 μg Sm (II, III) per g of calcium sulphate, to 54 min for the sample containing 0·10 μg Sm (II, III) per g. Merkader found the intensity of the fluorescence of samples containing 10 μg Sm (II, III) per g to be unaffected by the presence of iron (III), lead (II), and manganese (II). Europium, yttrium, or gadolinium reduced the intensity of fluorescence of a sample containing 10 μg Sm (II, III) per g of calcium sulphate by "two orders of magnitude" (to 1 per cent).

* Because of the lack of knowledge of the exact extent of reduction to the divalent state, this product is designated as $CaSO_4$—Sm (II, III).

VOL. 9 1957

Concentrations of 100 μg per g of ytterbium and praseodymium reduced the intensity of fluorescence of an equal amount of samarium by "one order of magnitude" (to 10 per cent?).

Experimental

The reagents and instruments were the same as those reported in another paper [1]. In addition to the recording spectrograph used previously, fluorimetric measurements were made using a filter photometer embodying an AH-4 mercury lamp, a Corning No. 5970 filter for excitation, and a 1P21 photomultiplier tube preceded by a Corning No. 3480 filter. This photometer was designed by J. R. TALLACKSON and C. B. PICKLE at Oak Ridge National Laboratory. The sensitivity of the instrument was adjusted each time before use against an arbitrary standard containing a uranyl salt in fused sodium fluoride.

Solutions of rare earths were the same as those employed previously [1]. Fluorophors were made by adding 1 ml of calcium chloride, equivalent to 0·100 g of calcium sulphate, to 5 ml of a 10 per cent solution of potassium sulphate containing the samarium (III). The precipitation was carried out at 80°C. After 15 min, the precipitate was filtered by suction and washed with water which had previously been saturated with calcium sulphate. The precipitate was then packed into a platinum dish and dried at 128°C. The surface of each sample was made uniformly concave by pressing it into the platinum dish with the end of a clean test tube. The sample was then ignited for 15 min at 750°C. Divalent samarium was produced by exposing the above samples to a beam of 3 MeV electrons from a Van de Graaff accelerator before measurement. The intensities recorded by the spectrograph were corrected for the response of the spectrograph by means of correction curves determined by SANGSTER and IRVINE [10]. In order to simplify the presentation of the results with regard to the amounts of samarium and other elements present in the fluorophor, it was assumed that the calculated amount of 0·1 g of calcium sulphate was always precipitated when stoichiometric amounts of calcium and sulphate were mixed, and that the precipitate carried completely the samarium or other rare earths present in the solution. Hence, the amounts referred to below can be converted to a "per gram" basis, often used by other investigators, by multiplying by 10.

Results

$CaSO_4$—Sm (III)

Irradiation with 2536 Å radiation produced no fluorescence at fluorophor temperatures of 20°, 60°, and 100°C for the following amounts of samarium (III): 0·0015, 0·015, 0·15, 1·5, 150, 900, and 1363 μg.

The spectrum of the fluorescence excited by 3650 Å is shown in Fig. 1. The positions of the samarium (III) bands found in the present investigation are listed in Table 1 together with those reported by earlier workers. It can be seen that cathode-ray excitation yielded essentially the same spectrum as excitation by 3650 Å, and that no significant shift of wavelengths occurred on heating the fluorophor from 20 to 100°C. On the other hand, it can be seen from the intensity values in Table 2 that changes of 20–25 per cent occurred in the relative intensities of the samarium (III) bands on heating the fluorophor from 20°C to 100°C.

Table 1. Locations of the samarium (III) bands in the spectrum of the fluorescence of a sample, prepared from a solution containing 1362 μg of samarium, when excited at 20, 60, and 100°C, by 3650 Å radiation as compared with results of other workers

Tomaschek [7]	Bruninghaus [2][a]	Lenard, Schmidt, and Tomaschek [4]	This study	
Wavelength (Å)	Wavelength (Å)	Wavelength (Å)	Wavelength (Å)	Wavenumber (cm^{-1})
—	5311 (*w*)	5300	absent	absent
5549	—	5560	5556 ± 4[c]	17998 ± 26
—	5592 (*w*)	—	5592 ± 0·5	17883 ± 3
5623 (7)[b]	5633 (*s*)	5630	5629 ± 1	17765 ± 6
—	—	—	5677 ± 7[c]	17615 ± 43
5861	5866 (*w*)	5855	5864 ± 2[c]	17593 ± 12
—	5905 (*w*)	5900	5909 ± 4	16923 ± 23
5956 (9)	5964 (*s*)	5950	5955 ± 2	16793 ± 11
6021–6036 (6)	6030 (*s*)	6040	6023 ± 1	16603 ± 5
6072	—	—	absent	absent
—	—	6180–6300	absent	absent
—	—	—	6383 ± 6[c]	15667 ± 29
6397 (2)	—	—	6403 ± 2[c]	15618 ± 10
6432 (7)	6435 (*vs*)	6425	6427 ± 1	15559 ± 5
6457 (6)	—	—	6454 ± 4[c]	15494 ± 19
6479 (3)	—	—	absent	absent
6504 (1)	—	—	6505 ± 7[c]	15373 ± 33
6541	—	—	absent	absent

[a] Cathode-ray excitation.
[b] In this column, numbers in parentheses are Tomaschek's estimates of relative line intensity. The most intense line is (9), while the weakest lines have no numbers.
[c] Very poorly defined in this drawing and generally so weak as to be doubtful.

Table 2. Average relative intensities and percentage change with temperature of analytically useful samarium (III) bands in a sample prepared from 5 ml of solution containing 1362 μg of samarium

Wavelength (Å)	Recorded relative intensity (Average for 3 temperatures)	Corrected averages[a]	Change, per cent	
			20–60[b]	60–100[c]
5629	603	618·0	−13·4	−9·4
5955	1000[d]	1410·0	−11·0	−10·2
6023	676	1178·0	−16·3	−10·8
6427	143	747·0	−4·2	−20·4

[a] Corrected by comparison against responses obtained using a standard lamp [10].
[b] Relative to intensity at 20°C.
[c] Relative to intensity at 60°C.
[d] Arbitrary standard.

VOL. 9 1957

Assuming a linear relationship between intensity of fluorescence and concentration of samarium, the intensity of the 5955 Å band indicated the lower limit of detection to be about 25 μg of samarium (III) in the solution of sample. (A limit slightly under 15 μg of samarium (III) was found in later studies.) Since this limit was considered to be much too high for the desired analytical purposes, no further work was done with this fluorophor.

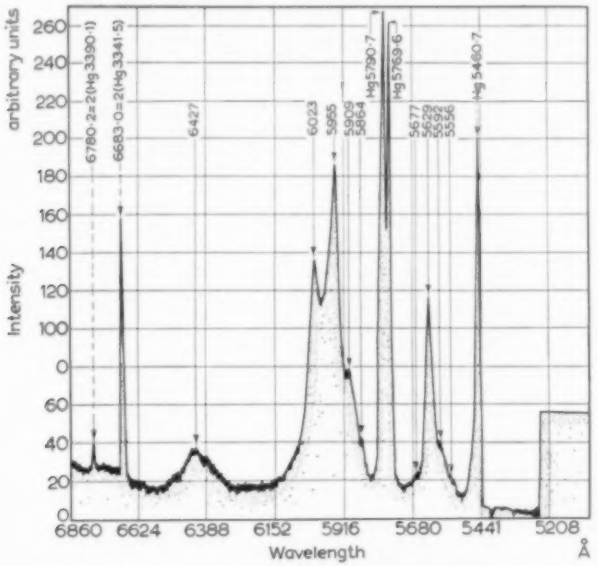

Fig. 1. Spectrum of calcium sulphate containing 1363 μg of samarium (III) under 3650 Å excitation at 20°C.

$CaSO_4$—Sm (II, III)

When a sample of calcium sulphate containing samarium (III) was subjected to 3 MeV electrons produced by a pressure-insulated Van de Graaff electrostatic accelerator [11], a fluorophor was formed which contained a mixture of samarium (III) and samarium (II). It exhibited weak fluorescence under 2536 Å radiation, intense fluorescence under 3650 Å, and, in certain samples, a weak phosphorescence.

Phosphorescence produced by electron bombardment. An orange-yellow phosphorescence that looked to the eye very much like the fluorescence excited by 2536Å was produced by bombardment with certain electron dosages. The decay of this phosphorescence in several of these phosphors was measured at 20°C with the fluorophotometer. Two fluorophors, prepared by precipitation from a solution containing 155 μg of samarium (III) followed by bombardment with 5×10^6 rep,* showed a phosphorescence having exponential decay. The half-life was calculated to be 92 and 93 min, respectively, while $7{\cdot}5 \times 10^{-3}$ min^{-1} was obtained in each case for alpha, the decay constant. As one might expect from the nature of

* Roentgen equivalent physical, or rep, is a term used to describe the power absorbed by the sample. One rep is equal to 83 erg/g of tissue. (The major application of the accelerator is to clinical work.) On the basis of the ionization produced in aluminium. Trump *et al.* [11] determined 10^6 rep to be equivalent to $1{\cdot}99 \times 10^6$ electrons/cm^2.

the decay, the phosphorescence was insensitive to changes in temperature, no visible change occurring on heating the sample to 100°C. The intensity of the phosphorescence, as measured with the fluorophotometer, without the use of ultra-violet radiation, was the same 30 min after electron bombardment as the fluorescence of samples prepared from solutions which contained 1·5 μg of samarium (III) and had been subjected to electron bombardments of $7{\cdot}0 \times 10^6$ rep. However, it is important to note that three other samples prepared under presumably identical conditions exhibited no detectable phosphorescence, whereas another sample, which contained 900 μg, did phosphoresce. Hence the conditions leading to phosphorescence have not been carefully defined by these few experiments.

At an intermediate level of 15·0 μg a sample bombarded with 5×10^6 rep showed a phosphorescence decay curve suggestive of power-law decay which could be resolved into two components. The short-lived component had a half-life of 16 min and a value of 43×10^{-3} min^{-1} for alpha; the long-lived component, a half-life of 124 min and a value of $5{\cdot}6 \times 10^{-3}$ min^{-1} for alpha. Since the decay curves were the same as those observed below for samarium samples containing europium, the possibility that this phosphorescence arose from europium contamination was considered. However, attempts to confirm the presence of europium by recording the spectrum were not successful because of the low intensity of the phosphorescence.

It should be noted that phosphorescence was absent when sufficiently low concentrations of samarium were present. Thus no phosphorescence was ever observed in samples precipitated from solutions containing 1·50 μg or less of samarium (III). One can only conclude that the phosphorescence was probably too weak to be detected if it was present.

A brief examination was made of the effect of the presence of different amounts of europium on the phosphorescence obtained from 15·0 μg of samarium upon irradiation with $5{\cdot}0 \times 10^6$ rep when europium in amounts of 0·0, 0·015, 0·15, 1·50, 15·0, and 150 μg were present in the sample solutions. The first five samples showed phosphorescence decay curves like those just described. The first four had the same decay constant: a half-life for the short-lived component of 22 min, and for the long-lived component 128 min. The fifth sample was only slightly different, the shorter half-life being 28 min. In the sixth sample no phosphorescence could be observed. That concentration of europium was sufficient, not only to quench the phosphorescence, but, as will be shown later, to affect gravely the fluorescence as well.

Finally, an observation which could profitably be explored in future studies, was the effect of ultra-violet radiation on the phosphorescence. After electron bombardment, one of the fluorophors, prepared from the solution containing 15 μg of samarium (III) and 15 μg of europium (III), was irradiated with 2536 Å and then 3650 Å and the respective fluorescence spectra recorded; then it was included with the other fluorophors in the measurements of the decay of phosphorescence. For each of the eight measurements taken in obtaining a decay curve, the intensity of the phosphorescence of this sample was half that of the other fluorophors, which had not been exposed to both 2536 Å and 3650 Å excitation, probably as a result of photoquenching [14]. No attempt was made to determine the relative efficiencies of 2536 Å and 3650 Å in quenching this phosphorescence.

VOL. 9 1957

Excitation of fluorescence by 2536 Å. The spectrum of the fluorescence excited in a previously bombarded sample by this radiation consisted of a continuum, which started at 5575 Å, peaked at 6157 Å, and ended at 6792 Å. The intensity of this fluorescence was too weak for analytical use. Basing an estimate on the spectra of four samples containing 15·0 μg of samarium each, the lower limit of detection was 5 μg. In view of this relatively low sensitivity, no further observations were made using 2536-Å excitation.

Excitation of fluorescence by 3650 Å. Fig. 2 shows the spectrum of the fluorescence of a sample containing 155 μg of samarium. The spectrum of the fluorescence

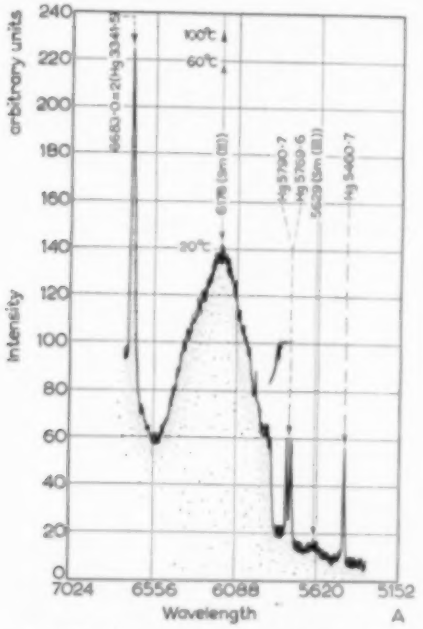

Fig. 2. Spectrum, under 3650 Å excitation, of calcium sulphate containing 155 μg o samarium. The sample had been ignited at 700°C for 10 min and exposed to $7{\cdot}0 \times 10^6$ rep before being measured at 20°C, 60°C, and 100°C.

consisted of a featureless, triangular-shaped band, lying between 5790 Å and 6683 Å, with a maximum at 6178 $\pm$ 4 Å (average of measurements on twenty-one spectra) for amounts from 1·5 to 155 μg of samarium and for fluorophor temperatures of 20°, 60°, and 100°C. Consequently, it can be concluded that no shift of band maximum occurred over these ranges of concentration and temperature.

Fig. 2 also shows that band intensity was dependent upon temperature, having been increased by 76 per cent on heating to 60°C, and another 6 per cent on further heating to 100°C. Cooling to −15°C eliminated the band.

The 5629 Å band of samarium (III) can still be seen in Fig. 2, showing that the reduction of samarium (III) to the divalent state was far from complete. A measurable 5629 Å band was also observed in the spectrum of a sample containing

15 μg Sm (II, III) which had been subjected to the maximum electron bombardment of $7{\cdot}6 \times 10^{-6}$ rep. As one would expect from the incompleteness of the reduction of samarium (III), the intensity of the fluorescence increased with the dosage of the electrons and, in the range from $5{\cdot}0 \times 10^6$ to $7{\cdot}0 \times 10^6$ rep, was proportional to the intensity of the electron bombardment.

Quantitative studies. Before attempting to set up a series of calibration curves, a study was made of the precipitation of the calcium sulphate under a variety of conditions. In each case the solution contained 1·5 μg of samarium and the solution containing calcium was the precipitant. Intensity measurements were made with the filter photometer except for the data on ignition temperature shown in Table 3.

Table 3. Effect of temperature of ignition on intensity of fluorescence at 6178 Å of 1·50 μg of samarium

Temperature of ignition (°C)	Intensity of fluorescence
500	314
600	265
700	360
800	356
900	100
1000	70
1100	19

Except where the effect of variations in the conditions were being studied, the preparative conditions were as follows: total volume of sample, 10 ml; temperature of sample just before precipitation, 80°C; concentration of potassium sulphate in the sample, 10 per cent by weight; temperature and time of ignition of the calcium sulphate, 800°C and 10 min; electron dosage, $7{\cdot}0 \times 10^6$ rep. Except where the solution volume was 50 ml or where the solution temperature was 20°C, the weight of calcium sulphate that precipitated was very close to 0·100 g, the amount one would obtain if the amount of dissolved calcium sulphate were negligible. The results of a study of variations in the conditions are outlined below.

1. Fluorophors precipitated from volumes of 5, 10, and 20 ml showed no significant differences in intensity of fluorescence. In the case of a 50-ml solution, barely enough calcium sulphate was recovered to cover the bottom of a platinum dish, but the intensity of the fluorescence was 17 per cent higher than that of fluorophors precipitated from the other three volumes.

2. Fluorophors precipitated at 90°C had a fluorescence intensity 16 per cent greater than those precipitated at 80°C, while precipitation at 75°C produced no significant difference. At 20°C, insufficient calcium sulphate was recovered to permit measurement of the fluorescence.

3. A fluorophor precipitated from 8 per cent potassium sulphate was 36 per cent less intense than samples precipitated from 9 per cent potassium sulphate, while a sample precipitated from solutions saturated with potassium sulphate was slightly more fluorescent (4·5) than the latter.

VOL. 9 1957

4. No difference was observed in the intensities of fluorescence of three fluorophors precipitated in solutions containing amounts of calcium ion equivalent to 0·050, 0·100, and 0·150 g of calcium sulphate.

5. Table 3 shows that the fluorophors ignited at 700° and 800°C exhibited the most intense fluorescence. There was no significant change in intensity when the ignition time was extended from 10 to 60 min at 800°C.

The above experiments were performed not as a means of explaining the mechanics of the precipitation process but only to ascertain the limits of variability which could be tolerated. The results indicated that variations of 5 per cent or less in the results might be anticipated by working in the ranges of 5–20 ml for sample volume, 75–80°C at the time of precipitation using 9–10 per cent potassium sulphate in the sample, and 700–800°C for ignition for a period from 10–60 min. Hence, no variable appears to require exceptional care in its adjustment.

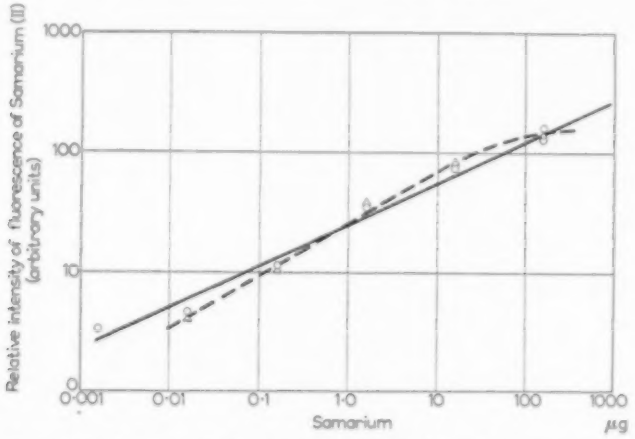

Fig. 3. Relationships between the intensity of the 6178 Å band of samarium (II) excited by 3650 Å and the amount of samarium (III) in the original solution. Samples were ignited at 700°C for 10 min and bombarded with $7{\cdot}0 \times 10^6$ rep.
○ Samples at 60°C measured on the spectrometer.
△ Samples at 20°C measured on the fluorophotometer.

Measurements of the intensity, using the spectrograph, of the 6178 Å peak of samarium (II) in the spectra of six samples covering the concentration range, 0·00155–155 μg samarium (II, III), gave a satisfactorily linear relationship between intensity of samarium (II) fluorescence and the amount of samarium (III) initially present in the sample solution (Fig. 3). However, when five of these same samples were measured on the fluorophotometer,* a less satisfactory curve, also shown in Fig. 3, was obtained. The exact cause was not ascertained, but it probably was due to a combination of factors including differences in the spectral sensitivities of the receivers and the monochromaticity of the energy striking the respective receivers. The lower limit of detection was calculated to be 0·0010 μg of samarium (III) in

* The 0·00155 μg sample was used as blank in this series of measurements, the original blank having been lost. However, the magnitude of the deflection for the 0·0155 μg sample indicated that a measureable deflection would have been obtained for the 0·0015 μg sample.

the original solution, when the fluorophor was measured by the spectrograph at a temperature of 60°C, or by the fluorophotometer at 20°C.

Table 4. Intensities of fluorescence of three sets of fluorophors precipitated from solutions containing 1·5 μg of samarium (III), bombarded with 3 MeV electrons and measured with the fluorophotometer

Set 1	Set 2	Set 3
7·0 × 10^6 rep	7·0 × 10^6 rep	5·0 × 10^6 rep
542	486	546
552	536	534[a]
576	542	538[b]
584	522	538[c]
	532	550[d]
	493	
564 ± 30[e]	518 ± 22	541 ± 8

[a] Sample solution also contained 0·015 μg of europium (III).
[b] Sample solution also contained 0·15 μg of europium (III).
[c] Sample solution also contained 1·5 μg of europium (III).
[d] Sample solution also contained 15 μg of europium (III).
[e] The uncertainty in each case is the standard deviation, calculated by the method of Dean and Dixon [13].

The precision obtained in the measurement with the fluorophotometer of three sets of fluorophors is shown in Table 4. These sets were prepared at different times from the same stock solutions. In each case the preparative conditions were the "standard" ones listed above, except that the electron bombardment was varied and, in one set (No. 3), varying amounts of europium (III) were present. All of the samples comprising one set were subjected to electron bombardment at the same time. The reproducibility of intensity within one set of samples varied from the standard deviation of 1·5 per cent for set No. 3 to 5·3 per cent for set No. 1. These intensity differences within a given set of samples are attributed primarily to the inability to reproduce exactly the macroscopic area of the sample by pressing it into the platinum dish with a test-tube, because the variability could be decreased, at some sacrifice of sensitivity, by restricting the area viewed by the photomultiplier so that the sample filled the entire area. Two other factors might also be involved. One is the inability to reproduce a microscopically uniform surface with the pressing technique. The other is the reproducibility of co-precipitation. Neither of these factors was isolated for evaluation.

It can be seen from Table 4 that the agreement between intensities of two sets of samples subjected to nominally the same electron dosages was poorer than the agreement within sets. This would appear to indicate that variations were occurring in the electron dosage actually obtained for a given setting of the Van de Graaff generator. Hence the need for bombarding simultaneously both standards and samples if the best possible precision is desired.

The effects upon the fluorescence of adding some extraneous elements to the solution of potassium sulphate before addition of 15·0 μg of samarium were also

VOL. 9 1957

explored briefly. Where precipitation occurred on addition of the extraneous element, the precipitate was not removed prior to precipitation of the calcium sulphate. The results in Table 5 showed that concentrations of lanthanum (III)

Table 5. Effect of different concentrations of some extraneous ions upon the intensity of fluorescence at 6178 Å of a sample containing 15·0 μg of samarium

Extraneous element	Concentration of extraneous element in sample solution (μg/ml)	Percentage of fluorescent intensity of sample containing 15·0 μg of samarium only[b]
None	Zero	100
La (III)	1400[a]	4·1
	140[a]	17
Ce (VI)	140[a]	113
	14	60
Ce (III)	1400[a]	28
	140[a]	16
Nd (III)	13·0	95
	1·3	101
	0·13	98
Eu (III)	21·4	92, 108
	2·1	102
	$2{\cdot}1 \times 10^{-1}$	100
	$2{\cdot}1 \times 10^{-2}$	100
	$2{\cdot}1 \times 10^{-3}$	99
Gd (III)	13·0	95
	1·3	96
	$1{\cdot}3 \times 10^{-1}$	100
Fe (III)	558	115
Co (II)	589	100
Ni (II)	587	100

[a] Precipitation occurred before formation of the calcium sulphate.
[b] The intensity of fluorescence of two fluorophors containing only 15·0 μg of samarium was 312 and 319 (arbitrary units).

and cerium (III), in approximately 100-fold excess, seriously quenched the samarium fluorescence. One would expect this behaviour to be typical of that for other trivalent rare earths. Neodymium (III), gadolinium (III), and europium (III), in about tenfold excess, showed virtually no interference, a result which one would again hope was typical of trivalent rare earths. Cerium (IV) was anomalous, the larger excess giving an increase, but the smaller a severe decrease in intensity. No detailed study was made of this effect. Table 5 also shows that 0·01 M cobalt (II) and nickel (II), both of which are often effective quenchers [12], were without effect, while 0·01 M iron (III) produced slight positive interference. The last finding is not in serious disagreement with MERKADER [5], who reported no interference from iron.

$CaSO_4Eu$ (II, III)

During the course of the interference studies it became evident that the procedure used for samarium was also quite sensitive for europium. Hence, a

number of runs were made using europium alone and effecting reduction by means of 3 MeV electrons from a Van de Graaff accelerator. Once again, the concentrations have been stated on the assumption that complete precipitation of the trivalent rare earth occurred.

Table 6. Average relative intensities of the europium bands in the spectra of four samples of europium (II, III) excited at 20°C with 2536 Å radiation

Wavelength[a] (Å)	Relative intensity at 20°C	Corrected average intensity at 20°C	Decrease on heating to 60°C (per cent)
2848 ± 6[b]	1000[c]	5220	12·2
5894 ± 3	391 ± 40	485	8·8
5918 ± 2	370 ± 31	476	13·0
5947 ± 3	293 ± 35	403	21·9
6126 ± 3	79·0 ± 9·5	170	8·3
6151 ± 1	396 ± 45	925	9·5
6170 ± 1	130 ± 12	308	5·9
6200 ± 3	370 ± 28	998	14·0
6950	49 ± 14[d]	1190	
7018	12[e]	314	

The effect of heating the samples to 60°C is also shown.
[a] Averages of ten spectra at 20°C and 60°C.
[b] Only band attributed to Eu (II).
[c] Arbitrary standard.
[d] Average of only two samples.
[e] Single sample.

VOL. 9 1957

Excitation by 2536 Å. In contrast to the weak continuum produced in the samarium (II, III) fluorophor by 2536 Å excitation, the europium (II, III) fluorophor gave a spectrum containing ten bands, most of them well defined, as shown in Fig. 4. The wavelength values listed in Table 6 were made at 20 and 60°C and represent the averages of ten spectra for samples of calcium sulphate containing 905, 90·5, 15·0, and 9·0 μg of europium (II, III). Nine of the bands are remarkably narrow and line-like, probably because they involve internal 4*f*-transitions protected from the crystal environment. The relatively broad tenth band at 3848 Å is probably due to a transition involving an external level which would be subject to perturbation by the crystal environment [9]. The 3848 Å band was therefore attributed to divalent europium; the other nine bands to trivalent europium. No significant shifts of wavelength occurred in europium (II, III) bands over this range of concentration. Moreover, there was apparently no change in wavelength produced by samarium, because the sample containing 15·0 μg of europium (II, III) also contained 15·0 μg of samarium (II, III). Its spectrum differed from the others only by the presence of an additional band, a weak one at 6891 Å.

The average relative intensities at 20°C of the europium bands of four samples, containing 9·0, 90·5, and 905·0 (two samples) μg of europium (II, III) respectively, are given in the same table. It can be seen that no significant change of relative intensity of the bands occurred over this concentration range. However, when one of the samples containing 905 μg of europium was heated to 60°C, the intensity of each of the bands decreased.

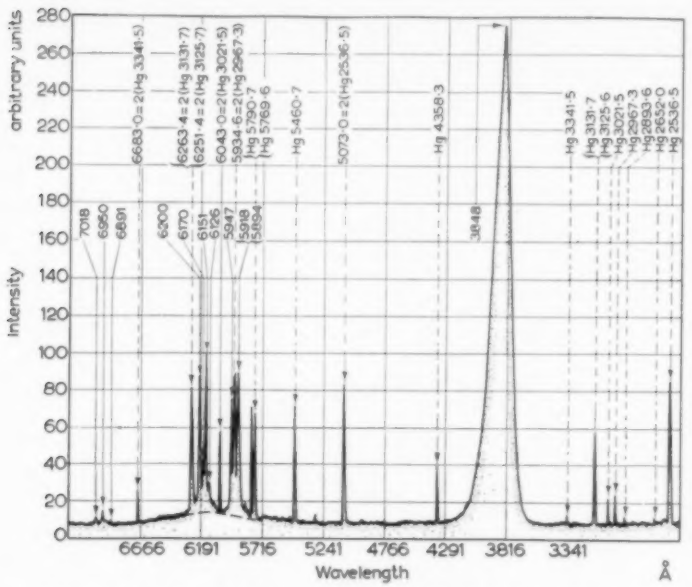

Fig. 4. Spectrum of calcium sulphate containing 150 μg of europium (II, III) and 15 μg of samarium (II, III) under 2536 Å excitation at 20°C.

In view of the fact that bands for both divalent and trivalent europium were present in irradiated samples, it was of interest to compare qualitatively the relative merits of each for determining europium using the limited amount of data available. The relationship between the intensity of the europium (II) band and the amount of europium (III) initially present in 7 ml of sample solution is recorded in Fig. 5. On the basis of the spectrum of the fluorophor prepared in a solution

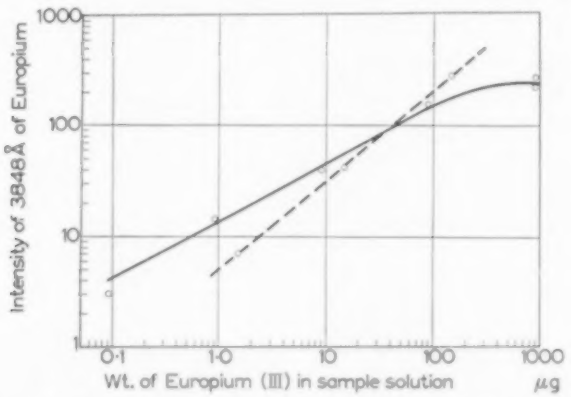

Fig. 5. Relation between the intensity of the europium band at 3848 Å and the amount of europium in the sample solution (2536 Å excitation at 20°C). $7{\cdot}0 \times 10^6$ rep, 700°C for 10 min.
— — — Fluorophors prepared in solutions containing only europium (III).
——— Fluorophors prepared in solutions containing 15·0 μg samarium (III) in addition to europium (III).

containing 0·090 μg of europium (III), the lower limit of detection for the 3848 Å band of europium (II) was estimated to be 0·060 μg of europium (III) in the original solution. The relationship between the intensities of the 5894, 5918, 6151, and 6200 Å bands of europium (III) and the weight of europium (III) in the sample solution are shown in Fig. 6. Judging from the spectrum of the sample prepared in a solution containing 0·90 μg of europium (III), the lower limit of detection to be obtained using these europium (III) bands was about 0·45 μg of europium (III) in the sample solution. Unfortunately, the data concerning precision cannot be stated, because duplicates were prepared only for one set of solutions containing 905 μg of europium (III).

Upon adding 15·0 μg of samarium (III) to samples containing different quantities of europium (III), it was found that no europium bands could be seen in the spectrum of the sample which contained the smallest europium concentration, 0·15 μg of europium (II, III). The results obtained for the other three fluorophors are also plotted in Fig. 6 so that the data for samples, with and without samarium, can be compared.

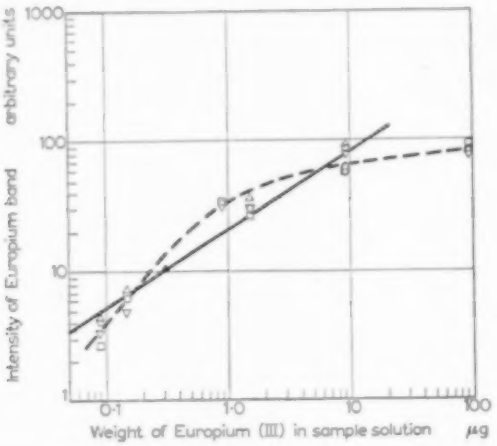

Fig. 6. Relation between the intensities of four europium bands and the amount of europium in the sample solution (2536 Å excitation at 20°C).

○ 5894 Å
▽ 5918 Å
△ 6151 Å
□ 6200 Å

— — — Fluorophors prepared in solutions containing only europium (III).
——— Fluorophors prepared in solutions containing 15·0 g samarium (III) in addition to europium (III).

The lower limit of detection in the presence of samarium (II, III) was the same for both the supposed europium (II) band and the four europium (III) bands listed above: namely, 0·50 μg of europium (II, III). For the 3848 Å band of europium (II), this represented a decrease in sensitivity of approximately eight times that achieved in the absence of samarium (II, III); whereas the sensitivity of the europium (III) bands was not significantly affected by the presence of the samarium (II, III).

VOL. 9 1957

The continuum which was described earlier as being characteristic of the fluorescence of samarium (II, III) under 2536 Å excitation was present in all of these fluorophors. In addition, the yellow phosphorescence described earlier was also present in most of the samples.

Excitation by 3650 Å. The spectrum of europium (III) excited by 3650 Å was recorded over the wavelength interval, 5460–6683 Å.* It contained the same seven wavelengths listed for this interval in Table 6 as wavelengths excited by 2536 Å. In addition, it contained one more band located at 5932 Å. The table also lists two longer wavelengths that were found after the study of the effect of heating had been completed. The relative intensities of the bands were the same as those excited by 2536 Å, but heating to 60°C produced a uniform decrease of 7·2 ± 3·0 per cent in all bands. A further decrease in intensity of 15·1 ± 3·7 per cent, relative to intensity at 20°C, was obtained on heating to 100°C.

The spectra obtained for the two fluorophors containing 905 and 90·5 μg of europium (II, III), respectively, permitted estimation of the lower limit of detection by the spectrograph to be about 20 μg of europium (III) in the sample solution. The lower limit of sensitivity obtained with the fluorophotometer, based upon the measurement of five fluorophors, was about 10 μg of europium (III) in the sample solution. This represents reasonably good agreement between the instruments.

Discussion

From an analytical point of view, the significant differences between the samarium (II, III) and the europium (II, III) fluorophors were as follows. Irradiation with 2536 Å excited no fluorescence due to samarium (III), only a weak continuum due to samarium (II), but a relatively intense fluorescence due probably

Table 7. Estimated lower limits of detection in terms of micrograms of samarium (III) or europium (III) in the original solution

Fluorescence measured	Excitation	
	2536 Å	3650 Å
Samarium (II)	5	0·0010
Samarium (III)	N.F.	15
Europium (II)	0·060	N.D.
Europium (III)	0·45	20

N.F.—not fluorescent.
N.D.—not determined because of interference from mercury lines.

to both europium (II) and europium (III). On the other hand, 3650 Å excited relatively weak fluorescence from samarium (III) and europium (III), but relatively intense fluorescence from samarium (II). The estimated lower limits of detection for samarium (II) and (III) and europium (II) and (III) are summarized in Table 7. Because the relative intensities of the two exciting wavelengths were

* The 3848 Å band of europium was not measured, because the presence of many highly intense lines in the spectrum of the AH-4 lamp on the high wavelength side of Hg 3650 Å precluded measurement of that band.

not determined, comparisons should, in the strict sense, be limited to the same excitation wavelength. However, these data do emphasize the advantages of using 2536 Å to excite europium (II), and 3650 Å to excite samarium (II). Thus determinations of both samarium and europium in a mixture should be possible using either a spectrograph or a filter fluorophotometer, providing that two sources of excitation were employed. Measurement of the intensity of the 3848 Å band of europium (II) excited by 2536 Å would permit determination of the original europium (III) content of the sample from which the fluorophor had been prepared. Then excitation with 3650 Å and measurement of the intensity of the 6178 Å band of samarium (II) would yield the samarium (III) content. Previous measurement of europium should permit correction for the contribution of europium (III) fluorescence to the intensity of the samarium (II) band. Measurement of the samarium (II) fluorescence should be made at 60°C to increase the intensity of samarium (II) fluorescence while decreasing that of europium (III) (and, incidentally, that for samarium (III) and europium (II) as well). In view of the fact that the effect of europium (II, III) upon the intensity of fluorescence of samarium (II) was considerably less than the effect of samarium (II, III) upon the intensity of fluorescence of europium (II, III), the use of the proposed method would be more suitable for the determination of samarium in the presence of small to moderate amounts of europium than for the reverse situation.

Acknowledgements—The authors are indebted to Professor R. C. Lord for the use of his recording spectrograph and to Professor J. G. Trump, of the Department of Electrical Engineering, for his permission to have samples bombarded by the Van de Graaff accelerator. The authors wish to thank Messrs. K. A. Wright and J. A. Anson for their co-operation in making the bombardments.

The authors wish to acknowledge joint sponsorship of this study by the Office of Naval Research and the Atomic Energy Commission.

VOL. 9 1957

References

[1] Peattie C. G. and Rogers L. B. *Spectrochim Acta* 1956 **7** 321.
[2] Bruninghaus L. *Ann. Chim.* (*Phys.*) 1910 **21** (8) 210, 519.
[3] Karlik B. and Przibram K. *S.B. Akad. Wiss. Wien.* 1937 **146** (IIa) 209.
[4] Lenard P., Schmidt F., and Tomaschek R. *Handb. Exp. Physik.* 1928 **23** 468.
[5] Merkader S. *S.B. Akad. Wiss. Wien.* 1940 **149** (IIa) 349.
[6] Tomaschek R. *Ann. Phys.* 1924 **75** 109.
[7] Tomaschek R. *Ibid.* 1927 **84** 329.
[8] Urbain G. *Ann. Chim.* (*Phys.*) 1909 **18** (8) 229.
[9] Butement F. D. S. *Trans. Faraday Soc.* 1948 **44** 617.
[10] Sangster R. C. and Irvine J. W. *J. Chem. Phys.* 1956 **24** (4) 670.
[11] Trump J. G., Wright K. A., and Clarke A. M. *J. Appl. Phys.* 1950 **21** 345.
[12] Kröger F. A. *Some Aspects of the Luminescence of Solids* Elsevier Publication, New York, 1948.
[13] Dean R. B. and Dixon W. J. *Anal. Chem.* 1951 **23** 636.
[14] Levevenz H. W. *Introduction to the Luminescence of Solids* John Wiley, New York, 1950.

Spectrochimica Acta, 1957, Vol. 9, pp. 323 to 331. Pergamon Press Ltd., London

A statistical study on the homogeneity of zinc-base spectrographic standards

ROBERT C. FRANK, JAMES E. DALLEMAND, and DAVID L. FRY
Research Staff, General Motors Corporation, Detroit, Michigan

(*Received* 28 *January* 1957)

Abstract—A lack of good zinc-base spectrographic standards from commercial sources prompted a co-operative programme between the General Motors Corporation and the National Bureau of Standards to attempt to cast six good heats of these standards.

A homogeneity study of the six heats is presented. A large number of spectrographic determinations were made using a direct-reading spectrograph and following a predetermined pattern. The results were then evaluated using a three-variable analysis of variance which indicated whether there was significant inhomogeneity of the minor constituents of the alloys. When the inhomogeneity was significant, the Duncan [1, 2] test was used to find homogeneous regions in the standards material which can be used satisfactorily.

Introduction

IT is a common practice when performing a quantitative analysis with an emission spectrograph to calibrate the spectrograph and the plates by using standards which contain known concentrations of the element concerned. One usually assumes that the concentration of the element is uniform throughout the standards material and by sampling a small portion of the standard material the specified concentration is the correct one. In the case of liquid standards this assumption is usually correct, but when the standards are in the form of solid chunks of metal the assumption may be rather poor. This is true because it is often very difficult to mix a number of molten metals into an alloy and keep them uniformly distributed until the entire mass has solidified. This inhomogeneity of the standards essentially puts a limit on the accuracy of spectrographic results which one can hope to obtain. A complete check of the homogeneity of a set of standards would require making determinations all over the surface and all through every standard. Since the standards material would then be all used up, the obviously more satisfactory procedure would be to make several determinations on several well chosen standards and make statistical inferences about the remainder. The more determinations one can make, the more sound will be the inferences.

In this study six heats of zinc-base spectrographic standards were cast through a co-operative programme between the General Motors Corporation and the National Bureau of Standards. Each heat was continuously cast in the form of about 100 consecutive square bars which were $1\frac{3}{4}$ in. on a side and about 40 in. long. Each of the six alloys contained eleven other elements besides the primary constituent, zinc. These elements and the approximate amount of each are listed in Table 3. In order to use the material for spectrographic standards it is intended that the bars be cut up into segments $\frac{1}{2}$ in. thick. More accurate values of the concentrations will be, of course, obtained by chemical certification.

The sampling for the lineal homogeneity study was made by choosing five $\frac{1}{2}$ in. segments each cut from one of the one hundred bars. These five segments were chosen from five different parts of the heat, i.e. one each was chosen from among the first and last bars of the heat and the other three from among the middle bars. Previous work on this type of casting led us to suspect that the concentration might be different in the end bars than it was in the centre bars. The bars were cast one after the other. Some elements have a tendency to precipitate out of the melt over a period of time, thus changing the concentration in bars cast at different times. The sampling for the transverse homogeneity study was made by making spectrographic analyses across the face of each of the segments. The analysis pattern for this study was suggested by ROBERT MICHAELIS of the National Bureau of Standards and is shown in Fig. 1.* The positions are well selected in

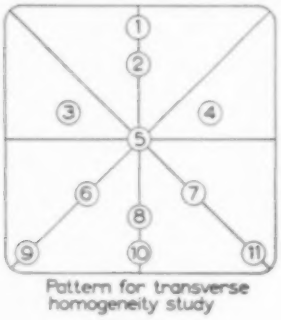

Fig. 1.

that it is expected that a composition pattern would reveal itself by changes at the centre, on the diagonals, or at the edges of the segment. The positions are always referred to by using the numbers shown in Fig. 1. Position 5 is in the centre. Positions 2, 3, 4, 6, 7, and 8 are on a circle with a $\frac{1}{2}$ in. radius. 6, 7, 9, and 11 lie on the diagonals and 3 and 4 half-way between the diagonal and the perpendicular bisectors of the edges. 1, 9, 10, and 11 lie $\frac{1}{8}$ in. from the edges.

Spectrographic conditions

The spectrographic analyses were made with an Applied Research Laboratories quantometer [3]. It is important in this type of homogeneity study to specify the source conditions, because the statistical tests used are essentially comparison tests in which the various effects are compared with the error of the method. The multisource [4], was used for all elements except aluminium and copper, and the high-voltage source was used for aluminium and copper. The source conditions are:

Multi-source:

40 μF, 430 μH, 50 ohms, 980 V
Sample negative
Volume of metal volatilized : 91×10^{-6} in^3

* Private communication.

VOL. 9 1957

High-voltage spark:

0·0075 μF, residual inductance for aluminium, 25 μH for copper
Residual resistance
8 R.F. amperes. 16,240 V
2 brk/half-cycle, unidirectional
Sample negative
Volume of metal volatilized: $1{\cdot}9 \times 10^{-6}$ in^3

Pre-burn: 20 sec. Exposure: 20 sec
Analytical gap: 3 mm. Counter electrode : $\frac{1}{4}$ in. graphite, 120° cone
Sample preparation: lathe with last cut 0·002 in. or less
Zinc internal standard line used

Using the multi-source conditions, eleven analyses were made on the face of each segment and each time the quantometer analysed for magnesium, lead, tin, cadium, iron, manganese, nickel, silicon, and chromium. After analysing the five segments for each heat, they were re-surfaced and analysed again in exactly the same positions; this was done in order to measure an effect which was chosen to be called the time effect. It was essentially a measure of the consistency of the quantometer over a period of time. The whole test was repeated again, using the high-voltage spark and analysing for aluminium, using residual inductance and then again for copper using 25 μH of inductance.

Statistical methods

The data for each of the eleven elements in each of the six heats had to be processed separately, so the analysis of variance was performed sixty-six times, once for each of the elements in the six heats. For the sake of expediency, we have coined the term heat-element to refer to any element in a given heat. A separate data sheet and a separate analysis of variance was made for each of the sixty-six heat elements. The data sheets were of the form shown in Table 1. The heads of the columns designate the heat and segment number and the rows are designated by the position numbers. The two numbers grouped together are the two analyses made in the same position but at different times. On each data sheet there were eleven rows each containing ten numbers, and these rows were used to measure the transverse homogeneity. There were five columns, each containing twenty-two numbers, and these were used to measure the lineal homogeneity. For the time effect, there were two sets of fifty-five numbers.

The first step in analysing the data was to obtain the means of the rows and of the columns. This gave us an estimate of the difference between the various positions and also between the various segments. In general, the difference between the segments was not too evident by simply looking at these means. However, in looking over the means of the rows, it appeared that in a large number of heat-elements the number 5 (centre) position had either the highest (Fe, Si, Mn, Ni, Cr) or lowest (Cd, Pb, Mg) concentration of the eleven positions. This occurred in so many cases and the concentrations for the number 5 position varied from the others by such a large margin that it was felt that the data for the number 5 position

should be removed before proceeding any further. In a casting of this type the centre of the bar cools slower than the outside edges and as a result some of the constituents tend to migrate either into or away from the centre, thus changing the concentrations. We, therefore, felt justified in removing the data for the number 5 position.

Table 1. Typical data sheet

Position	A-1		A-5		A-20		A-50		A-85	
1	0·076	0·067	0·069	0·066	0·073	0·070	0·073	0·063	0·070	0·069
2	0·071	0·066	0·071	0·062	0·069	0·068	0·075	0·069	0·066	0·064
3	0·070	0·065	0·068	0·066	0·068	0·066	0·069	0·067	0·068	0·063
4	0·067	0·066	0·071	0·066	0·069	0·067	0·072	0·068	0·068	0·064
5*	0·060	0·059	0·060	0·060	0·065	0·061	0·061	0·060	0·058	0·055
6	0·071	0·065	0·066	0·065	0·070	0·068	0·069	0·066	0·064	0·067
7	0·065	0·067	0·068	0·066	0·070	0·065	0·069	0·065	0·070	0·065
8	0·067	0·067	0·071	0·067	0·065	0·068	0·072	0·082	0·069	0·064
9	0·071	0·067	0·069	0·067	0·067	0·169	0·063	0·063	0·067	0·064
10	0·066	0·063	0·070	0·065	0·067	0·073	0·069	0·066	0·069	0·068
11	0·068	0·068	0·068	0·068	0·064	0·068	0·069	0·066	0·067	0·069

* Data for position 5 not used in analysis of variance.

The next step in the test was to perform the analysis of variance [5]. The analysis of variance technique is valuable in that it has the property of being able to separate the various effects in such a way that their significance can be tested independently of each other. There are three effects to be tested in this case. These are: transverse segregation, lineal segregation, and the time effect. Transverse segregation is indicated if the concentration means of the various positions on the surface of the segment are found to be significantly different from each other. Lineal segregation is indicated if the concentration means of the five segments are found significantly different from each other. The so-called time effect was not of primary interest in the study, but came as a byproduct of the analysis. A significant difference in the "time means" might be due to an instrument drift. It is probably not caused by the sample.

The mathematical model for the analysis of variance was

$$X_{ijk} = \mu + \rho_i + \nu_j + \tau_k + \pi_{ij} + \varepsilon_{ijk}$$

VOL. 9 1957

where X_{ijk} represents the kth measurement at the ith position on the jth segment.

μ = grand mean of the underlying distribution.

ρ_i = the deviation from the mean due to the effect of position i.

ν_j = the deviation from the mean due to the effect of segment j.

τ_k = the deviation from the mean due to the effect of time k.

π_{ij} = the interaction of the position and segment effect.

ε_{ijk} = a measurement of the error.

In an analysis of variance with three variables such as this, one would normally expect to have two other first-order interactions and a second-order interaction; but in this case, it was assumed that these interactions are zero in the model in order to form an estimate of the error or residual variance which would have a maximum number of degrees of freedom. Physical considerations seemed to make this assumption tenable.

Next, the following assumptions were made:

1. The true situation fits the mathematical model and in particular has the linearity property.

2. The $\sum(\varepsilon_{ijk}) = 0$, which means that the measurements are unbiased.

3. The error of the method is the same for all analyses made for a given heat element.

4. The errors are independently and normally distributed, and therefore also uncorrelated.

5. The three main effects, position, segment, and time, are fixed.

6. $\sum_i \rho_i = 0 \qquad \sum \nu_j = 0 \qquad \sum_k \tau_k = 0$

These assumptions are the ones usually made in an analysis of variance. In some cases where multiple observations are taken under each variable combination

Table 2. Analysis of variance table-fixed model

Source of variation	d/f	(MS)	$E(MS)$
Due to position (rows)	9	$MS(R)$	$\sigma^2 + K_1\phi(R)$
Due to segment (columns)	4	$MS(C)$	$\sigma^2 + K_2\phi(C)$
Due to time	1	$MS(T)$	$\sigma^2 + X_3\phi(T)$
Interaction ($R \times C$)	36	$MS(RC)$	$\sigma^2 + K_4\phi(RC)$
Error	49	$MS(E)$	σ^2

it is a fairly simple matter to check assumption 3 by the use of statistical tests due to BARTLETT and COCHRAN [6]. However, in this study none of the assumptions were easily checked quantitatively. It was felt by the experimenters that the assumptions were justified and the analysis was performed using them. The table for the fixed model of analysis of variance is given in Table 2. The d/f column is, of course, the number of degrees of freedom for each of the effects. The third

column is the calculated mean squares. These are calculated in the usual way. The sums of squares are calculated first, and then these are divided by the number of degrees of freedom to obtain the mean squares. The formulae for calculating the sums of squares are given in most of the textbooks on statistics.* The fourth column contains the expected mean squares which are the values to which the respective mean squares average in the long run (i.e. if the whole experiment were repeated many times).

The four hypotheses to be tested are:

1. $\phi(R) = 0$ There is no difference between the means of the rows.
   Test by calculating

$$F_1 = \frac{MS(R)}{MS(E)}$$

   Reject if $F_1 > F_\alpha(9, 49)$
2. $\phi(C) = 0$. There is no difference between the means of the columns.
   Test by calculating

$$F_2 = \frac{MS(C)}{MS(E)}$$

   Reject if $F_2 > F_\alpha(4, 49)$
3. $\phi(T) = 0$ There is no difference between the means for the two times.
   Test by calculating

$$F_3 = \frac{MS(T)}{MS(E)}$$

   Reject if $F_3 > F_\alpha(1, 49)$
4. $\phi(RC) = 0$ There is no interaction between the rows and columns.
   Test by calculating

$$F_4 = \frac{MS(RC)}{MS(E)}$$

   Reject if $F_4 > F_\alpha(36, 49)$

The $F_\alpha(n_1, n_2)$ is the F number from "Fisher's F Distribution" for the corresponding numbers of degrees of freedom n_1 and n_2. Tables of these numbers are found in most statistical textbooks. α is the significance level. The significance level was chosen to be 5 per cent and it indicates that no more than 5 per cent of the time we will reject the hypothesis when we should have accepted it.

The original data on the data sheets was punched into cards and a programme was prepared for the I.B.M. Card Programmed Calculator. The C.P.C. then performed the analysis of variance for each of the sixty-six heat elements. The results of these analyses are given in Table 3.

If the analysis of variance indicates that the material is inhomogeneous, then one is faced with the problem of determining whether there are homogeneous regions which can be used. In order to solve this problem one must compare the means of the rows or columns to determine if there are several that can be considered equal.

* See for example reference [6].

VOL. 9 1957

This must be done by comparing the means in pairs. There are several statistical tests which allow one to do this but the primary objection to most of them is that the error probability of wrongly rejecting the hypothesis of equality of all the means becomes very high as the number of means involved increases. DUNCAN's test has all of the desirable properties of an F test and yet at the same time allows one to make simultaneous comparisons between a large number of pairs of means in order to determine which are significantly different. It essentially evaluates all possible combinations of means in groups of two or more, testing each group as to both range and internal variation in comparison to their standard error.

Table 3. Results of the spectrographic analysis and of the analysis of variance

		Mg	Pb	Sn	Cd	Fe	Si	Mn	Ni	Cr	Cu	A
A	Significance	*T**	*RT*	*T**	*T**	*RC**	*T**	*C*		*C*	*T*	*C**
	Average	0·0678	0·00246	0·00105	0·000437	0·0321	0·0154	0·0238	0·0120	0·0139	0·0384	3·10
B	Significance	*R**	*C**	*R***T*	*T**		*RC*	*R***C**		*C*		*C***T**
	Average	0·0152	0·00281	0·000564	0·00159	0·105	0·0412	0·0380	0·0484	0·0384	0·0579	3·42
C	Significance	*R**	*R**	*R**						*T*	*T***C**	
	Average	0·0301	0·00782	0·00337	0·00598	0·0258	0·0159	0·00793		0·00266	0·158	3·67
D	Significance	*CT**	*CT**	*C***T**	*R***C**			*R***T**	*RC**	*R**	*CT**	*T**
	Average	0·00788	0·00511	0·00275	0·00389	0·0780	0·00301	0·00566	0·0211	0·00755	0·637	4·57
E	Significance	*R***T**	*R**(*RC*)*	*R***T*		*R*(*RC*)	*R***T**	(*RC*)			*RCT*	*RC*
	Average	0·0909	0·0134	0·0105	0·0131	0·0165	0·0680	0·000696	0·00371	0·000543	1·55	5·25
F	Significance	*R**				*R**	*R*					*C***T**
	Average	0·0317	0·00819	0·00381	0·00619	0·0228	0·0192	0·00564		0·00180	0·987	4·23

Significant interaction.—(*RC*)
Significant transverse segregation.—*R*
Significant longitudinal segregation.—*C*
Significant time effect.—*T*
*Significant at 1 per cent also.

The complete test will not be described here, but a few general remarks are in order concerning the form in which the results appear. In preparation for the test, the means are first ranked using code letters for convenience and to reduce the chance of bias. The largest mean is then at one end of the group and the smallest at the other. Brackets are drawn around the non-significant groups when the test is finished. An example of the bracketing is shown below.

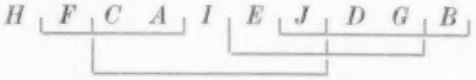

When the test is completed, any two means within a single bracket are not significantly different from each other. Since there are often several brackets, it is

often difficult to decide what to do with this information. In this test it was decided that there were certain positions on the segment which could be removed physically on the lathe or milling machine if they were found to be the chief cause of the inhomogeneity. For instance, the positions 9 and 11 lie on the corners of the segment and the 1 and 10 positions lie on the edge but halfway between the corners. If these were found to be the cause of the inhomogeneity, it was felt that they could be removed by cutting the segment down in a lathe. With this in mind, while looking over the results of the Duncan test, an attempt was made to find as many cases as possible where a bracket included all positions except the 1, 9, 10, and 11 positions. In some cases this was possible and in some cases one of the other positions would have had to be removed also in order to make the sample homogeneous. The Duncan test was also applied to the significant column effects in an attempt to determine which of the segments contributed to the lineal inhomogeneity. In this case it was most desirous to throw out either high or low numbered segments if possible because then either the last few or first few bars of the heat could be thrown away. If the bad ones were in the middle of the heat, one would not know exactly which ones or how many of the bars to throw away.

Results

Now let us consider the results of these two statistical tests. A complete tabulation of the results is given in Tables 3 and 4.

Since the time effect has nothing to do with the homogeneity of the standards, it will not be discussed here.

Interestingly enough, it turned out that there was a position-segment interaction effect in three of the heat-elements at the 5 per cent level. This could possibly mean that the concentration really was varying on the faces of the segments in a manner related to the segment number, or it could also mean that there is some fourth effect taking place which is not known. All three of the heat-elements were in the same heat so it is possible that the interaction is real.

Nineteen of the heat-elements showed a significant column or segment effect at the 5 per cent significance level. The Duncan test was applied to the significant nineteen, and in many cases it was possible to show that cropping the end bars from the heat would improve the homogeneity. However, after looking over the results, it was felt that five segments were probably not a sufficiently large sample to determine exactly where the heat should be cropped and a much more complete test should be made to determine where to crop the heat. For the forty-five heat-elements that showed no lineal segregation no further tests are necessary.

Probably the most important results of these statistical tests apply to the transverse segregation problem. Twenty-three of the heat-elements showed a row or position effect at the 5 per cent significance level. Table 4 is a table of these twenty-three segregated heat-elements. The second column contains the mean concentration of the element in that particular heat. This gives an estimate of the concentration level.

The third column contains the positions which one would like to discard on the basis of the Duncan test results in order to leave a piece of standards material which can be considered reasonably homogeneous. It is readily seen that, except

VOL. 9 1957

Table 4. Twenty-three significant heat elements

	μ	Duncan test discard positions
Al-E	5·25	4, 2, 6
Mg-B	0·0152	9, 11, 1, 10, 3
Mg-C	0·0301	9, 11, 1, 6, 7
Mg-E	0·0909	9, 11
Mg-F	0·0317	9, 11
Fe-A	0·0321	9, 10, 11, 6
Fe-E	0·0165	10, 11
Fe-F	0·0228	9, 11, 6, 7
Pb-A	0·00246	9, 1, 11
Pb-CD	0·00782	9, 1, 11, 10, 4
Pb-E	0·0134	8, 1, 10
Sn-B	0·000564	9, 10, 11, 3
Sn-C	0·00337	1, 10, 7
Sn-E	0·0105	1, 10, 6, 2
Cd-D	0·00389	9, 11, 10, 1, 2
Si-B	0·0412	10, 3
Si-E	0·0680	9, 11, 10, 1, 6
Si-F	0·0192	4, 3
Cr-D	0·00755	9, 11, 10, 1, 3
Ni-D	0·0211	9, 11, 10, 1, 4
Mn-B	0·0380	9, 10, 11
Mn-D	0·00566	9, 11, 1, 10, 6
Cu-E	1·55	9, 11, 1, 10

for a few cases, removal of the edge material, which would include positions 1, 9, 10, and, 11, would not leave the remainder homogeneous. However, we noted when looking at the ranked means that these edge positions were often on the ends of the ranks. One would, therefore, expect that removal of this edge material would at least improve the situation. Regardless of whether any extra material is physically removed, the results of the Duncan test indicate where one ought to spark on the *D* surface of the segment in order to get the most consistent results.

The final judgment of the twenty-three segregated heat-elements will ultimately lie in the hands of the person that uses them. It will depend to a very large extent upon his individual requirements. In cases where accuracy is extremely important, the best possible results can be obtained by confining oneself to a region mid-way between the centre and edges of the segment. As shown by the Duncan test, one is more apt to obtain homogeneous determinations in this region.

References

[1] Duncan D. B. *Virginia J. Sci.* 1951 **2** 171.
[2] Federer W. T. *Experimental Design* pp. 33–40. MacMillan, New York, 1955.
[3] Hasler Maurice F. *Spectrochim. Acta* 1953 **6** 69.
[4] Hasler Maurice F. and Dietert Harry W. *J. Opt. Soc. Amer.* 1943 **33** 218.
[5] Anderson R. L. and Bancroft T. A. *Statistical Theory in Research* McGraw-Hill, New York, 1952.
[6] Dixon W. J. and Massey F. J. *Introduction to Statistical Analysis* McGraw-Hill, New York, 1951.

Spectrochimica Acta, 1957, Vol. 9, pp. 332 to 340. Pergamon Press Ltd., London

The spectrographic determination of the rare earths

J. R. Butler
Imperial College of Science and Technology, London. S.W.7

(*Received* 1 *January* 1957; *in revised form* 6 *May* 1957)

Abstract—A d.c. arc method is described for estimating the rare earths in rare earth oxides separated from minerals. The spectrograph used is a specially constructed glass Littrow prism type with a dispersion of 2·7 Å/mm at 4000 Å; this is adequate for the determination of 15 of the 16 naturally occurring rare earths in oxides poor in Ce and 13 of the rare earths in oxides rich in Ce. The method and lines selected will be of varying use to other workers interested in the geochemistry of the rare earths depending on the spectrograph available.

Introduction

The lanthanons, which have atomic numbers 57–71 inclusive, are a highly interesting group of elements from the geochemical point of view as their chemical properties are so similar. They all produce trivalent ions which are progressively smaller with increasing atomic number between the modest limits of 1·14 Å for La^{+3} ($Z = 57$) and 0·85 Å for Lu^{+3} ($Z = 71$) although Ce^{+4}, Sm^{+2}, Eu^{+2}, Yb^{+2} and the complex oxides Pr_6O_{11} and Tb_4O_7 also exist. Moreover the lanthanons are frequently associated with Yt ($Z = 39$ and radius $Yt^{+3} = 0{\cdot}92$ Å) and occasionally with Sc ($Z = 21$ and radius $Sc^{+3} = 0{\cdot}81$ Å) and a chemical determination of the rare earths (i.e. the lanthanons together with Sc and Yt) presents great difficulties as the solubilities of their salts and derivatives differ so little.

X-ray spectrographic methods have been successfully used for determining the rare earths in minerals and rocks by Goldschmidt and Thomassen [1], Minami [2], and Sahama and Vähätalo [3]; and in post-war years Wylie [4] has been prominent in using a spectrophotometric method for rare-earth analysis of minerals, especially those rich in Ce. Optical spectrographic methods for the estimation of rare-earth impurities in samples artificially enriched with particular rare-earths have been described in recent years ([5,6], and other workers at Oak Ridge National Laboratory) and a useful method for determining Yt, La, Ce, Pr, Nd and Sm in monazites has also been proposed by Murata *et al.* [7], and used to give interesting geochemical data.

This paper describes a spectrographic method for the determination of all the rare earths, viz. Sc, Yt, La, Ce, Pr, Nd, Sm, Eu, Gd, Tb, Dy, Ho, Er, Tm, Yb and Lu in minerals such as gadolinite, samarskite or euxenite which are relatively poor in Ce, and of all the rare earths except Eu, Ho and Tm in minerals such as monazite which are rich in Ce. The material analysed was invariably the rare-earth oxides together with ThO_2 (hereafter called the oxides) which had been separated from the minerals. The presence of ThO_2 was found to have no effect in the determination of the rare earths and the tedious preparation of rare earths free from Th was thus avoided. Th was determined chemically by the method of Gordon *et al.* [8].

VOL. 9 1957

Apparatus

The spectrograph used was a fully automatic glass one designed by Professor R. MANNKOPFF and constructed by him in 1947 at Rothamsted Experimental Station, Harpenden, Herts. It embodies the autocollimation or Littrow principle and contains a 60° prism, a 30° half-prism and a lens of aperture 7·5 cm and focal length 190 cm for Na_D light. The spectrum from 3500 Å to 10,000 Å covers five 15 cm plates with dispersions as indicated in Table 1.

The limited plate length proved a disadvantage as there was no single setting which could be used to record suitable lines of *all* the rare earths. The determination of the rare earths using the excitation conditions and lines mentioned below would be more straightforward with, for example, a grating instrument with dispersion 2·5 Å per mm and a plate length of 25 cm.

Table 1. Limits of wavelength differences for separation of 0·1 mm on spectrogram

Wavelength (Å)	Wavelength limits (Å)
3500	0·18
4000	0·27
4500	0·40
5000	0·58
5500	0·80
6000	1·05

Excitation conditions

As the rare earths were to be determined in samples consisting entirely of rare-earth oxides with subsidiary ThO_2, a highly sensitive method was not required. Samples were mixed with an equal weight of 140 mesh carbon powder and approximately 15 mg were arced in carbon anodes having crater dimensions 5 mm deep × 1·5 mm diameter and external diameter 3·05–3·15 mm. A flat-bottomed carbon cathode 5 mm diameter was used as counter electrode. The current was maintained at 9 A and the electrode gap at 10 mm during the time needed for complete volatilization of the specimen—75 sec to 90 sec. The middle 5 mm of the arc column was focused on the collimator lens and a rhodium-on-quartz stepped filter of ratio 1·7 : 1 was placed in front of the slit. Kodak III F plates 15 cm × 10 cm were used to record the range 5000–6500 Å and Kodak IV J plates 15 cm × 10 cm were used to record the ranges 4200–4800 Å, 3750–4150 Å and 3500–3800 Å. For volatilization tests the faster Kodak III J plates were used. The recommended developing conditions were adhered to but plate gamma values were found not to be constant for plates with differing emulsion batch numbers.

Photometric procedure

Using an A.R.L. projection comparator-densitometer with a linear galvanometric scale deflections were noted for a clear portion of the plate (i_0) and the relevant line (i). These values were then used to obtain the transformed density, D_t, of the line

where D_t is given by $D_t = \log \frac{(i_0 - i)}{(i)}$ · Line intensities were compared at the usual (but arbitrary) transformed density of $D_t = 0{\cdot}48$ (corresponding to a normal density, D, of $D = 0{\cdot}6$ where $D = \log \frac{(i_0)}{(i)}$).

Table 2. Analytical lines

1 Lines for Ce-rich or Yt-rich oxides with sensitivities

2 Lines for Yt-rich oxides with sensitivities in absence of interference; see text for remarks on Sc and Eu lines

Analysis lines for Ce or Yt-rich oxides (Å)	Sensitivities (%)	Analysis lines for Yt-rich oxides* (Å)	Sensitivities in absence of interference (%)
Sc 5700·23	0·5	4325·01	0·05
Yt 4682·32	1·0		
La 4574·87	1·0		
Ce 4483·89	1·5		
Pr 3965·26	0·3	4468·71 (with $La_2O_3 < 15\%$)	1·0
Nd 4451·56	0·8		
Sm 4434·32	0·3		
Eu —	—	4435·53/60	0·05
Gd 4327·10	0·8		
Tb 4278·51	0·3		
Dy 4308·62	0·5	3914·87 (with $CeO_2 < 25\%$)	0·8
Ho —		4254·43 (with $CeO_2 < 10\%$ and Cr 4274·80 absent†)	0·6
Er 3892·69	0·5		
Tm —		4242·15 (with $CeO_2 < 10\%$ Cr 4242·7 absent)	0·6
Yb 3987·99	0·01		
Lu 4518·57	0·2		

* See text for remarks on Sc and Eu lines.

† Harrison [11] gives the arc intensities Cr 4254·3 = 5000 R. Cr 4274·8 = 4000 R.

The logarithm of the percentage relative intensity (log per cent relative I) of lines was calculated by obtaining D_t values nearest the standard values in adjacent steps and assuming the relation D_t versus log per cent relative I to be linear for the limited range. From the log per cent relative I values thus obtained $\log I_a/I_b$ values (where a and b refer to rare-earth lines from oxides A and B respectively) were calculated for a variety of combinations of lines from several different elements. $\text{Log} \frac{(\text{concentration A})}{(\text{concentration B})}$ i.e. $\log [A]/[B]$ was plotted against $\log I_a/I_b$ to constitute a working curve.

VOL. 9 1957

Spectrograms of Yt-rich oxides usually had negligible backgrounds but those of oxides with about 20 per cent CeO_2 had significant backgrounds and corrections became necessary especially for the weaker lines; the method of MITCHELL *et al.* [9] was used.

Line selection

The practical resolution distance on the photographic plate was taken as 0·1 mm corresponding to the differences in wavelengths shown in Table 1.

Dispersion of the prism instrument is, of course, non-linear, but a spectrogram showing all the arc lines of all the rare earths in the region 4200 Å–6000 Å would show an average of 3 lines per 0·1 mm independent, approximately, of wavelength.

The arc spectra of Sc, Yt, Eu, Yb and Lu are simple, being dominated by a few very strong lines but showing also a number of weak and very weak lines. Those of the remaining rare earths are complex with many lines of comparable strengths but without extremely sensitive lines; La, Ce, Pr, Nd, Sm and Gd show a preponderance of lines in the visible, whilst Tb, Dy, Ho, Er and Tm produce relatively more of their lines in the ultra-violet. Whether or not a line is sensibly free from interference (from other coincident or nearly coincident lines) depends partly on the composition of the oxides giving rise to the spectrogram. Oxides from monazite or apatite are normally rich in La, Ce and Nd, and the derived spectrograms are crowded with lines; oxides from gadolinite, euxenite or samarskite are rich in Yt and can contain more than 20 per cent Gd_2O_3 and up to 10 per cent Sm_2O_3 and 10 per cent Dy_2O_3, but they give spectrograms with substantially fewer lines.

The elements Tb, Ho and Tm never reach high concentrations in oxides separated from minerals, and consequently their weak lines very rarely interfere with lines of other rare-earth elements.

The tables and charts of GATTERER and JUNKES [10] and the wavelength tables of HARRISON [11] were studied in the range 3850 Å–6000 Å and Table 2, column 1 lists a selection of the lines found to be free from coincidence in spectrograms of oxides having such varied compositions as shown in Table 3, columns 1–7. In addition, the lines in Table 2, column 2 can be used for oxides rich in Yt and poor in Ce, etc., with the limitations indicated. The Sc and Eu lines are highly sensitive and interferences from Ce, Pr, Nd, Gd or Dy are usually rather weak. Thus the occurrence of a weak line in the Sc or Eu line position on the spectrogram precludes the presence of much of these elements since they both produce strong lines when present for a few tenths of one per cent. No suitable lines for Eu, Ho or Tm were found for materials rich in Ce.

Internal standards and standard mixtures

It has been shown by FASSEL and other authors [5,12,13] that the volatilities of the lighter lanthanons including Gd are closely comparable under their particular conditions of excitation. The relative volatilities of all the rare earths under the arc conditions described in this paper were checked by recording running plate spectrograms of standard mixtures of Specpure* oxides and measuring $\log I_a/I_b$ for the elements and lines given in Table 2.

* Specpure is the trade name given by Johnson Matthey Ltd. of London to spectroscopically pure materials which they prepare.

Sm and Eu were found to be the most volatile rare earths with Yb slightly less so; these were more volatile than the group Sc, Yt, La, Ce, Pr, Nd and Dy, which all showed strikingly similar volatilities. Tb, Ho and Tm followed this involatile group fairly closely, but Gd, Er and Lu volatilized erratically.

In many spectrographic procedures employing internal standardization the internal standard is not originally present in the material to be analysed or, if it is, then it occurs to a negligible extent. However, rare-earth minerals like gadolinite, yttrofluorite and yttrotungstite contain all the rare earths except Sc and Eu and the paucity of coincidence-free lines of Sc and Eu has precluded their use as internal standards. Thus the method proposed by Fassel [5] has advantages. Ce is

Table 3. Composition of standards Nos. 1–7

	1	2	3	4	5	6	7
Sc_2O_3	0·88	*	*	0·50	*	2·46	1·62
Yt_2O_3	33·63	43·88	76·60	3·89	50·19	13·86	70·47
La_2O_3	5·76	0·25	*	20·20	11·20	3·11	4·38
CeO_2	12·05	8·31	*	39·43	7·00	9·75	4·84
Pr_6O_{11}	5·65	1·04	*	1·84	1·86	8·09	0·94
Nd_2O_3	8·55	1·04	1·81	19·95	5·30	6·65	4·08
Sm_2O_3	7·02	7·31	1·77	2·27	2·10	10·05	1·21
Eu_2O_3	0·48	*	*	0·53	*	2·59	1·71
Gd_2O_3	7·04	24·20	3·63	2·27	3·51	10·05	1·21
Tb_4O_7	2·60	0·94	0·87	0·43	1·55	2·11	1·39
Dy_2O_3	4·66	9·95	10·41	3·05	5·01	10·09	1·55
Ho_2O_3	1·39	0·83	1·38	0·53	*	2·63	1·74
Er_2O_3	2·40	1·01	3·53	1·61	7·00	5·25	0·71
Tm_2O_3	1·88	*	*	0·51	*	2·85	1·65
Yb_2O_3	3·84	1·00	*	2·57	5·28	8·38	1·13
Lu_2O_3	2·17	0·24	*	0·42	*	2·08	1·37

estimated chemically and the oxides to be analysed spectrographically are mixed with additional CeO_2 to give a fixed concentration of CeO_2 in the mixture. Ce is then used as a fixed concentration internal standard for estimating Yt and Gd.

In the method to be described, chemical techniques for determining any of the rare earths are avoided and one or more rare earth is used as a variable or fixed concentration internal standard for other rare earths. For oxides poor in the lighter lanthanons and correspondingly rich in Yt and the heavier lanthanons it is to be expected that La and Ce will be less abundant than Pr or Nd and accordingly added La or added Ce was used as a fixed concentration or slightly variable internal standard. For oxides poor in Yt and rich in Ce, etc. added Yt can be used as an internal standard with a pure spectrographic method for estimating the original Yt content [14].

VOL. 9 1957

From the volatility data it seemed likely that Yt, La or Ce might be suitable internal standards for all the rare earths except Sm, Eu and Yb. However, satisfactory working curves were obtained for Ce/Yb, for Yt, La or Ce/Sm and, with mixtures containing below 10 per cent CeO_2 for Yt or La/Eu when Eu did not exceed a few tenths of one per cent (the Eu line is inconveniently dense for higher concentrations). Table 3 shows the compositions of some of the many standard mixtures prepared from Specpure oxides; the compositions *partly* resemble those of

Table 4. Composition of oxides from gadolinite, Hitterø, Norway

I(La) Estimations using added La as internal standard; range 4200 Å–4800 Å. Ho_2O_3 values ± 30 per cent

II(Dy) Estimations using original Dy as liaison internal standard; range 3850 Å–4150 Å

III(Ce) Estimations using added Ce as internal standard; range 3850 Å–4150 Å for Yb only and 4200 Å–4800 Å for others

IV Complete analysis. Percentage oxides in gadolinite (chemically) = 51·28 per cent.

An asterisk indicates below sensitivity and a dash absence of data

	I(La)	II(Dy)	III(Ce)	IV
Sc_2O_3	*	—	—	*
Yt_2O_3	57·0	—	61·20	59·1
La_2O_3	—	0·48	*	0·48
CeO_2	1·70	2·08	—	1·83
Pr_6O_{11}	*	0·66	—	0·66
Nd_2O_3	4·05	—	4·80	4·42
Sm_2O_3	3·31	—	3·42	3·36
Eu_2O_3	*	—	—	*
Gd_2O_3	6·53	—	6·98	6·75
Tb_4O_7	1·22	—	1·37	1·30
Dy_2O_3	8·00	—	8·25	8·12
Ho_2O_3	1·1	—	—	1·1
Er_2O_3	—	5·20	—	5·20
Tm_2O_3	0·8	—	—	0·8
Yb_2O_3	—	—	9·36	9·36
Lu_2O_3	0·83	—	1·02	0·92

oxides from apatite (No. 1), samarskite with added Ce (No. 2), gadolinite (No. 3), monazite (No. 4), euxenite with added La (No. 5) sphene (No. 6) and wiikite (No. 7). Spectrograms of these and other standards showed that the lines of Sc, Eu and Yb (Table 2) were inconveniently dense when the oxide concentrations exceeded a few tenths of one per cent.

In Yt-rich oxides (e.g. from euxenites or gadolinites) Sc and Eu are usually below the limits of detection (Table 2 column 2S) but Yb can often substantially exceed 1 per cent and it was found convenient to dilute the oxides in a mixture of 95 per cent Yt_2O_3 and 5 per cent CeO_2 and estimate Yb using the line pair Ce

3952·54 Å/Yb 3987·99 Å. (A similar dilution approach could be made for estimating appreciable Sc or Eu in oxides.) Ce was used as a slightly variable internal standard since the original oxides may contain sufficient CeO_2 to sensibly augment the CeO_2 concentration in the mixture of diluted oxides. Standard mixtures containing 0·01–1·00 per cent Yb_2O_3 and 4–6 per cent CeO_2 in Specpure Yt_2O_3 were prepared. The working curve for log I_{Ce}/I_{Yb} was straight for Yb_2O_3 concentrations between 0·04 and 0·40 per cent and CeO_2 concentrations of 4 to 6 per cent and within these ranges the standard deviation for a single determined value of log $[CeO_2]/[Yb_2O_3]$ was ± 7 per cent. The determination of Yb in oxides from a gadolinite is discussed later.

Spectrograms of standards including all those in Table 3 were used to obtain a variety of working curves with Yt 4682·32 Å, La 4574·88 Å and Ce 4483·89 Å as internal standard lines. The limited wavelength coverage of the spectrograph did not allow the recording of Ce 4483·89 Å and lines below 4000 Å on one plate, and the three lines of Yt, La and Ce were thus only of use for each other or for Nd 4451·56 Å, Sm 4434·32 Å, Gd 4327·10 Å, Tb 4278·51 Å, Dy 4308·62 Å and Lu 4518·57 Å for Yt- or Ce-rich oxides. Working curves for [Yt_2O_3 or La_2O_3 or CeO_2]/[B] were found to remain straight lines for at least a ten fold change in the ratio [Yt_2O_3 etc.]/[B] provided the concentration of Yt_2O_3 etc. or B was more than about twice the limit of detection for the line used (Table 2, column 1S); typical concentration ratio ranges can be derived from the data in Table 3. The standard deviations for a single determined value of log[Yt_2O_3 or La_2O_3 of CeO_2]/[B] were ± 7 per cent for Yt_2O_3, La_2O_3, Pr_6O_{11}, Nd_2O_3, Sm_2O_3 and Dy_2O_3, $\pm 8\frac{1}{2}$ per cent for Tb_4O_7, ± 9 per cent for Gd_2O_3 and ± 40 per cent for Lu_2O_3 (cf. its erratic volatilization characteristics); all these were for [Yt_2O_3 etc.] or [B] exceeding twice the detection limit. For low line densities when [Yt_2O_3 etc.] or [B] was below twice the sensitivity the standard deviations were slightly increased. Tentative working curves were also constructed for log [La_2O_3]/[Ho_2O_3 and Tm_2O_3] with La_2O_3 between 5 and 15 per cent, CeO_2 below 4 per cent and Ho_2O_3 and Tm_2O_3 between 0·2 and 2·0 per cent. High standard deviations are quoted for concentrations of Ho_2O_3 or Tm_2O_3 in oxides from gadolinite (Table 4) since there were relatively few points on the working curves due to lack of Specpure materials; the reproducibility of log I_{La}/I_{Ho} or I_{Tm} was, however, similar to that for log I_{La}/I_{Tb}.

For oxides rich in Yt added La_2O_3 (10 per cent) and added CeO_2 (20 per cent) were used as internal standards for estimating Yt, La, Ce, Pr, Nd, Sm, Gd, Tb, Dy and Lu; added La_2O_3 (10 per cent) was used as internal standard for estimating Sc, Eu, Ho and Tm. Spectrograms in the range below 4000 Å show lines of La, Ce, Pr, Dy and Er which are sensibly free from interferences provided CeO_2 is below 25 per cent in the oxides. No suitable Yt line was found and unfortunately La 3988·51 Å and Ce 3952·54 Å became inconveniently dense for concentrations exceeding 2 per cent La_2O_3 and 10 per cent CeO_2. Under these circumstances it was decided to construct working curves involving Dy 3914·87 Å as internal standard line to La 3988·51 Å, Ce 3952·54 Å, Pr 3965·26 Å and Er 3892·69 Å with a view to using Dy as a variable internal standard or liaison internal standard in estimating Pr and Er concentrations and low concentrations of La and Ce. Straight-line working curves were obtained for log [Dy_2O_3]/[B] with Dy_2O_3 between 3 and

VOL. 9 1957

15 per cent, La_2O_3 between 0·2 and 2·0 per cent, CeO_2 and Pr_6O_{11} between 1·0 and 10·0 per cent and Er_2O_3 between 1·5 and 15·0 per cent. The standard deviations for a single determined value of log $[Dy_2O_3]/[B]$ were ± 7 per cent for La, Ce and Pr and ± 17 per cent for Er (cf. its irregular volatilization characteristics). Pr and Er would be estimated in Ce-rich oxides by diluting in Yt_2O_3 to reduce the CeO_2 content to below 10 per cent and using Ce as liaison internal standard. The standard deviations for a single determined value of log $[CeO_2]/[B]$ from the relevant working curve were ± 7 per cent for Pr_6O_{11} and ± 17 per cent for Er_2O_3.

Determination of the rare earths in oxides from a gadolinite

Duplicate spectrograms of the oxides taken in the range 4150 Å–3850 Å showed convenient densities for lines of La, Ce, Pr, Dy and Er; that for Yb was extremely high. Using photometric measurements and the relevant working curves estimates were obtained for the concentration ratios of Dy_2O_3/La_2O_3, Dy_2O_3/CeO_2, Dy_2O_3/Pr_6O_{11} and Dy_2O_3/Er_2O_3. One portion of the oxides was mixed with Specpure La_2O_3 in the ratio 8 parts of oxides to 1 part La_2O_3 and the La-enriched oxides were arced and recorded in duplicate in the range 4200 Å–4800 Å. Using the working curve for the line pair La 4574·88 Å/Dy 4308·62 Å a value of 1·61 was obtained for the concentration ratio La_2O_3/Dy_2O_3 in the mixture. A preliminary estimate of 7·65 per cent Dy_2O_3 was obtained by ignoring original La_2O_3 content. This figure was then used to estimate original La_2O_3 in the oxides from the Dy_2O_3/La_2O_3 (original) concentration ratio obtained from the spectrogram in the range 3850 Å–4150 Å. This gave a preliminary estimate of 0·46 per cent for La_2O_3. An improved estimate was then made for Dy_2O_3 by allowing for the contribution of original La_2O_3 to the total La_2O_3 content in the La-enriched oxides. This gave a value of 7·94 per cent Dy_2O_3 which in turn led to an improved estimate of 0·48 per cent for La_2O_3. Estimates for the concentrations of several rare earths using La as internal standard are given in Table 4, column 1. The standard deviation for the Dy_2O_3 estimate was ± 5 per cent (duplicate spectrograms) and in estimating La, Ce, Pr and Er with Dy as internal standard it is to be noted that the Dy_2O_3 content was not known exactly; thus these estimates had standard deviations of ± 7 per cent for La_2O_3, CeO_2 and Pr_6O_{11} and ± 13 per cent for Er_2O_3 (duplicate spectrograms in both ranges). Values for the oxides from the gadolinite are shown in Table 4, column 2.

Further estimates of Yt_2O_3, Nd_2O_3, Sm_2O_3, Gd_2O_3, Tb_4O_7, Dy_2O_3 and Lu_2O_3 were made from duplicate spectrograms of a mixture of 4 parts original oxides and 1 part Specpure CeO_2; Ce 4483·89 Å was used as the internal standard line and the presence of 1·83 per cent CeO_2 in the original oxides (as estimated previously via La and Dy) was allowed for. Results are shown in Table 4, column 3.

Yb was estimated from a spectrogram of 2 per cent oxides in a diluent of 5 per cent CeO_2 and 95 per cent Yt_2O_3 since trial showed that this dilution led to a convenient density of Yb 3987·99 Å. Using the Ce/Yb line pair a value of 26·9 was obtained for the concentration ratio CeO_2/Yb_2O_3 and the Yb_2O_3 content in the original oxides was estimated as 9·36 per cent after taking into account the original CeO_2 content of the oxides.

Table 4, column 4, shows the complete analysis of the oxides. The summation of 103·41 is regarded as satisfactory; ThO_2 was determined as trace.

Determination of rare earths in Ce-rich and Yt-poor oxides

Analyses of oxides from monazite, apatite, etc., have not yet been performed in this laboratory but bearing in mind that many working curves were constructed using data from spectrograms of Ce-rich oxides it is considered permissible to adumbrate an approach to this analysis. In the range 4200 Å–4800 Å Yt, 4682·32 Å could be used as internal standard line in (i) a spectrogram of the oxides and (ii) a spectrogram of the oxides containing 50 per cent added Specpure Yt_2O_3 (on a carbon-free basis). Normally the oxides of monazite contain below 5 per cent Yt_2O_3 and this can be estimated by comparing the difference between the values of $\log I_{Ce\ 4483}/I_{Yt\ 4682}$ arising from the two spectrograms. This difference will be unique for a given original Yt_2O_3 content. If the preliminary estimate for original Yt_2O_3 is $5 \pm 0{\cdot}75$ per cent then the systematic error in estimating La_2O_3 etc. through Yt as an added internal standard will be minus 1·5 per cent. Pr and Er can be estimated in the range 3850 Å–4150 Å using Ce 3952·54 Å as liaison internal standard after suitable dilution of the oxides in Specpure Yt_2O_3.

Acknowledgements—This work was started at Rothamsted Experimental Station, Harpenden, Herts., and it is through the kindness of Sir William Ogg (Director) and Dr. Alex Muir (Deputy Director) that I have been able to continue using the spectrograph constructed there. I also wish to thank Miss Rosemary Hall for undertaking the thorium and total rare earths determinations. Dr. H. Neumann of the Geologisk Museum, Oslo, kindly supplied the gadolinite sample.

VOL. 9 1957

References

[1] Goldschmidt V. M. and Thomassen L. *Videnskapsselskapets Skr.* I, *Mat.-naturv. Kl.* 1924 No. 5.
[2] Minami E. *Nachr. Ges. Wiss. Göttingen* 1935 N.F. I No. 14, 155–170.
[3] Sahama Th. G. and Vähätalo V. *C.R. Soc. Géol. Finlande* 1939 13; 14.
[4] Wylie A. W. *Aust. J. Appl. Sci.* 1950 **1** No. 2, 164–71.
[5] Fassel V. A. *J. Opt. Soc. Amer.* 1949 **39** 187–193.
[6] Norris J. A. and Pepper C. E. *Analyt. Chem.* 1952 **24** 1399–1403.
[7] Murata K. J., Rose H. J., Jr., and Carron M. K. *Geochim. et Cosmochim. Acta* 1953 **4** 292–300.
[8] Gordon L., Vanselow C. H., and Willard H. H. *Analyt. Chem.* 1949 **21** 1323–5.
[9] Mitchell R. L., Scott R. O., and Farmer V. C. *Nature, Lond.* 1946 **157** 193–4.
[10] Gatterer A. and Junkes J. *Spektren der seltenen Erden* Vatican City, Specola Vaticana, 1943.
[11] Harrison G. R. *M.I.T. Wavelength Tables* John Wiley, New York, 1939.
[12] Fassel V. A., Cook H. D., Krotz L. C., and Kehres P. W. *Spectrochim. Acta* 1952 **5** 201–209.
[13] Fassel V. A. and Wilhelm H. A. *J. Opt. Soc. Amer.* 1948 **38** 518–526.
[14] Butler J. R. and Le Riche H. H. *Spectrochim. Acta* 1951 **4** 435–8.

Spectrochimica Acta, 1957, Vol. 9, pp 341 to 345. Pergamon Press Ltd., London

The NH stretching frequencies of primary amines

L. J. Bellamy and R. L. Williams
Explosives Research and Development Establishment, Waltham Abbey, Essex

(*Received* 27 *April* 1957)

Abstract—The symmetrical and asymmetrical NH stretching frequencies of primary amines in dilute solution are shown to be related by the expression $\nu_s = 345{\cdot}5 + 0{\cdot}876\ \nu_{as}$, for a range of 62 different compounds. The standard deviation of the symmetric frequency calculated in this way is 4·8 cm^{-1}. The relation holds good for co-ordination compounds in which the nitrogen atom acts as an electron donor and also for cases in which both NH links are equivalently bonded. When only one NH link is hydrogen bonded the asymmetry introduced leads to a breakdown of the relationship, and this has useful applications in the identification of different kinds of molecular association.

Introduction

Many specific groupings give rise to more than one characteristic infra-red absorption frequency, and a number of instances are known in which two or more frequencies of this type have been shown to be inter-related. This can arise from the dependence of both frequencies upon the same force constant, as in the asymmetric and symmetric frequencies of the —SO_2— group [1]; or from the dependence of the separate force constants upon the same variable, as in the relationships which exist between the various CH frequencies of the methyl halides [2] or between the carbonyl and C–O stretching frequencies of steroid acetates [3]. These last examples arise from the fact that changes in the inductive effects of substituent groups change both force constants to proportionate extents.

In all cases of this type it is essential that the frequencies chosen should be free from mass or coupling effects and from any dipolar interactions which may affect one frequency more than another. Although this limits the scope of this method, many important group frequencies comply with these requirements. In particular, the frequencies arising from the stretching motions of hydrogen atoms are usually free from mass or coupling effects because of the light mass of the hydrogen atom and the resulting high frequencies. We have therefore studied the symmetric and antisymmetric NH stretching frequencies of primary amines in solution to see whether any relation between them exists, and if so what effect hydrogen bonding has upon it.

The stretching frequencies of primary amines

Until recently very little work has been done on the stretching frequencies of primary amines, and such data as were available were discordant and obtained under conditions of low resolution. In the past few years however studies on a wide range of primary amines under high resolution have been made by a number of workers and the results obtained are strictly comparable between one laboratory and another. Thus, Califano and Moccia [4] have studied fourteen aromatic primary amines in dilute solution of carbon tetrachloride. Their results for aniline and for *m*-toluidine agree very well with those of Fuson, Josien *et al.* [5] and of

Chatt *et al.* [6,7] respectively. Fuson *et al.* have studied aniline in various solvents and at different concentrations in the same solvent. Chatt *et al.* have examined a number of primary amines, both alone and when chelated to platinum in co-ordination complexes when the monomeric NH stretching frequencies are lowered by about 200 cm^{-1}. Richtering [8] has also given data on the liquid and solution frequencies of aniline which agree well with previous workers. A small number of co-ordination compounds involving ethylene diamine have also been studied by Svatos *et al.* [9]. A wide range of data are therefore available which are highly concordant and which cover a wide frequency range. All these data have therefore been employed in the study of the possible relationship between the two NH stretching modes.

Results

All the above data [4–9] yield a simple linear relationship between the asymmetric and symmetric NH stretching frequencies for all cases of dilute solutions and liquids. A least-squares treatment shows that the two frequencies are related by the expression $\nu_s = 345{\cdot}5 + 0{\cdot}875\,\nu_{as}$. This equation is obeyed in the case of the studied 62 amines with a standard deviation of 4·8 cm^{-1}. This order of agreement is highly satisfactory, particularly in view of the fact that data from a number of laboratories have been used. This is in accordance with theoretical expectation which would also predict that the relationship would not be obeyed in situations in which the two NH links are non-equivalent. Thus 2-amino pyridine [10] in dilute solution in carbon tetrachloride obeys the relation within 2 cm^{-1} but in the solid state three frequencies are found. No selection of pairs of these gives agreement within 45 cm^{-1}, due to the fact that this compound cannot hydrogen bond in any way which would lead to equivalent NH links. Similarly in copper anthranilate inequality in the NH links is introduced by the intramolecular hydrogen bond; absorption occurs at 3280 cm^{-1} and 3126 cm^{-1}. The calculated symmetric frequency is nearly 100 cm^{-1} higher than this last value. Other instances of this difference in the behaviour of unsymmetrically bonded NH links are discussed below.

VOL. 9 1957

Discussion and applications

Provided due regard is paid to the limitations of this method it has several useful applications. It may for example be helpful in some cases in differentiating between compounds in which the NH frequencies are lowered by hydrogen bonding and those in which it is lowered by electron donation as in the co-ordination complexes. It has potentialities for the positive identification of primary amine groups in compounds such as the amino heterocyclics in which alternative tautomeric forms are possible, and it offers a useful guide as to whether or not a compound such as aniline is hydrogen bonded in the liquid state. Some possibilities of this type are discussed in more detail below.

(a) *Co-ordination complexes*

The most extensive studies of co-ordination compounds involving primary amines are due to Chatt *et al.* [6,7]. These workers have studied many compounds of the general type *trans* (L.am.Pt.X_2) where L is a suitable ligand, am. is a primary

amine, and X is a halogen atom. A smaller number of similar compounds have been studied in the solid state by SVATOS *et al.* [9], who have also examined a few hexavalent platinum complexes.

In dilute solutions of carbon tetrachloride the various co-ordination compounds listed by CHATT *et al.* [6,7] exist as monomers and obey the expression given above. In more concentrated solutions there is strong evidence from dissociation constant studies that they exist primarily as dimers and it has been suggested that these are linked by hydrogen bonds between one NH link of each molecule and a chlorine atom of the other. This suggestion is supported by the observed frequencies, which fall by about 100 cm^{-1} and appear near 3200 cm^{-1} and 3120 cm^{-1}. They are accompanied by a weaker absorption near 3300 cm^{-1} which suggests the presence of some additional species but there is little doubt that the principal absorptions originate in the dimer. The calculated ν_s frequencies, using the expression given above, diverge from those actually found by an average of 30 cm^{-1} which supports the view that a symmetrical hydrogen bonding is taking place. Similar discrepancies are found with solutions in carbon tetrachloride containing dioxane from which it would seem likely that it is not sterically possible for two dioxane molecules to bond to the same NH_2 group.

In the solid state the likelihood that compounds of this type will be able to form symmetrical and therefore equivalent hydrogen bonds is increased. The compound $Pt(en)Br_2$ for example (en = ethylenediamine) shows two bands [9] at 3270 cm^{-1} and 3210 cm^{-1} which agree precisely with the expression we have derived. $Co(en)_3Cl_3$ and $Pt(en)_2Cl_2$ also show a pair of absorptions [4] which conform within 3 cm^{-1} and 1 cm^{-1} respectively although in these cases a third band is present which may indicate some additional species. On the other hand in $(Co(en)_2Cl_2)Cl$ four bands are found [9], no combinations of which agree with the calculated values. In view of the likelihood of intramolecular bonding in this compound this is not unreasonable. A similar departure from the relationship is shown by other intramolecularly bonded complexes such as sodium and copper anthranilates and platinum glycinate.

The solid compounds of the type $L.am.Pt.X_2$ give multiple absorptions in the NH region [6,7] which cannot be interpreted unequivocally. A compound such as *trans* ($Pr_2S{\cdot}p\text{-}CH_3C_6H_4NH_2\ PtCl_2$) for example has six bands at 3274, 3217; 3246, 3200; 3174 and 3134. It is interesting to note however that these are capable of division into three pairs as shown, each of which obeys the relationship given. It is possible therefore that these represent the absorption of three distinct molecular arrangements, each with equivalent NH links.

(b) *Heterocyclic amines*

A good deal of spectroscopic work has been carried out on hydroxy and amino pyridines and pyrimidines with a view to differentiating between the possible tautomeric structures. It is known for example that many simple hydroxy compounds of this type exist wholly in the keto form [11,12]. In amino compounds the recognition of the structures present is more difficult. It is for example difficult to differentiate the δNH_2 deformation frequency from the heterocyclic ring vibrations which occur in the same region. The balance of evidence would however appear to favour the amino rather than the imino form in many cases [13,14].

In dilute solution in carbon tetrachloride 2-amino pyridine [15] absorbs at 3500 cm^{-1} and 3410 cm. The value for ν_s calculated from the 3500 cm^{-1} frequency is 3412 cm^{-1}. In benzene solution three bands appear at 3490 cm^{-1}, 3395 cm^{-1} and 3315 cm^{-1}. The first two which are clearly monomer bonds obey the frequency relation as before. The 3315 cm^{-1} band must correspond to some hydrogen bonding but it is interesting to note that the frequency pair 3395 cm^{-1}, 3315 cm^{-1} also obey the relationship so that the 3395 cm^{-1} absorption may be a composite of *as* and *s* absorptions from bonded and unbonded NH links.

4-Amino pyridine [15] in dilute solution also gives NH absorptions which follow the equation for monomeric amino groups, so also do 3-amino pyridine, 2- and 4-aminoquinoline, 2-aminopyrimidine and 2-aminothiazole which have been studied by Angyal and Wener [14]. These workers used only rock-salt optics but the high frequency range appears to have been calibrated with particular care and their values of aniline and 2-amino pyridine agree very well with those of workers using higher resolution.

This evidence therefore provides strong support for the view that the amino form is the normal structure of these compounds. In the solid state the NH frequencies of these materials do not follow the calculated values. This is to be expected as they are unlikely to be able to associate in any way which would lead to equivalent hydrogen bonds and this in no way affects the general conclusions.

(*e*) *Molecular association*

Liquid aniline absorbs at 3432 cm^{-1} and 3353 cm^{-1}, which represents a very marked frequency fall from the values of 3473 cm^{-1} and 3385 cm^{-1} in carbon tetrachloride [5]. There has been some discussion in the literature as to whether this shift is due to association through N—H . . . N bonds or to dielectric constant and dipolar effects in the liquid. Studies at various concentrations in carbon tetrachloride suggest that the latter explanation is correct as there is a steady shift to lower frequencies as the concentration is increased. This contrasts with the behaviour of pyrrole, for example which shows two separate absorptions attributed to the monomeric and bonded NH groups [16]. As N—H . . . N bonding in aniline would lead to non-equivalent NH links whereas dielectric constant effects would affect both NH links equally, the relationship described affords a simple method of differentiating between the two possibilities. The asymmetric frequency of 3432 cm^{-1} yields a calculated value of 3352 cm^{-1} for the symmetric mode and the excellent agreement indicates that association through hydrogen bonds is unlikely in this case. Similar results are given by liquid ethylenediamine [9].

References

[1] Bellamy L. J. and Williams R. L. *J. Chem. Soc.* 1957, 863.
[2] Bellamy L. J. and Williams R. L. *Ibid.* 1956, 2753.
[3] Jones R. N. and Sandorfy C. *Chemical Applications of Spectroscopy* p. 482. Interscience, New York, 1956.
[4] Califano S. and Moccia R. *Gazz. Chim. Ital.* 1956 **86** 1014.
[5] Fuson N., Josien M. L., Powell R. L., and Utterbach E. *J. Chem. Phys.* 1952 **20** 145.
[6] Chatt J., Duncanson L. A., and Venanzi L. M. *J. Chem. Soc.* 1955, 4461.
[7] Chatt J., Duncanson L. A., and Venanzi L. M. *Ibid.* 1956, 2712.

VOL. 9 1957

[8] Richtering H. *Z. Phys. Chem.* 1956 **9** 393.
[9] Svatos G. F., Curran C., and Quagliano J. V. *J. Amer. Chem. Soc.* 1955 **77** 6159.
[10] Shigorin D. N., Danyushevskii Y. L., and Goldf'arb Y. L. *Izv. Akad. Nauk SSSR Odtel Khim. Nauk* 1956 120.
[11] Tanner E. M. *Spectrochim. Acta.* 1956 **8** 9.
[12] Brown D. J. and Short L. N. *J. Chem. Soc.* 1953, 331.
[13] Short L. N. and Thompson H. W. *Ibid.* 1952, 168.
[14] Angyal C. L. and Wener R. L. *Ibid.* 1952, 2911.
[15] Costa G., Blasina P., and Sartori W. *Z. Phys. Chem.* 1956 **7** 123.
[16] Josien M. L. and Fuson N. *J. Opt. Soc. Amer.* 1954 **22** 1169.

OL.
9
57

6—(20 pp.)

Spectrochimica Acta, 1957, Vol. 9, pp. 346 to 356. Pergamon Press Ltd., London

Effects of polymorphism and influence of sample preparation on the infra-red spectrum of estradiol-17β*

ERIKA SMAKULA, AUGUSTUS GORI, and HERBERT H. WOTIZ
Department of Biochemistry, Boston University School of Medicine, Boston, Massachusetts

(*Received* 7 *January* 1957; *amended* 15 *April* 1957)

Abstract—It was shown by infra-red absorption spectra and X-ray diffraction powder patterns that estradiol-17β can exist in the amorphous form and in at least four different crystalline modifications with a common melting-point. It was also shown that these modifications are selectively interconvertible by various degrees of thermal and/or mechanical agitation. This property is disturbing in the various infra-red solid-state sampling techniques, which involve grinding, pressing, and heating, since it may lead to the spectrum of a different crystal form or to a mixed spectrum. X-ray diffraction patterns obtained from finely ground powders may suffer from the same effect. Thermal and mechanical conversion of several modifications into one common crystal form may prevent recognition of polymorphism by means of melting-point determinations or X-ray diffraction. Drastically different modes of hydrogen bonding characterize the infra-red spectra of the different modifications. Discussion of the spectra and band assignments are given.

VOL.
9
1957

INFRA-RED absorption spectra of organic compounds are sensitive to the physical state of the substance analysed as well as to specific crystal modifications [1, 2, 3]. Such spectral changes are due to the influence of intermolecular forces on the force constants of intramolecular vibrations. This influence is particularly evident in compounds with associating groups, which provide the opportunity for hydrogen bonding. The ability of the molecules of a compound to associate in alternate modes of hydrogen bounding of comparable stability can be expected to be a major cause of polymorphism, thereby causing differences in the solid-state spectra of polymorphous substances. Unless the compound can be analysed in the amorphous phase, the spectral identification of a polymorphous polyhydroxy compound requires standard spectra of all the possible crystal modifications. However, all solid-state sampling techniques may induce changes in crystal structure. The influence of the dielectric properties of solvents on the crystal structure is expected when a sample is deposited on a plate of sodium chloride from a solution. It was found that mechanical and thermal agitation may also give rise to a change in crystal structure. Mixed spectra of different modifications may be the result of such effects. The presence of the two hydroxyl groups (one phenolic, the other alcoholic) in estradiol-17β ($\Delta^{1:3:5\,(10)}$-estratriene-3:17β-diol) provides suitable conditions for different modes of hydrogen bonding and for several crystalline modifications. Four such modifications of estradiol-17β were prepared, and their sensitivity to thermal and mechanical agitation and their infra-red spectra were investigated.

* These studies have been carried out with the assistance of research grants and an institutional research grant from the American Cancer Society and from Aids for Cancer Research, Boston, Massachusetts.

Experimental

All spectra recorded here were taken on a Perkin-Elmer model 21 double-beam infra-red spectrophotometer with sodium chloride optics and using slit programme 927. All samples were prepared from a single lot of estradiol-17β (m.p. 178–179°C), which was found to be homogenous by paper chromatography.* Potassium bromide pellets were prepared in a 12-mm die, as described by SCHIEDT [4], using optical-grade potassium bromide powder.†

Melting-points reported were taken on a Fisher-Johns melting-point apparatus and have not been corrected.

X-ray powder diffraction patterns were recorded on Kodak X-ray film by a Phillips X-ray diffraction apparatus model 5001 of 114·59-mm diameter. Samples were placed in a glass capillary tube and were exposed for 12 to 14 hr to nickel-filtered copper radiation at 40 kV and 15 mA.

Results

Influence of solvents and of mechanical and thermal agitation on the preparation of the four crystalline modifications (A, B, C, D) and the amorphous form

Form A. This form was obtained by the following procedures:

1. Crystallization of the steroid from an ethyl acetate solution at room temperature.

Proof of the chemical identity of forms *B*, *C*, *D* and the amorphous form was obtained by converting each of them into form *A* by the above procedure.

2. Crystallization of the amorphous form over a period of several weeks.

3. Grinding of an amorphous sample or forms *B*, *C*, or *D*.

The speed of conversion was traced by the examination of Nujol mulls of the steroid. The samples were ground for successively longer periods, both as the powder and as a mull, and the increase of the spectral characteristics of form *A* and the decrease of those of any other form were observed. The grinding time necessary for the total conversion of form *B* to form *A* was relatively short, while the more rigid crystal structures *C* and *D* required longer manipulation.

Form B. This form was obtained by crystallization of forms *A*, *C*, or *D* from a methanol solution.

Form C. This form was obtained by the following two procedures:

1. Forced crystallization of a cooling melt of estradiol-17β by gentle rubbing.

2. Exposing forms *A*, *B*, or *D* to a temperature between 100°C and the melting-point.

Heating of form *A* or *B* on the stage of a Fisher-Johns melting-point apparatus from 95–170°C over a period of 10 min converted either of them completely into form *C* without intermediate melting. The time necessary for conversion within this range is inversely proportional to the temperature. Form *D* when deposited on the stage of the melting-point block at any temperature between 100°C and 160°C melted, then recrystallized immediately as form C. Systematic studies to determine transition points were not carried out. Preliminary studies indicated that form *B*, which contains stronger hydrogen bonds, required more energy than form *A* to be converted to form *C*. The conversion of all modifications to form *C* is the obvious reason for their common melting-point, preventing recognition of their polymorphic nature by melting-point determinations.

* The authors gratefully acknowledge the contribution of estradiol-17β from Dr. PEARLMAN of Schering, Inc.

† Harshaw Chemical Co., Cleveland, Ohio.

Form D. This form was obtained by the following three methods:

1. Vacuum evaporation of an ethyl acetate solution of estradiol-17β at 50°C.
2. Evaporation of an ethyl acetate solution of the steroid on a hot plate.
3. Rapid cooling of a melt.

Form *D* was very difficult to obtain and frequently several attempts were necessary to repeat the results. It appeared that repeated disruption of the crystal structure and of the more stable modes of hydrogen bonding was necessary to prevent rearrangement to forms *A* or *C*. Mixed spectra of forms *D* and *C* were frequently found.

Amorphous form. The general characteristic of the various crystalline modifications is the disappearance of all spectral differences when passing to the amorphous or liquid phase. Identical spectra of the amorphous form were obtained by the two methods below:

1. The melting of any one of the four crystal modifications between two rock-salt plates and subsequent cooling to room temperature.

The resulting glassy film was completely transparent to visual observation.

2. The heating to the melting-point of estradiol-17β of a potassium bromide pellet containing any of the four forms or their mixtures.

The transparency of the pellets, which was lost on heating, was restored by repeating the pressing procedure.

Spectra obtained from pellets before exposing them to this procedure were not always reproducible. This indicated that the crystalline modifications are sensitive to pressure as well as to grinding.

VOL.
9
1957

X-ray diffraction powder patterns

Specific X-ray diffraction photographs (Fig. 1) differing in position and intensity of the lines were obtained from forms *A*, *C*, and *D*. Form *B* gave a pattern identical to that of form *A*. It is obvious that the convertibility of crystal modifications by grinding will have a disturbing influence on X-ray diffraction patterns similar to that which it has on the infra-red spectra. The conversion of all forms to a common form may prevent recognition of polymorphism by X-ray diffraction. This may have been the reason for the failure to obtain an individual X-ray diffraction pattern for form *B*. The diffraction pattern obtained for form *A* is identical with the one published by Parsons and Beher [5].

Discussion

The spectra of all forms of estradiol-17β are presented in Fig. 2. Table 1 gives the band positions, estimated band intensities, band assignments, and references. Any reference to the authors of well-established band assignments has been omitted. They are excellently discussed by Bellamy [6], Brugel [7], and Jones and Sandorfy [8]. All spectra show absorption bands characteristic for phenols and alcohols. The assignment of bands as well as differences in intensities and positions, due to the influence of different modes of hydrogen bonding and molecular packing in the unit cells of the various crystal structures, are discussed according to the group frequencies. They are shown by the small-letter index in Table 1.

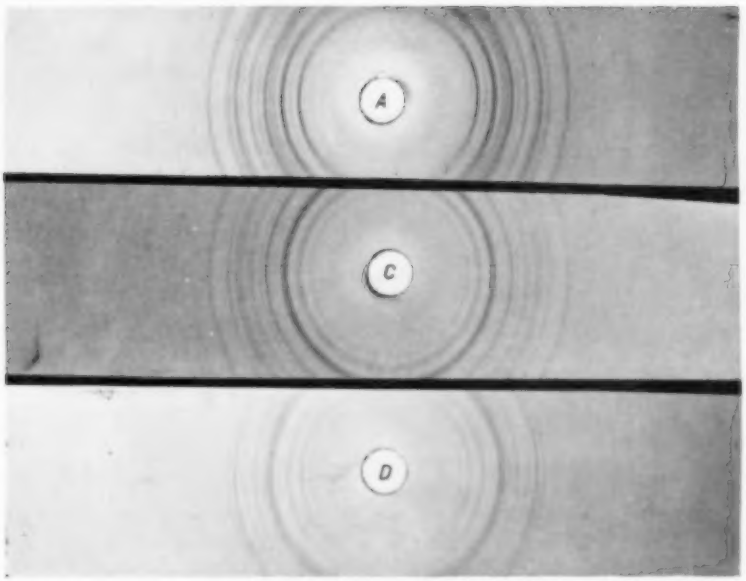

Fig. 1. X-ray diffraction powder patterns of crystal forms *A*, *C*, and *D*.

VOL.
9
1957

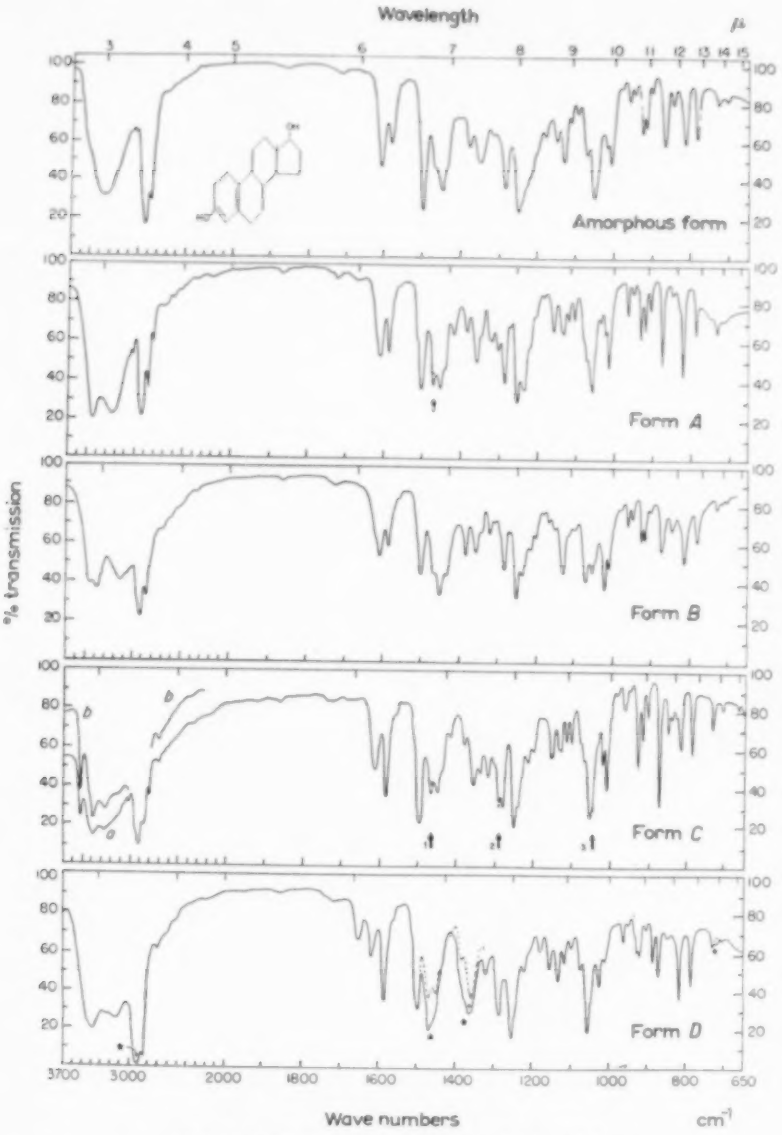

Fig. 2. Infra-red spectra of the various solid forms.

Amorphous form: Glassy melt.

Form A: Crystallized on a sodium chloride plate from a glassy melt. Arrow indicates increased intensity due to orientation.

Form B: Potassium bromide pellet.

Form C: (a) Crystallized on sodium chloride plate from Form *A*; Arrow 1 indicates intensity due to orientation; arrows 2 and 3 indicate intensities slightly decreased due to incomplete crystallization. (b) Nujol mull.

Form D: Nujol mull; asterisks indicate Nujol bands. Bands inserted in Nujol region are Form *D* bands of a rapidly cooled melt.

Table 1. Band assignments for the infra-red spectra of estradiol-17β
$\sim$ approximately; (*s*) strong; (*m*) medium; (*w*) weak; (*sh*) shoulder; (*b*) broad.
Frequencies in cm^{-1}

	Amorphous form	Form *A*	Form *B*	Form *C*	Form *D*	Band assignments	Reference
a	3600 (*sh*) 3510 (*sh*)					Terminal free and dimeric O—H stretching vibrations of chain or net-like molecular association complexes	[11]
				3525		Free O—H stretching vibration	
		3435	3450 3365	3390	$\sim$3400	Bonded O—H stretching vibrations Alcoholic self-association and phenolic self-association	
	$\sim$3345 (*b*)	3225		$\sim$3270	$\sim$3250	Mixed association of phenolic and alcoholic hydroxyl groups	
			3125	$\sim$3150	$\sim$3150		
	3020 (*w*) 3070 (*sh*)	3020 (*w*) 3060 (*sh*)	3020 (*w*) 3060 (*sh*)	3015 (*w*) $\sim$3050 (*sh*)	3015 (*w*) $\sim$3050 (*sh*)	Aromatic C—H stretching vibrations Aromatic C—H stretching vibrations	
	$\sim$2950 (*sh*) $\sim$2920 (*b, s*) 2860 (*m*)	$\sim$2950 (*sh*) $\sim$2920 (*b, s*) 2860 (*m*)	$\sim$2950 (*sh*) $\sim$1915 (*b, s*) 2855 (*m*)	$\sim$2950 (*sh*) $\sim$2915 (*b, s*) 2860 (*m*)	$\sim$2950 (*sh*) $\sim$2920 (*b, s*) 2860 (*m*)	Overlapping methyl and methylene stretching vibrations	
b		2805 (*w*)		2805 (*w*)		17 C—H stretching vibration (tentative)	
	$\sim$1860 (*b, w*) $\sim$1725 (*b, w*) $\sim$1670 (*b, w*)	$\sim$1860 (*b, w*) $\sim$1725 (*b, w*) $\sim$1670 (*b, w*)	$\sim$1860 (*b, w*) $\sim$1725 (*b, w*) $\sim$1670 (*b, w*)	$\sim$1860 (*b, w*) $\sim$1725 (*b, w*) $\sim$1670 (*b, w*)	$\sim$1860 (*b, w*) $\sim$1725 (*b, w*) $\sim$1670 (*b, w*)	Combination and overtone bands in agreement with 1:2:4-tri-substituted benzenes	
c					1652 (*m-w*)	Hydrogen bonded C=O stretching vibration (tentative)	
d	1608 (*m-s*) 1618 (*sh*)	1608 (*m*) 1618 (*sh*)	1608 (*m*) 1618 (*sh*)	1615 (*m*)	1608 (*sh*) 1618 (*m*)	Combination tone of two symmetric skeletal vibrations of the aromatic ring, infra-red active by reduced symmetry	[8]
e	1585 (*m*)	1585 (*m*)	1585 (*m*)	1585 (*m-s*)	1585 (*m-s*)	Fundamental aromatic ring vibration infra-red active by reduced symmetry	[8]
f	1500 (*s*)	1500 (*s*)	1500 (*m-s*)	1500 (*s*)	1500 (*m-s*)	Fundamental skeletal vibration	[8]
g	$\sim$1470 (*sh*) 1450 (*m-s*)	$\sim$1470 (*sh*) 1450 (*s*)	$\sim$1470 (*sh*) 1450 (*s*)	$\sim$1470 (*sh*) 1450 (*m-s*)	1470 (*m-s*) 1450 (*m-s*)	Unperturbed methylene bending vibrations	[21]

VOL. 9
1957

	~1435 (*sh*)	~1430 (*sh*)	~1435 (*sh*)	~1435 (*sh*)	~1435 (*sh*)	Skeletal vibration of the aromatic ring (tentative)	[22]
	1380 (*m*)	1380 (*w-m*)	1380 (*m*)	1380 (*w-m*)	1380 (*w-m*)	Bending vibration of angular methyl group	[21]
b		1418 (*w*)		1418 (*w*)		C-17 C—H bending vibration (tentative)	
h_1	1350 (*m, b*)	1357 (*m*) 1345 (*sh*)	1357 (*m*) 1345 (*sh*)	1358 (*m*) 1350 (*m-w*)	1367 (*sh*) 1357 (*m-s*) 1340 (*sh*)	Aromatic ring vibrations of B_1 symmetry, coupling partner of h_2	[23]
i	1284 (*m-s*)	1287 (*sh*) 1282 (*m-s*)	1290 (*sh*) 1282 (*m-s*)	1291 (*m-s*) 1280 (*m-s*)	1292 (*sh*) 1285 (*m-s*)	Unassigned complex band	
k	1250 (*s*)	1250 (*s*)	1250 (*s*)	1250 (*s*)	1250 (*s*)	Phenolic C—O stretching vibration	[23, 16]
h_2	1250–1200	~1237 (*sh*) 1231	1237	1242		Phenolic O—H bending vibration. Coupling partner of h_1	
	~1130 (*m*)	~1130 (*w-m*)	~1130 (*m-s*)	~1130 (*w-m*)	~1130 (*w-m*)	Two or more unresolved components. Rocking vibration of angular methyl group (tentative)	[25]
		1078 (*sh*)		1079 (*sh*)			
	1071 (*m*)	1070 (*sh*)	1069 (*m-s*)	1070 (*sh*)	1072 (*w*)		
l	1052 (*s*)	1054 (*s*)	1052 (*m*)	1054 (*s*)	1054 (*s*)	C-17 C—O stretching vibration	
a, l				1046 (*s, sh*)		free O—H bending vibration	
		1032 (*w*)					
	1019 (*w*)	1020 (*w*)	1020 (*s*)	1020 (*m-w*)	1023 (*m-w*)		
	1009 (*m*)	1011 (*m*)	1009 (*m*)	1011 (*m*)	1010 (*sh*)		
	962	961	959	963	964		
	947	947	947	948 (*sh*)	950		
	927	927	924	927	927		
	917	915	916	916	920		
	902	902	900	902	902		
c					886		
	867 (*m*)	872 (*m*)	872 (*m*)	872 (*s*)	971 (*m-w*)	Aromatic C—H out-of-plane deformation; one free hydrogen atom	
	847	845	845	849	848	Weak band; multiple overlapping on low frequency side	
	816 (*m*)	818 (*m-s*)	813 (*m-s*)	815 (*m*)	816 (*m*)	Aromatic C—H out-of-plane, in-phase deformation; two adjacent free hydrogen atoms.	
	784 (*m*)	784 (*w-m*)	780 (*m*)	785 (*m*)	786 (*m*)	Aromatic out-of-plane, out-of-phase C—H bending vibration (tentative)	
	731	730	727	731	730		
	705	705	703	707	706		
		~740 (*b, w*)	~775? (*b, w*)	~720 (*b, w*)	~720 (*b, w*)	Phenolic out-of-plane O—H bending vibration	[26]

(*a*). O—H stretching vibrations. Estradiol-17β is capable of hydrogen bonding involving one phenolic and one alcoholic hydroxyl group per molecule. There are three expected types of hydrogen bonds with their respective subtypes of dimeric and/or polymeric association as follows: Type I—alcoholic self-association; Type II—phenolic self-association; and Type III—mixed association of phenolic and alcoholic hydroxyl groups.

It has been established that the order of hydrogen bonds of types I, II, and III reflects the order of increasing bond strength and the order of decreasing frequency of absorption of the bonded O—H stretching vibration respectively; in binary systems type III bonding occurs preferentially [9, 10].

The broad structureless association band of the amorphous form is typical for polymeric association in liquids and concentrated solutions. The frequency range at half-width ($\sim$500 cm^{-1}) and the broad absorption maximum near 3345 cm^{-1} suggest an overlapping of absorption bands of types I, II, and III. The band corresponds in each of the four crystal forms to an individual group of sharper bands, which covers at half-width approximately the same frequency range (also $\sim$500 cm^{-1}). The random distribution of hydrogen bonds of various degrees of association in the disordered amorphous phase is precipitated selectively in the four crystal forms into several rigid modes of hydrogen bands of defined strengths.

The bands of each crystal form are overlapping and of multiple structure. Attempts to relate these bands to hydrogen bond modes of types I, II, and III encounter the following difficulties: The absorption regions of the three types of bonds are overlapping. An O—H stretching vibration of a higher state of aggregation (type I) may coincide in position with an O—H stretching vibration of a lower degree of association (types II and III) because of the selective nature of hydrogen bonding. The possibility also exists of an additional lowering of the bonded O—H stretching vibrations due to crystalline field effects. In the crystalline state, steroids with type I bonding only exhibit absorption bands as low as 3200 cm^{-1} [12]. Crystalline phenol with type II bonding only absorbs at 3210 cm^{-1} [13].

It is concluded that the absorption below 3200 cm^{-1} such as that which occurs in forms *B*, *C* and *D* is likely to arise exclusively from bond type III; absorption above 3500 cm^{-1} is likely to arise from a "free" O—H stretching vibration. Band assignments between 3500 cm^{-1} and 3200 cm^{-1} are subject to the overlapping of regions, as shown in Table 1.

Form *C* is the only modification which exhibits a "free" O—H stretching band at 3525 cm^{-1}. The 3525-cm^{-1} band is very sharp and is remarkable because of its steep high-frequency slope which starts below 3600 cm^{-1} and is quite different from the characteristic slanted high-frequency slope of all other modifications starting above 3600 cm^{-1}. In general, "free" O—H stretching vibrations are not observed in crystals unless steric hindrance is severe. The shift of about 100 cm^{-1} below the "free" O—H stretching vibration in dilute solutions may be caused in part by crystal lattice forces and in part by the participation of the oxygen of the hydroxyl group in a single-bridge dimer bond, the latter giving rise to the sharp absorption band at 3390 cm^{-1}. The assymetric high-frequency branch of this band indicates by its shoulders the presence of other components. The single-bridge dimer is

VOL. 9 1957

believed to be due to the alcoholic hydroxyl group, since the corresponding unbonded O—H bending frequency occurs in the expected region at 1046 cm^{-1} [14] and not near 1175 cm^{-1} (the position of the unbonded phenolic O—H bending frequency [15, 16]).

All five forms have in addition to the bands given in Table 1 an extremely broad low-intensity band, the maximum of which cannot be determined because of its overlap with the C—H stretching absorption. The presence of some exceptionally strong hydrogen bonds, as they occur in carboxylic acids, may account for this band.

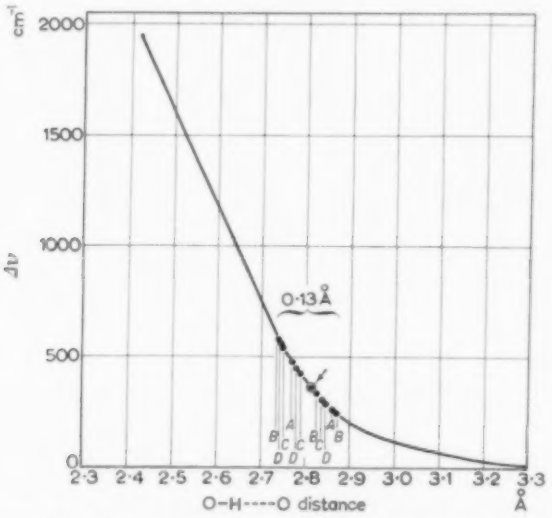

Fig. 3. Relationship of band lengths to frequency shift of the various types of hydrogen bonds in crystal modifications *A*, *B*, *C*, and *D* of estradiol-17β. These data were obtained from the graphs of LORD and MERRIFIELD [17] and NAKAMOTO, MARGOSHES, and RUNDLE [18]. The arrow indicates mean bond length as obtained from $\Delta\nu$ of the amorphous form.

LORD and MERRIFIELD [17] demonstrated a linear relationship between O—H $\cdots$ O distances which were obtained from X-ray studies in crystals, and the infra-red frequency shift $\Delta\nu$ of the lowered O—H stretching vibration of strongly bonded molecules. NAKAMOTO *et al.* [18], using experimental values for crystals, showed that for weaker hydrogen bonds the O—H $\cdots$ O distances increase exponentially as the bonded O—H stretching frequency approaches the unbonded.

A combined empirical graph by these authors, who assumed a value of 3700 cm^{-1} for the "free" O—H stretching vibration, was used in Fig. 3, to obtain an approximation of values of the O—H $\cdots$ O bond lengths, which correspond to the known $\Delta\nu$ values for the different bands in the various modifications. $\Delta\nu$ values are not exact because of the broadness and the multiple nature of the bands. The reference value of 3700 cm^{-1} has been retained. The values were all located in the region which deviates from the linear relationship and they varied between 2·87 Å and 2·74 Å (approximately 2·8 Å $\pm$ 2·5 per cent). The weak broad band of stronger hydrogen bonding present in all forms was not evaluated. $\Delta\nu$ of the amorphous

form, although not directly applicable to the graph, appears to correspond to a mean bond length of about 2·81 Å.

The rearrangement of hydrogen bonds from one modification to another involves small changes in total O—H · · ·O bond lengths. For example, a difference of about 100 cm^{-1} (0·03 Å) between the strongest hydrogen bond in form *A* and the strongest hydrogen bond in one of the other modifications amounts to a total change of bond length of about 1 per cent. This, however, corresponds to a variation of 10 per cent of the largest possible decrease in bond length (0·35 Å), since the smallest possible bond length in the case of symmetric hydrogen bonding appears to be 2·45Å [18, 19].

Lippincott and Schroeder [19] worked out a theoretical relationship between O—H · · · O bond lengths in crystals and calculated $\Delta\nu$. They used a simple linear model of the hydrogen bond which was represented by a potential function adequate to describe the properties of covalent bond. The above approximations give about the same values when obtained from the graph of these authors. They calculated the change of bond energy in terms of frequency shift as 1 kcal per 100 cm^{-1}. According to this value the rearrangement of hydrogen bonds from one modification to another involves changes in bond energies of about 1 kcal at most.

(*b*). A sharp well-resolved absorption band of low intensity near 2805 cm^{-1} was found to be of interest because of its concomitance with a well-resolved broad band of medium intensity at 1418 cm^{-1}. These two bands were found in forms *A* and *C* only. They may arise from a stretching and a bending vibration of the C—H group perturbed by the proximity of the C-17 hydroxyl group on the same atom. The bands are not usually seen in 17-hydroxylated steroids because of their low intensity. The specific association in crystal forms *A* and *C* may bring about a change in dipole moment which is sufficient to produce an intensity increase.

(*c*). Only in form *D* does there appear a broad low-intensity band at 1652 cm^{-1}. It is suggested that this band is due to a hydrogen bonded carbonyl stretching vibration, arising from a limited ketonization of the benzenoid ring

where intermolecular bonding in a crystal lattice has stabilized some of the molecules as the ketonic tautomer. The appearance of a new band at 886 cm^{-1} in a region associated with olefinic C—H deformation vibrations, further supports this assumption. For example, steroid-1:4-dienones are known to exhibit a prominent band at 887 cm^{-1} [20].

(*d,e,f*). All five forms possess a characteristic group of three bands (*d*, *e*, *f*) of varying intensities such as those found in aromatic compounds. Only the position of band *d*, located between 1608 cm^{-1} and 1618 cm^{-1} assigned to a combination tone of two skeletal ring vibrations [8] appears to be sensitive to intermolecular forces which differ in the various crystal structures and the amorphous form. This broad complex band is made up of two major components of strongly varying intensities at 1608 cm^{-1} and 1618 cm^{-1} and of two much weaker components which appear as shoulders at 1600 cm^{-1} and at 1630 cm^{-1}. The intensity of either component determines the frequency of the absorption maximum. The multiple structure may be

VOL. 9 1957

caused by the modifying influence of different concomitantly existing strengths of hydrogen bonding per unit cell of each modification. Overtones and combination tones can be expected to be more sensitive to perturbation than fundamental vibrations [8].

(*g*). The methylene bending vibration at 1470 cm^{-1} was found to be sensitive to orientation in forms *A* and *C*.

(*h*1, *h*2). A complex band (*h*1) near 1350 cm^{-1} consists of at least two components of varying intensities which are combined in one broad band in the amorphous form. A number of overlapping bands (*h*2) between 1250 cm^{-1} and 1200 cm^{-1}, differing in intensities and position in the different crystal forms, appear as a very broad diffuse composite in the amorphous form. These bands appear to be coupling partners of two vibrations according to a recent assignment by MECKE and ROSSMY [23]. These authors showed by deuteration studies with aromatic compounds that a band near 1350 cm^{-1} is one partner of the coupling of the phenolic O—H bending vibration, with a ring vibration of B_1 symmetry that is uninfluenced by substitution. The other partner absorbs near 1174 cm^{-1} or higher, depending upon the state of aggregation, and exhibits more "hydroxyl character" than does the first partner. In the different crystals the bending vibration of the phenolic O—H group appears selectively perturbed in intensity as well as in position by defined strengths of hydrogen bonding of types II and III. Because of strong band overlapping in the O—H stretching region they could not be correlated with the corresponding O—H stretching vibrations. In the amorphous phase the diffuse, broad composite of many overlapping bands, which merges with the low-frequency branch of the stable C—O stretching vibration (*k*), arises from randomly bonded O—H bending vibrations.

(*i*). A medium strong band near 1280 cm^{-1} is also sensitive to the specific crystal form. Its origin is not known.

(*k*). All forms of estradiol-17β exhibit a strong sharp absorption band at 1250 cm^{-1}, which is remarkably constant in position. The assignment of this band as a phenolic C—O stretching vibration [23, 16] prompts the assumption that the aromatic ring has a stabilizing influence on this vibration, thus making it insensitive to hydrogen bonding effects. The high-frequency slope of this band is stable for all forms, including the amorphous form. Strong overlapping occurs with the *h*2 bands on the low-frequency side.

(*l*). In the 1100-cm^{-1} to 1000-cm^{-1} region all spectra show absorption envelopes characteristic to each form. The strongest peak, which is considered to belong to the C—O stretching band of the 17 C—OH group, is sharp and is located at 1054 cm^{-1} for forms *A*, *C*, and *D*. It is near 1052 cm^{-1} with a broadened maximum in the amorphous form. The position of the C—O band appears to be influenced very little by hydrogen bonding. Form *B* shows exceptional absorption at 1052cm^{-1} with strongly reduced intensity and loss of identity of the C—O stretching vibration along with an increased intensity of bands at 1020 cm^{-1} and 1069 cm^{-1}. This unusual behaviour is not an orientation effect. The random distribution of particles is assured by their incorporation in a potassium bromide pellet. It is unlikely that resonance splitting of closely absorbing C—C and C—O stretching and O—H bending vibrations occurs, since it was not found in the other

modifications. There is no data available as to the effect of specific types of association on the intensities of valency vibrations.

Quinan and Wiberley [14] showed that C—O stretching and O—H inplane bending vibrations of alcohols absorb at approximately the same frequency in solutions, with the weaker O—H band usually being unresolved. This also seems to hold true for crystals. Only in form *C* does the frequency of the O—H bending vibration seem to be clearly recognizable as an inflection at 1046 cm^{-1} on the low-frequency side of the C—O band corresponding to the "free" O—H stretching vibration [14]. Form *D* again has the simplest absorption pattern, as it has in the 1250-cm^{-1} region.

A number of bands below 1000 cm^{-1}, the region of aromatic C—H out-of-plane bending vibrations and CH_2 rocking vibrations, have been listed without attempt to indicate their considerable intensity variations. They show small (0–5 cm^{-1}) frequency differences. Kletz and Price [24] pointed out that such small frequency variations may arise from repulsive forces between peripheral atoms which approach closer than their van der Waals' radii.

References

[1] Kendall D. N. *Anal. Chem.* 1953 **25** 382.
[2] Ebert A. A. and Gottlieb H. B. *J. Amer. Chem. Soc.* 1952 **74** 2806.
[3] Sinclair R. G., McKay A. F., and Jones R. N. *J. Amer. Chem. Soc.* 1952 **74** 2570.
[4] Schiedt U. *Z. Naturforsch.* 1952 **76** 270.
[5] Parsons J. and Beher W. T. *Anal. Chem.* 1955 **27** 514.
[6] Bellamy L. D. *The Infra-red Spectra of Complex Molecules* John Wiley, New York, 1954.
[7] Bruegel W. *Einfuehrung in die Ultrarotspektroskopie* Steinkopff, Darmstadt, 1954.
[8] Jones R. N. and Sandorfy C. Infra-red and raman spectrometry. *Physical Methods of Organic Chemistry* (Editor: Weissberger) Vol IX. Interscience, New York.
[9] Kuhn L. P. *J. Amer. Chem. Soc.* 1952 **74** 2492.
[10] Luettke W. and Marsen H. *Z. Electrochem.* 1953 **57** 680.
[11] Smith F. A. and Creitz E. C. *J. Res. Nat. Bur. Stand.* 1951 **46** 145.
[12] Jones R. N., Williams V. Z., Whalen M. J., and Dobriner K. *J. Amer. Chem. Soc.* 1948 **70** 2024.
[13] Sears W. C. and Kitchen L. J. *J. Amer. Chem. Soc.* 1949 **71** 4110.
[14] Quinan J. R. and Wiberley S. E. *Anal. Chem.* 1954 **26** 1762.
[15] Williams V. Z., Hofstadter R., and Herman R. C. *J. Chem. Phys.* 1939 **7** 802.
[16] Davies M. and Jones R. L. *J. Chem. Soc.* 1954 120.
[17] Lord R. C. and Merrifield R. E. *J. Chem. Phys.* 1953 **21** 166.
[18] Nakamoto K., Margoshes M., and Rundle R. E. *J. Amer. Chem. Soc.* 1955 **77** 6480.
[19] Lippincott E. R. and Schroeder R. *J. Chem. Phys.* 1955 **23** 1099.
[20] Jones R. N., Herling F., and Katzenellenbogen E. *J. Amer. Chem. Soc.* 1955 **77** 651.
[21] Jones R. N. and Cole A. R. H. *J. Amer. Chem. Soc.* 1952 **74** 5648.
[22] Depaigne-Delay A. and Lecomte J. *J. Phys. Radium* 1946 **7** 38.
[23] Mecke R. and Rossmy G. *Z. Elektrochem.* 1955 **59** 866.
[24] Kletz T. A. and Price W. C. *J. Chem. Soc.* 1947 644.
[25] Jones R. N., Nolin B., and Roberts G. *J. Amer. Chem. Soc.* 1955 **77** 6331.
[26] Davies M. *J. Chem. Phys.* 1948 **16** 274.

VOL. 9 1957

Spectrochimica Acta, 1957, Vol. 9, pp. 357 to 363. Pergamon Press Ltd., London

REPORTS OF MEETINGS

The Tenth Conference on Spectroscopy in the U.S.S.R.

Report based upon information supplied by V. V. NALIMOV and V. V. NEDLER, All Union Institute of Scientific and Technical Information, Moscow.

THE Tenth Conference on Spectroscopy, organized by the Spectroscopic Commission of the Department of Physical and Mathematical Sciences of the Academy of Sciences of the U.S.S.R., was held in Lvov (Ukrainian S.S.R.), from 4 to 14 July 1956. This conference is convened by the Commission for Spectroscopy in different republics of the Soviet Union every 2 years. The proceedings are printed in the *Bulletin of the Academy of Sciences of the U.S.S.R.** and the papers will be published in the *Proceedings of the University of the State of Lvov.*

There were 127 papers presented to the section on molecular spectra, and 165 to the section on atomic spectra.

Several papers dealt with the physical basis of spectral analysis, each devoted to a special aspect of the problem.

Papers concerned with the physical processes in the plasma included—The effect of the composition of the gas on the intensity of spectral lines with thermal excitation; Investigation of the conditions of ionization and excitation in the plasma of the arc discharge; Phase changes of temperature and degree of ionization in the high-voltage a.c. arc; Investigation of elementary processes in the torch discharge.

Electrode processes in the spark discharge, and the hydrodynamic theory of the formation of the flame were considered. It was shown that the formation and projection of the flame may be considered as an explosion of the surface layers of the metallic electrodes. The processes on the cathode and anode are different. The cathodic flame consists of streamers and comes from tiny patches, which rapidly appear and disappear; there are no streamers at the anode and the track starts from a fusion crater. The temperature of the flame leaving the electrode is obviously low, and activation of atoms occurs as the flame passes away from the electrode along the spark track.

The mechanism of entry of the electrode material into the luminous cloud of the condensed spark discharge was discussed, and the effect of cooling the electrodes upon line intensity was investigated. Some of the physical processes occurring in pulsed sparks were also considered.

The relation between the composition of the sample and of the radiating cloud was examined. The evaporation of the sample can be treated as an equilibrium

* *Bull. Acad. Sci. U.R.S.S. Ser. Phys.* 1937 **2** No. 2; 1940 **4** No. I; 1941 **5** No. 2–3; 1945 **9** No. 3,6 1947 **11** No. 4; 1948 **12** No. 4,5; 1950 **14** No. 4,5,6; 1953 **17** No. 5,6; 1954 **18** No. 2,6; 1955 **19** No. 1,2.

process and a thermodynamic treatment based on the theory of the evaporation of solutions can be applied.

Some authors have investigated the kinetics of the evaporation process and established the interesting fact that the total energy radiated at the characteristic frequencies of the element is dependent on its rate of evaporation.

Some data on the evaporation of binary alloys into the spark and arc and the dependence thereon of the temperature of the arc have been obtained.

A further group of papers dealt with methods of evaporation and the problem of the fractional evaporation of metals. Recently S. L. Mandelshtam, N. N. Semenov, and Z. M. Turovtseva published a new method for the determination of uranium in mixtures, called the method of evaporation. A vacuum method of evaporation, which combines fractional evaporation with accumulation of the evaporated mixture, and in many cases gives a marked increase in sensitivity, has also been developed. The role of "promoters," which increase the intensities of lines of other elements was examined. Some authors suggested that the action of these "promoters" depends on their stabilizing the burning of the arc and a reduced diffusion by the atoms of the element to be determined from the zone of the discharge; and that there is no relation between the effectiveness of the "promoter" and its rate of evaporation. Other authors held the opposite view.

Several papers described the use of radioactive indicators for investigating the evaporation of different elements contained in the sample to be analysed. In contrast with the normal method of determining the concentrations of elements from the relative intensities of their lines, the radioactivity of the residue gives a direct measure of the amount of an element which has not evaporated. This method was applied to investigate the effect of the total composition of the sample on the intensities of molybdenum lines, in the analysis of granites.

A number of papers dealt with the effect of the phase structure of metals and alloys, for example in cast iron or copper alloys, upon emission spectral analysis. The effect of a third component upon the analysis of binary alloys was also considered, and it was suggested that improvements could be obtained by introducing the sample as a powder into the gap between the electrodes. In the case of geological materials, an internal reference standard is sometimes added. For the analysis of ores of some rare-earth elements, or of scandium, a chemical pre-treatment is sometimes useful.

A few authors described work using photoelectrical recording methods. One method involving the simultaneous recording and comparison of two modulated light beams received by a single photomultiplier was explained. Steps to increase the stability of the photomultiplier by automatic regulation of the dynode voltages were suggested. The photoelectrical recording method has been applied in the analysis of phosphorus in steel.

A new development is the use of emission spectroscopy for the determination of gases in metals, e.g. oxygen or nitrogen in steel, or hydrogen in metals such as titanium, molybdenum and other alloys. Other advances in the experimental procedures included the possibility of carrying out spectral analysis directly in an electric arc steel smelting furnace, and portable equipment for the analysis of metal and slag in the furnace.

VOL. 9 1957

Among the detailed reports on specific analyses were those on steel, bronze, tungsten, molybdenum, niobium, tantalum, titanium, zirconium, cobalt, gold, tin, uranium, antimony, alkali metals and alkaline-earth metals. Other papers dealt with the analysis of cement, alundum, glass, corundum, slags, clays, and magnesite, metals in oils and metallic additives, trace components in phosphors etc.

In connection with the standardization of analytical methods, it was suggested that with slags, the best results are obtained in spectrographic analysis if the sample is first fused and then brought into solution. Factors such as plate development, arc temperature conditions, and other factors were considered.

The Eighth Annual Symposium on Spectroscopy

THE Eighth Annual Symposium on Spectroscopy sponsored by the American Association of Spectrographers in co-operation with the Milwaukee Society for Applied Spectroscopy and the Indiana Spectrographers Society, was held in Chicago, Illinois, from 29 April to 1 May 1957. The following papers were presented.

Time-resolved spectroscopy in spectrochemical analysis, A. BARDOCZ, Hungarian Academy of Sciences, Central Research Institute of Physics, Department for Spectroscopy.

Light radiated from transient spark discharges varies as the conditions vary in time in the source. The observation of the variation in time of the radiation emitted gives useful information concerning the excitation levels, variation in intensity, intensity ratios, pressure broadening, wavelength shift, Stark broadening, and self-absorption with time of the spectrum lines. This information can be obtained from time-resolved spark spectra taken with the intermediate of an electronically controlled high-precision spark source combined with a rotating-mirror optical system. From time-resolved spark spectra, spectrum lines suitable for analysis can be selected on a theoretical basis. In time-resolved spectra the continuous background originating at the beginning of the discharge is separated from the rest of the spectrum. The background-free spectrum, in addition to facilitating the construction of straight working curves without background correction is suitable for estimation of minor constituents in metals and alloys. Working curves for the estimation of impurities in aluminium are given. The background separated from the rest of the spectrum can be used in principle as internal standard in spectrochemical analysis.

Ultrasonics—a new tool? T. BULAT, Pioneer Central Division, Bendix Aviation Corp.

Applications of ultrasonic techniques in the laboratory were outlined.

Quantometric determination of phosphorus in steels, LOUNAMAA, NIILO, read by A. GOLDBLATT.

A method for the direct-reading determination of phosphorus in steel was described. Use of a constant time exposure rather than constant internal standard intensity provides analyses with a coefficient of variation of 4 per cent or less in the range of 0·02 to 0·08 per cent phosphorus.

X-ray spectroscopy in non-ferrous alloys, G. L. CRUMRINE, North American Smelting, Inc.

The use of the X-ray spectrograph in the analysis of non-ferrous alloys was reviewed. Problems involved, wet chemical checks, as well as the future aspects of the instrument's applications were presented.

A near infra-red study of fatty acids and some related compounds, P. Edmondson and R. Holman, Medical School, University of Minnesota.

The spectral absorption of a series of fatty acids and other lipids has been measured between 0·9 and 3·0 μ. By means of these spectra, band assignments have been made for many organic structures. Near infra-red spectra should simplify characteristics of many common chemical structures and may be valuable in the solution of many problems in lipid chemistry.

Infra-red analysis of synthetic waxes of the polychloronaphthalene type, L. Cencelj, University Chemical Laboratory, Ljubljana, Yugoslavia, read by L. Kaufmann.

Numerous isomers present in the wax are separated and identified by the combined techniques of absorption chromatography and infra-red analysis.

Identification and estimation of each isomer was made by comparing the spectra recorded under the same conditions for pure polychloronaphthalenes. In fractions having more than one isomer the relative content was estimated from the intensities of the corresponding bands for mixtures of pure isomers, since it is established that the intensity of some absorption bands in the 10–15 μ region is equal for all pure compounds.

Percentages of the various isomers are given. Where there is some doubt concerning the substitution in an isomer then the position of the absorption bands in the 11–14 μ region and the order of chromatographic elution are used to assign the correct position of the substituents.

Recent developments in infra-red instruments, V. J. King, Beckman Instrument Company.

Design and performance considerations of a double-beam, double-monochromator infra-red instrument were given.

The wavelength range from 0·5 μ to 35 μ can be covered by the selection of proper prism material incorporated in the integrated, easily changed, optical interchange units. Scattered radiation is less than 1 per cent. Instrument may be operated either single or double beam. Versatility and simplicity are stressed in overall instrument design.

VOL. 9 1957

The design and performance of a new infra-red spectrometer, J. Huley, Perkin-Elmer Corp.

Recent developments in infra-red at Baird-Atomic, Inc., Richard E. Reiss, Baird-Atomic, Inc.

Recent developments in infra-red instrumentation at Baird-Atomic were discussed. These developments include several new accessories. Particular attention was given to the KM-1 infra-red spectrophotometer and various components which may be added to increase the performance of this expandable instrument.

Use of X-ray spectroscopy for analysis of low atomic number elements, D. Miller, Philips Electronics, Inc.

The recent improvements in X-ray detectors make possible analysis of the elements in the sulphur-magnesium range which previously have not been possible by X-ray methods. A brief general discussion of the X-ray spectrographic method and instrumentation was followed by a description of the new flow counter X-ray detector. Data was presented showing limits of detectability for the various elements in the group being discussed. Calibration curves were shown for silicon in steels, aluminium alloys, silicon, calcium, aluminium and iron in cements, aluminium in bauxite, and chlorine in polyethylene.

Microspectrometry by X-rays, A. Engstrom, Department of Medical Physics, Karolinska Institutet, Stockholm, read by H. Hettel.

The use of X-rays for analytical purposes can be divided into three methodological groups defined after the interaction between X-rays and materials.

(a) Absorption
(b) Emission (fluorescence)
(c) Scattering

This communication presented techniques and applications of these principles to micro-

and histochemical problems. Amounts of substance as small as 10^{-12}–10^{-14} g can be analysed for certain components. The errors associated with the procedures were treated.

Determination of Rb and Cs by X-ray fluorescence, A. F. Vindeis Jr., Bell Telephone Laboratories.

An X-ray fluorescence method was described for the determination of Rb and Cs coprecipitated with potassiumtetraphenylborate. The cations are precipitated in dilute acid medium and filtered into $\frac{1}{2}$ in. discs of very pure, highly absorbent filter paper. The precipitate is then dispersed throughout the filter-paper pad with acetonitrile, acetone, or dimethyl formamide, and dried under an infra-red lamp. The filter-paper discs are then rotated in an aluminium sample-holder under the X-ray beam. A tungsten target X-ray tube is used as a primary source of X-ray, and is operated at 50 kV and 50 mA. A lithium fluoride analysing crystal is used to diffract the fluorescent radiation. The RbK_α and CsL_α radiation is used for the analysis lines. The method is sensitive to as little as 1 μg of Rb or Cs on the filter-paper pad. The standard deviation is 4·2 per cent with 5 μg and 2·9 per cent with 10 μg of Rb or Cs on the filter-paper pad. The method is applicable to from 1 to over 100 μg of Rb or Cs.

Spectrographic analysis by the evaporation method, S. Mandelshtam, Academy of Sciences Moscow, Russia.

Analytical curves for isotopic analysis, A. Striganow, Academy of Sciences, Moscow, Russia.

Application of atomic absorption spectroscopy to solids, M. E. Sikorski and P. L. Copeland, Armour Research Foundation.

The application of atomic absorbtion spectroscopy to the analysis of solids was reviewed. Advantages and limitations of the method were discussed and examples were given of applications of the method. Future possibilities were outlined.

Transient intensities in the spectrometric analysis of brass and nickel alloys, J. V. Hurwitz, Mines Branch, Ottawa, Canada.

A spectrographic study of the diffusion of B and Si into nickel, W. Tiffin, University of Florida.

The Quantovac: a direct-reading polychromator for the 1600 Å to 3000 Å region, G. Andermann, J. W. Kemp, and M. F. Hasler, Applied Research Laboratories, Glendale, California.

The Quantovac, which is basically a concave grating, vacuum spectrometer, suitable for work in the range from 1600 Å to 3000 Å, and equipped with a number of photoelectric detectors, was described in detail.

Its performance was evaluated particularly with reference to the measurement of carbon, sulphur, and phosphorus in ferrous materials, and new data were presented.

Its possible performance down to 1100 Å was discussed.

An arc method for sample transfer in spectrochemical analysis, C. J. Leistner, Allison Division, General Motors Corporation, Indianapolis, Indiana.

This paper included a survey of the foreign literature dealing with the sample transfer method for spectrochemical analysis. Emphasis was made on its application at the Allison Spectrographic Laboratory for quantitative and semi-quantitative evaluation of various jet-engine components.

Determination of silicon in cast iron, B. Kilberg, Deere and Company.

Sampling procedures were investigated and a selection was made of a procedure for cast iron that gives optimum results with regard to the determination of silicon as well as manganese and residual alloys in cast iron. A spectrographic procedure in which each reading is corrected for film contrast had also been worked out. A three-month correlation of spectrographic versus chemical analysis of silicon in cast iron was presented.

Observations on the spectrographic analysis of the heavy rare-earth elements, R. N. Kniseley, V. A. Fassel, W. F. Gordon, C. G. Tremmel, B. B. Quinney, R. W. Tabeling, and B. G. Hurd, Iowa State College, Ames, Iowa.

Emission spectrometric methods have been developed for the quantitative determination of rare-earth impurities commonly associated with purified Sm, Gd, Tb, Y, Tm, Yb, Lu, and Sc. Basically, the methods involved d.c. carbon arc excitation of rare-earth oxide-graphite mixtures, utilizing the unique similarity in excitation behaviour of many of the rare earths to provide a high degree of internal standardization. The problems encountered in rare-earth analysis were discussed in detail along with the presentation of the data relating to the individual methods.

Problem of direct reading in the ultra-violet vacuum region, Edgar Luscher, Institute of Technology, University of Lausanne.

For direct reading in the Schumman region of the electromagnetic spectrum there exist only two possibilities for detectors, namely Geiger-Müller counters and special photomultipliers with a thin quartz window (up to 1750 Å) or with fluorescent screen. Construction of Geiger-Müller counters and applications of photomultipliers were discussed. Descriptions of the mounting in vacuum or in an inert-gas atmosphere of spectrographs were given.

Spectroscopic instrumentation in the Soviet Union, Robert J. Meltzer, Bausch and Lomb Optical Company, Rochester, New York.

This paper described and illustrated those spectroscopic instruments developed in the Soviet Union which are in production as standard instruments rather than special-purpose instruments. They include instruments for emission spectroscopy; absorption spectroscopy in the ultra-violet, visible and infra-red; and Raman spectroscopy.

VOL. 9 1957

A new visual spectroscope for metal analysis, Wm. Rudin, Elesco Smelting Corp.

The installation and operation of the "Fuess Metal Spectroscope" were discussed. Various accessories to the instrument as well as its application to specific problems were given.

Analysis of heat-resistant alloys, Jack Rosza, National Spectrographic Laboratories.

The derivation of a method for the analysis of high-temperature alloys as well as various problems connected with the attainment of sensitivity for W and Cr as well as the method for obtaining the residual elements were discussed.

Effective line-widths in photographic spectral photometry, J. Junkes, S.J. and E. W. Salpeter, S.J., Astrophysical Laboratory of the Vatican Observatory, Castel Gandolfo, Italy; read by J. J. Devlin, S.J.

The width of any photographic image increases with increasing intensity and can be used for intensity measurements. The "effective width of a spectral line" is a photometric parameter. When the spectral line is symmetrically placed on the slit of a photometer, and the aperture of the slit is adjusted in such a way that a given amount of light is always transmitted, then this aperture is a measure of the width of the line and is called its "effective width."

Effective line-widths are related to opacities rather than to real line-widths, but they allow one to measure more of the photographic effect. Their logarithms combine with log E and log C in the same manner as do the densities, but they embrace greater intervals, as is shown by a few examples.

The measuring of these effective line-widths can be done with the usual densitometers, if only their slits can be opened wide enough, but for continuous work, an appropriate variable slit photometer is to be recommended, for which a new slit system, based on the parallelogram principle, is proposed.

A.c. arc method for the analysis of cast-iron alloys, M. J. TUMEY, Fabricast Division, General Motors Corp.

This paper represented the culmination of efforts to standardize all spectrographic methods for steel, cast iron, and nodular iron into one versatile method. This method has proved itself valuable in that all of the common types of cast iron, grey, perlitic, or nodular, as well as low-alloy steels can be analysed by the same method and using common working curves. The method is simple, easy to control, and fairly foolproof.

NOTICE OF MEETING

Conference on Molecular Spectroscopy

Preliminary Notice

THE Spectroscopic Panel of the Hydrocarbon Research Group of the Institute of Petroleum is organizing a Conference on Molecular Spectroscopy to be held at the Institution of Electrical Engineers in London on 27 and 28 February 1958. This is the second Conference to be arranged by the Panel and, as in the previous one held in October 1954, the programme will cover the whole field of spectroscopy, the emphasis being on the newer techniques and the more recent developments in instrumentation. The main topics to be discussed will be Nuclear Magnetic Resonance, Technical Developments, Intermolecular Forces and Factors Affecting Intensities of Absorption Bands. In addition there will be an open discussion on the organization of spectroscopic services in an industrial laboratory.

The papers contributed will be by invitation only and will be preprinted for circulation prior to the meeting. Application forms for membership of the Conference, together with further information, can be obtained from:

E. THORNTON,
Secretary, IP Spectroscopic Panel,
c/o The British Petroleum Co. Ltd.,
Chertsey Road,
Sunbury-on-Thames,
Middlesex.

It is hoped to arrange for modern British spectrometric equipment to be on exhibition during the Conference.

Announcement

Prof. M. KENT WILSON has kindly undertaken to serve as Acting Editor during the absence of Dr. MILLER, who is on sabbatical leave at Zurich until mid-1958.

Dr. B. F. SCRIBNER has kindly undertaken to serve as Acting Editor in the absence of DR. FASSEL, who is on sabbatical leave in India until early 1958.

Communications which would otherwise have been directed to Drs. MILLER or FASSEL can, therefore, be sent to the respective Acting Editors.

Papers to be published in future issues

S. Mandelshtam: Excitation of the spectrum in a spark discharge.

Michio Hayasha, Isao Ichishima, Takehiko Shimanarch, and San-ichiro Mizushima: Internal rotation in 1,2-dichloro-2-methylpropane.

M. St. C. Flett: Studies of the band near 3 μ in some hydroxy compounds.

A. Fiorenza and M. Lachin: La mesure de la "Largeur effective" des raies dans l'analyse des substances en poudre.

K. D. Mielenz: Zur Ausleuchtung von Spektrographen durch Zwischenabbildung der Lichtquelle.

William G. Fateley and Ellis R. Lippincott: Normal co-ordinate analysis of the vibrational spectrum of iron pentacarbonyl.

José R. Barceló: The infra-red spectrum of some metallic chelate compounds—I. Rubeanates.

K. Bunge: Materialabbau in Funkenentladungen. Experimentelle Untersuchungen an Zinkkathoden.

D. Hadži and D. Prevoršek: Infra-red absorption bands associated with the NH Group—III. Hydroxamic acids and derivatives.

P. J. Stone and H. W. Thompson: Vibrational band intensity of the hydroxyl group in phenols.

J. G. Hawkins, E. R. Ward, and D. H. Wiffen: Characteristic infra-red absorption frequencies of substituted naphthalenes.

J. Artaud, J. Blaise, and S. Gerstenkorn: Analyse isotopique du lithium par spectroscopie optique.

H. Schüler and E. Lutz: Organische moleküle in der Glimmentladung. Spektroskopische untersuchungen über das verhalten von Benzol, Toluol, Chlorbenzol Diphenyl und Benzylchlorid III.

J. B. Ainscough and J. Gaunt: The molecular structure of niobium pentachloride.

J. B. Ainscough and J. Gaunt: The molecular structure of antimony pentafluoride.

Urner Liddel and Edwin D. Becker: Infra-red spectroscopic studies of hydrogen bonding in methanol, ethanol and *t*-butanol.

F. Rosendahl: Untersuchung der statistischen Streuung der Restgehaltsbestimmung nach dem spektrochemischen zugabeverfahren.

Theodore L. Brown: The solvent effect in infra-red densities.

Eugene Lieber, T. S. Chao, C. N. Ramachandra Rao: The ultra-violet absorption spectra of substituted phenyl amino-1,2,3-triazoles.

R. E. Richards and J. B. Leane: Proton resonance spectra of some crystals containing nitrogen and fluorine.

D. C. McKean: Infra-red spectrum of tetramethylhydrazine.

Gilbert Michel and Georges Duyckaerts: Contribution à la spectrometrie Raman. II. Intensite de la raie du carbonyle aliphatique.

San-ichiro Mizushima, Akiko Yamaguchi, Tatsuo Miyazawa, Takehiko Shimanouchi: Normal vibrations of urea and urea-d_4.

O. S. Heavens, J. Ring, and S. D. Smith: Interference filters for the infra-red.

P. Krumholz: Spectroscopic studies on rare earths compounds. I. Instrumentation.

P. Krumholz: Spectroscopic studies on rare earths compounds. II. A comparative study of the absorption spectra of the neodymium ion in aqueous solution and in crystalline salts.

Editorial Note

The index to Volume IX will be published in Vol. X.

VOL.
9
1957

VOL.
9
957